AAPS Advances in the Pharmaceutical Sciences Series 8

Brian R. Moyer
Narayan P.S. Cheruvu
Tom C.-C. Hu *Editors*

Pharmaco-Imaging in Drug and Biologics Development

Fundamentals and Applications

aapspress
Springer

AAPS Advances in the Pharmaceutical Sciences Series

The AAPS Advances in the Pharmaceutical Sciences Series, published in partnership with the American Association of Pharmaceutical Scientists, is designed to deliver well written volumes authored by opinion leaders and authoritarians from around the globe, addressing innovations in drug research and development, and best practice for scientists and industry professionals in the pharma and biotech industries. For more details and to see a list of titles in the Series please visit
http://www.springer.com/series/8825

Brian R. Moyer • Narayan P.S. Cheruvu
Tom C.-C. Hu
Editors

Pharmaco-Imaging in Drug and Biologics Development

Fundamentals and Applications

aapspress Springer

Editors
Brian R. Moyer
BRMoyer & Associates, LLC
Bedford, NH, USA

Narayan P.S. Cheruvu
Covidien Inc.
Hazelwood, MO, USA

Tom C.-C. Hu
Health and Human Services
Office of the Assistant Secretary
of Preparedness and Response (ASPR)
Biomedical Advanced Research
and Development Authority (BARDA)
Washington, DC, USA

Additional material to this book can be downloaded from
http://extras.springer.com/978-1-4614-8247-5

ISSN 2210-7371 ISSN 2210-738X (electronic)
ISBN 978-1-4614-8246-8 ISBN 978-1-4614-8247-5 (eBook)
DOI 10.1007/978-1-4614-8247-5
Springer New York Heidelberg Dordrecht London

Library of Congress Control Number: 2013943597

Printed on acid-free paper

Springer is part of Springer Science+Business Media (www.springer.com)

Brian R. Moyer: To my wife, Carol, who has been an ever-strong influence in my life to always produce excellence, to our daughters, Lauren and Alycia, who always know that the dinner conversation will take a strange twist when Dad talks "science," to my parents Harold and Shirley, for the way of life they taught me, and, to my mentor in imaging, Dr. Thomas F. Budinger, who taught me the true art of "seeing" science and to really love the imaging world.

Narayan Cheruvu: To my wife, Lavanya, for her support and dedication to family, to my parents (Sri Rama Sarma Cheruvu and Lakshmi Rajyam Cheruvu), and to my mentors Prof. Darbha S. Sharma (at IT-BHU), Prof. K.V. Ramana Murthy (at Andhra University), and Dr. Tata N.V. Prasad (at Covidien Ltd).

Tom C.-C. Hu: To my wife, Vivian, for her understanding for numerous late evening writings, reviews, and evaluations. To our kids, Abigail and Joshua, for all the joys and blessings they bring to our lives. Being a parent is truly a humbling experience. To my family, Kuo-Chieh Hu, Mei-Tsen Li, Chih-Kao Hu, and Chih-Ching Hu for the unending support to my pursuit of scientific knowledge. To my mentors, Drs. Alan P. Koretsky, Chien Ho, Guy MacGowan, and Miguel Llinás,

Preface

Imaging sciences applied to medicine could be regarded as starting when the first histologic section was viewed or when Roentgen accidently took a picture of his hand by interfering with photons hitting a photographic plate. In the 1990s applications of PCR in gene mapping along with novel methods and automated systems for protein expression helped define the molecular basis of several pathologies and has led to many new ideas on how to track, treat, and follow disease. The revolution in how we look at disease has now created a time where "Pharmacology, and indeed pathology itself, is *Visible*." What do we mean by this statement? Alongside the development of such technologies as PCR and molecular biology revolution was another engineering and mathematics revolution, which when combined with the molecular biology advances has pushed the proverbial "Physician's Black Bag" into a whole new tool chest that opens up diagnostic and therapeutic potentials we only thought was possible in science fiction a few short years ago.

In this new twenty-first century, we are witnessing the creation of an expanding "biomarker" library, tools to "see" pathology as a dynamic, i.e., as it is progressing in situ, and not simply under the microscope on histology slides, the ability to measure treatment responses in vivo and to give doctors as well as patients a way to understand what their disease is and how it is responding to therapy. Consider the ultrasound image that is now a common "souvenir" of a pregnancy. The image used to be a blur of sound echoes translated to an electronic display and printed on a recording film, and now, due to better understanding of sound wave physics, mathematical computations providing high-resolution electronic signals and translated into high-definition displays (or "maps"), we not only recognize "a fetus," but the image created today introduces us to seeing a recognizable "brother or sister."

The late 1900s saw the revolution of 2-D (photo-type imaging) to 3-D projection imaging. The ability to create "bread slicing," otherwise known as "tomography," or serial projections of the body has revolutionized and personalized medicine. One can use x-ray computed tomography (CT) for anatomy, positron emission tomography (PET) and single photon emission computed tomography (SPECT) for functional distribution of radiotracers, magnetic resonance imaging (MRI) and magnetic

resonance spectroscopy (MRS) for metabolic and very high resolution (near micron resolution) of the "state of water" (fixed in place or flowing plus "seeing" the chemical state) and even ultrasound to view internally as if we were actually there such that we can rotate about "inside" as if we are in situ ourselves. The utility of the human-sized instruments we use in the clinic applied to small animal research is, however, poorly translatable, impractical, as well as cost prohibitive. While pharmaceutics are generally developed first from animal models to the eventual testing in the clinical subject or volunteer, imaging has recently reversed this path to head back to the laboratory to develop systems which are designed specifically, but with full clinical translational intent, for use in small animals.

Clinical development within "Pharma" (the collective pharmaceutical business) has fostered the need to miniaturize the practical imaging field for human to that useful for small mammals such as the mouse. Accomplishing technical reductions of human-sized imaging platforms to accommodate animal models has fostered, indeed required, technical advances in material and computational sciences. Novel new materials for scintillation detection has allowed for smaller platforms but indeed higher efficiency in photon capture. In nuclear medicine, smaller detectors and tight packing has led to very high resolution systems. Modern micro-electronics to improve signal separation, reduce signal cross-talk (i.e., random event errors, etc.), and high speed processor electronics for digital as well as analog computational activities, has allowed for very small animals to be imaged with very useful image quality. Computational improvements include complex algorithms which can collect and frame digital data, construct and statistically correct the image, translate to visual media (screen, film, digital, contrast variables, and signal intensity correction (isobar color pallets). These platform improvements provide the investigator with highly sensitive analytical tools to witness drug actions in small animals. The utility of quantifying anatomic regions and volumes of interest (ROI and VOI, resp.) in serial image collections can provide for dynamic assessments (time variance of a signal) in the test system (animal model). One can also perform dual mode imaging, i.e. co-positioning of two imaging platforms, to collect, for example, anatomy with function (i.e. CT with PET, MRI with PET, etc.). Multiplatform imaging can provide the pharmacologist with a novel "view" of drug or biologic targeting and/or response over the course of an ever-changing landscape related to a pathophysiology.

MRI (magnetic resonance imaging), MRS (magnetic resonance spectroscopy imaging; imaging of metabolites), optical probes of luminescence (luciferase based) or fluorescence (Quantum Dots, near infrared (NIR), and BRET imaging (self-illuminating probes) are all adding to the novel drug development armament. Laser excitation of in vivo sites of optical probe uptake allows for small animals (e.g., nude mice with modest translucence due to thin skin and target-to-light distance is minimally interference by scatter), and excitation of a probe by an outside light source can make the localized probe emit a response light at a different wavelength for remote ex vivo detection. The internal scatter and reflectance within the animal body can be determined in a semi-quantitative manner to provide a scatter- and attenuation-corrected uptake value to compare against controls.

The advent of hundreds of new, highly specific, target-oriented animal models of disease has allowed us to optimize both the performance of imaging platforms as well as the opportunity to optimize the animal models. Imaging scientists now have the molecular biology revolution to help define diseases not through the microscope but through the visualization of a pathology's pharmacodynamics, i.e., tracking and localizing disease processes using patho-specific biomarkers, probes, and chemical state. The recent additions of optical imaging with self-illuminating quantum dots (QDs), the advances in the libraries of knockout/in animal models, chemical analytical methods now applied to autoradiographic as well as in vivo imaging (MALDI and SIMS-MS and MRS imaging), have all made small regional in vivo sampling possible. The drug development paradigm is now shifting from the formalism of the pharmacology and toxicology paths of the last century that has served us well to a potentially revolutionary path which will reduce animal usage and obtain time rate of change of biomarker and physiologic responses to drugs and biologics and create new interventional strategies.

This book is intended to be a contribution to the understanding of imaging as may be practically applied to the regulatory advancement of drugs and biologics. The enormity of the subject matter, the diversity of imaging platforms, and the daily addition of biomarkers and imaging agents makes this volume "out of date" as soon as it is published. However, we invite the reader to delve into this subject matter with imagination and to take the knowledge collected from this volume to apply these technologies toward the regulatory approvals of his or her own diagnostic or therapeutic products.

The book is for practical purposes divided into the specific platforms used currently in nonclinical imaging and especially as applied to drug and biologics development. That is, following a general introduction to the imaging platforms of nonclinical imaging (Moyer; Chap. 1) we describe the laboratory environment (Stout; Chap. 2) and practical setup considerations (Klaunberg and Morris; Chap. 3) that must be examined to establish a functional and economical asset to the company or academic laboratory for investigations into the pharmacology and toxicology of new chemical entities. In Chap. 4, we introduce the reader to a large Pharma company's philosophical and practical uses of imaging (Freedman). We step away from imaging per se in Chap. 5 for a short lesson on the concept of animal dosing and allometric considerations in imaging studies (Moyer). Solon and Moyer (Chap. 6) takes us through a very old but still highly applicable imaging technique called "autoradiography" and he introduces many new applications and analytical approaches using NIMS, MALDI, and MRS in tissue slice analyses. Chapter 7 (Bradley and Wyant) takes us to a favorite topic in the imaging world: Oncology. The authors provide examples of several animal models as well as inform on the limits of imaging oncology targets and measurement of therapeutic efficacy endpoints in small animal models. They have provided examples of molecularly engineered imaging probes (i.e. Mabs, etc.) and animal models that may potentially show target specificity losses from genetic change in the tumor or in the genetics of the host animal. Chapter 8 (Loutsios et al.) discusses the imaging of labeled cells and methods to maintain functionality with the perturbation of radiolabeling.

Golding and Zaitseva (Chap. 9) discuss the role of imaging in infections and their studies using bioluminescent technologies. Keith et al. (Chap. 10) introduce us to the very difficult work of imaging in the BSL3 and BSL-4 environments where pathogens must be controlled and imaging systems must be isolated for maintenance as well as operator protection. Moyer et al. (Chapter 11) take us through the physics of MR and how images are produced but more importantly the limitations of MR in resolution, time rates of change of any given pharmaceutical, contrast agent or biomarker, and the high signal requirements needed for quantitative imaging in small animals. Chapter 12 (Venter et al.) discusses the principles and technologies of magnetic resonance spectroscopy imaging (MRSI) and how we can image in situ a chemical entity's metabolomics as a consequence of disease or pathology. Lastly, we offer a regulatory chapter (Chap. 13, Moyer et al.) where we cite the regulatory implications of image sensitivity, specificity, quality and reproducibility, core laboratory image reading, image charters, receiver–operator characteristics (ROC) analysis of sensitivity and specificity of an imaging technique, and examine the regulatory guidance documents that are written mostly for the development of imaging agents and contract agents but where we are attempting to "turn the coin over" and examine the other approach, e.g., use known imaging agents that are functionally related to a pharmaceutical to advance that drug or biologic to their own regulatory approvals.

We invite you to read these chapters not as "facts to take back" to the laboratory but rather as "ideas to apply" to your own specific situation, your animal model and pathology and clinical indication that you are investigating. The primary goal of the book is to strip down the complexities of imaging (the physics, computational requirements, and limitations), the assortment of nuclear, optical, MR, and other probes that may be applicable, and the assessment of "practicality" in bringing an imaging platform (or more than one as in combined modalities, i.e., PET and CT) into your own laboratory setting. Imaging can offer so much "visibility" to pharmacology and we do believe imaging technologies will offer any investigator an actual vision or understanding of the pathology they are studying. Use of imaging should result in more defined pathways toward regulatory approvals. The future advancements and improvements in imaging systems that are expected in the next few years will certainly move drug and biologics development with even more "clarity of next steps" for more rapid drug or biologic advancement to approval.

To our imaging colleagues, respectfully.

Bedford, NH, USA — Brian R. Moyer
Hazelwood, MO, USA — Narayan P.S. Cheruvu
Washington, DC, USA — Tom C.-C. Hu

Quotes

"We are experiencing a paradigm shift from anatomic towards biomarker (molecular imaging) as the primary means for assessing treatment response in Oncology"

quote from Dr. Steven Larson, 2005.

"The source and center of all man's creative power … is his power of making images, or the power of imagination."

Robert Collier, American motivational author, 1885–1950

"Logic will get you from A to B. Imagination will take you everywhere."

Albert Einstein, American Physicist, Nobel Laureate 1921, 1879–1955

"You cannot depend on your eyes when your imagination is out of focus."

Mark Twain, American Humorist, Author, 1835–1910

Contents

Contributors

Kottekkattu K. Balan Nuclear Medicine, Addenbrooke's Hospital, CUHNHSFT, Cambridge, UK

Laura Bollinger Integrated Research Facility, National Institutes of Allergy and Infectious Diseases, National Institutes of Health, Frederick, MD, USA

Daniel P. Bradley Millennium: The Takeda Oncology Company, Cambridge, MA, USA

Svetlana Chefer Integrated Research Facility, National Institutes of Allergy and Infectious Diseases, National Institutes of Health, Frederick, MD, USA

Narayan P.S. Cheruvu Covidien Inc., Hazelwood, MO, USA

Edwin R. Chilvers Division of Respiratory Medicine, Department of Medicine, University of Cambridge School of Clinical Medicine, Cambridge, UK

Alison M. Condliffe Division of Respiratory Medicine, Department of Medicine, University of Cambridge School of Clinical Medicine, Cambridge, UK

Kevin A. Douglass Department of Chemistry, Western Michigan University, Kalamazoo, MI, USA

Neda Farahi Division of Respiratory Medicine, Department of Medicine, University of Cambridge School of Clinical Medicine, Cambridge, UK

Immanuel Freedman GlaxoSmithKline, King of Prussia, PA, USA

Daniel Gillett Nuclear Medicine, Addenbrooke's Hospital, CUHNHSFT, Cambridge, UK

Hana Golding Division of Viral Products (DVP), Center for Biologics Evaluation and Research (CBER), Food and Drug Administration (FDA), Bethesda, MD, USA

Sarah Heard Nuclear Medicine, Addenbrooke's Hospital, CUHNHSFT, Cambridge, UK

Tom C.-C. Hu Health and Human Services (HHS), Office of the Assistant Secretary for Preparedness and Response (ASPR), Biomedical Advanced Research and Development Authority (BARDA), Washington, DC, USA

Nuclear and Radiological Engineering/Medical Physics Program, George W. Woodruff School of Mechanical Engineering, Georgia Institute of Technology, Atlanta, GA, USA

Demian R. Ifa Department of Chemistry, York University, Toronto, ON, Canada

Peter Jahrling Integrated Research Facility, National Institutes of Allergy and Infectious Diseases, National Institutes of Health, Frederick, MD, USA

Emerging Viral Pathogens Section, National Institute of Allergy and Infectious Diseases, National Institutes of Health, Bethesda, MD, USA

Lauren Keith Integrated Research Facility, National Institutes of Allergy and Infectious Diseases, National Institutes of Health, Frederick, MD, USA

Brenda A. Klaunberg NIH Mouse Imaging Facility, National Institute of Neurological Disorders and Stroke, National Institutes of Health, Bethesda, MD, USA

Chrystalla Loutsios Division of Respiratory Medicine, Department of Medicine, University of Cambridge School of Clinical Medicine, Cambridge, UK

H. Douglas Morris NIH Mouse Imaging Facility, National Institute of Neurological Disorders and Stroke, National Institutes of Health, Bethesda, MD, USA

Brian R. Moyer BRMoyer & Associates, LLC, Bedford, NH, USA

A. Michael Peters Clinical Sciences Imaging Centre, Brighton and Sussex Medical School, Brighton, UK

Jonathan Potts Clinical Sciences Imaging Centre, Brighton and Sussex Medical School, Brighton, UK

Prina Ruparelia Division of Respiratory Medicine, Department of Medicine, University of Cambridge School of Clinical Medicine, Cambridge, UK

Jurgen Seidel Integrated Research Facility, National Institutes of Allergy and Infectious Diseases, National Institutes of Health, Frederick, MD, USA

Chandra K. Solanki Nuclear Medicine, Addenbrooke's Hospital, CUHNHSFT, Cambridge, UK

Kishor Solanki Nuclear Medicine, Addenbrooke's Hospital, CUHNHSFT, Cambridge, UK

Jeffrey Solomon Integrated Research Facility, National Institutes of Allergy and Infectious Diseases, National Institutes of Health, Frederick, MD, USA

Eric G. Solon QPS, LLC, Newark, DE, USA

David B. Stout Biomedical Physics IDP, Molecular & Medical Pharmacology, Preclinical Imaging Technology Center, Crump Institute for Molecular Imaging, University of California, Los Angeles, CA, USA

Charlotte Summers Division of Respiratory Medicine, Department of Medicine, University of Cambridge School of Clinical Medicine, Cambridge, UK

David Thomasson Integrated Research Facility, National Institutes of Allergy and Infectious Diseases, National Institutes of Health, Frederick, MD, USA

Andre R. Venter Department of Chemistry, Western Michigan University, Kalamazoo, MI, USA

Jessica White Division of Respiratory Medicine, Department of Medicine, University of Cambridge School of Clinical Medicine, Cambridge, UK

Simon Williams Deptartment of Biomedical Imaging, Genentech, Inc., South San Francisco, CA, USA

Tim Wyant Millennium: The Takeda Oncology Company, Cambridge, MA, USA

Srikanth Yellayi Integrated Research Facility, National Institutes of Allergy and Infectious Diseases, National Institutes of Health, Frederick, MD, USA

Marina Zaitseva Division of Viral Products (DVP), Center for Biologics Evaluation and Research (CBER), Food and Drug Administration (FDA), Bethesda, MD, USA

Chapter 1
Imaging Platforms and Drug Development: An Introduction

Brian R. Moyer

Abstract Medical imaging over the last century contributed significantly in the knowledge of disease, disease mechanisms, and even in the molecular manipulation of disease with drugs and biologics. The discovery of how molecular biomarkers express, locate, change, and often drive physiologic processes has been greatly expanded using imaging. The advances in medicine from imaging have driven even more development of imaging platforms toward miniaturization for use in the nonclinical laboratory. The recent additions in the area of optical imaging with self-illuminating quantum dots (QDs), the advances in the libraries of knockout/in animal models, chemical analytical methods now applied to imaging (MALDI and SIMS-MS and MRS imaging) have made small regional in vivo sampling possible. The drug development paradigm is now shifting from the formalism of the pharmacology and toxicology paths of the last century that has served us well to a potentially revolutionary path which will reduce animal usage and obtain time rate of change of biomarker and physiologic responses to drugs and interventional strategies. This chapter is intended to be a broad overview of imaging platforms for the readers to introduce themselves into this subject matter and to come away with a new knowledge of these technologies and how they may assist in the advanced development of drug or biologics and toward regulatory approval.

Mr. Moyer is currently contracted to the Biomedical Advanced Research and Development Authority (BARDA), Health and Human Services (HHS), Washington, DC as Sr. Science Advisor, Project BioShield, Chemical, Radiologic and Nuclear Threats (CRN Group, through Tunnell Government Services (TGS), Bethesda, MD; He owns and operates his consulting firm, BRMoyer & Associates, LLC, out of Bedford, NH, specializing in imaging systems and approaches for drug development, radiation and chemical injury medical countermeasures, and pharmacokinetics and toxicokinetics of drugs and biologics.

B.R. Moyer (✉)
BRMoyer & Associates, LLC, 23 Hawk Drive, Bedford, NH 03110, USA
e-mail: bmoyernh@gmail.com

B.R. Moyer et al. (eds.), *Pharmaco-Imaging in Drug and Biologics Development*,
AAPS Advances in the Pharmaceutical Sciences Series 8, DOI 10.1007/978-1-4614-8247-5_1,

1.1 Molecular Medicine Has Arrived

"Modern medicine" has morphed into "Molecular Medicine" and it has taken on this new identity in part due to the capabilities of imaging. Where imaging used to mean the view through the microscope in 1800s, it became the view on the silver halide photographic plate in the time of the early 1900s. The advent of highly sensitive photographic emulsions and manufacturing of uniform films gave science the ability to perform autoradiographs of the distribution of radiopharmaceuticals in pathologic anatomy which added a physiologic "photo" onto the classic artwork of Frank Netter. This new "view" provided a way to discern pathology—an "outside-in" view—of internal structures. Autoradiography has changed over the years and is not simply histology slides with silver grains (see the chapter on Autoradiography; Chap. 5).

I place the advent of "modern" imaging at the hands of Hal Anger who exploited the known NaI crystal detectors for recording ionizing radiation to capture gamma photons from emitting radionuclides. He combined a packed array of photomultiplier tubes onto a large NaI crystal (approx. 10–15 cm diameter) and covered the crystal with lead shielding machined with a designed array of small holes (collimation). The result was a way to take a 3-D object with radioactivity dispersed in the volume and acquire an image that showed the 3-D object as a 2-D projection (i.e., a typical photograph) by collecting an electronic map of oscilloscope events (recorded positional scintillations on photographic film using a camera with an open aperture) which acquired for a period of time, provided a collection of events that as an aggregate, created an "image" of the distribution. Today, with hardware advancements and computational systems that were unimagined in the mid-1950s, we utilize novel chemistry and synthetic methods to create radiopharmaceuticals tagged with specific radionuclides which allow us to examine pathophysiology in three dimensions and over time. The use of even more regions of the electromagnetic spectrum from infrared (optical imaging) through radiowaves (MRI, fMRI, and MRS imaging; see Chaps. 11 and 12), we can diagnose disease and evaluate treatment success for, to name a few, cardiac disease, Alzheimer's disease, diabetes, cancer, infectious diseases, and so many other pathologies, but now with exceptional resolution in both space and time.

Alzheimer's disease was discovered in the 1800s through examination of postmortem brain tissues for the presence of amyloid. Today we can view amyloid deposition in vivo with noninvasive imaging platforms and novel molecular probe which have affinity for amyloid. We have an alternative as well by looking for a pharmacodynamic effect of amyloid deposition such as reduced glucose metabolism. Knowledge of either the extent of amyloid deposition itself or the manifestation of amyloid as reduced cognition or glucose utilization may potentially provide treatment strategies and also allow us to measure their effectiveness.

Molecular medicine is now the exploitation of patho-specific "biomarkers" to detect disease. Physicians can now "find, fight, and follow" disease (e.g., diagnose, treat, and measure success of treatment) using imaging and the need for new novel disease biomarkers is in high demand. This chapter introduces the reader to the history and significance of selected innovative physical and molecular biomarker

probes and the instruments that are now using these probes. The reader gains an appreciation of the cleverness and the scientific simplicity that imaging has brought to the toolbox of medical sciences in the fight against disease.

1.2 Molecular Medicine: What Is an "Image"

The intent of this book is to introduce the reader to the use of imaging in drug and biologics development by impressing upon the reader the wide array of tools now at their doorstep. Modern medicine has advanced to heights our scientific predecessors, even those of 20 years ago, could not foresee except in science fiction. Looking into the human body in three dimensions, with clarity and spectacular resolution, we can now watch the brain "think" with imaging tools such as functional magnetic resonance imaging (fMRI), see if a cognition deficit is regionally defined with glucose utilization, measure a heart variable such as blood flow (angiography) or metabolism (glucose or palmitate utilization), infection localization, cancer structure, metabolism and viability (CT, PET and thymidine analogs, MR, resp), and so much more. In some ways, however, the imaging field has been like the "blind man and the elephant" where one imaging modality defines one part of "the picture" and another modality defines another. In this scientific review we attempts to cover many of the modalities of medical imaging which have grown in clinical and non-clinical acceptance as both notional (exploratory) and definitive (regulatory body acceptance) laboratory tools to add to the drug development laboratory repertoire.

Biomarkers include the physical and chemical system responses to disease or injury like the expression of a protein or up (or down)-regulation of a receptor. Biomarkers include, for example, biologics that are used to monitor and direct therapy in chronic diseases such as cancer (e.g., carcinoembryonic antigen, CEA), diabetes (hemoglobin-Alc), and autoimmune disease (Rheumatoid factor). LaBaer (2005) outlines eight "biomarker rules", however, as this review focuses on imaging biomarkers, emphasizes his Rules #3, #4, and #8 which read, respectively: #3: "Consider the target and control populations carefully", #4: "focus on developing a sensitive and specific test …", and #8: "remember these samples come from people—and mice (and other animal models) are not people".

In "imaging" we do not refer to the probe as the "biomarker." Imaging biomarkers are the product or "view" as seen through an imaging system, with or without the use of a bioprobe, to define the expression, or "mark", of disease or injury. Biomarkers include changes in anatomy (i.e., bone density or tissue fluid balance), drug actions, receptor binding, genomic expression or adduct formation (DNA/RNA adducts), metabolite formations (metabolomics and proteomics), change in enzyme rates, urinary and blood related adducts (i.e., hemoglobin and albumin), organ and tissue uptake, cascade initiation, clearance of an initiating drug as well as the inhibition or acceleration of a secondary biologic expressions, and more. Indeed, biologic measures that can be validated as part of a drug effect or system response can be considered, with regulatory scrutiny, a "biomarker." The time course, identity, and relative abundance (signal) of biomarkers must be fully characterized in order

to use them as surrogate investigative measures in research or diagnosis (LaBaer 2005; Colburn 1995, 1997; Daniels and Hughes 1997; De Gruttola et al. 1997; Deyton 1996; Ellenberg and Hamilton 1989; Frank and Hargreaves 2003; DeMeyer and Shapiro 2003; Bocan 2010, Fleming and DeMets 1995). Bocan (2010) is a fine introduction on imaging biomarkers and the imaging platform technologies that are discussed in this volume.

A typical biomarker is not generally a step function, i.e. "ON" and then "OFF", but may be expressed as a step function when defined as a family of events that together are assigned a threshold limit for "ON" or "OFF". A urinary metabolite may appear rapidly as a biologic response, increase over time, and decline while urinary adducts, as a continuum of the response which can last for months before declining, may appear late. The presence of both as a family of events is a "biomarker". Biomarkers are best described and validated in terms of their pharmacokinetics with expression variables such as time to first appearance, or T_a, which is dependent on sensitivity of the assays, the slope of marker expression (rate to full expression which can be dose-dependent and nonlinear), T_{max} (time to maximum expression), C_{max} (maximal concentration at target or site of measurement), and washout (loss of effect or clearance of the biomarker, both expressed as a decay half-life). The reappearance of a biomarker upon repeated challenge may be limited due to receptor saturation (maximal binding), catabolism and resynthesis of the receptor as well as reinsertion into the receptor site, or depletion of expression (consumption rates and delay of replacement rates). Biomarkers must be measurable, their kinetics understood, and the link to their source validated.

Imaging is a scientific discipline which one can utilize the full electromagnetic spectrum from high energy gamma rays to low energy radiowaves and mathematically transforms the energy frequencies detected into a readable format—an "image"—to describe a natural phenomenon. In some respects, imaging is simply a "pattern recognition" tool used to describe pathologies or anatomical features through a translation process. An example of an image pattern is, for example, a "heat map" of selected genes which, as an aggregate expression, form a recognizable (sensitivity threshold) "pattern" representing "ON" and "OFF" genetic switches (Fig. 1.1). Figure 1.1, taken from one of my previous publications (Moyer and Barrett 2009), is such an example. Here peripheral blood (PB) metagene color profiles describe different gene expression patterns when the blood is exposed to chemotherapy or radiation therapy. Genetic array maps are used to show the expression levels of a family of specific genes in peripheral blood taken from healthy subjects where a gene is "ON" (yellow to red) or "OFF" (dark blue to light blue). Exposure of the PB to chemotherapy or radiation elicits specifically different expression patterns of metagene change suggesting shared and unique genetic responses to the stressors. The graphics on the right are "leave-one-out" depictions (mathematical transforms) of the heat map arrays (the "image") and provide, in this case, a way to demonstrate which specific gene expression patterns are for chemotherapeutic-treated versus radiation-treated PB. The heat map "image" is thus a tool to translate a biologic event or a physiologic change following a stimulus (drug or biologic action).

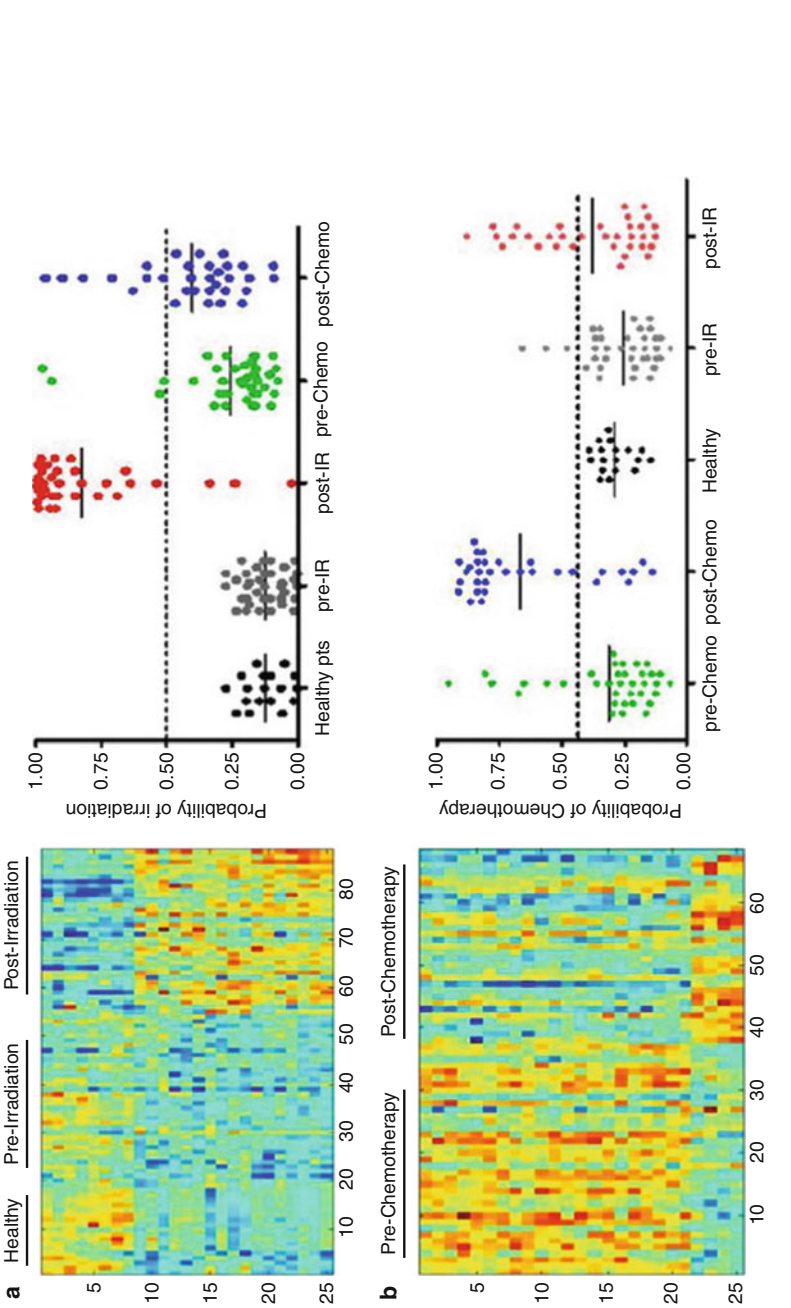

Fig. 1.1 Metagene expression patterns (*left side* images) displayed as "heat maps" where rows are specific peripheral blood (PB) samples and columns are specific genes. In chemotherapy or radiation therapy these genes display expression changes. The genetic expression maps for pre- and post-irradiation and pre- and post-chemotherapy are compared versus an untreated ("healthy") "normal" heat map. The graphic (*right*) is a "take-one-away" assay which is a mathematical representation of the five treatment groups. Thus the heat map"images" can provide discrete translatable data allowing interpretation of genetic changes. (courtesy: John Chute, Duke Univ and data from Dressman et al. 2007 and Meadows et al. 2008; Reproduced from Bioanalysis, May 2009, Vol. 1, No. 2, Pages 321–356 with permission of Future Science Ltd)

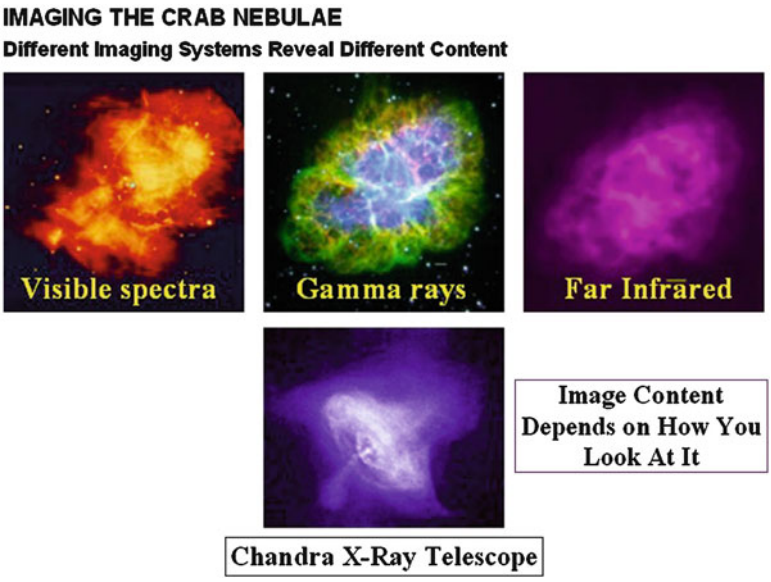

Fig. 1.2 False color renditions of the Crab Nebulae viewed using different wavelengths of the electromagnetic spectrum. While portions of the electromagnetic spectrum reveal amorphous structure, x-ray imaging uniquely reveals a vortex and physical structural detail. Each image is from the NASA *Astronomy Picture of the Day* web site http://antwrp.gsfc.nasa.gov/apod/astropix.html and assembled by the author for this depiction (Reproduced from Bioanalysis, May 2009, Vol. 1, No. 2, Pages 321–356 with permission of Future Science Ltd)

Imaging platforms are unique instruments which exploit the electromagnetic spectrum by varying temporal and quantitative measures created by the pharmacodynamics of biomarkers. Imaging, and the mathematical transform of images, can expand the physiologic limits of our eyes to see outside of the confines of the visible spectrum. Different wavelengths of energy can be used to describe different things not unlike a set of drill bits can be used to probe a target (a building board) so an objective (insertion of a screw) can be achieved. Conventional microscopy uses visible light energies but, to achieve the higher resolution of electron microscopy, one uses narrower wavelengths in the x-ray energies which can "see" smaller objects via a more defined diffraction of structural angles where the larger visible light wavelengths are impeded. Electron micrographs thus use high energy "light" to visualize structures where a lower energy "light" probe is incapable of discerning structures.

Selecting the right imaging system and probe (i.e., wavelength) is a universal tool and goes beyond biology with applications in virtually all scientific disciplines. An example taken from space sciences is depicted in Fig. 1.2. The figures describe the amorphous Crab Nebulae as viewed using different wavelengths (energies) of "light" (where "light" is the electromagnetic spectrum). When viewed using broad coverage wavelengths of light the structure of the nebulae is simply amorphous. Use of the Chandra x-ray telescope, however, reveals unique detail not seen with higher

(gamma) or lower resolving (microwave, infrared) energies. Viewing with the x-ray wavelength defines the structure as a swirling and axially- oriented vortex. The x-ray wavelength even allows viewing over time to see "motion" within the structure. Information derived from any imaging platforms thus depends on the system and each system will reveal different content.

1.2.1 Development of Imaging Sciences

Medical imaging had a rich history in the twentieth century, especially in the miniaturization of electronic systems, powerful and rapid computational systems, and molecular structure and synthetic capabilities which each has driven the development of imaging platforms. Specific examples of achievement over the past century include:

- 1900–1920s x-rays employed for imaging and applied as "health elixir"
- 1930s: Radioiodine thyroid functional uptake; x-ray "shoe fittings", Tc-99m discovery (a "man-made" low energy—144 keV—short half-life—6 h—isotope, easily capable of leaving the body and yet being absorbed by a NaI crystal); gamma counting
- 1940s: Geiger counter use for flow renograms/cell labeling C-14 and other biologic-relevant isotopes useful in the photosynthesis; tissue autoradiography (grain-counting histology); the Manhattan Project and the handling of nuclear materials
- 1950s: Radioisotope chemistry: Tc-99m conjugations; C-14 photosynthetic and metabolic studies; larger array detectors; accelerator sources of radionuclides
- 1960s: The Anger Camera; chelation chemistry; concept of positron camera; digital computing begins; computational programming, CT systems (Hounsfield units)
- 1970s–1980s: Trace metals (i.e., mercury in tuna fish) spawns novel isotope work; development of Mabs; novel animal models—SCID technologies; concepts of computational 3D imaging (tomography) allowing for PET/SPECT/CT/MR/US
- 1980s: Computational systems refinement/complexity; high capacity/rapid computer systems; PET synthetic chemistry; new positron radiotracers; high Tesla MR systems; PCR and molecular probes; recombinant proteins; knockout/in animals
- 1990s: Biomarkers: PCR defines pathologies; PEGylated proteins, peptides, Mabs and fragments, glycans, new chelation methods; exploitation of cancer biomarkers; image-guided radiotherapy; platform miniaturizations for animal studies
- 2000s: Molecular/optical imaging; Quantum dots; use of knockout mice
- *2010—The future:* Hybrid imaging technologies (MR-PET-CT); carbon nanotube probes and delivery systems and nanotechnology for drug delivery—more

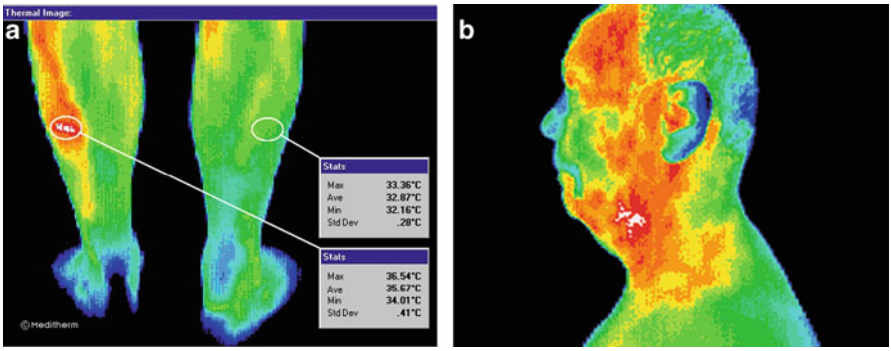

Fig. 1.3 Thermographic images—a pattern recognition "image" where increased blood flow is mapped. (**a**) Infrared (IR) thermogram of a patient suspected of a left side stress fracture of the fibula. This was not evident on a radiograph but DITI showed sufficient evidence of local pathology to justify a scintigraphic (nuclear medicine) image which diagnosed a stress fracture. (**b**) Inflammatory pattern in the neck region that correlated with a diagnosis of digastric lymph node inflammation with swelling. With permission: Meditherm®; web site: http://www.meditherm.com/thermography_default.htm

An imaging "biomarker" is intended to be a direct measure of a pharmacodynamic "effect" from a specific pathology or physiologic function. Images, as described earlier, are simply patterns. Conventional radiographic images, like photographs, are analog density patterns expressed as two dimensional views (2-D; *x* vs. *y*) of three dimensional objects (3-D; *x*, *y*, and *z* directions; i.e., "bread slice technology, or tomography) plus a time rate of change component. Modern imaging can collect either analog or digital data and, with the use of computer systems, display and quantify regions of interest off of an image to display or solve for rate constants. We can "see" (interpret) information from the 2-D displays but digital 3-D displays improve pattern recognition with the removal of confounding overlaid information (noise) and using digital picture element (pixel) values one can quantify the biomarker response and calculate statistical certainty from an image pattern.

As with the metagene genetic array "heat map" image described earlier, a thermal image of a biologic system is also a "heat map". Infections, inflammatory mediators, burns, or any other cause can initiate changes in localized blood flow which can be detected by infrared sensors. Thermography is an old military imaging system to find heat sources on the battlefield. Here the technology is refined with smaller sensors to see finite differences on the skin surface. Thermographic imaging has been adopted clinically due to its simplicity, use of various color displays (user preferences), large pixel arrays in the display of event rates (thermal emission in the infrared or long wavelength; 600–800 nm energies), and generally provides a quick clinical interpretation of inflammatory pathologies, for example, by increased skin blood flow. Thermography has been used in the evaluation of burns but there are limits in resolution with increased depth of the blood flow foci. A patient's localized increase in blood flow can be indicative of widely different sources of injury as can be seen in Fig. 1.3.

Biomarkers may be divided into four principle categories: (1) predictive, (2) prognostic, (3) diagnostic, and (4) dosimetric (adopted from Okunieff et al. 2008). "Predictive biomarkers" are those that suggest a certainty of a future event or known change to be evident in physiologic status and are available before a drug or action is applied to a target. High cholesterol is a predictive indicator of future heart disease. "Prognostic biomarkers" include those that foretell a future event and are available at the time of symptoms (pathology) or following a drug intervention. Prolonged elevation of plasma glucose after a meal is such a marker and indicates a prognosis of diabetes. This is different from "predictive" in that there is less involvement of a future event as the condition already exists. "Diagnostic biomarkers" are those that are common in clinical practice and available at the time of symptoms (pathology) or useful markers to follow a drug or biologic's action on a target. These types of markers facilitate a clinical decision to treat or not to treat. The use of ultrasound during a cardiac stress test is an imaging platform to assist viewing cardiac wall motion irregularities. Dosimetric biomarkers are those that represent outcomes of pharmacologic, radiologic, or other intervention (positive or negative over or under expression of a biomarker) in response to an event or stimulus. The drug-induced cardiac stress test is again an example where we could apply a pharmacologic agent instead of a treadmill. Adenosine, dipyridamole (Persantine), and dobutamine are the most widely available pharmacologic agents for cardiac stress testing. Table 1.1 describes the four categories of biomarkers and is an adaptation of work by Okunieff (2008) to describe these categories with respect to imaging.

Biomarkers which are useful in imaging reflect on a variety of targets, targeted tissues, and/or biological properties and characteristics as seen in the following:

- *Metabolism*—measure glucose utilization of tissues (brain, heart, tumors) using F-18 fluorodeoxyglucose (FDG)—obtain standardized uptake values (SUV)
- *Growth*—DNA turnover using thymidine uptake for turnover, F-18 FLT
- Organ or tumor size—CT /MR: anatomical, RECIST; PET/SPECT: functional domain of a tumor (living tissue vs. living plus necrotic combined
- *Vasculature*—MR (blood flow), MR and CT angiography, SPECT/PET for platelet adherence, clot formation, and inflammatory responses
- *Markers/receptors*—Mabs, peptides, aptamers, cell surface properties
- *Density differences*—CT for mass density, MR for water content and mobility
- *Physical reflectivity*—Ultrasound and bubble technologies for measuring flow and defining structures via edge detection
- *Heat*—thermal imaging where tumor tissue exhibits higher caloric consumption and emission of waste heat
- *Hypoxia*—xenon lung ventilation studies, and functional MR blood flow (fMRI)
- *Gene triggers/promoter sites*—optical tracers may be quantum dots or fluorescent probes or, for research purposes, genetically modified mice where a luciferase gene is inserted adjacent to a promoter site
- *Cell trafficking and cell surface properties*—glycan cell surface decoration and speciation, labeled cells can traffic differently and have different elimination kinetics due to infection; stem cell therapies can be followed to observe engraftment.

Table 1.1 Types of biomarkers and how they are used in imaging

Marker class	Definition	Example
Predictive	A biomarker available before a drug or action is applied to a target	Imaging: MRI In Multiple Sclerosis (MS) the brain exhibits physical changes in the white matter structures which are related to the water relaxivity within the brain (the magnetization state of water hydrogen can be detected as emission of radiowaves) (Phelps 2004; Fukushima et al. 2008)
Prognostic	A biomarker available after a drug or action is applied and which predicts a subsequent increase in risk of injury or change in pathologic state	Imaging: PET C-11 β-CFT uptake in the dopamine-rich regions of the substantia nigra is significantly reduced following exposure to the neurotoxin MPTP, a byproduct of improper chemical synthesis of methamphetamine (Cercignani et al. 2001; Filippi et al. 1998)
Diagnostic	A biomarker available at the time of symptoms (pathology) or following a drug or action on a target	Imaging: PET C-11 PIB as an indicator of amyloid deposition in the brain of suspected Alzheimer disease patients (Brooks 2004) Imaging: PET F-18 detection of suspected lung cancer with standard uptake value (SUV) of >5 (DaSilva et al. 1993); ischemic myocardium: animated gated PET and SPECT images (Christian et al. 2004; Rabinovici et al. 2007; Minn et al. 1995) Imaging: fMRI rCBF (regional cerebral blood flow) in regions of the brain during thought or physical movement—BOLD (blood oxygen level dependent) technique to localize flow change by stroke (Pineiro et al. 2002)
Dosimetric	A biomarker available after a drug or action is applied on a target and which a response can be related to the dose (or proportionality of an action) relative to a negative control	Imaging: Microscopy Chromosomal aberrations (dicentrics) using microscopic imaging (radiation dosimetry) (Anderson et al. 2006) Imaging: SPECT Application of cell trafficking In-111 WBCs recognizing changes in tissues, i.e., cytokines to elicit NK cell proliferative dose response; infections (Sinha et al. 2004)

Inclusive of definitions and examples of which image platform and/or imaging marker may be employed. Many imaging systems and how they are used are uniquely suited for specific tasks and use as a marker class (Table is adapted from Moyer and Barrett 2009)
Four other references elaborate further on these points: Wang and Deng 2010; Agdeppa and Spilker 2009; Eckelman 2003; and Sun et al. 2001

In theory, for a biomarker to serve as an effective end point or substitute for the clinical outcome, effects of intervention on the biomarker must reliably predict the overall effect on the clinical outcome. In practice, this requirement frequently fails (DeMeyer and Shapiro 2003). Any drug applied as a therapeutic also has the possibility that it may affect a clinical outcome by unintended, unanticipated, unrecognized, and potentially saturable mechanisms of action that operate independently of the disease process. Fleming and DeMets (1995) provide several examples of how selection of a biomarker may be incorrect and may actually be indicative of unrelated pathways and outcomes. Biomarker response can be confusing in the milieu of all the other potentially confounding biologic activities which, in turn, can alter biomarker responses. True biomarkers must be elicited by the intervention on a disease and then be reflective of the clinical outcome. In 2003, Eckelman (2003) published a detailed treatise on biomarker behavior by imaging knockout mice, e.g., genetically altered mice, i.e. a specific animal model generated for improved target specificity. Knockout mice were shown to have high utility by decreasing the "biologic noise" early in the drug discovery phases of nonclinical experiments and could be seen to reduce time, animal numbers, and cost by avoiding "classical" (but inherently more "noisy") pharmacologic models.

In 2003, Smith et al. (2003) provided a treatise on "*Biomarkers in Imaging: Realizing Radiology's Future*." Their sense of the science was that imaging of biomarkers was a definitive way to shorten the "bench to bedside" timeline. Imaging biomarkers may have an enormous potential to shorten the drug development timeline but they should never be considered a solution to every preclinical or clinical question. They also noted that imaging could be a successful tool in determining the PK and/or PD of new drug candidates. Imaging could be used to validate binding (measure rate constants) with respect to known cellular or organ-specific disease targets. Measurement of the effect of formulation change on in vivo distribution over time, specific targeting efficiencies, the time to C_{max} at the target, metabolism/catabolism rates, and even elimination rate would all be a huge cost savings if they could be determined in fewer animals needed to capture all these endpoints. Imaging also affords multiple views over time such as in cancer therapy (i.e., CT RECIST[1] and MRI measurements), or when the target is elusive or moving, i.e., heart motion and blood flow (US flow measures, cardiac imaging), or when the target is not anatomy but rather simply a function, i.e., thinking (regional brain blood flow with fMRI; PET correlations). Table 1.2 is adapted from their paper and describes, from my perspective, how imaging of biomarkers that can be used over various imaging platforms to improve the drug development timeline.

Table 1.3 describes the parameters that currently represent the path of drug development and the impact that an imaging biomarker may have on that parameter (adapted from Smith et al. 2003).

[1] RECIST: Response Evaluation Criteria in Solid Tumors (Therasse 2002).

Table 1.2 Role of imaging biomarkers in drug development and clinical medicine

Product development stage	Applicability of imaging biomarkers	Imaging modalities[a]
Target identification	YES	Molecular imaging, PET, SPECT, ARG
Target validation	YES	Molecular imaging, PET, SPECT, ARG
Lead candidate identification	LIKELY	Biomarkers would preferentially be specific or directly linked to the target pathology and not a surrogate or secondary indicator
Lead optimization	YES	Molecular imaging, PET, SPECT
Preclinical testing	YES	Molecular imaging, PET, SPECT, US, CT, OP, ARG
Clinical trials	YES	CT, MR, fMR, PET, SPECT, US, OP, TH, conventional radiography
Diagnosis	YES	CT, MR, fMR, PET, SPECT, US, OP, TH, conventional radiography
Patient monitoring	YES	CT, MR, PET, SPECT, US, OP, TH, conventional radiography
"Animal Rule" trials	YES	*Animal* Efficacy *Rule* (21 C.F.R. § 314.610, drugs; § 601.91, biologics); Examples: Radiation or chemical agent injury and Select Agents in BSL-3/4 environments to test therapeutics in animals where ethics prohibit the use of humans. Open to all imaging platforms

[a]*CT* computed tomography, *PET* positron emission tomography, *SPECT* Single photon emission computed tomography, *MR* magnetic resonance, *fMRI* functional magnetic resonance (blood flow), *OP* optical and fluorescent tracers, *ARG* autoradiography (whole body or histologic with grain counting), *TH* thermography; modified from: Smith et al. (2003)

Table 1.3 Biomarkers in imaging: traditional end points in drug development and the effect of use of an imaging biomarker

Parameter	Traditional biomarker measure	Imaging provides
Time to results	May be long, esp. mortality indices	Potentially SHORTER
Objectivity	May be low, esp., morbidity	Potentially INCREASED
Cost	High, esp., with long endpoints (animal housing, care and laboratory services	Relatively LOW cost
Ability for study blinding	May be difficult, esp. for devices	Relatively easy to perform blinding with images
Detect subtle change	Often low probabilities	Routinely available
Patient as own control	Possible to difficult	Often possible
Access to resources	Dedicated infrastructure, but often available, in-house validated assays for early development need technology transfer for full acceptance	Widespread, costs can be defrayed by routine clinical use of a platform and simple to do tech transfer of known platforms

Modified from Eckleman (2003); For a far more detailed table of high resolution, small animal imaging systems see Table 1.1 in a review by Rudin and Weissleder 2003

1.2.2 Selected Imaging Modalities, Biomarkers, and Drug Development

1.2.2.1 Computed Tomography

Computed tomography (CT) is one of the most widely used medical imaging technologies used to detect density differences and in vivo edge discrimination. The history of CT is really that of three histories[2]: (1) the history of tomography itself, (2) the development of the algorithms used to reconstruct the image, and (3) the development of high-speed digital computers. CT measures the density of objects and has units of density called Hounsfield units[3]. The initial prototype CT scanner used in clinical trials shown here had some less than inspiring specifications: scan time: 9 days, reconstruction: 2.5 h; print the image: 2 h; resolution: 80 × 80 (voxel elements for a 20 cm × 20 cm 2-D slice). The modern device is a rotating x-ray source surrounding an object (patient) where the instrument measures a fan beam of x-rays onto a set of detectors on the opposing side of the object. A series of x-ray projections around an object and the resulting absorption maps of the incident beam and reduction on the x-rays reaching the detectors (attenuation) is reconstructed to represent the interior of an object.

CT scans can, for example, measure bone density in assessing an osteoporosis patient. Therapeutic intervention with a drug to enhance bone formation or prevent bone loss can be measured over time using CT where the change in Hounsfield units (HU) of density serves as a biomarker of treatment success or failure. Also, detection of lung tumors or mammary tumors using CT represents a contrast change in regional HU relative to the air-filled lung regions or less dense fatty tissues of the breast. Radiotherapy, as incident beam radiation to treat the breast or lung tumors, will increase the water content of the lung tissues affected by the absorbed energy and lead to less contrast by CT over time until the tumors are killed and resolved. Changing to another imaging biomarker such as metabolic markers or perfusion markers can improve clinical observations during treatment.

CT, as well as standard x-ray imaging, can utilize contrast media to resolve objects such as tumors and vascular structures. The HU changes associated with the distribution of a contrast agent within a tumor or vascular system (i.e., carotid arteriography, deep leg venography, or coronary angiography) can be definitive in diagnosis. The utility of contrast agents is their added improvement in target-to-nontarget ratio (increased statistical discrimination) which can improve a clinical biomarker.

---

[2] http://www.bioclinica.com/blog/evolution-ct-scan-clinical-trials, The Evolution of CT Scan Clinical Trials, Stuart Jackson blog on July 22, 2011.

[3] The Hounsfield unit (HU) scale is a measure of the attenuation coefficients within an object in which the radiodensity of distilled water at standard pressure and temperature (STP) is defined as zero HU and the radiodensity of air at STP is defined as −1,000 HU. Muscle and bone will measure as HU exceeding 30 and 300 HU, on average, respectively.

While CT is a well-adopted imaging modality in both the clinical setting and the nonclinical laboratory, it is not of high interest other than as a marker of density in animal test systems and overlay in multi-modality imaging, i.e., with PET, SPECT, and optical probes. We will not have a chapter on CT except as a co-investigative tool for the imaging platforms discussed in this book.

It is important for the reader to recognize some imaging tools like CT have become so much a part of the clinical setting that their inherent risks are lost or ignored in their everyday use. CT in the USA has grown to where it has become a standard clinical tool, and is often seen as technically required for protection of physician liability. As such, CT has become a primary diagnostic at many institutions and it is used in excess with radiation dose complications due to overuse and accidents. Physicians have been known to ignore the concomitant dosimetry in favor of a "more precise" or "higher resolution" image. The New York Times in June 2011 provided an article on the overuse of CT scans in hospitals across the USA where they reported on the rate of duplicate chest CT scans (refer to: http://www.nytimes.com/2011/06/18/health/18radiation.html?pagewanted=all&_r=0). The link includes an interactive map (shown as Fig. 1.4) where one can select individual hospitals and view their respective chest CT scans per annum and how many are repeated: http://www.nytimes.com/interactive/2011/06/17/us/hospital-ct-scans.html?ref=health The dose of x-rays from a chest CT is not insignificant and doubling the patient's exposure and adding to their cumulative lifetime dose is a serious consideration.

It is imperative in this context, that the Reader understand, for each of the imaging modalities described in this book, that there are inherent benefits as well as risks for each and every modality described in this text. Each modality, its purpose and risks, must be considered in their nonclinical as well as clinical environments. The primary clinical risk for CT is with respect to ionizing radiation, but other imaging signal systems employ other kinds of risks including magnetic field effects, infrared heating, DNA intercalation or delivery of a biomarker at sufficiently high focus to initiate injury or delayed risk of injury. Users must always understand the risks to the animal handlers and any other imaging personnel.

1.2.2.2 Nuclear Medicine and Radiotracer Technologies

Autoradiography

One of the original biologic images was the 1896 image of Roentgen's hand with the delineation of the bone structure and the ring on his finger. The discovery that radiation could provide an image on photographic film led to many applications of contact radiography which matured to the modern slice technologies of CT, SPECT, PET, and MR mimicking the whole body slice to a more useful histologic tool, autoradiography, to show the biodistribution of radionuclides and radiolabeled biochemical entities.

One of the first techniques employed using radioactive materials was contact radiography. The technique added significantly to the field as an adaptive technology to histology (Caro and Tubergen 1962). Radiolabeled substances and their

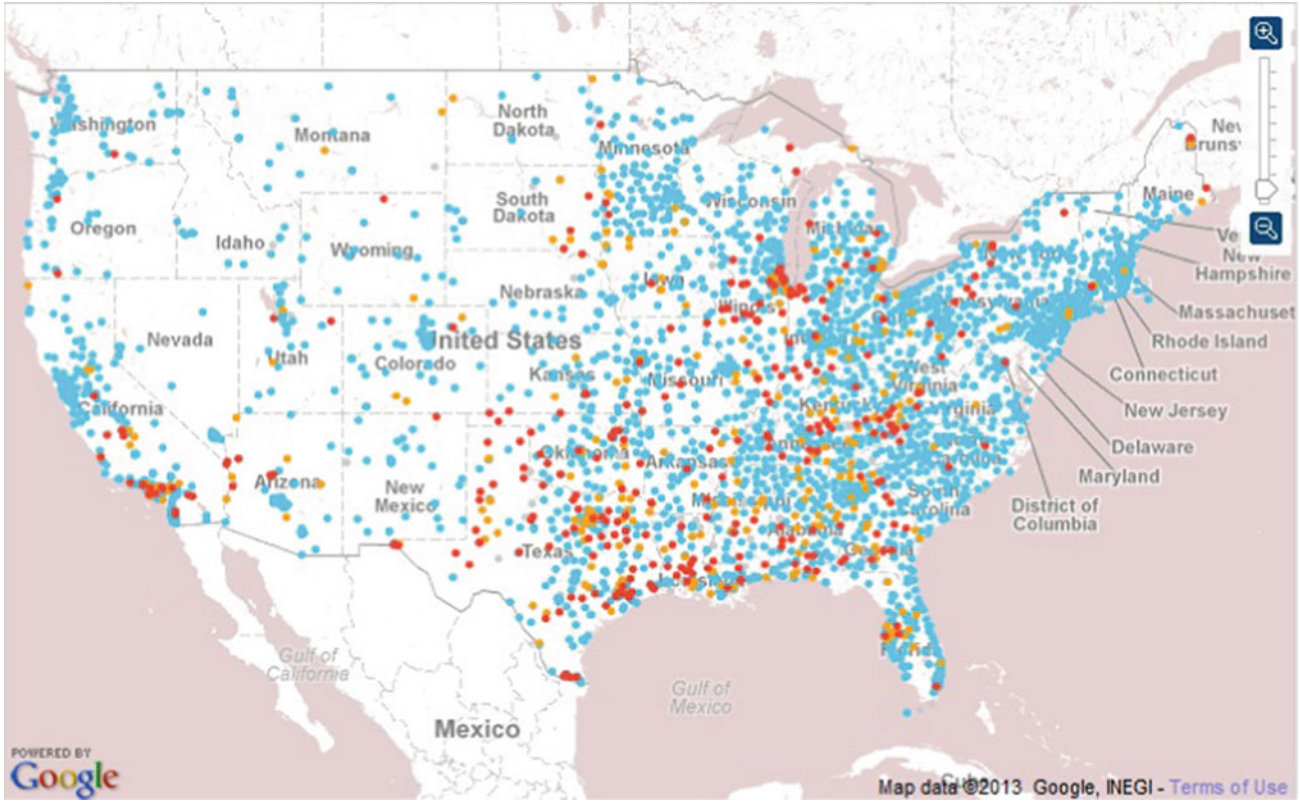

Fig. 1.4 Static image of an interactive map, from an article in the New York Times, of the United States showing each hospital in the USA with a color code for the rate of duplication of CT scans. The *blue dots* are below 20 %, *yellow* for a 20–40 % risk, and *red* are hospitals which are above a rate of 40 % per annum. Note the predominant regional location for RED is mostly in the middle states and southern states (Source: Center for Medicare and Medicaid Services; see link in text)

distribution following injection, or other mode of entry, can be "seen" using autoradiography. Radioactive tissue can be prepared as a histologic slide, immersed in a fine silver halide photographic emulsion. Exposure of the tissue section allows for silver grain formation over time and development of the slide, like a photo, and inspection of the slide by microscopy following standard histologic staining, can reveal the distribution of the radioisotope in the tissue. With the success of histologic plus radiotracer imaging, whole animal (body) autoradiography (WBA) was developed as a macro tool to map the tissue kinetics and biodistributions of drugs in whole animals. Highly engineered cryomicrotome devices for whole animal sectioning were developed to avoid "chatter" (change in section thickness) and provide uniform 20–50 μm sections over sample (carcass) distances of 10–30 cm (depending on the device) allowing the sectioning of small mammals such as the Cynomolgus or the Marmoset nonhuman primate. The devices as refrigeration units also sublimate thin sections overnight and the tissue section can then be placed in intimate contact with high resolution x-ray films or highly sensitive electronic photo-plates in direct contact systems (for beta emitting isotopes) such as the phosphoimager systems (Johnston et al. 1990; Solon 2002, 2007; Solon and Kraus 2002, and (http://www.perkinelmer.com/Catalog/Family/ID/Cyclone%20Plus%20Phosphor%20Imagers). Readers are directed to the chapter on Autoradiography which will provide a look at the modern analytical assays of this technique which still utilize whole body sections to quantitate regional distributions of molecular entities but with advanced analytical tools such as MALDI (matrix-assisted laser desorption/ionization mass spectrometric imaging) and NIMS methodologies (Solon et al. 2010). For a practical web-based review of autoradiography and especially as it relates to F-18 FDG PET vs. C-14 FDG imaging/quantitation, the Reader is directed to a full review provide through Loats, Inc., as "Application Notes—Metabolic Autoradiography" http://www.loats.com/AppNotes-2DeoxyGlucose.PDF.

As was indicated in a previous section, formulation changes often can lead to surprising changes in biodistribution of drugs. One such example was a cytokine I was working with which was formulated in sodium dodecyl sulfate (20 %) for solubility and the cytokine exhibited a pulmonary toxicity which was interpreted as a "normal" response for the indicated cell stimulations that were expected. Upon radiolabeling the cytokine and examining the immediate post-dosing distribution using whole body autoradiography (WBARG) of the radiolabel, it was observed that the protein was aggregating in vivo and that the aggregates were accumulating as punctate islands of radioactivity in the spleen (Fig. 1.5). Upon reformulation in a glycine buffer at the appropriate concentration to reduce in vivo aggregation, the spleen in thin section whole body autoradiography films were seen as uniform and toxicity, resulting from localized cytokine stimulation, was reduced significantly and there was a noted improvement in efficacy due to the resultant increase in the AUC and C_{max} parameter estimates (data not shown) which allowed the reduction in the effective dose and widened the cytokine's therapeutic index (TI).

Fig. 1.5 WBARG of a rat showing two serial adjacent sections (separated by about 300 μm) 4 h after being administered a cytokine radiolabeled with I-125. The image depicts the localized uptake (*dark grains*) in the spleen demonstrating RES clearance of protein aggregates. The cytokine was administered 4 h prior to the animal being euthanized and frozen for cryostat sectioning. The images show the aggregation of the protein and clearance via the splenic islands (white pulp by image—anatomy correlation (superimposed histology and image). The formulation effect of promoting in vivo aggregation led to RES clearance and focal stimulation at sites of aggregated protein which led to unwanted toxicities. Reformulation promoted a more uniform biodistribution and allowed for a reduction in the clinical dose for the same level of efficacy in an animal cancer model (personal archives)

Planar, SPECT, and PET Imaging

Nuclear imaging has become a standard noninvasive clinical tool to examine functional anatomy and functional processes. In the 1950s Hal Anger developed several of the first nuclear medicine imaging systems at Donner Laboratory at the University of California Berkeley (Wagner 2003). One of the first was the rectilinear scanner, a moving bed that traveled over an array of 64 photomultiplier tubes (four rows of 16 tubes) to provide a two dimensional "whole body" image (Fig. 1.6). An Am-241 photon source over the bed was used to provide a silhouette image of the object being scanned to allow for spatial identification of radioactivity in the image silhouette. He later created the first gamma "camera" (now known as an Anger camera) which was a large NaI crystal with an array of photomultiplier tubes. The array produced a 2-D map of counts from radioactivity impinging on the crystal and the camera was able to discern a planar image.

Fig. 1.6 Imaging laboratory at Donner Laboratory, University of California at Berkeley (circa 1972) where Hap Anger developed these two devices. (**a**) *To the left* is an original Anger camera and *to the right* is a whole body scanner. (**b**) An early WBS image (isotope unknown) with an Am-241 suspended above the patient serving to create a patient silhouette allowing for regional 2-D localization of the isotope in the body (images from the author's archives)

Radioisotopes with appropriate gamma energies for absorbance by 1 cm thick NaI detectors were sought as these had the appropriate efficiencies to use the devices. Energies below 50 keV had low capacity to escape deep tissues to interact with the detector and energies in excess of 250 keV were to energetic and would have low detector efficiencies (ability to create a scintillation event in the crystal). The 140 keV gamma emitting Tc-99m discovered by Nobel laureates Segre and Seaborg in 1939 (daughter isotope of Mo-99 decay) met the energy and half-life (6 h) need for the Anger camera and discoveries on ways to attach (chelate) Tc-99m to drugs, proteins, peptides, and other chemical entities had a dramatic effect in opening the door for nuclear medicine development.

The discovery of CT in the 1960s led to computational method to reconstruct images from projections and created the notion of imaging tomographic sections—"bread slices"—through the body (Friedland and Thurber 1996). Out of these computational methods and the known physical properties of isotopes emitting positrons (positive nuclear emissions which annihilate upon meeting an electron and resulting in the formation of two opposing gamma rays of 511 keV energies 180° in opposition) led to Positron Emission Tomography (PET). It was only a matter of time, and

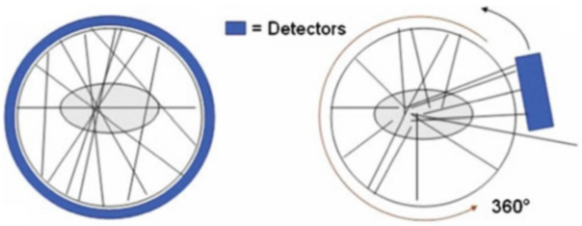

Fig. 1.7 PET and SPECT imaging systems. The PET system is depicted in the left image where a ring of detectors creates the array of positron coincident chords which are reconstructed into the PET "image"; The SPECT system is a single, double, or triple head (detector) camera where single photon tracks are collected. In both cases a reference scan is first obtained to determine the image's attenuation correction coefficients for each projected angle. (Reproduced from Bioanalysis, May 2009, Vol. 1, No. 2, Pages 321–356 with permission of Future Science Ltd.)

truly inventive reconstruction mathematics, to take single photon emission isotopes, like Tc-99m, Tl-201, and many others, and create a way to do 3-D imaging which we term Single Photon Emission Computed Tomography (SPECT). Three major textbooks on SPECT and PET imaging technologies have been published recently (Christian et al. 2004; Valk et al. 2003; Phelps 2004).

In PET, it is the emission of the 511 KeV gammas that results in (1) a sufficiently high enough energy to have low tissue absorption, (2) a physical reduction in scatter by only counting coincident events in a ring detector system, and (3) construction of a linear chord for coincident photons an the progressive overlay of these ring events creates a defined distribution of the chord representing the 3-D location of the radioactivity in the object (patient or animal). PET and SPECT systems differ as depicted in Fig. 1.7. For educational purposes the reader is directed to a web-based collection of PET and SPECT imaging studies where there are details on the way 3-D images are collected, processed, and interpreted clinically.[4]

PET and SPECT in the Molecular Imaging of Cancer

Imaging for the detection of cancer, from its first use with conventional chest x-ray and mammography, has been propelled by major advances in instrumentation molecular mechanisms of cancer. Imaging instrumentation and electronic noise and scatter correction algorithms have significantly improved resolution, data fidelity through computational advances, and the introduction of molecular probes has exceeded expectations and opened many new avenues of research. The Journal of Nuclear Medicine in 2008 has an entire issue dedicated to the molecular imaging of cancer (J Nucl Med, Suppl 2, 2008) and it introduced, as the first article in the issue,

[4] A Doctor's Guide to Nuclear Medicine, Barry E Chatterton, Sr. Dir., Nuclear Medicine, Royal Adelaide Hospital; http://www.rah.sa.gov.au/nucmed/nucmed/ncmd_docguide.htm.

the dramatic changes in nuclear imaging instrumentation (Pichler et al. 2008; Vastenhouw and Beekman 2007). Advances in PET and SPECT imaging, novel molecular probes, and the understanding of genetic diseases, biomarker expression/metabolism, etc., have all advanced the art and been instrumental in the defense of regulatory approval for several new therapeutics. A major treatise on the employment of molecular probes in PET/SPECT oncologic drug development was published in 2005 and covers essentially all areas of oncologic interest that may be investigated via nuclear medicine approaches (Kelloff et al. 2005).

Modern cancer imaging employs a wide variety of radiolabeled (for PET and SPECT) or contrast-labeled (for CT and MR) probes to image phenotypic expression of biomarkers. These probes include peptides, Mabs and Fab' fragments, aptamers, cell markers, growth markers, lipids, angiogenesis markers, metastatic markers, hypoxia markers, and several others. New imaging tools with higher resolution and the mathematics of image processing employed in planar, SPECT and PET modalities, MR and optical imaging platforms has revolutionized cancer medicine.

Three dimensional images of objects as small as the nude mouse are now possible using microSPECT (and microPET systems) and small regions can be resolved using projections of axial slices (coronal, sagittal, and transverse) (Vastenhouw and Beekman 2007). Both the MicroPET and MicroSPECT systems are marketed with the capability of doing CT imaging for the same specific slice to provide density correction (isotope attenuation correction) which facilitates image statistics correction for small animals. The Reader is directed to our chapter on cancer imaging which covers a wide variety of small animal systems applicable to the nonclinical drug development laboratory setting.

Drug and Biomarker Kinetics Using Nuclear Imaging

Imaging, particularly nuclear medicine and radiotracer technologies, provides a view of pharmacokinetic behavior of biomarkers as one can map the distribution, transit, targeting, and elimination of radiolabeled drugs. Nuclear medicine is unique in imaging as it can provide both anatomical and functional measures of biology. The "functions" that can be described using nuclear imaging include several important pharmacokinetic and pharmacodynamic expressions such as:

- The "**input function**": IV, IM, SQ, oral, nasal, lymphatic; input to organ systems
- The "**transit function**": gastrointestinal absorption and transit time, lymphatic flow, blood flow, mucosal transit
- The "**distribution function**": receptor-based elimination from the blood; oil–water coefficients, blood brain barrier, and other stops
- The "**binding function**": receptor affinity (Kd value), the "on-off rate"
- The "**time to effect**" and/or "**time to toxicity**" pharmacodynamic functions
- The "**degradation function**": enzyme kinetics, pH effect, metabolism

- The "**elimination function**": renal, hepatic, biliary, ventilation, sweat, e.g., geriatric differences (impaired renal or hepatic clearance); effects of concurrent medications (drug–drug interactions); pediatric (body surface area relationships)
- The "**allometric function**": pharmacokinetic parameter estimates based upon allometric scaling using body surface area, heart rate, etc.
- The integral of all these functions is what can be called the "**drug signature**"

Three mathematical methods are commonly practiced in the analysis of F-18 FDG drug kinetic behavior from images. These include the Logan Plot (Logan et al. 1990), the SUV (Standardized uptake value) (Christian et al. 2004; Phelps et al. 1979; Ferl et al. 2007; Krohn et al. 2007; Huang 2000; Keyes 1995), and the Reference Tissue Method (Sandella et al. 1998). The **Logan Plot** defines the kinetics of radiolabeled compounds in a compartmental system where the compartments are described in terms of a set of first-order, constant-coefficient, ordinary differential equations. The **Standardized Uptake Value**, or SUV, is a common method to define tumor metabolic rate for glucose in relative terms. It does not require an input function as does the Logan Plot. It relies upon uptake in a region of interest (tumor) standardized to total dose distribution (nontarget). The SUV method defines a region uptake against a reference (no uptake) tissue (brain = cerebellum; lung tumor = other lung region; heart = skeletal muscle). The SUV is typically done at one time point after a defined clearance but can be done dynamically. There are drawbacks to this method as described by Huang (2000) and Keyes (1995). The third methodology is the **Simplified Reference Tissue Method** or SRTM. This is a common method employing a reference ligand kinetic model but does not require an input function. The model assumes one compartment and requires a starting (reference) ligand kinetic model (example: erythrocyte uptake). The SMRT differs from SUV as it does not correct for nonspecific binding and typically uses the cerebellum as a reference (baseline) region-of-interest (ROI) for the input function term.

Each of these mathematical methods of image analysis has applications, with modifications, to a variety of biomarker candidates. The Readers are encouraged to read the chapters on Oncology and Allometrics which touch on these processes. The dose selection allometrics may not be important in use of radiotracers simply because these are typically non-physiologic doses, but rather in the use of the drugs under study using imaging where molar excess concentrations may be used in safety studies (or in the case of MR contrast agents), target saturation could occur, or differences in receptor occupancy through species specificity of the drug or biologic under study may be involved.

Imaging the Neuroendocrine System, Neuroantomy, and Function

PET is currently the preferred technology for state of the art brain metabolism imaging, CT is the preferred imaging modality for general anatomic imaging, and MRI is the current standard for brain imaging for specific water-mediated signaling. CT, while used extensively as a first pass imaging system is limited to anatomical injury

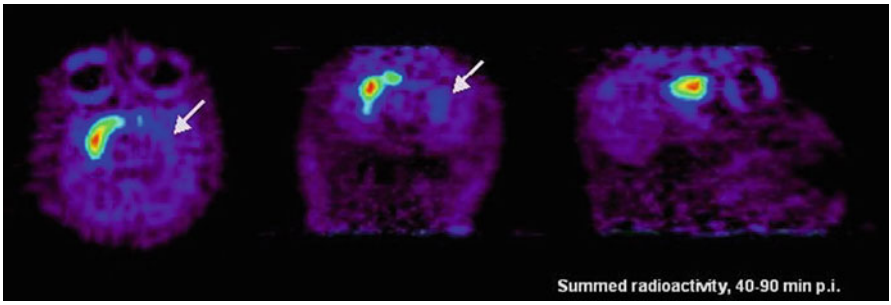

Fig. 1.8 Images of a nonhuman primate subjected to the neurotoxin MPTP which has a severe toxic effect of destruction of the substantia nigra in the mid-brain (6.5 kg Rhesus macaque). MicroPET P4 images at 2 weeks post-lesion induction using C-11 β-CFT shows 90 % denervation of the dopamine transporter in the substantia nigra; the normal contralateral side shows specific binding of the C-11 β-CFT. (Reproduced from Bioanalysis, May 2009, Vol. 1, No. 2, Pages 321–356 with permission of Future Science Ltd.)

assessment where displacement is measured by a range of densities from bone to air. Tissue contrast may identify clinically relevant targets such as distortion of structure from a tumor. The initial anatomic information aids in further imaging using PET or MRI systems. Sossi (2007) provides an excellent review of PET brain imaging describing new detectors, reconstruction algorithms, and the use of PET in movement disorders and Alzheimer's disease.

Brain damage was observed in the early 1980s in subjects using crudely synthesized methamphetamine which created a byproduct known as MPTP (Schober 2004). This byproduct is a neurotoxin to the dopamine centers of the brain and left drug abuse victims with an irreversible loss of their dopamine production (substantia nigra) and early Parkinson's symptomology. Figure 1.8 depicts a nonhuman primate with unilateral destruction of the substantia nigra using MPTP and imaging the brain 2 weeks later using C-11 β-CFT.[5] Movement disorders such as Parkinson's disease are studied using new radiotracer dopamine analogs. Two new biomarkers of dopaminergic neurologic diseases include C-11 β-CFT ([C-11]2-carbomethoxy-3-(4-fluorophenyl)-tropane) and C-11 tetrabenzine. A mouse model for PET imaging of MPTP-induced degeneration of dopaminergic neurons has been successfully developed using the radiotracer 18F-DTBZ, an analog of MPTP, and allows for evaluation of new Parkinsons disease therapies (Toomey et al. 2012).

Imaging Alzheimer's Disease

Alzheimer's disease (AD) is a dementia is characterized by the accumulation of Aβ-amyloid which serves accumulate over time and force denervation through cortical neuron separations plus impeding vascular flow. Amyloid deposition and confirmation of Alzheimer's Dementia had classically been detected only at death with

[5] β-CFT, is a cocaine-derived drug used in dopamine stimulation scientific research. CFT is a phenyltropane-based dopamine reuptake inhibitor.

confirmatory histologic staining of the brain with thioflavin stains and Oil Red O. Original imaging with F-18-FDG PET to detect regional brain usage of glucose helped define the actual regions of the brain affected first by amyloid deposition. Researchers at the University of Pittsburgh developed a thioflavin-like radiotracer called Pittsburgh Compound-B labeled with C-11 (^{11}C-PIB). C-11 PIB specifically binds to fibrillar amyloid-beta (Aβ) plaques (Mintun et al. 2006) and can help discriminate AD from frontotemporal lobar degeneration (FTLD), a non-Aβ amyloid form of adult dementia (Rabinovici et al. 2007). As mentioned earlier in this chapter, a new imaging agent for detection of amyloid with a longer half-life isotope, F-18 (2 h vs. 20 min) was recently approved by the FDA (AMYViD; a Lilly and AVID Pharmaceuticals venture). This new imaging agent is now art of the Lilly therapeutic drug venture for AD for testing their monoclonal Ab, Solanezumab, in the clinical setting using AMYViD as a POS diagnostic imaging agent. This is in line with the earlier statement of "Find, Fight and Follow" as a paradigm of developing diagnostics that can help with the therapeutic efficacy assessments.

Advances is the development of RNA aptamers has used them as biomarkers for imaging and the detection of AD (Ylera et al. 2002). High-affinity RNA aptamers against the βA4(1–40) have been isolated from a combinatorial library of $\sim 10^{15}$ different molecules. The apparent dissociation constants K_d of these aptamers for Aβ-amyloid are 29–48 nM, which is quite acceptable for nuclear imaging agents, especially if at that nanomolar concentrations, it does not elicit activation. Heiss and Herholz (2006) provide a review of brain receptor imaging and describe the increasing number of potential probes for neurologic biomarkers. In the field of autism, Williams and Minshew (2007) describe the impact that imaging would have on the study of autism and the potential to develop therapeutics to relieve this disease's increasingly social and financial impact. Esposito et al. (2008) describe their efforts in measuring neuroinflammation in AD using C-11 arachadonic acid and PET imaging. Imaging and molecular medicine are coming even closer in the article by Diehn et al. (2008) as they provide evidence that surrogate imaging probes may be able to be tied to specific gene expressions in brain cancers. Agdeppa and Spilker (2009) have provided a major review on imaging agent development and give an excellent overview of microdosing (as described above) and "theranostics", that is, compounds which are diagnostics at a low dose but turned into therapeutics at higher doses.

Imaging Infection and Inflammation and Imaging in BSL-3/4 Environs

Occult infection remains a difficult target for imaging. The biomarkers associated with infection such as C-reactive protein and cytokine expressions are all sufficiently nonspecific to not be adequate to use as a biomarker in the sense we have described earlier. The detection of appendicitis remains problematic. Labeled white blood cells or platelets with radioisotopes of In-111 or Tc-99m have been modestly successful but cells must be harvested from the patient, isolated, radiolabeled, reinjected, and then allowance of sufficient time is necessary for targeting as well as clearance (Arndt et al. 1993). A specific biomarker for definitive identification of

infection and inflammation is yet to be developed, however, In-111 WBCs, F-18 FDG, and F-18 FLT (fluoro-thymidine) are routinely used in clinical research as a first pass test.

The first use of a radiolabeled aptamer specifically for imaging inflammation was by Charlton et al. (1997). The aptamer was created to target human neutrophil elastase and was labeled with Tc-99m. The aptamer was able to image neutrophils in a rat inflammation model with a peak target-to-background ratio of approximately 4 at 2 h postinjection. Aptamer uptake was compared against conventional IgG methods, which has decidedly slower clearance but IgG agents demonstrated a two- to threefold greater absolute uptake versus the aptamer.

Bioluminescence applied to imaging of infection and inflammation is a major new avenue of nonclinical development and is covered in full in Chap. 9 by Hana Golding and Marina Zaitseva from the NIH and FDA on optical probes. The Reader is also invited to read Chap. 10 by Lauren Keith et al., from Ft. Detrick MD, where they have created an imaging theater with specially modified PET/SPECT/CT and MR imaging systems and added high-level safety procedures to study dangerous infectious organisms in the BSL-3 and BSL-4 environments.

Cell-labeling techniques have expanded well beyond the In-111-oxine labeling of white blood cells (Arndt et al. 1993; Sinha et al. 2004) and now techniques in bioluminescence and fluorescence allow for tumor angiography as well as confocal microscopy and imaging of vascular flow patterns, transient adherence and tumbling of cells in the vasculature in situ (Michalet et al. 2005). There is an outstanding review covering magnetic resonance techniques (esp. using paramagnetic T2* relaxation) and special probes like SPIO particles where one can resolve to 50 μm in live animals (Muja and Bulte 2009). Also the Reader is encouraged to review the work of Thurner and Sundgren (2008) for imaging of and diagnostics for slow virus infections.

Cardiac and Atherosclerosis Imaging

Nuclear medicine imaging of the heart and measuring cardiac performance has been a major goal of modern medicine. Biomarkers of cardiac imaging began with K-40 studies in the middle of the last century (History of nuclear medicine discoveries: http://www.thealaragroup.com/amh/historicalmomentsinnuclearmedicine.doc, Society of Nuclear Medicine History: http://interactive.snm.org/index.cfm?PageID=1107&RPID=10). PET imaging has employed a potassium analog, Rb-82, but it is a 75-s half-life positron emitter which is generator produced but has practical limitations (Santana et al. 2007). The advent of SPECT imaging brought another potassium analog, Tl-201, into clinical practice (Valk et al. 2003; Machac et al. 2006). PET imaging of cardiac sugar metabolism with F-18 FDG began in the1980s and is now a clinical imaging standard. Newer tracers for metabolic imaging of the heart, such as I-123 BMIPP, a fatty acid substrate (radioiodine-labeled 15-(*p*-iodophenyl)-3-(*R*,*S*)-methyl pentadecanoic acid (I-BMIPP), more accurately test the heart as fatty acids are the primary fuel for the cardiac muscle (Fukushima et al. 2008). Lack of uptake of I-123 BMIPP is a clinical sign of cardiac injury.

Research into radiolabeled biomarkers for vascular disease such as aneurysms, atherosclerosis, lipid accumulation in the vessel walls, and "unstable plaque" are all under development by big and small pharmaceutical companies. Radiolabeled lipids and lipid–DNA complexes have been investigated (Yamada et al. 1998; Niven et al. 2000). Platelet anomalies and deep vein thrombosis are explored using SPECT agents such as Tc-99m GPIIbIIIa peptide antagonists (Bates et al. 2003; Taillefer et al. 2000). An excellent resource on SPECT and PET cardiac imaging is available as web-accessible document from the American Society of Nuclear Cardiology.[6] The University of Kansas also has a web-accessible set of images with examples of F-18 FDG in full 3-D axial plane displays used for clinical diagnosis and they display gated studies of cardiac performance as animations.[7]

The ideal biomarker for myocardial perfusion will need to not interact with cardiac medications or pharmacological vasodilator stress agents and it must show myocardial avidity providing a high heart/background ratio. The biomarker should have a high extraction fraction with uptake directly proportional to myocardial blood flow over physiological as well as exercise or pathologic-induced stress uptake over normal ranges and the agent should lack redistribution from the heart (target loss) during the imaging period. No biomarker currently provides all these attributes. The four biomarkers of cardiac performance that are currently used in clinical practice include: Tc-99m Sestamibi (ion channel imaging), Tc-99m Tetrafosmin (ion channel imaging), Tl-201 (as a K analog), and F-18 FDG (glucose metabolism). As mentioned earlier, I-123 BMIPP is a myocardial fatty acid metabolism imaging agent that is now approved worldwide in the assessment of "ischemic memory" using SPECT (Koyama et al. 2011). "Ischemic memory" is a phenomenon where, even after weeks post-recovery from an acute myocardial ischemic event, heart muscle areas still retain diagnostic anomalies in fatty acid metabolism that remain at-risk of further infarction even after successful reperfusion (Mouchizuki et al. 2002).

New novel SPECT designs (U-SPECT and D-SPECT) have begun a revolution in the design of high-resolution SPECT systems for cardiac imaging (Vastenhouw and Beekman 2007; Gambhir et al. 2009). The novel D-SPECT camera technology uses nine collimated detector columns arranged in a curved configuration to conform to the shape of the left side of the patient's chest. The application of these newer designs has yet to be brought into the preclinical design with miniaturization. Potentially, both the U-SPEC and the D-SPECT molecular imaging technologies will be integrated with other existing modalities including CT, MRI, and ultrasound systems, providing high definition fused images.

---

[6] ASNC IMAGING GUIDELINES FOR NUCLEAR CARDIOLOGY PROCEDURES, Stress protocols and tracers Milena J. Henzlova MJ, Cerqueira MD, Hansen CL, Taillefer R, Siu-Sun Yao S-S, http://www.asnc.org/imageuploads/ImagingGuidelinesStressProtocols021109.pdf and, ASNC IMAGING GUIDELINES FOR NUCLEAR CARDIOLOGY PROCEDURES Single Photon-Emission Computed Tomography, Thomas A. Holly TA, Abbott BG, Al-Mallah M, Calnon DA, Cohen MC, DiFilippo FP, Ficaro EP, Freeman MR, Hendel RC, Jain D, Leonard SM, Nichols KJ, Polk DM, Soman P, http://www.asnc.org/imageuploads/ImagingGuidelineSPECTJune2010.pdf.

[7] Animation of gated F-18 FDG cardiac PET images (from the Univ. of Kansas Medical School, Nuclear Medicine Dept.: http://www.rad.kumc.edu/nucmed//clinical/pet_gated_fdg.htm and http://www.rad.kumc.edu/nucmed/clinical/PET_gated_FDG_3v_animated.htm.

Biomarkers of Tumor Hypoxia

Tumor hypoxia (necrotic center and attenuated by drug-induced apoptosis) has been a challenging biomarker for imaging (Krohn et al. 2008; Blankenburg 2008; Hiller et al. 2006). Reactive oxygen species (ROS) which arise due to anaerobic metabolism, radiation treatment, and the generalized reduction of drug permeation into tumors with anoxic regions are the principal issues in finding good probes. Gradient perfusion from the vascular supply (normoxic regions) to sites of active metabolism is highly regulated by tumor angiogenesis, apoptosis, and vascular integrity. Acute hypoxia must be reversed or the tissue physiologic condition moves to apoptosis or cell death. Chronic hypoxia will lead to an adaptive genomic change which will be "survival directed" and increase metabolic behavior to escape from hypoxic environments. Hypoxia is fast becoming as important a biomarker target in solid tumors as identification of glycolysis, angiogenesis, apoptosis, or distant metastases.

Identification of hypoxia has implications in many medical settings. The goal of tumor therapy must include the characterization of the tumor metabolic state and not simply its detection and sizing. Tumors show increased radiation sensitivity in the presence of oxygenation. This is termed the OER or oxygen enhancement ratio. Radiation therapy is best performed under oxygenated conditions as tumors are typically more radioresistant under hypoxic conditions and many tumors exhibit central necrosis due to hypoxia (Skarsgard and Harrison 1991; Verheij 2008). Tirapazamine, a hypoxic cytotoxin, is commonly used as a potentiator of radiotherapy in combination with the common chemotherapeutic cisplatin. For survival, hypoxic cells undergo genetic modifications to adapt to the stress of hypoxia including generation of mutant p53, glycolysis, and HIF-1. Understanding the heterogeneity of the tumor with respect to the regional hypoxia allows for a more successful irradiation plan, including more precise radiation dose delivery (enhancement) to hypoxic (radioresistant) regions, and a likely better outcome for the patient is possible. Tumor stage, grade, size poorly predict hypoxia so a nuclear or other imaging modality is an important part of therapy planning.

Krohn et al. (2008) have described the radiotracer F-18-labeled nitroimidazole F-18 FMISO as the choice for imaging tumor hypoxia. Other nitroimidazoles include FAZA, FETA, FETNIM, EF3, EF5, and IAZA. The methylthiosemicarbazone ATSM, labeled with Cu-64 (a longer half-life PET tracer with 0.53 day half-life), is a new imaging agent for hypoxia (Anderson and Ferdani 2009; Mankoff et al. 2008; Obata et al. 2003). Cu-64 ATSM is selective for hypoxic tissues due to the increase in the redox trapping mechanism in hypoxic cells. The agent accumulates avidly in hypoxic cells and remains in hypoxic areas within tumors, whereas in normoxic cells the product washes freely out providing contrast within the tumor body. Anderson and Ferdani (2009) have published a detailed treatise on Cu-64 PET agents.

MRI (directly or with contrast) imaging of hypoxia is also an alternative. Using fMRI and the BOLD signal of paramagnetic deoxyHb from O_2Hb one can see the regional hypoxia in the tumor (Evelhoch et al. 2000; Ferris et al. 2011). O_2-sensitive contrast agents, such as perfluorotributylamine, hexafluorobenzene, hexomethyldisiloxane, trifluoroethoxy-MISO can be used for MR imaging of hypoxic tumors.

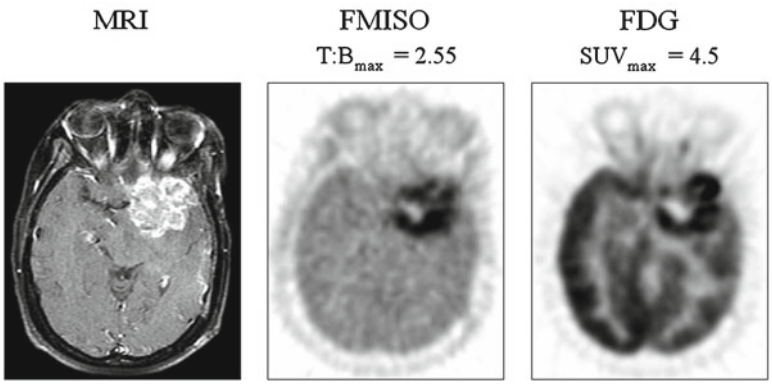

Fig. 1.9 Glioma imaging with MRI, F-18 MISO, and F-18 FDG: *Left*: anatomy by MRI, MRI imaging of a glioma with MR contrast agent reveals the tumor location. *Middle image*: PET image of F-18 MISO uptake in the tumor hypoxic center; *Right image*: PET image of F-18 FDG showing uptake in the tumor periphery (active growth region). The hypoxic FMISO-avid region is concentric and within the FDG uptake and both surrounding the tumor's actual necrotic core. The necrotic core is absent of both tracers. Courtesy: (Reproduced from Bioanalysis, May 2009, Vol. 1, No. 2, Pages 321–356 with permission of Future Science Ltd)

Also, lactate is a metabolic waste that is a result of hypoxia and lactate signal can be detected by MR spectroscopy, NIR, and bioluminescent probes and ESR (the electron spin resonance line width is sensitive to O_2) can delineate poorly oxygenated areas.

Hypoxia is an important aspect of stroke, myocardial hypoxia (stunned myocardium), diabetes, infection, arthritis, transplantation hypoxia, and other conditions. F-18 MISO data analysis requires only a single image at approximately 2 h postinjection (intravenous) and uptake is not generally limited by blood flow. F-18 MISO uptake is the same in most normal tissues and, unlike FDG, no arterial input function sampling or metabolite analysis is required or needed for quantitation. Synthesis of F-18 MISO can be accomplished in high yield via modification of the FDG Box technology. Figure 1.9 shows a glioma imaged with F-18 FMISO and the difference in the hypoxia image from that of FDG is also shown for comparison. The glioma structure is viewed using MR and the regional metabolic differences of two biomarkers (glycolysis and hypoxia) are evident with F-18 MISO uptake setting within the borders of the FDG image.

1.2.2.3 Magnetic Resonance Imaging, Functional MRI, and Mass Spectroscopy Imaging

Magnetic resonance imaging (MRI) and magnetic resonance spectroscopy (MRS) are not new players in imaging but they are in terms of biomarkers. MR is basically an imaging tool which utilizes radiowave emission in response to the action of an

imposed magnetic field, *B*o, on a biologic system. An excellent textbook on MR imaging and spectroscopy has been published by Westbrook et al. (2005) entitled *MR in Practice*. MR is almost universally an anatomical tool but it is capable of measuring metabolites using resonance spectroscopy (MRS). MR does not measure anatomy in the same sense that CT does with measuring density. MR measures the state of water. Ice and water are actually quite different in "structural" terms where liquid water has a mobility, or T2 relaxation time (stated as "apparent diffusion constant" or ADC) of 3,000 ms, while ice has a T2 relaxation time of 0.019 ms, more than 5-orders of magnitude. Tumors also demonstrate T2 ADC values which, under sufficient power (gauss) of an MR imaging system, can discriminate water mobility in muscle (ADC = 0.54 ms) versus tumors (ADC = 0.74 ms). Normal tissues range from 0.595 to 0.237 for brain to intestine, respectively, and thus if a tumor has a sufficiently different "water structure" (ADC value), a tumor may show a discrimination from normal tissues. Indeed, we can think of MR as a way to measure water mobility change as an effect of radiation or chemotherapy exposure or to drug therapy. ADC maps are parametric images of the apparent diffusion coefficients of diffusion weighted to create images. The term "apparent" refers to the dependence of these coefficients on factors other than prior molecular mobility. ADC maps are also called diffusion maps and represent a distinct biomarker of successful chemotherapy. They can also be a biomarker image of stroke as the changes in brain ADC with absence of flow can markedly be detected using this technique and can also show recovery of the neural area if intervention is successful (Schlaug et al. 1997; Chenevert et al. 1997; Morse et al. 2007; Ross et al. 2003). Other applications are in cardiac apoptosis (Hiller et al. 2006) and, as described earlier in this chapter, cell labeling and tracking using MR imaging in animal models of disease using paramagnetic probes and novel iron-tagged and gadolinium-tagged contrast agents (Muja and Bulte 2009).

The Reader is asked to read the chapters on Oncology Imaging and the chapter on Autoradiography where MALDI is discussed and also the chapter on MRS Imaging, where the physics of MR is further explained and the engagement of MRS applied to imaging is fully covered by Venter and his colleagues, respectively.

Functional MRI and Blood Flow in the Brain and Lungs

While anatomical images with MR are viewed as high resolution, a lower resolution MR tool has been developed for brain blood flow imaging, functional MR imaging (fMRI). fMRI is an imaging technique to measure blood flow (BF) and blood oxygenation BO) where increased flow and increased oxygenation are fundamentally "interpreted" as neurologic activation, or "stimulated" by reason of BF enrichment. This technique has particular implications as a biomarker tool in psychiatry, stroke (Pineiro et al. 2002), and neuropharmacology and there is an excellent review in animal studies by Ferris et al. (2011).

fMRI scans display changes in BF using the phenomenon of oxygen enhancement of the local water—blood—signal. In essence, "thinking" (use of a brain region)

promotes (increases) blood flow to a region of the brain where the increased BF suggests neurologic activation. A test to stimulate recall of a memory, for example, may increase BF to the hippocampus, a brain region known to be important for memory. Measurement of the BF changes thus has a role in the assessment of cognition and may help in diagnosis of memory loss, AD, or neurologic deficits from other causes.

Hyperpolarized gases are also a tool of imaging with MR. Dugas et al. (2004) describe hyperpolarized Helium 3 (^{3}He) in mice where they were investigating the flow of gases in and out of the lung. The murine lung field is indeed small and requires the high resolution of MR coupled with appropriate mechanical ventilation that can be used in imaging (Hedlund and Johnson 2002). With respect to MR, lung imaging provides two major challenges: (1) lungs are typically low in water content (use CT if you want to find consolidations) and (2) the air–tissue interfaces of bronchioles and arterioles reduce sensitivity due to variations in the magnetic susceptibility (causes short T2 and T2*relaxation times; see Chap. 11 for physics of MR). Hyperpolarized helium-3 introduced directly into the gas exchange regions of the lung allows for high-quality imaging of the lung, even in small mammals. What is imaged is the ADC (apparent diffusion coefficient; see Chap. 11) which is greater that controls by as much as 25 % in elastase-induced emphysema murine models which is a sufficient "delta" to allow for determination of efficacy of a drug or biologic to reduce such a change. This approach has been used for emphysema models using the pig, dog, guinea pig, rat, and mouse. Human studies to evaluate lung gas exchange using this technique have been employed clinically and, as described previously in this chapter, one can now image smaller animals with system miniaturizations.

Ultrasound Imaging

Ultrasound imaging, or sonograms, is a technique that utilizes sound waves to exploit a property of the tissues such as edges or discontinuity of density (Riess 2003; Wirtzfeld et al. 2005). In some respects, it is similar to CT, but with decidedly poorer resolution, in what it can detect. Imaging advancements in the technique through instrumentation, image reconstruction and the use of contrast agents (microbubble agents) can aid in the discrimination of edges and detection of anomalous surrounding tissues. The imaging technique can detect "biomarkers" of pathology such as blood clots (Cogo et al. 1998), kidney stones, tumors of the breast (calcium grains in breast DCIS), and in the abdomen, and it can be used for ventricular wall thickness and wall motion. While this imaging modality has many clinical indications, it has only limited small animal drug development applications and will not be covered in this book where we want to focus on imaging platforms that offer demonstrated translational capability and can more likely contribute to product licensure or approval. Readers are encouraged to seek more information on such topics as fluorocarbon-based injectables (Riess 2003), cardiac wall motion (Nagel et al. 1999), and a transgenic prostate cancer mouse model (Wirtzfeld et al. 2005). Nagel et al. have provided an excellent review of MRI imaging of

ischemia-induced wall motion abnormalities. They used high-dose dobutamine for evaluation by stress MRI (DSMR) and then compared their outcomes against dobutamine stress echocardiography (DSE). They did find that DSMR yielded a significantly higher diagnostic accuracy compared to DSE which, while not unexpected, the DSE was still equally diagnostic.

Several different antibody- or peptide-targeted microbubbles have been successfully tested for visualizing receptors overexpressed on tumor blood vessels and on atherosclerotic plaques (Kiessling et al. 2012). Kiessling et al. reported the first molecularly targeted microbubble formulation to diagnosis and localize prostate cancer was entering a Phase 0 trial. Other potential uses of the microbubbles technologies include thrombolytic therapy and enhancement of drug delivery across biologic barriers (i.e., the BBB).

Optical Tomography, Quantum Dots and Luminescence Imaging

Optical imaging systems are the current "vogue" in the nonclinical animal imaging laboratory as the systems are simple, relatively good resolution in the murine models, and the technique has had major advancements in chemical fidelity of test agents which have improved light persistence and reduction of image noise.

One of the problems with commonly used luminescent or fluorophore probes in histology and microscopy imaging is their rapid light emission decay following an excitation pulse. Colloidal semiconductors, or quantum dots (QDs), are single crystal nanoparticle whose size and shape can be closely controlled (Medintz et al. 2005; Michalet et al. 2005, So et al. 2006; Frangioni 2006). The size controls their absorption and emission and they have been designed to show prolonged light emission decay time. When a QD is linked to a biomolecule it can be used as a probe in a tissue section or in vivo using a light capture imaging platform. The pharmaceutical probe emits a characteristic wavelength of light upon absorbance of an excitation pulse (light/laser or other source). The photon signal decay of a QD which is internalized in a cell is markedly persistent from that of the same, but unconjugated, fluorophore where the QD signal can last well beyond 180 s versus a near complete decay of emitted light by 60 s for the internalized flurophore (Lopez 2003; Wu et al. 2003).

QDs can be synthesized from a variety of semiconductor materials, i.e., CdSe, CdS, CdTe, InAs, PbSe, and more. A detailed review of the QD technology, their synthesis and light-emitting properties, was published in 2005 by Michalet. QDs have a unique size-dependent property of releasing specific wavelengths of light in the near infrared (>700 nm) when an incident wavelength of light by a tuned laser at another wavelength excites the nanoparticle. QDs are being used in multiple probes for tissue microscopy, especially confocal microscopy, for imaging structures deep into tissue or are in a flow situation and are now being explored for in vivo imaging of surface structures and tumors in nude mice. QDs do produce strong background autofluorescence, have self-absorption, and significant light loss by tissue scatter of emitted photons. Figure 1.10 depicts a cartoon of a

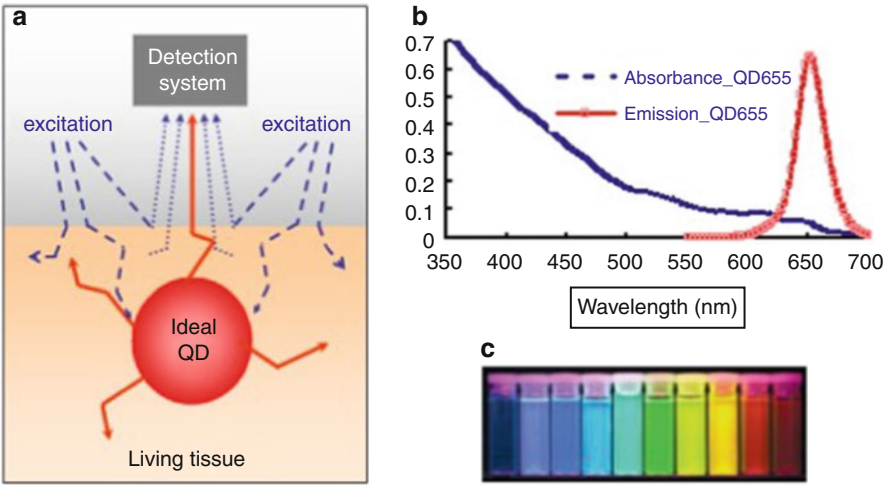

Fig. 1.10 Tunable quantum dots (QDs) for optical imaging. (**a**) An idealized quantum dot that may target a biologic entity uniquely can be tagged with a reporter or receptor-binding entity (i.e., DNA, iRNA proteins, Mabs, peptides, other binding entities). The QD does require external illumination to have an emission line. (**b**) is the incident excitation spectra (*sloping line*) and the resulting unique photopeak of the QD (30–50 nm FWHM) and, (**c**) examples of the emission colors which are dependent on the QD core size between 2 and 9.5 nm. Emission wavelengths range from 400 to 1,300 nm. (Courtesy: Jinghong Rao, Stanford University, Molecular Imaging Laboratory, Stanford, CA; with permission)

QD in tissue with an incident light excitation and the resultant emission scatter. A graph of excitation energy spectra versus the unique emission wavelength of the QD is also shown. The tunable QD emission color characteristics are principally based upon the nanoparticle size and they typically range from 2 to 9.5 nm. The emission light ranges from 400 to 1,350 nm with each emission peak having a full width at half maxima of about 30–50 nm.

Little incident light is available for QD excitation at nonsuperficial locations. New QD designs are *trifunctional* having tags of light-emitting products such as luciferase (LUC8) and the high-affinity probe for localizing the QD complex and a means of auto-excitation. The binding portion of a QD complex to a receptor can trigger the bioluminescent complex to excite the associated QD due to separation distances and the QD becomes the energy acceptor from the donor luciferase light (rather than external visualization of the luciferase) and the QD becomes activated emitting its own signature wavelength. Trifunctional structures allow QDs to work without the need for an external (ex vivo) excitation source (laser). This new technology is called BRET, or Bioluminescence Resonance Energy Transfer, which has excellent potential to allow for deep tissue in vivo excitation of QDs and detection via specific wavelength directed laparoscopy or other techniques. BRET, or self-illuminating QDs, is described in Fig. 1.11 (So et al. 2006; Frangioni 2006).

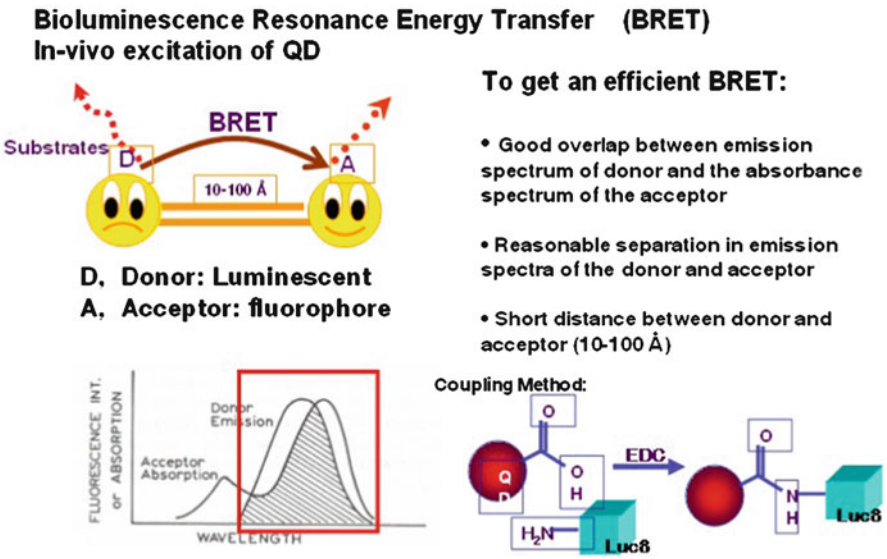

Fig. 1.11 BRET technologies are potentially useful for obtaining higher energy QD emission than from luciferase itself. Deep in vivo tissue excitation of QDs from non-external laser excitation is the main advantage of BRET QD probes. (Courtesy: Jinghong Rao, Stanford University, Molecular Imaging Laboratory, Stanford, CA; with permission)

1.3 Summary

This brief introductory chapter has hopefully set the stage for the Reader to venture to each of the upcoming chapters which will cover specific aspects of imaging platforms in the drug discovery and development laboratory. Appendix 1 of this chapter attempts to format a wide variety of imaging applications, the platforms and selected authors. The Reader should also visit the references listed at the end of this chapter (and all the references of each chapter) as although they are cited for specific reasons in the body of this chapter, there are many additional and important imaging suggestions and procedures that the Reader may find informative. The last chapter of this book will hopefully address any regulatory questions the readers may have and we invite all readers to query any of our authors. We have discussed several examples of ways to image specific biologic processes as well as use of selected biomarkers, but it is an impossible task to list or discuss all the possibilities and ideas that are being generated about the uses of imaging as they are published faster than this book can be published. In some ways this book will be outdated nearly by the time it is published. This text will be published in print and electronically to allow for updating these technologies Imagination is the only limit at this time. The editors and the authors of this book recognize the value of imaging in drug and biologics development and all also understand that no one image platform tells the

story of a drug or biologic and not one text can either. The Editors have created a resource and we are hopeful you will find important and practical imaging ideas which move your product(s) to approval.

The following key points are for you remember as you explore the chapters of this book as any new imaging platform, or any new imaging probe, should be examined under these critically important caveats or precepts:

- Biomarkers assessed by imaging essentially fall into four categories: (1) predictive, (2) prognostic, (3) diagnostic, and (4) dosimetric.
- Useful imaging targets or biomarkers need to be "causal", i.e. they must be mechanistically related, plausible, and proximal to a disease endpoint to provide accurate, confirmatory, and supportive evidence of a therapeutic intervention's efficacy.
- Biomarkers exploited in imaging can represent biochemical/anatomical/pathological process(es) or be representative specific pharmacological response(s) to therapeutic intervention.
- Biomarkers can serve as surrogate markers or replace a conventional clinical endpoint for efficacy and/or toxicity if the linkage is validated and the relation defensible.
- Biomarkers can accelerate drug development and decision making if used appropriately in the right models, species, and under the appropriate-controlled conditions.
- Biomarkers can provide a mechanistic bridge between preclinical study outcomes and clinical trial results.
- From a regulatory perspective, biomarker development must be validated prior to utilization in a proposed drug development plan.
- The Prentice criteria (Prentice 1989; Fleming and DeMets 1995; Campbell 2006), a unifying statistical approach for surrogate marker validation must be satisfied (Wagner et al. 2006), that is, a surrogate for a true endpoint must yield a valid test of the null hypothesis of no association between treatment and the true response. This criterion essentially requires the surrogate variable to "capture" any relationship between the treatment and the true endpoint.
- It is becoming clear that future clinical endpoints will not be univariate (single outcomes or single biomarker reads) but rather composite endpoints and a multivariate approach.
- Clinical medicine needs better ways to measure individual responses in pivotal clinical trials rather than simple mean analysis, perhaps using biomarker probes will be beneficial.
- Biomarker use in medical practice may help create individualized, i.e. personalized, medicine, and the regulatory process is a critical consideration (Woodcock 1997).
- Imaging is such a diverse technique to measure biomarkers. Physical properties, metabolism, pharmacokinetic and pharmacodynamic responses, and physiologic status can all be measured now with high resolution, minimal intervention, and high predictive clinical value.

- Lastly, nonclinical and clinical imaging platform may not, and are likely to not, provide equivalent outcomes. One must consider the "imaging equivalence" across species in drug and biologic development is a measure of the imaging physics, the product and probe chemistry, and the species translational fidelity.

Appendix 1. Selected Biomarkers and Interventional Probes Useful in Imaging[a]

Biomarkers/imaging targets (used in drug development)	Tracer or probe	Imaging modality	Suggested citations (see the full ref. listing)
Sugar and lipid metabolism:	F-18 FDG	PET	Phelps; Valk;
Cancer chemo/ radiation therapy	–	MR T2	Huang,
Cardiac metabolism	F-18 FDG	PET	
	C-11palmitate;C-11-choline	PET	
Brain metabolism/flow	N-13 ammonia/Rb-82	PET	
Lung cancer (SSTR+)	Tc-99m Depreotide		
Pancreatic cancer	Ga-68 DOTA-NOC or	SPECT	
Brain chemistry	F-18 DOPA	PET	
HDL and LDL metabolism	Tc-99m HDL and LDL	SPECT	
Free fatty oxidation rates	C-11 acetate	PET	
Blood flow (*vascular*):		PET	
BOLD signal–oxygenated Hgb		fMR (@ 3T[b])	Ferris
Cardiac and brain perfusion	Rb-82, O-15 H_2O; *N*-13 ammonia	PET SPECT	
Vascularobstruction/ aneurysms	Tc-99m ECD *Neurolite®		
Blood cells or labeled albumin	Gd contrast; Fenanoparticles	MR SPECT	
	In-111 oxine; Tc-99m HMPAO		
Apoptosis	Tc-99m Annexin V		Schlaug
Stroke/hypoxia	ADC change	MR	Krohn,
Elastase-induced emphysema	Hyperpolarized Helium-3	MR	Corbett; Dugas
Cardiac:			
Glucose metabolism	F-18 FDG	PET	Phelps
Perfusion	Rb-82, *O*-15 H_2O; *N*-13 ammonia	PET	
Fatty acid metabolism	I-123 BMIPP; I-124	SPECT; PET	

(continued)

Biomarkers/imaging targets (used in drug development)	Tracer or probe	Imaging modality	Suggested citations (see the full ref. listing)
Cationic pumps	Tc-99m—Sestamibi	SPECT	Machac
	Tc-99m Tetrofosmin	SPECT	Machac
	Tc-99m furifosmin (Q12)	SPECT	
	Tl-201	SPECT	Machac
Acetylcholinesterase	C-11 Edrophonium C-11 Pyridostigmine	PET	
DNA synthesis	F-18 FLT C-11 FMAU Br-76 BFU	PET	Lu
Inflammation/infection:			
Neutrophil elastase	Apatamer interference	SPECT	Charlton
White blood cells	In-111-oxine	SPECT	Sinha
Neuroinflammation		SPECT/PET	Deyton
HIV		PET	Esposito
Cell labeling	Various. Incl BLI.QD	SPECT/PET/BLI	
Generalized/focal infections	FDG/FLT	PET	Van Waarde
Muscarinic receptor:			
M2	F-18 FP TZTP	PET	Eckelman
Dopamine transporters	C-11 Cocaine	PET	Eckelman
Dopaminergic/Serotonin:			
D2 receptor	O-15 U91356a C-11 Raclopride C-11 β-CFT C-11 β-CIT C-11 β-CNT	PET	Eckelman
Dopamine metabolism:			
D1 receptor	O-15 SKF82958	PET	Eckelman
Benzodiazepine receptor	O-15 Lorazepam	PET	Eckelman
NMDA receptor (dopamine release)	C-11 Raclopride	PET	Eckelman
5-HT1A receptor	C-11 NMSP	PET	Eckelman
	F-18 FCWAYS		Eckelman
5-HT2A receptor	F-18 Setoperone	PET	Eckelman
Neurologic disease:		PET	Klunk
Alzheimer's disease (AD)	F-18 FDG; C-11 PIB;		Sossi
Aβ-amyloid	AMYViD; F-18 FDDNP; Fe accumulation	PET, MR T2	Esposito
Neuroinflammation	C-11 Arachidonic acid ADC change (with contrast)	MR	
Glioma	F-18 FDG	PET	
Pheochemocytoma	I-123/I-124 MIBG	SPECT/PET	
Multiple sclerosis	ADC changes	MR	

(continued)

Biomarkers/imaging targets (used in drug development)	Tracer or probe	Imaging modality	Suggested citations (see the full ref. listing)
Bone:			
Density/metastases	NaF (F-18); F-18-FLT	CT; PET	
Marrow cellularity	In-111 HPAMO WBCs	SPECT	
	Diffusion weighted MR	MR	
	F-18 FDG. F-18-FLT	PET	
Cancer and Tumor Hypoxia:			
Hypoxia	F-18 FMISO	PET	Krohn
	Other nitroimidazoles: FAZA, FETA, FETNIM, EF3, EF5, IAZA; Cu-64-ATSM		
	O_2-sensitive MR contrast BOLD agents: Perfluorotributylamine, Hexafluorobenzene, Hexomethyldisiloxane, Trifluoroethoxy-MISO	MR	
	Lactate MRS as a consequence of hypoxia:	MRI, NIR, BLI	
	O_2-line width sensitivity	ESR	
Glioblastomas	F-18 FDG	PET	
	I-123/I-124 MIBG	PET	
Prostate	I-123-MIP-1095	SPECT	
Pheochromocytoma	C-11 Me-CGS 27023A	PET	
Matrix metalloproteinases	C-11 Me-halo-CGS 27023A	PET and BLI	
	C-11 Biphenylsulfonamide	PET	
Luciferase-PET probes (for mice)	C-11 D-luciferin methyl ester	PET/BLI	
	C-11 D-luciferin methyl ether	PET/BLI	
Renal function:			
Renal stones	contrast	CT; MR	
Renal flow	Tc-99m inulin	SPECT	
Tubular secretion	In-111 DTPA	SPECT	
Bowel function:			
Obstruction/torsion/ transit time	X-ray (with contrast), CT	CT, US	
Appendicitis	In-111 WBCs, peptides	SPECT, PET, CT, US, MR	
Diffusion-weighted MR	DW-MR		
Hepatic function:			
Biliary flow	Tc-99m HYNIC-GC	SPECT	

(continued)

Biomarkers/imaging targets (used in drug development)	Tracer or probe	Imaging modality	Suggested citations (see the full ref. listing)
Genitourinary function/cancers:			
Cervical cancer Prostate cancer	Cu-64 DOTA-Cetuximab	PET	Anderson
Lung function/cancers:			
Fibrosis	(ROI scoring; HU measures)	CT	
Ventilation	Xe-133, Tc-99m MAA	SPECT	
SSTR + lung cancer	Cu-64-TETA-octrotide	PET	
Vascular disease and function:			
LDL	Gd-DTPA-SA-LDL	MR	
DVT (deep vein thrombosis) and pulmonary embolism	Tc-99m IIbIIIa receptor antagonists	SPECT	
Aneurysms	Gd-MS-325/vascular contrast	MR	
Angiography/Venography	X-ray contrast	CT	Taillefer;
GI flow/distortions	Microbubbles	US	Bates

Abbreviations: *NIR* near infrared, *BLI* bioluminescent imaging, *ESR* electron spin resonance, *OI* and *QD* optical and quantum dot, *PET* positron emission tomography, *SPECT* single photon emission computed tomography, *CT* computed tomography, *Planar* single projection nuclear image, *US* ultrasound, *MR* magnetic resonance, *fMR* functional MR using the BOLD (blood oxygen level dependent)

[a]The listing is not meant to be exhaustive and does not intentionally exclude other innovative probes

[b]3T: 3 Tesla (3T) magnetic field strength required

References

Agdeppa ED, Spilker ME (2009) A review of imaging agent development. AAPS J 11(2): 286–299. doi:10.1208/s12248-009-9104-5

Anderson CJ, Ferdani R (2009) Copper-64 radiopharmaceuticals for PET imaging of cancer: advances in preclinical and clinical research. Cancer Biother Radiopharm 24(4):379–393

Anderson RM, Sumption ND, Papworth DG, Goodhead DT (2006) Chromosome breakpoint distribution of damage induced in peripheral blood lymphocytes by densely ionizing radiation. Intrnl J Rad Biol 82(1):49–58

Arndt JW, Van der Sluys VA, Blok D, Griffloen G, Verspaget HW, Lamers CBHW, Pauwels EKJ (1993) Prospective comparative study of Technetium 99m-WBCs and Indium-111 granulocytes for examination of patients with inflammatory bowel disease. J Nucl Med 34: 1052–1057

Baek H-M, Chen J-H, Nalcioglu O, Su M-Y (2008) Letter to the editor. Choline as a biomarker for cell proliferation: Do the results from proton MR spectroscopy show difference between HER2/neu positive and negative breast cancers? Int J Cancer 123(5):219–1221

Bates SM, Lister-James J, Julian JA, Math M, Taillefer R, Moyer BR, Ginsberg JS (2003) Imaging characteristics of a novel Technetium Tc-99m–labeled platelet glycoprotein Iib/IIIa receptor

antagonist in patients with acute deep vein thrombosis or a history of deep vein thrombosis. Arch Intern Med 163:452–456
Blankenburg FG (2008) In-vivo detection of apoptosis. J Nucl Med 49:81S–95S
Bocan T (2010) Platform imaging biomarkers: applications across pre-clinical drug discovery with a focus on neuroscience, oncology, cardiovascular and future horizons. Am Pharm Rev 13(5): 16–21
Brooks DJ (2004) Neuroimaging in Parkinson disease. NeuroRx 1(2):243–254
Brouwers AH, Laverman P, Boerman OC, Oyen WJ, Barrett JA, Harris TD, Edwards DS, Corstens FH (2000) A^{99m}Tc-labelled leukotriene B4 receptor antagonist for scintigraphic detection of infection in rabbits. Nucl Med Commun 21(11):1043–1050
Brown AP, Citrin DE, Camphausen KA (2008) Clinical biomarkers of angiogenic inhibition. Cancer Metastasis Rev 27:415–434
Cai W, Chen X (2008) Multimodality molecular imaging of tumor angiogenesis. J Nucl Med 49:113S–128S
Campbell G (2006) Surrogate endpoints: a regulatory view; http://www.amstat.org; web link: http://www.amstat.org/meetings/fdaworkshop/presentations/2006/Greg%20Campbell%20Surrogate%20Endpoints.ppt
Caro LG, Van Tubergen RP (1962) High-resolution autoradiography. I. Methods. J Cell Biol 15:173–182
Cercignani M, Bozzali M, Iannucci G, Comi G, Filippi M (2001) Magnetization transfer ratio and mean diffusivity of normal appearing white and grey matter from patients with multiple sclerosis. J Neurol Neurosurg Psychiatry 70:311–317
Charlton J, Sennello J, Smith D (1997) In vivo imaging of inflammation using an aptamer inhibitor of human neutrophil elastase. Chem Biol 4:809–816
Chenevert TL, McKeever PE, Ross BD (1997) Monitoring early response of experimental brain tumors to therapy using diffusion magnetic resonance imaging. Clin Cancer Res 3:1457–1466
Christian PE, Bernier DBR, Langham JK (eds) (2004) Nuclear medicine and PET: technology and techniques, 5th edn. Mosby, St. Louis
Cogo A, Lensing AW, Koopman MMW (1998) Compression ultrasound for diagnostic management of patients with clinically suspected deep vein thrombosis: prospective cohort study. BMJ 316:17–20
Colburn WA (1995) Surrogate markers and clinical pharmacology. J Clin Pharmacol 35(5): 441–442, comment 464–470
Colburn WA (1997) Selecting and validating biologic markers for drug development. J Clin Pharmacol 37(5):355–362
Corbett JR, Ficaro EP (2004) Gated SPECT and the visual gold standard: gold standard or not? J Nucl Med 42(11):1639–1642
Daniels MJ, Hughes MD (1997) Meta-analysis for the evaluation of potential surrogate markers. Stat Med 16(17):1965–1982
DaSilva JN, Kilbourn MR, Domino EF (1993) In vivo imaging of monoaminergic nerve terminals in normal and MPTP-lesioned primate brain using positron emission tomography (PET) and [^{11}C] tetrabenazine. Synapse 14:128–131
De Gruttola V, Fleming T, Lin DY, Coombs R (1997) Perspective: validating surrogate markers–Are we being naive? J Infect Dis 175(2):237–246
DeMeyer G, Shapiro F (2003) Biomarker development. The road to clinical utility. Curr Drug Discov 12:23–27
Deyton L (1996) Importance of surrogate markers in evaluation of antiviral therapy for HIV infection. JAMA 276(2):159–160
Diehn M, Nardini C, Wang DS, McGovern S, Jayaraman M, Liang Y, Aldape K, Cha S, Kuo MD (2008) Identification of noninvasive imaging surrogates for brain tumor gene-expression modules. Proc Natl Acad Sci USA 105:5213–5218
Dougan H, Weitz JI, Stafford AR, Gillespie KD, Klement P, Hobbs JB, Lyster DM (2003) Evaluation of DNA aptamers directed to thrombin as potential thrombus imaging agents. Nucl Med Biol 30:61–72

Dressman H, Muramoto GG, Chao NJ, Meadows S, Marshall D, Ginsburg GS, Nevins JR, Chute JP (2007) Gene expression signatures that predict radiation exposure in mice and humans. PLoS Med 4:1–9

Dugas JP, Garbow JR, Kobayashi DK, Conradi MS (2004) Hyperpolarized 3He MRI of mouse lung. Magn Reson Med 52:1310–1317

Eckelman WC (2003) The use of PET and knockout mice in the drug discovery process. Drug Discov Today 8:404–410

Ellenberg SS, Hamilton JM (1989) Surrogate endpoints in clinical trials: cancer. Stat Med 8(4): 405–413

Esposito G, Giovacchini G, Liow J-S, Bhattacharjee AK, Greenstein D, Schapiro M, Hallett M, Herscovich P, Eckelman WC, Carson RE, Rappoport SI (2008) Imaging neuroinflammation in Alzheimer's disease with radiolabeled arachidonic acid and PET. J Nucl Med 49:1414–1421

Evelhoch JL, Gillies RJ, Karczmar GS, Koutcher JA, Maxwell RJ, Nalcioglu O, Raghunand N, Ronen SM, Ross BD, Swartz HM (2000) Applications of magnetic resonance in model systems: cancer therapeutics. Neoplasia 2:152–165

Ferl GZ, Zhang X, Wu H-M, Huang S-C (2007) Estimation of the ^{18}F-FDG input function in mice by use of dynamic small-animal PET and minimal blood sample data. J Nucl Med 48:2037–2045

Ferris CF, Smerkers B, Kulkarni P, Caffrey M, Afacan O, Toddes S, Stolberg T, Febo M (2011) Functional magnetic resonance imaging in awake animals. Rev Neurosci 22:665–674

Filippi M, Horsfield MA, Ader HJ, Barkhof F, Bruzzi P, Evans A, Frank JA, Grossman RI, McFarland HF, Molyneux P, Paty DW, Simon J, Tofts PS, Wolinsky JS, Miller DH (1998) Guidelines for using quantitative measures of brain magnetic resonance imaging abnormalities in monitoring the treatment of multiple sclerosis. Ann Neurol 43:499–506

Fleming TR, DeMets DL (1995) Surrogate end points in clinical trials: are we being misled? Ann Intern Med 125(7):605–613, comment. 1996; 126(8), 667

Frangioni JV (2006) Self-illuminating quantum dots light the way. Nat Biotechnol 24(3):326–328

Frank R, Hargreaves R (2003) Clinical biomarkers in drug discovery and development. Nat Rev Drug Discov 2:566–580

Friedland GW, Thurber BD (1996) Perspective: the birth of CT. AJR Am J Roentgenol 167:1365–1370, and, http://www.bioclinica.com/blog/evolution-ct-scan-clinical-trials The Evolution of CT Scan Clinical Trials, Stuart Jackson blog on July 22, 2011

Fukushima Y, Toba M, Ishihara K, Mizumura S, Seino T, Tanaka K, Mizuno K, Kumita S (2008) Usefulness of 201TlCl/ 123I-BMIPP dual-myocardial SPECT for patients with non-ST segment elevation myocardial infarction. Ann Nucl Med 22(5):363–369

Gambhir SS (2006) Using radiolabeled DNA as an imaging agent to recognize protein targets. J Nucl Med 47(4):557–558

Gambhir SS, Berman DS, Ziffer J, Nagler M, Sandler M, Patton J, Hutton B, Sharir T, Haim SB, Haim SB (2009) A novel high-sensitivity rapid-acquisition single-photon cardiac imaging camera. J Nucl Med 50:635–643

Hansen CL, Goldstein RA, Akinboboye OO, Berman DS, Botvinick EH, Churchwell KB, Cooke CD et al (2007) Myocardial perfusion and function: single photon emission computed tomography. J Nucl Cardiol 14:e39–e60

Hedlund L, Johnson G (2002) Mechanical ventilation for imaging the small animal. ILAR J 43:159–174

Heiss W-D, Herholz K (2006) Brain receptor imaging. J Nucl Med 47:302–312

Hiller K-H, Waller C, Nahrendorf M, Bauer WR, Jakob PM (2006) Assessment of cardiovascular apoptosis in the isolated rat heart by magnetic resonance molecular imaging. Mol Imaging 5:115–121

Huang SC (2000) The anatomy of SUV (standardized uptake value). Nucl Med Biol 27:643–646

Huang J, Chang C, Lee I, Sutcliffe JL, Cherry SR, Tarantal AF (2008) Radiolabeling rhesus monkey CD34+ hematopoietic and mesenchymal stem cells with ^{64}Cu-Pyruvaldehyde-Bis(N4-Methylthiosemicarbazone) for micro-PET imaging. Mol Imaging 7(1):1–11

Inoue T, Kato T, Uchida T, Sakuma M, Nakajima A, Shibazaki M, Imoto Y, Saito M, Hashimoto S, Hikichi Y, Node K (2005) Local release of C-reactive protein from vulnerable plaque or coronary arterial wall injured by stenting. J Am Coll Cardiol 46(2):239–245

Jaffer FA, Nahrendorf M, Sosnovik D, Kelly KA, Aikawa E, Weissleder R (2006) Cellular imaging of inflammation in atherosclerosis using magnetofluorescent nanomaterials. Mol Imaging 5:85–92

Johnston RF, Pickett SC, Barker DL (1990) Autoradiography using storage phosphor technology. Electrophoresis 11:355–360

Kelloff GJ, Krohn KA, Larson SM, Weissleder R, Mankoff DA, Hoffman JM, Link JM, Guyton KZ, Eckelman WC, Scher HI, O'Shaughnessy J, Cheson BD, Sigman CC, Tatum JL, Mills GQ, Sullivan DC, Woodcock J (2005) The progress and promise of molecular imaging probes in oncologic drug development. Clin Cancer Res 11(22):7967–7985

Keyes JW (1995) SUV: standardized uptake or silly useless value? J Nucl Med 36:1836–1839

Kiessling F, Fokong S, Koczera P, Lederle W, Lammers T (2012) Ultrasound microbubbles for molecular diagnosis, therapy, and theranostics. J Nucl Med 53:345–348

Koyama K, Akashi YJ, Kida K, Suzuki KK, Ishibashi Y, Musha H, Banach M (2011) Relevance of 123I-BMIPP delayed scintigraphic imaging for patients with angina pectoris – A pilot study. Arch Med Sci 7(3):428–432

Krishna R (ed) (2006) Dose optimization in drug development, from the series "Drugs and the pharmaceutical sciences",.Swarbrick J (exe. ed.), Taylor & Francis Group, LLC, New York/London; web link: http://www.google.com/url?sa=t&rct=j&q=&esrc=s&source=web&cd=1&ved=0CDMQFjAA&url=http%3A%2F%2Fslib.phys.msu.ru%2Fsl%2F79%2FKrishna%2520R.%2520-%2520Dose%2520Optimization%2520in%2520Drug%2520Development%2C%2520Vol.%2520161%2520(2006)(293s).pdf&ei=CJJgUbaaPMfD4AO98YCADw&usg=AFQjCNH6qbVW13B8rgEwmkCcB0z9C8J8YQ&sig2=_I3Q1IQ82s3eymUepazvEg&bvm=bv.44770516,d.dmg&cad=rja

Krohn KA, Muzi M, Spence AM (2007) What is in a number? The FDG lumped constant in the rat brain. J Nucl Med 48:5–7

Krohn KA, Link JM, Mason RP (2008) Molecular imaging of hypoxia. J Nucl Med 49:129S–148S

LaBaer J (2005) So, you want to look for biomarkers. Introduction to the special biomarkers issue. J Proteome Res 4:1053–1059

Logan J, Fowler JS, Volkow ND, Wolf AP, Dewey SL, Schlyer DJ, MacGregor RR, Hitzemann R, Bendriem B, Gatley SJ, Christman DR (1990) Graphical analysis of reversible radioligand binding from time-activity measurements applied to [*N*-^{11}C-methyl]-(−)-cocaine PET studies in human subjects. J Cereb Blood Flow Metab 10:740–747

Lopez JC (2003) Quantum leap for quantum dots. Nat Rev Neurosci 4:163

Lu L, Samuelson L, Bergstrom M, Sato K, Fasth K-J, Langstrom B (2002) Rat studies comparing C-11-FMAU, F-18 FLT and Br-76 BFU as proliferation markers. J Nucl Med 43:1688–1698

Machac J, Bacharach SL, Bateman TM, Bax JJ, Beanlands R, Bengel F, Bergmann SR, Brunken RC, Case J, Delbeke D, DiCarli MF, Garcia EV, Goldstein RA, Gropler RJ, Travin M, Patterson R, Schelbert HR (2006) Positron emission tomography myocardial perfusion and glucose metabolism imaging. J Nucl Cardiol 13:e121–e151

Mankoff DA, Link JM, Linden HM, Sundararajan L, Krohn KA (2008) Tumor receptor imaging. J Nucl Med 49:149S–163S

Marchetti F, Coleman MA, Jones IM, Wyrobek AJ (2006) Candidate protein biodosimeters of human exposure to ionizing radiation. Int J Radiat Biol 82:605–639

Meadows SK, Dressman HK, Muramoto GG, Himburg H, Salter A, Wei ZZ, Ginsburg G, Chao NJ, Nevins JR, Chute JP (2008) Gene expression signatures of radiation response are specific, durable and accurate in mice and humans. PLoS Med 3:690–701

Medintz IL, Testsuo-Uyeda H, Goldman ER, Mattoussi H (2005) Quantum dot bioconjugates for imaging, labeling and sensing. Nat Mater 4:435–446

Michalet X, Pinaud FF, Bentolila LA, Tsay JM, Doose S, Li JJ, Sundaresan J, Wu AM, Gambhir SS, Weiss S (2005) Quantum dots for live cells, in vivo imaging, and diagnostics. Science 307:538–544

Minn H, Zasadny KR, Quint LE, Wahl RL (1995) Lung cancer: reproducibility of quantitative measurements for evaluating 2-[F-18]-fluoro-2-deoxy-D-glucose uptake at PET. Radiology 196:167–173

Mintun MA, LaRossa GN, Sheline YI, Dence CS, Lee SY, Mach RH, Klunk WE, Mathis CA, DeKosky ST, Morris JC (2006) [^{11}C]PIB in a nondemented population. Potential antecedent marker of Alzheimer disease. Neurology 67:446–452

Molecular imaging of cancer: from molecules to humans (2008) J Nucl Med 49(Suppl 2):1S–195S

Morse DL, Galons JP, Payne CM, Jennings DL, Day S, Xia G, Gillies RJ (2007) MRI-measured water mobility increases in response to chemotherapy via multiple cell death mechanisms. NMR Biomed 20:602–614

Mouchizuki T, Murase K, Higashuino H, Miyagawa M, Sugawara Y, Kikuchi T, Kezoe J (2002) Ischemic "memory image" in acute myocardial infarction of I- 123BMIPP after reperfusion therapy: a comparison withTc-99m pyrophosphate and Tl-201 dual-isotope SPECT. Ann Nucl Med 16(8):563–568

Moyer BR, Barrett JB (2009) Biomarkers and Imaging: the physics and chemistry of imaging biomarkers. Bioanalysis 1(2):321–356

Mueller-Lisse UG, Scherr MK (2007) Proton MR spectroscopy of the prostate. Eur J Radiol 63(3):351–360

Muja M, Bulte JWM (2009) Magnetic resonance imaging of cells in experimental disease models. Prog Nucl Magn Reson Spectrosc 55:61–77

Nagel E, Lehmkuhl H, Bocksch W, Klein C, Vogel U, Frantz E, Ellmer A, Dreysse S, Fleck EE (1999) Noninvasive diagnosis of ischemia-induced wall motion abnormalities with the use of high-dose dobutamine stress MRI: comparison with dobutamine stress echocardiography. Circulation 99:763–770

Niven R, Pearlman R, Wedeking T, Mackeigan J, Noker P, Simpson-Herren L, Smith JG (2000) Biodistribution of radiolabeled lipid-DNA complexes and DNA in mice. J Pharm Sci 87(11): 1292–1299

Obata A, Yoshimoto M, Kasamatsu S, Naiki H, Takamatsu S, Kashikura K, Furukawa T, Lewis JS, Welch MJ, Saji H (2003) Intra-tumoral distribution of ^{64}Cu-ATSM: a comparison study with FDG. Nucl Med Biol 30(5):529–534

Okunieff P, Chen Y, Maguire DJ, Huser AK (2008) Molecular markers of radiation-related normal tissue toxicity. Cancer Metastasis Rev 27(3):363–374

Orlova A, Nilsson FY, Wikman M, Widström C, Ståhl S, Carlsson J, Tolmachev V (2006) Comparative in vivo evaluation of iodine and technetium labels on anti-HER2 affibody for single photon imaging of HER2 expression in tumors. J Nucl Med 47(3):512–519

Oyajobi BO, Munoz S, Kakonen R, Williams PJ, Gupta A, Wideman CL, Story B, Grubbs B, Armstrong A, Dougall WC, Garrett IR, Mundy GR (2007) Detection of myeloma in skeleton of mice by whole body optical fluorescence imaging. Mol Cancer Ther 6(6):1701–1708

Perket JM (2009) Mass spectacle: making the most of mass spectrometry imaging. The Scientist 23(3):61, http://www.the-scientist.com/?articles.view/articleNo/27190/title/Mass-Spectacle/

Phelps ME (ed) (2004) PET: Molecular imaging and its biological applications. Springer-Verlag, New York, USA

Phelps ME, Huang SC, Hoffman EJ, Selin C, Sokoloff L, Kuhl DE (1979) Tomographic measurement of local cerebral glucose metabolic rate in humans with (F-18)2-fluoro-2-deoxy-D-glucose: validation of method. Ann Neurol 6:371–388

Pichler BJ, Wehrl HF, Judenhofer MS (2008) Latest advances in molecular imaging instrumentation. J Nucl Med 49(Suppl 2):5S–23S

Pineiro R, Pendlebury S, Johansen-Berg H, Matthews PM (2002) BOLD signal in stroke altered hemodynamic responses in patients after subcortical stroke measured by functional MRI. Stroke 33:103–109

Prentice RL (1989) Surrogate endpoints in clinical trials: definition and operational criteria. Stat Med 8:431–440

Rabinovici GD, Furst AJ, O'Neil JP, Racine CA, Mormino EC, Baker SL, Chetty S, Patel P, Pagliaro TA, Klunk WE, Mathis CA, Rosen HJ, Miller BL, Jagust WJ (2007) C-11 PIB PET

imaging in Alzheimer disease and frontotemporal lobar degeneration. Neurology 68:1205–1212
Riess JG (2003) Fluorocarbon-based injectable gaseous microbubbles for diagnosis and therapy. Curr Opin Colloid Interface Sci 8:259–266
Ross BD, Moffat BA, Lawrence TS, Mukherji SK, Gebarski SS, Quint DJ, Johnson TD, Junck L, Robertson PL, Muraszko KM, Dong Q, Meyer CR, Bland PH, McConville P, Geng H, Rehemtulla A, Chenevert TL (2003) Evaluation of cancer therapy using diffusion magnetic resonance imaging. Mol Cancer Ther 2:581–587
Rudin M, Weissleder R (2003) Molecular imaging in drug discovery and development—Review. Nat Rev Drug Discov 2:123–131
Sampath L, Kwon S, Ke S, Wang W, Schiff R, Mawad ME, Sevick-Muraca E (2007) Dual-labeled trastuzumab-based imaging agent for the detection of human epidermal growth factor receptor 2 overexpression in breast cancer. J Nucl Med 48:1501–1510
Sandella A, Ohlsson T, Erlandsson K, Strand SE (1998) An alternative method to normalize clinical FDG studies. J Nucl Med 39(3):552–555
Santana CA, Folks RD, Garcia EV, Verdes L, Sanya R, Hainer J, DiCarli MF, Esteves FP (2007) Quantitative ^{82}Rb PET/CT. Development and validation of myocardial perfusion database. J Nucl Med 48:1122–1128
Schlaug G, Seiwert B, Benfield A, Edelman RR, Warach S (1997) Time course of the apparent diffusion coefficient (ADC) abnormality in stroke. Neurology 49:113–119
Schober A (2004) Classic toxin-induced animal models of Parkinson's disease: 6-OHDA and MPTP. Cell Tissue Res 318:215–224. doi:10.1007/s00441-004-0938-y
Shapiro D, Thibault P, Beetz T, Elser V, Howells M, Jacobsen C, Kirz J, Lima E, Miao H, Neiman AM, Sayre D (2005) Biological imaging by soft x-ray diffraction microscopy. Proc Natl Acad Sci USA 102:15343
Sinha P, Conrad GR, Shyamashree SS (2004) Localization of In-111 white blood cells in rhabdomyolysis. Clin Nucl Med 29:367–369
Skarsgard LD, Harrison I (1991) Dose Dependence of the Oxygen Enhancement Ratio (OER) in Radiation Inactivation of Chinese Hamster V79-171 Cells. Rad Res 127(3):243–247
Smith JJ, Sorenson AG, Thrall JH (2003) Biomarkers in imaging: realizing radiology's future. Radiology 227:633–638
So M-K, Xu C, Loening AM, Gambhir SS, Rao J (2006) Self-illuminating quantum dot conjugates for in-vivo imaging. Nat Biotechnol 24(1):339–343
Solon E (2002) Correspondence: continued discussion of quantitative whole-body autoradiography in the pharmaceutical industry. Survey results on study design, methods and regulatory compliance. J Pharmacol Toxicol Methods 48:187–189
Solon E (2007) Autoradiography: high resolution molecular imaging in pharmaceutical discovery and development. Expert Opin Drug Discov 2(4):1–12
Solon EG, Kraus L (2002) Appraisal of state-of-the-art: quantitative whole-body autoradiography in the pharmaceutical industry. Survey results on study design, methods, and regulatory compliance. J Pharmacol Toxicol Methods 46:73–81
Solon EG, Schweitzer A, Stoeckli M, Prideaux B (2010) Autoradiography, MALDI-MS, and SIMS-MS Imaging in pharmaceutical discovery and development. AAPS J 12(1):11. doi: 10.121208/s12248-009-9158-4
Sossi V (2007) Cutting edge brain imaging with positron emission tomography. Neuroimaging Clin N Am 17:427–440
Stollman TH, Scheer MGW, Leenders WPJ, Verrijp KCN, Soede AC, Oyen WJG, Ruers TJM, Boerman OC (2008) Specific imaging of VEGF-A expression with radiolabeled anti-VEGF monoclonal antibody. Int J Cancer 122:2310–2314
Sun Z, Ng KH, Ramli N (2001) Editorial: biomedical imaging research: a fast emerging area for interdisciplinary collaboration. Biomed Imaging Interv J 7(3):1–3

Taillefer R, Edell S, Innes G, Lister-James J (2000) Acute thromboscintigraphy with ^{99m}Tc-apcitide: results of the phase 3 multicenter clinical trial comparing Tc-99m-apcitide scintigraphy with contrast venography for imaging acute DVT. J Nucl Med 41:1214–1223

Thakur ML (1995) Radiolabeled peptides: now and the future. Nucl Med Commun 16:724–732

Therasse P (2002) Measuring the clinical response. What does it mean? Eur J Cancer 38: 1817–1823

Thurner MM, Sundgren PC (2008) Imaging of slow viruses. Neuroimaging Clin N Am 18: 133–148

Toomey JS, Bhatia S, Moon LT, Orchard EA, Tainter KH, J. Lokitz SJ, Terry T, Mathis JM (2012) PET Imaging a MPTP-Induced Mouse Model of Parkinson's Disease Using the Fluoropropyl-Dihydrotetrabenazine Analog [18F]-DTBZ (AV-133). PLoS One 7(6):e39041. doi:10.1371/journal.pone.0039041

Valk P, Bailey DL, Townsend DW, Maisey MM (eds) (2003) Positron emission tomography: basic science and clinical practice. Springer, London

Van Waarde A, Cobben DCP, Suurmeijer AJH, Maas B, Vaalburg W, deVries EFJ, Jager PL, Hoekstra HJ, Elsinga PH (2004) Selectivity of 18F-FLT and 18F-FDG for differentiating tumor from inflammation in a rodent model. J Nucl Med 45:695–700

Van Westreenen HL, Cobben DCP, Jager PL, van Dullemen HM, Wesseling J, Elsinga PH, Plukker JT (2005) Comparison of ^{18}F-FLT PET and ^{18}F-FDG PET in esophageal cancer. J Nucl Med 46: 400–404

Vastenhouw B, Beekman F (2007) Submillimeter total-body murine imaging with U-SPECT-I. J Nucl Med 48:487–493

Verheij M (2008) Clinical biomarkers and imaging for radiotherapy-induced cell death. Cancer Metastasis Rev 27:471–480

Wagner H (2003) History notes. Hal Anger: nuclear medicine's quiet genius. J Nucl Med 44: 26N–34N

Wagner JA (2006) Bridging preclinical and clinical development: biomarker validation and qualification, Chapter 3. In: Krishna R (ed) Dose optimization in drug development, from the series "Drugs and the pharmaceutical sciences", Swarbrick J (exe. ed.), Taylor & Francis Group, LLC, New York/London, pp 35–44; web link: http://www.google.com/url?sa=t&rct=j&q=&esrc=s&source=web&cd=1&ved=0CDMQFjAA&url=http%3A%2F%2Fslib.phys.msu.ru%2Fsl%2F79%2FKrishna%2520R.%2520-%2520Dose%2520Optimization%2520in%2520Drug%2520Development%2C%2520Vol.%2520161%2520(2006)(293s).pdf&ei=CJJgUbaaPMfD4AO98YCADw&usg=AFQjCNH6qbVW13B8rgEwmkCcB0z9C8J8YQ&sig2=_I3Q1IQ82s3eymUepazvEg&bvm=bv.44770516,d.dmg&cad=rja

Wang Y-X, Deng M (2010) Medical imaging in new drug clinical development. J Thorac Dis 2:245–252

Westbrook C, Roth CK, Talbot J (eds) (2005) MRI in practice, 3rd edn. Blackwell, Malden, MA

Wheeler KT, Wang L-M, Wallen CA, Childers SR, Cline JM, Keng PC, Mach RH (2000) Sigma-2 receptors as a biomarker of proliferation in solid tumours. Br J Cancer 82:1223–1232

Williams DL, Minshew NJ (2007) Understanding autism and related disorders: what has imaging taught us? Neuroimaging Clin N Am 17:495–509

Wirtzfeld LA, Wu G, Bygrave M, Yamasaki Y, Sakai H, Moussa M, Izawa JI, Downey DB, Greenberg NM, Fenster A, Xuan JW, Lacefield JC (2005) A new three-dimensional ultrasound microimaging technology for preclinical studies using a transgenic prostate cancer mouse model. Cancer Res 65(14):6337–6345

Woodcock J (1997) An FDA perspective on the drug development process. Food Drug Law J 52(2):145–161

Wu X, Liu H, Liu J, Kari N, Haley KN, Treadway JA, Larson JP, Ge N, Peale F, Bruchez MP (2003) Immunofluorescent labeling of cancer marker Her2 and other cellular targets with semiconductor quantum dots. Nat Biotechnol 21:41–46

Yamada T, Matsumori A, Tamaki S, Sasayama S (1998) Myosin light chain I grade: a simple marker for the severity and prognosis of patients with acute myocardial infarction. Am Heart J 135(2 Pt 1):329–334

Chapter 2
Imaging in Drug Development: Animal Models, Handling and Physiological Constraints

David B. Stout

Abstract In this chapter we delve into the primary components and operational issues that need to be considered in the setup and operation of a dedicated animal imaging facility with the use of PET, SPECT, CT, MR, and other platforms. The special conditions required for successful animal models, needs of the animals during imaging, and the avoidance of environmental and physiologic artifacts to the images are discussed.

2.1 Introduction

Preclinical molecular imaging research using animals typically focuses on measuring a metabolic process associated with a disease using PET, SPECT, or optical methods, often in conjunction with an anatomical imaging modality such as MR or CT (Phelps 2000). The purpose is to elucidate diagnostic or treatment options for a disease, then translate those findings into human applications. It is vital to understand whether the measurement being made is relevant, since handling conditions can alter the in vivo distribution of the imaging probe (Fueger et al. 2006).

With the advent of imaging systems suitable for work with mice, most preclinical research now utilizes mice or rats, which often provide very useful indications of what will happen in humans (Stout and Zaidi 2009). However there are situations where these animals have differences from humans that could be important. For example, rodents typically metabolize substances much more rapidly than humans,

D.B. Stout, Ph.D. (✉)
Biomedical Physics IDP, Molecular & Medical Pharmacology, Preclinical Imaging Technology Center, Crump Institute for Molecular Imaging, University of California, 570 Westwood Plaza, Los Angeles, CA, USA
e-mail: dstout@mednet.ucla.edu; http://labs.pharmacology.ucla.edu/stoutlab/imaging.html

B.R. Moyer et al. (eds.), *Pharmaco-Imaging in Drug and Biologics Development*, AAPS Advances in the Pharmaceutical Sciences Series 8, DOI 10.1007/978-1-4614-8247-5_2,

resulting in shorter circulating blood times, and if investigating the metabolism of a radiolabeled drug, the metabolites (including the radiotracer) may be cleared faster resulting in higher radioactive dose to bladder wall than might be estimated using other species. For preclinical imaging work, perhaps most important of all is that the biodistribution of imaging agents can be markedly altered based on how the animals are treated and how the data are both created and analyzed. Anesthesia, heating, and other factors alter physiological conditions (Fueger et al. 2006; Lee et al. 2005; Toyama et al. 2004), which in turn alter the images of metabolism obtained from PET scans by altering both distribution and kinetics of metabolism. There are often multiple choices for constructing PET and SPECT images (i.e., filtered back projection, ordered subset expectation maximization [OSEM], maximum a posteriori [MAP]), and the way images are analyzed can be quite subjective.

Characterization of how labeled imaging agents behave in vivo can be determined in several ways, including single imaging sessions, imaging the same animal multiple times, sacrificing animals at various time points for whole-body static (in situ) images, or individual tissue gamma counting for organ quantitation (percent of injected dose; %ID) or histologic/*en face* (liquid photographic emulsion) autoradiography (see Chap. 6 by Solon and Moyer). Whether optical, PET, SPECT, or MR methods are used, except in rare cases, anesthesia is essential to ensure the animals stay immobile during the imaging process. All anesthetic agents alter physiology, which in turn alters in vivo metabolism (Toyama et al. 2004). The question is what these effects upon the experiment at hand are and what can be done to control, minimize, measure, or remove those effects on the process under investigation.

This chapter will describe factors that can alter metabolism and measurements made in vivo. There are multiple ways to mitigate, measure, or control these factors, and the best method depends upon the specific experimental conditions. An example of the process of taking an imaging probe from idea to FDA approval through investigational new drug (IND) approval is presented as an example of how various preclinical investigation methods can be combined to take an imaging agent from an idea to clinical application and how one may utilize such agents in new novel drug and biologic discovery and development.

2.2 Animal Models

The choice of animal model to use depends on many factors, including availability of an appropriate model of the human disease, size with respect to the imaging system capabilities and resolution, overall operating cost, animal housing considerations, and perhaps whether the species of choice is well characterized for the type of experiment and data analysis required. In some cases, use of endangered species and animals commonly kept as pets is constrained by both regulatory and safety concerns. In some cases, drugs and biologics for treating certain threats (smallpox, anthrax, radiation, chemical warfare agents, or select agents (National Select Agent

Registry, CDC, http://www.selectagents.gov/select%20agents%20and%20toxins%20list.html)) have only animal models to demonstrate efficacy since testing in humans would be unethical (see the Animal Rule: 21 CFR 314.600 for drugs; 21 CFR 601.90 for biological products; http://www.fda.gov/downloads/Drugs/GuidanceComplianceRegulatoryInformation/Guidances/ucm078923.pdf).

Larger species, such as dogs, primates, or pigs, have advantages with respect to how well they lend themselves to observation and measurements of small structures. The limited resolution of imaging systems means that a larger object may be the only way to measure certain structures, especially in imaging substructures of the brain. Large animals have bigger blood pools that may be needed for rapid and frequent blood time-activity sampling and metabolite analysis. Surgical interventions are easier and most veterinarians or medical doctors are able to work easily in larger animals.

The drawback to larger animals includes high cost, difficulty in handling, and that they often can be imaged only using human imaging systems. There may be regulatory barriers to imaging animals and humans in the same system or difficulty with availability of scanner time (clinical use over animal use) and radioisotope selection. Many primates are endangered, and even with breeding colonies there are often high costs and safety issues that preclude using primates. Perhaps the biggest limitation is the small number of studies, usually just one or two, that can be done per day compared to smaller species using miniaturized PET and SPECT systems. Furthermore, larger animals require expensive and large caging systems and require careful handling for physical safety, since there may be biological pathogens and parasites that could be transferred to humans, such as hepatitis and tuberculosis.

There are times when the only justifiable species to use may be primates. One example is the study of Parkinson's disease, where biochemical, behavioral, and in vivo metabolic information can be obtained. The larger size of primates enables visualization of the caudate and putamen brain structures, which in turn allows for earlier and more accurate detection of the disease. Further, primates replicate the human disease very well using a neurotoxin-induction model that does not affect rodents (Leenders et al. 1988).

Small animals such as mice and rats have a number of advantages. The entire animal can often be imaged all at once, making it far easier and more accurate to measure biodistribution of probes and radiation dosimetry. Smaller animals are less expensive and easier to handle, and large numbers can be housed together and imaged in a short time. The smaller sizes also afford less scatter, attenuation, and less radioactivity needed for imaging, which also reduces personnel exposure. Mice in particular are available with a wide range of genetic knock-in and knockout genes, thus can be used to look at many different genetic conditions. The availability of immune-compromised SCID and nude mice and rats enables oncology research using human tumor lines, which means that experimental results should ideally translate directly to human use.

However, rodents are not always the ideal option because surgical interventions, blood sampling, and injections are not easy. The small size means that in general only organ-level measurements are possible using most methodologies, and long

scan times are likely necessary to obtain high-resolution MR images. In some cases, rodents are not well matched to humans for certain diseases. One example is the lack of a gallbladder in rats making gastrointestinal imaging and studies where biliary clearance is important difficult to investigate and interpret.

2.3 Animal Handling

From the time animals are received from a vendor until completion of the project, there are many steps where environmental conditions must be carefully considered. A well-designed imaging center or neighboring coordinated facilities are necessary to conduct the necessary procedures to create the animal models (Fig. 2.1). For imaging work, heating, anesthesia, pathogen control, positioning, and post-imaging disposal are necessary to acquire useful data in a safe and effective manner. Even before work begins, animals must be acclimatized to their surroundings to reduce the stress of transport (Conour et al. 2006; Jennifer Obernier and Baldwin 2006).

For genetic and oncology work, there are biosafety concerns for viral vectors, human tumor cell lines, and potentially carcinogenic or biohazardous chemotherapy agents. An appropriately furnished location is essential to safely work with these agents, monitor tumors, and conduct any surgical interventions. Local regulations vary widely, but the general requirements can be considered to be a barrier facility with proper ventilation, biohazardous capabilities, and perhaps a surgical area with anesthesia and heating support.

Depending on local requirements, it may be necessary to quarantine or isolate animals based on their health status, immune condition, or due to the use of

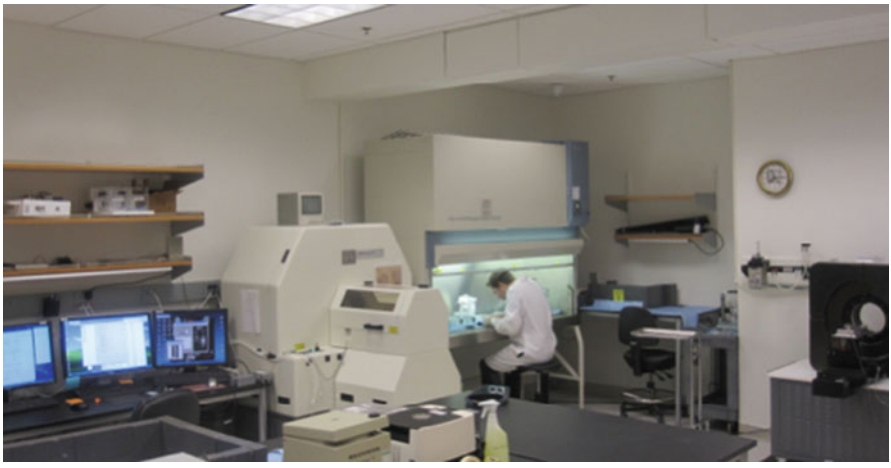

Fig. 2.1 Good ergonomic design puts everything in close proximity where needed and uses space for radiation safety where possible. The biosafety cabinet is located between the PET and CT systems, with the computers located to one side to avoid radiation exposure

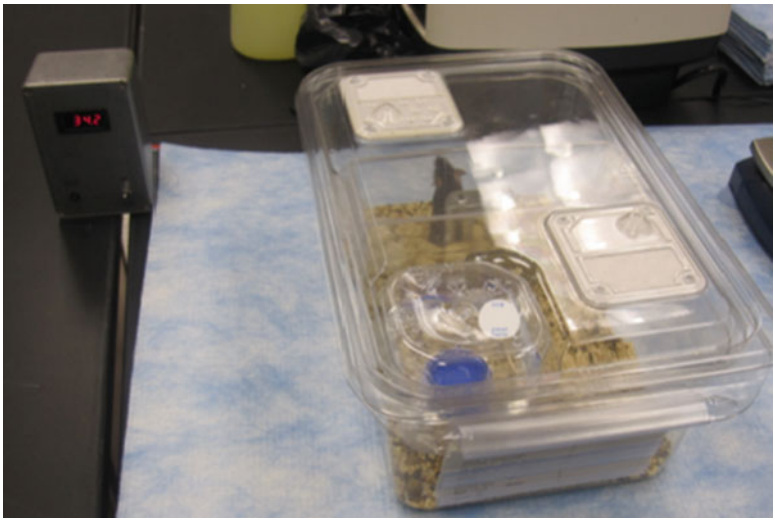

Fig. 2.2 Heating plates are located throughout the imaging center, positioned wherever animals are located. Preheating animals ensures minimal brown fat activity and a stable reproducible environment essential for reproducible metabolic data

infectious or select agents (see Chaps. 9 (Golding and Zeitseva) and 10 (Keith et al.) on imaging infections with optical probes and under regulated biosafety level (BSL-3/4) containment, resp). Quarantine may be due to disease or parasites or might be due to the use of neurotoxins or other biohazardous agents that may be excreted and pose a handling risk. The space requirements for this can pose a serious problem and might prevent experiments if no suitable locations are available. One option frequently used is the use of disposable microisolator cages (Fig. 2.2), where each animal is in an enclosed space without exposure to adjacent cages. This requires the use of individually ventilated cage racks (IVC) and cage changing using a biosafety cabinet and proper barrier techniques. One caveat is that IVC housing systems can create or exacerbate cold stress in animals, which may have deleterious or unexpected consequences upon translational research.

For imaging work, nearly all studies are done with animals under anesthesia. This is necessary to acquire sufficient data over a period of time to create a useful image where mobility affects positional information while it is being acquired by an imaging platform. Animals might be imaged dynamically from the time of injection or may be allowed a period of time for uptake and nonspecific agent clearance prior to a brief static imaging session. For dynamic work, typically 1 h is sufficient for mice and F-18 (positron isotope; ~2 h physical half-life)-labeled probes; however, this is highly dependent on the imaging agent, its biologic half-life in the species of interest, and its physical half-life. For experiments requiring longer times to observe specific biomarker signals, often animals will be injected with isotope having 12–72 h half-lives and the animals imaged multiple times over several days. For static imaging work, there may be relatively large numbers of animals being imaged

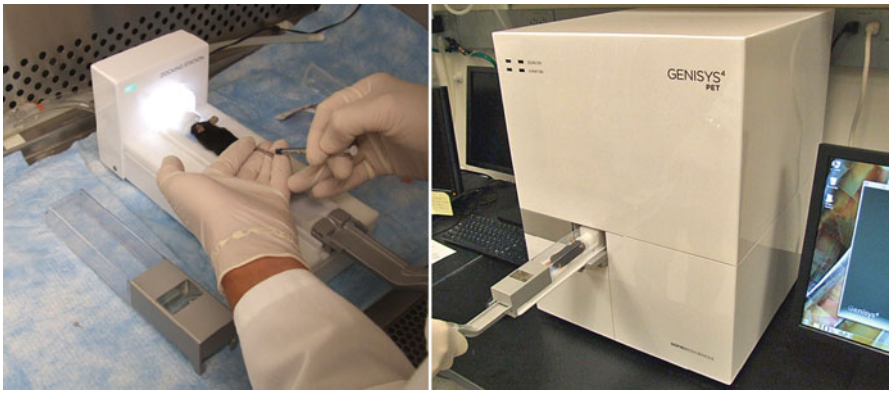

Fig. 2.3 This system has no lines to connect for the chamber, a simple plug and scan configuration. The system has both X-ray and photographic imaging components; thus, anatomical information is provided and CT imaging may not be necessary. The system has video monitoring of animal that provides a readout of the respiration rate, thus providing information to adjust anesthesia accordingly

together. These animals might be injected with short-lived isotopes such as F-18 and imaged multiple times over the course of several weeks using repeated injections.

Ideally the imaging systems will have proper physiological support systems for establishing and maintaining a reproducible metabolic state. To date, few systems provide these features, despite the importance of stable physiology for measuring changes in metabolism. Several equipment vendors have started offering heating and anesthesia options, along with imaging chambers; however, most are still unfortunately third-party additions to the system. Recently a new system has become available that integrates anesthesia, heating, chambers, and a prep station for comprehensive PET imaging for mice (Fig. 2.3).

To keep track of all the animals, data files, billing, and usage information, a database is essential (Fig. 2.4). The archival system, animal identification, and session information can be part of the database, making it simple and easy to track information for each experiment. Password protection and access strategies can be put into place to enable restricted and flexible access to both the database information and image data. The example shown in Fig. 2.4 is used to create session information, billing reports, usage reports for grants, oversight committees, and other needs, along with features for archival and retrieving of data.

To aid in accurate data analysis and animal safety, reproducibility of positioning is highly desired. This can be accomplished through the use of imaging chambers designed to deliver anesthesia, heating, and reproducible positioning (Suckow et al. 2009). Properly designed chambers can provide a pathogen-free environment necessary for working with immune-compromised rodents typically used for oncology research (Fig. 2.5). To facilitate high throughput of animals in a cost-effective manner, the anesthesia systems ideally should be simple and easy to use without requiring adjustable flow meters.

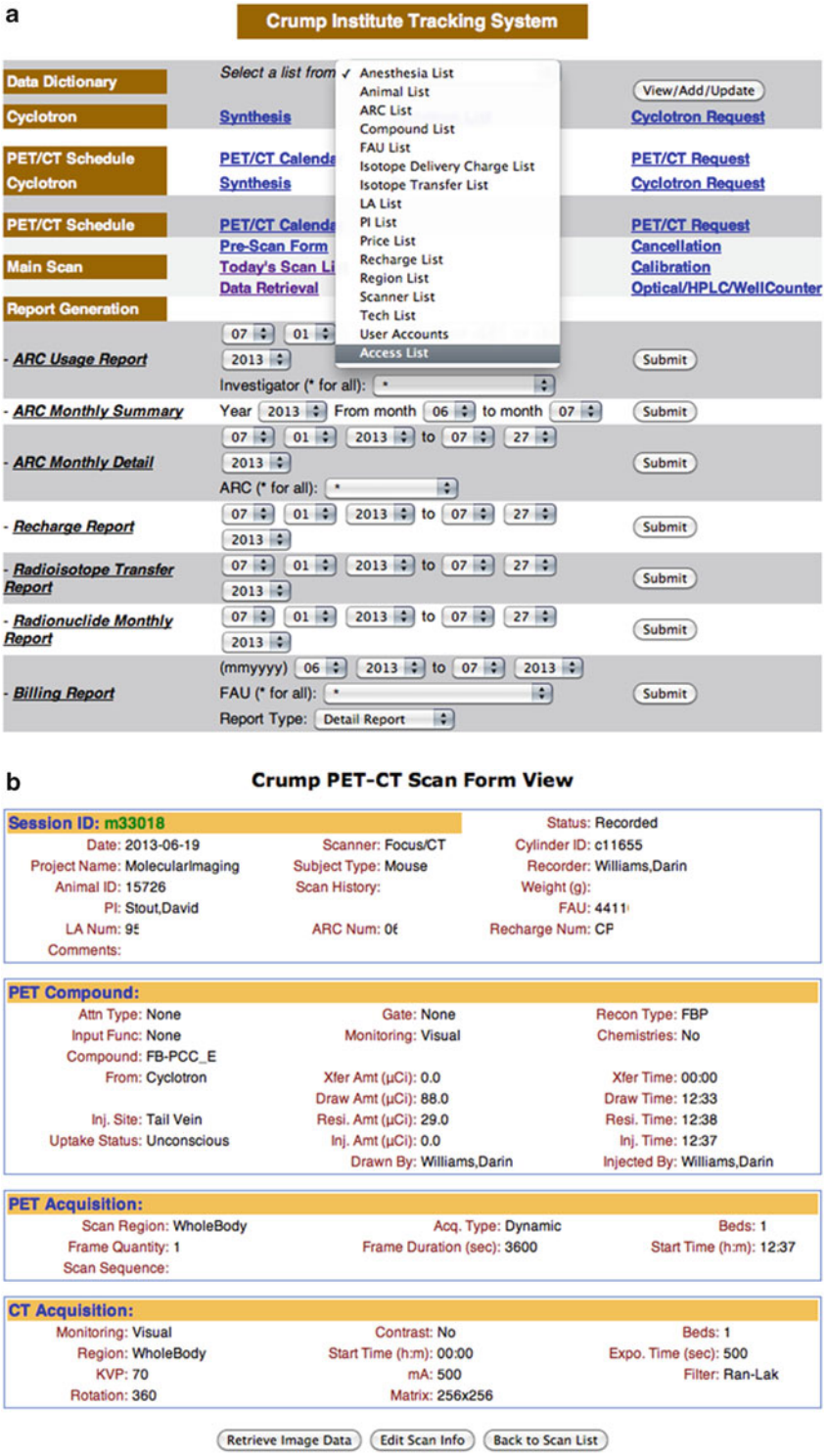

Fig. 2. 4 An easy to use image archiving strategy is essential. Database must include all relevant data related to the experiment, both for investigator's subsequent image analysis and for reports generated for various regulatory agencies and grant reviews

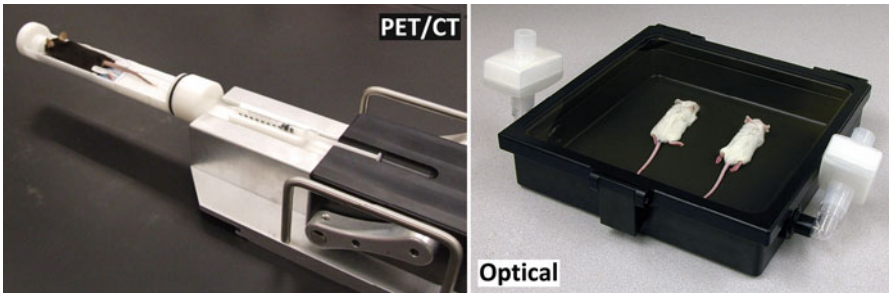

Fig. 2.5 The microPET-CT imaging chamber provides reproducible positioning, constant gas anesthesia, multimodality imaging capability (PET, CT, MR), barrier for immunocompromised mice and rats, and temperature control. The optical chamber provides gas anesthesia and barrier conditions

2.4 PET/CT

The logistics of imaging multiple animals in a short period of time requires good ergonomic design of the workspace (Stout et al. 2005). Our center primarily images immune-compromised animals; thus, we conduct all of our animal preparation work in biosafety cabinets. To avoid mistakes, use of two gas anesthesia boxes is recommended to separate injected from non-injected animals (Fig. 2.6). Heating should be provided for cages, induction boxes, work areas, chambers, and recovery areas to ensure mice are properly warmed to facilitate good blood flow and stable enzymatic activity. Without heating, animals will rapidly become hypothermic under anesthesia, and this will alter physiology and any metabolic measurements. This can result in poor blood flow to peripheral and subcutaneous tumors and will highly activate brown fat in the neck region (Baba et al. 2007) (Fig. 2.7). Mice thermoregulate body temperature via tail blood flow, so the ability to inject and deliver probes via tail vein injections depends on both tail and body temperature.

The injection of an imaging agent can be quite challenging. The small volume, typically 50–200 μl, small size of the mouse, and high energy of PET radiation mean that use of a shielded syringe is not feasible or practical. The better option to reduce the hand dose of the animal handler is to practice and become proficient in quickly injecting mice using an unshielded syringe. Most injections are made into the tail vein of animals. However, intraperitoneal or retro-orbital injections are sometimes possible depending on the experimental conditions.

One major complication with injecting in the tail is the unknown amount of radioactivity which extravagates and is left in the tail. Usually the injection location is not within the field of view of the imaging system, and the amount left behind is unknown, is highly variable, and can be quite significant. This complication can lead to highly inaccurate estimates of the total injected dose for subsequent

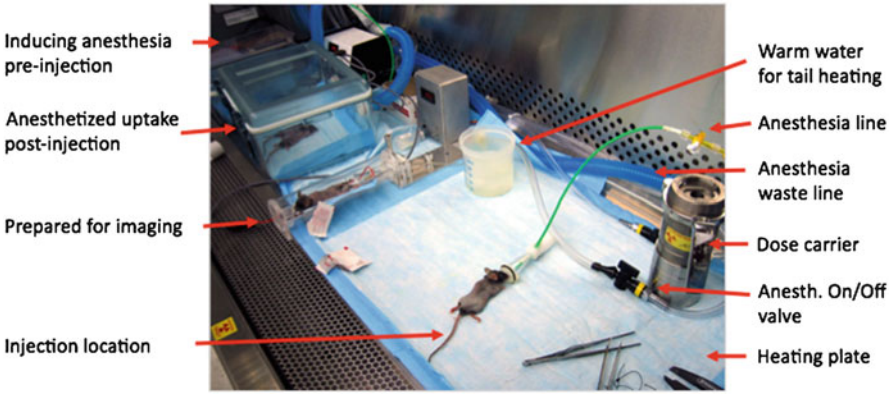

Fig. 2.6 Usually several mice are undergoing injection, uptake, and preparation for imaging at the same time. With the demands of anesthesia, injection, chamber assembly PET scanning, CT scanning, and recovery happening in each 12 min block of time, the process needs to be straightforward and everything within easy reach. Set-it and forget-it arrangements for heating and anesthesia are essential

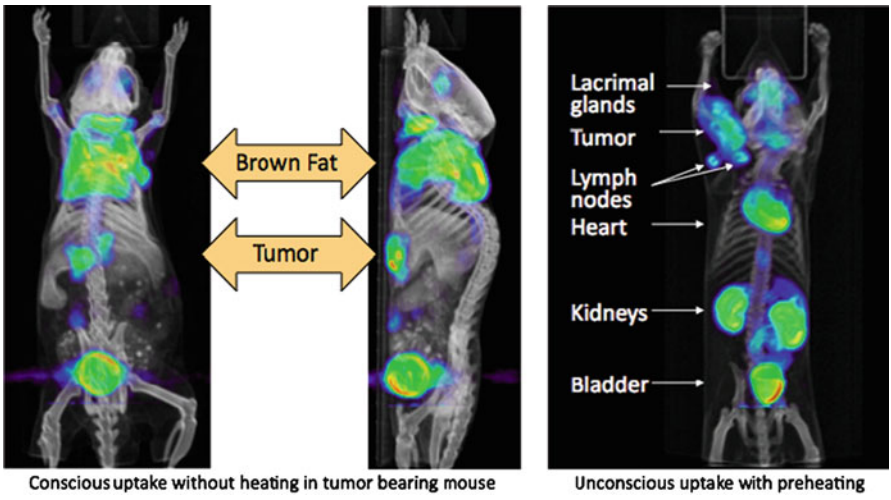

Fig. 2.7 Cold animals compensate by activating brown fat, a highly metabolically active tissue that can mask nearby FDG signals. Proper preheating can eliminate this signal

quantitative analysis. Practice and developing good injection expertise or the use of a catheter to inject can reduce the residual activity. If accurate injection activity is needed, it is best either to measure the tail activity or to quantify based only on what is present in the body, excluding the tail activity since it was not bioavailable for metabolic determinations.

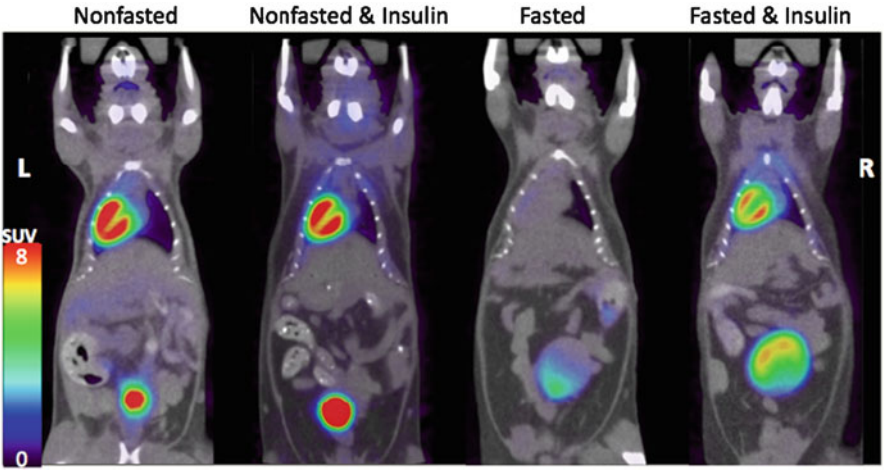

Fig. 2.8 Endogenous glucose competes with FDG for tissue uptake. In the heart, fatty acid versus glucose utilization plays a big role in myocardial tracer uptake

How animals are injected, treated, and handled can dramatically alter the uptake pattern of imaging probes. An example of this is the ability of heart myocardium muscle to switch from glucose to fatty acids as an energy source (Fig. 2.8). If mice are fasted, the heart uptake of FDG can be essentially switched off (Kreissl et al. 2011). This might be unwanted for cardiologists but could be ideal for looking at signals in the lungs. Another example for oncologists is the uptake of imaging probes in peripheral subcutaneous tumors. If animals are hypothermic, blood supply is constricted to preserve core body temperature, so probe uptake may be dramatically reduced due to temperature rather than intervention (Fueger et al. 2006). Often tumors are placed on the upper flank to avoid bladder signals. However, with FDG there can be extremely high brown fat uptake in the neck region that may interfere with tumor measurements (Fig. 2.7). Many imaging probes cross through cellular membranes by active transport, which is subject to competition by endogenous compounds, such as glucose or amino acids. Often probes are specifically retained by phosphorylation by enzymes, which are known to be linked to temperature and circadian rhythm (Jilge 2004). Rodents thermoregulate their body temperature based on blood flow in the tail, which may alter tail injection clearance and blood pressure and flow.

2.5 Biodistribution and Radiation Dosimetry

When developing a new imaging agent, the most common experiment is to look at where the radioactivity goes over time. These biodistribution studies can be relatively short, 1–2 h, or may require multiple imaging sessions over time, based on the pharmacokinetics of the labeled probe. Rodents can usually be imaged safely for

1–2 h; however, longer times are possible if subcutaneous saline is given to help keep the animals hydrated. Many small molecules will clear fairly rapidly in rodents within 1 h, either by renal kidney excretion or through hepatobiliary excretion via the gallbladder from liver through the gastrointestinal tract. Most F-18-labeled probes will rapidly accumulate in the bladder. It is important to understand the elimination process, in order to design the targeted uptake region to avoid these structures. For example, tumors are best placed in the upper flank or shoulder region, rather than anywhere near the bladder. Labeled peptides or antibodies typically require many hours or even days for specific targeting and clearance of nonspecific signal; thus, these experiments will require imaging over the course of several days (Kenanova et al. 2005).

Biodistribution data is typically expressed as the amount of injected dose in each organ over time. This requires knowing the amount that was injected, the amount in each organ over multiple time points, and the organ weight (i.e., percent injected dose, %ID, and %ID/gm over time). As mentioned before, knowing how much was injected is not as simple as measuring what was in the syringe, but rather how much activity was available to the body over time, disregarding anything remaining at the injection site. When dynamic imaging is started from the time of injection, a simple way to check on the injection quality is to look at the whole-body total activity over the course of the imaging session. Since the activity is decay corrected for the isotope half-life by the image reconstruction software, the total activity seen in the image over time should rapidly reach a peak and stay constant over time. If the activity rises, then there is leaching in of activity from outside the field of view (typically from the tail injection site), as the animal is not capable of generating radioactivity on its own.

With the knowledge of the amount of radioactivity in each organ over time, determining radiation dosimetry is fairly straightforward. By removing the isotope decay correction, the number of disintegrations over the course of imaging can be determined. Presuming that changes in biodistribution are fairly complete by the end of the imaging time, then one can safely assume that the remainder of the radioactivity will stay in the same location. By taking the last biodistribution time point and assuming no change in location, one can compute the number of disintegrations for the next five or so half-lives, which will account for over 95 % of any dose. Integrating the total dose over time, the dose per organ can be determined, and the dose per injected activity amount can be established. The term used for the number of disintegrations in any given organ is called the "residence time," which is a function of both the biological and physical half-lives of the labeled probe. Using Olinda, the only FDA-approved dosimetry software package, the amount of dose delivered to each organ can be determined (Stabin et al. 2005). From this data, the maximum safe injectable dose for humans can be determined and used to obtain approval for first use in human studies with new imaging probes.

Animals provide a reasonably accurate estimation of human radiation dosimetry (Seltzer et al. 2004). Although historically primates or larger animals have been used, it turns out mice provide reasonable and slightly conservative estimates. An advantage to mice is that since the entire animal can be observed at once, better temporal sampling is acquired for all organs at the same time.

2.6 Metabolic Profile and Toxicology

It is vital to keep in mind that nuclear medicine images, whether SPECT or PET, provide information only about the location of the isotope decay. Excluding positron range, the images show where the isotope was located, but not what atom it was attached to at the time. A decayed and recorded photon event in an imaging system could have come from either free isotope, a metabolite, or from the intact labeled imaging probe. Without knowing the metabolic profile of the imaging agent, there is no way to know what the image signal actually represents. For this reason, it is imperative that the metabolic fate of the injected probe be carefully studied in vivo before any claims are made about the performance of the imaging agent.

Characterization of a labeled probe is typically accomplished by taking blood samples over time and examination using high-pressure (or performance) liquid chromatography (HPLC). Imaging probes can remain unchanged in vivo or may be phosphorylated or metabolized into a different molecule. Retention times of known standards measured via UV absorption versus the retention times of the radioactive peaks indicate the metabolic fate in vivo. Understanding what the images are showing is essential to understanding the experimental results.

When the time comes to move an imaging probe into human application, it is necessary to ensure that there are no toxicological effects of the imaging probe resulting from normal metabolism. Toxicology testing is accomplished by injecting generally 100× the normal expected mass amount of the imaging agent into animals and observing the physiology for any changes. It is not necessary to inject radiolabeled probe, so this work can be done using the unlabeled substance itself. Given that most PET imaging agents are used in picomolar or nanomolar concentrations, toxicology testing is often accomplished using only 1–2 μg of the compound. This tiny amount of material is difficult if not impossible to detect by any means other than having it labeled with radioactivity. To date, no probe examined by or known by the author has elicited any physiologically recorded response or safety issues following injection at the concentrations expected for routine imaging use.

Since toxicology testing can be very rigorous and expensive, it is worth making the distinction between testing required for FDA approval of a new agent and what is required for preliminary first use in human (FIH) studies. For initial evaluation, testing in rats is ideal as the species is sufficiently large to acquire blood samples prior to injection, immediately after injection and at 2 h postinjection. These blood samples are examined for any changes, and it is important to separate changes normally found with anesthesia from those that might possibly occur due to the injected agent. The rats are examined frequently over several hours to look for any physiological changes in temperature and heart and respiratory rates. This preliminary data is sufficient to show lack of any effect and to obtain initial approval for first use in humans for compounds already approved by the FDA.

When the time comes to seek FDA approval under the investigational new drug application (IND) for more routine use in humans or for a new molecule not previously approved, more stringent toxicology testing conducted under regulatory mandated good laboratory practices (GLP) is required. The guidelines for these

procedures are available through the FDA website (http://www.fda.gov/Drugs/DevelopmentApprovalProcess/HowDrugsareDevelopedandApproved/ApprovalApplications/InvestigationalNewDrugINDApplication/default.htm). These requirements are similar to the cGMP requirements for producing radiolabeled human use probes and describe the need for careful monitoring and validation of each step in the process. An independent auditor must review the data to make sure everything is conducted according to plan and that any deviations are properly documented. Toxicology testing at this level is often quite expensive and until recently has required evaluation in two separate species. As will be explained below (and Chap. 13 of this volume), another option is to develop in-house services as opposed to the more expensive contract research companies.

2.7 Radiochemistry

It is worth noting the distinction between the conditions now required by the FDA for imaging probe production for human use versus nonhuman use. Since December 2011, all production of labeled imaging agents used in humans must follow cGMP requirements laid out by the FDA (Norenberg et al. 2011). Production of preclinical research probes generally falls under the US Pharmacopeia regulations, though this is not clearly defined for preclinical work intended for eventual human use authorization. Given the high cost differential between various production options, it is important to know ahead of time what conditions are required for regulatory approvals.

2.8 From Idea to IND: The Story of FAC

At the author's institution, a decision was made to develop a new PET imaging probe targeting immune system cancers for diagnostic purposes. One of the strengths of an academic institution is the availability of a diversity of expertise from multiple fields. A group of people was assembled and given a deadline of several months to identify candidates for looking at upregulated receptors in the activated immune system. We wanted to specifically look at only what was activated in a disease state, not in normal metabolic function. Using various tests, including microarray gene mapping, literature knowledge, and various in vitro tests, we arrived at a candidate molecule, called 2′-deoxy-2′-[18F]-D-arabinofuranosylcytosine (D-FAC). This gemcitabine analog is a specific substrate for deoxycytidine kinase (dCK) receptors, which are upregulated in activated lymphoid organs (Radu et al. 2008; Laing et al. 2009). The imposition of a deadline was useful incentive to move quickly, as was the presence of a leader (Dr. Michael Phelps) who kept everyone focused on meeting the goal in a time-efficient manner.

With the knowledge that there were several stereoisomers of the FAC molecule, we examined each of them with in vitro cell and in vivo preclinical studies to decide

the best candidates for subsequent human work. We examined three of the isomers in depth, including metabolic profiling and in vivo biodistribution and toxicology testing. We were able to synthesize the probes, investigate in mouse models and begin investigations in humans within 9 months, a staggering feat compared to historical trends of 10 years or more. For the second isomer, we did this in only 6 months. With further investigations using human subjects, we moved on to filing with the Food and Drug Administration (FDA) via the investigational new drug (IND) process, obtaining approval 30 days after submission. The third isomer was also submitted, in case it turns out that this isomer works better in humans compared to rodent results.

To accomplish this effort in such a short time, the right people, skills, and equipment were needed. Our group has a long history of developing new PET imaging agents, along with careful characterization of the biological fate in vivo and going through the approval process. For preclinical work, we had already put into place expedited approval processes, imaging equipment and procedures, and developed biodistribution and dosimetry services. We moved quickly by knowing how to make the regulatory system work in an expedited manner and from having the tools and techniques honed that would enable us to quickly acquire, analyze, and move forward with additional experiments.

One reason it has been fairly straightforward to obtain FDA approval is that PET probes are not a drug intended to treat any disease but rather an imaging agent used at only one dosage. For this reason, and since PET agents are used in vanishingly small concentrations (often nano- or picomolar), we sought approval using only one species (rat) and one dosage for toxicology. Simplifying the submission and providing only the relevant required testing results meant that the approval process was faster and much more economical. Estimates are that we obtained approval at less than 10 % of the usual costs for new IND filings for therapeutic indications.

The key to successful imaging probe development is an effective and efficient preclinical imaging infrastructure together with good radiochemistry and clinical support. These three often separate groups must work together to make and evaluate imaging probes and then move them through the regulatory process. We added our campus veterinary group to this triad, which helped establish good laboratory practices (GLP) for the toxicology testing program that would have been too difficult and expensive to pursue without their help. With the establishment of GLP toxicology testing, together with the approvals for animal work established through the preclinical imaging center, we now offer this service campus-wide and on a contract basis to outside parties.

Several services were added to the preclinical imaging center, namely, autoradiography, biodistribution, radiation dosimetry, and toxicology testing. These were added because the complexity, expertise required, and coordinated nature of conducting the studies would have been extremely difficult for any one faculty member to manage. Often these services are used intensely, but infrequently, so the knowledge and skills can be lost as students or postdocs rotate through labs or staffing changes occur.

Autoradiography support was added by purchasing a microtome for tissue sectioning and a whole-body slicing system. The whole-body cryotome was very useful in observing where the labeled probe went at various times with resolution down to the cellular level (Stout and Pastuskovas 2011). This was particularly important for FAC, as the gut uptake observed in the PET images was localized to the intestinal villi due to blood transport and receptor binding rather than transit of hepatobiliary excretion from the gallbladder into the GI tract. Although not used frequently, autoradiography was a crucial step to take in the process of identifying exactly what was being observed in the PET images. Autoradiography can provide detailed radioactivity distributions, down to about 25 μm, which is far greater resolution than nuclear medicine-based approaches (see Chap. 6 for more details on autoradiography applications). The reader is encouraged to read Chap. 6 (Solon and Moyer) for a full treatise on autoradiography.

Biodistribution kinetic information is readily obtained from dynamic PET or SPECT imaging by experienced personnel. The process of creating the optimal set of images to capture the changing distribution patterns takes time and skill, both with image reconstruction and image analysis. From this information, estimates of translating the animal biodistribution kinetic data to human radiation dosimetry can be measured. Olinda, the successor to MIRDOSE, is the only FDA-approved dosimetry program, which is used to determine the maximum safe allowable radiolabeled imaging agent dose for use with humans (Stabin et al. 2005). Fortunately mice usually provide a conservative estimate of a safe injectable radiation dose, since the limiting organ for many imaging agents is typically the bladder wall where renal elimination and persistence of a high concentration of radiolabel is most often evident. Mice often metabolize and eliminate into urine the radiolabel from imaging agents much faster than humans, so the maximum safe injection values we determine are often lower than what is later determined from human studies.

For toxicology, we took a two-step approach: simple tests for previously FDA-approved molecules via the Radioactive Drug Research Committee[1] (RDRC) approval and GLP level testing for IND filing with the FDA. To validate that there were no measurable changes in heart rate, respiration, temperature, or blood chemistry, we inject 100× the expected dose into five rats and monitored them for 1 h, followed by necropsy reports at 2 weeks. The amount of injected agent was 1.2–1.6 μg. At this low a concentration, it is not surprising that we saw no changes in physiological parameters. We did see some drift in the blood chemistry measurements over time, which we confirmed using saline injections in control animals to be related to anesthesia rather than any effect from the injected agent. These preliminary toxicology tests, together with biodistribution and dosimetry measurements in mice, were sufficient to satisfy RDRC requirements for first use in humans, for up to 30 patients.

An interesting and important note is that the probe that we found worked best in mice was not the one that works best in humans, at least not so far in our limited investigations.

[1] http://www.fda.gov/Drugs/ScienceResearch/ResearchAreas/Oncology/ucm196481.htm.

This is one reason that it is important to pursue multiple imaging isomers and to begin work in humans as rapidly as possible. Considerable time, money, and resources can be spent in preclinical models which might not replicate well in humans. By moving drug development rapidly into human use, we can better know where to devote our time and effort for other clinical and preclinical research. A similar finding was noted by the group at UC Davis (Gagnon et al. 2009), where the predictions based on in vitro testing did not lead to the best candidate in vivo. Since they evaluated a range of different compounds, they were able to identify ones that were most suitable to move forward into human testing.

Once the ideal candidate was determined, the next step was to assemble the tests required for IND filing. The major requirement was GLP level toxicology testing. Where we could have pursued one agent together with one control group, we chose instead to evaluate three agents at once. This saved having to test two additional control groups, thus by pursuing all three agents at the same time; we spent 33 % less for the testing of four groups instead of six. Conducting the testing in-house, even with invasive surgeries to directly measure blood pressure, we spent ~$160K for four groups, both sexes, one species. We were prepared with animal use approvals to investigate a second species, but ultimately we were not required to do so.

To accomplish these tasks, instead of obtaining regulatory approvals for a specific investigator, we decided instead to create an animal use protocol for the imaging center which included all the necessary testing steps. Investigators can readily pursue their own research under their own approvals, but now they can also ask for these tests to be done and do not need to devote their lab's personnel, time, and resources to carrying out these tasks. These tests are often infrequent, so having central staff trained and able to consistently carry out the tasks save having to train new students, staff, or postdocs in various labs who may turn over between tests. All the necessary steps can be put into one protocol and maintained ready for any group to use as needed.

In addition to the preclinical work to evaluate the dosimetry and toxicology, the IND filing required a description of the mechanism of action (MOA), metabolic fate, and a detailed description of the synthesis conditions (IND CMC requirement). For use in humans, a plan of action such as a clinical protocol and expected outcomes of that trial are required, along with any previous information about use in humans (i.e., outside of FDA jurisdiction).

The regulatory environment is a considerable hurdle and can at times become a substantial roadblock to research. Working together with these oversight agencies, a fast-track system can be established for adding new imaging agents to approved protocols. When one considers that everything done in an imaging experiment is essentially identical to previous imaging work, other than what is within the injection syringe, adding a new agent that is usually in the nanomolar range should be a simple authorization that does not require a full committee review of each agent. For a more detailed view of the regulatory landscape for imaging in general, please see Chap. 13 on Regulatory Issue with Imaging.

2.9 Summary

Successful and accurate preclinical data acquisition in support of regulatory authorization for a novel imaging agent requires a well-designed and well-integrated imaging center that supports all the logistical elements of the process. Attention to detail is critical, as a seemingly minor problem may invalidate the entire filing process, requiring additional work. Good design for flow of people; animals; radiation usage, including human subject dosimetry estimation; and data management can help to ensure that standardized procedures are followed, appropriate data are collected, and optimal physiological conditions for metabolic imaging are followed.

Once data has been acquired, processing of images into useful metabolic information requires in-depth knowledge of the imaging systems and image reconstruction and a clear understanding of the physiology of the selected animal models. For FDA filings to use a new imaging probe in humans, a careful understanding of the regulatory requirements and documentation of the entire experimental process is essential. The scope of knowledge required will almost certainly require a team effort of people with a variety of skills, including physics, biology, radiochemistry, statistics, dosimetry, and regulatory compliance. While managing to meet all these requirements is daunting, once the process has been created and documented, subsequent work can become fairly routine.

References

Baba S, Engles J, Huso D, Ishimori T, Wahl R (2007) Comparison of uptake of multiple clinical radiotracers into brown adipose tissue under cold-stimulated and nonstimulated conditions. J Nucl Med 48:1715–23

Conour L, Murray K, Brown M (2006) Preparation of animals for research - issues to consider for rodents and rabbits. ILAR J 47:283–93

Fueger BJ, Czernin J, Hildebrandt I, Tran C, Halpern BS, Stout DB, Phelps ME, Weber WA (2006) Impact of animal handling on the results of FDG-PET studies in mice. J Nucl Med 47(6): 999–1006, PMID 16741310

Gagnon K, Hausner S, Marik J, Abbey JC, Marshall J, Sutcliffe J (2009) High-throughput in vivo screening of targeted molecular imaging agents. Proc Natl Acad Sci USA 106:17904–909

Jennifer Obernier J, Baldwin R (2006) Establishing an appropriate period of acclimatization following transportation of laboratory animals. ILAR J 47:364–9

Jilge B, Kunz E (2004) The laboratory mouse. Elsevier Academic https://store.elsevier.com/product.jsp?isbn=9780080542539&pagename=search

Kenanova V, Olafsen T, Crow D, Sundaresan G, Subbarayan M, Carter N, Ikle D, Yazaki PJ, Chatziioannou A, Gambhir S, Williams L, Shively J, Colcher D, Raubitschek A, Wu A (2005) Tailoring the pharmacokinetics and positron emission tomography imaging properties of anti–carcinoembryonic antigen single-chain Fv-Fc antibody fragments. Cancer Res 65:622–45

Kreissl M, Stout DB, Wong K-P, Wu H-M, Caglayan E, Ladno W, Zhang X, Prior J, Reiners C, Huang S-C, Schelbert HR (2011) Influence of dietary state and insulin on myocardial, skeletal muscle and brain [18F]-fluorodeoxyglucose kinetics in mice. EJNMMI Res 1:8

Laing RE, Walter MA, Campbell DO, Herschman HR, Satyamurthy N, Phelps ME, Czernin J, Witte ON, Radu CG (2009) Noninvasive prediction of tumor responses to gemcitabine using positron emission tomography. Proc Natl Acad Sci USA 106(8):2847–2852

Lee K-H, Ko B-H, Paik J-Y, Jung K-H, Yong Y-C, Kim B-T (2005) Effects of anesthetic agents and fasting duration on 18FDG biodistribution and insulin levels in tumor-bearing mice. J Nucl Med 46:1531–36

Leenders KL, Aquilonius S-M, Bergström K, Bjurling P, Crossman AR, Eckernas S-A, Gee AG, Hartvig P, Lundqvist H, Långström B, Rimland A, Tedroff J (1988) Unilateral MPTP lesion in a rhesus monkey: effects on the striatal dopaminergic system measured in vivo with PET using various novel tracers. Brain Res 445:61–67

Norenberg J, Schwarz S, VanBrocklin H (2011) FDA cGMP requirements for PET drugs. J Nucl Med 52:16N

Phelps M (2000) PET: the merging of biology and imaging into molecular imaging. J Nucl Med 41:661–681

Radu CG, Shu CJ, Nair-Gill E, Shelly SM, Barrio JR, Satyamurthy N, Phelps ME, Witte ON (2008) Molecular imaging of lymphoid organs and immune activation by positron emission tomography with a new [18F]-labeled 2′-deoxycytidine analog. Nat Med 14:783–788

Seltzer MA, Jahan SA, Sparks R, Stout DB, Satymurthy N, Dahlbom M, Phelps ME, Barrio JR (2004) Radiation dose estimates in humans for (11)C-acetate whole-body PET. J Nucl Med 45(7):1233–1236, PMID 15235071

Stabin M, Sparks R, Crowe E (2005) OLINDA/EXM: the second-generation personal computer software for internal dose assessment in nuclear medicine. J Nucl Med 46:1023–7

Stout DB, Pastuskovas C (2011) In vitro methods for in vivo quantitation of PET and SPECT imaging probes: autoradiography and gamma counting. In: Kiessling F, Pichler B (eds) Small animal imaging. Springer, Berlin/Heidelberg, pp 347–60

Stout DB, Zaidi H (2009) Preclinical multimodality imaging in vivo. PET Clin 3:251–273

Stout DB, Chatziioannou A, Lawson T, Silverman R, Phelps ME (2005) Small animal imaging center design: The Crump Institute at UCLA. Mol Imaging Biol 7(6):1–10, PMID 16261425

Suckow CE, Kuntner C, Chow PL, Silverman RW, Chatziioannou AF, Stout DB (2009) Multimodality rodent imaging chambers for use under barrier conditions with gas anesthesia. Mol Imaging Biol 11(2):100–106

Toyama H, Ichise M, Liow J-S, Vines D, Seneca N, Modell K, Seidel J, Green M, Innis R (2004) Evaluation of anesthesia effects on 18FDG uptake in mouse brain and heart using small animal PET. Nucl Med Biol 31:251–56

Chapter 3
Considerations for Preclinical Laboratory Animal Imaging Center Design, Setup, and Management Suitable for Biomedical Investigation for Drug Discovery

Brenda A. Klaunberg and H. Douglas Morris

Abstract In vivo imaging techniques are rapidly becoming routine procedures for biomedical research and drug/biologics development. Imaging is an outstanding tool for noninvasively testing the response to therapy by examining animals as whole organisms. Many kinds of imaging platforms are now commercially available, and many are optimized for smaller species. Before beginning construction for a centralized in vivo imaging facility, one must first define the requirements and limitations of the facility. The planning should involve laboratory animal veterinarians, investigators, imaging specialists, occupational health specialists, and administrators. Considerations include the animal models of interest, the scientific questions to be addressed, inclusion of radiochemistry (PET/SPECT), select agent use (BSL requirements), logistics and laboratory flow, and personnel safety within the imaging environment. Architects must incorporate functional design into the technical requirements and building aesthetics. The limitless variables prevent the production of a step-by-step imaging center design manual; however, we suggest a foundation of advice learned from our experiences with the National Institutes of Health Mouse Imaging Facility. Magnetic resonance imaging is an infrastructure-dependent platform and is a recommended base to start facility design. The importance of preplanning and clear communications for success cannot be overemphasized.

B.A. Klaunberg, M.S., V.M.D. (✉) • H.D. Morris, Ph.D.
NIH Mouse Imaging Facility, National Institute of Neurological Disorders and Stroke, National Institutes of Health, 10 Center Drive, B1D-69, Bethesda, MD 20892, USA
e-mail: klaunbeb@mail.nih.gov

B.R. Moyer et al. (eds.), *Pharmaco-Imaging in Drug and Biologics Development*,
AAPS Advances in the Pharmaceutical Sciences Series 8, DOI 10.1007/978-1-4614-8247-5_3,

Abbreviations

BAS	Building automation system
CT	Computed tomography
ECG	Electrocardiogram
EEG	Electroencephalogram
FDG	2-[^{18}F]fluoro-2-deoxy-D-glucose
HVAC	Heating, ventilating, and air conditioning
LAN	Local area network
MHz	Megahertz
MPW	Medical pathological waste
MRI	Magnetic resonance imaging
NHP	Nonhuman primate
PET	Positron emission tomography
PPE	Personnel protective clothing and equipment
RF	Radio frequency

3.1 Introduction

Biomedical research requires periodic glimpses of the inner workings of an organism. This may be accomplished by a variety of means to determine the effects of disease or treatment. Animal research plays a key role in the advancement of medicine and drug discovery. In the past, as researchers developed animal models of human diseases, dissection at important timepoints enhanced our understanding of those diseases and their treatments. Old experimental designs included cohorts of animals large enough to sacrifice subsets of subjects along the course of the timeline to observe effects. Each individual animal was considered part of the whole, and another set of animals served as untreated or sham controls. A modern approach to the same experiment now includes in vivo imaging. Imaging allows the researcher to observe biological processes in the animal in a noninvasive fashion and document those changes over time in an individual. The ability to use an animal as its own control and observe the effects of disease or treatment noninvasively results in the use of fewer animals. Imaging provides excellent anatomical, physiological and/or functional details in individuals because it more closely resembles the use of human models (who are not sacrificed during experimental timepoints). Additionally, the use of fewer animals results in a significant reduction in the cost of research, probably totaling in the millions of dollars overall.

Preclinical in vivo imaging modalities span a wide range of options from low-resolution anatomical scanners up to devices capable of measuring specific molecular functions on a cellular level. In the context of drug discovery, it may be prudent to include as many options as possible. This would allow for investigation of

unanticipated effects, both beneficial and detrimental. In fact, it may lead to new discoveries as occasionally occurs with drug development.

The Food and Drug Administration (FDA) requirements for new drug approval include safety and efficacy testing in two animal species prior to being used in clinical trials. An ideal design for a drug development imaging center would allow for imaging of multiple species of animal models. Unfortunately, imaging devices optimized for larger species may not generate acceptable data for smaller species, thus commanding the need for double the amount of equipment. But if money and space were unlimited, this would be the ideal situation. As budgets tend to be restricted, one should carefully consider what equipment could serve multiple species most efficiently. The services of an experienced imaging consultant may be money well spent.

The experimental animal varieties and types of imaging equipment will define the remainder of the imaging center's design. These are the two most important decisions and must be made first and before any other considerations. Thoughts for future expansion will allow for flexibility once researchers are familiar with imaging methods and its utility. Preclinical imaging technologies are continually advancing, and an ideal imaging facility will include sufficient design flexibility (and space) to expand and incorporate new techniques such as imaging of transgenic animals (Budinger et al. 1999). Species-specific housing designs may be found in any laboratory animal facility design and planning guide. We attempt to point out the species-specific issues worth consideration when designing an imaging facility.

Providing a step-by-step guide for designing an animal imaging center is nearly impossible; however, based upon our experiences with the National Institutes of Health Mouse Imaging Facility, we will offer advice for an ideal laboratory animal imaging center. This paper will be divided into five major sections: (1) facility design (including general considerations, animal support, MRI-specific considerations, and miscellaneous topics), (2) animal imaging support, (3) personnel, (4) imaging equipment, and (5) data management. MRI is heavily infrastructure dependent. MR imagers require particular structural specifications in the building and trained personnel to operate and maintain the equipment, and the MRI environment brings unique occupational safety hazards. Because of its restricting conditions, we use MRI as the limiting factor for the rest of the facility design. It is often easier to incorporate other imaging devices as the facility expands without the need for major construction, as is usually the case with MRI. We lend advice specific to various aspects of design as appropriate. Generic discussion of other topics leaves the facility planners to accommodate the unique and specific needs of the facility; however, we suggest that an ideal imaging facility for drug development includes research and technical support for imaging optimization, contrast enhancement and intellectual collaboration, technical expertise for animal procedures, and an informatics division. A successful facility design is the result of attentive forethought toward facility short- and long-term goals and future plans and collaborations with specialists in the various aspects of the center components.

3.2 Facility Design

Countless factors influence the function and design of an in vivo animal imaging facility. This paper will explore what we consider the four major topics in facility design. The first discusses general facility needs for employees involved in animal research. Much of this discussion applies to any types of workspace, office space, storage space, restrooms, break rooms, and conference rooms, building environmental parameters, and the pathways which animals and humans take to get to various locations. Animal imaging support, including procedure rooms, housing, and euthanasia, is discussed in the second section. The third major topic focuses on the design specifics associated with MRI. These include structural requirements, tools and magnet location, as well as MRI magnet room environmental concerns and cryogen gas usage and storage. Lastly we explore assorted ancillary equipment that is useful in the imaging and animal research areas (biological safety cabinets, chemical fume hoods, autoclaves) and various other safety issues (radiation, biological).

3.2.1 General Facility Considerations

When planning a preclinical imaging center, always remember the prime directive: to image numerous animals with high-quality data as easily and efficiently as possible. This includes minimizing stress to the experimental animals as well as the employees. Key decisions will determine several building design factors: the types of imaging animals and their proximity to the imaging facility; the traffic patterns relative to animal entry, room layouts, and loading docks; and the use of modules or blocks constituting repetitive design. Incorrect assumptions, inaccurate information transfer, and lack of communication may result in planning errors (Ruys 1990). Communication mistakes and erroneous professional judgment, including failure to ensure that all assumptions upon which decisions are made are correct assumptions, are more difficult to guard against and could prove catastrophic in accomplishing a successful design. Soliciting the opinions of knowledgeable and experienced consultants may prevent the need for costly corrections of design errors. Do not assume that the architect is familiar with all the functions of a research animal facility. Be sure to communicate functional design priorities with a clear explanation of the reasoning behind the design to ensure the architect's understanding. Aesthetics have no value if the building design does not support an efficient workflow, and project success depends on the architect's comprehension of the functional design criteria. Keep all communications clear and concise. Summarize all discussions in writing for all parties, emphasizing the functional goals and reiterating the rationale for the design layout (purpose, workflow) at the risk of redundancy.

The imaging center planning committee should include a variety of people with several areas of expertise. Laboratory animal veterinarians experienced with each of the desired imaging species and managing the required support staff will be knowledgeable in logistics of animal transportation, preparation areas, emergency support, and meeting the requirements of AAALAC accreditation (if desired). Specialists with expertise in citing the various desired imaging modalities can point out the specific building design requirements needed for the equipment and support areas. The input of an occupational health specialist will prove invaluable for a healthy work environment as well as a design to accommodate imaging pathogens with higher designations. Imaging scientists will offer insight into some of the ancillary support equipment that may enhance the imaging environment. Examples of supplementary equipment and space may include planning for an area to perform surgical procedures prior to imaging, perfusion fixation for post-imaging histology, a room for euthanasia and tissue harvest, and a clinical laboratory area for time-sensitive assays that may need to be run immediately prior to, during, or after imaging (blood gasses, ammonia levels, clotting factors, blood levels of drugs or metabolites). Inclusion of an administrator, human resource person, or someone otherwise nonaffiliated with imaging may offer a unique and valuable perspective for personnel requirements and visitors to the center. It is easy to get tunnel vision regarding the desired imaging goals and overlook "normal" requirements for the employees such as break rooms.

Traffic Patterns. When planning corridors and access points, consider all people, animals, and equipment (corridor width) that will need to get from one place to another. Ideally the animal housing facility is incorporated within the imaging center or conveniently adjacent. Animal transportation can cause physiological stress (and therefore confound physiological imaging data) so it is best to keep travel time, distances, and environmental factors to a minimum. Plan for easy, direct routes from building entrances to preparation areas and imaging suites. Additionally, locate imaging areas such that people and animals do not pass through other imaging areas to arrive at the designated location. A perfect scenario would include an animal prep and recovery area adjoining each distinct imaging area. These imaging areas would have solid walls and doors to provide physical barriers to prevent any cross contamination when multiple imaging devices are being used simultaneously. Additionally, attention to study flow improves efficiency when there is adequate working space such that one animal can be prepped while one is being imaged and another is recovering.

Remember to place the personnel offices (with a dedicated human entrance) outside of the animal imaging areas. Working with laboratory animal species generally requires the use of personal protective equipment (PPE) to protect both the animals and employees from any cross contamination or allergens. It is not practical to have areas where PPE is required and areas where PPE is not required (offices) within the same sections of a building. Areas designated for animal work and people have different environmental requirements with regard to temperature, humidity, air exchange, and relative air pressure. Keep the animal imaging and procedural areas

physically separated from the human areas to maintain the most effective and convenient animal biosecurity and occupational health standards.

Designated corridors for animal transportation to and from imaging and procedure areas and restricted corridors for human traffic only are ideal. This separation will help to minimize the potential of one species posing an infectious disease threat to another species. Old world nonhuman primates (NHP) may carry endemic herpes viruses that can be deadly to new world NHP and humans (Coulibaly et al. 2004, Gay and Holden 1933; Loomis et al. 1981; Weigler 1992; Wilson et al. 1990). Additionally, humans are a significant risk to both old and new world NHP with regard to measles and tuberculosis. The risk of infectious pathogen exchange may be somewhat reduced between human and rodent species, but risk still exists. Additionally, it has been demonstrated that laboratory workers may develop allergies or asthma to rodents (Aoyama et al. 1992; Bardana 1992; Chan-Yeung and Malo 1994; Hollander et al. 1997) so it is best to prevent unnecessary occupational exposure to allergens.

Cross contamination of murine pathogens can be prevented through good practices and management strategies. A preclinical imaging center may serve rodents of varying health status. While a strict barrier facility tolerates no murine pathogens, it may be impractical to try to maintain barrier status for imaging animals unless the imaging equipment is located within the barrier. Conventional housing facilities offer some leniency with regard to pathogen tolerance and may facilitate movement of animals to and from imaging more easily. Animals of various levels of immunocompetency may be needed for cancer studies and other immunomodulatory drug research, as well as animals purposely infected with pathogenic organisms that require containment. Consider all these factors when planning corridors within the facility. An example of an imaging facility design is offered in Fig. 3.1.

Supply Storage Rooms. Storage space is often in short supply and comes at a premium price. When planning a new imaging facility, be sure to consider all aspects of the facility operations to ensure adequate storage space allocation. It may be beneficial to define these areas as “support space” instead of “storage space” to make certain its value is not depreciated. Each imaging suite should have designated areas for frequently used consumable items such as personal protective equipment (PPE), gloves, disposable drapes, syringes, and needles. The amount of space within each room may vary by imaging equipment type, as some devices require minimal supplies. Contrast agents, emergency support drugs, anesthetics, sterile eye lubricants, and other pharmaceuticals would also be ideally located within the imaging suite. Spare boxes of paper hand towels, gauze sponges, and tape could be stored in each room. These types of consumables could easily be stored under laboratory bench tops or within portable storage cabinets. Lockable storage is always desirable and may be required. Dedicated storage rooms are needed for larger quantities of consumables and general supplies since they can require quite a bit of space. It is likely not practical to order small weekly quantities

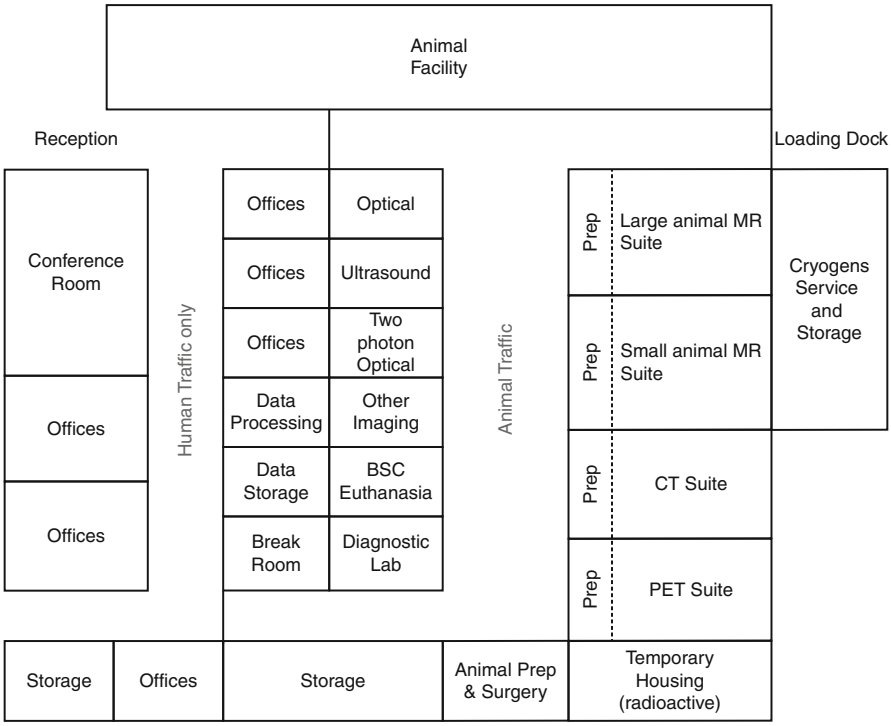

Fig. 3.1 An example layout for an in vivo imaging center, including suites for multiple imaging methods and support spaces. Note that the center separates human spaces from animal spaces and the access pathways between these areas. This is critical to maintain hygiene and pathogen transmission controls. Imaging suites should be dedicated to a single modality to reduce problems with dual scheduling. Small prep areas should be dedicated spaces in each suite to prep an animal for imaging studies independent of any particular preparation in the biomedical study

of provisions. Garbage bags, medical pathological waste (MPW) containers, empty sharps containers, clean mop heads, etc., will all need a larger storage area and may also require safety shielding for radiopharmaceutical waste, animal carcasses, and tissue that are being held for counting/processing. Remember to allow storage space for administrative supplies such as CDs and DVDs, printer paper, toner cartridges, pens, notepaper, and files.

Hazardous chemical storage (including cleaning solutions) will require special consideration such as fire and explosion proof cabinetry. OSHA and your Department of Occupational Health and Safety will determine the requirements. It may be useful to over-anticipate current needs to allow for greater flexibility for future experiments.

Each specific imager will have its own unique storage needs. Most MRI magnets are superconducting and thus necessitate allocated space to store large cylinders of

cryogens such as liquid helium and liquid nitrogen. This storage area requires easy access to a loading dock for cylinder exchanges and liquid gas refills. Various imaging accessories such as MRI gradients and coils should be conveniently stored near the magnets for easy access, including magnet safe tools and devices. Space within magnet rooms is often ideal so storage cabinets or shelves could be built in during construction. Remember to consider the best location for a loading dock to receive animals and supplies.

Administrative and Personnel Offices. An imaging facility requires skilled people to run the scanners and maintain daily operations of the facility. Each employee needs a space for desk work and their personal belongings and to eat lunch. Strategic locations of office space in close proximity to workspace will provide a pleasant work environment while meeting the demands of the center. Senior laboratory staff and scientists, principal investigators, and facility managers should all have private offices, and upper level personnel should be provided enough space to have collaborative or private discussions. Animal imaging technical support staff (veterinarians, technicians) may have double duties within the housing facilities and imaging suites. Depending on where they spend most of their time, office/desk space may be located within the imaging or housing facility. If animals are maintained in a barrier, it is more practical to have support staff office space adjacent to the barrier, but if personnel are dedicated to the imaging facility, then desks within the facility are more practical. Consider space allotment for visiting scientists and other temporary personnel such as postdoctoral fellows and graduate students. Remember to include storage space for common office supplies, fax/copy machines, and mailboxes. Reference manuals, standard operating procedures, and animal study proposals should be located in a secure, employee-accessible area.

Break rooms are a welcome addition to each floor of a busy facility. Personnel need space to safely consume food and beverages outside the imaging and animal areas. Sound buffers are desirable so that employees can enjoy a brief respite from loud imaging equipment and support areas. Since break rooms are gathering places, a white board, tack board, table, and chairs will provide a comfortable environment and an opportunity to discuss issues or post announcements. Since dining is the primary function of the break room space, the room is ideally equipped with a refrigerator, microwave, countertop, and a sink for washing hands and dishes. In the age of "green thinking," cabinets will provide space for reusable mugs, dishes, and silverware, and if space allows, a dishwasher is a welcome convenience. Remember to set aside space for waste and recycling containers of appropriate volumes.

Restrooms and Showers. Restrooms are required in any type of building and should meet Americans with Disabilities Act (ADA) requirements. Central locations for restrooms allow minimal disruption to the workday's activities. The size of the facility and number of employees will dictate the number and locations of restrooms. Showers may be necessary within the animal housing facility but are

optional for an imaging facility. Their necessity should be discussed with the laboratory animal veterinarian and occupational health specialist.

Conference rooms are valuable meeting rooms and can serve multiple functions. A conference room is an ideal location for invited speaker presentations, scientific discussions with investigators, sales representatives, journal club, employee training, and orientation and continuing education. The size of the imaging facility and number of researchers will suggest the number of conference rooms needed. The room should be equipped with state-of-the-art audiovisual equipment (adequate for large media file presentation), appropriate lighting control, and sound buffering for efficient communication. Access to the Internet via hardwire or wireless communication is necessary in the current world of cloud computing. Conveniently located electrical outlets are necessary to provide power to laptop computers or other devices such as vender equipment demonstrations. A dry erase board or blackboard is convenient for illustrating discussions.

A comfortable conference room is an ideal location for a laboratory animal imaging resource library. The bookshelves offer pleasant room aesthetics and the quiet room a refuge for study. The library's textbooks and manuals are also handy for quick reference sources during meetings. The conference room is ideally located in a quiet section of the building near personnel offices and outside of any restrictive areas that may contain magnet fringe fields or radiation hazards.

Environmental Considerations. Zoned control for temperature and humidity is desirable in the design of an animal imaging facility. Humans and animals have different environmental requirements than do equipment and computer areas. Both humans and animals will appreciate humidity levels between 30 and 70 %, but independent supplies and controls for human areas and animal areas are needed to meet the individual requirements of the experimental animals and personnel. Animal room temperatures range between 65 and 85 °F, but the animal species will dictate the desired ambient temperature so there may be different set points for different rooms. Most important is the ability to maintain the animal room temperature within 2 °F of the set point (Institute for Laboratory Animal Research 2011; Hessler and Leary 2002).

Computer rooms and many types of associated imaging equipment generate a lot of heat during daily operations. Stand-alone supplemental air conditioning is recommended for these areas to avoid overwhelming the building automation system (BAS). It is also a cost-effective alternative to overdesigning the BAS when these heat-generating areas are only a fraction of the entire building. The specific environmental requirements for specific imaging platform suites are defined in the manufacturer's siting recommendations.

Air exchange rates and relative air pressures are an important environmental control for air quality and biological security. Generally areas occupied by personnel maintain positive air pressures relative to corridors to prevent entrance of airborne hazards. By the same token, animal areas are usually adjusted to negative pressures

to contain animal odors, allergens, and potential pathogens. These parameters can certainly be set and adjusted after the building construction is finalized, but careful thought during the planning stages may help to avert any major HVAC renovations at a later date.

3.2.2 Animal Housing and Imaging Support

A preclinical imaging center is ideally located next to an animal holding facility. This ensures convenience for researchers and minimizes transport time for animals. Multiple species will be needed for drug development, and each has its own husbandry requirements. Regulated species necessitate an extra level of planning (such as outdoor exercise pens for canines). Guidelines for animal housing facility planning and construction can be found in many sources and will not be discussed in great detail here (Institute for Laboratory Animal Research 2011; Hessler and Leary 2002). Do consider the need to bring in animal models from outside sources. With numerous genetically manipulated mouse models available, it may be more appropriate for a study to use a model that is not available from a commercial source (i.e., from researchers in academia). The health status of outside sources may differ from that of the main colony, so quarantine areas and the ability to isolate populations are paramount and must be planned accordingly. The laboratory animal veterinarian can offer practical advice during the planning phase.

Housing and Holding Rooms. While animal housing and holding space is vital to a well-planned imaging facility, for the purposes of this document, we assume that the animal housing location is immediately adjacent to the imaging areas. Specific requirements and recommendations for each animal species can be found in several references (Institute for Laboratory Animal Research 2011; Hessler and Leary 2002) and are beyond the scope of this chapter. It may be appropriate to incorporate a small temporary housing area for smaller species like rats and mice if serial imaging will take place during a short period of time (6–24 h). Additionally, it may be beneficial to house radioactive animals from PET/SPECT studies within the PET/SPECT imaging area until the radiation emissions return to a safe level. It is sometimes permissible to house animals on bench tops for brief periods, but the environmental controls in imaging areas may not match the species requirements. If space allows the facility to provide "normal housing" identical to the home housing facility, it may help to minimize any anxieties the animals may have associated with the new imaging domain as well as maintain any microenvironmental controls. Additionally, if the home housing facility is a 10 min walk from the imaging suite, but the temporary housing space is within 1 min, its proximity adds to study/work efficiency. Temporary housing should use the same equipment as the home facility to facilitate interchangeable parts. A mouse or rat cage could be used for transporting the animal to the imaging suite in toto and then placed in the temporary housing rack without the need for a cage change. This temporary housing space could be located in a prep area adjacent to an imager or in a separate nearby location.

For both the home housing rooms and temporary rodent housing area, position the room away from loud and repetitive noise as it can produce deleterious effects on mice (Turner et al. 2005, 2007). If temporary housing areas exist within the imaging facility, appropriate accommodations for husbandry supply storage, cage changing, cage/wash washing, etc., all come into play. This may be avoided by utilizing the home housing facilities resources or use of disposable caging systems.

Procedure Rooms. General anesthesia is usually required to immobilize animals during imaging sessions, so every imager will need some type of animal procedure area. The complexity of the preparation space is defined by the imaging modality. For example, bioluminescence and fluorescence optical imaging is a relatively simple procedure compared to other modalities. An anesthetized animal is placed on an imaging platform (or under an imaging probe or microscope) and an image acquired over seconds to minutes. It may be necessary to inject a substrate (i.e., luciferin), but a small area where animals can be anesthetized, injected, and fur removed may suffice. On the other end of the complexity scale is MRI. After being anesthetized, animals are positioned on an imaging platform (or bed in a clinical scanner), an external heat source is positioned (if not built into the platform), sensors for physiological monitoring are applied, intravenous access established (if dynamic contrast study or blood draws for drug or biomarker kinetic analysis), and then the imaging coil is secured in place (or the animal is placed within a coil). For small animals such as rats and mice, this all may be done on a properly equipped bench top, but larger animals will need sufficient space for personnel to be able to properly prepare and have access to the animal for MR imaging. Larger animals are often intubated and ventilated, so allow space for stationary or portable large ventilators. Our facility performs a large number of NHP brain imaging procedures, and the animal is often positioned within a head stabilizer that is also used with stereotaxic coordinates for surgical procedures. Accurate animal positioning is critical to acquiring useful data and cannot be casually applied. Additionally, consider an emergency scenario: do personnel have enough room to perform cardiopulmonary resuscitation or rapid anesthetic induction, if needed? Ideally, the procedure room is located adjacent to each imaging room. It may be possible to design a shared space for several imagers, but this could hinder any simultaneous imaging on neighboring scanners. Cross contamination could also be a variable in a shared space.

Each procedure room/area should be equipped with the necessary tools for general anesthesia, imaging and associated procedures, and emergency situations. The basics for inhalation anesthesia include an induction chamber or induction drugs, precision vaporizer and vehicle gasses, intubation tubes or face masks, and ventilator (depending on species). Maintenance of normal physiological parameters is most important, so an external heat source and physiological monitoring equipment are also needed. All equipment used in proximity of scanners must be MRI compatible if preparing an animal for MRI, or low-density, low photon attenuation equipment for PET or SPECT. Emergency drugs and life support equipment and drugs should be conveniently located and readily accessible. An adequate method of handling waste anesthetic gasses is required to meet OSHA standards and assure personnel safety. Procedure rooms are a convenient location for eye wash stations

and NHP bite and scratch kits. Consultation with the laboratory animal veterinary staff during planning will ensure that the rooms are appropriately stocked and functionally designed.

If imaging will occur immediately prior to or after a surgical procedure, it may be useful to provide a surgical area. Larger animals require a properly designed dedicated surgical area. If imaging facility space is not available for a dedicated surgery suite, then surgical procedures are best done in the home housing facility. For smaller animals, transportation under anesthesia is much more challenging, so the ability to perform surgery and imaging in neighboring rooms is advantageous. If possible, follow the same guidelines for designing a small animal surgical suite as would be used for regulated species. This not only assures a suitable surgical environment for small animals but allows for future flexibility should a surgical area be needed for a regulated species.

Euthanasia. Euthanasia techniques should be done as painless and stress-free as possible and performed in such a way to minimize any animal distress and anxiety prior to loss of consciousness. Stressed animals emit alarm pheromones that can affect other animals within a room, thus propagating the distress and anxiety (Brechbühl et al. 2008). If euthanasia will be performed in awake animals, an isolated room should be dedicated for euthanasia procedures to comply with international standards (AVMA 2013; Institute for Laboratory Animal Research 2011). The home housing facility will surely be equipped for these procedures so it may not be needed in an imaging facility. Animals under general anesthesia for imaging can easily be euthanized under the same anesthesia to avoid the necessity of a dedicated area. Additionally, it is aesthetically better than recovering the animal from anesthesia and then performing euthanasia. Space to perform perfusion fixation and tissue harvests at the time of necropsy are discussed in other sections. A cold room or freezer for carcass disposal may be convenient to investigators in the imaging facility, and its size should be coordinated with the species undergoing the imaging studies as well as the rate of animals needing these disposal sites.

3.2.3 Magnet (MRI)-Specific Facility Designs

Location. MRI magnets have specialized building and environmental requirements. The architect or engineer needs to work closely with the end users and the MRI manufacturers to determine the structural details required for the instruments. Instrument makers provide detailed installation documentation to end users and the facility engineers to assure a successful installation and operation. The magnetic field in and around the MRI magnet can inactivate or alter life support devices such as pacemakers, neurostimulators, and insulin pumps. The location of MRI scanners must be carefully considered and planned such that the magnetic fields surrounding these instruments (fringe fields) do not interfere with other equipment or present a health hazard to personnel. Fringe fields of neighboring instruments may overlap,

but the manufacturing engineers should be consulted before finalizing plans. A magnetic field of 5 gauss is the FDA limit for the general public including people with pacemakers or other internal devices (Erdogan 2002; Faris and Shein 2006; Shinbane et al. 2007; Expert Panel on MR Safety 2013). The 5 gauss (G) fringe (peripheral to the magnet core) field lines should be well marked and protected from inadvertent access. Areas that personnel or visitors may use (hallways, offices, restrooms) must be located outside of all 5G contours. In addition to electromagnetic instruments, static MR imaging magnets must be isolated from large moving metal masses such as elevators. The latest American College of Radiology (ACR) MR safety guidelines should be consulted prior to start of any major MRI project. Though written for scanning of human patients, most of the major points also apply for preclinical imaging subjects (Expert Panel on MR Safety 2013).

Structural Considerations. Depending on the equipment's specifications, MRI magnets may be located within electromagnetically shielded rooms. This forms a physical isolation of the magnet that isolates and protects the magnet and personnel from safety hazards. The RF shielded room is specifically to isolate the MRI platform from the surrounding electromagnetic spectrum in the RF frequency range. MRI uses RF to generate images, and RF from other devices (such as physiological monitoring equipment) can interfere with imaging. The shielded room also serves to decrease the level of ambient noise generated by the operation of the MRI to operators outside the room. Special acoustical design features may be required to mitigate the transfer of sound and vibration through the structure to adjacent areas. Pits may be needed for the larger pieces of equipment. Many MRI scanners are located on basement or ground levels due to the weight of the instruments. The floors of scanner rooms may require reinforcement to support weights from 200 to 20,000 kg (44,200 lbs). Access and clearance, both vertical and horizontal, around the equipment must be carefully planned for equipment requirements, maintenance, and initial delivery and setup. The weight and size of these instruments may require that they be lowered into their resting places by a crane through a specially designed roof hatch opening. This is another reason that it may be practical to locate the imaging equipment outside the main footprint of the building. In all cases, it should be considered to have an installation access pathway for the magnet into the shielded room or the MRI suite outside of a standard or wide standard door. It is most likely that end users will want to exchange or upgrade the MRI as technological developments and user sophistication makes a newer instrument or instrument modifications an attractive possibility.

Cryogen Gasses. The large majority of MRI magnets are superconducting, so special cooling requirements will be determined by the specifications of the instrument. Consideration must be given to the access and storage of liquid gas Dewar flasks with the clearance needed to add cryogens to the devices. Typical cryogens are liquid helium and liquid nitrogen. These inert gasses pose a threat of asphyxiation if released in an enclosed space with poor ventilation, so each magnet room must include an oxygen sensor at standard head height that alarms when oxygen levels fall below normal limits (usually 18 %). If possible a method of

increasing ventilation in the MRI room during cryogen service operation should be included. All superconducting MRIs include manufacturer-mandated emergency ventilation from the magnet in case of a failure. The design engineer or architect must comply with these safety requirements when installing the emergency vent system.

Environmental Considerations. MRI suites require stable temperature and humidity control in the vicinity of the magnets and the supporting electrical equipment room. The design of the control systems must be coordinated with the mechanical systems design such as HVAC, plumbing, and other support services to minimize environmental condition fluctuation across magnets. The typical MRI room will require constant monitoring of temperature, humidity, and oxygen levels. Humidity requirements must be coordinated with the equipment manufacturer but will usually be around 20–25 % with minimal fluctuation. Requirements of the dehumidification system requirements should be listed with the system used.

Work Areas and Tools. Besides the magnet room itself, several operational spaces are needed. The ancillary equipment such as power supplies, RF amplifiers, gradient power supplies, and magnet cryogenic refrigerators are located close to the magnet room itself. The requirements for this operational equipment can be as large and specific as the magnet itself. Depending on the type of MRI system, the location can be within the publically precluded fringe field which allows a more efficient use of space. The operator console area should be able to support the scanner console and observer space. The console area is where the MRI scans are configured, initiated, and monitored. It is ideal to have additional workspace adjacent to the console area for laptops or analytical workstations. Animal preparation workspace must also be considered. Simple surgical instruments such as scissors, scalpels, and needles can become life-threatening projectiles if taken too close to the magnetic field. Additionally, repairs and periodic maintenance within the magnet room will require use of nonmagnetic tools (including screwdrivers, wrenches, scissors). Nonmagnetic tools (e.g., beryllium-copper alloy or titanium) are an additional expense that cannot be dismissed as unnecessary because standard instruments made of stainless steel and iron are rendered useless in the magnet room if not outright dangerous depending on proximity to magnet. Nonmagnetic light sources (such as flashlights) and cleaning supplies (brooms, mops, and buckets) are another necessity. Due to the magnetic field, there are significant safety hazards associated with working in the MRI environment. We recommend required safety training for all personnel and facility users.

3.2.4 Additional Facility Design Considerations (PET/SPECT, etc.)

Radiation Safety. Ionizing radiation is a useful tool for imaging functional processes with positron emission tomography (PET) or single photon emission

computed tomography (SPECT) and targeted tissue studies using autoradiography. Its use warrants special consideration during building planning phases and should involve a radiation safety specialist. The management of radioactive reagents, animals, and radioactive waste must satisfy nuclear regulatory requirements as well as any local and institutional policies. This includes restricted areas to prevent unauthorized entry and lockable storage containers. Reagent preparation areas, space for a scintillation counter, waste storage, record keeping, and decontamination chemicals (laboratory surfaces and skin contamination) must all be considered.

The half-lives of many commonly used PET radionuclides are short lived (some only minutes to hours) so commercially available imaging probes are often limited (e.g., 2-[^{18}F]fluoro-2-deoxy-D-glucose (FDG); half-life of 109 min (Vijayakumar et al. 2006). These short-lived isotopes require space for a nearby radiochemistry (radiosynthesis) laboratory, and a cyclotron to produce custom radionuclides is an ideal laboratory situation. Delivery routes of the radioactively labeled probes, whether custom or commercially produced, must be designed to minimize personnel exposure and transportation time and facilitate emergency procedures in the event of a spill.

Animals given radiolabeled probe may require special housing which can include metabolic caging to capture urine and fecal excretions for metabolic or kinetic analyses. It may be useful to incorporate temporary rodent housing within the imaging areas to allow decay to safe levels before returning animals to home facilities. For larger species, it may be prudent to plan for housing radioactive animals away from the main facility to avoid exposure to non-treated animals and to staff while an animal may await multiple images to follow the biodistribution. Animal waste, bedding, etc., may require special handling and must be taken into account during the planning phase.

Occasionally, radioactive reagents may be used during other types of imaging for later validation of imaging methods (e.g., autoradiography, longer-lived tracers, i.e., C-14, S-35, I-125). These methods require similar consideration for reagent preparation areas, space for a scintillation counter, autoradiography filming (potential need for a darkroom for film or liquid photographic emulsions) or phosphorimager methods, isotope accounting, study record keeping, dosimetry, and decontamination chemicals. The reader is encouraged to also see the chapter on autoradiography techniques included in this volume.

Animal Biosafety. The option to perform research involving the use of infectious pathogens and biohazardous reagents should be determined in the planning stages of the facility design. Specific environmental controls must be incorporated in the building design in order to achieve adequate biosecurity. Additionally, the specific pathogen status of the experimental animals must be considered. With the explosion of genetically manipulated mouse models (and other species), researchers may want to bring animals from noncommercial sources into the facility for their research. Containment (quarantine facilities) and transportation routes should be considered

during planning phases to minimize contamination potentials. Biosafety works in two directions: preventing animals or people from being exposed to a known research-associated biohazard (viral vectors, toxic metabolites) and preventing research animals from inadvertent exposure to environmental hazards (employees with influenza, immunocompromised animals and opportunistic pathogens). When allocating appropriate workspaces and storage for biohazardous materials during planning phases, give special consideration for decontamination procedures in the event of a biosecurity breach. This could include facilities for autoclaving of bedding and waste in the case of infectious disease imaging. The reader is encouraged to read the chapter in this volume on BSL-3 and BSL-4 nuclear and MR imaging.

Laminar flow hoods provide a unidirectional air flow at a fixed velocity that creates a protective "air curtain" within the hood. Several different types of biological safety cabinets (BSC) exist, each with varying levels of protection. Class I BSCs offer protection to personnel and the environment, but not the object within the cabinet. These are often used for procedures that have potential to create hazardous aerosols or equipment enclosure such as centrifuges. All class II BSCs are designed to protect the contents within the hood from contamination, as well as the personnel and environment (Chosewood and Wilson 2009).

3.3 Animal Imaging Support

The use of laboratory animals in drug discovery cannot be entirely avoided. In order to collect useful imaging data, it is imperative to minimize or prevent movement during acquisition for many in vivo imaging devices. Although it is possible to train some animals to accept restraint during certain imaging sessions through reward training, most animals are imaged under general anesthesia. Anesthesia allows the researcher to position a relaxed animal for optimal imaging data, minimizes motion artifact, and eliminates any animal stress or fear during restraint. This "animal normalization" tends to promote more uniform image data, especially in neurotransmitter imaging or functional MRI (blood flow; blood oxygen level-dependent imaging, BOLD). The facility's laboratory animal veterinarian will serve an important role in determining the best anesthetic protocols for each type of experiment. The following section will examine anesthesia equipment in the imaging environment, physiological monitoring equipment, and useful ancillary resources for imaging studies.

3.3.1 Anesthesia Equipment

We are currently fortunate to have choices of many safe, effective, and reasonably priced anesthetic options for the laboratory animal. There are many injectable

agents to achieve various levels of restraint or a surgical plane of anesthesia, and some are even rapidly reversible. Additionally, there are also several approved inhalational anesthetics. Every drug has a desired effect as well as potentially undesirable secondary effects. Researchers should discuss the experiments in detail with the laboratory animal veterinarian so the veterinarian can design an anesthetic protocol to minimize undesired effects that could impact results.

Inhalation anesthesia has many advantages over an injectable agent. Small animals such as rodents can be anesthetized with minimal stress of handling. They are gently placed in an anesthesia induction chamber, and the anesthetic agent is delivered by a gas vehicle, such as 100 % oxygen or oxygen-enhanced gas mixtures. Once the rodent is unconscious and unresponsive, they can be maintained under anesthesia with the aid of a nosecone. It is possible to intubate rodents, but aside from the technical challenges of correctly placing a rodent intubation tube, we found it more problematic due to respiratory secretions clogging the airways. Details about rodent anesthesia can be found in many sources (Fish et al. 2008).

For larger species, general anesthesia is usually achieved by administering an injectable induction agent, but we still prefer using an inhalant anesthesia during in vivo imaging. The single most important advantage of inhalant anesthesia in the imaging environment is the ability to rapidly adjust the level of anesthesia remotely (preferred design is outside the imaging room). Once an animal is positioned within a scanner for optimal imaging, it is not efficient to stop a scan in order to administer another dose of anesthetic agent. Several additional advantages of inhalational anesthesia include the following: it has physiological properties of minimal metabolism and rapid clearance which make it relatively safe to use in healthy and compromised animals, it provides an ability to titrate to effect, and it is not a controlled substance. Disadvantages of inhalational anesthetics include the required use of expensive precision delivery vaporizers that must be cleaned and calibrated annually, accessible sources of delivery gasses (oxygen, medical air, nitrogen, nitrous oxide), potential need for a species-related ventilators (larger species), and management of waste anesthetic gasses (WAG).

Injectable anesthetic agents offer many conveniences. The drugs are portable, and some can be administered by a variety of routes (intravenous, intraperitoneal, subcutaneous, oral). For brief periods of restraint during short imaging sessions (with no painful procedures), injectable anesthetics may be suitable. Disadvantages of some injectable anesthetics are that once given, the dose cannot be adjusted; the resultant effects are sometimes unpredictable and variable in individuals; and the drug must be metabolized by the body making any impairment to metabolism (renal, hepatic, or circulatory systems) prolong its clearance. Poor clearance can lead to toxic exposures over time, and some of these anesthetic drugs are schedule II controlled substances and require special handling and accounting. An exception to the disadvantages of injectable class of anesthetics is propofol. Propofol is ultrarapidly metabolized and easily titratable to effect, and its cost has come down in recent years. The use of propofol could prove to be just as safe as an inhalant anesthesia under certain circumstances except that it requires a continuous intravenous

infusion to maintain general anesthesia. While this may be easily achieved in larger species, it is challenging in rodents.

We recommend that all imaging areas be designed to incorporate use of inhalant anesthesia. Access to sources of anesthetic delivery gasses (oxygen, medical air, nitrogen, nitrous oxide) is required. Central sources of gas piped through the facility will provide convenience to users. Consider planning for an area to generate house oxygen. Waste anesthetic gas (WAG) is an occupational hazard so methods for its management must be considered during planning (US Dept of Labor 2013). A centralized vacuum that vents to the rooftop after passing through some filtration is an excellent way to handle WAG. Depending on the species to be imaged, the facility may need several different ventilators and associated equipment. Facility plans for storage areas when these devices are not in use are advised. Before purchasing any laboratory equipment, remember that some items may need to be MRI compatible.

3.3.2 Physiological Monitoring

Several modes of in vivo imaging prevent direct visualization of animals while in the device for scanning. In order to ensure that the animal is alive, physiologically stable, and at the proper level of anesthesia, it is important to utilize physiological monitoring equipment. The animal species will determine the type of monitoring equipment that can be used. Human and veterinary devices work well for larger species, but rodents and animals with heart rates above 300 beats per minute (and breathing rates above 60 breaths per minute) require specialized equipment. Technology has finally caught up to the demand so that now there are several physiological monitoring devices that can reliably measure heart rate, respiratory rate, body temperature, and pulse oximetry in rodents and they can be easily found by key word web searches. Other physiological parameters that may be measured include electrocardiogram (ECG), electroencephalogram (EEG), and respiratory wave patterns. Blood pressure, end-tidal carbon dioxide ($ETCO_2$) levels, anesthetic gas levels, and blood gasses (O_2, CO_2) can be measured in larger species noninvasively, but such measures are currently challenging for rodents. Fiber optic pressure monitors exist for measuring arterial/venous blood pressures in mice. The challenge always lies in catheter placement in the smaller rodent species.

Anesthesia is known to interfere with the brain's homeostatic control of core body temperature. It is important to plan for the use of supplemental heat to keep animals warm during imaging. Several options are available for patient warming such as warmed air devices or warmed circulating water pads. Before installing any warming or physiological monitoring devices, be sure to consult with the imaging specialist. It is important to determine if the device may introduce noise into the image data; additionally, it must be safe to use in the imaging environment (MRI). Wires and tubes attached to the animal may need to be connected to a central unit outside the imager so their route must be considered. Electronics are often

connected through a patch panel for MRI. Detailed anesthetic records should be maintained for every animal regardless of the species to help with image interpretations or to understand anomalous results.

3.3.3 Ancillary Support

During drug development, all aspects of efficacy and safety will likely be explored as best as possible. Equipment used to examine various physiological parameters may be located in laboratory space or the housing facility. It may also be convenient to consider having a diagnostic laboratory with microscopes, serum chemistry machines, hematocrit centrifuges, and complete blood count analyzers located near the imaging suites. While the animal is under anesthesia for imaging, the potential exists to collect tissue samples (such as blood), and rapid processing is usually beneficial if not required. Noninvasive blood pressure monitors and electrocardiograms may be useful to compliment the imaging data.

When imaging is at the experimental endpoint, it is possible to perform the euthanasia before recovery from imaging anesthesia. This is aesthetically more pleasant for animal care staff. A chemical fume hood conveniently located near the imaging suite will also facilitate perfusion fixation procedures without the need to recover the animals and transport them to another location.

3.4 Personnel

A successful laboratory animal imaging center requires a team approach to personnel which have a variety of skill levels and skill sets to efficiently and successfully master the tasks at hand. An ideal imaging laboratory will be self-contained in terms of critical core personnel such that any problem or opportunity can be addressed in a timely fashion to minimize downtime. The ideal facility would employ imaging specialists, animal support technicians, computer information technologists, and building staff appropriate for the installation. These different positions are discussed below in piece.

Imaging Specialists. Generally each imaging modality needs some imaging specialist to lead operations, planning, and technical developments on each modality. Depending on the modality, the level of training will vary. In an imaging facility that does technical development and research in addition to providing routine imaging services, additional expertise is required. To facilitate the scientific collaborations and nurture the advancement of the animal imaging technologies, doctorate-level researchers are necessary. The physics, chemistry, and biology peculiar to each imaging modality can be uniquely singular from the other imaging methods in the facility. Specialized training will be required to be

proficient at any imaging method so staffing and regular trainings are expected to maintain proficiency and reproducibility across studies. For MRI, the specialist should be skilled in the physics of the imaging process in order to develop new methodologies as required. For CT, PET, or SPECT, the specialist will need training regarding the physics of the imaging process, radiation safety and measurement, and knowledge of chemistry and physiology to develop new methods and application of radiopharmaceuticals and contrast agents. Specially trained personnel are needed to maintain the imaging magnets, CT systems, optical platforms, autoradiographic equipment, and PET/SPECT scanners. All modern imaging modalities are heavily dependent on cutting edge computer technology and data handling/storage to operate the scanners, reconstruct the data into useful images, and process the images into physiological relevant information. This can be accomplished via service and maintenance contracts with the vendors or other providers at the expense of imaging time delays (and disruption to imaging studies) that may occur if personnel are not in house. If funding will allow, specialists employed in each of the imaging modalities are ideal, but the reality is that motivated and skilled personnel may also perform adequately on more than one imaging method.

Animal support personnel are a critical element in the success of any imaging center. Technicians are needed to perform imaging procedures, anesthesia, catheterization, and other assorted surgical procedures, as defined by the study needs and the center SOPs. Technicians may be trained to run specific or routine imaging procedures in order to free up intellectual time for the imaging physicists. Husbandry personnel and support staff are required to maintain the animal housing facility and are a key element in maintaining the colony veterinary care. A small facility may require some cooperative technical staff for husbandry tasks, but a larger facility should have dedicated teams to handle each workload area. Veterinarians and veterinary technicians are vital to maintaining the health of the animal colonies and imaging subjects. Again, the number of personnel needed will be dictated by the number and variety of animals housed within the center, and a properly designed facility will aid in reducing staffing costs due to redundancies, gown changings, supply maintenance, etc.

Computer Information Technology (CIT). All imaging methods covered in this chapter create a digital record of the image, and a number of computers are required in the generation, recording, and interpretation of the imaging data. In addition to running the operational software for imaging devices, computers are needed for data management and personnel needs (email, ordering supplies, record keeping). Our experience suggests creation of an in-house or local network facilitates data storage and manipulation, so it is necessary to retain dedicated personnel capable of maintaining the network computer equipment. Although computer downtime will inevitably occur, this time should be kept to a minimum with the presence of dedicated CIT staff. Specific tasks of data processing personnel are discussed in another section.

Housekeeping and building maintenance services are necessary for a fully functioning facility employing numerous personnel. This includes waste removal, cleaning of imaging facilities, and animal preparation rooms. This is not a substitute for the standard animal hygiene and biohazard preparation of a bench space prior to and post performing an animal procedure. High traffic areas of animal movement or mixed functions need to be disinfected routinely to control disease vectors and transmission. Environmental conditions such as room temperature and humidity must be carefully controlled for all operational spaces such as scanner rooms, computer rooms, and animal housing rooms. Fluctuations outside of normal ranges should be corrected as quickly as possible, so building maintenance personnel should be available at any time. It is imperative that all support personnel be trained in safety procedures around the imaging equipment, including contract personnel.

Unique MRI Personnel Safety Considerations. The hazards associated with working around a high magnetic field are due to the difficulty of containment and the interaction of the concomitant field with items that are used in the normal course of a modern laboratory. Because of these hazards, employees should be carefully screened for contraindications to the MRI environment. The American College of Radiology (ACR) has very strict guidelines on who may be allowed to undergo an MRI scan. These guidelines should be considered with all personnel operating in and around the MRI magnet. The same contraindications the ACR is concerned about apply to MRI staff due to their exposure to the high magnetic field environment. Personnel with cardiac pacemakers, neurostimulators, aneurysm clips, stents, cochlear implants, drug pumps, or other metallic implants, including shrapnel, should not work in close proximity to the magnets unless they are cleared by direct consultation with appropriate MRI safety personnel. Metallic implants can shift within tissue if too close to the magnetic field. Working implanted devices may be inactivated in the magnetic fields which could result in a fatal accident (Erdogan 2002; Faris and Shein 2006; Shinbane et al. 2007). Many newer surgical devices and tools are MRI compatible, and personnel can safely work in the magnetic field, but this needs to be cleared by the appropriate MRI safety official (Shellock 2007). Warning signs should be posted in highly visible areas all around the facility to warn people of the magnetic environment. As stated earlier, magnets are best located in isolated areas where people may not inadvertently wander into the magnetic fields.

3.5 Imaging Equipment

A brief overview of several in vivo imaging methods follows, but details about each technique are beyond the scope of this paper. We advise the facility planners to further educate themselves on each of the techniques or consult with a specific imaging platform expert before making final decisions. Included in the following

brief in vivo imaging introduction are magnetic resonance imaging (MRI), X-ray computed tomography (CT), positron emission tomography (PET), ultrasound (US), and optical (OP) imaging. Other chapters in this volume will describe these and other modalities, lending nuances which each author brings on their respective discipline.

Magnetic resonance imaging (MRI) is a powerful, three-dimensional imaging modality that uses the property of nuclear spin in certain isotopes of elements to form anatomical images (Haake et al. 2000). Due to the expense of the MRI instrumentation (usually on the order of 0.5–1.5 million US dollars) and the environmental design requirements, the modality is usually placed in a shared imaging facility to maximize use. MR images are most structurally sensitive to soft tissue (e.g., nerves, muscle, blood) and can detect a large range of physiological conditions beyond static anatomy such as blood flow, perfusion, functional brain activity, or white matter orientation in the CNS or musculature (Kwong et al. 1992; Tseng et al. 1999; Mori and Zhang 2006) with minimal changes to imaging conditions for the preclinical subject. In general, MRI does not require contrast agents for images, but many contrast agents have been developed and are available clinically per specific FDA-approved indications but may be used experimentally to exploit a new drug or biological mechanism of action in the regulatory path of drug development.

As with all imaging techniques, MRI is sensitive to motion during the scan interval (acquisition period). The length of this scan interval—from seconds to minutes—makes accounting for animal motion such as respiration or cardiac motility an imperative. Periodic motion such as these can be mitigated using a form of synchronized acquisition or "gating" to time the movements during the scan such that the animal is always in the same position relative to the time of actual scanning interval. These gating methods can be either prospective, timing the scan only for a certain phase in the respiratory and/or cardiac cycle, or retrospective, whereby image data is selected for reconstruction based on the place in the cycle that it was acquired. Such gating techniques can provide stop motion cine loops of cardiac phases to provide direct measurements of cardiac wall motion, ejection fraction, and heart muscle perfusion (de Crespigny et al. 1991; Rose et al. 1994). Similarly to cardiac gating, respiratory gating is used to reduce or eliminate motion triggered by lung inflation/expiration and diaphragm movement. Respiratory gating is useful for mitigating motion transmitted within the abdomen and thoracic cavity, though most motion can be suppressed if scanning during the end-tidal respiration interval which is similar to a "breath-hold."

An exciting application in MRI is tracking of individually labeled cell populations in vivo. This has a number of uses in disease and injury processes particularly in the novel stem cell sciences. Stem cells are trackable in deep tissues or optically opaque tissues in the living animal over time (Epstein et al. 2002; Frank et al. 2003; Shapiro et al. 2004). The reader is encouraged to refer to the appropriate chapters in this volume on cell labeling and tracking.

X-ray computed tomography (CT) uses a series of radiographic images, acquired at different angles around the animal, to mathematically reconstruct a three-dimensional image of the subject (Paulus et al. 2000). The method of operation for most in vivo small animal imaging X-ray tomography scanners is to have the X-ray source and detector rotate around the animal synchronously. These images can be 2D or 3D giving the area of the detector, with individual slices, overlapping volumes or an entire volume being reconstructed and processed to form a 3D image of the preclinical animal from head to toe. These high-resolution CT systems are called "micro-CT" to describe the resolution of the images which range from 10 to 95 μm isotropic. The scanners are much smaller in size and in voxel volume than human clinical CT scanners (Jiang et al. 2000). Due to differences in absorptivity of X-rays, CT excels at visualization of bone structures when in proximity of soft tissue (muscle, connective tissue, etc.) or air. The fundamental physical interaction in X-ray imaging is the absorption or scattering of the X-ray by the electrons of the nucleus. The denser the tissue or the higher the number of electrons, then the greater the absorption, for example, calcium in bone absorbs more than carbon in fat. This property can be effectively used to visualize bony structures, fat tissues, or air spaces due the very high contrast between these materials. For materials that have little intrinsic contrast, i.e., the liver, the use of contrast agents can be quite useful in producing image contrast that is biologically meaningful (i.e., cysts or tumor locations). For X-ray CT, these contrast agents have a high atomic number element, usually iodine, attached to a molecule with the useful osmotic properties and penetration in tissue. Most contrast media available in human practice can be adapted for small animals when taking into account changes in blood volume, renal clearance rate, and other relevant factors (see the chapter in this volume on allometrics). Many other preclinical contrast media are available that give a much larger range of studies than the media adapted from medical practice. Many of these preclinical contrasts are based on a variety of nanoparticle technologies that can include therapeutic drug loads in addition to imaging contrasts. Such applications can include localization of tumors, vascular tree imaging, renal clearance, and hepatic structure (Bakan et al. 2002; Vera and Mattrey 2002; Weber et al. 2004).

Positron emission tomography (PET) forms an image based on radioisotope decay of a compound administered to the animal before initiating scanning (Cherry 2004). Radioisotope imaging methods can be very specific due to the low natural background radiation. PET isotopes emit a positron, which forms two opposed gamma rays (photons) upon annihilation with a local electron. This physical 180° oppositional detection provides a physical collimation which increases the statistical certainty of localization and a high signal-to-noise ratio (SNR) from otherwise scatter photons reaching the detectors. Limitations to radiation exposure require that the PET tracer agents be of a low concentration (i.e., high specific radioactivity and low mass for nonphysiological actions). Consequently, due to this low mass requirement and the inherent physics of positron annihilation source location, PET image resolution is lower than some of the other main volumetric imaging methods

like MRI and CT (Cherry 2006). A commonly used PET tracer is 2-[18F]fluoro-2-deoxy-glucose (FDG) for monitoring glucose metabolism and locating areas of high glycolytic activity. This is used in applications such as localizing metastatic tumor load and exceptional brain activity (and glucose consumption) such as during seizures. As glucose is metabolized throughout the body at some level, FDG PET provides an image with some relevant anatomy visualized. More target-specific PET agents can target cell surface binding sites or specific gene-expression products that are more generally sparse, and due to high efficiency, targeting the agent does not provide "anatomic" positioning and thus requires an additional imaging method for useful anatomical references such as MRI and CT (Beyer et al. 2000; Yaghoubi and Gambhir 2006). Current preclinical or "micro-PET" scanners have an image resolution of below 1 mm which is still much larger than competing scanner resolutions from MRI or CT which are submillimeter (Shao et al. 1997; Catana et al. 2006). PET agents have highly specific requirements to accurately and reproducibly synthesize products with cyclotron-produced isotopes and a very short shelf life. Commercial imaging products are available for certain widely used compounds (e.g., FDG). Often a laboratory is limited to production of specific agents such as FDG and a few others, which can travel well upon production to remote imaging facilities that do not have synthetic capabilities. Laboratory preparation of PET agents requires access to a particle accelerator to prepare the PET isotope prior to reacting with the target pharmaceutical for use as a radiotracer.

Single photon emission computed tomography (SPECT) estimates the distribution of radioactivity from an injected radiotracer (non-positron; single photon emission isotopes) injected typically into the bloodstream. Like a PET tracer, the radiotracer distributes in the body based on differences in perfusion and affinity of the tracer compound to the local microenvironment. The SPECT camera acquires a number of radioactivity maps, or projections, from a series of angular views. The spatial radioactivity distributions serve as the input for a mathematical transformation that produces a three-dimensional distribution of the radiotracer. Radiation dosage is not an intrinsic limit in preclinical animal imaging: high-resolution SPECT scanners use extreme collimation techniques to create higher-resolution images. Recently, combined SPECT-CT scanners or SPECT-MRI scans have been developed to reduce the demands of the SPECT system to produce an anatomically detailed map (low-dose CT radiographs, essentially, using an external rotating source for a photon attenuation scheme to correct for tissue density and photon scatter), utilizing the anatomical information from the co-registered imaging technique (Ji et al. 2010; Goetz et al. 2008). Applications for SPECT include preclinical models to recreate clinical conditions of stroke by using Tc-99 sestamibi, a cationic isonitrile that locks into mitochondria of intact uninjured cells, where the animal is imaged following coronary artery ligation to investigate infarct recovery. This example is being used for novel agents to facilitate recovery from strokes or reperfusion injury (Liu et al. 2002, 2004).

Ultrasound (US) imaging is produced from sound waves, and the resultant echoes at tissue interfaces (organ to organ, tissue to blood, etc.) to generate

two-dimensional images in real time. The frequency of the sound wave produced has a direct relation to the image resolution formed. Clinical ultrasound (up to ~14 MHz) is an excellent modality for observing moving organs and tissues such as cardiac wall motion, blood flow in major vessels, and certain anatomical structures such as fetuses. Preclinical US has advanced to higher frequencies (up to ~55 MHz) to produce near microscopic resolution images (~50 μm) of mice noninvasively for highly visualized structures near the surface (Foster et al. 2000, 2002; Zhou et al. 2004). Interactive applications of ultrasound imaging can include image-guided cardiac inoculations of cells and injections of mouse embryos (Slevin et al. 2006).

Volumetric ultrasound is possible by combining multiple 2D images with a registration algorithm to form a 3D image (Solberg et al. 2007). Using additional constraints, it is possible to evolve a 3D image in time to produce a 4D (3 spatial, 1 time) image (Yagel et al. 2007). Preclinical uses of 3D ultrasound can include such applications as cardiac evaluation and cancer diagnosis (van den Bosch et al. 2006; Badea et al. 2007; Correale et al. 2007; Mitterberger et al. 2007). The immediacy and lack of special facility requirements for ultrasound imaging is a strong support for including it in any imaging suite.

Optical Imaging. A plethora of optical imaging scanners, projectors, and spectrometers are available for laboratory animals. Optical imaging capitalizes on the physical properties of light (generated by various mechanisms) and at various wavelengths to generate two-dimensional images or in limited cases three-dimensional images or tomograms.

Laser Doppler imaging (LDI) is a simple and useful tool for assessing blood flow in patients and animals (Bohling et al. 2006; Humeau et al. 2007). LDI utilizes the Doppler shift in the reflectance of hemoglobin to produce images of blood flow below the tissue surface. LDI is limited due to the shallow depth of penetration, the exiting light, and the time required to raster scan over a surface to produce an image. The technique is useful to evaluate perfusion during healing, surgery, and other circumstances. Though limited in their capabilities, LDI scanners are inexpensive, produce short scan times, and have no special environmental requirements.

Fluorescence imaging uses a fluorescent chemical moiety or fluorophore and excitation light source and a wavelength sensitive detector. The method leverages the rich background of light microscopy and the labels, techniques, and specific fluorophores that have been built over decades of investigation and have recently been adapted to in vivo preclinical imaging (Graves et al. 2004; Hassan and Klaunberg 2004; Montet et al. 2007). The numbers of applications are too numerous for this chapter; however, a few examples include cell trafficking, tumor diagnosis, and staging. The technique does have to contend with many of the naturally fluorescent compounds within the animal's body, and this can interfere with signal location and quantitation (Hoffman and Yang 2006; Zacharakis et al. 2006). A number of in vivo fluorescence imaging devices are commercially available. Unlike radioactive techniques, fluorescence imaging devices require minimal environmental conditions and have been engineered to be easy to operate. The limits to the technique can be stretched to allow placement of a minimally invasive fiber optic within an animal

to observe a fluorescent signal in vivo at cellular resolution (Al-Gubory and Houdebine 2006; Pelled et al. 2006; Snedeker et al. 2006).

Bioluminescence imaging (BLI) produces a light signal via a biochemical reaction (Sato et al. 2004; Zhao et al. 2005; Shinde et al. 2006). This method is intrinsically preferred in a reporter gene study for tumor growth and metastasis, cell trafficking, or intracellular function. As no external light source is required to produce a signal, quantitation can be more strictly used in this technique. All visible light methods suffer from photon diffusion and local variable tissue absorbance. BLI has the advantage that known anatomical absorbance and light path information can be used to overcome these limitations to some degree. The device is similar to the in vivo fluorescence imager (black box with camera) and is routinely easy to operate. The reader is encouraged to read the chapter on BLI included in this volume.

3.6 Data Management

A well-managed imaging facility may have available scanner time booked in excess of 70 % over the operating day. It is great to have plenty of business, but this starts to reduce available time. Time is required to perform system maintenance, quality assurance checks, cleanup, and data analysis for scans in the center. Most imaging studies have a number of data points to be taken from each scan, and most of those have to be interpreted by a trained observer. A clinical radiologist spends all day looking at hundreds of images and dictates out the results that are rarely more than a simple linear measurement or a perceived hyper- or hypo-intensity at a certain location in an image. The resolution of most preclinical imaging methods means that it generates 10- to 100-fold more data than a standard clinical scan, with increased demand for more intensive processing. Most MRI scans create hundreds of megabytes of image data to gigabytes. Almost all micro-CT scans create tens of gigabytes of data. This puts an increased demand for moving data off the limited storage space of scanners and into the hands of the researchers and technician who are interpreting this information often using remote data analysis stations. Unless the local imaging facility is a service, where animals are submitted and reports are delivered, much of the data analysis and interpretation will be in the hands of the researchers whose animals are the experimental model. It is important to make the movement of image data as seamless and simple as possible while maintaining good backup discipline. It is also imperative that other supporting data, i.e., animal anesthesia and drug use and timing and handling, also be collected and reported with the image data.

The acquisition of the imaging data is actually a fraction of the time necessary to process, analyze, and interpret the data. Therefore, it is important to have the capacity to absorb the inflow from the imaging devices and hold the data for processing until the project is completed when the data can be safely archived for future retrieval. Otherwise, it is quite possible for the nonclinical investigator or the analyzing staff to find themselves virtually overwhelmed in data, and this can lead to

processing and interpretive errors and loss of study integrity which is needed for regulatory filings.

Data processing and management need to be included at initial planning stages for an imaging center. In vivo imaging can produce enormous volumes of digital data in short time. A whole body mouse CT scan of 35 μm resolution produces 5 Gb of radiographic projection data and 2 Gb of reconstructed image data in the course of a 20 min experiment. A micro-MRI of a whole brain at 35 μm creates a 1.05 Gb data file with a 0.5 Gb reconstructed image. These examples illustrate the need for the ability to control the flow of information from scanners. The imaging data is collected from each scanner in a usually proprietary format that is designed for the most efficient use by the scanner software and requires a subsequent reconstruction operation to transform the collected data into a usable image. The reconstruction requirements vary based on the type of imaging modality, the complexity of the acquisition, and the scalability of the algorithm processing the data. Some processes are handled well with personal computers, and others require an array of parallel processors or recently designed graphic processor units (GPUs). Data transfer over fast network connections eliminates the need to produce multiple disk copies for transport and provides for faster data reconstruction and analysis. Robust networks also ease the task of keeping robust and up-to-date backups in case of accidental data deletion or scanner failure.

Data analysis in the ideal imaging facility will use data management technicians and aid investigators with data processing and analysis. Generally the data analysis can require more time to analyze and evaluate than collection of said data. A busy facility may find it difficult for imaging specialists to find the time away from data collection to provide in-depth instruction and help with analysis. An image analysis specialist or team is a valuable asset in these cases where taking time away from data collection is a detriment. Additional prudent assets to the imaging facility would include a veterinary radiologist to assist with interpreting image data in a veterinary clinical context, and robust statistical analysis would be aided with the addition of a biostatistician. In our experience, most facility users have no or limited experience interpreting anatomical images, analyzing three-dimensional data sets, or using the analysis software which in many cases have a steep learning curve. Generally, facility users fall into one of three classes: (1) just give me the results, (2) help me with the hard analysis, or (3) teach me how to do it myself. The first class of investigators has no interest in the analysis and prefers just to have the processed results given to them. In this case, the imaging facility is operating as a service and as such should be sufficiently and expertly staffed to produce a reasonable flow of reliable information. In the second class, the imaging specialists or data analysts teach the investigators the portion of the analysis that is quick to pickup and performs the difficult part out of expediency. The third class is the most confident in their abilities and wants to fully control the flow of information into their experiments. If the imaging facility offers analysis as part of the imaging service, then such recognition as coauthorship on any publications may not be necessary. It is strongly advised that these arrangements be settled before any

scanning study is commenced as a good management practice. For investigators, that perform the analysis and processing independently, it is necessary to provide computer workstations for the express purpose of independent analysis as these computers usually have extreme processing, memory, and storage demands placed upon them by the analysis software. Another incentive is the cost of many software packages may exceed the budget of investigators. Avoiding duplication of software helps to reduce pressure on research laboratory as well as biotech/corporate laboratory budgets. Also the analysis team can use these workstations for training and collaboration with investigators and aid in the production of publication quality images and presentations.

Data Storage. As pointed out earlier, the amount of data that can be generated in a busy facility can be very large. The storage and management of the image data for investigators should be decided early in the planning process. Data discipline should be adhered to throughout the facility to avoid a backlog on scanners with insufficient space for new experiments. Investigators need to be provided with a copy of their image data in the format that is most useful (CD, DVD, portable device). A large facility should forgo this approach and have a central storage facility. Clinical radiology departments utilize centralized PACS (Picture Archiving and Communications Systems) for storage and local distribution. Most preclinical software has very limited export capability for these types of systems, and usually there is a loss of image information in terms of image modality details. For this reason, the ideal imaging facility would have an independent and imaging modality neutral data center to store and distribute imaging data. This can be as simple as a centralized server with adequate disk space or as complex as an array of storage systems for each imaging modality.

3.7 Summary

Planning, designing, and implementing a preclinical animal in vivo imaging facility are no small undertaking. The team of designers and key investigators need to understand all aspects of the functional facility and use the knowledge to guide the architects and builders. It is necessary that experienced personnel be included in the planning stages to avoid costly mistakes in later phases. A smooth workflow will be easy to maintain in a well-designed imaging center. A shared facility is the most common implementation of a multimodal imaging center as the large capital costs of equipment, personnel, and overhead make this the most efficient use of resources. Added benefits of a shared facility will be fostering cross-disciplinary collaborative projects, conservation of resources, reduced duplication of effort and equipment, and production of competitively outstanding data. An ideal imaging facility needs to provide state-of-the-art in vivo imaging equipment and have animal housing resources in the nearby area and preparation areas with surgical capabilities to reduce transportation trauma to and from imaging sessions. The imaging center

design needs to include the following elements: trained personnel, staff workspaces and offices, animal short-term housing and imaging support areas, adequate building requirements to accommodate specific imaging types such as MRI, and allowances to incorporate good safety practices for biological and radiation agents.

The constituent imaging devices in the center need to reflect the goals of the user community and satisfy the needs for the ongoing research studies. In the case of a limited budget, facility planners should choose the most essential modalities for the facility operation based on highest anticipated need. For the lucky few with a large or unlimited budget, the facility should reflect the most versatility to use imaging technology to attack a research problem with a wide area of imaging devices. Up-to-date anesthesia and physiological monitoring equipment are critical to maximize animal safety and validity of research results. Imaging technical development requires specialized staff to produce high-quality data beyond canned manufacturer protocols. Additional support staff, including housekeeping services (training in safety and hazards is required) and veterinary care, is necessary for successful facility to maintain focus. Data management must be accounted for in planning to have a successful flow of information to the completion of imaging projects. Through the use of deliberative planning with facility designers and experienced imaging experts, the current and future requirements of facility users, with good continuing management, will produce a highly utilized and ultimately successful preclinical in vivo imaging facility.

Acknowledgements The views, opinions, and findings contained in this report are those of the authors and do not reflect official policy or positions of the U.S. Department of Health and Human Services, the National Institutes of Health, or the United States Government.

References

Al-Gubory KH, Houdebine LM (2006) In vivo imaging of green fluorescent protein-expressing cells in transgenic animals using fibred confocal fluorescence microscopy. Eur J Cell Biol 85(8):837–845

Aoyama K, Ueda A, Manda F, Matsushita T, Ueda T, Yamauchi C (1992) Allergy to laboratory animals: an epidemiological study. Br J Ind Med 49(1):41–47

American Veterinary Medical Association (2013) Guidelines for the euthanasia of animals, 2013th edn. https://www.avma.org/KB/Policies/Pages/Euthanasia-Guidelines.aspx. Accessed 25 Mar 2013

Badea R, Socaciu M, Lupşor M, Moşteanu O, Pop T (2007) Evaluating the liver tumors using three-dimensional ultrasonography. A pictorial essay. J Gastrointestin Liver Dis 16(1):85–92, Review

Bakan DA, Lee FT Jr, Weichert JP, Longino MA, Counsell RE (2002 May) Hepatobiliary imaging using a novel hepatocyte-selective CT contrast agent. Acad Radiol 9(Suppl 1):S194–S199

Bardana EJ Jr (1992) Occupational asthma and related conditions in animal workers. In: Bardana EJ Jr, Montanaro A, O'Hollaren MT (eds) Occupational asthma. Hanley & Belfus, Philadelphia, PA

Beyer T, Townsend DW, Brun T, Kinahan PE, Charron M, Roddy R, Jerin J, Young J, Byars L, Nutt R (2000) A combined PET/CT scanner for clinical oncology. J Nucl Med 41(8):1369–1379

Bohling MW, Henderson RA, Swaim SF, Kincaid SA, Wright JC (2006) Comparison of the role of the subcutaneous tissues in cutaneous wound healing in the dog and cat. Vet Surg 35(1):3–14

Brechbühl J, Klaey M, Broillet MC (2008) Grueneberg ganglion cells mediate alarm pheromone detection in mice. Science 321(5892):1092–1095

Budinger TF, Benaron DA, Koretsky AP (1999) Imaging transgenic animals. Annu Rev Biomed Eng 1:611–648

Catana C, Wu Y, Judenhofer MS, Qi J, Pichler BJ, Cherry SR (2006 Dec) Simultaneous acquisition of multislice PET and MR images: initial results with a MR-compatible PET scanner. J Nucl Med 47(12):1968–1976

Chan-Yeung M, Malo JL (1994) Aetiological agents in occupational asthma. Eur Respir J 7: 346–371

Cherry SR (2004) In vivo molecular and genomic imaging: new challenges for imaging physics. Phys Med Biol 49(3):R13–R48

Cherry SR (2006) The 2006 Henry N. Wagner lecture: of mice and men (and positrons)—advances in PET imaging technology. J Nucl Med 47(11):1735–1745

Chosewood LC, Wilson DE (ed) (2009) Biosafety in microbiological and biomedical laboratories, 5th edn. United States Department of Health and Human Services, Public Health Service, Centers for Disease Control and Prevention, National Institutes of Health. HHS Publication No. (CDC) 21-1112. Revised 2009

Correale M, Ieva R, Balzano M, Di Biase M (2007) Real-time three-dimensional echocardiography: a pilot feasibility study in an Italian cardiologic center. J Cardiovasc Med (Hagerstown) 8(4):265–273

Coulibaly C, Hack R, Seidl J, Chudy M, Itter G, Plesker R (2004 Oct) A natural asymptomatic herpes B virus infection in a colony of laboratory brown capuchin monkeys (Cebus apella). Lab Anim 38(4):432–438

de Crespigny AJ, Carpenter TA, Hall LD (1991) Cardiac tagging in the rat using a DANTE sequence. Magn Reson Med 21(1):151–156. doi:10.1002/mrm.1910210119

Epstein FH, Yang Z, Gilson WD, Berr SS, Kramer CM, French BA (2002) MR tagging early after myocardial infarction in mice demonstrates contractile dysfunction in adjacent and remote regions. Magn Reson Med 48(2):399–403

Erdogan O (2002) Electromagnetic interference on pacemakers. Indian Pacing Electrophysiol J 2(3):74–78

Expert Panel on MR Safety, Kanal, E., Barkovich, A. J., Bell, C., Borgstede, J. P., Bradley, W. G., Froelich, J. W., Gimbel, J. R., Gosbee, J. W., Kuhni-Kaminski, E., Larson, P. A., Lester, J. W., Nyenhuis, J., Schaefer, D. J., Sebek, E. A., Weinreb, J., Wilkoff, B. L., Woods, T. O., Lucey, L. and Hernandez, D. (2013) ACR guidance document on MR safe practices. Magn Reson Imaging 37:501–530. doi:10.1002/jmri.24011

Faris OP, Shein M (2006) Food and Drug Administration perspective: magnetic resonance imaging of pacemaker and implantable cardioverter-defibrillator patients. Circulation 114(12):1232–1233

Fish RE, Brown MJ, Danneman PJ, Karas AZ (eds) (2008) Anesthesia and analgesia in laboratory animals, 2nd edn. Academic/Elsevier, New York

Foster FS, Pavlin CJ, Harasiewicz KA, Christopher DA, Turnbull DH (2000) Advances in ultrasound biomicroscopy. Ultrasound Med Biol 26(1):1–27, Review

Foster FS, Zhang MY, Zhou YQ, Liu G, Mehi J, Cherin E, Harasiewicz KA, Starkoski BG, Zan L, Knapik DA, Adamson SL (2002) A new ultrasound instrument for in vivo microimaging of mice. Ultrasound Med Biol 28(9):1165–1172

Frank JA, Miller BR, Arbab AS, Zywicke HA, Jordan EK, Lewis BK, Bryant LH Jr, Bulte JW (2003) Clinically applicable labeling of mammalian and stem cells by combining superparamagnetic iron oxides and transfection agents. Radiology 228(2):480–487

Gay FP, Holden M (1933) The herpes encephalitis problem. J Infect Dis 53:287–303

Graves EE, Weissleder R, Ntziachristos V (2004) Fluorescence molecular imaging of small animal tumor models. Curr Mol Med 4(4):419–430, Review

Goetz C, Breton E, Choquet P, Israel-Jost V, Constantinesco A (2008) SPECT low-field MRI system for small-animal imaging. J Nucl Med 49(1):88–93

Haake EM, Brown RW, Thompson MR, Venkatesan R (2000) Magnetic resonance imaging: physical principles and sequence design. Wiley, New York

Hassan M, Klaunberg BA (2004) Biomedical applications of fluorescence imaging in vivo. Comp Med 54(6):635–644

Hessler JR, Leary SL (2002) Design and management of animal facilities. In: Fox JG, Anderson LC, Loew FM, Quimby FW (eds) Laboratory animal medicine, 2nd edn. Academic Press/ Elsevier, New York, pp 909–953

Hoffman RM, Yang M (2006) Whole-body imaging with fluorescent proteins. Nat Protoc 1(3):1429–1438

Hollander A, Heederik D, Doekes G (1997) Respiratory allergy to rats: exposure-response relationships in laboratory animal workers. Am J Respir Crit Care Med 155:562–567

Humeau A, Steenbergen W, Nilsson H, Strömberg T (2007) Laser Doppler perfusion monitoring and imaging: novel approaches. Med Biol Eng Comput 45(5):421–435

Institute for Laboratory Animal Research (2011) Guide for the care and use of laboratory animals, 8th edn. National Academy Press. http://www.nap.edu/catalog.php?record_id=12910. Accessed 26 Mar 2013

Ji C, van der Have F, Gratama van Andel H, Ramakers R, Beekman F (2010) Accurate coregistration between ultra-high-resolution micro-SPECT and circular cone-beam micro-CT scanners. Int J Biomed Imaging 2010:654506. doi:10.1155/2010/654506

Jiang Y, Zhao J, White DL, Genant HK (2000) Micro CT and micro MR imaging of 3D architecture of animal skeleton. J Musculoskelet Neuronal Interact 1(1):45–51

Kwong KK, Belliveau JW, Chesler DA, Goldberg IE, Weisskoff RM, Poncelet BP, Kennedy DN, Hoppel BE, Cohen MS, Turner R et al (1992) Dynamic magnetic resonance imaging of human brain activity during primary sensory stimulation. Proc Natl Acad Sci USA 89(12):5675–5679

Liu Z, Kastis GA, Stevenson GD, Barrett HH, Furenlid LR, Kupinski MA, Patton DD, Wilson DW (2002) Quantitative analysis of acute myocardial infarct in rat hearts with ischemia-reperfusion using a high-resolution stationary SPECT system. J Nucl Med 43(7):933–939

Liu Z, Barrett HH, Stevenson GD, Kastis GA, Bettan M, Furenlid LR, Wilson DW, Pak KY (2004) High-resolution imaging with (99m)Tc-glucarate for assessing myocardial injury in rat heart models exposed to different durations of ischemia with reperfusion. J Nucl Med 45:1251–1259

Loomis MR, O'Neill T, Bush M, Montali RJ (1981) Fatal herpesvirus infection in patas monkeys and a black and white colobus monkey. J Am Vet Med Assoc 179(11):1236–1239

Mitterberger M, Pinggera GM, Pallwein L, Gradl J, Frauscher F, Bartsch G, Strasser H, Akkad T, Horninger W (2007) The value of three-dimensional transrectal ultrasonography in staging prostate cancer. BJU Int 100(1):47–50

Montet X, Figueiredo JL, Alencar H, Ntziachristos V, Mahmood U, Weissleder R (2007) Tomographic fluorescence imaging of tumor vascular volume in mice. Radiology 242(3):751–758

Mori S, Zhang J (2006) Principles of diffusion tensor imaging and its applications to basic neuroscience research. Neuron 51(5):527–539

Paulus MJ, Gleason SS, Kennel SJ, Hunsicker PR, Johnson DK (2000) High resolution X-ray computed tomography: an emerging tool for small animal cancer research. Neoplasia 2(1–2): 62–70, Review

Pelled G, Dodd SJ, Koretsky AP (2006) Catheter confocal fluorescence imaging and functional magnetic resonance imaging of local and systems level recovery in the regenerating rodent sciatic nerve. Neuroimage 30(3):847–856

Rose SE, Wilson SJ, Zelaya FO, Crozier S, Doddrell DM (1994) High resolution high field rodent cardiac imaging with flow enhancement suppression. Magn Reson Imaging 12(8):1183–1190

Ruys T (ed) (1990) Handbook of facilities planning, vol 1: laboratory facilities. Wiley, New York.

Sato A, Klaunberg B, Tolwani R (2004) In vivo bioluminescence imaging. Comp Med 54(6): 631–634

Shao Y, Cherry SR, Farahani K, Meadors K, Siegel S, Silverman RW, Marsden PK (1997) Simultaneous PET and MR imaging. Phys Med Biol 42(10):1965–1970

Shapiro EM, Skrtic S, Sharer K, Hill JM, Dunbar CE, Koretsky AP (2004) MRI detection of single particles for cellular imaging. Proc Natl Acad Sci USA 101(30):10901–10906

Shellock FG (2007) Comments on MR heating tests of critical implants. J Magn Reson Imaging 26:1182–1185
Shinbane JS, Colletti PM, Shellock FG (2007) MR in patients with pacemakers and ICDs: defining the issues. J Cardiovasc Magn Reson 9(1):5–13, Review
Shinde R, Perkins J, Contag CH (2006) Luciferin derivatives for enhanced in vitro and in vivo bioluminescence assays. Biochemistry 45(37):11103–11112
Slevin JC, Byers L, Gertsenstein M, Qu D, Mu J, Sunn N, Kingdom JC, Rossant J, Adamson SL (2006) High resolution ultrasound-guided microinjection for interventional studies of early embryonic and placental development in vivo in mice. BMC Dev Biol 6:10
Solberg OV, Lindseth F, Torp H, Blake RE, Nagelhus Hernes TA (2007) Freehand 3D ultrasound reconstruction algorithms—a review. Ultrasound Med Biol 33(7):991–1009, Review
Snedeker JG, Pelled G, Zilberman Y, Gerhard F, Müller R, Gazit D (2006) Endoscopic cellular microscopy for in vivo biomechanical assessment of tendon function. J Biomed Opt 11(6): 064010
Tseng WY, Reese TG, Weisskoff RM, Wedeen VJ (1999) Cardiac diffusion tensor MRI in vivo without strain correction. Magn Reson Med 42(2):393–403
Turner JG, Bauer CA, Rybak LP (2007) Noise in animal facilities: why it matters. J Am Assoc Lab Anim Sci 46(1):10–13
Turner JG, Parrish JL, Hughes LF, Toth LA, Caspary DM (2005) Hearing in laboratory animals: strain differences and nonauditory effects of noise. Comp Med 55(1):12–23
United States Department of Labor (2013) Occupational Safety and Health Administration. Waste anesthetic gasses. http://www.osha.gov/SLTC/wasteanestheticgases. Accessed 25 Mar 2013
van den Bosch AE, van Dijk VF, McGhie JS, Bogers AJ, Roos-Hesselink JW, Simoons ML, Meijboom FJ (2006) Real-time transthoracic three-dimensional echocardiography provides additional information of left-sided AV valve morphology after AVSD repair. Int J Cardiol 106(3):360–364
Vera DR, Mattrey RF (2002) A molecular CT blood pool contrast agent. Acad Radiol 9(7): 784–792
Vijayakumar V, Ali S, Briscoe EG, Bertolino P, Rahman A (2006) Detection of viable myocardium by FDG SPECT predicts major adverse cardiac events in patients with coronary artery disease and left ventricular dysfunction. World J Nucl Med 5(2):74–78
Weber SM, Peterson KA, Durkee B, Qi C, Longino M, Warner T, Lee FT Jr, Weichert JP (2004) Imaging of murine liver tumor using microCT with a hepatocyte-selective contrast agent: accuracy is dependent on adequate contrast enhancement. J Surg Res 119(1):41–45
Weigler BJ (1992) Biology of B virus in macaques and human host: a review. Clin Infect Dis 14(2):555–567
Wilson RB, Holscher MA, Chang T, Hodges JR (1990) Fatal Herpesvirus simiae B (B virus) infection in a patas monkey (Erythrocebus patas). J Vet Diagn Invest 2:242–244
Yagel S, Cohen SM, Shapiro I, Valsky DV (2007) 3D and 4D ultrasound in fetal cardiac scanning: a new look at the fetal heart. Ultrasound Obstet Gynecol 29(1):81–95
Yaghoubi SS, Gambhir SS (2006) PET imaging of herpes simplex virus type 1 thymidine kinase (HSV1-tk) or mutant HSV1-sr39tk reporter gene expression in mice and humans using [18F] FHBG. Nat Protoc 1(6):3069–3075
Zacharakis G, Shih H, Ripoll J, Weissleder R, Ntziachristos V (2006) Normalized transillumination of fluorescent proteins in small animals. Mol Imaging 5(3):153–159
Zhao H, Doyle TC, Coquoz O, Kalish F, Rice BW, Contag CH (2005) Emission spectra of bioluminescent reporters and interaction with mammalian tissue determine the sensitivity of detection in vivo. J Biomed Opt 10(4):41210
Zhou YQ, Foster FS, Nieman BJ, Davidson L, Chen XJ, Henkelman RM (2004) Comprehensive transthoracic cardiac imaging in mice using ultrasound biomicroscopy with anatomical confirmation by magnetic resonance imaging. Physiol Genomics 18(2):232–244

Chapter 4
Pharmaco-Imaging in Translational Science and Research

Immanuel Freedman

Abstract Examples of pharmaco-imaging in translational science and research include whole body infrared imaging of normal healthy mouse, magnetic resonance imaging of normal healthy mouse calf muscle, and magnetic resonance imaging of relapsing-remitting multiple sclerosis patient brain. Rationales, experimental design, study outcomes, and conclusions are presented.

4.1 Introduction

Within GSK Biopharm & Immuno-inflammation Pharmacoology, studies are performed on biopharmaceutical compounds in preclinical models such as mice, rats, and monkeys, as well as humans from First Time in Human to Post-Marketing (phases I–IV).

Aligned with the vision of GlaxoSmithKline Clinical Pharmacology, Modeling, and Simulation to establish model-based technology as a core element of the drug development process, the Biopharm & Immuno-inflammation Pharmacology group integrates pharmacokinetics, pharmacodynamics, modeling, simulation, and biometrics into the selection, global development, and registration of drugs for the betterment of patients.

Mechanistic pharmacometric models, typically based on nonlinear mixed modeling methods, may enable translation between compounds, species, phases, therapeutic areas, and indications, considering their similarities and clinically significant differences, and translation of terms in mathematical models.

I. Freedman (✉)
GlaxoSmithKline, King of Prussia, PA, USA
e-mail: immanuel.q.freedman@gsk.com

B.R. Moyer et al. (eds.), *Pharmaco-Imaging in Drug and Biologics Development*,
AAPS Advances in the Pharmaceutical Sciences Series 8, DOI 10.1007/978-1-4614-8247-5_4,

Noninvasive methods such as imaging may increase the number of observations that can be made without significantly perturbing the biological system by invasive blood draws or stressful biopsies. This chapter discusses specific examples of pharmaco-imaging methods with demonstrated value in internal and regulatory decision-making.

4.2 Specific Examples: Example 1: Whole Body Infrared Imaging of Normal Healthy Mouse

4.2.1 Rationale

Osteoarthritis (OA) is a widely prevalent joint disease with a high unmet medical need that represents a substantial economic burden. In OA, cartilage metabolism outpaces anabolic regeneration with consequent destruction of cartilage. Aggrecan is a key structural component of cartilage, responsible for elasticity, water content, and structural integrity. ADAM TS 5 is an enzyme expressed by chondrocytes that degrades aggrecan, and ADAM TS 5 activity is linked to the development and progression of OA in both mouse models and human OA.

This section discusses pharmaco-imaging methods that demonstrate preclinical target engagement and pharmacokinetics and provide translational guidance for an unspecified monoclonal antibody (mAb) directed against ADAM TS 5.

4.2.2 Materials and Methods

4.2.2.1 Animal Model: Normal Healthy Hairless (SHK1) Mouse

Mouse IgG1 isotype control (MOPC21) or unspecified anti-ADAM TS 5 monoclonal antibody (mAb) was labeled with IR800 green fluorescent dye in phosphate-buffered saline (PBS) solution. They were administered to normal healthy hairless (SHK1) mice via the intraperitoneal (IP) or intra-articular (IA) route ($n = 6$/group) as follows:

• Mouse IgG1 isotope control	225 μg in 200 μL	PBS IP
• Anti-ADAM TS 5 mAb	225 μg in 200 μL	PBS IP
• Mouse IgG1 isotype control	50 μg in 15 μL	PBS IA
• Anti-ADAM TS 5 mAb	50 μg in 15 μL	PBS IA

The mice were serially imaged at 800nm wavelength, bled following administration, and $n = 3$ mice/group were sacrificed at 8 days and 60 days after dose. The in vivo time course of whole body mAb biodistribution and total and ADAM TS 5-specific pharmacokinetics in serum was determined by near-infrared imaging on the LI-COR Odyssey scanner (LI-COR Biosciences:NE).

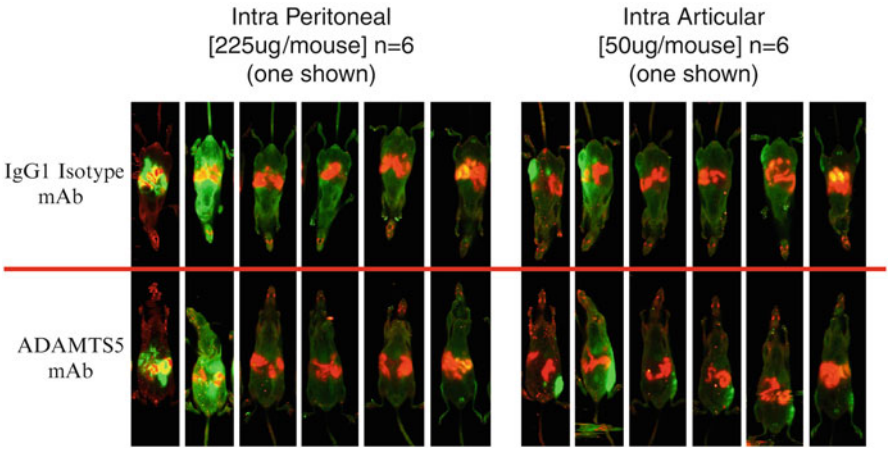

Fig. 4.1 Image sequence showing time course of single-dose IgG1 isotype mAb and anti-ADAM TS 5 mAb biodistribution in SHK1 mouse at 0.5, 24, 72, 168, 672, and 1,344 h after dose

4.2.2.2 Standard Curves

Qualitative standard curves for IR800-labeled IgG1 isotope control (MOPC21) and anti-ADAM TS 5 mAb were imaged according to the following protocol at serial dilutions from 1:1 to 1:32 for initial concentrations of 299 and 319 μg/mL, respectively.

- Co-incubate 10 μL of labeled mAb in PBS with 10 μL protein A/G beads (Thermo Scientific:IL) for 30 min at 25 °C in a 96-well v-bottom microtiter plate.
- Add 100 μL PBS.
- Centrifuge plate and aspirate liquid.
- Wash beads 3× with 100 μL PBS and aspirate liquid.
- Read plate on LI-COR Odyssey imaging system.

4.2.3 Results and Discussion

4.2.3.1 Whole Body Biodistribution

Figure 4.1 shows the time course of whole body biodistribution for one of $n=6$ mice, suggesting a longer half-life for the anti-ADAM TS 5 mAb dosed at 50 μg IA than 225 μg IP.

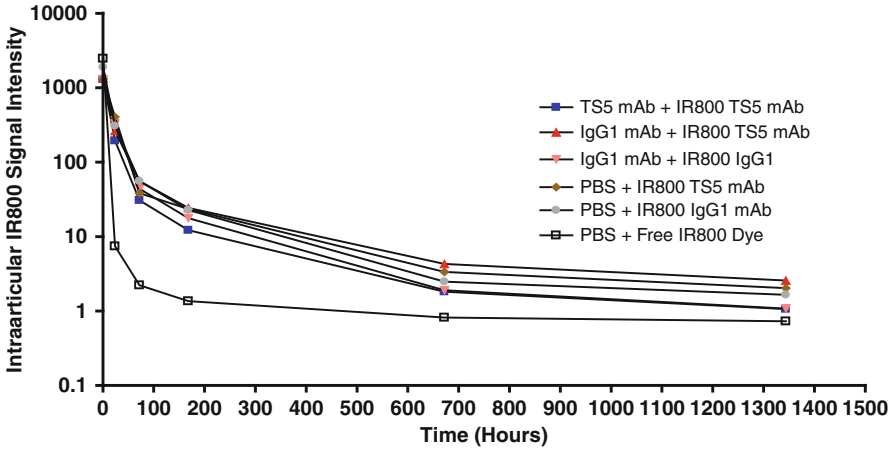

Fig. 4.2 Labeled mAb pharmacokinetics after unlabeled mAb administration

Table 4.1 Labeled mAb pharmacokinetics after unlabeled mAb administration

Compound	$t_{½,\alpha}$ (h)	$t_{½,\beta}$ (h)
TS5 mAb + IR800 TS5 mAb	12.7	511
IgG1 mAb + IR800 TS5 mAb	9.13	221
IgG1 mAb + IR800 IgG1	39.6	NC
PBS + IR800 TS5 mAb	13.1	483
PBS + IR800 IgG1 mAb	8.1	89.2
PBS + IR800 PBS	2.87	101

NC not calculated

4.2.3.2 Labeled mAb Challenge After Unlabeled mAb Administration

Figure 4.2 shows the time course of anti-ADAM TS 5 mAb pharmacokinetics following 0.2 mg unlabeled mAb on day 1 and 0.1 mg labeled mAb on day 1 administered via the IA route. Compartmental pharmacokinetic analysis with WinNonlin 5.2 software (Pharsight:NC) yields a two-compartment linear model with nominal distributional half-life $t_{½,}\alpha$ and terminal half-life $t_{½,}\beta$ according to Table 4.1.

4.2.3.3 Translation to Human

Table 4.1 and Fig. 4.2 suggest target engagement since the anti-ADAM TS 5 mAb has longer half-life than the IgG1 isotype control at the same dose. By allometric scaling of passive processes (Savage et al. 2004; West et al. 1997), a nominal 483 h terminal half-life for the fluorescent signal from 0.1 mg *total* anti-ADAM TS 5 mAb

dosed via the IA route to 25 mg mouse scales to 60 kg human according to $(60{,}000/25)^{1/4} \times 483$ h = 3,380 h (140 days), while a nominal 89.2 h terminal half-life for the 0.1 mg IgG1 isotype control scales to 624 h (26.0 days), in reasonable agreement with a typical 21-day serum terminal half-life for non-binding mAb in human.

4.2.3.4 Limitations

Limitations of this method include (a) the animal size is limited to the physical size of the Odyssey scanner, (b) continuous observations in vivo require gas anesthesia, and (c) the fluorescent signal strength standard curve is qualitative.

4.3 Example 2: Magnetic Resonance Imaging of Normal Healthy Mouse Calf Muscle

4.3.1 Rationale

Myostatin is a secreted protein that inhibits muscle differentiation and growth. Encoded by the myostatin gene (MSTN), myostatin is produced in skeletal muscle cells and circulates in blood as free mature myostatin and as an inactive latent complex of the myostatin C-terminal dimer and other proteins including its propeptide. Mature myostatin acts on muscle tissue by binding a cell-bound activin R2 receptor. Humans lacking a functional MSTN gene, MSTN knockout, and conditional knockout mice gain muscle mass, while transgenic mice that overexpress MSTN selectively in skeletal muscle lose muscle mass.

Overexpression of myostatin may be implicated in human muscle-wasting diseases including hip fracture and cancer cachexia. A therapeutic humanized mAb that binds mature myostatin may increase human muscle mass by competitive antagonism of the muscle growth inhibition that occurs when mature myostatin binds the activin R2 receptor.

This section discusses pharmaco-imaging methods that demonstrate preclinical target engagement and pharmacokinetics and provide translational guidance for an unspecified monoclonal antibody (mAb) directed against mature myostatin.

4.3.2 Materials and Methods

4.3.2.1 Animal Model: Normal Healthy ♂ C57BL/6 Mouse

Mouse IgG2a isotype control or an unspecified murine mAb (10B3) directed against mature myostatin was administered to normal healthy ♂ C57BL/6 mice 8 weeks

old, via the intraperitoneal (IP) route on days 0, 4, 7, 14, and 21 at 10 mL/kg concentration for day 0 to reduce dose volume and 5 mL/kg for the remaining doses, $n = 6$/group, as follows:

• Mouse IgG2a isotope control	30 mg/kg IP (Group 1)
• Anti-myostatin mAb (10B3)	3 mg/kg IP (Group 2)
• Anti-myostatin mAb (10B3)	30 mg/kg IP (Group 3)

The mice were serially imaged by magnetic resonance image (MRI) on a weekly basis for 12 weeks following initial dosing. Contours were manually drawn around muscle, excluding bone and subcutaneous fat. Calf muscle volumes were recorded weekly, and cardiac septum and left ventricular wall thickness were recorded based on an average of three measurements at the day 0 and weeks 2, 4, and 12 time points. Serum pharmacokinetic samples and animal body weights were collected weekly from day 0 to week 12. Tissue samples including leg and heart muscles were collected for analysis at week 4.

4.3.2.2 MRI Instrumentation and Method

A Bruker BioSpec 4.7T 40 cm MRI Scanner (Bruker: MA) scanned the mice. The scans were enhanced with T2 contrast enhancement, using a multi-echo spin-echo sequence based on Rapid Acquisition with Refocused Echoes (RARE) factor of 4. Four averages were obtained, with repetition time 1,500 ms and echo time 8 ms. Motion suppression was enabled. The matrix size was 256×192 with field of view 4×4 cm. The slice thickness was 0.75 mm and total acquisition time 4′48″ for each calf muscle observation.

4.3.3 Results and Discussion

Figure 4.3 shows the percent change from baseline for calf muscle volume from day 0 to week 12 with treatment period from day 0 to week 4 and washout period from weeks 4 to 12.

4.3.3.1 Pharmacometric Model Development

Serum pharmacokinetics of the10B3 mAb obtained from a satellite study of male C57BL/6 dosed with 0.1, 1, or 10 mg/kg single dose IP ($n = 4$/time point) were well described by a mamillary model with (1) depot, (2) serum, and (3) peripheral compartments. In Fig. 4.4, the PK model is described by absorption rate constant (Ka), central volume of distribution (V1), linear clearance (K), Michaelis-Menten maximal velocity (Vm) and serum concentration at half-maximal velocity (Km)

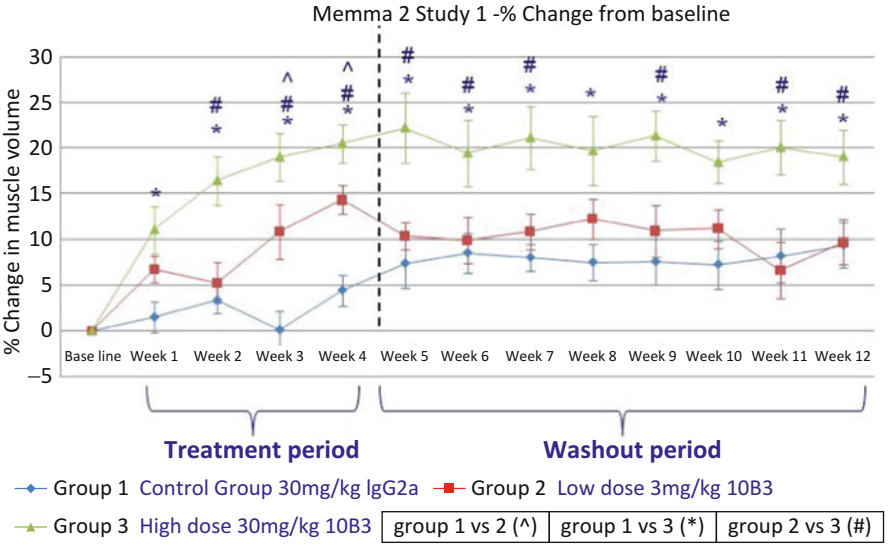

Fig. 4.3 Calf muscle volume percent change from baseline from day 0 to week 12 with treatment period from day 0 to week 4 and washout period from weeks 4 to 12 for C57BL/6 male mice dosed with 3 or 30 mg/kg 10B3 or IgG2a control IP on days 0, 4, 7, 14, and 21

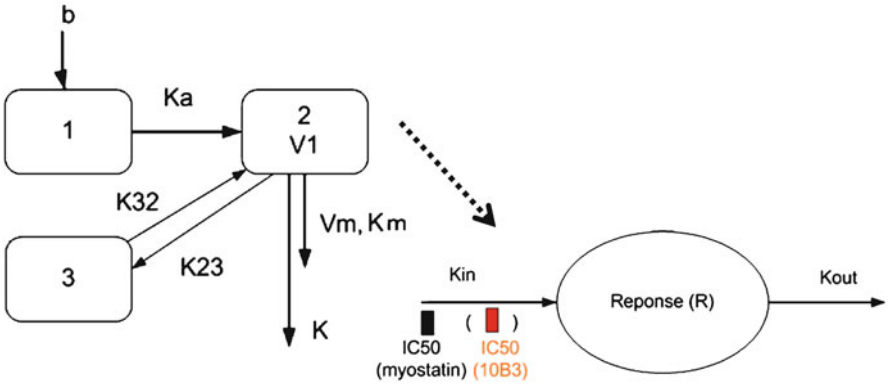

Fig. 4.4 Sequential indirect response pharmacometric model with competitive antagonism

(Gibiansky et al. 2008), central-to-peripheral rate constant (K23), and peripheral-to-central rate constant (K32).

Since the mAb (10B3) is a competitive antagonist of a negative regulator of muscle growth (myostatin), the time course of calf muscle growth in male C57BL/6 mice was well described by a sequential indirect response pharmacometric model (Sharma and Jusko 1998) developed in NONMEM VI software (ICON: NJ). The model structure is depicted in Fig. 4.4, where 10B3 antagonizes the negative muscle growth regulation of myostatin in terms of Loewe additive response.

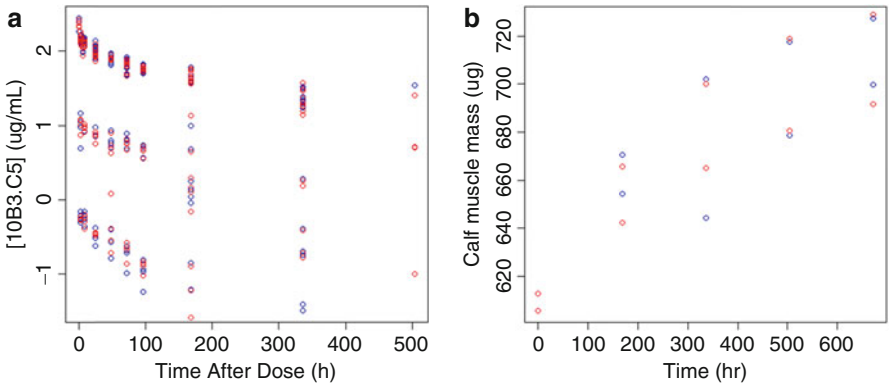

Fig. 4.5 Observed and predicted mean (**a**) PK in male C57BL/6 mice dosed with 0.1, 1, or 10 mg/kg IP single dose ($n=4$/time point) and (**b**) calf muscle volume PD profile in male C57BL/6 mice dosed with 3 or 30 mg/kg on days 0, 4, 7, 14, and 21 ($n=6$/group) (*blue* observed, *red* predicted)

The natural muscle growth response is produced at an input rate constant (Kin) and turns over at output rate constant (Kout). Myostatin inhibits muscle growth with serum concentration at half-maximal inhibition (IC50,myostatin) while 10B3 antagonizes myostatin at half-maximal concentration (IC50, 10B3); PD model parameters include the maximal inhibition of muscle growth (Imax) and maximal muscle growth (Emax). Since the mice are growing, the PD model may not be in initial homeostasis.

Figure 4.5 shows good agreement between the observed and predicted mean PK profile in male C57BL/6 mice dosed with 10B3 0.1, 1, or 10 mg/kg IP single dose ($n=4$/time point) and observed and predicted calf muscle volume PD profiles in male C57BL/6 mice dosed with 10B3 3 or 30 mg/kg IP on days 0, 4, 7, 14, and 21.

The maximal lean muscle mass decrease versus increase of soleus, gastrocnemius, quadriceps, and tibialis anterior muscle for sedentary myostatin transgenic and conditional knockout mice relative to wild-type mice at necropsy was well described by a straight line of slope 0.706 ± 0.198, with adjusted $R^2 = 0.79$. The muscle mass increase is in qualitative agreement with the mean cross-sectional area of Type 2 muscle fiber in C57BL/6J mouse soleus, gastrocnemius, and tibialis anterior muscles (Fig. 4.6) (Augusto et al. 2004).

4.3.3.2 Translation to Human

The target therapeutic profile requires that efficacious treatment of patients with 25 % muscle loss should reverse the muscle loss within 24 weeks of treatment with onset of clinical benefits within 5 weeks after first dose.

Each parameter in the PK/PD model was translated from 25 g mouse to 70 kg human according to allometric scaling of passive processes (Mager et al. 2009) to

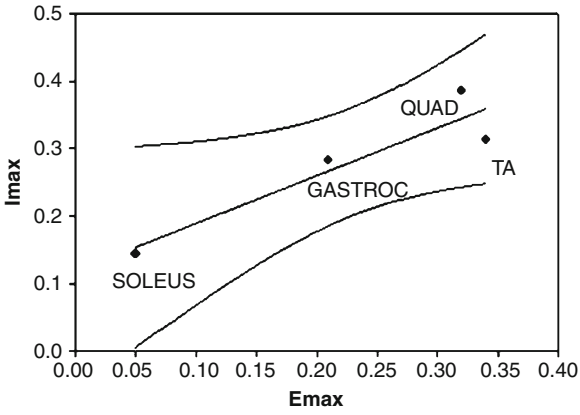

Fig. 4.6 Maximal muscle mass decrease (Imax) versus increase (Emax) for sedentary myostatin transgenic and conditional knockout mice. The *curved lines* represent a 90 % prediction interval

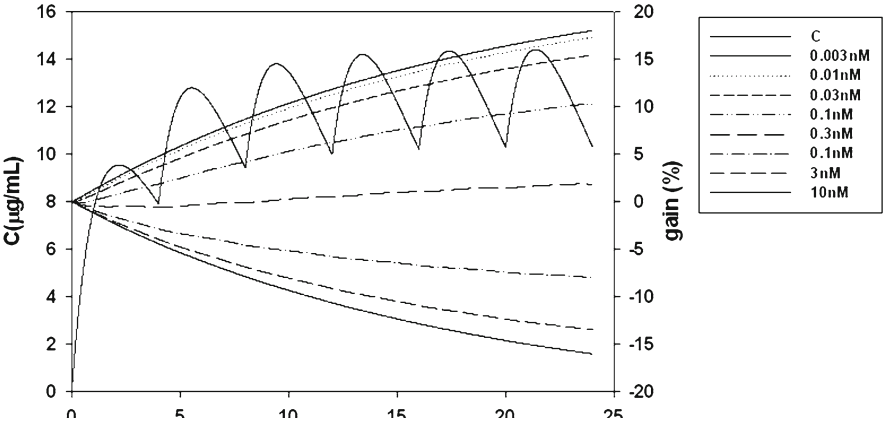

Fig. 4.7 Predicted gain in gastrocnemius muscle mass by design IC_{50} for 70 kg human disease model dosed with 5 mg/kg every 4 weeks for 24 weeks

provide a predictive PK/PD model using Berkeley Madonna software (University of California, Berkeley, CA).

Figure 4.7 shows the PK and predicted gain in gastrocnemius muscle mass for a 70 kg diseased human with initial myostatin levels sufficient for almost maximal muscle wasting (25 %), dosed with 5 mg/kg every 4 weeks for 24 weeks of a prospective humanized mAb directed against myostatin, where the linear regression shown in Fig. 4.6 translated the predicted gain in tibialis anterior (calf) muscle mass to gastrocnemius muscle mass.

According to the target therapeutic profile, efficacious treatment with therapeutic mAb directed against myostatin may require the development of a humanized mAb with 0.03–0.1 nM affinity.

4.3.3.3 Limitations

Limitations of this method include (a) the MRI instrumentation may limit the size of animal that may be imaged, (b) the development of a pharmacometric model requires mechanistic understanding of the biological effect and drug metabolism, and (c) translation of the pharmacometric model to human requires assumptions about scaling and careful consideration of interspecies similarities and differences.

4.4 Example 3: Magnetic Resonance Imaging of Relapsing-Remitting Multiple Sclerosis Patient Brain

4.4.1 Rationale

Multiple sclerosis (MS) is a multifocal, heterogeneous, progressive neurological disease characterized by inflammation, demyelination, and gliosis of the central nervous system (CNS). Although the etiology of MS remains unknown, convergent lines of genetic, immunological, and epidemiological evidence suggest that tissue injury results from a misdirected immune response triggered by "nonself" antigens that mimic constitutive peptides of myelin. Relapsing-remitting multiple sclerosis (RRMS) is specifically characterized by unpredictable exacerbation of symptoms (relapse), followed by periods of remission, during which any deficits from the relapse may recover with or without sequelae.

Ofatumumab is a novel IgG1κ lytic monoclonal antibody (mAb) that specifically binds to the human CD20 antigen of which expression is restricted to B lymphocytes from the pre-B-cell stage to the plasmacytoid immunoblast stage only. A recent trial with an anti-CD20 mAb (rituximab) demonstrated that targeting B cells reduces the number of gadolinium-enhancing (GdE) T1 lesions and the relapse rate in relapsing-remitting multiple sclerosis (RRMS). Ofatumumab has been shown to be both well tolerated and efficacious in several diseases, including a small, placebo-controlled trial in RRMS known as OMS11502 (also known as GEN414) (Sorensen et al. 2010).

This section discusses pharmaco-imaging methods that demonstrate clinical target engagement and pharmacokinetics and provide guidance for the design of clinical trial OMS112831 in relapsing-remitting multiple sclerosis patients by translation of ofatumumab from rheumatoid arthritis to relapsing-remitting multiple sclerosis.

4.4.2 Materials and Methods

1. Human model: patient with relapsing-remitting multiple sclerosis.
2. Imaging method and materials.

Subjects received monthly MRI brain scans from screening to 48 weeks after first dose, followed by an individualized follow-up period. Imaging analysts counted the number of new T1 Gd-enhancing lesions and new or enlarging T2 lesions at each scan relative to the previous scan.

4.4.3 Results and Discussion

Study OMS112831 is a double-blind, placebo-controlled, parallel-group study that will investigate the safety and efficacy of a subcutaneous formulation of ofatumumab in the treatment of subjects with RRMS. The primary objective of the study is to investigate efficacy as assessed by magnetic resonance imaging. Other objectives will include evaluation of tolerability/safety, dose-response relationship, pharmacokinetics, pharmacodynamics, exposure-response, as well as other clinical endpoints.

Figure 4.8 shows raw summary statistics for ofatumumab study OMS115102 (GEN 414) that highlight the minimal amount of observed new MRI lesion activity following administration of IV ofatumumab in both the week 0–24 and week 24–48 treatment periods. Although driven largely by one subject with 88 lesions, the mean number of new T1-weighted GdE lesions for the overall placebo group was 9.69 lesions. The effect of ofatumumab on total T1-enhancing lesions, new and/or enlarging T2 lesions, and new T1 hypointense lesions with very low MRI activity in treated subjects was similar to that seen on new T1 GdE lesions.

The only available data on subcutaneous ofatumumab administered to human is from the study OFA110867 in rheumatoid arthritis (RA) patients. The majority of adverse events (AEs) in OFA110867 were mild or moderate in intensity. Post-injection systemic reactions (PISRs) were more frequent for the combined active (13/27; 48 %) than placebo (2/8; 25 %) group. Overall, safety data indicate that doses up to 60 mg SC single dose were well tolerated with acetaminophen and antihistamine pre-treatment.

At the relatively low doses projected in study OMS112831, no lesion count dose-response information is available for ofatumumab in any clinical or preclinical model. We designed the trial by clinical trial simulation by translating a pharmacometric disease model for subcutaneously administered ofatumumab from RA to RRMS.

4.4.3.1 Pharmacometric Model Development in Patients with Rheumatoid Arthritis

Data from a rheumatoid arthritis (RA) single SQ dose study (study OFA110867) and a pharmacometric model derived from models submitted to BLA 125,326 form the basis of dose predictions for this protocol. The RA study is the starting point for modeling for four reasons:

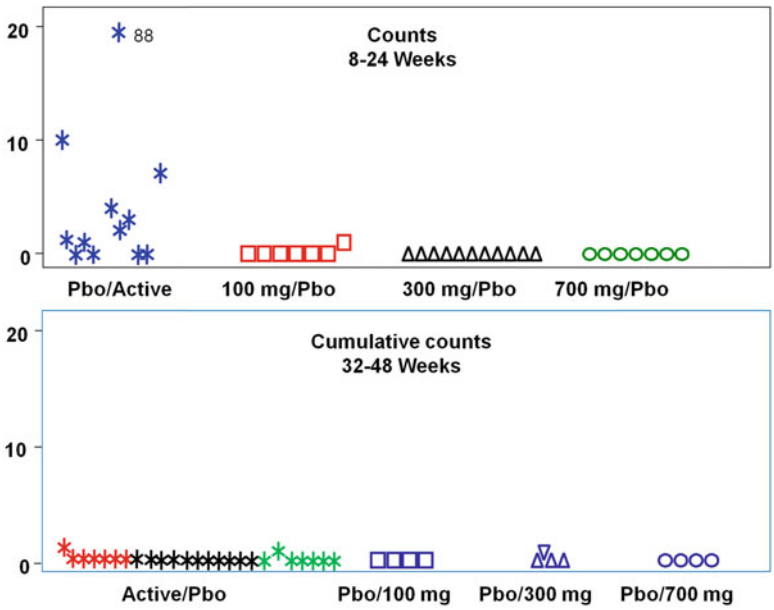

Fig. 4.8 Raw summary statistics for OMS115102 cumulative new T1 Gd-enhancing lesions

- OFA110867 is the only subcutaneously administered ofatumumab study available.
- A unified PK/PD model has been developed from an IV model reported to the FDA for RA, CLL, and FL indications, and this model well describes the relationships between dose, instantaneous concentration, and peripheral CD19+ B-cell count for the RA population.
- The OMS115102 concentration and CD19+ B-cell data do not permit detailed modeling of this PK/PD relationship from OMS115102 data alone.
- The relationship between bioavailability and dose may be complicated by the likelihood that ofatumumab substantially depletes lymphatic B cells before entering systemic circulation.

The choice of the study OFA110867 as basis for modeling likely reflects a conservative viewpoint relative to RRMS. First, the placebo cohort of the OFA110867 study shows peripheral CD19+ B-cell counts that increase with time and may not be in homeostasis because of systemic inflammation related to aggressive lymphoproliferation. Therefore, the same dose to MS patients may result in somewhat higher systemic concentration of ofatumumab and more depletion of peripheral B cells because the peripheral B cells may not proliferate so rapidly in MS as in RA.

4.4.3.2 Translation to Patients with Relapsing-Remitting Multiple Sclerosis

Depleting the $CD20^+$ B-cell subset reduces the supply of mature B cells (including pathogenic B cells) for migration across the blood-brain barrier, clonal expansion, and differentiation into plasma or memory cells.

Kuenz et al. reported that cerebrospinal fluid (CSF) B cells correlated with early brain inflammation in multiple sclerosis including number of GdE lesions, while Petereit et al. observed that reduction in lesion number correlated with reduction in CSF B-cell count (Kuenz et al. 2008; Petereit and Rubbert-Roth 2009).

Kuenz et al. further reported that "new focal white-matter lesions appear to develop following new waves of inflammation, involving immune cells which enter the brain from the peripheral blood and cause major blood-brain barrier leakage mediated by matrix metalloproteinases (MMP)." Sormani et al. reported that the statistical distribution of new GdE lesions observed during a 24-week period was well described by a negative binomial distribution with expected value $\mu = 13.0$ and over-dispersion parameter $\Theta = 0.52$ in RRMS patients not required to have enhancing brain lesions at baseline with monthly MRI scanning over 24 weeks (Sormani et al. 2001).

These observations support the notion that selective recruitment of immune cells across the blood-brain barrier occurs in almost discrete events with an average inter-event interval of about 22 weeks, according to a Gamma-Poisson mixture model. The Sormani et al. model provides a statistical link for the mean rate of incidence of new GdE lesions and pharmacometric model predictions of the reduction in count of peripherally activated pathogenic B or T cells that have migrated into the CSF.

Petereit and Rubbert-Roth showed that the observed rituximab plasma to CSF concentration ratio for subjects with a normal blood-brain barrier is about 0.1 %; the expectation for ofatumumab is similar (Petereit and Rubbert-Roth 2009). Normal healthy serum to CSF ratios are about 230:1 for albumin and 369:1 for IgG in the absence of intrathecal IgG synthesis (Tourtellotte 1975). Hence, for subjects with moderate to severe impairment of the blood-brain barrier corresponding to an albumin index of 14–30 (Cook 2006), the ofatumumab plasma to CSF concentration ratio is predicted to be in the range of about 0.87 % to about 1.87 %, based on the *assumption* that plasma to CSF ratios are reasonably close to serum to CSF ratios.

The pharmacometric model therefore postulates a mechanism of lesion formation based on selective recruitment of a very small fraction of pathogenic immune cells across the blood-brain barrier. A key assumption of the kinetics argument is that, if peripheral B cells are implicated in production of the pathogenic immune cells, the production rate of pathogenic immune cells may reasonably be proportional to the instantaneous peripheral B-cell count. If the pathogenic immune cells that have migrated across the blood-brain barrier are implicated in the development of lesions, it is a reasonable kinetic assumption that the production rate of inflammatory (GdE) lesions be proportional to their count, so the cumulative number of inflammatory lesions may be proportional to the exposure to these pathogenic immune cells in CSF.

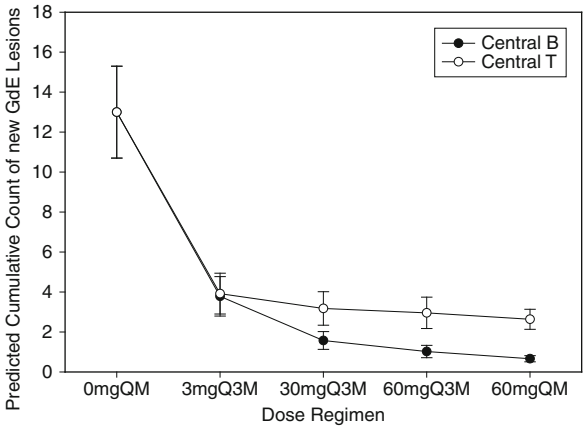

Fig. 4.9 Predicted geometric mean and standard error of estimate of cumulative new Gd-enhancing lesion count over 24 weeks, based on predicted count of peripherally activated pathogenic B or T cells that have migrated into CSF

The model assumes that the T cells are antigen-primed CD4+ cells of CD45RO CCR7^{+} phenotype with mean proliferation and disappearance rates according to Table 2 of Macallan et al. (2004). The uptake rate constants for pathogenic T- or B-cell migration across the blood-brain barrier were based on the respective in vitro migration rates in the presence of both TNF-α and IFN-γ cytokines reported by Alter et al. (2003).

The pathogenic memory B cells are considered to turnover in CSF at the rate estimated for peripheral CD19^{+} B cells in study OFA110867 and to be cleared by ofatumumab by the antibody-dependent cell-mediated cytotoxicity (ADCC) pathway at a rate corresponding to in vitro studies.

The model assumes that pathogenic memory B cells will not proliferate unless they encounter a specific antigen or nonspecific infection that triggers proliferation via antigen binding or toll-like receptor 9 (TLR9) pathways. The model further assumes that the instantaneous mean incidence rate of GdE lesions is proportional to the count of peripherally activated pathogenic T or B cells present in CSF.

The initial distribution of peripheral CD19+ B cells is drawn from a lognormal distribution with expected value $\mu = 198$ GI/L and standard deviation 0.403 on the logarithmic scale obtained by a maximum likelihood fit to the baseline peripheral CD19+ counts observed for the 100 mg cohort of study OMS115102 in RRMS subjects.

Figure 4.9 shows the predicted geometric mean and standard error of new GdE lesions based on the reduction of pathogenic T and B cells present in CSF that have been selectively recruited across the blood-brain barrier via adhesion and the negative binomial distribution for RRMS patients not required to have enhancing brain lesions at baseline, as reported by Sormani et al. (2001).

The pharmacometric model may explain delayed relapse in terms of CSF pathogenic B or T cell proliferation triggered by specific antigen exposure or external event such as infection. In principle, repopulation of peripheral immune cells is necessary but not sufficient for relapse to occur. An external stimulus may be required to trigger rapid proliferation and relapse even after repopulation of CSF B or T cells.

A low uptake rate constant may explain delayed repopulation of pathogenic immune cells in CSF including B cells and T cells. The natural rate of central memory immune cell turnover may explain delayed eradication of pathogenic immune cells from CSF.

4.4.3.3 Dose Rationale

While the 3, 30, and 60 mg single SQ doses were all well tolerated in study OFA110867, the 3 mg single dose was the most tolerable. The OMS112831 study investigates the use of a single 3 mg dose ("conditioning dose") prior to a 30 mg or 60 mg dose in half of the subjects receiving those doses. The intent of the single SQ 3 mg conditioning dose is to reduce cytokine-release reaction to subsequent larger doses by depleting peripheral $CD20^+$ B cells by about 50 % over about 6–9 days, thereby enhancing tolerability.

The purpose of the 3 mg SQ arm is to explore the efficacy of sub-depleting doses (<95 % depletion of peripheral B cells) and to provide information helpful to dose-response and exposure-response modeling. According to the predictive pharmacometric model, the expected reduction of new enhancing T1 lesion burden at week 24 for subjects dosed with placebo at week 0 and 3 mg SQ at week 12 is 55.2 % with 90 % confidence interval 44.7–67.4 %, a response that was observed with currently available first-line MS disease-modifying therapies in their phase II studies. Rituximab data suggest that efficacy in suppressing lesions was maintained through repletion to peripheral B-cell levels ~30 % of LLN (Hauser et al. 2008).

The choice of 30 mg dosed quarterly was because it is the lowest quarterly dose which is likely to continuously maintain at least 95 % peripheral $CD20^+$ B-cell depletion in at least 90 % of the subjects. The choice of 60 mg as the upper dosing cohorts was based on findings that this dose displayed similar peripheral B-cell depletion to 100 mg (the highest dose tested in OFA110867) while appearing to have better tolerability. For the 60 mg monthly cohort, the expected rate of peripherally activated T- and B-cell migration across the blood-brain barrier is very small based on the predicted extensive peripheral B-cell depletion. Although moderate B-cell depletion in the CSF (and perhaps CNS) is possible via ADCC in accordance with the sigmoid Emax model of Bleeker et al., the expectation is that it will not be robust or complete (Bleeker et al. 2007). The 60 and 30 mg arms are expected to deplete peripheral B cells to reduce activation of pathogenic T and B cells (via reduced antigen presentation or regulatory T-cell augmentation) to levels similar to those expected for the efficacious dose in OMS115102 100 mg Q2Wx1. Although the present study duration is only 24 weeks, Fig. 4.10 shows the predicted survival curve for the time to replete peripheral blood CD19+ B cells to LLN (110 cells/μL) after dosing RRMS subjects with SQ ofatumumab in a clinically realistic scenario of treatment discontinuation after one full year of real-world treatment, when steady state has been reached. Note that for doses greater than 3 mg SQ, the predicted time to repletion of peripheral $CD19^+$ B cells to lower limit of normal (LLN: 110 cells/μL) after the last dose exceeds (approximately) 20 weeks. In study OFA110867,

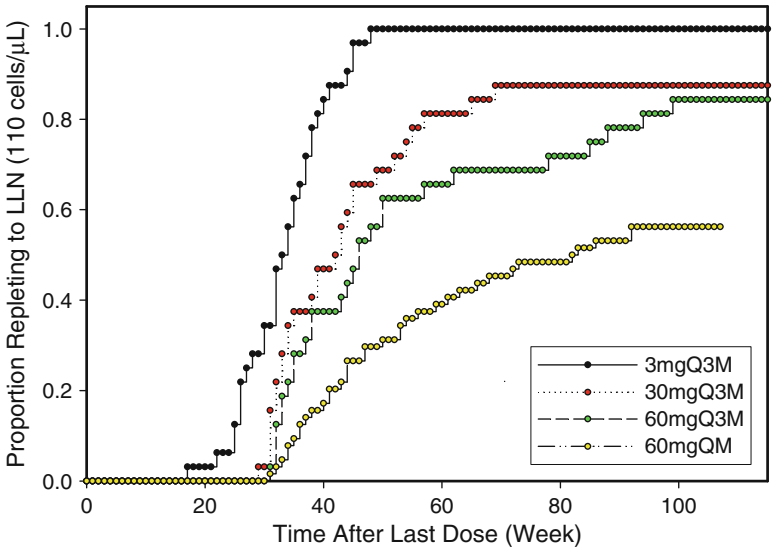

Fig. 4.10 Predicted survival curve for the time to replete peripheral blood CD19+ B cells to LLN (110 cells/μL) in a clinically realistic scenario of treatment discontinuation after 1 full year of real-world treatment

the shortest time to the start of repletion was about 43 days for the 3 mg and 30 mg doses and 57 days for the 60 mg dose, comparable with typical life span of a mature circulating B cell. The OMS112831 doses support dose selection for phase III studies. The predictive pharmacometric model supports a monotonic relation between mean reduction in new enhancing T1 lesion burden and cumulative dose, with 90 % prediction interval including ofatumumab dosed at 10 mg Q3M SQ to 40 mg Q3M SQ for the dose that results in >90 % reduction in new enhancing T1 lesion burden. Repetition of these doses at 3-month intervals, or the lesser of time to repletion of B cells to peripheral LLN, allows partial repletion of peripheral B cells and may provide some level of adaptive immunity against infections (including JC virus variants) that may trigger relapse by opening the blood-brain barrier or by activating pathogenic immune cells expressing TLR9.

4.4.3.4 Limitations

Limitations of this method include (a) the development of a pharmacometric model requires mechanistic understanding of the biological effect and drug metabolism and (b) translation of the pharmacometric model to human requires assumptions about scaling and careful consideration of interspecies similarities and differences.

4.5 Conclusions and Future Directions

Each example highlights the role of pharmaco-imaging to provide noninvasive pharmacodynamic or pharmacokinetic:parmacodynamic (PK/PD is a standard nomenclature) assessments in clinical and preclinical drug development. The detailed relation between short-term assessments and long-term disability measured by clinical score remains to be firmly established in longer-term studies, for translation of muscle hypertrophy in young, growing mice to clinical scores of disability in the sarcopenic hip-fracture patient population and for the relation between lesion counts and clinical scores of long-term disability status such as the Expanded Disability Status Scale (EDSS) in the relapsing-remitting multiple sclerosis patient population.

Acknowledgments The ADAM TS 5 PK study was designed by a GlaxoSmithKline(GSK) team including Elefante, L.; Freedman, I.; Larkin, J.; Liu, F.; Lohr, T.; Matheny, C.; and White, J.

The anti-myostatin PK/PD study "memma2" was designed by a GSK team including Ashman, S.; Chagani, K.; Freedman, I.; and Reid, J.

The OMS112831 study was designed by a GSK team including Bhangu, S.; Carranza, J.; Derosier, F.; Depew, C.; Edwards, T.; Freedman, I.; Grove, R.; Hall, A.; Herrera, P.; Hill-Zabala, C.; Lopez, M.; Nichols, L.; Rogers, R.; Schifano, L.; Schindielorz, A.; Sue-Ling, K.; Tolson, J.; and Watson, D.

References

Alter A, Duddy M, Hebert S et al (2003) Determinants of human B cell migration across brain endothelial cells. J Immunol 170(9):4497–4505

Augusto V, Padovani CR, Campos GER (2004) Skeletal muscle types in C57BL/J mice. Braz J Morphol Sci 21(2):89–94

Bleeker WK, Munk ME, Mackus WJM et al (2007) Estimation of dose requirements for sustained in vivo activity of a therapeutic human anti-CD20 antibody. Br J Haematol 140:303–312

Cook SD (2006) Evidence for an infectious etiology of multiple sclerosis. In: Cook SD (ed) Handbook of multiple sclerosis, 4th edn. Taylor & Francis, New York

Gibiansky L et al (2008) Approximations of the target-mediated drug disposition and identifiability of model parameters. J Pharmacokinet Pharmacodyn 35(5):573–591

Hauser SL, Waubant E, Arnold DL et al (2008) B-cell depletion with rituximab in relapsing-remitting multiple sclerosis. N Engl J Med 358:676–688

Kuenz B, Lutterotti A, Ehling R et al (2008) Cerebrospinal fluid B cells correlate with early brain inflammation in multiple sclerosis. PLoS One 3(7):e2559

Macallan DC, Wallace D, Zhang Y et al (2004) Rapid turnover of effector memory CD4+ T cells in healthy humans. J Exp Med 200(2):255–260

Mager DE, Woo S, Jusko WJ (2009) Scaling pharmacodynamics from in vitro and preclinical animal studies in humans. Drug Met Pharmacokinet 24(1):16–24

Petereit HF, Rubbert-Roth A (2009) Rituximab levels in cerebrospinal fluid of patients with neurological autoimmune disorders. Mult Scler 15(2):189–192

Savage VM et al (2004) The predominance of quarter-power allometric scaling in biology. Funct Ecolo 18(2):257–282

Sharma A, Jusko W (1998) Characteristics of indirect pharmacodynamics models and applications to clinical drug responses. Br J Clin Pharmacol 45(3):229–239

Sorensen PS, Drulovic J, Havrdova E (2010) Magnetic resonance imaging (MRI) efficacy of ofatumumab in relapsing-remitting multiple sclerosis (RRMS)—24-week results of a phase II study. In 26th Congress of the European Committee for Treatment and Research in Multiple Sclerosis (ECTRIMS), Oct 13–16, 2010 , Gothenburg: SE

Sormani MP, Bruzzi P, Rovaris M et al (2001) Modelling new enhancing MRI lesion counts in multiple sclerosis. Mult Scler 7:298–304

Tourtellotte WW (1975) What is multiple sclerosis? Laboratory criteria for diagnosis. In: Davison AN, Humphrey JH, Liversedge AL et al (eds) Multiple sclerosis research, HMSO, London, p 9

West GB, Brown JH, Enquist BJ (1997) A general model for the origin of allometric scaling laws in biology. Science 276(5309):122–126

Chapter 5
The Role of Pharmacokinetics and Allometrics in Imaging: Practical Issues and Considerations

Brian R. Moyer

Abstract "Disease" can be best defined as a complex array of biological activities which are all relational to the underlying changes in the normal physiology of the species. The study of disease from infections to tumors, from mice through various species, is fraught with significant differences in tissue and organ blood flow, organ sizes, physiologic functional differences, metabolic biomarkers, structural uniqueness ("lock and key" receptor specificity), varied and unique immunologic responses, and indeed all of these partake in some manner in the control and definition of each species. The goal of imaging is to provide either some key biomarker or metabolite that provides translational time–activity responses or anatomical distinctions over time that reflect the natural history (NHx) of a disease or ways to describe the biologic changes that are in question as a result of pathology. Allometric analysis thus may be necessary in the selection of dosing where target saturation may be important, species show variation in target affinities, imaging is time dependent and physiologic "clocks" vary, and many other considerations. This chapter attempts to describe such situations as well as currently used approaches.

5.1 Introduction: Dose Selection in the Nonclinical to Clinical Settings

In 2006 a clinical trial was held for a new monoclonal antibody, a humanized IgG4/kappa monoclonal Antibody (Ab), that binds to the human CD28 receptor. As an IgG4 Ab it binds with low affinity to Fc-receptors and does not mediate ADCC or CDC activity. The antibody under study was TGN1412 sponsored by TeGenero AG

[*] **Electronic supplementary material** The online version of this chapter (DOI 10.1007/978-1-4614-8247-5_5) contains supplementary material, which is available to authorized users.

B.R. Moyer (✉)
BRMoyer & Associates, LLC, 23 Hawk Drive, Bedford, NH 03110, USA
e-mail: bmoyernh@gmail.com

B.R. Moyer et al. (eds.), *Pharmaco-Imaging in Drug and Biologics Development*,
AAPS Advances in the Pharmaceutical Sciences Series 8, DOI 10.1007/978-1-4614-8247-5_5,

(Rellahan 2009). Six subjects in a Phase 1 dose escalation trial received the drug at a starting dose of 0.1 mg/kg. The subjects were separated in time by 10 min each for their dose. The dose was determined to be a non-risk dose from work performed in animal studies. All six subjects elicited adverse events within 90 min post dose administration and these became progressively worse with organ failures by 21 h post administration. Suntharalingam et al. (2006) described the cytokine storms elicited in these patients over the initial day of events. The animal to human dose translation was not effective and the result was a superagonistic anti-CD28 antibody. Where a typical T-cell receptor (TCR) activation requires two signal functions (TCR engagement followed by co-stimulatory receptor engagement, i.e., C80/86 engagement), TGN1412 was capable of directly stimulating the TCR via the CD28 site without a co-stimulatory requirement resulting in an uncontrolled cytokine storm. The injuries in this trial were not caused by product impurities, product quality—the injuries were due to the product's in vivo human bioactivity—a function that was controllable by a better predictive starting dose. As we move imaging into the realm of preclinical testing of especially biologics for approval, the PK dose translation must be respectfully considered.

Could this unfortunate event have been predicted pharmacologically and an appropriate dose surmised using allometrics? That is debatable, but in the imaging world we are faced with risk of human dose extrapolation from animals all the time as we are employing many different assumptions of product safety and efficacy into the clinical setting. This chapter is intended to introduce the reader to the concept of dose scaling and minimization of risk in determining the appropriate dose of an imaging agent with respect to dosimetry for nuclear imaging agents, and safety for those imaging agents requiring higher molar quantities for their practical applications. Prediction of animal safety of a given product is a textbook all to itself but we will touch here on ways of thinking and expressing drug safety that should be part of every imaging scientist's vernacular. Estimating the inter species differences in drug behavior has been a challenge for many years (Boxenbaum 1984). Taking the comparative measurements of rate constants, receptor affinities, physiologic differences in clearance, and many other parameters allows the drug developer to have a relatively good estimate for the starting dose in human studies but it remains a "work-in-progress" discipline (Radziszewski et al. 2009).

The use of imaging in drug or biologics development is clearly to identify supporting mechanisms of action and demonstration of positive alterations in the natural history of disease in response to the use of a therapeutic (Moyer and Barrett 2009). Figure 5.1 describes the connectivity of pharmacokinetic (PK) and pharmacodynamic (PD); and toxicokinetic (TK) activities at a high level. It should be noted that the prominent point of connectivity in the figure is "time". The issue of a single point in time—even compared to a baseline value—may not be sufficient to defend the outcome of an imaging endpoint in support of a regulatory filing for approval of a drug or biologic, potentially even for an IND. Imaging, like PK, PD, and TK should be exploited with relation to time.

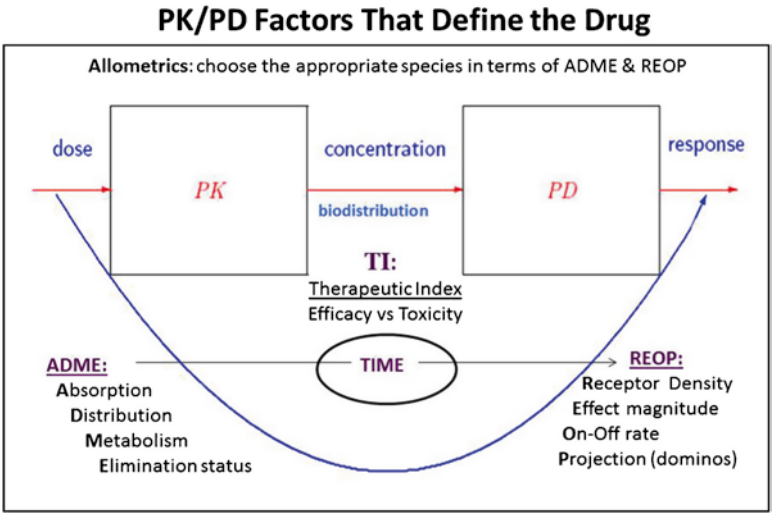

Fig. 5.1 A schematic portrayal of the relationship of PK (ADME terms) and PD (REOP terms) on the in vivo biological activity of a drug, biologic or xenobiotic. ADME (absorption, distribution, metabolism, elimination), TI (Therapeutic Index; see Muller and Milton 2012) and REOP (receptor occupancy, response or effect magnitude, binding avidity, and projection or cascade effects) are key elements in the description of a drug and biologic's behavior in different species

5.2 Pharmacokinetics and Toxicokinetics: Importance in Imaging

A dose of a "drug" enters the body and is affected by factors of physical chemistry and biology from solubility through uniqueness of binding to a pharmacologic target. These activities are concentration dependent, dispersedly controlled to a unique biodistribution by actions of molecular charge, solubility, nonspecific binding and blood flow (biodistribution), pathophysiology affecting biological binding (enhanced or decreased), and governed by the coincident activity of elimination which decreases the drug's bioavailability. PK analysis tells you how to interpret, and indeed predict, your PD and TK observations.

Pharmacokinetics is indeed a mathematical attempt to define biology in engineering terms. The input–output models of environmental scenarios, manufacturing control systems, electronic bread-board designs, and ***BIOLOGY*** are all capable of being described in mathematical terms. Figure 5.1 implies this relationship and the insight of the time rate of change of a drug or biologic allows us to predict exposure of a target to a drug where a concentration-dependent response, or a pharmacologic dynamic outcome, can be predicted. The binding affinity of a receptor for a specific

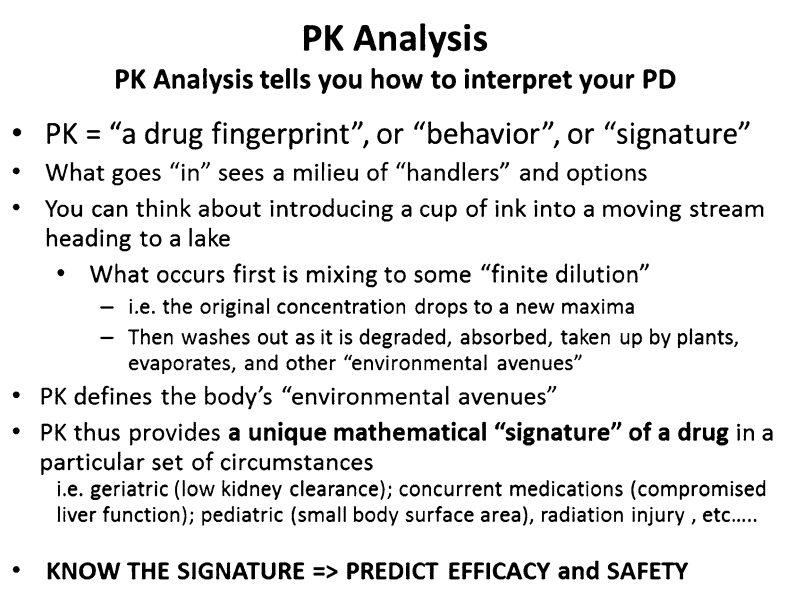

Fig. 5.2 Drug signature. The ability to define a drug or biologic's unique "signature", e.g., behavior in a defined biologic system (i.e., murine, canine, NHP, human models, etc.), is an important key to the proper selection of an imaging platform as well as use of imaging tracers or contrast agents in nonclinical studies. A close and analytic inspection of the "environment" a drug is to be introduced (aka the specific pathology) and the relationship the dose has in describing or assisting in drug development of human-need pharmaceuticals is not to be minimized

drug may be known to occur in vitro at the micromolar (μM) range. Following administration by some route of entry (IV, IM, SC, IP, PO, etc.[1]), a distribution of a drug or biologic occurs to some limit of the concentration and at the target the drug or biologic may never achieves a specific molar concentration (i.e., under dosing) due to species metabolic capability, alternate affinities lower affinities but far more abundant nonspecific targets and which have a more flow-dependent availability or elimination (species related renal and hepatic blood flow, immunologic consumption, etc.). The prediction of a pharmacokinetic response, i.e., the assignment of specific pharmacokinetic terms called "parameters", each of which have mathematical relationships to each other provides us with the ability to predict pharmacodynamic or toxicologic responses (Boisell et al. 2008). Through the determination of a "drug signature", as defined by these parameter estimates in Fig. 5.2, we have a unique tool to define drug responses, biologic activity and, in totality, the pharmacodynamics of biochemical entities.

The absorption and elimination of a drug or biologic is defined using a time–activity profile with examples defined in Fig. 5.3. The administration of a drug or biologic into a species of choice results in a concentration gradient from the point

[1] IV, IM, SC, IP, PO, etc. refer to intravenous, intramuscular, subcutaneous, intraperitoneal, orally, etc., respectively.

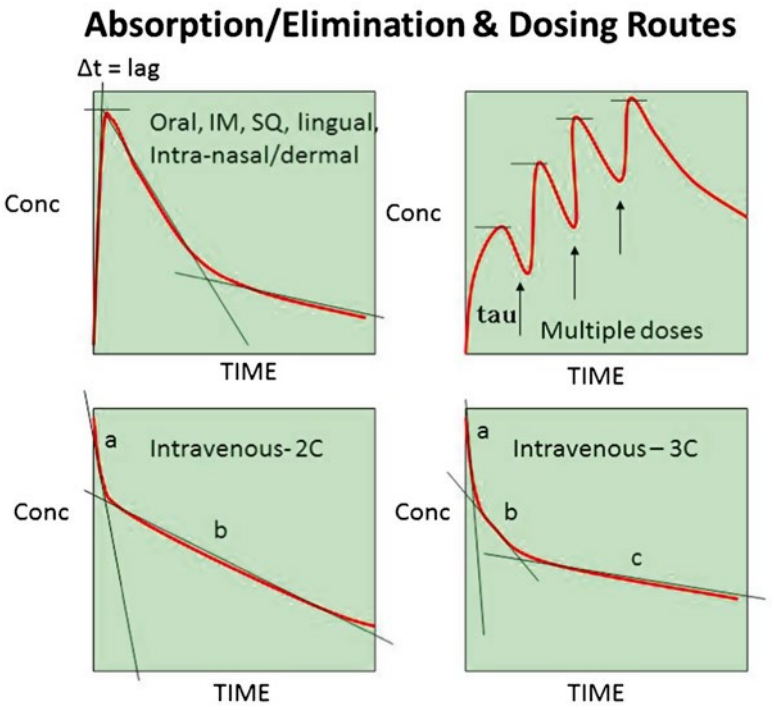

Fig. 5.3 Examples of the kinetic behavior of drug and biologics where we can express the change in time vs. change in concentration of "*x*" in volume or target "*y*" and these profiles can be described mathematically. The time–activity (time-conc) profile is the core of what imaging is trying to describe

of entry that moves immediately into both distributive and an elimination functions. An intravenously administered drug is an instantaneous delivery to the blood pool but the "instantaneous" is a bit misleading as, we recall from Fig. 5.2, a dilution of the concentrated "dose" has to occur in that "space" (region, compartment, pool, volume, etc.).

Physiologic approaches in pharmacokinetics interpret biology in an engineering manner where a flow diagram (Physiologic-Based Pharmacokinetic Modeling; PBMK; Fig. 5.4a, b) links an event-driven cascade (i.e., "dominos"; re. REOP, Fig. 5.2) where the tissues and organs of a species have finite boundaries of tissue weights, volumes, and rates of blood flow that contribute to a drug or biologic's unique "drug signature" (PK profile). To add to this complexity is the concept of drug-specific transporters. For a full treatise on the involvement of drug transporters and their importance in drug kinetics the reader is directed to the work of Giacomini and Sugiyama (2010). The PKPD paradigm is best described using a block diagram that in many ways ignores many subtle considerations in biologic systems such as immunologic consumption and indeed we can add a compartment for such an elimination mode. Similarly, we would add a new flow tag called "leak" showing product

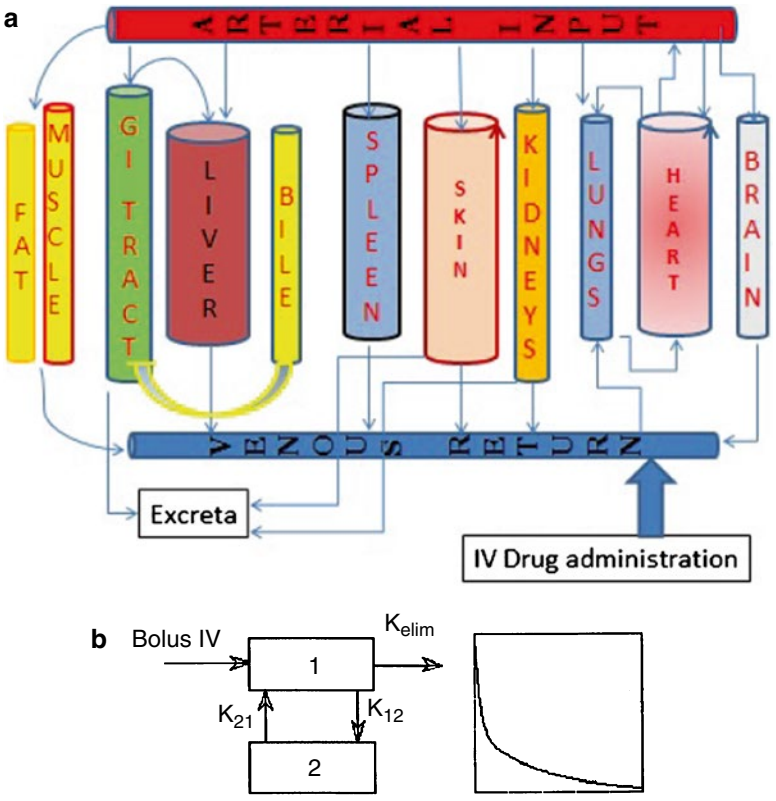

Fig. 5.4 A physiologic flow diagram translated to compartment modeling. (**a**) The PBPK model (physiologic-based pharmacokinetics) approach (A) bridges the input function of a drug or biologic added to the venous side (or arterial side) and the partition of the drug distribution by blood flow (physical compartments), the fractional distribution of the bolus into tissues (pharmacologic compartments), and metabolic behavior (chemical-dependent compartment) as defined by fractional organ flow, organ size, the rate constants across or into the organ system, and ratio of the organ to organ body weight or surface area. (**b**) A simple translation of the physical compartment model in A to define rate constants (*arrows*), as an engineering flow diagram, results in a biphasic time versus concentration elimination curve

loss occurring in a flow diagram of a manufacturing process or a municipal water system that has a broken pipe and loss "X" to the expected flow of total effluent is accounted. The use of a drug or biologic is highly dependent on the pathology of interest and potentially other ongoing pathologies. An example was presented by Jaehde and Sorgel (1995) where they discussed the changes in PK parameter estimates in burn patients where the volume of distribution can be altered by changes in protein binding or a change (enlargement) in extracellular fluid volumes. Clearance can also change due to tubular secretion glomerular filtration, hepatic blood flow, drug metabolizing activity, protein binding, and new additional elimination pathways. Animal models for burns will vary considerably with major differences in allometric considerations.

Table 5.1 Physiologic parameters associated with seven representative species which are commonly used in medical imaging studies

Parameter	Mouse	Hamster	Rat	Rabbit	Monkey	Dog	Human
Body weight, g	22	150	500	2,330	5,000	12,000	70,000
Compartment Volumes, mL							
Plasma	1.0	6.48	19.6	70	220	500	3,000
Muscle	10	–	245	1,350	2,500	5,530	35,000
Kidney	0.34	1.36	3.65	15	30	60	280
Liver	1.33	6.89	19.55	100	135	480	1,350
GI Tract	1.5	12.23	11.25	120	230	480	2,100
Gut lumen	1.5	–	8.8	–	230	–	2,100
Heart	0.095	0.63	1.15	6	17	120	300
Lungs	0.12	0.74	2.1	17	–	120	–
Spleen	0.1	0.54	1.3	1	–	36	160
Marrow	0.6	–	–	47	135	120	1,400
Plasma Flow Rate, mL/min							
Plasma	4.38	40.34	84.6	520	379	512	3,670
Muscle	0.5	–	22.4	155	50	138	420
Kidney	0.8	5.27	12.8	80	74	90	700
Liver	1.1	6.5	4.7	177	92	60	800
Gut	0.9	5.3	14.6	111	75	81.5	700
Heart	0.28	0.14	1.6	16	65	60	150
Lungs	4.38	28.4	2.25	520	–	512	–
Spleen	0.05	0.25	0.95	9.0	–	13.5	240
Marrow	0.17	–	–	11	23	20	120

Table content adapted from: Mordenti 1986

Table 5.1 describes several physiologic parameters of selected species, including human. The body weights of seven species are described along with tissue and fluid compartment pool volumes and plasma flow rates for several selected tissues (compartments). Physiologic flow models are developed using laboratory animals and in principle allow one to scale up (using terms of engineering) to make predictive implications of drug behavior in humans (and other species; aka, predictive allometrics). The cancer therapeutic methotrexate has been extensively examined using these tools (refs from Table 5.1). The drug follows a multi-compartment distribution, linear protein binding, strong saturable protein binding, entero-hepatic recirculation, and other perturbations on physiologic functions and as such.

5.3 Concepts of Allometry (Dose Translation) in PK Analysis

Animal species commonly used in preclinical imaging studies (i.e., mice, rats, rabbits, monkeys, and dogs) do not always eliminate drugs at the same manner or rates that are observed in humans. Typically, the smaller the mammal the more rapid the species will eliminate drugs relative to that of larger mammals (O'Flaherty 1989;

Table 5.2 The Determination of the Km value for relational determination of doses across selected species; refer to the FDA Guidance 2005

Body Surface Area (BSA) and the Km Factor: Linearizing the PK Parameters			
The most common "Rosetta Stone" for species allometrics is body surface area (BSA)			
Adult human BSA = 1.6–1.7 m^2; rat = 0.025 m^2; mouse = 0.0066 m^2			
Species	**Body weight, kg**	**Surface area, m-sq**	**Km factor, kg/m-sq**
Mouse	0.02	0.0066	3.0
Rat	0.15	0.025	5.9
Monkey	3.0	0.24	12
Dog	8.0	0.40	20
Human, Child	20	0.80	25
Human, Adult	60	1.6-1.7	37

See the FDA Guidance (5541fnl.pdf; pg 7; July 2005)
To determine the dose from a mouse to a human:
Human dose equivalent (HDE) = 2nd species dose (mg/kg) × (Species Km/Human Km)
If the Murine dose for efficacy is 20 mg/kg = 20 mg/kg × 0.025 kg = **0.5 mg/mouse**
HDE = 20 mg/kg × (3/37) = 20 mg/kg × 0.081 = > 1.62 mg/kg × 70 kg = **113.4 mg/human**

Table 5.3 Development changes in body composition reported as percentage of total body mass (data from: Alcorn and McNamara 2003)

Age	Body mass (kg)	Water	Protein	Fat
Newborn, full term	3.5	74	11	14
4 months	7.0	61.5	11.5	27
12 months	10.5	60.5	15	24.5
Adult	70	55–60[a]		

[a]Obesity decreases the percentage of total body water

Mordenti 1986). Using this kind of information about species variance in drug elimination, drug elimination across species has been shown to be predictable, scalable and, in engineering terms, obeys the power equation $\boldsymbol{Y = aW^b}$. Early reports on pharmacokinetic scaling across species normalized the x- and *y*-axes to illustrate some degree of superimposability of the respective pharmacokinetic curves. The ultimate goal is to predict human pharmacokinetics and this superimposability was useful but not mathematically useful. The power function approaches have allowed unique expression of human parameter estimates to be determined. The allometry concept provides models beyond pharmacokinetics as models of cardiovascular functions also behave in power functions where energy of flow and turbulence are dissipated toward "terminal tubes" do not structurally or histologically vary with body size (capillary networks are in general, conserved). Allometry via power functions thus also provides a complete analysis of scaling relations for mammalian circulatory systems that appears to be in agreement with data (West et al. 1997). In more general terms, allometric models help predict structural and functional properties of vertebrate cardiovascular and respiratory systems, plant vascular systems, insect tracheal tubes, and other complex distribution networks.

Tables 5.2 and 5.3 are important and very useful key approaches that are used in dose translation allometry. The FDA has endorsed the Km (kg/m-sq) allometric

approach as well as other techniques including PD response analysis (i.e., unique cytokine dose responses across species). Body surface area is one approach that is used as a dose and cross-species dose normalizing method has been found to be highly successful in aligning dose linearity across species (Pinkel 1958; Rall and North 1953; Bachmann et al. 1996; Baker et al. 2002; Krasovskii 1976; Lindstad and Schaeffer 2002; Mahmood 1998, 2000, 2005, 2007; Mahmood and Balian 1996; Mahmood and Green 2003; FDA Guidance 2005; Tang and Meyershon 2006; Reagan-Shaw et al. 2007; Dedrick 2009).

Table 5.2 describes, in part, the method advocated by Reagan-Shaw et al. (2007). In some cases, however, drug doses are prescribed not in terms of micrograms per kg but in terms of micrograms per unit area, specifically body surface area (usually in terms of square meters, i.e., m^2). Such is the case for the colony stimulating factor GM-CSF (Sanofi; Sargramostim, Leukine™). The conversion of m^2 doses across species can utilize the Km values described in Table 5.2 (above) but translation of height and weight into body surface area (BSA) of small animals has been a difficult and challenging relational task. I have explored using a mix of three human height–weight exponential methods to calculate the BSA of animals such as the rhesus macaque and they include: the Haycock, the Mosteller, and the DuBois methods (refer: http://www.halls.md/body-surface-area/refs.htm). The DuBois method was further adapted for the rhesus macaque by Liu and Higbee (1976) where they added a slight correction factor using a skull to anus measurement. Taking the three BSA equations and making a mean BSA measure has been a better way to define the dose for the rhesus macaque and works for other species as well within limits defined by the species anatomy. A working copy of an EXCEL worksheet/tool using these three BSA equations for dose conversion to a second species based on input of only height and weight measures is provided to the Reader via the Springer web link. (http://link.springer.com/book/10.1007/978-1-4614-8247-5). The EXCEL tool also contains the details of the surface area equations and the FDA dosing guidance is also embedded.

The role of pharmacokinetics in imaging was historically ignored for nuclear tracers used in PET, SPECT and especially the original planar imaging platforms used in nuclear medicine as they all rely on tracer biology. “Tracer biology”, or the notion of a drug effect measurable using a miniscule mass of a drug to elicit an image of a chemical entity binding to a target, is a classic property of high-specific radioactivity nuclear medicine drugs and biologics.[2] Most drugs and biologics, however, are not necessarily operating in the nanomolar or lower range. The concept of a “Phase 0” study, i.e., a low dose of a radiolabeled imaging agent (Hung 2009), is allowed because this kind of trial purportedly has little pharmacologic risk, while operating at sub-pharmacologically active doses of the chemical entity (the “red box”; Fig. 5.5). The dose is often conducted at the nanomolar range (or less) of

[2] Specific radioactivity is the ratio of the radioactive isotope, i.e., Tc-99m, to the cold (stable) isotope, i.e., Tc-99, in, for example, Ci/mmol. A high-specific radioactivity product is needed for a Phase “0” study to reduce the mass.

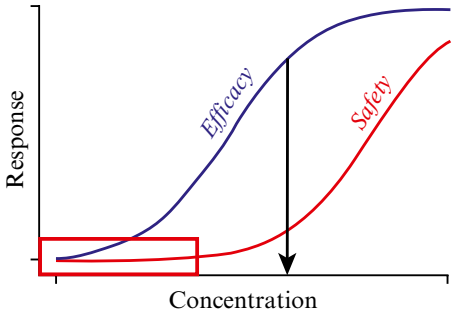

Fig. 5.5 Defining the dose for a Phase "0" study. The sigmoidal response curves for efficacy versus safety. The bold black arrow represents the dose for the maximal therapeutic index (TI) value. Phase "0" nuclear imaging studies are conducted purportedly at doses within the red box. What defines the "**red box**" is data from animal studies where no physiologic response is observed yet binding is demonstrated either in vitro or in vivo using the intended nuclear imaging product and imaging tool. The challenge is the dose translation of the animal dose to human which is critical to avoid any concentration "shift to the right" and resultant appearance of safety concerns

product which is capable of binding to specific receptors, generally neurologic targets, but not sufficient in eliciting a pharmacologic response.

A drug or biologic's integrated preclinical PK/PD package should be designed to be relevant in the human condition or disease and designed to establishes a derivable relationship between drug exposure and the mechanism of action (i.e., a selected biomarker). This relationship is critical in the selection of first dose(s) in humans. The pharmacokinetics of all drugs should be understood sufficiently to allow for comparative translation of the drug exposures across species. In terms of imaging, this is principally related to avoidance of target receptor saturation or poor biodistribution which alter target uptake or washout (e.g., on-off rate) statistics (voxel-related image content) which may distort interpretation of images over time. For high plasma drug concentrations (i.e., Cp >> Km), the saturable clearance function approaches a limiting value (Vmax), and at relatively low concentrations will represent a first-order elimination rate (Vmax/Km). A major source of the nonlinear elimination (and sometimes distribution; see Williams 2012) of antibodies is receptor-mediated clearance (RMCl) or target-mediated drug disposition (TMDD).

For antibodies that exhibit complex nonlinear kinetics, model-based dose selection can avoid the potential limitations of simpler methods that are often associated with inappropriate (and potentially wrong) assumptions. The development of a TMDD model for a specific kind of antibody in rats and monkeys and its translation for predicting the minimal anticipated biological effect level (MABEL) in humans is an excellent example of how allometrics plays an important role in safety (Mager 2012). In his chapter on the PK and PD of antibody-based therapeutics, Mager describes the testing of a large range of dose levels (0.1–100 mg/kg) of this antibody in rats and monkeys, and where no significant adverse events were ultimately observed (the no observable adverse event level; NOAEL, was determined for both species). The study resulted in determining the minimal human dose that is

predicted to show high target occupancy along with a 100-fold safety factor based on body surface area scaling.

On the other hand, when applying a simple receptor occupancy (RO) equation,

$$\left[\mathrm{RO}\% - C\mathrm{p}0 * 100\right] / \left[K\mathrm{d} + C\mathrm{p}0\right] \tag{5.1}$$

One should select the dose which provides a small 10 % receptor occupancy. This low dose estimate using minimal receptor occupancy is likely associated with failing to consider turnover processes and other inappropriate assumptions, such as rapid binding conditions and drug concentrations in far excess of the receptor ($C\mathrm{p} >> K\mathrm{d}$). Organ sizes and many physiological processes, such as renal clearance, scale across species according to a well-known power–law relationship (Adolph 1949; Rall and North 1953; Pinkel 1958; Mordenti 1986; Holford 1995; Bachmann et al. 1996; Mahmood and Balian 1996; West et al. 1997; Baker et al. 2002; Wajima et al. 2002; Mahmood 2005; Tang and Mayershon 2006; Reagan-Shaw et al. 2007; Savage et al. 2008; Dedrick 2009):

$$Y = aW^b \tag{5.2}$$

Where, a PK parameter of interest, i.e., clearance, Cl, has a relational basis to body weight (W) to a power value which typically rests in the domain of 3/4 or 0.75 (Mahmood and Green 2003). Drug clearance and body size as a means of allometry in the literature over 2000–2007 is provided as a fine review by McLeay et al. (2012). Interspecies conversions of toxicity seem best met by means of a power function of the body weight raised to the power of 2/3 to 1, where 1 is a direct weight-based scaling. The US EPA in the late 1980s used the 2/3 power to distinguish environmental toxic waste effects on various wildlife and it remains a practical approach today. The appropriate basis for an interconversion of dose across species is dependent on the mechanism of action (MOA) of a chemical, on its intrinsic metabolism, the developmental stage of the species in question, and on the dose pattern (dose schedule, pattern of exposure) (O'Flaherty 1989). Kinetically equivalent doses are defined as those doses that produce either equal concentrations in the plasma compartment or at the receptor (or target) sites or an equally integrated dose over time as in mass/unit volume/unit time to a target receptor or tissue across each species mean body weight. The two terms "dose concentration" and "dose exposure" are not always equivalent. It very important to consider that conversion of doses or dose rates from smaller to larger species is often realistic on a body surface area or ¾ power basis EXCEPT ***when first-order elimination and capacity limited production of an active metabolite coexist.*** In such cases, the peak concentration (i.e., Cmax) may not be sufficiently predictive of exposure (i.e., AUC) even though they are mutually dependent PK parameters.

Use of a fractional power of body weight to scale adult therapeutic doses to pediatric-equivalent PK doses, and to scale doses administered to test animals in drug development to the doses used in human clinical trials, has now become widely accepted and is translates more efficiently and accurately (except in the bolded

conditions described above) upon the log transform of Eq. 5.2 which has the property of a linear relationship (a straight line) following a log transform, where:

$$\log(y) = \log(a) + b * \log(W); \quad \text{or,} \quad \text{simply}: Y = mx + b \tag{5.3}$$

It is relevant to note that this approach has several attractive features:

- It is simple to use.
- Requires establishment of the drug blood or plasma concentration–time data.
- Requires knowledge of elimination pathways (i.e., geriatrics may have depressed Cl).
- Important, in most cases, to know if the product has plasma or blood component binding.
- Data analysis is generally straightforward.
- The use of either a power function of parameters of interest versus a normalization denominator of either body weight or body surface area (BSA) on a log–log scale.
- The equation for a straight line—term "b" as the slope representing the rate of change for the parameter versus the change in body weight or BSA.
- Compartmental analysis (CA; Simpson 2011) vs. non-compartmental analysis (NCA; Stepniewska 2011),
  - CA models can be complex and lengthy processes.
  - NCA models are less restrictive than fitting CA.
  - NCA methods do not require specialty software for analyses.
  - NCA criteria for best fit minimizations include

    Ordinary least squares
    Weighted least square
    Maximum likelihood estimation (MLE)

- *Three PK parameter estimates which are regularly used for allometry are also useful for imaging:*
  Clearance, *Volume of Distribution*, and the *Elimination Half-Life.*

Allometry based on organ sizes, or physiological volumes, tends to have the exponent as directly proportional, or $b = 1$. Physiological times, or the duration of physiological events (e.g., heartbeat and breath duration, lifespan or turnover times of endogenous substances or processes), typically scale across species with b values around 0.25. These interspecies relationships are based it seems from the fractal nature of biological systems (West et al. 1997; West and Brown 2005).

Chappell and Mordenti (1991) were the first to apply allometric scaling to therapeutic proteins. They applied the scaling to five compounds, one of which was an anti-CD4 IgG1 antibody. Exponents for total systemic clearance and the volumes of distribution (central compartment and steady-state value) were in agreement with the expected theoretical values. Mahmood (2004) confirmed that simple allometry may be used for most proteins in a review of predicted total clearance values of 15 therapeutic proteins from interspecies scaling.

Table 5.4 Examples of power functions used in allometrics

Power functions that relate species		
Physiologic power functions		
Power functions with: $Y = aW^b$		
Physiologic function	**Power function**	**Units**
Urine output	$=(0.0064)W^{0.82}$	mL/h
Ventilation rate	$=(120)W^{0.74}$	mL/h
Cr clearance	$=(4.2)W^{0.69}$	mL/h
Inulin clearance	$=(1.74)W^{0.77}$	mL/h
Heartbeat period	$=(1.19\times10^{-5})W^{0.27}$	h
Nephron number	$=(2600)W^{0.62}$	Count
Tidal volume	$=(6.2\times10^{-3})W^{1.01}$	mL
Kidney weight	$=(0.0212)W^{0.85}$	g
Heart weight	$=(6.6\times10^{-3})W^{0.98}$	g
Blood volume	$=(0.331)W^{1.09}$	mL (or g)

Power functions can relate specific organs and physiologic functions. Several investigative targets are currently defined where we have the allometric power function to exploit

This mechanistic approach predicted a starting dose of approximately 0.008 mg/kg which is much lower than established NOAEL in toxicity studies, but is more reasonable than the use of simple target occupancy calculations which do not also include the physiologic perturbations on the dose. An efficacious dose level was also predicted using the scaled model, and this study highlights how complex processes such as TMDD may limit the use of simple dose selection techniques and the need for more appropriate model-based algorithms to ensure clinical safety and efficacy.

Important to imaging is the ability to evaluate the time rate of change of some physiologic or metabolic parameter of interest. The importance of imaging in yielding the necessary statistics, resolution, and individual animal or patient evaluation is probably the most sought out technology in medicine for its personalized diagnostics. Table 5.4 describes several investigative physiologic and pharmacokinetic parameter targets where we have the allometric power function to exploit. Figure 5.6 demonstrates the utility of using a common pharmacokinetic parameter test, renal clearance of antipyrine, for drug comparative kinetics across species (REF). Onthank et al. (2005) provides a wealth of background on the clearance of drugs as relates to species and translational biology.

5.4 PK Parameter Estimates and Applications in Imaging

Zhao et al. (2009) describe an overview of imaging surrogates used for measuring tumor responses to therapy. It is important to recognize that there are allometric relationships of tumor responses and it may be necessary to know the therapeutic drug doses which may affect drug/biologic distribution and clearance. PET tracers have been created for metabolic imaging where we can evaluate the metabolic rate

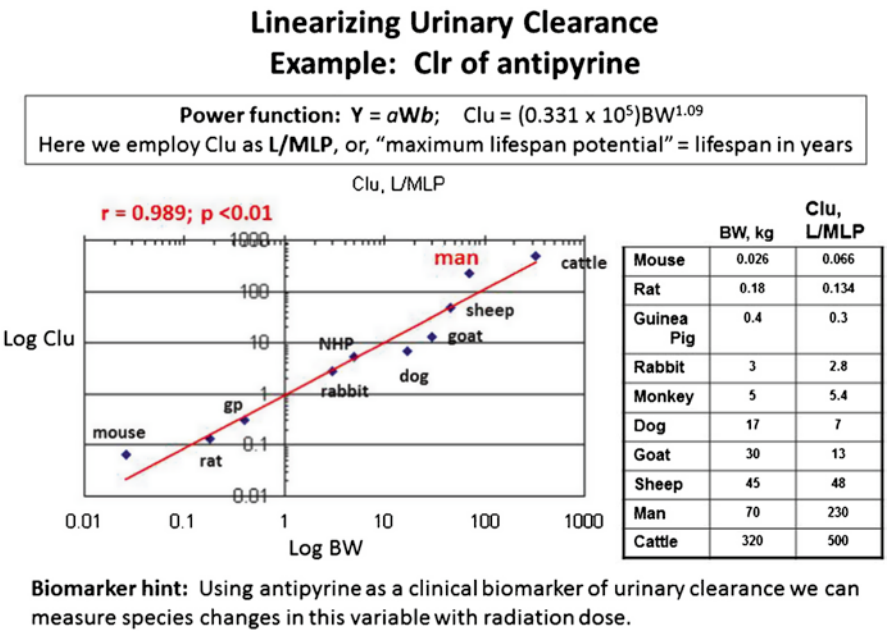

	BW, kg	Clu, L/MLP
Mouse	0.026	0.066
Rat	0.18	0.134
Guinea Pig	0.4	0.3
Rabbit	3	2.8
Monkey	5	5.4
Dog	17	7
Goat	30	13
Sheep	45	48
Man	70	230
Cattle	320	500

Fig. 5.6 Antipyrine renal clearance. A graphic portrayal of the linear relationship of clearance of antipyrine across species. Such a linear relationship can be exploited to demonstrate cross species drug clearance changes relative to the known antipyrine clearance estimates

of glucose uptake, i.e., F-18 fluorodeoxyglucose (Hanaoka et al. 2008), or the uptake in a progenitor cell proliferative environment such as the bone marrow using DNA precursor analogs, i.e., F-18 fluorothymidine (Menda et al. 2010). Figure 5.7 is an example of how the PET-derived SUV values (i.e., the PD response) are changing with the introduction of a therapeutic (chemotherapy or radiation effects on bone marrow) and this "delta" can be quite variable across species ability functionally respond to therapeutic interventions. Species differences and specific sensitivities to novel drugs and biologics can be measured using the terms of specific uptake values (SUVs) which represents a ratio to baseline expected values. As has been discussed throughout this chapter "baseline expected outcomes", that is the species to species correlations of drug behavior, should be thought of as allometrically defined and employing allometrics gives us avenues in imaging to uniquely confirm species differences in radiotracer distribution and elimination pathways in drug research. In the case of MR imaging, and especially in metabolic (MRS) studies, utilization of a stable isotope approach can markedly improve the efficiency and accuracy of bioavailability, tissue distribution, tissue elimination and bioequivalence studies particularly for highly variable drugs in formulations that are qualitatively and quantitatively the same as well as for quality by design (QbD) investigative studies (Parr et al. 2012; Williams 2012).

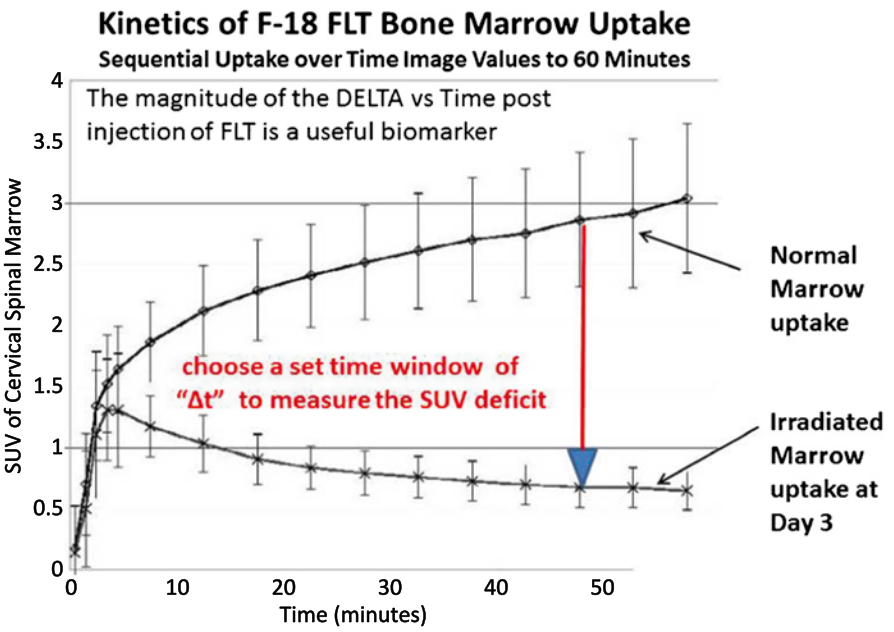

Fig. 5.7 Marked depression of F-18 FLT in irradiated progenitor cell uptake in human bone marrow following radiation. The SUV value is seen to be depressed following irradiation. Examination of effectiveness of progenitor stimulating drugs (cytokines) to induce proliferation in this setting may have alterations in drug clearance or distribution induced by the complex pathophysiology of radiation hematopoietic injury (with permission, L Boles-Ponto, Univ of Iowa and from: Menda et al. 2010)

Glucose use of the lung can be compared by bilateral functional comparisons. An example is the use of FDG to evaluate the efficacy of various doses and clearance behaviors when using tobramycin. A study by Dolovich and Labiris (2004) examined tobramycin therapy before and after 28 days of inhaled tobramycin therapy (160 mg twice daily) in patients. Control groups of cystic fibrosis and nonactive sarcoidosis showed mean glucose use in the lung (SUV values) of 1.3 mcmol/g×h (95 % confidence interval, CI, of 0.55–2.10). and 2.8 mcmol/g×h (95 % CI 2.65–2.99). Normal glucose use in the lung averages 1.2 mcmol/g×h (95 % CI 0.94–1.46). Patients with nonactive sarcoidosis have a significantly higher lung glucose use than normal. Despite the presence of chronic sputum neutrophilia, lung glucose use was not elevated in patients with CF and did not change with inhaled tobramycin therapy (Dolovich and Labiris 2004). Williams (2012) provides an excellent treatise on tissue distribution of protein therapeutics and molecular probes as described through imaging.

Allometry of cell therapeutics remains a challenge to define, especially in the imaging employing radiolabeled or SPOI-labeled cells for PET and SPECT or MRI imaging, respectively, and green fluorescent protein (GFP) or luciferase labeling of cells for bioluminescent imaging. (Huang et al. 2008) discussed the role of cell quantities and cell burden of label. The specific radioactivity of Cu-64 as a PET tracer has deleterious effects from cold copper[3] as well as from cell burdens of high-specific radioactivity where the cell viability falls off with excesses of >1 μmol of Cu-64/mL of labeling cocktail. They studies these effects in fetal monkey and recombinant mesenchymal stem cells (rhMSC) where they labeled these cells with 0–230 pmol Cu/mL as Cu-64-PTSM (Pyruvaldehyde-*Bis*-N4-Methylthiosemicarbazone) and showed no significant differences in cell viability, growth, or differentiation. The most deleterious effect came from the highest specific activity studies. The time frame from preparation to its use as a PET tracer is a critical measure. Studies on CD34+ cells labeled in excess of 1 h post labeling can show reduced cell functionality. Cell radioactivity may be deleterious to cell survival or function, i.e. proliferation, when radiolabeled in excess of 40 μCi/mL. Typical cell radiolabeling is done with incubation in the presence of a stock cell-supporting milieu with 20 μCi/mL of the desired radiolabel added to $\sim 5 \times 10^5$ cells. Allometric conversion of cellular therapeutic doses are not as yet fully investigated and this remains a major hurdle for future cell therapy programs and prediction of human safety.

5.5 Conclusions

There are some important features of allometric scaling for the prediction of human drug clearance from animal data and their application to imaging agents. I take the efforts of Mahmood and Green (2003), Mahmood (2007) in defining allometric principles as especially succinct in identifying important first principles for imaging and I recommend reading and understanding his important contribution to the field. First, the exponents of simple allometry have no physiological meaning. These are mathematical manipulations that may bear no real meaning to the physiology of the test species. Second, the exponential elements of clearance for a given drug are not universal and depend on the species under study generating these clearance values. Third, the impact of plasma protein (and other nonspecific) binding on the allometric scaling and indeed the human protein binding can be exquisitely different and challenging to predict. Fourth, in vitro binding and scaling solely on this is fraught with error due to metabolism and renal elimination (reduction in drug availability). Fifth, the attraction of a fixed exponential across species is often favorably viewed and sought to simplify the estimations. Caution is warranted. Sixth, external factors such as study designs, analytical errors, physiochemical properties may have significant impact on allometric determinations.

[3] Copper concentrations at 5 micromolar (μM) may stimulate respiratory and collapse of the membrane potential of mitochondria.

The predicted starting dose for a Phase 0 imaging study should be viewed as simply "predicted" and not "absolute" or "established" and thus the use of any imaging contrast agent or tracer product in the trial shall include protocol definitions for proper safety controls, timing of doses, and availability of supportive care. The understanding of PK allometry as applied to imaging is new and often discounted but the use of this tool can provide significant advantage to the product success and future market opportunities. The Reader is encouraged to review Chapter 13 on the FDA and regulatory aspects of allometry, Phase "0" studies, and much more. Further, the Reader is asked to refer to the FDA Guidances related to medical imaging (FDA Guidance for Industry 2004, 2005, 2006, 2010) as these will provide further insight on how drug and biologic development using imaging technologies and how they can be aided through exploring interspecies allometry.

References

Adolph EF (1949) Quantitative relations in the physiological constitutions of mammals. Science 109:579–585

Alcorn J, McNamara PJ (2003) Pharmacokinetics in the Newborn. Adv Drug Deliv Rev 35:667–6986

Bachmann K, Pardoe D, White D (1996) Scaling basic toxicokinetic parameters from rat to man. Environ Health Perspect 104:400–407

Baker SD, Verweij J, Rowinsky EK, Donchower RC, Schellens JH, Grochow LB, Sparreboom A (2002) Role of body surface area in dosing of investigational anticancer agents in adults, 1991–2001. J Nat Cancer Inst 94:1883–1888

Boisell J-P, Ribba B, Grenier E, Chapuisat G, Dronne M-A (2008) Modeling methodology in pathophysiology. Prog Biophys Mol Biol 97:28–39

Boxenbaum H (1984) Interspecies pharmacokinetic scaling and the evolutionary-comparative paradigm. Drug Metab Rev 15:1071–1121

Chappell WR, Mordenti J (1991) Extrapolation of toxicological and pharmacological data from animals to humans. Adv Drug Res 20:1–116

Dedrick RL (2009) Animal scale-up. www.cc.nih.gov/researchers/training/principles/pdf/ph1.pdf

Dolovich M, Labiris R (2004) Imaging drug delivery and drug responses in the lung. Proc Am Thorac Soc 1:329–337

FDA, Guidance for Industry: Developing Medical Imaging Drug and Biological Products, Part1, Conducting Safety Assessments 5742prt1.pdf; Part 2: Clinical Indications, 5742prt2.pdf; Part 3: Design, Analysis, and Interpretation of Clinical Studies; 5742prt3.pdf;2004. http://www.fda.gov/downloads/RegulatoryInformation/Guidances/UCM126051.pdf

FDA Guidance for Industry: Establishment of a Safe Starting Dose for Therapeutics. http://www.fda.gov/downloads/Drugs/Guidances/UCM078932.pdf. July 2005

FDA Guidance for Industry: Investigators, and Reviewers. Exploratory IND Studies. Publication: 7086fnl.pdf;2006. http://www.fda.gov/downloads/Drugs/GuidanceComplianceRegulatoryInformation/Guidances/ucm078933.pdf

FDA, Guidance for Industry: Determining Whether Human Research Studies Can Be Conducted Without an IND; 2010. http://www.fda.gov/downloads/Drugs/GuidanceComplianceRegulatoryInformation/Guidances/UCM229175.pdf

Giacomini KM, Sugiyama Y (2010) Chapter 2. Membrane Transporters and Drug Response, in, Goodman and Gilman, The Pharmacological Basis of Therapeutics, Brunton L, Chabner B, Chabner BA, Knollman B (Eds). pp 41–70. McGraw-Hill.com. http://www.google.com/url?sa=t&rct=j&q=&esrc=s&source=web&cd=1&ved=0CCIQFjAA&url=http%3A%2F%2Fbooks.

mcgraw-hill.com%2Fmedical%2Fgoodmanandgilman%2Fpdfs%2FCHAPTER2.pdf&ei=_Ix5UMH9AqWR0QHhsIHwCQ&usg=AFQjCNGrBX_e08ptpVuP7G9Pqs6K-Bsp0Q
Hanaoka K, Hosano M, Usami K, Yamazue Y, Sumita M, Komeya Y, Tsuchiya N, Im S-W, Okada M (2008) FDG uptake in bone marrow after G-CSF administration in patients with malignant lymphoma. J Nucl Med 49(Suppl):249P
Holford NHG (1995) The target concentration approach to clinical drug development. Clin Pharmacokinet 29(5):287–291
http://www.google.com/url?sa=t&rct=j&q=&esrc=s&source=web&cd=5&ved=0CEYQFjAE&url=http%3A%2F%2Fwww.medlib.am%2FFulltexts%2FDEVELOPMENT%2520of%2520Antibody-Based%2520Therapeutics%2520Translational%2520Considerations%25202012.pdf&ei=uxkEUbaVBebl0gH3koHAAw&usg=AFQjCNEsYgzowdRivcb5LeaxV_7ij9h9kg&bvm=bv.41524429,d.dmQ&cad=rja
Huang J, Chang C, Lee I, Sutcliffe JL, Cherry SR, Tarantal AF (2008) Radiolabeling rhesus monkey CD34+ hematopoietic and mesenchymal stem cells with Cu-64-pyruvaldehyde-Bis(N4-methylthiosemicarbazone) for MicroPET imaging. Mol Imaging 7(1):1–11
Hung JC (2009) The Exploratory IND (Phase 0) Concept. Ann Nucl Med Sci 22:93–100
Jaehde U, Sorgel F (1995) Clinical pharmacokinetics in patients with burns. Clin Pharmacokinet 29:15–28
Krasovskii GN (1976) Extrapolation of experimental data from animals to man. Environ Health Perspect 13:51–58
Liu CT, Higbee GA (1976) Determination of body surface area in the rhesus monkey. J Appl Physiol 40(1):101–104
Lindstad SL, Schaeffer PJ (2002) Use of allometry in predicting anatomical and physiological parameters in mammals. Lab Anim 36:1–19
Mager DE (2012) Application of pharmacokinetic/pharmacodynamic modeling in the development of antibody-based therapeutics. In: Tabrizi MA, Bornstein GG, Klakamp SL (eds) Development of antibody-based therapeutics. Translational considerations. Springer Science+Business Media, New York, pp 285–302, Chapter 11
Mahmood I (1998) Integration of in-vitro data and brain weight in allometric scaling to predict clearance in humans: some suggestions. J Pharm Sci 87:527–529
Mahmood I (2000) Interspecies scaling: role of protein binding in the prediction of clearance from animals to humans. J Clin Pharmacol 40:1439–1446
Mahmood I (2004) Interspecies scaling of protein drugs: Prediction of clearance from animals to humans. J Pharm Sci 93(1):177–185
Mahmood I (2005) Interspecies scaling of clearance, interspecies pharmacokinetic scaling: principles and application of allometric scaling. Pine House Publishers, Rockville, MD
Mahmood I (2007) Application of allometric principles for the prediction of pharmacokinetics in human and veterinary drug development. Adv Drug Deliv Rev 59:1177–1192
Mahmood I, Balian JD (1996) Interspecies scaling: Predicting clearance of drugs in humans: three different approaches. Xenobiotica 26:887–985
Mahmood I, Green MD (2003) Selection of the first-time dose in humans: comparison of different approaches based on interspecies scaling of clearance. J Clin Pharmacol 43:692–697
McLeay SC, Morrish GA, Kirkpatrick CMJ, Green B (2012) The relationship between drug clearance and body size: Systematic review and Meta-Analysis of the literature published from 2000 to 2007. Clin Pharmacokinet 51(5):319–330
Menda Y, Boles Ponto LL, Dornfeld KJ, Tewson TJ, Watkins GL, Gupta AK, Anderson C, McGuire S, Schultz MK, Sunderland JJ, Graham MM, Buatti JM (2010) Investigation of the pharmacokinetics of 3′-deoxy-3′-[^{18}F]-fluorothymidine uptake in the bone marrow before and early after initiation of chemoradiation therapy in head and neck cancer. Nucl Med Biol 37(4):433–438
Mordenti J (1986) Man versus Beast: Pharmacokinetic scaling in mammals. J Pharm Sci 75(11):1028–1040
Moyer BR, Barrett JA (2009) Review: biomarkers and imaging: physics and chemistry for noninvasive analyses. Bioanalysis 1(2):321–356

Muller PY, Milton MN (2012) The determination and interpretation of the therapeutic index in drug development. Nat Rev Drug Discov 11:751–761

O'Flaherty EJ (1989) Interspecies conversion of kinetically equivalent doses. Risk Anal 9(4): 587–598

Onthank DC, *Prediction of* "*First dose in human*" *for radiopharmaceutical/imaging agents based on allometric scaling of pharmacokinetics in pre-clinical animal models*, Ph.D. Dissertation, Worchester Polytechnic Institute. Dec 2005. http://www.wpi.edu/Pubs/ETD/Available/etd-011006-132234/unrestricted/2Onthank-Dissertation.pdf. Accessed 26 Apr 2013

Parr A, Gupta M, Montague TH, Hoke F (2012) Re-introduction of a novel approach to the Use of stable isotopes in pharmacokinetic studies. AAPS J 14(3):639–645

Pinkel D (1958) The use of body surface area as a criterion of drug dosage in cancer chemotherapy. Cancer Res 18:853–856

Rall DP, North WC (1953) Consideration of dose-weight relationships. Proc Soc Exp Biol Med 83:825–827

Reagan-Shaw S, Nihal M, Ahmad N (2007) Dose translation from animal to human studies revisited. FASEB J 22:659–661

Rellahan B (2009) The TeGenero Incident March 13, 2006 UK; TGN1412—a superagonist anti- CD28 antibody, FDA presentation. Division of Monoclonal Antibodies, Office of Biotechnology Products, CDER, 2009. http://www.ctti-clinicaltrials.org/resources/2009-fda-clinical-investigator-training-course/Rellahan%20case%20study.pdf . Accessed 5/6/2013

Radziszewski W (2009) Estimating Starting Dose and Dose Range for First in Human Study. Merck Research Laboratory. http://mediaserver.aaps.org/meetings/09AM/Slides/11.12.09_Thu/403%20B/0900/Waldemar%20Radziszewski.pdf

Simpson J (2011) Compartmental Pharmacokinetic Analysis. The University of Melbourne. https://www.wwarn.org/sites/default/files/CompartmentalModelling.pdf

Stepniewska K (2011) Non-Compartmental Pharmacokinetics. WWARN. https://www.wwarn.org/sites/default/files/NonCompartmentalAnalysis.pdf

Suntharalingam G, Perry MR, Ward S, Brett SJ, Castello-Cortes A, Brunner MD, Panoskaltsis N (2006) "Cytokine storm" in a Phase 1 trial of the anti-CD28 monoclonal antibody TGN1412. New Engl J Med 355:1018–1028

Savage VM, Deeds EJ, Fontana W (2008) Sizing up allometric scaling theory. PLOS Computat Biol 9(e1000171):1–17

Tang H, Mayershon M (2006) A global examination of allometric scaling for predicting human drug clearance and the prediction of large vertical allometry. J Pharm Sci 95:1783–1799

Wajima T, Fukumura K, Yano Y, Oguma T (2002) Prediction of human pharmacokinetics from animal data and molecular structural parameters using multivariate regression analysis. J Pharm Sci 91:2489–2499

West GB, Brown JH (2005) The origin of allometric scaling laws in biology from genomes to ecosystems: towards a quantitative unifying theory of biological structure and organization. J Exp Biol 208:1575–1592

West GB, Brown JH, Enquist BJ (1997) A general model for the origin of allometric scaling laws in biology. Science 276:122–126

Williams S-P (2012) Tissue distribution studies of protein therapeutics using molecular probes: molecular imaging. AAPS J 14(3):389–398

Zhao B, Schwartz H, Larson SM (2009) Imaging surrogates of tumor response to therapy: Anatomic and functional biomarkers. J Nuc Med 50:239–249

Chapter 6
Quantitative Imaging Using Autoradiographic Techniques

Eric G. Solon and Brian R. Moyer

Abstract Autoradiography (ARG) is a powerful, high resolution, quantitative molecular imaging technique used to study the tissue distribution of radiolabeled xenobiotics in biological models. ARG involves the close apposition of solid specimens containing radiolabeled substance to a detector layer, such as photographic emulsions, film, phosphor imaging plates, and direct nuclear imagers/counters and the two basic types include: Macro-autoradiography, which is imaging of organs, organ systems, and/or whole-body sections (WBA); and micro-autoradiography (MARG), which provides localization of radioactivity at the cellular level. The basic technique is more than 60 years, but it remained largely qualitative due to the limited linear range of quantification offered by nuclear emulsion detection systems. However, recent technologies have revolutionized the techniques of WBA and made quantification of radioactivity in tissues possible. WBA and MARG techniques provide drug researchers with quantitative tissue concentration data and a high resolution visual location of those drug or biologic concentrations in intact organs, tissues, and cells of laboratory animals. In addition, novel techniques such as matrix-assisted laser desorption imaging mass spectrometry (MALDI-MSI), and Secondary Ion Mass Spectrometric (SIMS) imaging can positively identify the molecular identity and image the spatial distribution of the parent drug and/or their metabolites in the same samples used for whole-body and micro-autoradiography. This chapter presents an overview of the techniques and reviews the use of QWBA, MARG, MALDI-MS, SIMS, and tissue extraction and liquid chromatography/mass spectroscopy (LC/MS) in the pharmaceutical industry.

E.G. Solon (✉)
QPS, LLC, 110 Executive Drive, Suite 7, Newark, DE 19702, USA
e-mail: eric.solon@qps.com

B.R. Moyer
BRMoyer & Associates, LLC, 23 Hawk Drive, Bedford, NH 03110, USA
e-mail: bmoyernh@gmail.com

B.R. Moyer et al. (eds.), *Pharmaco-Imaging in Drug and Biologics Development*,
AAPS Advances in the Pharmaceutical Sciences Series 8, DOI 10.1007/978-1-4614-8247-5_6,

6.1 Introduction

Autoradiography (ARG) is an elegant collection of high resolution imaging techniques that enable the qualitative and now quantitative assessments of drug localization in tissues and cells or lab animals. The techniques have been used to support drug discovery and development for over 60 years in both academia and industry are widely used to study the absorption, distribution, metabolism, and elimination properties (ADME) of large and small molecule drugs in organs, tissues, and cells of lab animals. The techniques rely on the use of radiolabeled test compounds, which provide the most accurate method for the quantitative and qualitative assessment of the parent drug and its metabolites in biological samples. The use of radiolabeled compounds is the most efficient method for determining drug disposition and metabolite identification, despite attempts to use nonradioactive techniques. ARG involves the close apposition of solid specimens containing radiolabeled substance to a detector layer, such as photographic emulsions, film, phosphor imaging plates, and direct nuclear imagers/counters. The two basic types include: Macro-autoradiography, which is imaging of radioactivity in organs, organ systems, and/or whole-body sections and which includes qualitative whole-body autoradiography (WBA) and quantitative WBA (QWBA); and micro-autoradiography (MARG), which provides localization of radioactivity at the cellular level. The basic techniques remained largely qualitative due to the limited linear range of quantification offered by nuclear emulsion detection systems (e.g., X-ray film). However, in 1975 phosphor imaging technology (Luckey 1975) revolutionized the techniques of WBA and made quantification of radioactivity in tissues possible because it offered a robust method to quantify radioactivity over a wide linear range (5–6 orders of magnitude). This technique is more accurately referred to as quantitative whole-body autoradiography (QWBA) or also as whole-body autoradioluminography (WBAL) (Potchioba et al. 1995).

The use of radiolabeled compounds is the most efficient tool for quantitatively examining the ADME properties of drugs, but researchers are attempting to utilize newer techniques, such as compounds labeled with florescent tags (Mitra and Foster 2008), and mass spectroscopy (MS) techniques despite some limitations. Reliable and sensitive quantitation of florescent-labeled compounds has not been consistently achieved due to background and matrix effects, and image resolution is much less than provided by imaging by QWBA. Another limitation of fluorescently labeled compounds is that sometimes the relatively large florescent tag can alter the activity and/or binding of the compound due to the size and possible chemical modifications. Consequently, the pharmaceutical activity of each fluorescently labeled compound should be verified before it is used to study ADME characteristics to ensure that accurate data will be obtained. Nevertheless, florescent compounds are widely used as an in vivo imaging tool in drug discovery to screen the localization of compounds in organs and tumors of xenograft animal models.

Mass spectroscopy is also used to gather ADME information related to quantitation and molecular identification, but its use is also limited (Michnowicz 2011).

Although MS can provide reliable tissue quantitation, it requires much more work to get that data because appropriate standards are required and the organ extraction process, efficiency, and possible matrix effects need to be considered and influence accurate assessments of tissue concentrations. These issues often confound the true tissue-level quantitative data, and can't match the quality of data provided by radiolabeled compounds and quantitative autoradiography imaging techniques. However, the techniques of MALDI-MS and SIMS have improved over the past 10–15 years and offer the ability to identify and semi-quantify both parent compounds and/or their metabolites in whole-body and individual tissue sections (Solon et al. 2010).

For years the use of radiolabeled compounds and QWBA have become the gold standard for determining tissue distribution characteristics of drugs and it has remained the best option because it provides the most efficient way to visually localize and quantify the amount of a chemical entity throughout the body, and in discreet organs, tissues, and cells of laboratory animals.

WBA, which refers to the original technique developed by Sven Ullberg in the mid-1950s, relied on a film detection system/imaging system. Dr. Ullberg first published the use of WBA while studying in situ biodistribution of ^{35}S-Penicilin (Ullberg 1954) in 1954. The basic technique of WBA entails the administration of a radiolabeled test compound [most often hydrogen-3 (^{3}H) or carbon-14 (^{14}C) isotopes] to labs animals (e.g., rodents and nonhuman primates) followed by euthanasia and freezing the carcasses of animals at different time points after drug administration. The frozen intact carcasses are cryosectioned (at 30–50 μm thickness) at different levels through the carcass to capture all tissues, and the sections are imaged *en face* (in contact) using X-ray film. The technique remained qualitative for about 25 years because film is not a linear detection system that could be easily used for quantitation. It wasn't until after 1979 when phosphor imaging technology (Luckey 1975) was used to quantitatively image beta radiation in solid samples. The technology was quickly adopted by large pharmaceutical companies who applied the technology to well-established WBA techniques that were being used to supplement organ distribution studies that were performed by organ excision, homogenization and/or combustion, and liquid scintillation counting (LSC) of radioactivity. QWBA, which could be performed in much less time (days as opposed to weeks or months) and provided true tissue-level quantitation, was quickly adopted and validated by the pharmaceutical industry (Coulston and Carr 2000; Solon and Kraus 2002) and it has all but replaced the classical analysis of organ homogenates by LSC. QWBA is now widely accepted as the best technique to determine the tissue distribution of new drug entities and it is accepted by regulatory agencies around the world.

MARG is a qualitative autoradiographic histology technique that utilizes a photographic media for detection (e.g., nuclear/photographic emulsion) to spatially locate drug-derived radioactivity at the cellular level in organ/tissue samples that have been removed from lab animals given radiolabeled test compounds. Fresh tissue or organ samples are snap-frozen, cryosectioned (at 4–10 μm thickness) and exposed to nuclear imaging emulsion that has been applied to glass microscope

slides (Stumpf 2005). The sections are allowed to expose the emulsion-coated slides and then the slides are developed like film, stained, and examined under a light microscope to visually identify the localization of the drug-derived radioactivity at the microscopic level. This chapter describes the techniques of QWBA, MARG, MALDI-MS, and SIMS and presents examples of how they have been used in the pharmaceutical industry.

6.2 Tissue Concentration Determinations Using Phosphor Imaging and QWBA

Sven Ullberg, who was the founder of the QWBA technique, first published his work in 1954 (Ullberg 1954). His original methods begin with the administration of a radioactive test substance (beta particle emitter) to a lab animal, where typical doses of radioactivity range from 100 to 200 microcuries (μCi)/kg. The dose of radioactivity can vary greatly depending on the isotope, dose route, availability of the radiolabeled material, and/or other considerations, but the radiopurity of the compound being administered is perhaps the most important considerations because it is directly related to the accurate quantitation of the compound being studied.

Radiopurity defines the percentage of the test molecule in a preparation that is radiolabeled versus the percentage of radiolabeled degradation products, and/or other radioactive contaminants present in a given lot of a radiolabeled test article. The desired radiopurity of a test compound should be 97 % or higher, whenever possible, to assure that the quantitative results reflect the amount/concentration of the test compound (and/or its metabolites), but not degradation products and/or contaminants. The in vivo stability of the radiolabel on the compound of interest is also very important so that the quantitative results accurately reflect the amount of the radiolabeled drug and/or its metabolites. In vivo instability of a radiolabeled drug can be a source of gross over and/or underestimations of the tissue concentrations if it is not properly characterized for each sample analyzed in a QWBA and/or MARG study. Stably labeling test molecules with ^{14}C in known positions usually results in the most reliable test molecules for QWBA and MARG. In contrast, labeling of small molecules with ^{3}H and large molecules with ^{125}I is often less stable and it is crucial to monitor their stability in vivo, when quantitative results are needed (Solon 2007). In general, small organic molecules are labeled with ^{14}C, ^{35}S, or ^{3}H, and larger molecules, such as proteins, and peptides, are labeled using ^{125}I (and sometimes ^{35}S), owing to the related molecular structures (Hahn 1983). It is common for tritium-labeled drugs to undergo some degree of hydrogen-exchange with water in vivo (Kim et al. 2004; Hesk and McNamara 2007). Thus, it is important to verify the stability of the ^{3}H label in vivo by obtaining plasma and/or urine at the time of euthanasia from the animals being used for QWBA and/or MARG (Kim et al. 2004). The extent of in vivo stability can be determined by measuring the concentration of radioactivity in fresh (wet), and evaporated samples of plasma and/or

urine obtained from the animals to be analyzed. If radioactivity in the fresh (wet) samples is more than the dried samples, then it is likely that there was an exchange of ^{3}H from the ^{3}H-drug with endogenous water and the resulting tissue concentration data obtained by QWBA (and/or dissection and liquid scintillation analysis) must be interpreted more carefully and/or corrected.

Similar considerations are required when radiolabeling large molecules with ^{125}I, which is now the case in the biotech industry, where there is increased interest in determining the ADME characteristics of large molecule biopharmaceuticals. This has become more important, as researchers now rely on the use of ^{125}I-labeled test articles and QWBA to determine the tissue distribution of biotech entities, such as antibodies, peptides, and proteins. Currently, ^{125}I QWBA appears to provide the highest resolution and most quantitative method for determining tissue distribution of large molecules because it is either not possible, and/or extremely expensive to radiolabel these molecules with ^{14}C or ^{3}H. (Although it is also possible to analyze organ/tissue homogenates with extraction and LC/MS techniques, those assays are time consuming and require a lot of sample processing, which undoubtedly affects the accuracy of quantitation.) However, the stability of ^{125}I labeling on large molecules is subject to bio-dehalogenation in vivo, and results in relatively high concentrations of free ^{125}I, which often vary at different time points after dosing (Sinsheimer and Shum 1981). Therefore, the determination of drug concentrations in tissues using ^{125}I labeled molecules must be considered as semiquantitative due to the inevitability of measuring free ^{125}I along with the test article. Furthermore, the tissue concentration data of ^{125}I-labeled compounds obtained for the thyroid, stomach, kidneys, mammary gland, salivary gland, thymus, epidermis, and choroid plexus must be interpreted more carefully because these organs contain a sodium-iodide symporter that is involved in the organification, and/or elimination of free ^{125}I (Venturi and Venturi 1999). Consequently, they will contain the free and/or organified ^{125}I, which is not drug-related and may provide misleading results. One way to reduce that effect is to administer non-radiolabeled sodium-iodide to test animals prior to dosing with the ^{125}I-labeled drug. This reduces the uptake of free ^{125}I into those tissues, thus reducing the confounding effects on tissue quantitation of the test drug (Solon 2007). This also may act to shunt free ^{125}I to the kidneys thus facilitating clearance and elimination and reducing the effects of free plasma ^{125}I on tissue quantitation. Even though this technique will reduce the background "noise" of free ^{125}I on quantitation, it does not eliminate the effect and the concentrations of free ^{125}I in the body must be characterized to better understand the true drug-derived concentrations in tissue. To characterize free ^{125}I versus drug-bound ^{125}I, investigators may use trichloroacetic acid (TCA) protein precipitation of plasma (and sometimes tissues) to determine the ratio of protein-precipitable ^{125}I versus free ^{125}I (Solon 2007). That ratio can then be used to correct tissue concentrations obtained using QWBA. This does not account for the further possibility of in vivo binding of free ^{125}I to animal proteins and/or distinguish between parent drug, metabolites, and degradation products. To address those questions, further analysis of plasma and/or tissues may be performed using extraction techniques followed by gel-electrophoresis, thin-layer chromatography, ELISA, and/or specialized mass spectroscopy techniques.

To these ends, the selection of the radiolabel for a specific test compound for use of determining drug tissue concentrations is one of the most important steps for QWBA, and/or any quantitative technique that relies on the use of radiolabeled test articles. Nevertheless, each step of the process for QWBA is also important for the accurate quantitation of tissue concentrations and the following descriptions of QWBA procedures will discuss these considerations.

Each step of processing after animals have been administered the radiolabeled compound can also effect tissue quantitation, and these include euthanasia, carcasses freezing, embedding, cryosectioning, section dehydration, exposure to phosphor imaging plates, image qualification and calibration, and image analysis. The initial step of euthanasia should be conducted in a manner that will not have detrimental effects on tissue distribution. One such example is the use of CO_2 inhalation for euthanasia. If a goal of a study is to examine brain concentrations of a drug or biologic, CO_2 administration should be avoided as is commonly known to disrupt brain permeability and the quantitative results may be altered. Thus, most investigators will use an overdose of a barbiturate and/or inhaled anesthetic such as isoflurane rather than CO_2. In any case, animals are euthanized at different time points after dosing and their carcasses are snap-frozen for processing. The most common freezing technique for QWBA is performed by submerging the euthanized or deeply anesthetized animal into a container of hexane and dry ice, which attains a temperature of approximately −70 °C (Solon and Kraus 2002). Freezing times may vary from lab to lab however, it is generally agreed that the optimal time for rats and mice (body weights ranging from 30 to 250 g) is 15–30 min and about an hour for larger animals such as dogs and monkey (body weights ranging from 3 to 6 kg). Animals may be frozen in a variety of positions (see Fig. 6.1a) ranging from holding the tail of the animal and dipping it into the hexane–dry ice bath to putting the animal into some sort of positioning frame in an attempt to maintain body positions, which enables uniform presentation for sectioning and image analysis in later steps. Frozen carcasses are then freeze-embedded in a block of embedding media (typically 1–5 % carboxymethylcelluose) and the blocked animal is then cryosectioned in a large field cryomicrotome. Most animals are sectioned in a saggital orientation for whole-body sectioning, but in some cases a cross-sectional orientation (ventral to dorsal) may better serve the investigator and is a more common format for human PET/SPECT as well as CT and MR imaging. Such may be the case where only head structures are being studied and serial frontal sections through the head of a rat are required. In such cases, adjustments may be needed during the embedding procedure to ensure that the head is properly oriented (Caution: carboxymethylcellullose is relatively opaque). During embedding there is some risk of thawing and so technicians must ensure that the hexane–dry ice bath used for this purpose has been precooled to facilitate quick freezing of the embedding media. It is also a good practice to include a set of 3–4 radiolabeled standards at a single concentration (e.g., 0.5 μCi/g of blood, plasma, or other media) that are placed at intervals alongside of the carcass into each block to serve as section thickness indicators that will assure section thickness uniformity for quantitative analysis during image analysis (see Fig. 6.1b). One tissue that works well for this is the brain where it can be easily

Fig. 6.1 (**a**) A rat carcass being frozen in a hexane–dry ice bath. (**b**) A partially cryosectioned cat carcass inside a Leica CM3600 Cryomacrocut microtome, blue co-embedded ^{14}C quality control standards for verifying section thickness. (**c**) Dehydrating rat whole-body sections on collection tape. (**d**) Dehydrated, rat whole-body sections, ^{14}C-blood calibration standards, a phosphor imaging plate and an exposure cassette ready for exposing. (**e**) The image calibration function screen of the MCID image analysis software showing how image density values produced by the calibration standards are plotted against the known concentrations of radioactivity in the co-exposed ^{14}C calibration standards

homogenized with a radiolabel standard and when cut retains shape and relative thickness (beta energy attenuation) even under dessication. The use of quality control standards for verifying section thickness uniformity is important (Solon and Kraus 2002), especially when there are several different people performing sectioning for a study. This is because of the possibility that different people can produce sections of different thickness based on how they pull the sections during sectioning. It is important to control for this because if a section is thicker at one end or another then the resulting quantitation will be compromised and inaccurate. This is most important when the data will be used for submission to regulatory authorities and the quality must be assured.

Whole-body sections are collected onto adhesive tape at section thicknesses of generally 20–50 μm using a large cryomicrotome (e.g., Leica CM 3600®, Nussloch, Germany) and the sections on tape are dehydrated (usually inside the microtome chamber by cold sublimation) (see Fig. 6.1c). The handling of dehydrated whole-body sections during the exposure to phosphor imaging plates is another area that requires attention. Care must be used to avoid unnecessary bending and/or contact with the tissue on the tape which can lead to sample loss (flaking and chipping). A common source of artifacts come from bending sections while handling them during exposure to imaging plates, X-ray film, and/or direct detectors. For example, this can result in the relocation of radioactivity from the sample on the collection tape if the sample undergoes flaking of intestinal contents that may contain particles of highly radioactive material (e.g., dosing material and/or ingesta containing radioactive bile from the liver) and/or other tissue. Contamination across the whole-body section can produce images that are difficult to analyze later and may invalidate all previous work if it is extensive. The dried sections may then be mounted on cardboard backing, and are then placed into exposure cassettes in close contact (*en face*) with phosphor imaging plates (or X-ray film), along with a set of radioactive calibration standards (see Fig. 6.1d).

Calibration standards are typically a series of blood aliquots (or brain as discussed earlier) that have been spiked with radioactivity (Schweitzer et al. 1975) to produce a range of concentrations (e.g., at 0.0001–10 μCi/g blood). It is important to realize that the standards used must match the section thickness of the whole-body sections to be analyzed otherwise the calibration values will not match the samples and the resulting quantification will be incorrect. Reusable commercially available calibration standards are available, but must be validated and usually require recalibration against standards made under the conditions for which they will be used (i.e., using lab-prepared standards that have been sectioned at the same thickness used for QWBA and using standards that reflect a similar tissue matrix such as blood).

Typical sample exposure times for phosphor imaging plates are anywhere from 3 to 7 days for ^{14}C and similar isotopes, but once again this depends on the nature of the isotope and anticipated amount of radioactivity in the sections. After the appropriate exposure time, the imaging plates are scanned in a phosphor imager. Modern day phosphor imagers can scan imaging plates at a variety of resolutions (i.e., to

generate images that have different pixel sizes) that range from 10 to 1,000 μm. Most labs conducting QWBA studies use a scan resolution of 100 μm, which produces digital image files that are approximately 15,000 megabytes (for an imaging plates that measures approximately 40 × 40 cm). However, the size of the acquired data (image) files depends on the size of the imaging plate used, which can vary from a plate that is approximately 20 × 20–40 × 40 cm. The higher the resolution, the larger the file size, and thus the digital data storage capacity of the laboratory must be considered.

The digital autoradiographic (a.k.a. autoradioluminographs when the image is obtained using phosphor imaging) images are then accessed using an image analysis software that is capable of analyzing autoradiographic images and several software packages are commercially available. In order for an image to be acceptable for the determination of tissue concentrations data, the analyst must assure that each section used to create the image was uniformly thick. An analysis of the density values obtained from the co-embedded internal section thickness standards that were collected along with each section facilitates that need. Acceptance criteria, such as making sure that the image densitometry readings of all internal standards are within 10 % of each other, can serve that purpose. Only sections that conform to the criteria established by the lab should be used for image analysis and tissue quantitation or faulty data may be unknowingly obtained. Next, each autoradiograph must be calibrated such that the densitometry readings of the grey-scale levels directly relate to the concentration of radioactivity visualized in the image of each tissue to be analyzed. The phosphor imager used to collect the digital image assigns a grey-scale density value to individual pixels, which is directly related to the radioactive concentration from the region of the sample. For example, a Typhoon 9410® (GE Healthcare) has a linear dynamic range of 100,000:1. The pixel and/or mean pixel density value for a given area of the image can be related to concentrations of radioactivity in tissue by image analysis software that interpolates the sample density reading from a calibration curve of known radioactivity concentrations from co-exposed calibration (see Fig. 6.1e).

There are several imaging systems that can be used for the drug in situ distribution analysis of QWBA samples and they include phosphor imaging, which is the most commonly used today, and direct beta imagers. Phosphor imaging technology has its limitations, such as sample exposure time, use for ^{3}H or other weak beta emitters, image resolution (pixel size), lower limits of detection (0.06 dpm/mm^2 of ^{14}C), lower limits of quantitation (~ 2,220 dpm/g/0.5 mm^2 image region from sections that are ~ 40 μm thick section), effects and sources of background radiation, image plate scanning time, and digital image file size and storage (Kolbe and Dietzel 2000). In drug discovery and development, fast sample analysis is an important key to success and is also one reason why WBA was not used as much before phosphor imaging which enabled much shorter exposure times. Currently typical exposure times still require 3–14 days for ^{14}C and ^{3}H, and so there is still room for improvement. Weak beta emitters like ^{3}H usually require a longer exposure time and 7–14 days is routine. Another limitation of phosphor imaging of ^{3}H is the need to use

special imaging plates that can only be used once because they lack the protective coating that allows the weak beta to interact with the sensors that is typically present on plates used to image ^{14}C or higher energy isotopes. Direct imagers such as the Beta imager (Biospace Mesures, Paris France) have improved this by offering real-time imaging, without the need for imaging plates, however, even this can require an overnight acquisition time and often only a few sections from only 1 small animal can be imaged at a time (Breskin 2000). As a result, it can still require about 10 days of imaging time. Furthermore the sample holder can accommodate only about 3–4 whole-rat-body sections, whereas a large format phosphor imaging plate can image up to 8–10 whole-rat-body sections.

Image resolution is another limitation, but one that may not be a big issue for imaging at the tissue level. Current phosphor image scanners (made by Fuji, Kodak, and GE Healthcare) have the capability to scan imaging plates so that an image may have pixel sizes that are anywhere from 10 × 10–1,000 × 1,000 μm. Thus it is acceptable for determining quantitative data at the tissue level but does not reflect actual single cell uptake like liquid emulsion methods which are far more intimate with histologic specimens.

The determination of tissue concentrations from autoradiographic images relies on the quality of the processes that produced the image, which is why every step of a QWBA study is important and impacts the quality of the image to be analyzed. Quantification is performed using image densitometry analysis. A standard curve is constructed from the integrated responses of densitometry values/mm^2 of the pixels of each image of the calibration standards (that were co-exposed with the sections imaged) with the known concentrations of radioactivity of each standard (in μ-Curies [μCi] or mega-Becquerels [MBq] of radioactivity/g of standard) that were determined using an LSC assay. Figure 6.1f shows a computer screen with a curve that was obtained from the densitometry values of images of the calibration standards integrated against the known concentrations of radioactivity in each standard. The concentrations of radioactivity in each standard, and subsequently each tissue, are determined as μCi/g, or MBq/g, which can then be converted to μg equivalents of drug per gram sample (μg equiv/g) using the specific activity of the administered radiolabeled drug (expressed as μCi/mg or MBq/mg). A lower limit of quantification (LLOQ) can then be applied to the data. There are different methods for determining the LLOQ for QWBA analysis and may be based on background measurements (e.g., 3× the mean of 10 background readings), or using the lowest calibration standard that can be reliably used on the calibration curve. Response curves determined for image analysis calibration are often generated using a weighted, 1st degree, polynomial, linear equation (1/densitometry value/mm^2). A numerical estimate of goodness of fit of the standard values on the curve is often provided by the image analysis system as a relative error, where the absolute value for the relative error of each calibration standard is ≤ 0.250 to be accepted.

An example of a standard curve calculation is provided below.

$$\text{Response} = a_1 \times \text{Concentration} + a_0$$

Where:

$$\begin{aligned}\text{Response} &= \text{Densitometry value as provided by the software / area of tissue mm}^2\\ \text{Concentration} &= \text{standard concentration}\left(\text{in } \mu\text{Ci / g or MBq / g}\right)\\ a_1 &= \text{slope}\\ a_0 &= \text{y} - \text{intercept}\end{aligned}$$

The relative error for each standard is calculated using the standard curve according to:

$$\text{Relative Error} = \frac{\text{nominal concentration } (\mu\text{Ci / g}) - \text{calculated concentration } (\mu\text{Ci / g})}{\text{nominal concentration } (\mu\text{Ci / g})}$$

Individual tissue sample concentrations are then calculated according to:

$$\text{Concentration } (\mu\text{g equivalents / g of tissue}) = \frac{\text{Concentration from std. curve } (\mu\text{Ci / g})}{\text{Specific Activity } (\mu\text{Ci / g})}$$

An LLOQ and upper limit of quantitation (ULOQ) can be based on the lowest (e.g., 0.0001 μCi/g) and highest (e.g., 10 μCi/g) standards used in the calibration curve. The equation used to determine the LLOQ and ULOQ would then be:

$$\text{LLOQ} = \frac{\text{Density} - \text{Standard (e.g., 0.0001 } \mu\text{Ci / g)}}{\text{Specific Activity (in } \mu\text{Ci / } \mu\text{g)}}$$

$$\text{ULOQ} = \frac{\text{Density} - \text{Standard (e.g., 10 } \mu\text{Ci / g)}}{\text{Specific Activity (in } \mu\text{Ci / } \mu\text{g)}}$$

The LLOQ may also be determined as a function of the background where 2× and 3× background are used; however, this may affect the determination of tissue pharmacokinetic data due to the acceptance or rejection of data that is considered to be below the LLOQ (Solon and Lee 2002).

Tissue concentrations are obtained selecting regions of interest of the autoradiograph that correspond to each tissue of interest and therefore it relies on the use of an image analysis system that is capable of precisely sampling regions of an autoradiograph that corresponds to each tissue of interest. The person performing the image analysis needs to have a very good knowledge of animal anatomy, interpreting tissue distribution patterns and artifacts, and possess a complete knowledge of the entire process so that they can recognize such things as improper dosing, freezing, sectioning, section melting or faulty dehydration, and section thickness inconsistencies.

At this point it is worth discussing the image analysis software used for QWBA.

To date, there are only about three major providers of software that are being used for industrial pharmaceutical QWBA analysis. The three most popular

software systems being used for QWBA are AIDA™ (Raytest Isotopenmessgeräte GmbH, Straubenhardt, Germany), Seescan 2™ (LabLogic Systems Limited, Sheffield, UK), and MCID™ (InterFocus, Linton, UK). These software packages offer good image sampling tools, region of interest (ROI) tracking, and powerful algorithmic calibration features that lend themselves to use for regulatory purposes. Image contrasting features also help to identify tissues with very low or very high concentrations during image analysis. One recent improvement made by Raytest in their AIDA™ software is that which easily co-registers the autoradioluminograph with a color image of the actual whole-body sections (obtained from a conventional scanner). This enables the user to identify regions to quantify on the color image of the actual section while the software samples the autoradioluminographic image. This is useful when tissue concentrations are very low, and for beginner autoradiographers, who may be less experienced in sampling autoradiographs. However, it can lead the analyst into a false sense of security where artifactual radioactivity can contaminate adjacent regions of the specimen and, if careful attention is not paid, the analyst can easily and unknowingly sample regions that have been contaminated with high radioactivity, thus obtaining inaccurate results. Another feature offered by AIDA™ and Seescan2™ are extra features that help address regulatory compliance issues with the capability to add notes and secure audit trails to aid in documentation. All three systems have procedures in place to maintain data integrity to match quantitative values to specific regions of the images sampled.

6.3 The MARG Technique and Theoretical Feasibility of Tissue Concentration Determinations

Micro-autoradiography is a histological technique where radioactivity from within a small cellular, tissue, or organ sample is imaged using a glass microscope slides that have been coated with a photographic emulsion to record the spatial distribution of radioactivity at the cellular level. The first micro-autoradiographic data were produced by Lacassagne in 1924 (Lacassagne and Lattes 1924), which led to further work by Bélanger and Leblond (Bélanger and Leblond 1946), who poured liquid photographic emulsion onto histological sections to reveal the location of radioactive substances in the tissues. Joftes and Warren (1955) revised that technique and dipped slides into photographic emulsion, which gained wide use due to its ease of manipulation and reproducibility. Although, if diffusible radiolabeled compound are utilized, not unlike many pharmaceutical drugs, the results can be questionable due to the relocation of the radiolabeled substance, which results in relocation artifacts that can confound results and thus has discouraged its use in the pharmaceutical industry. However, in 1964 Appleton (Appleton 1964) first developed the technique of collecting cryosections onto slides covered with strips of dried emulsion using a thaw mounting technique. This required tissue sectioning and collection to be conducted in a darkroom and under safelight conditions, which required a high level of skill. The use of cryopreservation and cryosectioning remains critical

to the study of diffusible substances because it maintains the spatial locale of the radiolabeled substance in the matrix whereas liquid tissue fixation steps often solubilize and relocate diffusible test articles. However, when substances are tightly bound to cellular structures (e.g., receptor proteins), positive results may still be obtained from samples processed using conventional histology techniques. Further refinement of MARG techniques occurred during the 1960s by Caro (Caro 1961) and shortly after by Stumpf and Roth (Stumpf and Roth 1964) who made additional improvements to establish receptor autoradiography as a more reliable technique. This established the basis for the current MARG techniques. Numerous elaborations on the techniques have been presented by different investigators (Nagata 1997), but the basic principals have remained unchanged for >40 years. Today, as in the past, the MARG technique is very difficult to master, which continues to hamper its use. Researchers must use caution when reviewing the literature and relying on articles that used the emulsion dipping technique and claim quantitative data.

MARG begins with the administration of a radiolabeled substance (typically ^{3}H, ^{14}C, ^{35}S, or ^{125}I) to lab the animal, which is then euthanized, exsanguinated, and tissues are dissected and snap-frozen in isopentane that is chilled with liquid nitrogen. The tissue is then cryosectioned at −20 °C (or the optimal cutting temperature for a given tissue/organ), to obtain 4–10 μm thick sections. Then, under darkroom conditions, sections are thaw-mounted onto dry glass microscope slides that have been pre-coated with nuclear photographic emulsion. The slides are placed into a light-tight box with desiccant and allowed to expose for an appropriate amount of time. Figure 6.2 presents a pictorial summary of the methods used for MARG. The collection of cryosections onto dry, pre-coated slides, while under darkroom conditions, is a key step developed by Appleton and it eliminates the possibility of diffusion of soluble compounds, which can happen during slide and section dipping into an aqueous emulsion (Baker 1989). Following exposure, the slides are developed in a manner similar to developing photographic film before being stained using conventional histological staining protocols. This may include immunostaining techniques that can provide positive co-localization of drug-derived radioactivity to known cell types, receptors, and/or other structures/markers for which antibody staining protocols exist (Stumpf 2003).

In theory it is possible to determine the amount of radiolabeled compound in MARG preparations and there are several examples in the literature of investigators attempting to obtain quantitative data from MARG preparations. A few methods have been proposed to determine subcellular concentrations of drugs. These methods, which date back to the late 1960s, have been presented in books by Stumpf (Stumpf 2003) and Baker (Baker 1989). One of the earliest methods, which was known as the "Restricted Method" was based on the analysis of structures of similar shape and size (Salpeter et al. 1969) and was used to describe the distribution of silver grains in sections of ^{3}H-noradrenalin labeled nerve terminals. A second "Restricted Method" was also based on the analysis of structures of similar shape, but dissimilar sizes (Downs and Williams 1984). This method established a "universal curve" and required that the two-dimensional structures associated with

Fig. 6.2 (**a**) Snap-freezing of fresh tissue sample on a cryostat sample holder. (**b**) A Leica CM3050 Cryostat for cryosectioning of sample and collection onto slides pre-coated with emulsion. (**c**) Dip Miser slide coating cup (Electron Microscopy Sciences, Inc.), Kodak emulsion, black slide exposure box, Drierite desiccant and a coated slide. Slides are dipped into liquid emulsion heated in the Dip Miser and allowed to dry. Sections are collected onto the pre-coated slides and tissue sections are exposed in a sealed black slide box with desiccant at 4 °C. (**d**) Slides are developed using Kodak Developer and Fixer. (**e**) Slides may be stained as usual. (**f**) Examples of slides that have been stained; note the bottom slide shows how emulsion picks up stain, while the upper slide has no emulsion coating (from Solon, in Braddock 2012)

radioactivity were of similar shape. An "Unrestricted Method" or "Circle Method" was developed by Williams in 1969 (Williams 1969). This tested the hypothesis that radioactivity was randomly distributed and it ascribed values for relative concentrations. It also attempted to account for a lack of precision of the restricted models. A second "Unrestricted Method" known as the "Hypothetical Grain" method was developed by Blackett & Parry in 1973 (Blackett and Parry 1973). This method has five stages that include: (1) overlay screen preparation, (2) collection of "hypothetical grains" and construction of a "Cross-fire" matrix, (3) collection of

real-grain data, (4) fitting of hypothetical and real-grain data using chi-square, and (5) modification of the matrix until an "acceptable fit" is obtained.

Each of these methods claimed to be able to estimate the number of molecules in subcellular regions if the specific silver grain yield (average number of disintegrations to produce 1 silver grain) was determined. The proposed calculations consider exposure time, specific activity, silver grain yield (dependent on sample uniform cut method conditions), section thickness, volume of the compartment, and "other parameters", which are very difficult to control due to the various artifacts inherent in this very sensitive technique. High sensitivity techniques require extremely consistent and careful preparation, especially because the current MARG techniques rely on many manual and "artful" steps. The uniformity of the detection media (i.e., the production and use of manually emulsion-coated slide) is unknown and not characterized in all examples reviewed in the literature. Tissue absorption of radioactivity is also rarely considered or characterized and the number of cells counted/quantified must be sufficient for robust statistical analysis. Variable background and background subtraction can also invalidate results. There are no tissue section thickness quality control standards and/or internal calibration standards used in MARG. Changes in daily cosmic and background radiation can adversely affect the results of an entire study, which can take weeks to months to obtain. Furthermore there are no internal standards, and/or calibrators to assure the quantitative results are valid, so the technique is often dismissed when scrutinized by scientists in other bioanalytical disciplines. In short, most pharmaceutical researchers do not have the resources available to develop routine MARG procedures to enable and/or validate MARG as a quantitative technique, thus its use in the pharmaceutical industry has been limited.

In the future, technology may help to solve some of these problems if the detection media (e.g., emulsions) can be more uniformly produced and made to have inherently linear quantitation. Technology may also help to develop easier methods of collecting uniformly thick tissue sections that can be automatically mounted onto slides for processing. Although this would be quite a challenge due to the varying matrices to be sectioned (e.g., hard bone, adipose, and eyes). Dependable micro-sized calibration and quality control standards that can be co-exposed with every section would also need to be developed to assure reproducibility of quantitation.

Finally, new methods would need to enable a significant reduction in the amount and types of artifacts that are produced. Currently, the following types of artifacts must be controlled: (1) effects on emulsion by slight variations in light, humidity, temperature, tissue characteristics, fixation, freezing, chemicals, pH, developer, fixer, and miscellaneous debris in developer solutions; (2) tissue condition (e.g., freezing technique, fixation, autolysis, sectioning temperature, improper section mounting); (3) light leaks; (4) latent image fading; (5) reticulation of emulsion; (6) positive chemography; (7) negative chemography; (8) deviations of pH in processing fluids; (9) pressure artifacts; (10) ice crystals on knife; (11) crystalline deposits from developing process (Stumpf 2003). Some of these are more easily controlled than others, but together they require a high level of skill by the analyst to overcome and the presence of any can invalidate months of work. Until methods and/or technologies can be developed that can better control tissue section and

emulsion uniformity and also reduce the sources of and occurrence of artifacts, the current technique will remain strictly qualitative and will prove to be daunting for routine use in pharmaceutical discovery and development. The lack of new developments in MARG methods have continued to make MARG an underutilized technique in drug discovery and development, but when performed correctly the results can be of utmost value in promoting a drug candidate and in answering some pivotal questions for pharmaceutical investigators.

6.4 Tissue Concentration Determinations Using MALDI-MS

As previously discussed QWBA is an established technology for assessing pharmacokinetic and distribution properties of radiolabeled drug candidates in laboratory animals and is therefore widely applied in pharmaceutical research, but those results reflect total radioactivity and do not positively identify the compound(s), which could be parent drug and/or a metabolite(s). For this reason, QWBA data are often combined with compound identification data obtained from tissue extracts and other bioanalytical techniques, such as LC/MS/MS. LC/MS identification is either based on the exact mass of the analyte, or more often by fragmenting the ions in the MS instrument and measuring the specific fragment ion pattern (also termed MS/MS). In contrast to WBA, this technology delivers high identification specificity, but spatial resolution is limited to the size of the tissue sample being homogenized and extracted. To that end, the combination of the two techniques is used to gain specific compound and metabolite distribution information.

Over the last 20 years a relatively new technology called matrix-assisted laser desorption ionization mass spectrometric imaging (MALDI-MSI) (McDonnell and Heeren 2007) has been developed and is beginning to be used by the pharmaceutical industry to support ADME studies (Rohner et al. 2005; Stoeckli et al. 2007; Khatib-Shahidi et al. 2006). The technology combines the advantages of two techniques: The spatial resolution and quantitative capabilities of QWBA, and the compound identity specificity of mass spectrometry. MALDI-MSI may utilize the same whole-body or individual organ sections obtained from lab animals given either a radiolabeled and/or a non-radiolabeled compound. First, the sections must be dehydrated before the introduction in the vacuum chamber of the mass spectrometer, and second, the analytes must be transferred to the gas phase and ionized to allow a measurement. Thousands of mass spectra are acquired from a raster of positions over the sample. These spectra are assembled into a data set, from which one can extract multiple specific distributions of a particular mass. From the selection of available surface desorption mechanisms, MALDI (Karas et al. 1987) is currently most widespread. The MALDI technique requires a matrix in order to desorb and ionize the analytes from the surface upon impact of laser pulses. From the wide variety of different matrices and matrix application protocols, the manual application of α-cyano-4-hydroxycinnamic acid solution using a conventional thin-layer chromatography sprayer represents a robust and reproducible method.

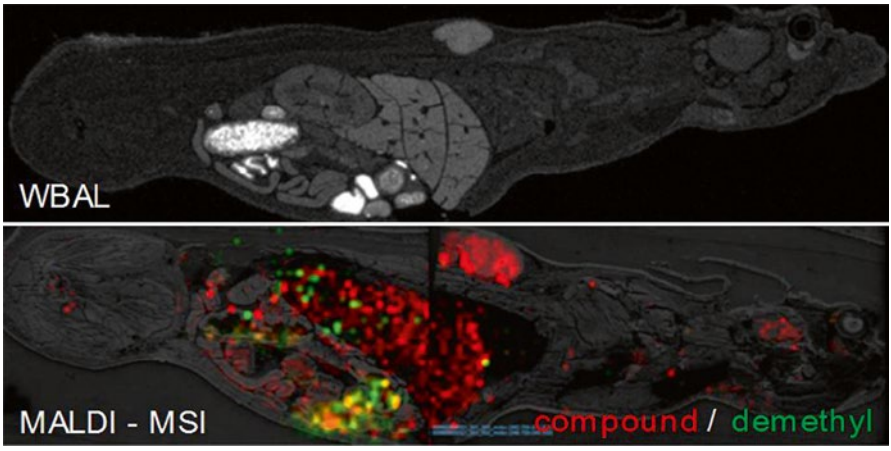

Fig. 6.3 Comparison of WBA and MALDI-MSI results obtained from the same compound-dosed animal. MALDI MSI allows distinguishing between compound (*red*) and its metabolites (*green*, co-localized with compound *yellow*), label-free and simultaneous (Taken from Solon et al. 2010)

If properly applied, this matrix leads to excellent sensitivity for a large number of compounds desorbed from tissue sections. The matrix-coated sections are then rastered over with a laser in the mass spectrometer, acquiring either spectra over the mass range of interest or multiple MS/MS spectra of the analytes of interest. The latter mode is especially suited for simultaneous imaging of a compound and its metabolites since both are often known in advance and, in addition, MS/MS images offer a high confidence in the specificity of the result. Such an image acquisition may take from 10 min up to several hours, depending on the imaging resolution. A typical experiment on a rat section with a raster of 0.5 mm takes about 1 h.

The dataset is visualized and analyzed using dedicated software written by the author, which is available for free download at http://www.ms-imaging.org. For each of the masses of interest a specific MS image is calculated and displayed similar to WBA images. The advantage of MSI is its high specificity, which allows the assignment of exact distributions for any analyte of choice. Images of multiple analytes may also be combined in a single red-green-blue image to allow an information-rich display of the distribution data (Fig. 6.3).

MALDI-MSI offers unmatched sensitivity and allows ionization of a wide substance range and, in addition, a broad selection of commercial instruments is available. Two major advantages of this technology include: radiolabeled compounds are not required because the mass and the fragmentation pattern are intrinsic properties of each molecule, which are detected by the mass spectrometer; and a mass spectrometer can acquire full spectra (or multiple MS/MS transitions) from the same sample, which allows for the simultaneous analysis of hundreds of analytes. These key advantages have inspired the development of the technology, which was specifically developed to examine drug distribution studies. The label-free

simultaneous detection of parent drug, and its metabolites has offered a powerful alternative to the well-established technologies of quantitative autoradiography.

Alternative desorption technologies suitable for mass spectroscopy imaging (MSI), which includes surface sampling (Van Berkel et al. 2008), and desorption electrospray (Wiseman et al. 2008) are also being developed, but will not be discussed here. Secondary ion mass spectrometry (SIMS) (Burns 1982) operates in a different spatial resolution regime and is described in the following section.

MS images obtained by the process described above do not consider analyte specific ion suppression effects by the biological matrix and therefore give only qualitative information on the analyte distribution. Since these suppression effects can by quite dramatic (up to 95 % signal loss were observed), additional experiments are required to evaluate and compensate for these effects. One method (Stoeckli et al. 2007) is to measure a control section homogeneously coated with compound. The resulting image displays the analyte suppression at every single location. This information, together with an internal standard spiked on the section of the dosed animals, allows a quantitative assessment of the analyte concentration. This method compensates suppression at the tissue level and not on single pixels, since all the pixels in the same tissue are normalized by the same correction factor obtained in the control experiment. A more accurate quantification can be achieved by coating sections with a stable isotope-labeled analyte before processing and then calculating the peak ratio for each pixel.

The need to obtain quantitative spatial bioanalytical data by MSI has increased over the past few years and new methods have been developed to address the limitations of quantification using MSI. Specifically, improvements are needed for reproducibility, tissue-specific ion suppression, and molecule-specific ionization yield. A recent advance in tissue quantitation of parent drug and metabolites using MALDI-MSI and radiolabeled compounds has been developed and is known as the "Modified Approach" (Hamm et al. 2012; Stauber 2012). The "Modified Standard" approach, which uses a radiolabeled compound (or an analog molecule with similar properties as the target molecule to normalize its signal on tissue or on the slide), and a calibration curve obtained using same conditions has enable scientists at Imabiotech, Inc. to quantify the amount of molecules within tissue while addressing the limitations of MSI. Currently this approach has only been successful using compounds with molecular weights of > 3,000 Da, but with further refinement the ability to quantify small molecules may be realized.

6.5 Tissue Concentration Determinations Using SIMS

In recent times SIMS-MSI has offered a complementary or alternative method to MALDI-MSI for the acquisition of higher spatial resolution images directly from biological tissue, although the technology has been used for several years in analysis of surface films and polymers. SIMS has been used successfully for the bioanalysis and imaging of tissues and cells with sub-micrometer spatial resolution and with a minimum amount of sample preparation (Heeren et al. 2006).

The SIMS ionization process utilizes a beam of ions that are directed to desorb ions from atoms, clusters, and molecules on a tissue surface that are then measured by quadrupole or time of flight mass spectrometry. The tissue material is removed by sputtering and is thus locally destroyed to obtain material for analysis. The sputtered products include atoms, molecules, and molecular fragments characteristic of the surface composition within each sample sputtered by the ion beam. Sensitivity is achieved by the secondary ion sputtering process and yields depend upon the nature, energy and incident angle of the primary ion beam as well as the properties of the target tissue and the application of any yield enhancement steps such as a metal or organic matrix coating (McDonnell et al. 2006). Images are then acquired at a resolution of a few hundred nanometers due to the use of primary ion sources that can be focused to spot sizes of ≤ 50 nm, which is far superior to that of MALDI-MSI.

The steps of SIMS image analysis and acquisition include: sample preparation of the sample (i.e., sectioning of tissues, freeze fracturing of cells to provide samples stable under high vacuum conditions which are required for SIMS analysis); ionization of the sample by the primary ion beam; mass separation (predominantly by TOF); ion detection in positive or negative polarity modes; and data handling and image processing.

The techniques requires the use of polyatomic ion sources such as Au_n^+, Bi_n^+, SF_5^+ and C_{60}^+ , which are commercially available, are easy to use, and which have long half-lives (Walker 2008). These ion sources produce larger secondary ion yields, thus reducing sample damage, and subsequent molecule fragmentation in comparison to the traditionally used liquid metal ion sources, such as gallium and indium, which produce fewer peaks above m/z 100 (Nagy et al. 2005). This increase in mass range means SIMS-MSI is ideally applicable for drug, metabolite, and lipid analysis.

SIMS technology is available in two platforms: static SIMS and dynamic SIMS. Static SIMS uses a low intensity primary ion beam, which removes a few monolayers of the surface, but generates larger mass fragments. Dynamic SIMS utilizes a higher intensity primary ion beam, which results in an increased secondary ion production, but with increased fragmentation of molecular species. SIMS can also be used for depth profiling analysis of tissues because it destroys surface through analysis thus resulting in the sputtering of species from deeper within the tissue sample (Todd et al. 2001). However, issues may occur such as with brain tissue analysis where deeper profiling was not possible due to low lipid concentrations at deeper levels (Jones et al. 2007).

Sample-coating methods, which have the potential to significantly increase the secondary ion yield, and thus the sensitivity of the analysis as well as enabling the ionization of larger lipids and peptides (Touboul et al. 2007), and two methods known as matrix-enhanced SIMS (ME-SIMS) and metal-assisted SIMS (MetA SIMS) have been used successfully. The application of an organic acid matrix has been shown to significantly increase the signal intensity of larger analytes directly from tissue (McDonnell et al. 2006), and for larger molecules (>5 kDa) the signal to noise ratio of ME-SIMS drops dramatically in comparison to MALDI (Heeren et al. 2006). Intact proteins, that have been purified and are at high concentrations, have

been observed up to 17 kDa, thus sample preparation is important, especially regarding the ultimate crystal size of the matrix, and its application method, which may become the limiting step for high spatial resolution imaging analysis. It is important to note that for ME-SIMS the ion yields will be determined by the matrix application process (i.e., tissue extraction and co-crystallization), and thus there is a significant loss of surface specificity in relation to the regular "surface sputtering" SIMS.

Studies have shown that coating the sample with a thin layer of metal (typically in the region of 1–5 nm) such as silver or gold increases the secondary ion yield of intact molecular ions (McDonnell et al. 2005). Conclusive reasoning for this is as of yet unconfirmed although the migration of analytes onto metal "nano islands" and the ability of the metal to act as a catonizing species (Delcourte and Bertrand 2004; Keune and Boon 2004; Delecorte et al. 2003) have been proposed. As the metal is sputter coated onto the tissue there is no risk of analyte spreading and thus loss of spatial information which may occur with the application of a wet organic matrix. The main problem encountered with MetA SIMS is the observation of ions in the resulting spectra in the form of metal adducts which may prove difficult to assign to specific analytes and analyte fragments.

6.6 Drug Discovery Case Studies

WBA (and to a much lesser extent MARG) has been used in the pharmaceutical industry since it was first introduced in the mid-1950s; however, it was not used extensively because it usually took weeks to months to obtain the images, which could be only for qualitative use. Autoradiographs often supported organ homogenate LSC data and only provided clues about the relative distribution to tissues, which were not be provided by LSC of organ homogenates. In the late 1980s large pharmaceutical companies and a limited number of large contract research organizations began developing and using phosphor imaging and WBA in drug discovery to help answer questions related to drug discovery, but it was not widely used by the industry because the instrumentation was very expensive. In the early to mid-1990s the Society for Whole-Body Autoradiography (SWBA) and the European Autoradiography Club (now called the European Society for Autoradiography [ESA]) raised awareness about the value of WBA and QWBA in pharmaceutical research, and regulators began asking for these studies to support drug registration. At the 1994 meeting of the SWBA, the utility of QWBA was obvious and presentations ranged from the disposition of ^{14}C-β-guanidinoproprionic acid in rats[2] to the determination of [^{14}C]risedronate in rat bone (Solon et al. 2010). The use of MARG was also discussed at these early meetings and several examples were presented by scientists from Monsanto, and labs at SUNY Stony Brook and Brookhaven National Laboratory, the latter of which discussed the use of MARG to study the prevention of renal ischemia using ^{99}Tc-RGD peptide. Although many of these presentations were rarely published, abstracts were circulated and word of mouth quickly spread about the use of QWBA and MARG to scientists in the field. Since then the use of

QWBA and MARG to support drug discovery efforts has increased and it is now commonly used to screen lead compounds for progression to development and to answer specific questions related to tumor, brain, and skin penetration, fetal transfer, tissue retention, unusual routes of elimination (ocular, intestinal, saliva, sweat, hair), hormone/enzyme redistribution due to drug affects, effects of enzyme induction/inhibition, drug–drug interactions, formulation comparisons, in vivo compound solubility, differential metabolite distribution, and interspecies comparisons to name a few.

Discovery ADME studies are often designed to include two groups of animals. One group (n = 3) is used to determine mass balance and excretion patterns and another group to determine tissues distribution. The samples obtained from these experiments can also be used to examine metabolism profiles and identification. A typical group for QWBA analysis, which may utilize only 4–6 rats, may include both oral (PO) and intravenous (IV) dose routes. Usually there is only one animal per time point and a few time points post-dose (typically at the expected time of expected maximal plasma concentration and 24 h post-dose), but this can provide a wealth of information. These studies may also include a third group of animals to provide individual tissues for possible MARG analysis, which could be conducted at any time during discovery and/or development. A separate group of animals to supply tissue samples for MARG is needed because the freezing step used for QWBA is relatively slow and leads to poor microscopic morphology.

Discovery ADME studies are valuable because they not only help to answer specific questions, but they also provide a snap-shot of overall tissue distribution that can be used to better design a more definitive tissue distribution study and can alert toxicologists and pathologists to potential safety issues. The image data can also be used later on during drug candidate selection to choose the discovery candidate with the best tissue distribution profile and/or to follow-up on new questions that often arise during discovery and development.

There has been a resurgent interest in the use of MARG in drug discovery, especially in the areas of ocular (Solon et al. 2010), brain (Solon 2007), and skin (Rauvast and Mavon 2006) distribution, where low but efficacious tissue concentrations can be localized at the cellular level to help scientists understand the action of their test compounds. This resurgence has been partially attributed to the availability of MARG as a contract service because the technique requires highly skilled scientists who are enabled to maintain their expertise by performing the procedures on a routine basis. The use of MARG requires a technical and scientific understanding of histology, drug disposition, and the use of radioactivity. Histology expertise normally fall into the Toxicology/Pathology departments of pharmaceutical companies, and the use of radioactivity is unfamiliar and often not allowed. As a result, these studies are usually conducted in a drug metabolism/pharmacokinetic (DMPK) department where the scientists are familiar with using radioactivity, but unfortunately most do not have a good understanding of histology and/or anatomy and physiology. This is another reason that MARG has been underutilized in the pharmaceutical industry. QWBA and MARG have been used to study a variety of compounds that include antibodies, liposomal compounds,

nanoparticles, oligonucleotides, peptides, proteins, radiopharmaceuticals, and small organic molecules (Solon 2007).

QWBA is an excellent tool to understand how chemical entities are absorbed and eliminated from not only the body, but most importantly into and out of discreet tissue compartments, which includes target organ(s)/tissue(s). Many researchers are familiar with the analysis and utility of plasma PK as an indicator of drug exposure, however target tissue PK profiles are often very different from plasma PK. Discovery QWBA and MARG studies can help scientists by providing in situ drug concentration data specifically for target tissues. In addition to gaining information about tissue PK, QWBA not only provides information about renal and biliary excretion, but it also reveals unanticipated routes such as intestinal secretion, hair, tears, salivia, seminal fluid, lymphatic fluid, cerebrospinal fluid, and/or sweat. Figure 6.4 shows an example of a drug that was observed to be secreted into the intestinal lumen after an IV dose. This small study was conducted to investigate why radioactivity was observed in feces of bile-duct cannulated rats given a single IV dose of a radiolabeled drug in a discovery mass balance study (Solon et al. 2002). QWBA showed drug-derived radioactivity in the intestinal tract at early time points, which indicated a small, but significant portion of the drug-derived radioactivity was being secreted directly into the lumen of the gastrointestinal tract as well as in bile and urine.

QWBA has been used to examine the distribution of xenobiotics through placental transfer into the fetus and the same samples have also been used for analysis of metabolites that are present in various tissues to provide detailed information about the ADME profile of a test article. An example of this is a study of fetal and maternal tissue distribution of ^{14}C-azidothymidine (^{14}C-AZT) after a single intravenous administration to a pregnant female rat (Solon 2007). QWBA revealed differential distribution of ^{14}C-AZT-derived radioactivity in fetal and maternal brain and liver (Fig. 6.5). Concentrations of radioactivity in fetal brain and liver were higher than in the adult. Fetal and maternal tissues were also obtained by necropsy of an additional pregnant rat for MARG and metabolite profiling by radio-HPLC. Figure 6.6 shows the MARG results which revealed the histological details of the different localization patterns.

To further characterize the different patterns of distribution, samples of fetal and maternal brain and liver were homogenized, extracted, and analyzed by radio-HPLC to obtain a metabolite profile of each tissue and differences were identified (Fig. 6.7). Further analysis using mass spectroscopy techniques can provide identification of these metabolites. This combined approach can help answer questions regarding pharmacokinetics, pharmacodynamics, and toxicology.

A second example of using this combined approach was demonstrated in a proof of concept study that was conducted to demonstrate how a small integrated study could provide preliminary ADME data related to Paclitaxel (Taxol) and its

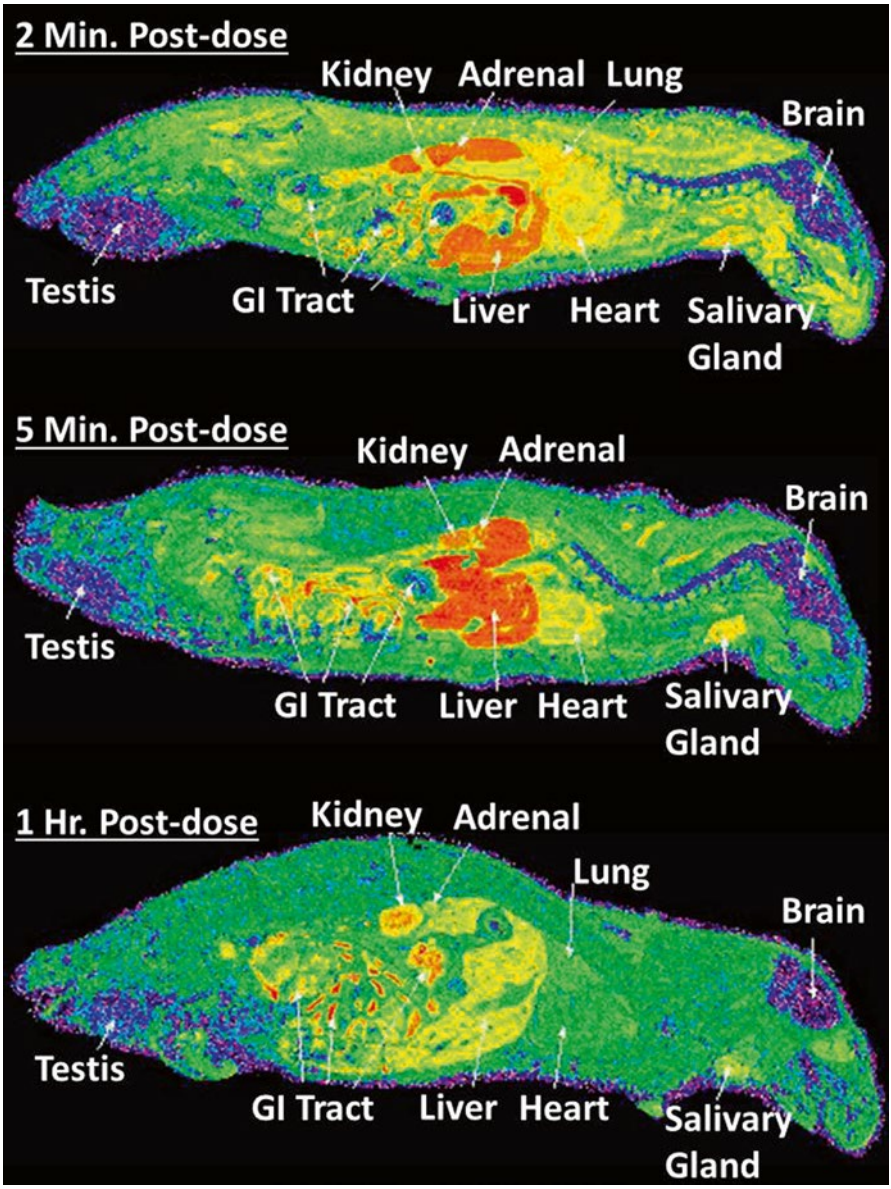

Fig. 6.4 Intestinal secretion. Autoradiograph of bile-duct cannulated rats given an IV dose of a ^{14}C-labeled drug. QWBA demonstrated intestinal secretion as an unanticipated route of elimination. The *red* color in the gastrointestinal (GI) tract is a high amount of drug-derived radioactivity (from Solon et al. 2002)

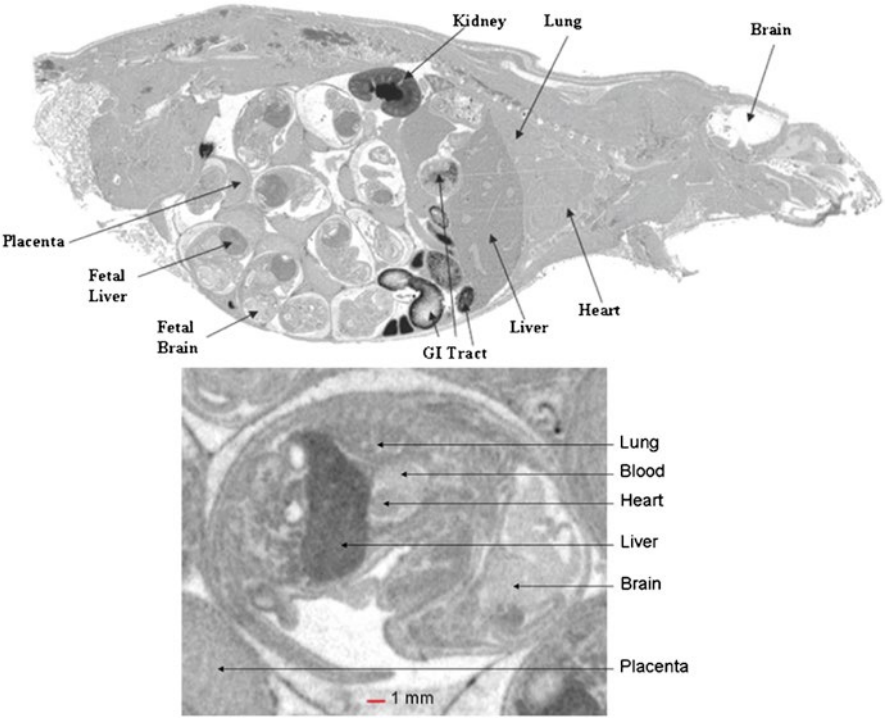

Fig. 6.5 Whole-body autoradioluminographs of a pregnant rat (*top*) and a 17-day-old fetus (*bottom*) showing differential distribution of ^{14}C-AZT-derived radioactivity in liver and brain (from Solon 2007)

metabolites by combining QWBA, liquid chromatography and flow through scintillation radiodetection (LC/FSD), and liquid chromatography and dual mass spectroscopy (LC/MS/MS) (unpublisheds data, Solon). ^{14}C-Taxol was given to four rats and blood, plasma, excreta and carcasses were collected for analysis of excretion and tissue distribution patterns. Samples of liver, kidney, spleen, heart, lung, skeletal muscle, and bone marrow were collected from the carcasses during sectioning for QWBA and were extracted and analyzed by LC/MS/MS to identify metabolites in tissues and plasma at each time point post-dose. Figure 6.8 shows the QWBA results, which showed differential distribution of drug-related radioactivity in the kidney, liver, and brain at the later time points, which was helpful in further elucidating the metabolism.

QWBA also showed relatively high concentrations in the central nervous system and testis, which prompted further analysis that identified potentially neurotoxic metabolites. LC/FSD/MS/MS data showed that low specific activity hindered LC/FSD profiling; however, the absolute amounts of drug-derived compounds were adequate for LC/MS/MS identification and two hydroxylated metabolites were found in low amounts in the liver, lung, kidney, and blood and an unknown

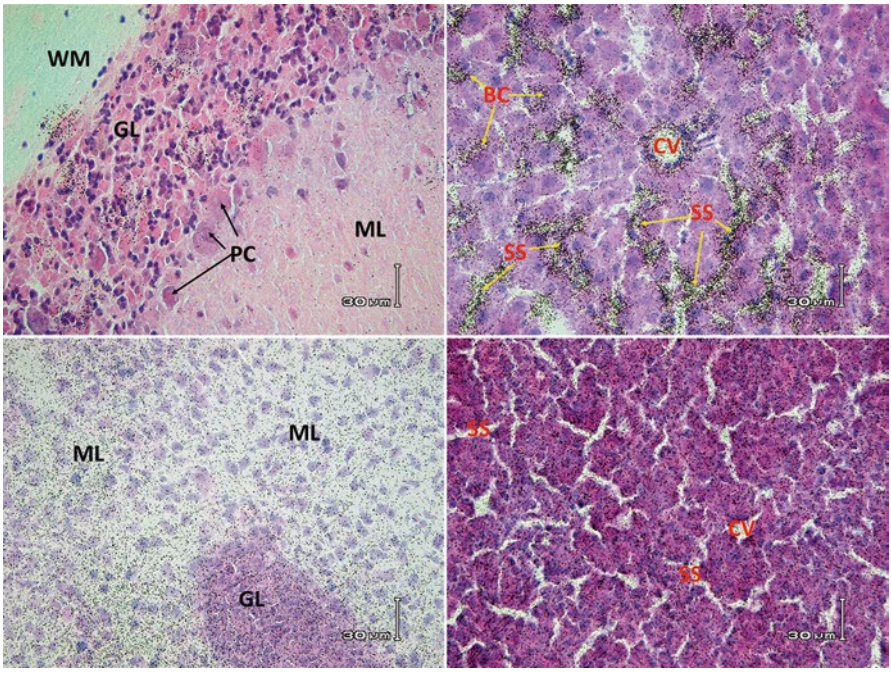

Fig. 6.6 Photomicroautoradiographs of the cellular localization of ^{14}C-AZT-derived radioactivity in the brain and liver of a pregnant rat (*top left* and *right*, respectively) and in the brain and liver of a 17-day-old fetus (*bottom left* and *right*, respectively) (Hematoxylin & Eosin Stain, 400×; ML = Molecular Layer, GL = Granular Layer, WM = White Matter, PC = Purkinje Cells) (from Solon 2007)

metabolite was found in urine. The developmental toxicity of Taxol has been known for over a decade before this proof of concept study was conducted however the exact cause has not been known for several more years. If a complete radiolabeled ADME study was run during the development of Taxol the metabolite ID and profiling may have pointed out this liability very early on development.

Understanding the clearance of compounds is paramount to developing a new drug and QWBA is an excellent technique that shows clearance and/or retention from every compartment of the body and as such it is useful in identifying tissue(s) that may pose a potential safety risks. Figure 6.9 shows an example of how QWBA analysis of two rats clearly demonstrated the retention of a discovery drug candidate that showed poor recovery in a discovery mass balance study. In this example, plasma data alone showed clearance from that compartment within 24 h, but QWBA images and tissue concentration data showed retention of drug-derived radioactivity in practically all tissues and no further work was conducted on developing the compound (Solon et al. 2002).

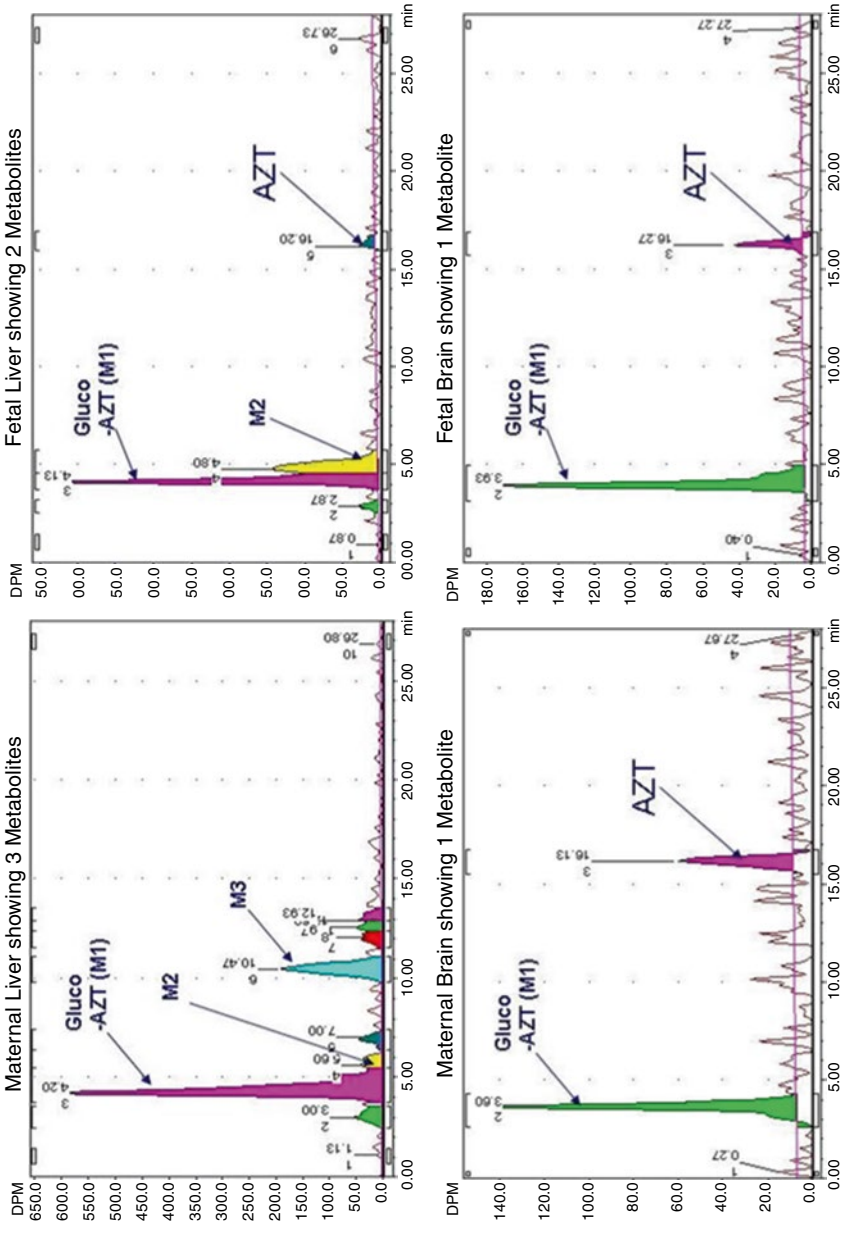

Fig. 6.7 Radiochromatographs showing the metabolite profiles obtained from maternal and fetal liver and brain samples after a single intravenous administration of ^{14}C-AZT

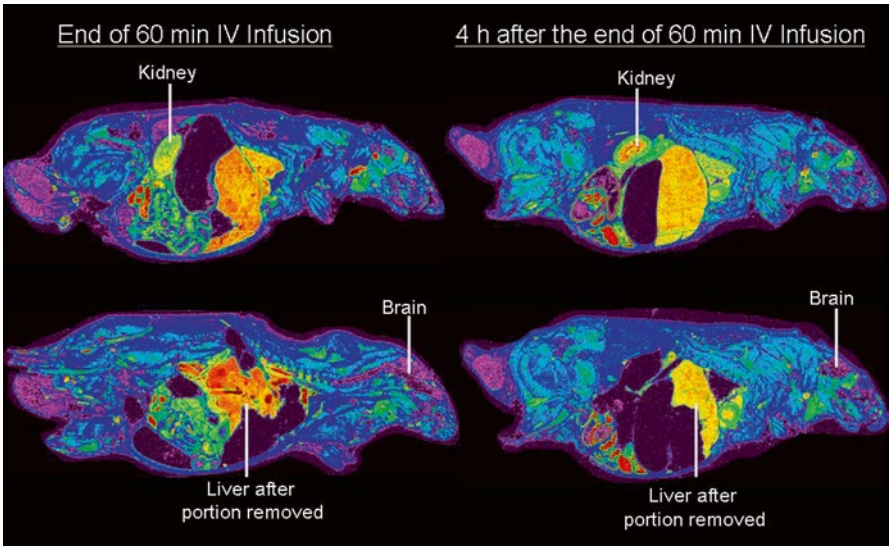

Fig. 6.8 Autoradiographs of ^{14}C-Taxol in rats after a 60 min infusion. Portions of liver, kidney, spleen, heart, lung, skeletal muscle, and bone marrow were removed and analyzed by LC/MS/MS and LC/radioflow detection to profile and identify metabolites (Solon, Unpublished Data)

Conversely, QWBA can also reveal the tissue distribution characteristics of high clearance drugs and/or the effects of enzyme induction, which may end or prolong further development of the drug. Figure 6.10 shows the resulting distribution pattern of a drug that induced its own metabolism and clearance (Solon et al. 2002). The data obtained at 24 h after the last of five daily oral doses of the same drug showed that the elimination after multiple dosing was more rapid than after a single dose and thus tissue exposure was notably lower. In most cases, this would end further development of the compound; however, concentrations in the heart, liver, and intestinal tract were present, which may be high enough to be efficacious for specific therapeutic treatments.

QWBA is often used in drug discovery to answer a variety of questions and/or to understand issues related to drug–drug interactions, inhibition and induction of metabolism, and the effects of drug transporters. These studies may utilize genetically modified animals such as p-glycoprotein knockout models, or the intentional use of specific drugs that are known to induce or inhibit specific metabolic enzymes. Figure 6.11 shows the effect of aminobenzotriazole (ABT), which is an indiscriminate inhibitor of P450 enzymes, on the tissue distribution of an aromatase inhibitor designed to treat cancer (Solon et al. 2002). This example showed researchers that a metabolite of the drug was able to penetrate the brain, which was an intended target, while the intact parent compound did not. This could be a benefit or liability depending on the nature of the metabolite, but this simple two animal study pointed out a potential toxicity issue that might need to be considered while moving the drug candidate through discovery.

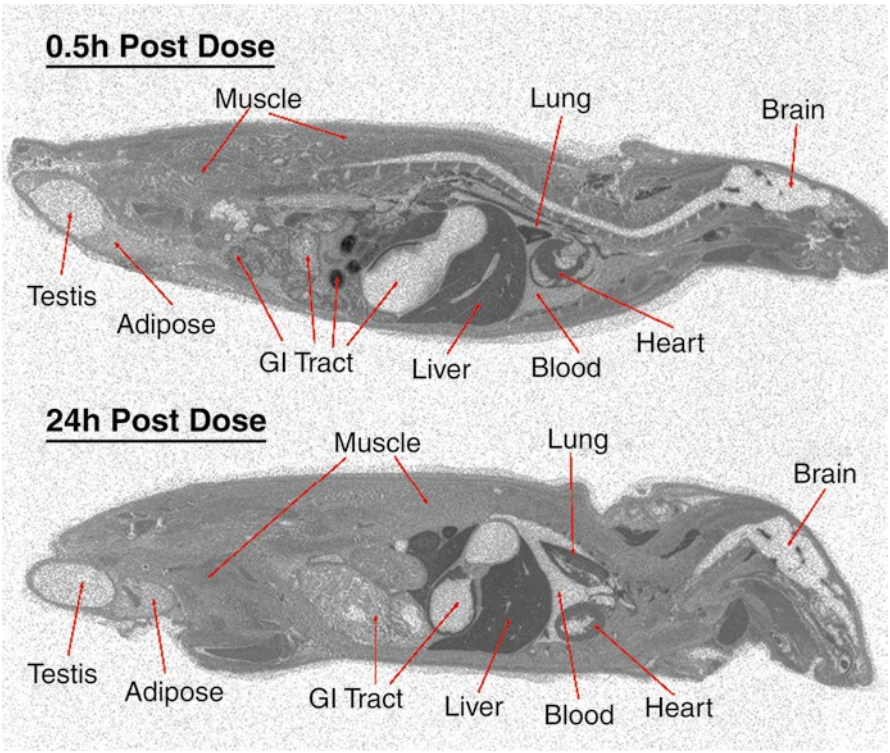

Fig. 6.9 Retention of drug-derived radioactivity in rat tissues. Whole-body autoradiographs of two rats given similar IV doses of a ^{14}C-labeled compound and were sacrificed at 0.5 (*top*) and 48 (*bottom*) h post-dose. Autoradiographs showed little or no decline in the amount of drug-derived radioactivity in tissues at 48 h post-dose, while blood concentrations were below quantifiable limits (from Solon et al. 2002)

It is crucial to determine the penetration and exposure of antibiotics into target tissues as early as possible to ensure that a given compound will be efficacious. This is especially true when the tissue to be treated is difficult to penetrate (e.g., brain, testis, bone). Figure 6.12 shows an autoradiograph of the distribution of ^{14}C-dalbavancin into bone and related tissues that can be infected by methicillin-resistant Staphylococcus after related surgical procedures and/or other trauma (Solon et al. 2007). In this study rabbits were given a single IV dose of ^{14}C-dalbavancin and one rabbit each was euthanized at various time points up to 336 h post-dose. The leg of each rabbit was frozen, sectioned, and examined using quantitative autoradiography, which showed that high concentrations of dalbavancin rapidly penetrated bone marrow, epiphyseal plate, periostium, and articular cartilage up to 336 h after the single dose. These data suggested that dalbavancin would be clinically useful in treating bone and joint infections.

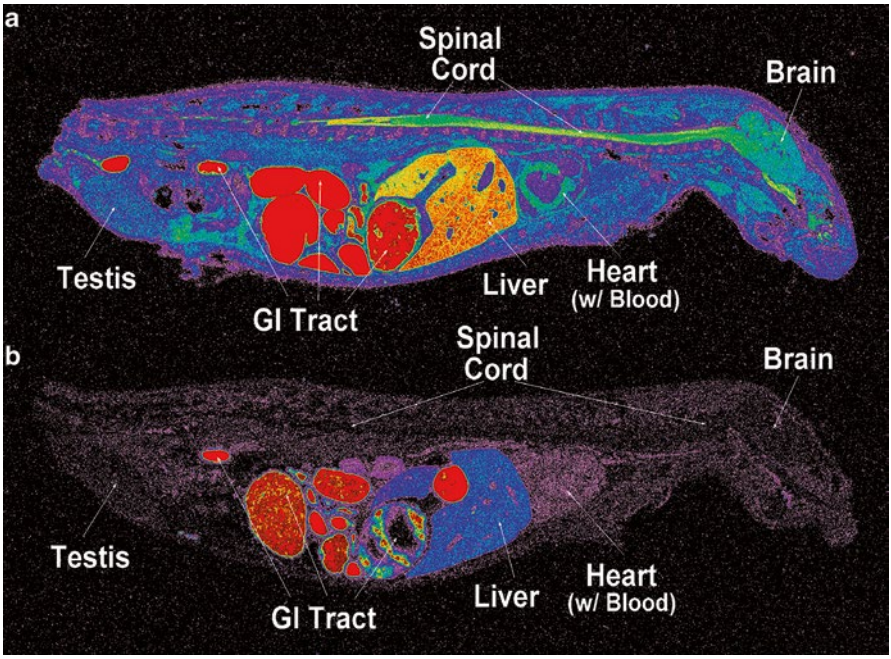

Fig. 6.10 Autoradiographs of a ^{14}C-drug in rat before and after enzyme auto-induction and tissue distribution. (**a**) Whole-body autoradiograph of drug-derived radioactivity in a rat at 24 h after a single oral dose of a ^{14}C-labeled drug. (**b**) Whole-body autoradiograph of drug-derived radioactivity in a rat at 24 h after the last of five daily oral doses of the same drug (days 1–4 administered unlabeled drug, day 5 administered ^{14}C-labeled drug) (from Solon et al. 2002)

The utilization of quantitative phosphor imaging and MARG to study drug distribution in individual complex organs such as the eye, skin, and blood vessels has helped many investigators gain a better understanding of their drug candidates and has become a strategy to select lead compounds. The use of the two technologies offers a powerful combination to obtain a high resolution image of the distribution into very discreet tissue compartments while providing reliable quantitative data on tissue concentrations. Figure 6.13 shows a phosphor image of a dog eye after treatment with a radiolabeled test article and MARG images that shows detailed qualitative distribution at the cellular level. In this example the test article was applied topically and tissue concentrations in the sclera, cornea, iris, conjunctiva, uveal tract, aqueous and vitreous humors, and lens were determined using the phosphor images obtained from sections adjacent to the sections used for MARG (Solon 2013).

These techniques were used by Miyaji et al. (Miyaji et al. 2011) to examine the distribution of a novel δ-protein kinase C inhibitor, which was reversibly conjugated to a cell penetrating peptide (KAI-9803) in rats. In this study the authors used both QWBA and MARG to show that KAI-9803 was delivered to target cells in the liver, heart, and kidney.

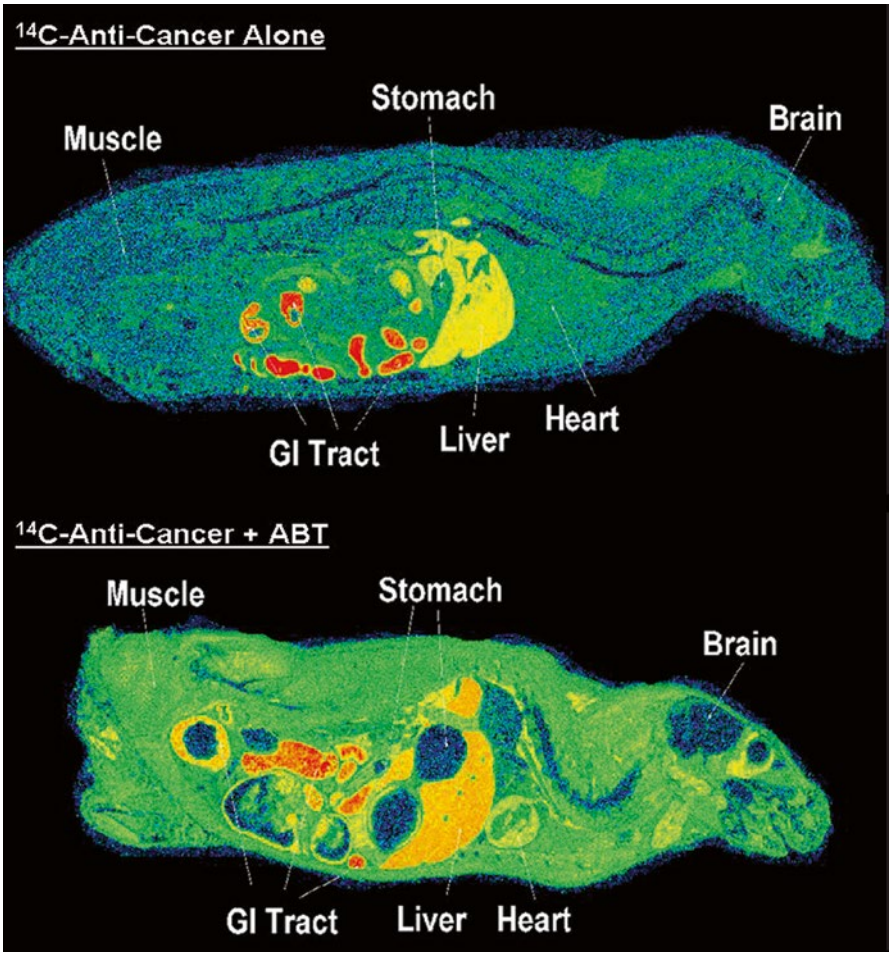

Fig. 6.11 Rat whole-body autoradiographs of ^{14}C-anticancer drug before and after metabolism inhibition by ABT. ABT decreased tissue:blood ratios ratio from 0.96 to 0.11 and showed that brain radioactivity was probably due to metabolite instead of parent drug, and suggested that more intestinal receptors were occupied by the parent molecule instead of metabolite (from Solon et al. 2002)

Serial whole animal sections can demonstrate not just the distribution of a radiolabeled or photonically labeled (see luciferase and QD sections) NCEs. Studies of cytokine stimulation of DNA synthesis (^{14}C-thymidine incorporation) have also been very useful in studying the pharmacodynamic responses of biologic therapeutics. Following cytokine administration the body undergoes a cascade of immunostimulatory events which can trigger such outcomes as cytokine storms not unlike that experienced in patients administered the Tegenro immunotherapeutic antibody. The extent of a cytokine or biologic entity immunostimulation versus the

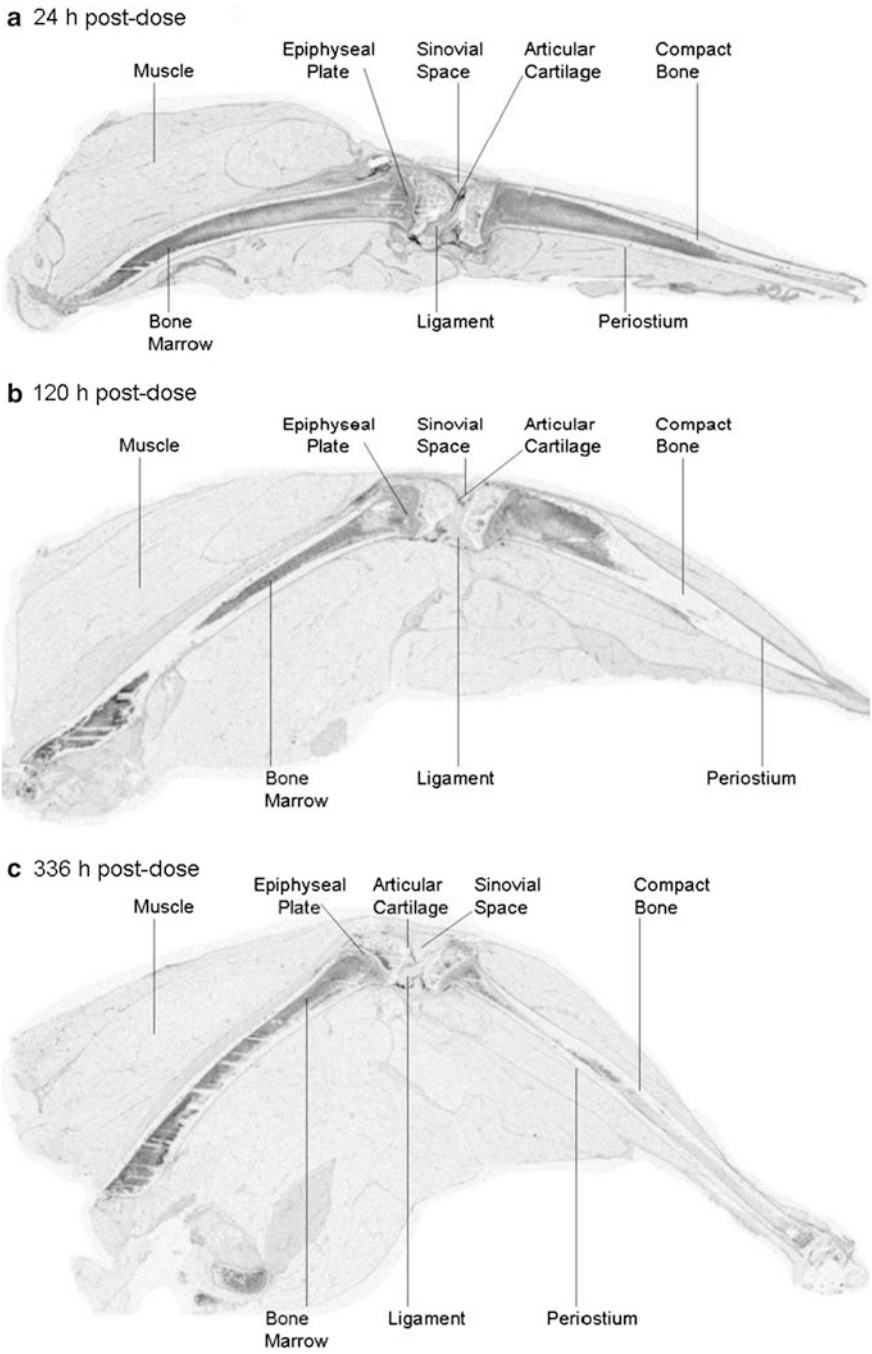

Fig. 6.12 Autoradiographs of ^{14}C-dalbavancin distribution in the hindleg of a male rabbit after a single IV dose at 20 mg/kg rabbit. Drug-related radioactivity was apparent at 24 h after a single dose (**a**), and was observed in tissue at 120 h (**b**) and up to 336 h (**c**) after a single dose (from Solon et al. 2007)

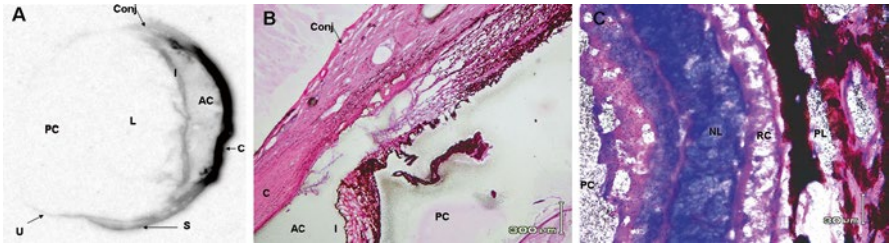

Fig. 6.13 Phosphor image of a dog eye (*A*) and micro-autoradiographs of the anterior eye structures (*B*) and posterior eye structures (*C*) after a topical administration of a ^{14}C-labeled test drug showing the localization of drug-derived radioactivity in cornea (C), iris (I), conjunctiva (Conj), posterior chamber (PC), anterior chamber (AC), uveal tract (U), lens (L), nuclear layer (NL), rods and cones (RC), and pigmented layer (PL). Radioactivity in (*A*) appears as a grey-scale image where black is high radioactivity and white is background. Radioactivity in (*B*) and (*C*) appears as black grains on the hematoxylin- and eosin-stained cryosections (From Solon 2013)

programmed dose escalation, and the extent of the stimulation out in time following administration, are key development milestones toward clinically acceptable conditions. The role of a cytokine, its mechanism of action, and the steps required to arrest such stimulatory activities also must be mapped and characterized.

To that end, a study examined the DNA synthetic activity following a clinically relevant immunostimulatory dose of a cytokine in a murine strain (unpublished data). Mice were given the cytokine at $T=0$, and at 24, 48, and 72 h post cytokine administration the animals were administered a labeling dose of ^{14}C-thymidine to map the extent of DNA synthetic areas relative to naive controls. Figure 6.14a (Panel A and B) and Fig. 6.14b (Panel A and B) represent the biodistribution of DNA synthetic activity at 24 and 72 h after cytokine stimulation (with similar serial sectioning of a control mouse in A). We will not cover the labeling method as this is relatively standard in such analyses. However, it is important to note in these images the relative increase in non-hematopoietic along with the other normally stem cell progenitor synthetic tissues, such as the gastrointestinal tract crypt cells and bone marrow. The DNA precursor demonstrates a uniform hematopoietic and gastrointestinal uptake in both sets of controls (A panels) and the uptake and expression of DNA synthesis continues well beyond the clearance of the intravenously administered cytokine, which in this study, and at the dose administered, had an

Fig. 6.14 (continued) (RES) clearance via the spleen. Note the high accumulation in the *white* pulp islands of the spleen seen as punctate accumulations located in situ. A. Five serial 30 μm sections of a rat at 4 h post-injection of the cytokine. B. The serial spleen images seen in the whole animal sections is depicted next to the histology image of an H&E-stained spleen demonstrating the *purple* islands of nuclear stained white cells. Spleen histology courtesy of: http://wahoo.nsm.umass.edu (free image). Full systemic blood clearance is noted in the cardiac chamber image in section 5 along with the void in the portal vein in the liver (images from Moyer; unpublished data)

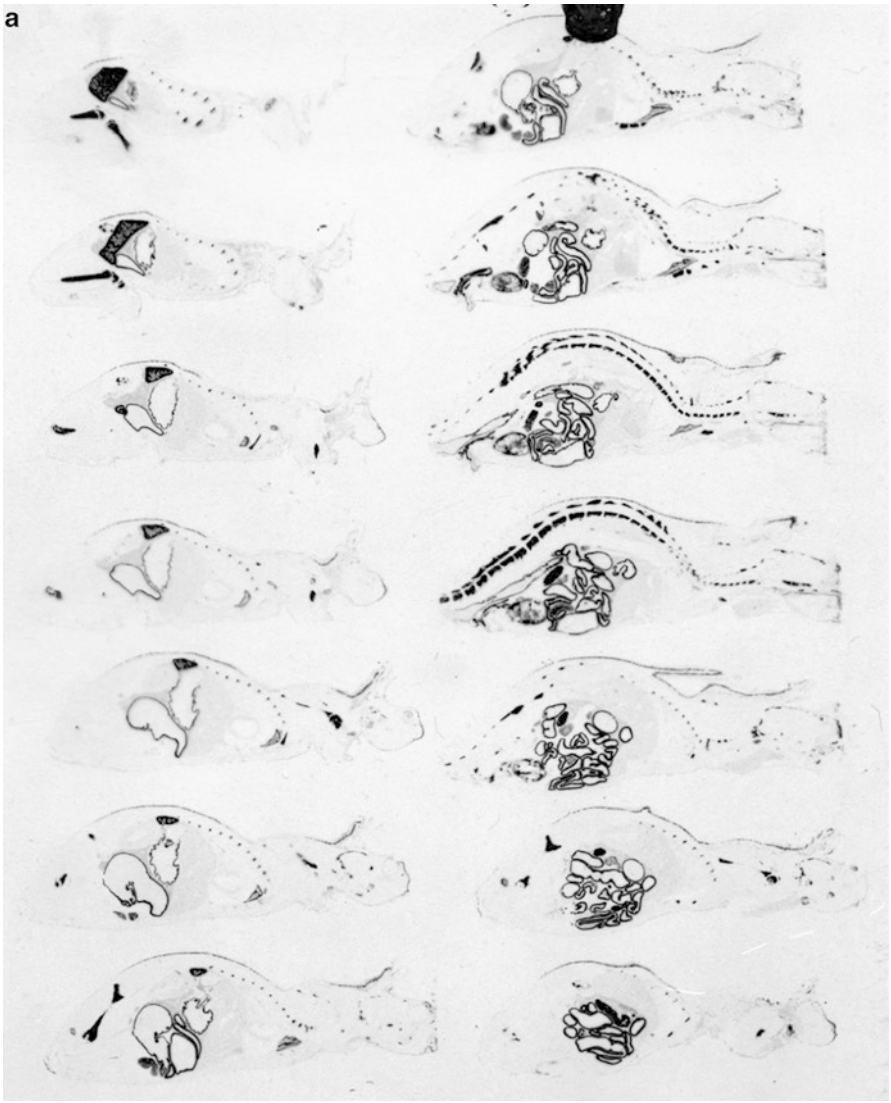

Fig. 6.14 (**a**) Serial 20 μm sections (L → R) through mice (Control and Cytokine-stimulated) at 24 h. Immunosynthetic changes in the mouse at 24 h following a stimulatory administration of a clinical dose of a cytokine at $T=0$. Animal sacrifice was at 2 h post thymidine at 24 h post cytokine. A. Control (unstimulated) mouse at 24 h after vehicle; B. Cytokine-stimulated mouse at 24 h. Images are of the distribution of C-14 Thymidine uptake representing stimulation of DNA synthesis. Note the heavy uptake in the normal animal is primarily associated with bone marrow, spleen, and GI, while the stimulated mouse has much more universal stimulation of DNA synthesis (from Moyer; unpublished data). (**b**) The same experiment as Fig. 14.a, but the thymidine tracer was administered at 72 h post stimulation (or vehicle). A. Control (unstimulated) mouse at 72 h post vehicle. B. Cytokine-stimulated mouse at 72 h post cytokine. Note the extensive DNA stimulation remains "ON" (a "PD effect") even out to 72 h post cytokine administration. Serial whole mouse sagittal sections (20 μm) from the *left side* to the *right side* of each animal (spleen is in the first *upper left* section). (from Moyer; unpublished data). (**c**) Example of a cytokine formulation that resulted in an unpredicted in vivo clumping of the protein followed by rapid reticuloendothelial

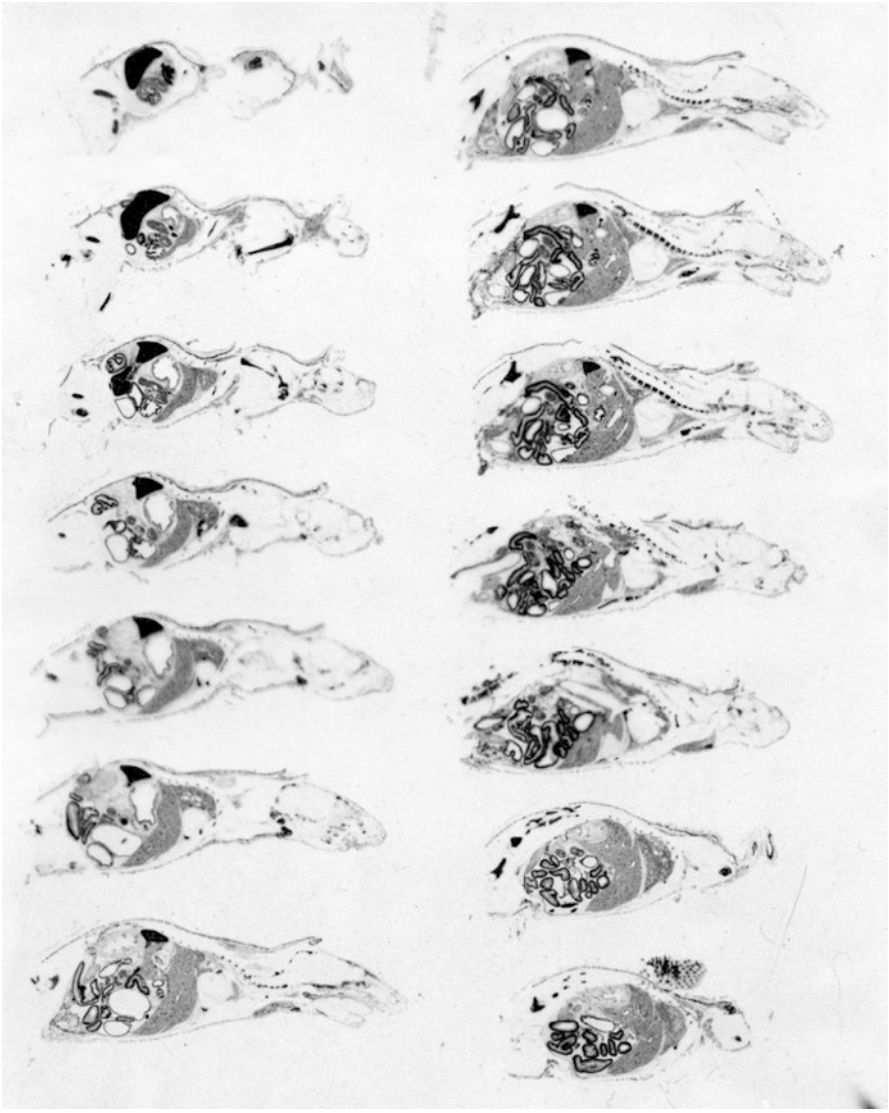

Fig. 6.14 (continued)

intravenous half-life of only 2 h yet immunosynthetic activities remain highly active well into 72 h post cytokine administration and in the multiple non-hematopoietic and gastrointestinal tissues. Organ distribution of radiotracers or water content and diffusibility (diffusion tensor imaging of MR, see Chap. 11) are also accomplished by dissection and LSC, and imaging of dissected organ approaches. An example of an imaging of a dissected organ was used in a program of drug development to

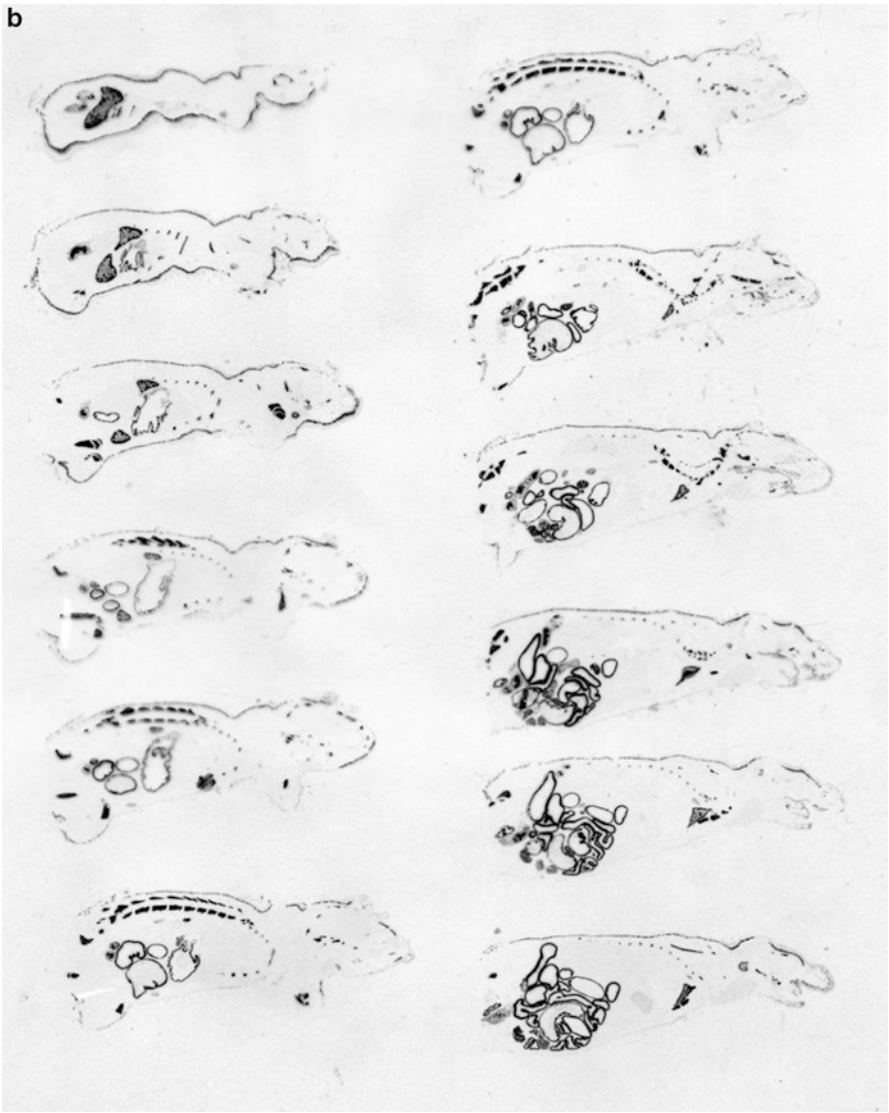

Fig. 6.14 (continued)

image cholesterol-laden plaques in arterial segments. This was a program to develop a somatostatin analog, which binds to highly expressed SSTR receptors in the underlying injured vascular tissue, which is capped by cholesterol deposition. The New Zealand White (NZW) rabbit has historically been used as a model of cholesterol deposition on arterial walls. The natural history of aortic arch injury by cholesterol (and also by aortic stripping injury by balloon catheterization) in this animal model has been used in the study of atherosclerotic disease.

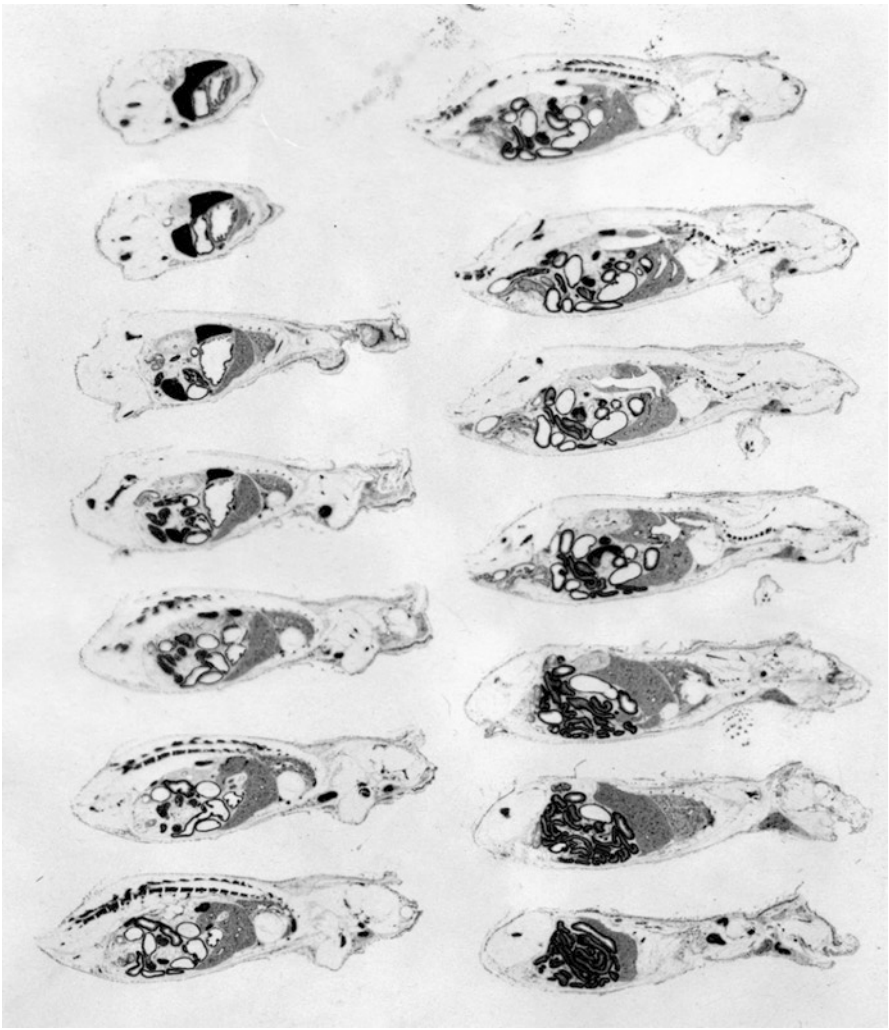

Fig. 6.14 (continued)

In the late 1980s it was noted that somatostatin receptors were expressed in vascular tissue and that they are up- and downregulated dependent on the state of arterial injury (unpublished data, Moyer). Early injuries of plaque deposition and vascular damage by attenuation of feeder blood flow (weeks to 4 months) following balloon catheterization for endothelial stripping of the distal artery and/or high cholesterol (1–3 % of the daily herbivore diet) are shown in Fig. 6.15.

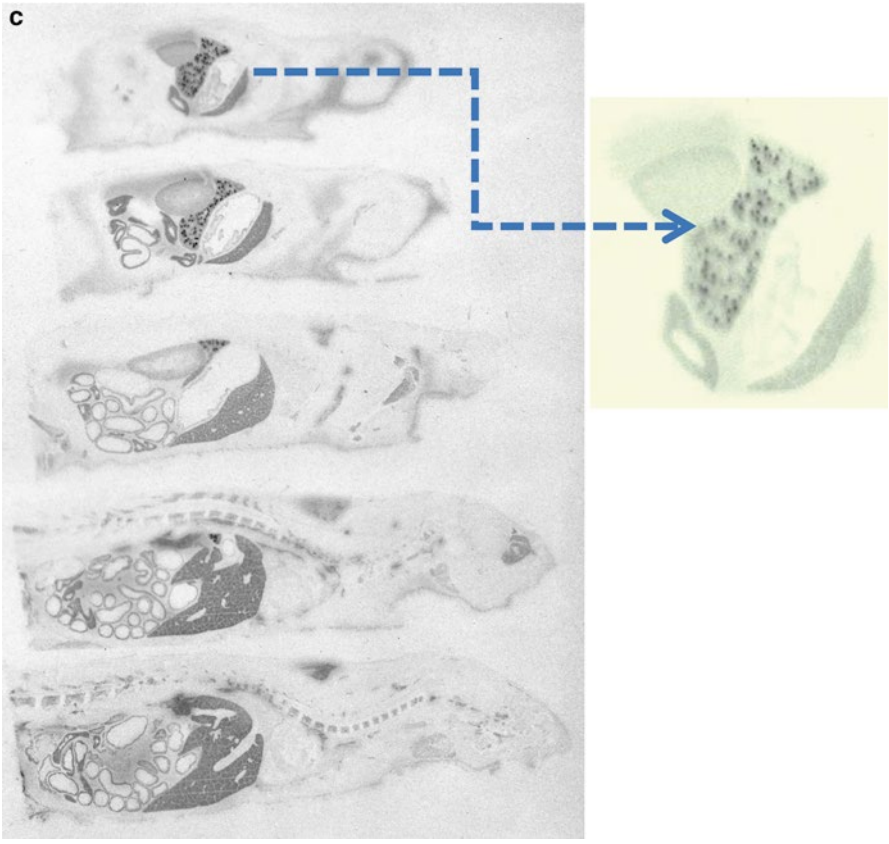

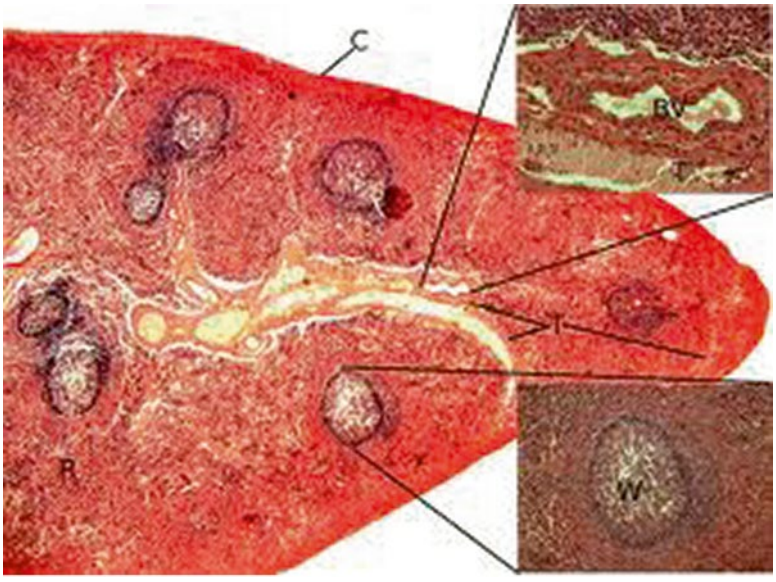

Fig. 6.14 (continued)

Fig. 6.15 An example of both ex vivo gamma camera and *en face* film imaging (i.e., radiograph) of aortic (atherosclerosis-test and control) and esophageal (NEG control tissue) isolates. The upper image depicts three tissue explants from three NZW rabbits (two test and one control) where cholesterol-fed rabbits exhibited a thick adherent depot of plaque over the aortic arch vascular wall. A Tc-99m SST (somatostatin) receptor (−R) antagonist peptide under development at the time was for development of a diagnostic imaging test to detect SSTR upregulation associated with aortic injury from chronic cholesterol exposure in the diet resulting in injured arterial walls. The peptide showed dramatic uptake in the cholesterol-laden aortic arch relative to associated (parallel and coincidently imaged in vivo) control tissue (>7 % ID/g versus <0.2 % ID/g), the uninjured esophagus. The issue of further development was hampered by the lack of an ability to associate a progressive SSTR expression relative to the cholesterol uptake with the natural history. It was found that as the animals experienced prolonged exposure and progressively injured more of the arterial segment, there was not a consistent or predictable expression of the SSTR signal along the arterial segment. Early disease was seen to show SSTR expression that would aid in predictive diagnostic but late stage disease, the more common to be seen clinically, diminished in SSTR signal proportionally to the extent of underlying vascular injury (Moyer, unpublished data)

6.7 Quantitative Imaging for Drug Development

The determination of tissue distribution of new drugs is often required by regulatory agencies for new drug registration and for their development. In the mid-1990s regulatory agencies, such as the Japanese Ministry of Health and the US FDA, made formal statements about the acceptability of QWBA data for new drug registration (Solon and Kraus 2002) and QWBA has become the technique of choice because the data provides much more detailed information than the former organ homogenate techniques.

Tissue PK information not only provides researchers with a way to examine detailed compartmentalized drug concentration information, but it also enables the determination of specific target tissue PK/pharmacodynamic (PK/PD) modeling, and the estimation of human tissue radiation exposure during human radiolabeled studies that are needed to examine human drug metabolism. Prior to the implementation of QWBA, organ dissection and LSC assays provided only a rough estimate of organ exposure to radiation and unfortunately less accurate tissue exposure information. This becomes important when a radiolabeled drug is retained in a discreet tissue within an organ with heterogenous tissue composition, such as the eye, kidney, and adrenal glands. In these cases the actual tissue concentration would be underestimated by LSC assay of organ homogenates because high concentrations in a discreet tissue would be diluted by low concentrations in surrounding tissues in an organ homogenate. This could lead to incorrect decisions about drug and/or radiation exposure.

Furthermore, classical dissection/LSC organ distribution studies often used an insufficient number of time points to reliably determine PK parameters for many organs. This was primarily a resource decision because organ homogenate studies require the use of three animals per time point due to the inherent variability introduced by organ collection (i.e., variable trimming and exsanguination at necropsy) and the extensive sample processing required for that technique. QWBA, which utilizes intact animals that have not been processed to any great extent, has shown much less variability (Coulston and Carr 2000; Solon and Kraus 2002) and so these studies are designed to include the analysis of more time points, which lead to more reliable PK data for more tissues. A typical, well-designed QWBA tissue distribution study includes the use of one animal per time and 8–12 time points. The study may also include extra animals that are maintained on the study after the QWBA data from the initial time points are examined. Most studies are designed such that the last animal carcass is collected at 5–7 days after a single dose administration. Another general guideline is to set the last time point to be at least 10 times the drug half-life in plasma, but researchers must consider that tissues will probably have very different half-lives and often it is many times longer than the half-life observed in plasma. To ensure that elimination can be verified from all tissues an extra animal may be added to the study such that it could be analyzed at a time point after the main study data have been examined. This provides researchers with an opportunity to determine the elimination of drug-related radioactivity from tissues that may retain it much longer than other tissues. This is especially useful if a drug and/or its

metabolites associate with melanin in pigmented tissues, such as the retina of the eye, meninges of the central nervous system, and pigmented skin, which could pose a radiation safety concern to humans during a clinical radiolabeled study (Roffey et al. 2007). In these situations, it is not unusual to see very slow elimination from pigmented tissues that can last for several weeks.

Male pigmented rats are used most often for tissue distribution studies, however, the animal model that best represents the expected pharmacokinetics in humans should be used whenever possible. This includes the examination of placental transfer of radiolabeled drugs in lab animals, such as that conducted at the Walter Reed Army Institute of Research (Li et al. 2008), who used QWBA to further clarify embryotoxicity of artesunate and its metabolite dihydroartemisinin in pregnant rats. Their work highlighted the importance of obtaining knowledge about partitioning of xenobiotics after introduction into the body and how that data can be used in the assessment of physiology-based pharmacokinetic modeling.

QWBA is routinely performed using all types of laboratory animals, which includes mice, hamsters, rats, guinea pigs, rabbits, ferrets, cats, dogs, and nonhuman primates. The large format cryomicrotome used for QWBA can adapt to any carcass or portion of a carcass that can fit into a frozen block that is approximately 40 cm long by 15 cm wide by 15 cm high. This added versatility provides for interspecies comparisons, which, for example, can be useful when researchers need to compare tissue PK parameters of the toxicology model (e.g., rat, mouse, or dog) to the pharmacology/efficacy model (e.g., guinea pig, rabbit, cat). This can be very valuable in explaining different results across species and was used by Pharmacia and Upjohn to study the pharmacokinetics of latanoprost in the cynomolgus monkey (Sjöquist et al. 1999). In this study radiolabeled latanoprost was administered topically to the eye of monkeys and QWBA was performed. The results revealed that drug-derived radioactivity had traveled through the lachrymal ducts and that high concentrations were present in the gastrointestinal tract, kidney, liver, blood, bile, and urine.

Researchers are often faced with a decision regarding where to place a radioactive label for their development studies. One important consideration is whether or not the isotope placement will enable the tracking of a particular metabolite and/or if a particular metabolite will be retained for a longer period of time than another. To help address this researchers sometime perform a QWBA tissue distribution study using a test article that has been labeled in two different places and then dosing two separate groups of animals to compare the tissue distribution patterns and PK of the drug-derived radioactivity from the two versions of the radiolabeled test article.

Figure 6.16 shows some of the results of such an experiment where a tissue distribution study in rats was conducted for Compound X (Solon 2013). Two batches of Compound X were prepared and each was labeled with ^{14}C at different positions on the molecule because Compound X had two known metabolites that were from two different parts of the molecule.

The two versions of the ^{14}C-labeled compound were administered to two groups of rats and tissue concentrations determined using QWBA analysis. The goal was to

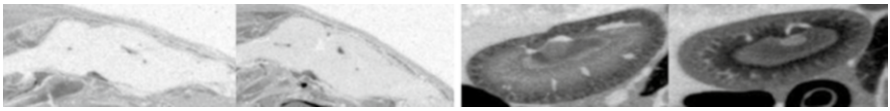

^{14}C-Label A ^{14}C-Label B ^{14}C-Label A ^{14}C-Label B

Time	Brain (cerebellum)		Brain (cerebellum)		Kidney (cortex)		Kidney (medulla)	
	Label A	Label B	Label A	Label B	Label A	Label B	Label A	Label B
1 hr	0.088	0.229	0.070	0.201	7.820	6.036	4.917	8.296
2 hr	0.089	0.407	0.076	0.353	6.368	7.962	5.391	10.446
4 hr	0.072	0.600	0.074	0.526	5.477	7.596	4.512	12.891
8 hr	0.050	0.604	0.037	0.606	2.810	4.708	2.848	4.809
24 hr	BQL	0.257	BQL	0.298	0.435	0.715	0.440	0.685
48 hr	BQL	0.134	BQL	0.145	0.141	0.268	0.166	0.191
72 hr	NI	0.094	NI	0.088	0.097	0.222	0.065	0.138
7 Day	NI	0.046	NI	0.048	NI	0.093	NI	0.050
10 Day	NI	0.030	NI	0.028	NI	0.056	NI	0.037
14 Day	NI	NI	NI	NI	NI	0.040	NI	BQL

Fig. 6.16 Distribution of dual radiolabeled compound in rat kidney (concentrations shown in **µ**g equivalents of ^{14}C-drug/g tissue; BQL = below quantifiable limits; NI—not identifiable in image [i.e. BQL]). Two batches of the parent molecule were prepared and each was labeled with ^{14}C at two different positions on the molecules so that the metabolites could be imaged and tissue concentrations determined using QWBA. The goal being to determine specific tissue exposure to each metabolite to address safety concerns (from Solon 2013)

track the tissue distribution of the radioactivity associated with each metabolite and parent drug and to correlate specific tissue exposure to each metabolite in an attempt to address safety concerns. It also helped investigators to see if the radioactivity from one of the radiolabeled versions would be eliminated faster than the other, which would provide decreased radiation exposure to humans during a clinical radiolabeled study. In this example, the concentration of drug-derived radioactivity from Label A in brain tissue were approximately half that observed after administration of Label B. Differential distribution was also observed in the kidney cortex and medulla. The resulting human estimations of radiation exposure to brain and the different tissues of the kidney obtained using the two versions of the radiolabeled compound were substantially different and helped to guide the choice of radiolabel for the human study as well as providing clues to the localization of a metabolite responsible for potential safety concerns.

Regulatory agencies are also concerned with the safety of substances used as drug carriers and/or to facilitate the sustained release of drugs and QWBA has been used to track the released drug as well carries, such as liposomes. Willis et al. examined the distribution of [1-^{14}C] -2-erucoyl)-DEPC DepoFoam® Formulation (Pacira Pharmaceuticals, Inc., San Diego, CA) in rats and showed that it was widely distributed and metabolized via normal pathways (Willis et al. 2011). This multivesicular liposome product was widely distributed, after a subcutaneous injection, and relatively high concentrations were found in lymph nodes and brown adipose (see Fig. 6.17).

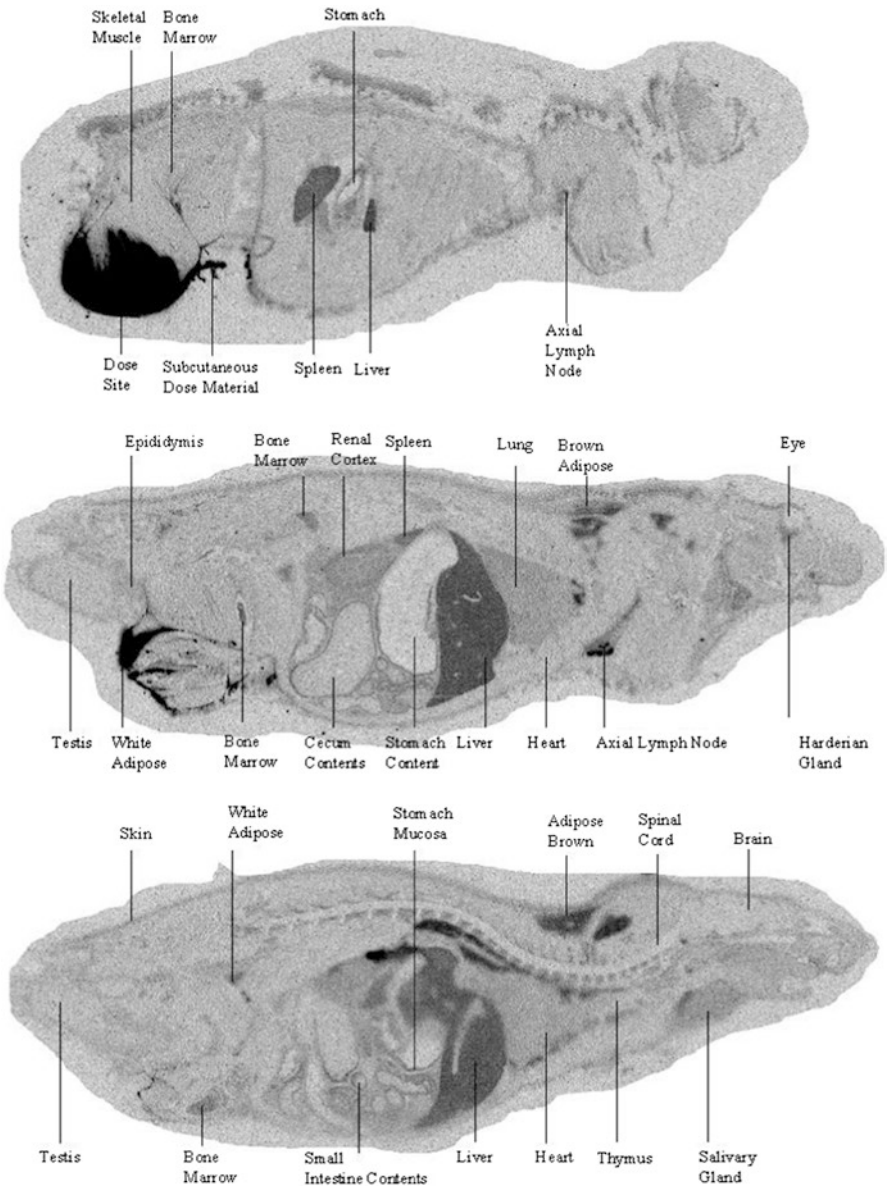

Fig. 6.17 ^{14}C-DepoFoam® in rats after a subcutaneous injection. Whole-body autoradiographs at 2 days after single subcutaneous administration of ^{14}C-DEPC in DepoFoam® formulation (from Solon 2013)

6.8 MALDI-MSI Case Studies

MALDI-MSI of compounds and metabolites is currently being applied to support ADME studies during drug discovery and development in combination with established methods, but it can also be used to examine biomarkers in the form of proteins

and lipids. An example of the latter was demonstrated by Sparvero et al. (Sparvero et al. 2012) who used MALDI-MSI to improve spectral and spatial resolution, sensitivity and specificity in identifying a low abundance of lipid species in tissue sections used for microscopy. Their work may lead to new discoveries in lipid metabolism, and biomarkers associated with area-specific alterations or damage from stress and/or diseases, such as traumatic brain injury, acute lung injury, or other such conditions. In a related sense, Schober et al. (Schober et al. 2012), who were also interested in examining the spatial distribution of proteins, used a trypsin spraying device to digest tissue sections which were then analyzed by MALDI-MSI to detect the resulting peptides from within myelin. Tryptic peptides in tissue were spatially resolved at 50 μm and several tryptic peptides of myelin-matched known spatial distributions. Additionally, numerous other tryptic peptides were identified. MALDI-MSI images were generated with a mass range of $\Delta m/z = 0.01$ μ. Their work also showed that MS images with lower selectivity could result in misleading information about the spatial distribution of tryptic peptides. They concluded that their methods significantly improved spatial resolution of tryptic peptides using a low-ppm mass accuracy in a single experiment, which provided highly reliable and specific information.

The most commonly used application of MALDI-MSI for drug discovery and development has been to identify the parent drug and metabolites in tissues and that is well demonstrated in work done by Prideaux et al. (Prideaux et al. 2011) when they used it better understand drug efficacy of a drug to treat tuberculosis (TB) and how efficiently certain drugs reached the site of action. These researchers applied MALDI-MSI to image the distribution of the second-line TB drug moxifloxacin at different time points after dosing. They were able to monitor selected multiple ion transitions of moxifloxacin in tuberculosis-infected rabbit lung biopsies in less than 15 min per tissue section. They also used a reference standard during the matrix spraying process that enabled normalization of the ion-suppressing effects of the inhomogeneous lung tissue. They found that the drug accumulated in granulomatous lesions at levels higher than that in surrounding lung tissue from 1.5 h post-dose until the final time point. They validated their MALDI-MSI findings of moxifloxacin distribution against quantitative LC/MS/MS analysis of lung and granuloma extracts from adjacent biopsies taken from the same animals. They concluded that non-homogeneous drug distribution occurred within the granulomas and that the caseum had very low levels compared to the cellular granuloma regions. This study also demonstrated that MALDI-MSI a rapid and sensitive method for analyzing the distribution of anti-TB compounds and they have applied this approach to their routine assessments in future studies.

Investigators at imabiotech have shown, in an application note imabiotech (Hamm et al. 2012), that the utility of Quantitative Mass Spectometry Imaging (QMSI) to evaluate the amount of mouse insulin in 10 μm thick sections of mouse pancreas on a glass slide on which they placed micro-droplets of human insulin at varying concentrations to serve as calibrators. They analyzed the samples using an AutoFlex speed LRF MALDI-TOF mass spectrometer (Bruker Daltonics, Bremen, Germany) equipped with a Smart beam II laser used at a repetition rate of 1,000 Hz that was optimized to detect insulin. A diagram of the workflow is presented in Fig. 6.18 and the calibration curve and image of the standards is presented in Fig. 6.19.

The resulting images (shown in Fig. 6.20) corresponded to the distribution of normalized mouse insulin and showed response of the molecule in tissue.

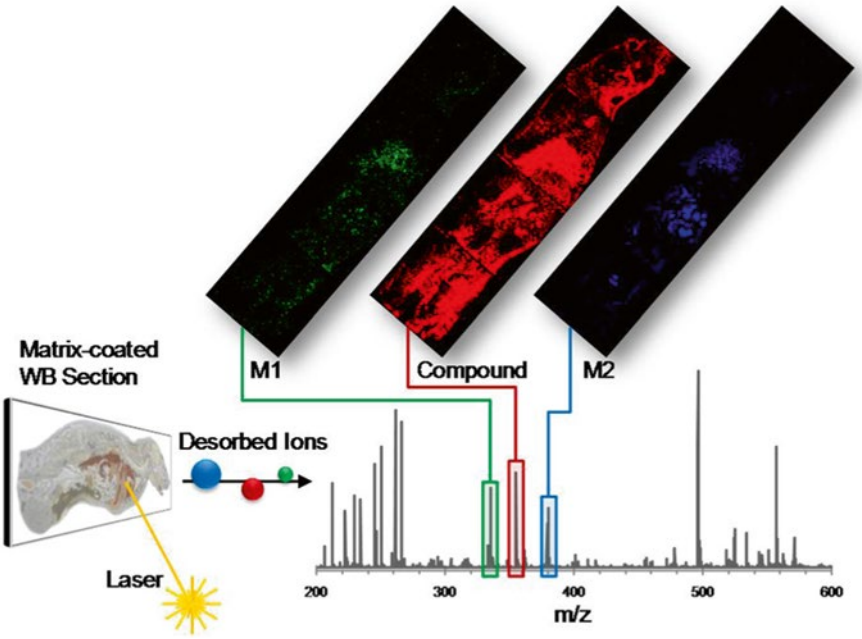

Fig. 6.18 MALDI-MSI Quantitation Workflow Diagram MALDI MS Imaging process. Analytes are simultaneously desorbed from the animal section in a defined raster. Out of the acquired spectra specific molecular images are calculated (from Solon et al. 2010)

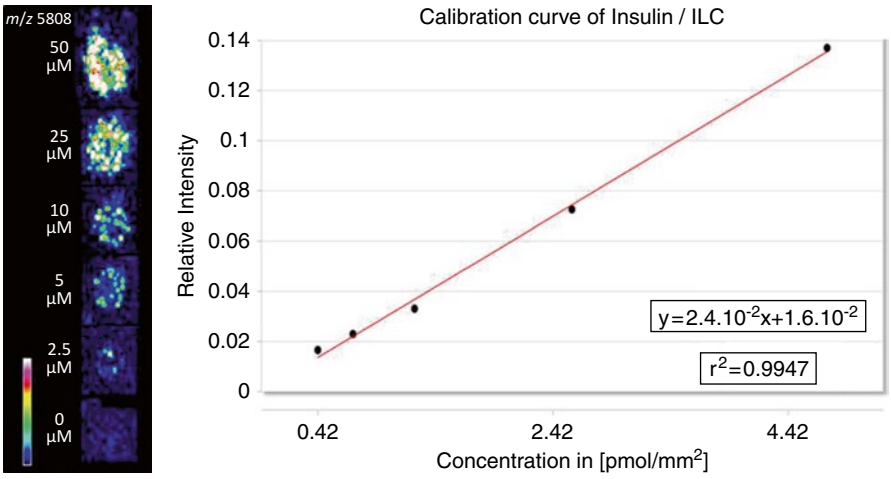

Fig. 6.19 MALDI-MSI Quantitation calibration curve and image of calibration standards from Quantinetix™ (from Hamm et al. 2012)

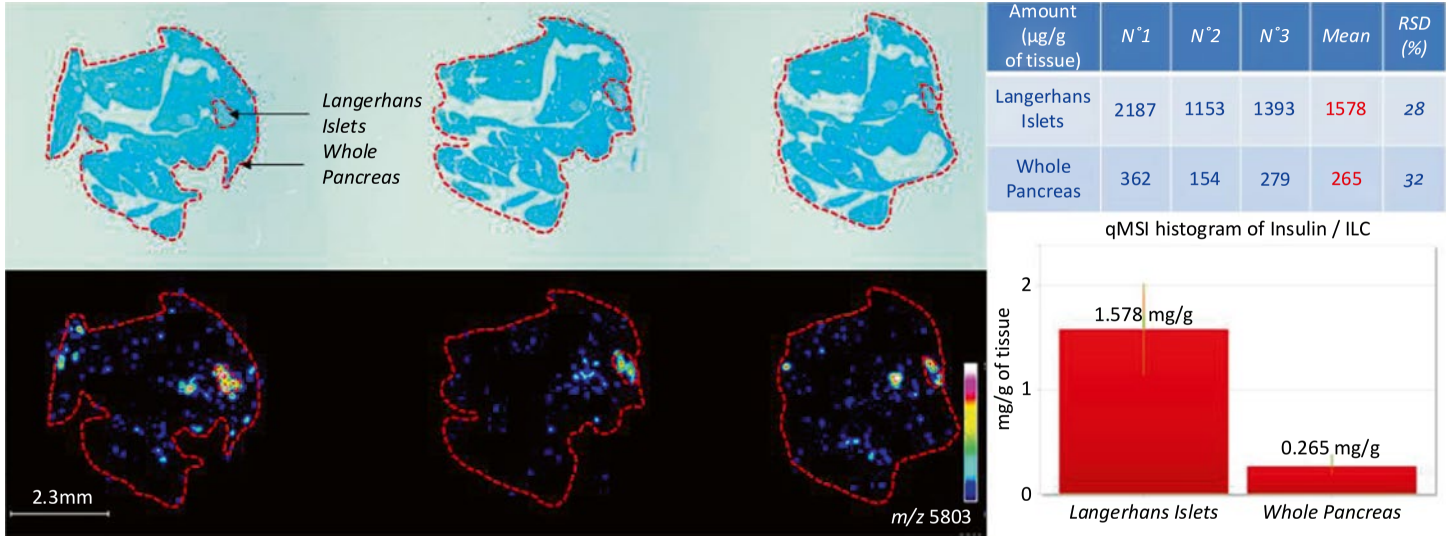

Fig. 6.20 MALDI-MSI Image of distribution of normalized mouse insulin and response of the molecule in tissue. The tissues were stained with methylene blue to show the islets of Langerhans on tissue section (*light blue* region of the optical image) (from Hamm et al. 2012; with permission)

The tissues were subsequently stained with methylene blue to show the islets of Langerhans on tissue section (light blue region of the optical image of Fig. 6.20). The technique showed that insulin was mainly localized to the Islets of Langerhans islets, which is site of peptide translation. Glucagon-related ions (*m/z* 3,483) were also observed on mass spectra from the Islets of Langerhans, but it was not quantified in the study. The concentration of mouse insulin in whole pancreas tissue was determined to be approximately 260 μg/g of tissue. The study showed that there was an inter-sample mean variation of 30 %, which is a widely accepted criteria for the study of biological samples using mass spectrometry imaging.

In conclusion the field of MALDI-MSI has been well-developed over the last 10 years and it is now being used to quantitatively evaluate small and large molecule drugs and to examine biomarkers during the drug discovery and development. However, compared to QWBA methods, MALDI-MSI requires much more time to obtain a complete PK profile of the 30–40 tissues routinely measured for drug distribution studies. Nevertheless, as methods and technologies of MALDI-MSI improve, the use of radiolabeled drugs and QWBA for determining tissue distribution may be replaced by MALDI-MSI-based technologies in the future.

6.9 SIMS: Sub-Micrometer Cellular and Tissue Imaging in Drug Discovery

Previous molecular imaging analysis of individual cells required fluorescent labeling of the molecule of interest, which is problematic due to limited available anti-lipid antibodies and alterations in the lipid chemical properties due to insertion of fluorescent probes (Debois et al. 2007). SIMS has been applied to the imaging of elements in cells at high-spatial resolution (Maier et al. 2002; Chandra et al. 2000), but analyzing elements in isolation only provides limited information to the biochemist who is usually more concerned with larger biomolecules and/or compounds.

Due to the advancements in primary ion source technology, it is also possible to acquire high spatial resolution microprobe images of important biological molecules in individual cells, and both static and dynamic SIMS have been used for this purpose. Lipids and sterols are the predominantly analyzed species, examples of which include cholesterol (Strick et al. 2002), sphingomyelin (Ostrowski et al. 2007) and phosphatidylcholine (McQuaw et al. 2007). Recent studies utilizing these capabilities include the analysis of cellular membrane components to understand the behavior and function of the major lipid constituents and separate research groups have imaged individual glial (Fletcher et al. 2008) and neuroblastoma (Parry and Winograd 2005) cells (as shown in Fig. 6.21). Relative semiquantitative SIMS imaging analysis of cholesterol has been reported in the membranes of macrophage cells treated to contain elevated levels of cholesterol with respect to control cells (Strick et al. 2002). These authors observed a statistically significant signal increase of over 100 % in images from the treated cells by using the signal of $C_5H_9^+$ (at *m/z* 69) as an internal standard.

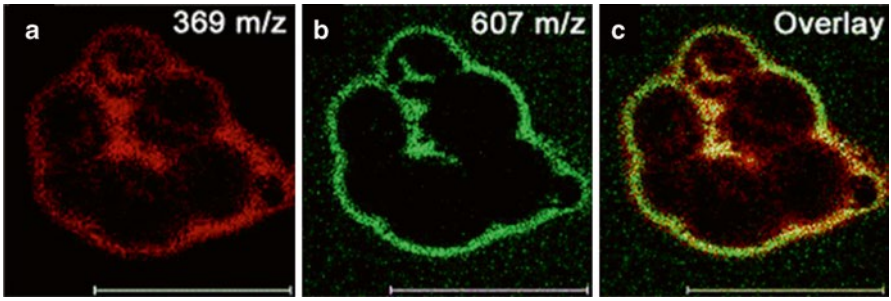

Fig. 6.21 SIMS Images of individual neuroblastoma cells after deposition of 1 nm gold. (*a*) Cholesterol [M-OH]. (*b*) Diacyglcerol. (*c*) Overlay showing the co-localization of the two species. Scale bar 100 **μ**m (From Solon et al. 2010 as adapted with permission from Parry and Winograd 2005; with permission)

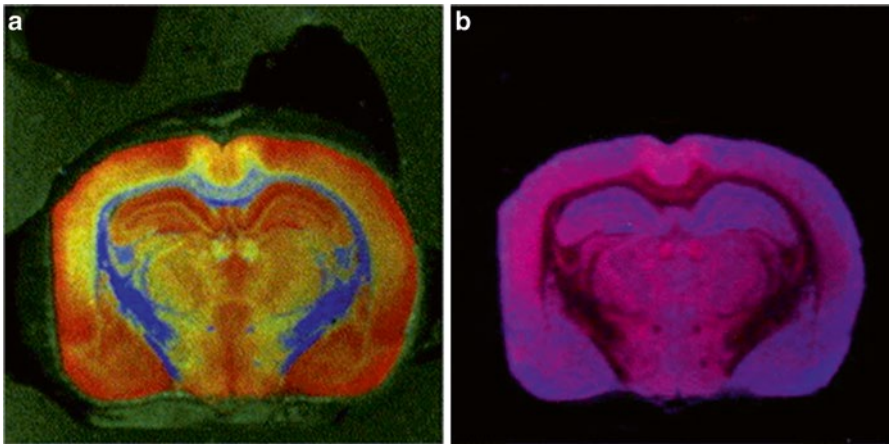

Fig. 6.22 Negative ion SIMS Images obtained from a rat brain section using a Bi3+ primary ion source. Analysis window is 256 × 256 pixels, pixel size 70 × 70 μm. Color overlays show the different localizations of the following negative ions: (**a**) *m/z* (255 + 283, *red*), *m/z* 892 (*green*), and *m/z* 771 (*blue*); (**b**) *m/z* 255 (*blue*) and *m/z* 283 (*red*) (from Solon et al. 2010 as adapted with permission from Altelaar et al. 2006; with permission)

Lower resolution imaging, that encompasses a larger imaging window, can be used for the localization of molecules over larger tissue areas (e.g., biopsy sections) or even sections of entire organs. Imaging SIMS technologies have been applied to a wide range of biological tissues including whole brain sections (as shown in Fig. 6.22) (Altelaar et al. 2006), aorta (Touboul et al. 2005), liver (Malmberg et al. 2007), kidney (Debois et al. 2009), muscle (Nygren et al. 2005), and skin (Magnusson et al. 2008).

Lipids remain the major analyte class investigated with larger window SIMS imaging and one such example is the localization of globotriaosylceramide and digalactosylceramide as biomarkers of Fabry disease in skin and kidney biopsies of

patients (Magnusson et al. 2008). Clear accumulations of both lipids were observed in patients in comparison to healthy volunteers as well as co-localization with the distribution of vitamin E and cholesterol.

In an effort to better understand tuberculosis (TB) drug efficacy and how efficiently certain drugs reach their site of action, Prideaux et al. (Prideaux et al. 2011) used MALDI-MSI to image the distribution of the second-line TB drug moxifloxacin within tuberculosis-infected rabbit lung biopsies at various times after dosing. They found that the drug accumulated in granulomatous lesions at higher concentrations than in surrounding lung tissues. They also validated their findings by analyzing lung and granuloma extracts from adjacent biopsies obtained from the same animals using quantitative LC/MS/MS analysis. Non-homogeneous drug distribution was observed in granulomas, and very low levels were observed in the caseum.

6.10 Regulatory Considerations

Regulatory agencies in developed countries have played pivotal roles in the development of new drugs and these agencies have made great progress to harmonize their requirements to approve new drugs. Communication among members of the US FDA, European Union, World Health Organization, Japanese Ministry of Health, and other regulatory agencies around the world has vastly improved since the early 1980s and now many of the requirements to register new drugs are very similar. Furthermore, developing countries can now more easily model their new drug approval processes after those in the developed nations due to technologies such as the internet and outreach organizations such as the World Health Organization.

Although most regulatory agencies do not require tissue distribution information during the drug discovery phase, it is often helpful for researchers to have some radiolabeled ADME data prior to elevating a drug into the development phase. Early ADME data can alert researchers to potential issues such as those discussed earlier. For companies that focus on out-licensing of their new drugs a limited ADME package is also a good sales tool that gives prospective buyers and/or collaborators information to make better decisions on how to proceed into a deal. The decision to perform and include preclinical radiolabeled ADME study data in an Innovative New Drug (IND) application is usually up to the pharmaceutical company and most companies will include that data if it is available. However, it is not required unless a human radiolabeled study will be run prior to or during Phase I studies, and in that case a human radiation dosimetry estimation, which relies on animal tissue distribution data, must be performed and the FDA has issued a guidance for that situation (US FDA 2010).

Today most regulatory agencies require that pharmaceutical companies include preclinical radiolabeled ADME studies as part of New Drug Applications (NDA) applications. This is because they provide the best data for choosing the toxicology models and doses, and they provide insight into human metabolism for safety evaluation. Thus, better decisions can be made about tissue exposures of the parent compound and its metabolites. Furthermore, it is absolutely necessary to perform

preclinical radiolabeled tissue distribution studies in nonclinical models prior to human radiolabel studies so that human radiation dosimetry estimates can be made.

Of course there are exceptions to the rule that radiolabeled studies need to be conducted for NDAs. The most common exception is when the new drug is to treat a life-threatening disease such as terminal cancer or orphan diseases. In these cases, limited tissue distribution studies may be performed, but they are usually to confirm that targeted tumor and/or other possible therapeutic targets will be adequately exposed to the test drug. Otherwise efficacy and toxicology studies are usually adequate to enable the conduct of further clinical studies.

6.11 Conclusion and Future Perspectives (Taken from Solon 2013)

The impact of the use of radiolabeled compounds for studying tissue distribution has been enormous over the history of drug discovery and development. The use of autoradiography image analysis has all but replaced the former techniques of organ homogenate LSC analysis in less than two decades. Autoradiography has been proven time and again to extend the knowledge of drug disposition by providing true tissue-level concentration data that details tissue exposures and helps to guide the decisions about drug safety, pharmacology, efficacy, and can help solve the challenges that can turn a chemical into a useful drug that saves lives. Until technology can offer efficient ways to quantify chemical entities in complex matrices, such as the multitude of tissues in the human body, radiolabeled compounds will need to be used as the most efficient way to do this job. Whole-body and micro-autoradiography techniques will continue to be utilized to uncover the mysteries surrounding tissue distribution of new drugs. This is because newer in vivo radio-imaging modalities, such as positron emission topography or florescence imaging (*30*) cannot offer the same high resolution and length of tracking time provided by stable, low energy ^{14}C- and tritium-labeled compounds. Furthermore, the new applications of MALDI-MS imaging and secondary ion mass spectrometric imaging (SIMS) technologies, which can identify non-radiolabeled parent drug molecules and metabolites in tissue samples, cannot yet be used to provide quantitative data. This is due to the various matrix effects imposed by each tissue type, which need to be accounted for in order to provide reliable quantification and this is not thought to be possible for many years to come.

References

Altelaar AFM, Klinkert I, Jalink K, de Lange RPJ, Adan RAH, Heeren RMA, Piersma SR (2006) Gold-enhanced biomolecular surface imaging of cells and tissue by SIMS and MALDI mass spectrometry. Anal Chem 78:734–742

Appleton TC (1964) Autoradiography of soluble labeled compounds. J Royal Micro Soc 83:277–281

Baker JRJ (1989) Autoradiography: a comprehensive review. Royal microscopical society, microscopy handbooks 18. Oxford Science, Oxford, pp 30–32
Bélanger LF, Leblond CP (1946) A method for locating radioactive elements in tissues by covering histological sections with a photographic emulsion. Endocrinology 39:8
Blackett NM, Parry DM (1973) A new method for analyzing electron microscope autoradiographs using hypothetical grain distributions. JCell Biol 57:9–15
Breskin A (2000) Advances in gas avalanche radiation detectors for biomedical applications. Nucl Instr Meth A454:26–39
Braddock M (2012) Biomedical Imaging. In: The Chemistry of Labels Probes and Contrast Agents. Chapter 6. RSC Publishing, Cambridge, UK, pp 309–342
Burns MS (1982) Applications of secondary ion mass-spectrometry (Sims) in biological-research: a review. J Microsc 127:237–258
Caro LG (1961) Electron microscopic radiography of thin sections: golgi zone as a site of protein concentration in pancreatic acinar cells. J Biophys Biochem Cytol 10:37
Chandra S, Smith DR, Morrison GH (2000) Subcellular imaging by dynamic SIMS ion microscopy. Anal Chem 202:217–229
Coulston F, Carr CJ (eds) (2000) The validation of radioluminography for use in quantitative distribution studies. Regul Toxicol Pharmacol 31(2):S1–S62
Debois D, Brunelle A, Laprevote O (2007) Attempts for molecular depth profiling directly on a rat brain tissue section using fullerene and bismuth cluster ion beams. Int J Mass Spectrom 260: 115–120
Debois D, Bralet MP, Le Naour F, Brunelle A, Laprevote O (2009) In situ lipidomic analysis of nonalcoholic fatty liver by cluster TOF-SIMS imaging. Anal Chem 81:2823–2831
Delcourte A, Bertrand P (2004) Interest of silver and gold metallization for molecular SIMS and SIMS imaging. Appl Surf Sci 231:250–255
Delecorte A, Bour J, Aubriet F, Muller JF, Bertrand P (2003) Sample metallization for performance improvement in desorption/ionization of kilodalton molecules: quantitative evaluation, imaging secondary ion MS, and laser ablation. Anal Chem 75:6875–6885
Dl J, Warren S (1955) Simplified liquid emulsion radioautography. J Biol Photogr Assoc 23(4):145–150
Downs AM, Williams MA (1984) An improved approach to the analysis of autoradiographs containing isolated sources of simple shape: method, theoretical basis and reference data. J Microsc 114:143–156
Fletcher JS, Rabbani S, Henderson A, Blenkinsopp P, Thompson SP, Lockyer NP, Vickerman JC (2008) A new dynamic in mass spectral imaging of single biological cells. Anal Chem 80:9058–9064
Hahn EJ (1983) Autoradiography: a review of basic principles. Am Laborat 15:64–71
Hamm G, Porreaux L, Stauber JJ (2012) www.imabiotech.com/Toward-Quantitative-Imaging-Mass.html; Imabiotech Application Note #MSI-01
Heeren RMA, McDonnell LA, Amstalden E, Luxembourg SL, Altelaar AFM, Piersma SR (2006) Why don't biologists use SIMS? A critical evaluation of imaging MS. Appl Surf Sci 252:6827–6835
Hesk D, McNamara P (2007) Synthesis of isotopically labelled compounds at Schering-Plough, an historical perspective. J Label Comp Rad 50:875–887
Jones EA, Lockyer NP, Vickerman JC (2007) Depth profiling brain tissue sections with a 40 keV C60+ primary ion beam. Int J Mass Spectrom 260:146–157
Joftes Dl, Warren S (1955) Simplified liquid emulsion radioautography. J Biol Photogr Assoc. 23(4):145–150
Karas M, Bachmann D, Bahr U, Hillenkamp F (1987) Matrix-assisted ultraviolet laser desorption of non-volatile compounds. Int J Mass Spectrom Ion Proc 78:53–68
Keune K, Boon JJ (2004) Enhancement of the static SIMS secondary ion yields of lipid moieties by ultrathin gold coating of aged oil paint surfaces. Surf Interface Anal 36:1620–1628
Khatib-Shahidi S, Andersson M, Herman JL, Gillespie TA, Caprioli RM (2006) Direct molecular analysis of whole-body animal tissue sections by imaging MALDI mass spectrometry. Anal Chem 78(18):6448–6456

Kim H, Prelusky D, Wang L, Hesk D, Palamanda J, Nomeir A (2004) The importance of radiochemical analysis of biological fluids before and after lyophilization from animals dosed with [3H]-labeled compounds in drug discovery. Am Pharm Rev 7:44–48

Kolbe H, Dietzel G (2000) Technical validation of radioluminography systems. Regul Toxicol Pharmacol 31(2):S5–S14

Lacassagne A, Lattes J (1924) R'éparitiondu polonium (injecté sous la peau) dans l'organisme de rats porteurs de griffes cancereuses. C R Séance Soc Biol 90:352–353

Li Q, Si Y, Smith KS, Zeng Q, Weina PJ (2008) Embryotoxicity of artesunate in animal species related to drug tissue distribution and toxicokinetic profiles. Birth Defects Res B Dev Reprod Toxicol 83:435–445

Luckey G (1975) US Patent 3,859,527

Magnusson Y, Friberg P, Sjövall P, Dangardt F, Malmberg P, Chen Y (2008) Clinical lipid imaging of human skeletal muscle using TOF-SIMS with bismuth cluster ion as a primary ion source. Clin Physiol Funct Imaging 28:202–209

Maier O, Oberle V, Hoekstra D (2002) Fluorescent lipid probes: some properties and applications (a review). Chem Phys Lipids 116:3–18

Malmberg P, Börner K, Yun C, Friberg P, Hagenhoff B, Mansson JE, Nygren H (2007) Localization of lipids in the aortic wall with imaging TOF-SIMS. Biochim Biophys Acta 1771:185–195

McDonnell LA, Heeren RMA (2007) Imaging mass spectrometry. Mass Spectrom Rev 26(4): 606–643

McDonnell LA, Piersma SR, Altelaar AFM, Mize TH, Luxembourg SL, Verhaert PDEM, van Minnen J, Heeren RMA (2005) Subcellular imaging mass spectrometry of brain tissue. J Mass Spectrom 40:160–168

McDonnell LA, Heeren RMA, de Lange RPJ, Fletcher IW (2006) Higher sensitivity secondary ion mass spectrometry of biological molecules for high resolution, chemically specific imaging. J Am Soc Mass Spectrom 17:1195–1202

McQuaw CM, Zheng L, Ewing AG, Winograd N (2007) Localization of sphingomyelin in cholesterol domains by imaging mass spectrometry. Langmuir 23:5645–5650

Michnowicz J (2011) Mass spectrometry in drug discovery and development. Nat Rev Drug Discov 1:651–651

Mitra S, Foster TH (2008) In vivo confocal fluorescence imaging of the intratumor distribution of the photosensitizer mono-l-aspartylchlorin-e61. Neoplasia 10(5):429–438

Miyaji Y, Walter S, Chen L, Kurihara A, Ishizuka T, Saito M, Kawai K, Okazaki O (2011) Distribution of KAI-9803, a novel δ-protein kinase C inhibitor, after intravenous administration to rats. Drug Metab Dispos 39(10):1946–1953

Nagata T (1997) Techniques and application of microscopic autoradiography. Histol Histopathol 12:1091–1124

Nagy G, Gelb LD, Walker AV (2005) An investigation of enhanced secondary ion emission under Au(n)+(n=1–7) bombardment. J Am Soc Mass Spectrom 16:733–742

Nygren H, Börner K, Malmberg P, Tallarek E, Hagenhoff B (2005) Imaging TOF-SIMS of rat kidney prepared by high-pressure freezing. Microsc Res Tech 68:329–334

Ostrowski SG, Kurczy ME, Roddy TP, Winograd N, Ewing AG (2007) SIMS imaging of cholesterol in membranes of fluorescently identified single cells. Anal Chem 79:3554–3560

Parry S, Winograd N (2005) High-resolution TOF-SIMS imaging of eukaryotic cells preserved in a trehalose matrix. Anal Chem 77:7950–7957

Potchioba MJ, Tensfeldt TG, Nocerini MR, Silber BM (1995) A novel quantitative method for determining the biodistribution of radiolabeled xenobiotics using whole-body cryosectioning. J Pharmacol Exp Ther 272(2):953–962

Prideaux B, Dartois V, Staab D, Weiner DM, Goh A, Via LE, Barry CEIII, Stoeckli M (2011) High-sensitivity MALDI-MRM-MS imaging of moxifloxacin distribution in tuberculosis-infected rabbit lungs and granulomatous lesions. Anal Chem 83(6):2112–2118

Rauvast V, Mavon A (2006) Transfollicular delivery of linoleic acid in human scalp skin : permeation study and microautoradiographic analysis. Int J Cosmet Sci 28(2):117–123

Roffey SJ, Obach RS, Gedge JI, Smith DA (2007) What is the objective of the mass balance study? A retrospective analysis of data in animal and human excretion studies employing radiolabeled drugs. Drug Metab Rev 39:17–43

Rohner TC, Staab D, Stoeckli M (2005) MALDI mass spectrometric imaging of biological tissue sections. Mech Aging Dev 126:177–185

Salpeter MM, Bachmann L, Salpeter EE (1969) Resolution in electron microscope radioautography. J Cell Biol 41:1–40

Schober Y, Guenther S, Spengler B, Römpp A (2012) High-resolution matrix-assisted laser desorption/ionization imaging of tryptic peptides from tissue. Rapid Commun Mass Spectrom 26(9):1141–1146

Schweitzer A, Fahr A, Niederberger W (1975) A simple method for quantitation of 14C-whole-body autoradiograms. Appl Radiat Isotopes 33:329–333

Sinsheimer JE, Shum YY (1981) Biodehalogenation and metabolism of 125[I]-4-iodobiphenyl. J Pharm Sci 70(5):546–549

Solon E (2007) Autoradiography: high-resolution molecular imaging in pharmaceutical discovery and development. Expert Opin Drug Discov 2(4):503–514

Solon E (2013) Use of radioactive compounds and autoradiography to determine drug tissue distribution. Chem Res Toxicol 25(3):543–555

Solon E, Kraus L (2002) Quantitative whole-body autoradiography in the pharmaceutical. Survey results on study design, methods and regulatory compliance. J Pharmacol Toxicol Methods 43:73–81

Solon EG, Lee F (2002) Methods determining phosphor imaging limits of quantitation in whole-body autoradiography rodent tissue distribution studies affect predictions of 14C human dosimetry. J Pharmacol Toxicol Methods 46:83–91

Solon E, Balani SK, Lee FW (2002) Whole-body autoradiography in drug discovery. Curr Drug Metab 3:451–462

Solon EG, Dowell JA, Lee J, King SK, Damle BD (2007) Distribution of radioactivity in bone and related structures following administration of [14C]dalbavancin to New Zealand white rabbits. Antimicrob Agents Chemother 51(8):3008–3010

Solon EG, Schweitzer A, Stoeckli M, Prideaux B (2010) Autoradiography, MALDI-MS, and SIMS-MS imaging in pharmaceutical discovery and development. AAPS J 12(1):11–26

Sparvero LJ, Amoscato AA, Dixon CE, Long JB, Kochanek PM, Pitt BR, Bayir H, Kagan VE (2012) Mapping of phospholipids by MALDI imaging (MALDI-MSI): realities and expectations. Chem Phys Lipids 165(5):545–562

Stauber JJ (2012) Quantitation by MS imaging: needs and challenges in pharmaceuticals. Bioanalysis 4(17):2095–2098

Stoeckli M, Staab D, Schweitzer A (2007) Compound and metabolite distribution measured by MALDI mass spectrometric imaging in whole-body tissue sections. Int J Mass Spectrom 260(2–3):195–202

Strick R, Strissel PL, Gavrilov K, Levi-Setti R (2002) Cation-chromatin binding as shown by ion microscopy is essential for the structural integrity of chromosomes. J Cell Biol 155:899–910

Stumpf WE (2003) Drug localization in tissues and cells. Library of Congress Control Number 2003105179. IDDC Press

Stumpf WE (2005) Drug localization and targeting with receptor microscopic autoradiography. J Pharmacol Toxicol Methods 51:25–40

Stumpf WE, Roth LJ (1964) Vacuum freeze drying of frozen sections for dry-mounting high resolution autoradiography. Stain Technol 39:219–223

Sjöquist B, Uhlin A, Byding P, Stjernschantz J (1999) Pharmacokinetics of latanoprost in the cynomolgus monkey. 2nd communication: repeated topical administration on the eye. Arzneimittelforschung 49:234–239

Todd PJ, Schaff TG, Chaurand P, Caprioli RM (2001) Organic ion imaging of biological tissue with MALDI and SIMS. J Mass Spectrom 36:355–369

Touboul D, Kollmer F, Niehuis E, Brunelle A, Laprevote O (2005) Improvement of biological time-of-flight-secondary ion mass spectrometry imaging with a bismuth cluster ion source. J Am Soc Mass Spectrom 16:1608–1618

Touboul D, Roy S, Germain DP, Chaminade P, Brunelle A, Laprevote O (2007) MALDI-TOF and cluster-TOF-SIMS imaging of Fabry disease biomarkers. Int J Mass Spectrom 260:158–165

U.S. Food and Drug Administration (2010) Guidance for Industry and Researchers, The Radioactive Drug Research Committee: Human research without an investigational new drug application. http://www.fda.gov/Drugs/GuidanceComplianceRegulatoryInformation/Guidances/default.htm. Accessed 09 Nov 2011

Ullberg S (1954) Studies on the distribution and fate of 35S-Labelled benzylpenicillin in the body. Acta Radiol Suppl 118:1–110

Van Berkel GJ et al (2008) Liquid microjunction surface sampling probe electrospray mass spectrometry for detection of drugs and metabolites in thin tissue sections. J Mass Spectrom 43(4):500–508

Venturi S, Venturi M (1999) Iodide, thyroid and stomach carcinogenesis: evolutionary story of a primitive antioxidant. Eur J Endocrinol 140:371–372

Walker AV (2008) Why is SIMS underused in chemical and biological analysis? Challenges and opportunities. Anal Chem 80:8865–8870

Williams MA (1969) In: Barer R, Cosslett VE (eds) Advances in optical and electron microscopy. Academic, New York, pp 219–272

Willis RC, Richard B, Los K, Willis B, Ward K, Rios V, Strzemienski P, Solon E, Logue A, Lordi A, Onel E (2011) Quantitative whole-body autoradiography following single subcutaneous injection of [1-14C]-2-erucoyl)-DEPC DepoFoam® formulation in rats. Presented at the 38th Meeting of the Controlled Release Society, Presentation 124, 30 July–3 August 2011

Wiseman JM, Ifa DR, Zhu Y, Kissinger CB, Manicke NE et al (2008) Desorption electrospray ionization mass spectrometry: imaging drugs and metabolites in tissues. Proc Nat Acad Sci USA 105(47):18120–18125

Chapter 7
Preclinical Imaging in Oncology: Considerations and Recommendations for the Imaging Scientist

Daniel P. Bradley and Tim Wyant

Abstract Oncology remains a major focus of the pharmaceutical industry, and they are investing heavily in the forward effort to move drugs and biologics through development to regulatory approval. The discovery and early preclinical development throughput for safety, tumor cell binding, and in vivo biodistribution are hindered by the complications and the uniqueness of frequently contrived xenobiotic animal models, generally in murine strains. Animal numbers for adequate sensitivity, tumor heterogeneity of response, and metabolism make for high tumor-to-tumor variance in growth and response. The throughput of studies (tumor growth periods), powering studies sufficiently for decisional steps in product advancement, and the general "how do we do the human translation" all contribute to the major costs in this arm of the pharmaceutical business. Imaging offers many advantages to help solve, or at least allay, these issues. Imaging can pinpoint the tumor uptake heterogeneity, it can reduce the numbers of animals as quantitative assessments can be done on fewer animals, it allows for each animal to serve as its own control, and it allows multiple time point sampling in the same animal(s) during the tumor gestation, eruption, and time window for optimal therapeutic intervention. This chapter will hopefully guide the reader through multiple examples of how to investigate tumor biology using imaging in the nonclinical environment and hopefully will provide useful approaches and ideas for inclusion in their oncology programs.

D.P. Bradley, Ph.D. (✉) • T. Wyant, Ph.D.
Millennium: The Takeda Oncology Company, Cambridge, MA, USA
e-mail: Daniel.bradley@mpi.com

B.R. Moyer et al. (eds.), *Pharmaco-Imaging in Drug and Biologics Development*,
AAPS Advances in the Pharmaceutical Sciences Series 8, DOI 10.1007/978-1-4614-8247-5_7,

7.1 Introduction

Advances in targeted therapies in oncology have necessitated more specific biomarkers to be developed to aid in patient selection, targeted design, and prediction to response, e.g., biomarkers representative of pathway activation/inhibition such as KRAS, EGFR, ALK (Ou et al. 2012; Vincent et al. 2012), and cell-surface markers (CD30 for SGN35 and HER2 for Herceptin) (Zieba et al. 2012). Furthermore, as the hallmarks of cancer origin and in situ expression become better understood, new measurements and even new measurement tools for these oncologic hallmarks will be developed as they are uncovered (Hanahan and Weinberg 2011).

Biomarkers of oncology (and other areas as well) are typically identified as participating in a mechanism of action (MOA), or emerge as a result of the MOA, and thus are developed at the later discovery stage of a targeting new chemical entity (drug/biologic/tracer molecule) as a consequence of the target interaction. Once a drug–target interaction (binding or response) is recognized, the biomarker is rigorously tested and qualified (i.e., validated) in the context of a targeted therapy, i.e., regulatory approval directed efficacy and safety studies for testing in a phase 1 clinical trial. Pharmacodynamic biomarkers, which are often in the imaging realm, are typically used early in phase 1 and 2 trials. Response markers for a successful cancer therapeutic, e.g., tumor size reduction can be measured using CT or MR using criteria such as RECIST—Response Evaluation Criteria In Solid Tumors (see http://www.eortc.be/recist/). Tumor size reductions via product (test agent)-induced apoptosis/necrosis may encourage continued development of the product. Recent draft FDA guidance on the development of companion diagnostics (CDx; a diagnostic used to direct a specific therapy) recommends parallel development of the CDx from the time the need for a companion is identified and through the same registration trials being completed for the drug approval for the selected drug/biologic disease indication (in vivo (imaging) CDx, e.g., the FDA-approved Novartis' product Exjade® in the treatment of iron overload in non-transfusion dependant thalassemia (NTDT)). FerriScan®, an MR imaging agent, is used in studies to select patients for therapy and to manage their Exjade® therapy. FerriScan® provides the needed measure of liver iron concentration (LIC) necessary for Exjade's safe and effective use; see http://www.haemoglobin-gstt.org/images/14/127/ferriscan%20and%20monitoring%20forum%20may%2009.pdf.

Conventional biomarkers include those that are extracted from directly biopsied material, typically the tumor or surrogate tissue, e.g., associated supportive or co-localized tissues or plasma. Samples are subsequently analyzed with various diagnostic or other analytical techniques such as simple histology, immunohistochemistry, FISH (fluorescent in situ hybridization), and PCR and blotting techniques for detecting genetic change, mutational events, and aberrant protein expression.

One of the more promising current techniques developed to exploit biomarkers (physiologic as well as pharmacologic) is imaging. Imaging has long been used in clinical practice to assess solid tumor response to chemotherapy (e.g., RECIST using CT or MRI). However, the use of targeted imaging agents as probes

(e.g. EC20 for folate receptor imaging) or endogenous contrast (e.g., DWI or DCE-MRI) based upon tumor functionality has expanded the opportunity of using imaging platforms to address questions involving molecular responses as well as potentially screening patients for specific therapeutic regimens using biomarker selection strategies. Biomedical imaging sciences offers specific advantages to conventional biomarker assessment requiring interventional sampling. The capability of noninvasive measurements, longitudinal assessments, multiple lesion identity or discovery in the whole body, parametric mapping on individual tumors to extract info on therapeutic response heterogeneity, and the ability to capitulate on multiple clinical parameters extracted in one imaging session are major clinical improvements we have witnessed in clinical practice over the past few decades.[1] The nondestructive nature of imaging allows scientists and physicians to measure dynamic parameters associated with functional and intact systems, e.g., vascular hemodynamics and pathway activation/inhibition.

In addition to the above, imaging sciences offer a potential to address some of the challenges faced currently with companion diagnostics. For example, Knowles and Wu (2012) noted that the use of trastuzumab (an anti-HER2 therapeutic antibody) in patients is only 20–30 % effective in a subpopulation of HER2-positive breast cancer patients as determined by immunohistochemistry or fluorescent in situ hybridization at initial diagnosis. In the situation of breast cancer metastases, HER2 expression is only inferred from the primary lesion. Whole body imaging may in the future play a role in identifying patients with HER-positive metastases expressing differing levels of the HER2 target, and thus imaging may be able to predict favorable outcomes from use of expression-specific directed therapeutics.

One must be cognizant of the fact that no one biomarker is "king," and typically in drug development, a comprehensive and complimentary biomarker strategy is more likely necessary to predict therapeutic success and accelerate development. The clinical goal is to improve probability of success in the selection of the appropriate therapy for the discovered oncologic expression and in the appropriate patient. Indeed, as the reader moves through this chapter, they must always consider the reproducibility and validation of the imaging technique in the context of the clinically relevant animal models that best mimic the human cancer in question, dose of the therapeutic and the reporter CDx, timing of image acquisitions during disease progression and treatment to indicate treatment success (or failure), and quantitation of the benefits (or lack thereof) and risks (if known) of pharmacological intervention.

Again, biomedical imaging has long been used in patient management in oncology. Anatomical or structural scanning, where a dimension or dimensions of target lesions are measured with of the utility of the World Health Organization's (WHO) RECIST1.0 (http://www.recist.com/) using CT or MR imaging (and now RECIST1.1 (and soon Positron Emission Response Criteria in Solid Tumors PERCIST using PET technologies)), which allows for quantitative response measurements via solid tumor size changes. However, more recently with the advent of targeted therapies, tumor imaging techniques have stepped into a new, and potentially very large,

[1] For example, FDG-PET and CT, MRI (DWI and MRS).

territory where we have novel functional or molecular uptake/washout readouts. Definitions were recently described at the Society of Nuclear Medicine 2010. This international body of nuclear imaging scientists and physicians was recently renamed as SNM Molecular Imaging, or SNMMI, partly in recognition of the expansive growth of nuclear medicine and its armament of novel molecular imaging agents (now including nonnuclear optical imaging), quantitative image processing computational systems, and the wide expanse of research activities including:

- *Molecular imaging agents*: "Probes" used to visualize, characterize, and quantitate biological processes in living systems. Both endogenous molecules and exogenous probes can serve as molecular imaging agents.
- *Molecular imaging instrumentation*: The platform technologies that "comprises tools that enable visualization and quantification in space and over time of signals from molecular imaging agents."
- *Molecular imaging quantification*: The science of computational determination of regional concentrations of molecular imaging agents and biological rate constants/pharmacokinetic/pharmacodynamic parameters. Further, molecular imaging quantification provides measurements of processes acting at molecular and cellular levels. Quantification is a key element of molecular imaging requiring a clear understanding on the origin of data and the limitations as well as the expectations of image analyses, especially as we control for inter- and intrasubject comparisons.

Describing these three listed elements in full goes well beyond the scope of this chapter, but the reader should explore other chapters in this volume where they may find information on molecular imaging platforms not included in this treatise including DCE-MRI (dynamic contrast enhanced-MRI) and DCE-CT for antiangiogenics, fluorodeoxyglucose PET (FDG-PET) in glycolytic-targeted therapies, and Octreoscan for somatostatin receptor participation in cancer physiology (Velikyan et al. 2010). A recent review examines the role of functional and molecular imaging in predicting response to specific therapies (Morse and Gillies 2010), and more advanced MI techniques are described by Pysz et al. (2010).

As we review biomedical imaging in the context of preclinical oncology models, it is important to consider and research the cohabitation of imaging probes that are also useful in other clinical endpoints, particularly in non-oncology disease areas, e.g., FDG-PET used in heart disease, atherosclerosis, and Alzheimer's research and DCE-MRI used in arthritis and inflammatory diseases.

This chapter will introduce the reader to small animal imaging technologies and techniques typically useful for oncology research and will attempt to expound on the techniques embedded in translational principles. Biomedical imaging research labs are becoming major partners with oncology research units across academic and pharmaceutical industry sites. Some reference will also be made to those novel agents used in MRI, PET, SPECT, US, and other platforms, but we will not cover the complex chemistry involved in the generation of these conventional and novel products. We recommend for a treatise on nuclear medicine applicable pharmaceuticals, the fine work written by Vallabahajosula ("Molecular Imaging: Radiopharmaceuticals for PET and SPECT"; Springer 2009; http://www.springer.com/medicine/nuclear+medicine/

book/978-3-540-76734-3) and for MRI contrast agents the treatise by Yim et al. (2011) ("Review Article: MRI Contrast Agent-Based Multifunctional Materials: Diagnosis and Therapy"; Journal of Nanomaterials, 2011, Article ID 747196, 11 pg; http://www.hindawi.com/journals/jnm/2011/747196/). For ultrasound (US) contrast agents, please refer to the ACR Guidelines: ACR Manual on Contrast Media, 8, 2012; ACR Committee on Drugs and Contrast Media, http://www.acr.org/~/media/ACR/Documents/PDF/QualitySafety/Resources/Contrast%20Manual/FullManual.pdf.

This chapter will examine several techniques that can be reasonably used within several models of interest in oncology. Finally, while many methods exist to measure similar biological and pharmacological processes, some techniques are simply better suited than others (e.g., DCE-MRI vs. DCE-CT where the former lacks the risk of the absorbed dose from ionizing radiation using radio waves alone as the means of image signal collection).

7.2 Animal Models: Use and Preparation

The most common species used in preclinical oncology is the immunocompromised mouse. This model includes strains such as the nude (nu/nu), SCID, and NOD-SCID mouse (Firestone 2010). The selection of choice of the use of a specific strain can be dictated by many factors and resources exist that have updated their comprehensive lists of the different models and their protocol-desirable characteristics, e.g., http://cancermodels.nci.nih.gov/camod/. The immunocompromised background of these strains necessitates meticulous protocols to limit the exposure of animals to environmental factors that could compromise their general well-being and risk of nosocomial infections. As such, appropriate personal protective equipment and good lab practice is to be followed to reduce inherent risks to the animals. Not all imaging labs can perform under controlled environments or operate in a "barriered" facilities and the incorporation of such skill sets involves extensive training and equipment (there are exceptions, e.g., MI http://molecularimaging.com/) (Note: For a complete treatise on imaging facilities for infection studies with Select Agents, please see Chap. 10 (Keith et al.) where the reader can be introduced to imaging in BSL-3/4 facilities and the details of these imaging procedures).

While preclinical imaging technologies generally share the same engineering and physics principles as its clinical counterpart, in almost all cases small animal subjects have to be immobilized via inhalational and/or injectable anesthetics. With anesthesia, the operator must consider physiological monitoring to ensure appropriate depth of anesthesia and in the case of PET, SPECT, MRI, or Optical to allow for the collection of data in a manner that may allow for gated (physiologic event triggered) acquisition. Multimodal data capture can be improved by integrated bed design as demonstrated by Nelson et al. (2011), to allow registration of images collected using different axial modalities especially when images are not collected in the same gantry. Cradle or "sled" systems that incorporate ECG, respiration, and temperature monitoring sensors are now used in a preclinical setup (Fig. 7.1a) in conjunction with the use of appropriate and validated monitoring instrumentation (Fig. 7.1b).

Fig. 7.1 (**a**) DAZAI system where specific beds are molded to mice of differing body weights and the resulting "sled" is fitted with ECG, respiration, and thermocouple sensors for full physiological monitoring of an animal's well-being while under anesthesia. (**b**) SAII system integrated with the DAZAI system, the SAII monitoring hardware allows the physiological signals to be electronically traced and stored; furthermore, integrating this system into the MRI or PET hardware enables the operator to gate/trigger acquisitions to cardiac and/or respiration cycles

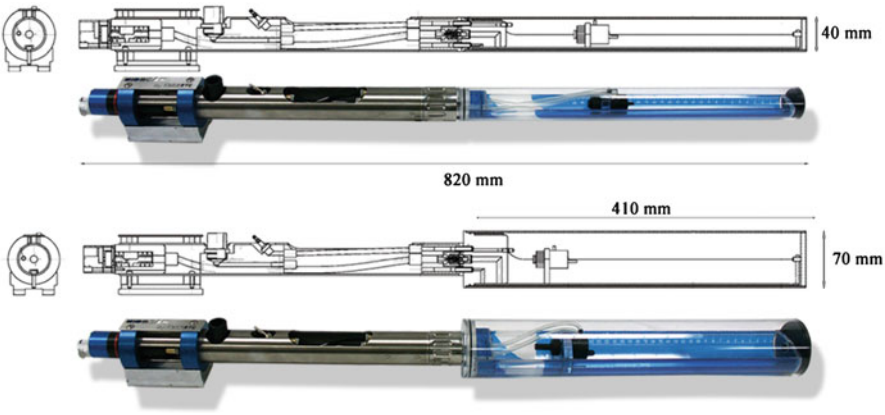

Fig. 7.2 Examples of the tubular designs that are for animal holding and "insertion" via a contained environment into an imaging system. These are applicable to small as well as large animals. Also, see Chap. 10 on BSL-3/4 laboratory imaging requirements

Other systems exist that permit use in either barriered or non-barriered facilities, e.g., bioscan-barriered cradles (Fig. 7.2). Such systems permit the transfer of animals from barriered facilities into "dirty" (i.e., uncontrolled or allowed to be contaminated) imaging platforms/imaging labs, all the while limiting the animal and animal handlers exposure to pathogens.

Where anesthesia is not appropriate and yet immobilization is preferred, there are instances where rats have been habituated to scanner systems and complex cradle designs can be of assistance. However, most animals are typically restrained while conscious using ear and mouth bars and/or body harnesses (Ferris et al. 2011). The appeal of conscious imaging has primarily been driven by the need for "awake" conditions for functional MRI (fMRI) and pharmacological stimulated MRI (phMRI)[2] communities where functional MRI uses blood oxygenation level dependent (BOLD) blood flow responses to measure regional blood flow changes due to imposed stimuli. BOLD responses can often be attenuated/altered by anesthetics (Hodkinson et al. 2012). A limited number of oncology studies have explored the effects of anesthesia on basal physiological measurements using MRI (Baudelet and Gallez 2004) and bioluminescence (Schnell et al. 2010) in rats with xenograft tumors. In experimental design it is typical to have a size and time matched control

[2] fMRI (functional magnetic resonance imaging) relies on the hemodynamic response and exploits the magnetic susceptibility differences between hemoglobin in its two different oxygenation states (deoxy- and oxyhemoglobin), and during neuronal activation there is a vascular response associated that can "flood" the neural region with oxygenated blood and increase the signal measured on T2* weighted imaging—this activation can come about from visual, motor, physiological stimuli. phMRI (or pharmacological MRI) uses the same imaging technique, but instead of an environmental stimuli, the subject receives a pharmacological stimulus that is thought to activates/inhibits brain centers.

or vehicle arm to understand the impact of the procedure on the "control" parameters being examined. However, careful consideration must be made when studying biological processes under different anesthetic states (Kersemans et al. 2011a). Anesthetic usage under conditions of animal termination (or non-recovery) may be done, but limits of duration may be governed under local animal license authorities, and consultation with these authorities should be considered when designing your studies. The authorities often will allow for longer scan times in these cases (1–2 h); however, in recovery-directed procedures where the animal will regain consciousness after the scan, careful consideration and ethical approval has to be sought when scanning with recovery. Furthermore the frequency of scanning and number of times each animal is exposed to anesthesia (and ionizing radiation in the case of PET and CT (see below)) has to be carefully considered when designing longitudinal studies; thus while "using each animal as its own control" is often cited as a great advantage of noninvasive imaging if that animal is under stress and not eating, grooming, or out of sync in its sleep–wake cycle, the data recovered from each scan and noise added could get progressively worse and be unreproducible and unreliable.

7.2.1 Major Modalities Used in Preclinical Oncology Drug Discovery: Principles, Limitations, and Applications

Many biomedical imaging laboratories exit in universities and pharmaceutical companies as core or central labs, and some exist within disease area departments (e.g., neurology, oncology, cardiovascular). Institutions without such facilities often exploit the small animal imaging CROs that exist across the globe. However, integrated imaging facilities have the advantage of exploiting proprietary novel animal models and procedures, unhindered access to different supportive functions (e.g., DMPK, molecular pathology, histology, chemistry, pharmacology, toxicology) and novel therapies being developed. Below, a number of the key translational modalities will be described, and examples in the oncology setting will be presented. Magnetic resonance imaging, positron emission tomography, and single photon emission computed tomography will be described. Firstly, MRI typically exploits the endogenous contrast brought about by the magnetic properties of the proton residing in H_2O—multiparametric acquisitions are one of the greatest benefits of MRI, plus non-ionizing radiation. MRI offers exquisite spatial resolution for anatomical imaging and more advanced uses now allow the measurement of many different physiological events in normal and diseased tissues. Second, PET relies on the administration of a positron-emitting isotope typically attached to a small molecule or via chelation on to larger molecules. While ^{18}F- FDG remains the cornerstone of oncologic PET examinations, more "boutique" isotopes are making inroads due to both ready complexation with common chelators (e.g., ^{68}Ga and DOTA, DTPA) and independence from cyclotron infrastructure. Finally SPECT, like PET, relies on gamma-emitting isotopes but instead detects the emissions directly (rather than through the annihilation process as in PET). Similarly, radiolabeled probes are

used that are either nonspecific (e.g., blood flow using Tc-99m hexamethylpropyleneamine oxime (Tc-99m HMPAO)), absorbed by certain cell types (e.g., bone uptake using Tc-99m methylene diphosphonate), or a targeted to specific cell-surface markers (e.g., ^{111}In trastuzumab). All these modalities will be described in more detail below.

7.2.1.1 Magnetic Resonance Imaging (MRI)

Often referred to as a "conventional anatomical imaging" procedure, magnetic resonance imaging (MRI; formerly termed nuclear magnetic resonance, NMR) provides exquisite soft tissue contrast without exposing the subject to harmful ionizing radiation. However, many "functional" and "molecular" MRI techniques exist including those that measure changes associated with hemodynamic responses in fMRI and antiangiogenic treatments in oncology, to metabolic profiling of spatially distinct regions of tumors (magnetic resonance spectroscopy (MRS)) and the onset of cell death during stroke or cytotoxic therapies to name but a few—methods successfully used in clinical and nonclinical subjects.

The body is made up largely of water molecules (H_2O), and it is the hydrogen atoms of the water molecules that possess a property exploited under high magnetic fields, e.g., the atom is essentially a magnet with a positive pole (the nucleus or singular proton) and a negative pole (the singular electron). The odd number of protons, ^{1}H, presents with a nonzero spin that results in NMR properties. In an applied magnetic field, B_0, two spin states arise (high and low energy) and transition between these two energy states can be induced by absorption of electromagnetic energy (B_1) generated by a radiofrequency (RF) coil at a specified frequency unique to the nuclei under investigation.[3] After excitation there is a loss of energy termed "relaxation" and this loss is governed by specific properties of the sample. The loss from relaxation is measured by the same or separate RF coil proximal to the sample. Longitudinal (T1) relaxation is the process by which the spin system returns to equilibrium state releasing energy back into its surrounding environment or "lattics" after the removal of the B_1 field. Transverse or spin–spin (T2) relaxation describes the rate of which the spins diphase due to inter- and intramolecular interactions after B_1 has been turned off. During the excitation period a series of additional magnetic fields which form a "gradient" through the sample and thus when applied creates an encoded spatial relationship of the signals and allows the operator to utilize spatially unique volumes to provide their own respective relaxation energy loss. This information created by manipulation of the RF power, timing (single or repeated application), shape, and duration of the RF and gradient pulses gives rise to the different "weighting" of volume elements within an MRI image. For a review of MR imaging

[3] It is not just 1H-containing molecules that can be studied with MRI but also the elements of P, C, N, Na, F, etc.

in the mouse using a variety of MR pulse sequences and methods, the reader is directed to Pautler (2004).

Small animal MRI systems from 1.5 to 17 Tesla (T; SI term of magnetic field strength) have been used for a variety of study objectives; the higher the Tesla (B_0), the greater the signal to noise ratio (SNR)—however, as field increases so does the size of the physical laboratory footprint of the system. Most preclinical systems lie in the range of 4.7 T (200 MHz)–9.4 T (400 MHz)—lower field systems can be more advantageous when imaging T1 and T2 signals. Susceptibility artifacts or noise introduced by small RF-induced susceptibility relaxation loss of hydrogens associated with nonspecific molecular entities can also be a problem at higher field (refer to Chap. 11 (Moyer, Hu and Williams) for a short treatise on the MRI operational physics and their controls).

The major advantage of MRI is the ability to acquire multiple contrast endpoints in a single imaging session, and this can be done with no injection of exogenous agents. For example, T1, T2, ADC (apparent diffusion coefficient), and MRS data can all be acquired in a single imaging session of a target lesion. Other advantages include the avoidance of ionizing as used by CT, SPECT, and PET where ionizing radiation provided their interpretive signal. Thus, MRI use provides multiple imaging sessions without deleterious absorbed ionizing radiation to the subject. Additionally, hardware can be modified to improve SNR (signal to noise ratio) and temporal resolution. For the former, this can be accomplished using different RF coil configurations termed volumetric, surface, or phased array (Doty et al. 2007), and cryo-cooled RF (B_1) systems are available by different vendors and custom-built in engineering laboratories. Finally, multiple nuclei of interest can be measured using decoupled RF coils tuned to the respective resonant frequency of the targeted nuclei, e.g., ^{1}H for lactate and ^{31}P for ATP measurements, respectively.

MRI has historically been reserved for the physicist applying their knowledge in a biological context; many vendors offer customized acquisition routines to trigger relaxation losses of specific targeted tissues or molecular entities that need to be optimized on site, and this requires pulse sequence coding and an in-depth knowledge of MRI physics. However, more vendors are releasing user friendly and ”target-ready” acquisition routines for high-throughput imaging of genetically engineered murine models using standard MRI parameters, e.g., T1W (T1-weighted) or T2W (T2-weighted) imaging. Preclinical imaging vendors are also offering systems with clinical operating systems to aid in translation of imaging techniques from the animal model laboratory to the clinical bedside. Furthermore, some of the newer systems even negate the need for dedicated areas of operation. For example, most high field superconducting magnets weigh more than 6–10 K pounds and possess a “stray field” that limits the proximity for monitoring equipment (i.e., cardiovascular system measuring devices such as ECGs) and other electronic devices (phones, watches, and other nonexperimental associated devices). Newer systems, are lighter and can be even described as benchtop devices (however, these are currently limited to 0.5–1 T) and can be applied when high-throughput genotyping of genetically engineered mouse models or chronic disease measurements are required for example. These smaller and lighter systems and potentially “open” systems (most

are ring systems that can be claustrophobic in clinical settings) also some do not require cryogenic cooling, i.e., repeated filling with liquid nitrogen (e.g., those produced by http://www.mrsolutions.co.uk/products/benchtop/).

Physiological, physical, and hardware-associated artifacts can often compromise the quality of MRI data and thus affect the fidelity and clinical interpretations of mathematically reconstructed images. While not to concern the new user of MRI, there are many type of artifacts that can be attributed to different sources. Some examples are listed in http://www.mritutor.org/mritutor/artifact.htm/, and this chapter cannot detail all of these (refer to Chap. 11 (Moyer, Hu, Williams and Morris) in this book and also see Smith and Nayak 2010).

Many scientific publications provide good examples of how MRI has been used in preclinical models of oncology; the simplest applications of MRI are when it is used as a tool for identifying lesion location, size, volume, and morphology, i.e., anatomical criteria. However, more advanced acquisition examples include those that acquire multiparametric maps to either determine basal differences between tumors of a different genotype or detect acute changes in the tumor physiology following drug action.

Considerations on small animal imaging in a recent and comprehensive review (Barnes et al. 2012) on dynamic contrast enhanced-MRI (DCE-MRI) can easily translate across different modalities. DCE-MRI is applicable when one wishes to study therapeutic agents that target the vasculature, but it also has value when studying imaging endpoints that rely on tracer delivery. For example, PET requires the administration of a labeled molecule and typically this molecule is trapped through an enzymatic reaction leading to metabolic stasis (e.g., ^{18}F FDG and the hexokinase failure to metabolize the deoxy form of glucose leading to the drug being "static" in situ allowing for image acquisition) or binds to a surface antigen (e.g., ^{89}Zr-Herceptin). For both of these examples, the drugs are delivered via the vasculature and the fractional delivery over time to the tumors (termed the "input function") allows mathematical measures and a way to understand those factors important in affecting tracer uptake. Measurements of the vasculature fractional distribution can be made with specific vascular agents (e.g., Gd-DTPA) or surrogate measurements can be derived from dynamic acquisitions of the targeted tracer. Different hemodynamic constituents associated vascular perfusion, vascular volume, vascular permeability and intra- and extravascular compartments can be extracted from DCE-MRI with different compartmental modeling routines (McGrath et al. 2009).

Diffusion-weighted MRI (DWI) exploits the endogenous diffusion properties of H_2O; in principle and in the context of oncologic endpoints, the assumption is based on the two major compartments in the microenvironment of a tumor having different diffusional properties, the extra- and intracellular space (ECS and ICS, respectively). Indeed, on induction of cell death, through apoptosis or necrosis, the change in the ratio of the two compartments can lead to a dramatic change in water diffusion paths, and this can be detected using DWI and be predictive for tumor shrinkage (Heijmen et al. 2013). For a comprehensive review of DWI applications and concepts, see Neil (2008) and Padhani et al. (2009).

While not "imaging" per se, magnetic resonance spectroscopy (MRS) exploits the NMR properties of spinning nuclei (for a full treatise on MRS-applications in

imaging, see Chap. 12 by Venter et al. in this volume). With the advent of metabolomics (the global quantitative assessment of endogenous metabolites within a biological system), noninvasive assessment of the cancer metabolome (inherent in situ metabolism and catabolism) is emerging as a powerful tool to measure this feature during disease progression, differentiating between benign and malignant lesions, and changes associated with tumor metabolism resulting from applied targeted therapies (Serkova et al. 2007; Spratlin et al. 2009). For a more detailed review of these imaging approaches and the importance of other factors affecting MRI image interpretations in basic preclinical research, see Albanese et al. (2012).

7.2.1.2 Positron Emission (Computed) Tomography (PET)

A compound labeled with a positron-emitting radionuclide, i.e., ^{11}C, ^{13}N, ^{15}O, ^{18}F, ^{64}Cu, and ^{82}Rb, is introduced into the body, usually by intravenous injection, to facilitate a rapid and high fractional dose input function to the desired anatomical target. When one of the radionuclide atoms decays, a positron is emitted from the nucleus and travels a very short distance and is annihilated with interaction with an electron resulting in the formation of two gamma rays. The mass of the two annihilating particles is converted into gamma energy forming two 511 keV gamma rays which oppose each other directionally by 180°. A positron emission tomography scanner consists of a ring, or multiple rings, of gamma-ray detectors that register coincident gamma ray "hits" in specific timing windows to define the near location of their origin in the body via a chord construct across the ring. By collecting large numbers of gamma-ray pair/coincident events (typically 10^6–10^7) and using computed tomography chord reconstruction methods, transverse cross-sectional images of the original 3D volume (a patient or a test animal) can be created. The frequency of chord crossover saturation points reflects the concentration of the positron-emitting radionuclide in the body slice as defined by the ring detector number, event resolution, and correction of photonic attenuation. For other detailed PET systems applications see Chaps. 2, 3, 4, 8, and 10 and also Jones (1996).

Advantages of PET, versus other imaging modalities in small animal cancer studies, are in its quantitative nature and very high sensitivity. The versatility for radiolabeling small molecules with PET radiotracers, including therapeutic agents (Bahce et al. 2013), is rapidly emerging as a tool that can be used to noninvasively assess whole body pharmacokinetic (PK) and pharmacodynamic (PD) parameters and can be used whether or not the level of tracer uptake corresponds to or depends upon the presence of activating tumor receptor mutations. Commonly used isotopes in PET are typically short-lived (minutes to hours), e.g., ^{18}F, ^{68}Ga, ^{11}C, and ^{15}O. However, the introduction of ^{64}Cu and ^{89}Zr as a longer-lived positron-emitting radioisotopes (half-lives of 12.7 and 78.4 h, resp.) that can be chelated and conjugated to Ab's has changed evaluation methods for Ab therapeutics. Antibody therapeutics typically exhibit long-lived biologic half-lives (re., PK), and they can now be labeled and imaged in both animal and human systems under conditions to measure their pharmacokinetic changes and the pharmacodynamic changes resulting in

their tumor-specific targets (Verel et al. 2003). Furthermore, where methods have been established using long-lived SPECT radioisotopes (e.g., ^{111}In and Tc-99m), positron emitters are slowly making inroads into the "hours post injection" territory currently favored using SPECT due to the improved PET radiochemistry with ^{89}Zr the more quantitative nature of PET.

^{111}In -DOTATOC, a somatostatin receptor (SSTR) ligand, has long been used for studying neuroendocrine tumors using SPECT. Emerging data suggests SST analogs labeled with ^{68}Ga as a PET radiotracer offers improved specificity and sensitivity (Buchmann et al. 2007). Preclinical evidence continues to emerge for ^{68}Ga as PET tracer demonstrating acceptable chelation chemistry (i.e., high specific radioactivity with limited radiolysis) allowing longer imaging and ability to reveal biological properties of targeted tissues (Breeman et al. 2011).

Preclinical examples of PET in cancer research are spread across radiolabeled small molecules, pathway targeted agents, antibodies, antibody fragments, and peptides (Aboagye 2005). A number of papers are highlighted below.

FDG-PET and other tracers have been evaluated in multiple tumors for general characterizing of target receptor avidity to the tracer (Kd or binding constants; Hill plots) or physiologic uptake (SUV or standard uptake value) and to measure the tracer kinetics in the context of acute therapeutic treatment (tumor apoptosis, shrinkage, etc.):

$$\mathrm{SUV} = r / (a' / w),$$

where r is the radioactivity activity concentration (kBq/ml) measured by the PET scanner within a region of interest (ROI), a' is the decay-corrected amount of injected radiolabeled FDG (kBq), and w is the weight of the patient (g) (Kinahan and Fletcher 2010).

For example, F-18 FDG, F-18 FLT, 18F-18 FET, and F-18FCH SUVs were evaluated in the recent paper by Ebenhan et al. (Ebenhan et al. 2009) and correlating the imaging data with tumor dissection, histology, and immunohistochemistry analysis of Ki67 (a marker of proliferation), Proliferating Cell Nuclear Antigen (PCNA), and Caspase-3. Some of the conclusions and highlights of this work are captured thus:

- Low and heterogeneous tracer uptake in experimental tumors represents a complicating factor for proper PET data interpretation.
- ^{18}F FDG imaging gives low tumor and low tumor edge (typically the metabolically active invasive border) tracer uptake, especially in human tumor xenografts in murine models.
- The murine models with the highest ^{18}F FDG uptake for the syngeneic orthotopic group (B16/BL6 strains) or SC (subcutaneous) xenograft group (U87 MG) showed the lowest ^{18}F FLT (fluorothymidine, a DNA targeting tracer) uptake for that group.
- ^{18}F FLT imaging appeared to provide the best imaging parameters (signal to noise) across all models.
- The correlation of ^{18}F FLT uptake with the proliferation markers Ki67 or PCNA was, however, relatively weak.

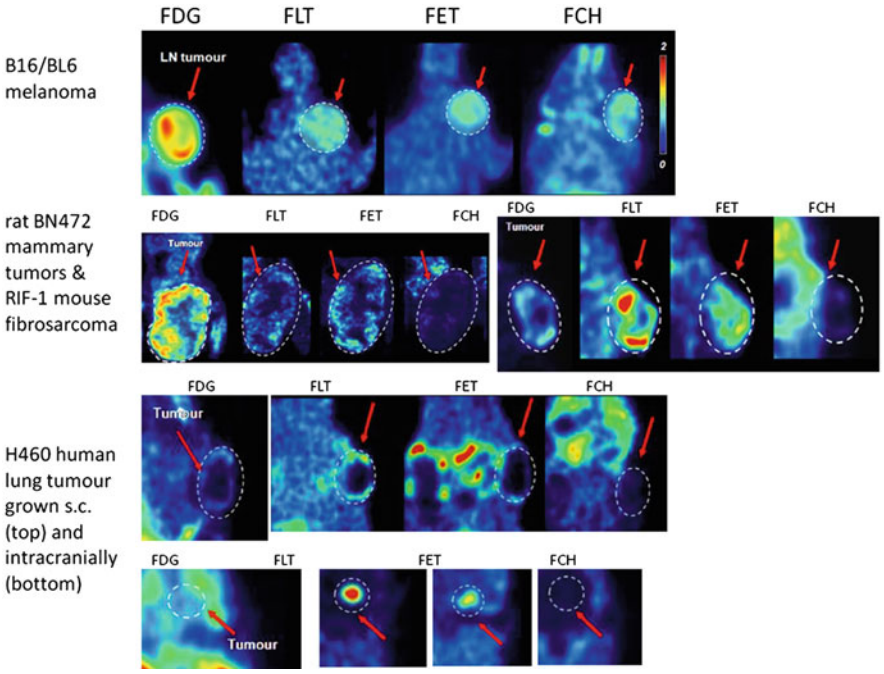

Fig. 7.3 Different tumor types and their avidity for different PET tracers (extracted and modified from Ebenhan et al. (2009); with permission)

- A very strong correlation between ^{18}F FLT uptake and tumor caspase-3 expression was observed (Fig. 7.3).

As is well known from the clinical setting, tumor response evaluated using the traditional RECIST (Response Evaluation Criteria in Solid Tumors; Therasse et al. 2006) alone is limited because many tyrosine kinase inhibitors (TKIs) do not lead to a detectable or statistical lesion shrinkage when first evaluated in small patient cohorts designed into a phase 1 clinical trial. Emerging preclinical FDG-PET, and clinical studies as well (McArthur et al. 2012), has demonstrated, in the context of novel targeted therapies, that modulating pathways associated with glycolysis can be used as an acute PD marker or one that also predicts for radiological outcome (Nguyen et al. 2011; Pantaleo et al. 2010). As with other modalities, when investigating imaging endpoints using preclinical models, central necrosis of solid tumors can confound therapeutic drug outcome results and careful consideration must be made on the mode of analysis or stipulate the starting size and rate of growth of tumors that are to be studied.

Complex chemical synthetic paths for radiolabeling with ^{11}C and the short half-life of ^{11}C have limited the utility of this tracer in imaging of therapeutic molecules. However, recent improvements in the radiochemistry have increased this tracer use. For example, erlotinib can be labeled with ^{11}C (Memon et al. 2009) and examined

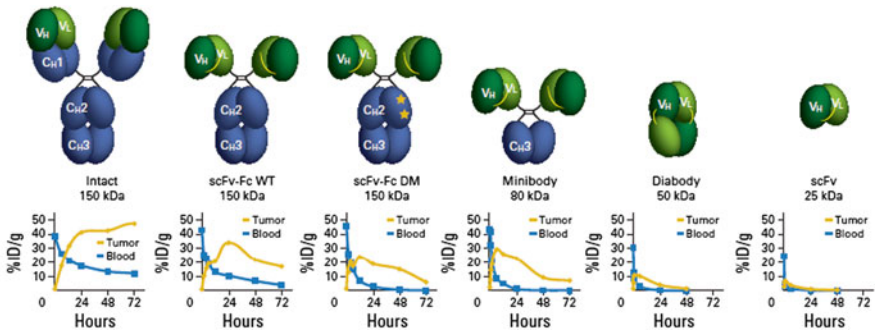

Fig. 7.4 Examples of changes in pharmacokinetic patterns that may occur with changes in antibody structure. The half-lives of immuno-PET imaging agents can be modified by (1) deleting constant domains to create fragments of varying size (single-chain Fv [scFv]-Fc, minibody, and diabody) or (2) by mutations that modify interactions with the FcRn receptor (scFv-Fc H310A/H435Q double mutant [DM]). For intact antibodies, imaging at 96–168 h provides optimal contrast. Antibody fragments such as scFv-Fc wild type (WT; 72–120 h), scFv-Fc DM (12–48 h), minibodies (8–48 h), and diabodies (4–8 h) are capable of obtaining high-contrast images at earlier time points (From Knowles and Wu (2012); with permission)

in multiple cell lines in vivo with different levels of EGFR expression and activity. Dynamic micro-PET has showed that HCC827 tumors have higher ^{11}C erlotinib uptake and retain the radioactivity significantly longer as compared with A549 and NCI358 tumors. However, the target tumor %ID/g is still relatively low (max uptake of 3.7 %ID; percent of injected dose). These results though have led to the quantitative measure of ^{11}C erlotinib uptake in patients with non-small cell lung carcinoma (NSCC) and found that it was significantly higher in tumors with EGFR-activating mutations (Bahce et al. 2013).

The more favorable PET radiotracer, ^{18}F, has a longer half-life (2 h vs. 20 min for ^{11}C) and also has complex radiochemistry for erlotinib, but the final step is the addition of F-18 which has advantages of specific activity but simply does not have a high enough yield for imaging. Ritter's group at Harvard, however, have improved the design and synthesis of an organometallic complex made from fluoride that behaves as an electrophilic fluorination reagent, and the use of the reagent for the synthesis of F-18-labeled small molecules via late-stage fluorination has been a breakthrough for high specific activity yields (Lee et al. 2011a).

Immune-positron emission tomography (immune-PET), i.e., imaging with intact antibodies, has shown success clinically in diagnosing and staging cancer. Engineered antibody fragments, such as "diabodies," "minibodies," and single-chain Fv (scFv)-Fc fragments, have been successfully employed for immune-PET imaging of cancer cell-surface biomarkers in preclinical models and are poised to bring same-day imaging into clinical development due to clearance kinetics (Knowles and Wu 2012) (Fig. 7.4).

7.2.1.3 Single Photon Emission Computed Tomography (SPECT)

For the physics of SPECT, the reader is referred to Groch and Erwin (2000), and in the context of small animal imaging and SPECT, see Franc et al. (2008) and Seo et al. (2013). Briefly, SPECT measures γ-rays directly after radionuclide emission, thereby gaining a theoretical advantage in spatial resolution over PET, for which resolution is currently limited by the fundamental processes of positron emission and positron–electron annihilation which occur away from the actual nuclear site of origin of the positron. SPECT uses many radiopharmaceuticals which are widely applied in clinical nuclear medicine and often have longer half-lives than most PET isotopes and therefore can be obtained from central radiopharmacies. Small animal SPECT studies generally cost less than other small animal imaging methods, such as small animal PET or small animal MRI. However, in contrast to PET the attenuation of detectable photons by soft tissue is estimated to be up to 50 % when imaging I-125 and up to 25 % when imaging Tc-99m in "rat-sized" objects thus leading to a potential decrease in the targeting sensitivity.

The main reasons for the advantage of SPECT, compared with PET, in brain imaging are the ability to push the spatial resolution to below 1 mm by fine-tuning the pinhole characteristics, the availability of longer-lived isotopes, and the high specific activity of most no-carrier-added SPECT tracers. Many PET tracers, particularly those labeled with ^{11}C, have a low specific activity which may lead to significant occupancy of the target site by the tracer itself to levels where there may be possible pharmacologic effects.

Recent developments of tumor-targeted SPECT radiotracers for imaging of cancer diseases has recently been reviewed in Müller and Schibli (2013), and considerations associated with tissue penetration, high affinity to the tumor-associated target structure, specific uptake and retention in the malignant lesions, and rapid clearance from nontargeted tissues and organs are addressed.

Examples of In-111 for larger (Abs) and Tc-99m for smaller molecules used in preclinical studies in oncology are many. One of the most advanced and exciting Tc-99m agents is that developed for folate imaging as part of a companion diagnostic package. Use of targeted therapy requires identification of patients whose tumors express a specific molecular target. Preclinical evaluation has been reported by Reddy et al. (2004). The folate receptor, which is over expressed by many primary and metastatic cancers, is an example of one system that can be successfully exploited for drug delivery. Folate-based radioligand labeled with In-111 was introduced and phase I/II clinical trials of In-111-diethylenetriaminepentaacetic acid-folate (In-111-DTPA-folate) were conducted in FR-positive ovarian cancers. However, plans to commercialize In-111-DTPA-folate were hampered by the high cost of In-111 and its suboptimal clinical applicability (i.e., long radiochemical half-life). Using a Tc-99m-folate conjugate, experiments were conducted to compare the biodistribution of intraperitoneal versus intravenous Tc-99m-EC20 and on the accessible targeting of both subcutaneous and intraperitoneal FR-positive tumors and to improve Tc-99m-EC20's TBR (tumor-to-blood ratio) co-injected versus pre-injected folic acid was also investigated. Preparation, radiochemical purity, yield, specific

activity, binding affinity, and tissue distribution studies were performed. Part of the qualification process in the preclinical models is to investigate differential levels of membrane-associated FR expression; 4T1, 4T1-pico, and M109 cells were used as tumor models for the assessment of Tc-99m-EC20 uptake; indeed net uptake of Tc-99m-EC20 in each of these tumors was proportional to their respective FR levels. Furthermore, FR-positive tumors are equally accessed by folate-targeted agents in a manner that is independent of both the tumor location and the route of dose administration. Nevertheless, many solid tumors have poorly formed vasculatures with intermittent blood flow and large distances between functional blood vessels and in the center of large tumors, increased interstitial pressure gradients cause radial fluid flow from the center to the periphery. Other factors, including foods (e.g., does the food or food metabolites contain competing products) and the critical mass of unlabeled peptide and the labeling specific activity (kBq/g), significantly affect uptake of peptide-based radioligands (Velikyan et al. 2008, 2010).

A major disadvantage of iodine-123 (I-123)-labeled monoclonal antibodies (MAbs) for SPECT imaging is the rapid diffusion of iodotyrosine from target cells after internalization and catabolism of the radioiodinated MAbs. In contrast, the chelated moieties remain intact longer in the systemic vasculature and are not subject to deiodination and offer a higher residualization. Indeed, assuring there is minimal metabolic processing of the radiolabeled product into radiolabeled subfragments (i.e., degradation) is the key consideration in reducing retention of antibodies (and confusing fragmentation) within the cell and reduces interpretive challenges of multiple product PK uptake, residency, and elimination profiles to the images (Shih et al. 1994).

Translation between SPECT and PET, for example, In-111 of DOTA-conjugated biological moieties can offer easier and cheaper data than that obtained by the PET equivalent trivalent ions. DOTA and DTPA avid SPECT radiometals (e.g., In-111) may be used for initial evaluation of a series of biological targeting moieties (BTMS; e.g., peptide, antibody, antibody fragments); once selection of an optimal BTM, the investigator may then move to the shorter-lived PET radioisotope. Anecdotal evidence suggests the distribution properties of the SPECT, and PET chelated radiometal may not greatly differ.

7.2.1.4 Computed Tomography (CT)

Like MRI, CT is often simply associated with anatomical imaging. Indeed, its use is most commonly identifying pathological lesions via alteration or distortion in normal structures. However, after administration of iodinated contrast agents—where conventionally this is used to enhance contrast (by absorption and attenuation of X-rays) in statically acquired images—more recently the i.v. administration of these agents can be followed with dynamic acquisitions where vascular hemodynamics and fine vascular structures related to flow impedance (atherosclerosis, etc.) can be resolved.

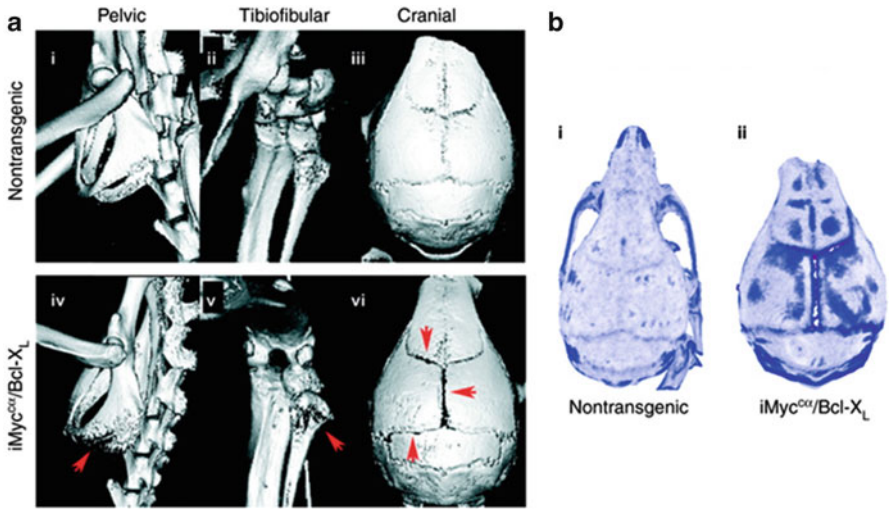

Fig. 7.5 (**a**) Osteolytic bone disease in the iMyc^{Cα}/Bcl-X$_L$ GEM model of de novo PCM. Unlike in age-matched nontransgenic (B6 × FVB/N) F$_1$ mice (*i–iii*), ex vivo CT imaging revealed evidence of osteolytic bone disease (*red arrows*) in the pelvic bone (*iv*), tibiofibular complex (*v*), and cranium (*vi*) of iMyc^{Cα}/Bcl-X$_L$ mice by approximately 110 days of age. (**b**) Increases in bone surface roughness and focal osteolytic lesions, which extended beyond the area of suture widening, were observed in 110-day-old iMyc^{Cα}/Bcl-X$_L$ mice (Lee et al. 2011b; with permissions)

CT uses X-rays to generate cross-sectional, two-dimensional images of the body. Images are acquired by rapid rotation of the X-ray tube a full 360° around the subject. The transmitted radiation is measured by a ring of sensitive radiation detectors located on the gantry around the subject.

Earlier publications of micro-CT in oncology animal models mainly explored skeletal changes associated with tumor dissemination and metastasis. A recent example was reported in complex GEMMS (http://www.ncbi.nlm.nih.gov/pubmed/15967710) models where spatial and temporal dynamics of lesion manifestation were unknown (Lee et al. 2011b). See Fig. 7.5 for a view of such distortion of bone from tumor invasion and displacement.

Like dynamic contrast enhanced-MRI (DCE-MRI), DCE-CT can offer parameters associated with hemodynamic constituents underlying vascular function in different disease states (e.g., atherosclerosis and tumors). Indeed, recently these two modalities have been compared in a rat tumor model (Ng et al. 2012). While both modalities had good reproducibility, their derived parameters were not equivalent. The latter could, in some part, be attributed to different sized molecular agents used and temporal resolution of the different modalities. However, other preclinical investigations have successfully used DCE-CT in the context of acute changes after antiangiogenic therapies (Cyran et al. 2012; Tai et al. 2010) (Fig. 7.6).

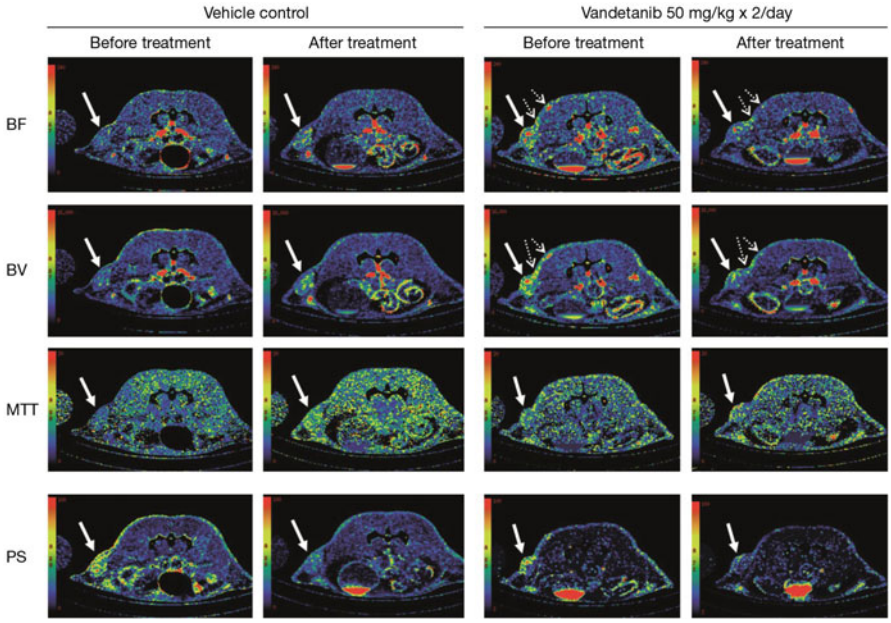

Fig. 7.6 Representative blood flow (BF), blood volume (BV), mean transit time (MTT), and permeability surface (PS) area maps of a transaxial section through the tumor of one vehicle- and one vandetanib-treated non-hypovascular tumor before and after treatment. In the BF, BV, MTT, and PS maps, values from 0 to 240 ml/min per 100 g, from 0 to 16 ml/100 g, from 0 to 20 s, and from 0 to 100 ml/min per 100 g, respectively, are coded according to the rainbow color scale. The parametric maps, in particular BF and BV, show the level of angiogenic activities in the tumor and adjacent tissue as indicated by *solid* and *dotted arrows* respectively (Images from Tai et al. (2010); with permission)

There are more CT cameras in clinical practice as stand-alone systems and as combined PET/CT systems versus combined or with MRI systems, and this is in part the motivation for preclinical studies with CT as the translational possibilities are perhaps greater than that with DCE-MRI. However, the CT radiation risk (Brenner and Hall 2007) in humans that exists is far greater when dynamic data is acquired compared to static acquisitions. Although methods are being introduced to reduce radiation exposure (*Image Gently*™ program out of the SNMI), the impact on sensitivity to hemodynamic changes has still to be determined (Kim et al. 2011). Limited literature exists for animal studies and the risks of radiation exposure from CT scans (Boone et al. 2004), but careful consideration is recommended in longitudinal studies (Willekens et al. 2010; Kersemans et al. 2011b) as these protocols are intended to be translated to human clinical use and radiation risk must be considered.

Multimodality has not been described in this chapter; however, PET/CT and SPECT/CT are the major multimodal techniques applied in preclinical oncology (Kapoor et al. 2004). Fundamentally, the combination of functional/molecular

Table 7.1 Names and intended physiologic targets of PET tracers[a] often used in clinical oncology and in laboratory studies using small animals are listed (Smith et al. 2012)

^{18}F FDG	Glucose metabolism/localization
3-F-18 Fluoro-3-deoxythymidine	Tumor proliferation
^{11}C Choline/^{18}F fluorocholine	Choline metabolism
^{18}F Fluoro-L-DOPA	Neuroendocrine tumors
^{18}F Fluoroethyltyrosine	Amino acid transport
^{18}F AH111585 (F18 fluciclatide)	Angiogenesis
^{18}F FACBC	Amino acid transport
^{18}F FMISO	Hypoxia
^{18}F HX4	Hypoxia
^{18}F EF5	Hypoxia
^{64}Cu ATSM	Hypoxia
^{68}Ga DOTATATE	Neuroendocrine tumors
^{18}F FES	Estrogen receptor
^{18}F RGD-K5	Angiogenesis
^{68}Ga BNOTA-PRGD2	Angiogenesis
^{18}F Paclitaxel	Multidrug resistance
^{89}Zr Bevacizumab	VEGF
^{18}F VM4-037	Carbonic anhydrase IX
^{89}Zr Cetuximab	EGFR
^{18}F FFNP	Progesterone receptor
^{64}Cu DOTA-U3-1287	HER3
^{18}F BAY94-9392	Amino acid transport
^{124}I NM404	Brain glioma
^{124}I cG250	Carbonic anhydrase IX
^{18}F ML-10	Apoptosis
^{11}C Lapatinib	Her2
^{18}F Annexin V	Apoptosis
^{18}F FAC	Tumor proliferation
^{11}C Verapamil	P-gp expression

The reader is encouraged to review the appropriateness of each agent, particularly biologics, which may exhibit species specificity in target binding in an animal system

[a]This list is not intended to be exhaustive and many agents are continuing to be added to this list

imaging with anatomical registration enables the investigator to work with high confidence in advanced disease models, e.g., orthotopic or genetically engineered mouse models with spontaneous lesion development. Beyond these is the recent introduction of PET/MRI (Cherry 2009). The latter has recently overcome some exquisite engineering complications associated with PET-associated electronics operating under conditions of high magnetic fields while still retaining spatial resolution and quantification capabilities.

7.2.1.5 Radiotracers/Radiopharmaceuticals ("Tracers")

The reader is encouraged to review this section with added information from the National Library of Medicine regarding radiotracers (ref: http://www.ncbi.nlm.nih.gov/books/NBK5330/). Table 7.1 describes several radiotracers created for PET imaging.

7.3 Animal Models Useful in Cancer Therapeutic Development

The reader is encouraged to examine a general review of the animal models used in cancer research over the years; see Frese and Tuveson (2007) and the earlier paper of Marx (2003).

In oncology preclinical studies, the most common publication of data when new targeted therapeutics are presented is the chemical structure of the new molecule, binding data from in vitro IC50s in multiple cell lines, and a mechanism of action treatise on how the molecule performs in vivo in these different lines as subcutaneous (SC) xenograft masses studied on the flank of immunocompromised species and other murine strains of choice. The SC xenograft efficacy protocol is typically represented by short-term (~21 days) tumor growth kinetics measured with calipers in three axial directions creating a tumor mass volume estimate. The treated arms of studies are compared to a standard-of-care and vehicle treatment, and the "tumor versus control" response metrics (size, orientation, visual appearance, etc.) are reported. Much criticism has been laid upon the ATCC SC xenograft models approach as there has been actually limited predictability realized to date for translational therapeutic efficacy and even for a translational basis of drug exposure (Johnson et al. 2001). The inherent "homogeneity" of the xenograft cells and the lack of the "normal" stromal and vascular component architectures at the onset make the xenograft models somewhat questionable for modeling the in situ nidus of tumor development. However, results from Voskoglou-Nomikos et al. (2003) suggest under the right conditions and when multiple models or tumor panels are used, these models may be useful in predicting the phase II clinical trial efficacy performance of cancer drugs and biologics.

Syngeneic cells benefit from being able to be used in animals whose immune system remains intact, and that this kind of cell system can play a large part in making a tumor response clinically relevant. The models are to date limited and the argument is that one is treating rat or mouse cancer cells and that the mutations may not be preserved or activated/inhibited in a manner similar to that of the human equivalent malignancy (de Jong and Maina 2010). It is imperative we always remember we are dealing with "models" and that there will be intrinsic differences from the human clinical experience that must be considered.

However, for qualifying imaging biomarkers in the context of a pharmaceutically targeted agent, if one can presume the mechanism of action (MoA) of these agents

is preserved through to the intended clinical population, then these models add value. For example, DCE-MRI systems, a measurement used to confirm acute hemodynamic changes after antiangiogenic treatments, have been useful preclinically and clinically in a number of cases. While only anecdotal, the changes observed in syngeneic lines or SC xenografts using the same type of contrast agents and similar acquisition routines appear to match that observed in a clinical context. In support of this, we first see that Lee et al. (2006) observed the reduction in tumor vascularity correlated significantly with improved clinical outcomes in patients with advanced colorectal cancer and liver metastases. They went onto assess the biomarkers used in the clinical trials and applied these markers in an orthotopic, syngeneic mouse model: C57BL/6 mice injected in the ear pinnae with murine B16/BL6 melanoma cells which metastases to the cervical lymph nodes; a change from baseline in the MRI-measured DCE-MRI parameter for the B16/BL6 melanoma model after treatment with PTK/ZK appeared to correlate well with antitumor activity of the agent. Through PK/PD modeling of the mouse B16/BL6 melanoma model MRI-initial area under the curve measures appear to be predictive of both tumor response and the pharmacodynamic effects of PTK/ZK in patients at equivalent drug exposures (Lee et al. 2006). Secondly, in two SC xenograft models Lovo (human colorectal carcinoma) or C6 (rat glioma) tumors, treated with Cediranib (RECENTIN, AZD2171), a highly potent inhibitor of the tyrosine kinase activity associated with all three vascular endothelial growth factor (VEGF) receptors, and imaged with DCE-MRI at baseline and 2 h after the final dose (3 doses, given at 2, 26, and 50 h), showed acute changes in two DCE-MRI parameters (Bradley et al. 2009), and these observations could be translated to that observed in the phase I clinical study of AZD2171 in patients with advanced solid tumors (Drevs et al. 2007). The observations revealed pharmacodynamic time-, dose-, and exposure-related decreases in the initial area under the curve, again defined as the DCE-MRI data collected over 60 s post-contrast arrival in the tissue (i.e., iAUC60).

Patient-derived xenografts (PDX), where fresh surgical tumor tissue is obtained and implanted subcutaneously or orthotopically in mice, are emerging as a new addition to the battery of preclinical models to test targeted agents. PDX are thought to more faithfully recapitulate the molecular diversity, cellular heterogeneity, and histology seen in patient tumors albeit the issues described earlier of actual tissue initiation. Differences in targeted therapy response rates between patient-derived tumor tissue and xenografts have been observed (Jin et al. 2012). However, limitations do exist and must be considered in the context of availability of other preclinical models (Kopetz et al. 2012). Limited literature exists where imaging PDX is specifically described (Germanos 2011, WMIC Abs P779).

Xenografts, syngeneic cell lines, and PDX can be inoculated orthotopically; this mode of implantation is more complex but may better recapitulate the microenvironment of what may be expected in the clinical context, e.g., stromal infiltration and delivery barriers of therapy as well as nutrients and vascular access. Extensive literature exists where imaging of orthotopically implanted tumors has revealed response to treatment using noninvasive measurements. Hoff et al. (2012) showed

the utility of simultaneously acquiring DCE- and DW-MRI data in an orthotopically implanted model of glioma; imaging pre- and post-VEGF-Trap (aka., Aflibercept) treatment showed acute changes in both DCE as well as DW derived parameters that were corroborated by histopathological findings. Furthermore, the impact of tumor growth on the tumor implantation sites were examined by Zechmann et al. (2007) where DCE-MRI and ^{1}H-MRS were assessed and compared between the two sites (orthotopic vs. subcutaneous); indeed, some tumor lines show comparable parameter changes and some are different.

Emerging data suggests that genetically engineered mouse model systems (GEMMS) better predict therapeutic responses and PK than the more traditional xenograft tumor systems (Chesi et al. 2012; Combest et al. 2012). Furthermore, Yuneva et al. (2012) have shown that the metabolic profile of the tumor depends on both the genetic lesion and tissue type. A most comprehensive assessment of a GEMM was by (Chen et al. 2012); understanding that while patients are often stratified by a single oncogenic driver mutation, the impact of coexisting genetic mutations, especially the loss of tumor suppressors, had not yet been fully explored. Comparison of F-18-FDG avidity, quantified by the standardized uptake value (SUV) calculation in lung cancers across three different genotypes showed an overall higher FDG uptake in both KRAS/p53 and KRAS/Lkb1 tumors compared to simple KRAS tumors alone. Expression of the glucose transporter GLUT1 was elevated in KRAS/Lkb1 mutant tumors, consistent with an increased baseline FDG-PET SUV signal. To determine if this finding was applicable to human patients, FDG avidity in nine patients with KRAS-mutated lung cancer was examined (Yuneva et al. 2012). Tumors from three patients positive for LKB1 immunostaining had a mean maximum SUV (SUV_{max}) of 2.33, whereas tumors from six patients negative for LKB1 immunostaining had a mean SUV_{max} of 8.75, a near fourfold difference.

7.4 Summary

In conclusion, biomedical imaging is becoming an integral biomarker in drug discovery and development. As illustrated in this chapter, the different modalities can reveal functional and physiological parameters otherwise unattainable by conventional methods. These measurements can be used when new animal models are developed and to follow acute pharmacodynamic changes during drug treatment. Furthermore, translational science (“bench to bedside”) and the use of clinically relevant modalities and appropriate clinical endpoints allow the researcher to qualify a novel/conventional biomarker in a selected preclinical model and, assuming preservation of MoA of the therapy, allow for the development of novel drug entities which can be utilized in their respective clinical oncology scenarios with the same expected targeting and tumor outcomes using the model-defined imaging techniques.

References

Aboagye EO (2005) Positron emission tomography imaging of small animals in anticancer drug development. Mol Imaging Biol 7:53–58

Albanese C, Rodriguez OC, Vanmeter J, Fricke ST, Rood BR, Lee Y, Wang SS, Madhavan S, Gusev Y, Petricoin EF, 3rd, et al (2012) Preclinical magnetic resonance imaging and systems biology in cancer research: Current applications and challenges. Am J Pathol

Bahce I, Smit EF, Lubberink M, van der Veldt AA, Yaqub M, Windhorst AD, Schuit RC, Thunnissen E, Heideman DAH, Postmus PE et al (2013) Development of [11C]erlotinib positron emission tomography for in vivo evaluation of epidermal growth factor receptor mutational status. Clin Cancer Res Off J Am Assoc Cancer Res 19:183–193

Barnes SL, Whisenant JG, Loveless ME, Yankeelov TE (2012) Practical dynamic contrast enhanced MRI in small animal models of cancer: data acquisition, data analysis, and interpretation. Pharmaceutics 4:442–478

Baudelet C, Gallez B (2004) Effect of anesthesia on the signal intensity in tumors using BOLD-MRI: comparison with flow measurements by Laser Doppler flowmetry and oxygen measurements by luminescence-based probes. Magn Reson Imaging 22:905–912

Boone JM, Velazquez O, Cherry SR (2004) Small-animal X-ray dose from micro-CT. Mol Imaging 3:149–158

Bradley DP, Tessier JJ, Lacey T, Scott M, Jürgensmeier JM, Odedra R, Mills J, Kilburn L, Wedge SR (2009) Examining the acute effects of cediranib (RECENTIN, AZD2171) treatment in tumor models: a dynamic contrast-enhanced MRI study using gadopentate. Magn Reson Imaging 27:377–384

Breeman WAP, De Blois E, Sze Chan H, Konijnenberg M, Kwekkeboom DJ, Krenning EP (2011) (68)Ga-labeled DOTA-peptides and (68)Ga-labeled radiopharmaceuticals for positron emission tomography: current status of research, clinical applications, and future perspectives. Semin Nucl Med 41:314–321

Brenner DJ, Hall EJ (2007) Computed tomography — an increasing source of radiation exposure. N Engl J Med 357:2277–2284

Buchmann I, Henze M, Engelbrecht S, Eisenhut M, Runz A, Schäfer M, Schilling T, Haufe S, Herrmann T, Haberkorn U (2007) Comparison of 68Ga-DOTATOC PET and 111In-DTPAOC (Octreoscan) SPECT in patients with neuroendocrine tumours. Eur J Nucl Med Mol Imaging 34:1617–1626

Chen Z, Cheng K, Walton Z, Wang Y, Ebi H, Shimamura T, Liu Y, Tupper T, Ouyang J, Li J et al (2012) A murine lung cancer co-clinical trial identifies genetic modifiers of therapeutic response. Nature 483:613–617

Cherry SR (2009) Multimodality imaging: beyond PET/CT and SPECT/CT. Semin Nucl Med 39:348–353

Chesi M, Matthews GM, Garbitt VM, Palmer SE, Shortt J, Lefebure M, Stewart AK, Johnstone RW, Bergsagel PL (2012) Drug response in a genetically engineered mouse model of multiple myeloma is predictive of clinical efficacy. Blood 120:376–385

Combest AJ, Roberts PJ, Dillon PM, Sandison K, Hanna SK, Ross C, Habibi S, Zamboni B, Müller M, Brunner M et al (2012) Genetically engineered cancer models, but not xenografts, faithfully predict anticancer drug exposure in melanoma tumors. Oncologist 17:1303–1316

Cyran CC, Von Einem JC, Paprottka PM, Schwarz B, Ingrisch M, Dietrich O, Hinkel R, Bruns CJ, Clevert DA, Eschbach R et al (2012) Dynamic contrast-enhanced computed tomography imaging biomarkers correlated with immunohistochemistry for monitoring the effects of sorafenib on experimental prostate carcinomas. Invest Radiol 47:49–57

de Jong M, Maina T (2010) Of mice and humans: are they the same?—implications in cancer translational research. J Nucl Med 51:501–504

Doty FD, Entzminger G, Kulkarni J, Pamarthy K, Staab JP (2007) Radio frequency coil technology for small-animal MRI. NMR Biomed 20:304–325

Drevs J, Siegert P, Medinger M, Mross K, Strecker R, Zirrgiebel U, Harder J, Blum H, Robertson J, Jürgensmeier JM et al (2007) Phase I clinical study of AZD2171, an oral vascular endothelial growth factor signaling inhibitor, in patients with advanced solid tumors. J Clin Oncol 25: 3045–3054

Ebenhan T, Honer M, Ametamey SM, Schubiger PA, Becquet M, Ferretti S, Cannet C, Rausch M, McSheehy PMJ (2009) Comparison of [18F]-tracers in various experimental tumor models by PET imaging and identification of an early response biomarker for the novel microtubule stabilizer patupilone. Mol Imaging Biol 11:308–321

Ferris CF, Smerkers B, Kulkarni P, Caffrey M, Afacan O, Toddes S, Stolberg T, Febo M (2011) Functional magnetic resonance imaging in awake animals. Rev Neurosci 22:665–674

Firestone B (2010) The challenge of selecting the "right" in vivo oncology pharmacology model. Curr Opin Pharmacol 10:391–396

Franc BL, Acton PD, Mari C, Hasegawa BH (2008) Small-animal SPECT and SPECT/CT: important tools for preclinical investigation. J Nucl Med 49:1651–1663

Frese KK, Tuveson DA (2007) Maximizing mouse cancer models. Nat Rev Cancer 7:645–658

Germanos M (2011) In vivo longitudinal 2-deoxy-2-[18F]fluoro-D-glucose (FDG) PET characterization of primary human tumor explant xenografts in mice. World Molecular Imaging Congress P779

Groch MW, Erwin WD (2000) SPECT in the year 2000: basic principles. J Nucl Med Technol 28:233–244

Hanahan D, Weinberg RA (2011) Hallmarks of cancer: the next generation. Cell 144:646–674

Heijmen L, Ter Voert EEGW, Nagtegaal ID, Span P, Bussink J, Punt CJA, de Wilt JHW, Sweep FCGJ, Heerschap A, van Laarhoven HWM (2013) Diffusion-weighted MR imaging in liver metastases of colorectal cancer: reproducibility and biological validation. Eur Radiol 23: 748–756

Hodkinson DJ, De Groote C, McKie S, Deakin JFW, Williams SR (2012) Differential effects of anaesthesia on the phMRI response to acute ketamine challenge. Br J Med Med Res 2: 373–385

Hoff BA, Bhojani MS, Rudge J, Chenevert TL, Meyer CR, Galbán S, Johnson TD, Leopold JS, Rehemtulla A, Ross BD et al (2012) DCE and DW-MRI monitoring of vascular disruption following VEGF-Trap treatment of a rat glioma model. NMR Biomed 25:935–942

Jin K, Lan H, Cao F, Han N, Xu Z, Li G, He K, Teng L (2012) Differential response to EGFR- and VEGF-targeted therapies in patient-derived tumor tissue xenograft models of colon carcinoma and related metastases. Int J Oncol 41:583–588

Johnson JI, Decker S, Zaharevitz D, Rubinstein LV, Venditti JM, Schepartz S, Kalyandrug S, Christian M, Arbuck S, Hollingshead M et al (2001) Relationships between drug activity in NCI preclinical in vitro and in vivo models and early clinical trials. Br J Cancer 84:1424–1431

Jones T (1996) The imaging science of positron emission tomography. Eur J Nucl Med 23: 807–813

Kapoor V, McCook BM, Torok FS (2004) An introduction to PET-CT imaging1. Radiographics 24:523–543

Kersemans V, Cornelissen B, Hueting R, Tredwell M, Hussien K, Allen PD, Falzone N, Hill SA, Dilworth JR, Gouverneur V et al (2011a) Hypoxia imaging using PET and SPECT: the effects of anesthetic and carrier gas on [Cu]-ATSM, [Tc]-HL91 and [F]-FMISO tumor hypoxia accumulation. PLoS One 6:e25911

Kersemans V, Thompson J, Cornelissen B, Woodcock M, Allen PD, Buls N, Muschel RJ, Hill MA, Smart SC (2011b) Micro-CT for anatomic referencing in PET and SPECT: radiation dose, biologic damage, and image quality. J Nucl Med 52:1827–1833

Kim SM, Haider MA, Milosevic M, Jaffray DA, Yeung IWT (2011) A method for patient dose reduction in dynamic contrast enhanced CT study. Med Phys 38:5094–5103

Kinahan PE, Fletcher JW (2010) PET/CT standardized uptake values (SUVs) in clinical practice and assessing response to therapy. Semin Ultrasound CT MR 31:496–505

Knowles SM, Wu AM (2012) Advances in immuno-positron emission tomography: antibodies for molecular imaging in oncology. J Clin Oncol 30:3884–3892

Kopetz S, Lemos R, Powis G (2012) The promise of patient-derived xenografts: the best laid plans of mice and men. Clin Cancer Res Off J Am Assoc Cancer Res 18:5160–5162

Lee L, Sharma S, Morgan B, Allegrini P, Schnell C, Brueggen J, Cozens R, Horsfield M, Guenther C, Steward WP et al (2006) Biomarkers for assessment of pharmacologic activity for a vascular endothelial growth factor (VEGF) receptor inhibitor, PTK787/ZK 222584 (PTK/ZK): translation of biological activity in a mouse melanoma metastasis model to phase I studies in patients with advanced colorectal cancer with liver metastases. Cancer Chemother Pharmacol 57:761–771

Lee E, Kamlet AS, Powers DC, Neumann CN, Boursalian GB, Furuya T, Choi DC, Hooker JM, Ritter T (2011a) A fluoride-derived electrophilic late-stage fluorination reagent for PET imaging. Science 334:639–642

Lee EC, Fitzgerald M, Bannerman B, Donelan J, Bano K, Terkelsen J, Bradley DP, Subakan O, Silva MD, Liu R et al (2011b) Antitumor activity of the investigational proteasome inhibitor MLN9708 in mouse models of B-cell and plasma cell malignancies. Clin Cancer Res 17: 7313–7323

Marx J (2003) Building better mouse models for studying cancer. Science 299:1972–1975

McArthur GA, Puzanov I, Amaravadi R, Ribas A, Chapman P, Kim KB, Sosman JA, Lee RJ, Nolop K, Flaherty KT et al (2012) Marked, homogeneous, and early [18F]fluorodeoxyglucose-positron emission tomography responses to vemurafenib in BRAF-mutant advanced melanoma. J Clin Oncol 30:1628–1634

McGrath DM, Bradley DP, Tessier JL, Lacey T, Taylor CJ, Parker GJM (2009) Comparison of model-based arterial input functions for dynamic contrast-enhanced MRI in tumor bearing rats. Magn Reson Med 61:1173–1184

Memon AA, Jakobsen S, Dagnaes-Hansen F, Sorensen BS, Keiding S, Nexo E (2009) Positron emission tomography (PET) imaging with [11C]-labeled erlotinib: a micro-PET study on mice with lung tumor xenografts. Cancer Res 69:873–878

Morse DL, Gillies RJ (2010) Molecular imaging and targeted therapies. Biochem Pharmacol 80: 731–738

Müller C, Schibli R (2013) Single photon emission computed tomography tracer. Recent Results Cancer Res 187:65–105

Neil JJ (2008) Diffusion imaging concepts for clinicians. J Magn Reson Imaging 27:1–7

Nelson GS, Perez J, Colomer MV, Ali R, Graves E (2011) Facilitating multimodal preclinical imaging studies in mice by using an immobilization bed. Comp Med 61:499–504

Ng CS, Waterton JC, Kundra V, Brammer D, Ravoori M, Han L, Wei W, Klumpp S, Johnson VE, Jackson EF (2012) Reproducibility and comparison of DCE-MRI and DCE-CT perfusion parameters in a rat tumor model. Technol Cancer Res Treat 11:279–288

Nguyen Q-D, Perumal M, Waldman TA, Aboagye EO (2011) Glucose metabolism measured by [^{18}F]fluorodeoxyglucose positron emission tomography is independent of PTEN/AKT status in human colon carcinoma cells. Transl Oncol 4:241–248

Ou S-HI, Bartlett CH, Mino-Kenudson M, Cui J, Iafrate AJ (2012) Crizotinib for the treatment of ALK-rearranged non-small cell lung cancer: a success story to usher in the second decade of molecular targeted therapy in oncology. Oncologist 17:1351–1375

Pantaleo MA, Nicoletti G, Nanni C, Gnocchi C, Landuzzi L, Quarta C, Boschi S, Nannini M, Di Battista M, Castellucci P et al (2010) Preclinical evaluation of KIT/PDGFRA and mTOR inhibitors in gastrointestinal stromal tumors using small animal FDG PET. J Exp Clin Cancer Res 29:173

Padhani AR, Liu G, Mu-Koh D, Chenevert TL, Thoeny HC, Takahara T, Dzik-Jurasz A, Ross BD, Van Cauteren M, Collins D et al (2009) Diffusion-Weighted magnetic resonance imaging as a cancer biomarker: consensus and recommendations. Neoplasia 11:102–125

Pautler RG (2004) Mouse MRI: concepts and applications in physiology. Physiology (Bethesda) 19:168–175

Pysz MA, Gambhir SS, Willmann JK (2010) Molecular imaging: current status and emerging strategies. Clin Radiol 65:500–516

Reddy JA, Xu L-C, Parker N, Vetzel M, Leamon CP (2004) Preclinical evaluation of (99m) Tc-EC20 for imaging folate receptor-positive tumors. J Nucl Med 45:857–866

Schnell C, Arnal S, Barbé S, Becquet M, Garcia-Echeverria C, Cozens R (2010) 261 Effects of isoflurane anesthesia on bioluminescence measurements: impact on pharmacological assessment of anti-tumor activity of chemical entities. Eur J Cancer Supplements 8:85

Seo Y, Jiang H, Franc BL (2013) Preclinical SPECT and SPECT/CT. Recent Results Cancer Res 187:193–220

Serkova NJ, Spratlin JL, Eckhardt SG (2007) NMR-based metabolomics: translational application and treatment of cancer. Curr Opin Mol Ther 9:572–585

Shih LB, Thorpe SR, Griffiths GL, Diril H, Ong GL, Hansen HJ, Goldenberg DM, Mattes MJ (1994) The processing and fate of antibodies and their radiolabels bound to the surface of tumor cells in vitro: a comparison of nine radiolabels. J Nucl Med 35:899–908

Smith TB, Nayak KS (2010) MRI artifacts and correction strategies. Imaging Med 2(4):445–457

Smith G, Carroll L, Aboagye EO (2012) New frontiers in the design and synthesis of imaging probes for PET oncology: current challenges and future directions. Mol Imaging Biol 14: 653–666

Spratlin JL, Serkova NJ, Eckhardt SG (2009) Clinical applications of metabolomics in oncology: a review. Clin Cancer Res 15:431–440

Tai JH, Tessier J, Ryan AJ, Hoffman L, Chen X, Lee T-Y (2010) Assessment of acute antivascular effects of vandetanib with high-resolution dynamic contrast-enhanced computed tomographic imaging in a human colon tumor xenograft model in the nude rat. Neoplasia 12:697–707

Therasse P, Eisenhauer EA, Verweij J (2006) RECIST revisited: a review of validation studies on tumour assessment. Eur J Cancer 42:1031–1039

Velikyan I, Beyer GJ, Bergström-Pettermann E, Johansen P, Bergström M, Långström B (2008) The importance of high specific radioactivity in the performance of 68Ga-labeled peptide. Nucl Med Biol 35:529–536

Velikyan I, Sundin A, Eriksson B, Lundqvist H, Sörensen J, Bergström M, Långström B (2010) In vivo binding of [68Ga]-DOTATOC to somatostatin receptors in neuroendocrine tumours–impact of peptide mass. Nucl Med Biol 37:265–275

Verel I, Visser GWM, Boellaard R, Stigter-van Walsum M, Snow GB, Van Dongen GAMS (2003) 89Zr immuno-PET: comprehensive procedures for the production of 89Zr-labeled monoclonal antibodies. J Nucl Med 44:1271–1281

Vincent MD, Kuruvilla MS, Leighl NB, Kamel-Reid S (2012) Biomarkers that currently affect clinical practice: EGFR, ALK, MET, KRAS. Curr Oncol 19:S33–S44

Voskoglou-Nomikos T, Pater JL, Seymour L (2003) Clinical predictive value of the in vitro cell line, human xenograft, and mouse allograft preclinical cancer models. Clin Cancer Res 9: 4227–4239

Willekens I, Buls N, Lahoutte T, Baeyens L, Vanhove C, Caveliers V, Deklerck R, Bossuyt A, De Mey J (2010) Evaluation of the radiation dose in micro-CT with optimization of the scan protocol. Contrast Media Mol Imaging 5:201–207

Yim H, Seo S, Na K (2011) MRI contrast agent-based multifunctional materials: diagnosis and therapy. J Nanomater 11 page

Yuneva MO, Fan TWM, Allen TD, Higashi RM, Ferraris DV, Tsukamoto T, Matés JM, Alonso FJ, Wang C, Seo Y et al (2012) The metabolic profile of tumors depends on both the responsible genetic lesion and tissue type. Cell Metab 15:157–170

Zechmann CM, Woenne EC, Brix G, Radzwill N, Ilg M, Bachert P, Peschke P, Kirsch S, Kauczor H-U, Delorme S et al (2007) Impact of stroma on the growth, microcirculation, and metabolism of experimental prostate tumors. Neoplasia 9:57–67

Zieba A, Grannas K, Söderberg O, Gullberg M, Nilsson M, Landegren U (2012) Molecular tools for companion diagnostics. N Biotechnol 29:634–640

Chapter 8
Use of Radiolabelled Leukocytes for Drug Evaluation in Man

Chrystalla Loutsios, Neda Farahi, Charlotte Summers, Prina Ruparelia, Jessica White, Jonathan Potts, Chandra K. Solanki, Kishor Solanki, Sarah Heard, Daniel Gillett, Kottekkattu K. Balan, Alison M. Condliffe, A. Michael Peters, and Edwin R. Chilvers

Abstract The endeavour to radiolabel or simply "label" autologous leukocytes has been a major clinical need. The endeavour to improve the labelling conditions and minimise interventional stresses and maintain cell functionality has been the driving objective. This chapter focuses on novel techniques used in this laboratory to radiolabel leukocytes, examples of the clinical indications that such labelled products might be informative, and how we can use these labelled cells in clinical situations to describe the life cycle behaviour (transit times and migratory capacity) of these labelled cells. Labelling techniques which preserve leukocyte functionality will assist in the development of new anti-inflammatory agents, anti-infectives, and indeed any drug or biologic where their clinical use may have an effect on these cells. Examples of labelling methods and clinical scenarios with imaging are described for conditions such as abscesses, ARDS, COPD, rheumatoid arthritis, inflammatory bowel disease, and vasculitis.

A. Michael Peters and Edwin R Chilvers are Joint Senior Authors.

C. Loutsios (✉) • N. Farahi • C. Summers • P. Ruparelia • J. White
A.M. Condliffe • E.R. Chilvers
Division of Respiratory Medicine, Department of Medicine, University of Cambridge School of Clinical Medicine, Cambridge, UK
e-mail: cl545@medschl.cam.ac.uk

J. Potts • A.M. Peters
Clinical Sciences Imaging Centre, Brighton and Sussex Medical School, Brighton, UK

C.K. Solanki • K. Solanki • S. Heard • D. Gillett • K.K. Balan
Nuclear Medicine, Addenbrooke's Hospital, CUHNHSFT, Cambridge, UK

B.R. Moyer et al. (eds.), *Pharmaco-Imaging in Drug and Biologics Development*, AAPS Advances in the Pharmaceutical Sciences Series 8, DOI 10.1007/978-1-4614-8247-5_8,

8.1 Introduction

The use of radioactive isotopes to label autologous leukocytes is an established technique with numerous clinical applications. It is used for cell kinetic studies, to localise and quantify sites of inflammation and infection, and has applications in the pharmaceutical industry as a non-invasive means of testing the effects of drugs on the life cycle of these cells.

Leukocytes play a vital role in the innate immune system and form the body's primary defence against infection and parasites; they are also important mediators of inflammation. Recent studies suggest their involvement in a variety of other processes including adaptive immunity, tumour progression, and even the formation and propagation of deep venous thrombosis (Von-Bruhl et al. 2012). Using radiolabelling techniques, the migration characteristics of leukocytes can be determined in several pathological conditions including lung and inflammatory bowel disease (IBD) and infections such as solid abscesses, renal sepsis, and orthopaedic infections. Cells of the innate immune system include granulocytes (neutrophils, eosinophils, and basophils), mast cells, monocytes, macrophages, and natural killer (NK) cells. Leukocytes of the adaptive immune system provide a more specific response to antigen and include lymphocytes (B and T cells).

Autologous human leukocytes are purified from a peripheral blood collection (generally 80 mL or more) and radiolabelled with a radioactive isotope (radioisotope, radionuclide; one which is known for its specific energies applicable to the imaging system intended, i.e. planar, positron emission tomography (PET), or single-photon emission computed tomography (SPECT) systems) before being reinjected into the individual donor. A combination of peripheral blood sampling and imaging then allows the quantitative analysis of cell kinetics, distribution, and fate. The quantification of leukocyte migration can be achieved by several techniques ranging from body fluid sampling through to complex imaging modalities using gamma cameras, which provide two- or three-dimensional images of the radiation detected. More recently, SPECT has used the gamma radiation emitted from radionuclides such as technetium (Tc-99m), indium (In-111), and thallium (Tl-201) and others, to generate a three-dimensional image of radioactivity in vivo providing high-resolution digital images which can also provide quantitative assessment of regional localisation (termed region of interest, or ROI).

The use of radiolabelled leukocytes to quantify and localise infection and inflammation in vivo provides a platform to test non-invasively the effects of existing and novel drugs and is therefore highly relevant to the pharmaceutical industry. As well as continued innovation in this field, other approaches for labelling cells, particularly stem cells, include the use of superparamagnetic iron oxide (SPIO) nanoparticles in combination with magnetic resonance imaging (MRI). Cell labelling techniques include receptor-mediated endocytosis whereby a ligand is added to the surface of the SPIO nanoparticle, which then binds to the cell surface before being internalised (Gupta and Gupta 2005). Although there are several potential applications for human disease, many of the studies remain experimental in animal models.

8.2 Leukocyte Preparations and Radiolabelling Techniques

The purification of leukocytes from whole blood is divided into stages with the initial isolation of buffy coat leukocytes containing mixed leukocytes and platelets. Further purification allows the isolation of granulocytes, lymphocytes, and monocytes. It is then possible to further isolate eosinophils from granulocytes. Once purified, cells are incubated with the selected radiolabel before being re-injected into the donor.

Granulocytes prepared in the absence of autologous plasma become metabolically active and adhere to the lung capillary endothelium when re-injected causing delayed transit through the lung, low recovery in the blood, and increased liver uptake (Saverymuttu et al. 1983a). It is therefore vital to purify cells in the continuous presence of autologous plasma to minimise ex vivo activation and preserve their physiological behaviour once re-injected. Primed and activated neutrophils demonstrate shape change characterised by the formation of a broad, flattened protrusion known as a lamellipodium through changes in the actin cytoskeleton (Downey 1994). Such shape change also affects the deformability of these cells and as a consequence delays their transit through the narrow pulmonary capillary bed (Hogg 1994).

The protocol for isolating and radiolabelling leukocytes has been previously documented (Frier 1994) and is illustrated in Fig. 8.1. A wide-bore 19G butterfly is used (reduces shear stresses on the cells that can lead to activation) to withdraw up to 160 mL whole blood into a syringe pre-filled with the anticoagulant acid–citrate–dextrose (ACD), which unlike heparin does not cause leukocyte aggregation or promote adherence to plastic centrifuge tubes (Ellis 2011). Hetastarch is then added to promote erythrocyte sedimentation. After 30–60 min in the presence of hetastarch, two separate layers of cells are discernible, the lower containing erythrocytes, which is discarded, and the upper layer of leukocyte- and platelet-rich plasma (PRP). This plasma is carefully removed and centrifuged at $150 \times g$ for 5 min to generate the leukocyte pellet and a supernatant of PRP. The leukocyte pellet contains granulocytes (neutrophils and eosinophils), peripheral blood mononuclear cells (PBMCs) including monocytes, lymphocytes, and macrophages in addition to some discernible contamination with platelets and erythrocytes. The cells in this upper layer are termed "buffy coat" leukocytes. The PRP supernatant is removed and centrifuged at $1{,}500 \times g$ for 5 min to leave a platelet pellet and provide for a useful cell-free plasma (CFP) supernatant which is retained. The CFP is used to resuspend the mixed leukocyte pellet and is also used when applying selected Percoll gradients necessary to purify the granulocytes into desired enrichments of specific cell types.

Further purification of the leukocyte pellet to isolate granulocytes requires the use of discontinuous iso-osmotic Percoll gradients. Percoll is made of colloidal silica particles that have been coated in polyvinylpyrrolidone (PVP). It is mixed with sodium chloride before being diluted with autologous CFP to prepare 50, 60, and 65 % solutions. Two millilitres of each gradient solution are then gently layered, in a specific order of decreasing density, in a sterile 10 ml tube and the position of each gradient is marked.

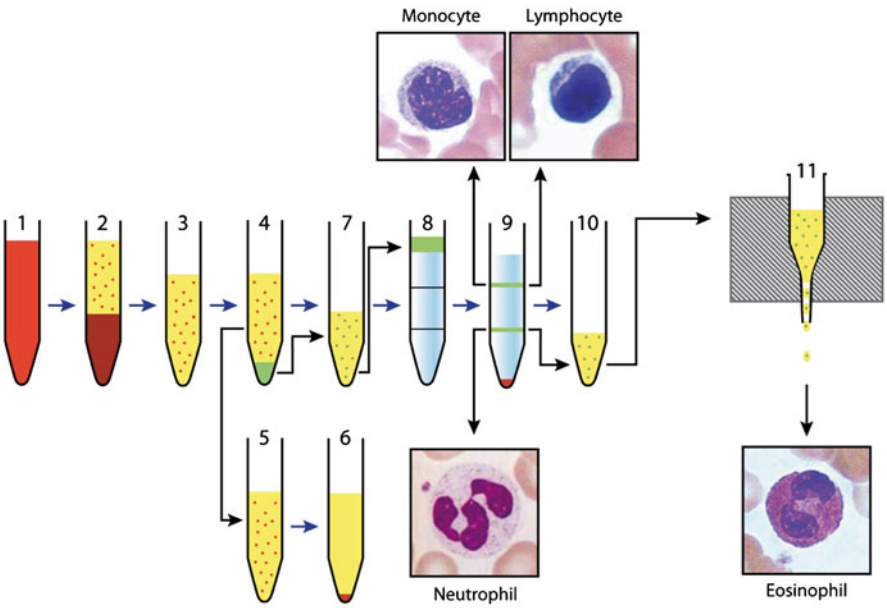

Fig. 8.1 Leukocyte isolation. (1) Whole blood in ACD. (2) Sedimentation of erythrocytes following the addition of hetastarch. Upper layer of leukocyte- and platelet-rich plasma. (3) Leukocyte- and platelet-rich plasma carefully removed from erythrocytes. (4) The generation of the leukocyte pellet (*green*) and supernatant of platelet-rich plasma following centrifugation at 150×*g* for 5 min. (5) Platelet-rich plasma supernatant is removed and centrifuged at 1,500×*g* for 5 min to generate (6) a platelet pellet (*red*) and the cell-free plasma (CFP) supernatant. (7) The leukocyte pellet is re-suspended in CFP. (8) Discontinuous Percoll gradients layered in decreasing density with leukocytes (*green*) overlaid. (9) Following centrifugation at 150×*g* for 5 min, PBMCs settle at the upper 50 % gradient interface and granulocytes at the lower 50–60 % interface. Contaminating red cells are found at the base of the tube. (10) Granulocytes are removed and re-suspended in CFP and incubated with immunomagnetic anti-CD16 antibodies. (11) Granulocytes are passed through a magnetic column which retains CD16-positive neutrophils and allows purified eosinophils to be collected

The leukocytes, suspended in CFP, are carefully overlaid onto the gradients and the tube is centrifuged at 150×*g* for 5 min. Following centrifugation, several distinct layers are visible and different cell types found at each of the three gradient interfaces. At the upper 50 % interface, the less dense platelets and PBMCs including lymphocytes and monocytes can be recovered and either used for research or discarded. The denser granulocytes settle at the 50–60 % interface and may be carefully withdrawn using a wide-bore pipette tip to minimise shear force damaging the cells. Contaminating erythrocytes may be visible at the base of the tube. The granulocytes are re-suspended in 3 mL buffer containing 0.5 % CFP and centrifuged at 150×*g* for 5 min. The supernatant is withdrawn and the granulocytes again re-suspended gently in 3 mL buffer containing 0.5 % CFP.

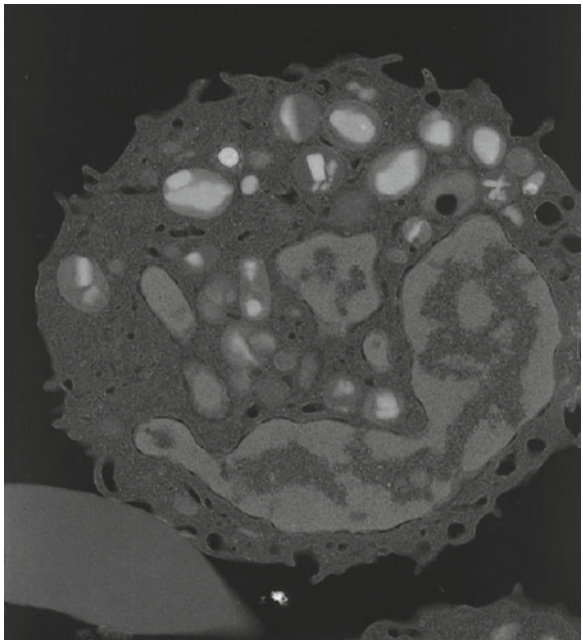

Fig. 8.2 Electron micrograph of a purified eosinophil showing the absence of cell surface CD16 antibody-coated immune-magnetic beads, which will only stain positive with neutrophils

If collection is desired, eosinophils can then be purified from the granulocyte fractions by negative selection using immunomagnetic anti-CD16 antibodies which retain CD16-positive neutrophils when passed through a magnetic column (Hansel et al. 1991) (Fig. 8.1). Purified eosinophils will therefore not stain positive for CD16 (Fig. 8.2).

Following isolation, cells are re-suspended in CFP and radiolabelled by incubation with an appropriate radioisotope, and at a desirable specific radioactivity for the intended imaging parameters of interest, for at least 15 min. The choice of radioisotope is dependent on its half-life and photon abundance required for the duration of the study without exposing the subject to excess radiation to stay within required limits of absorbed dose. The total effective dose received by subjects is dependent on the radionuclide used, whether additional imaging such as CT is incorporated into the protocol, and the organs exposed. 8 MBq of In-111 for example is used to label purified eosinophils used in planar gamma camera imaging, which gives an effective dose of 3.6 mSv to the subject. 200 MBq of Tc-99m used to label cells to be imaged with SPECT/CT gives an effective dose of 2 mSv. A low-dose CT thorax, if imaging the chest, will contribute an additional 3 mSv to the dose the subject receives.

The radioisotope in its ionic form cannot permeate the cell membrane and must therefore be complexed to a lipophilic chelator (ligand) with high affinity that results in an in vivo stable complex to allow the passive diffusion of the ligand–radioisotope complex into the cells of interest. This ligand must reach its target tissue without significant binding to plasma proteins and must not, at the dose of ligand extracted, either be toxic to its target cell or result in toxemias to the individual.

Early pioneer imaging of inflammation with Cr-51-labelled leukocytes was limited by this isotope's low labelling efficiency, high elution rate from the labelled cells and the infection locale, and poor emission characteristics of gamma radiation (high-energy gamma rays), all of which led to suboptimal imaging (Froelich and Swanson 1984). Its long half-life of 27.7 days also led to the use of other isotopes being favoured. Subsequent techniques involved the use of Ga-67-citrate to directly label inflammatory processes. Following injection, Ga-67-citrate binds to circulating transferrin (as an iron analogue) and extravasates within inflammatory sites due to increased vascular permeability where it binds to lactoferrin released from leukocytes or to siderophores produced by bacteria (Froelich and Swanson 1984). Following intravenous administration, 10–25 % of Ga-67-citrate is excreted by the kidneys within 24 h. There is slower excretion via the gastrointestinal tract and the remainder of the radioisotope localises predominantly in the liver and skeleton (Hoffer 1980). Such background tissue uptake resulting in increasing intra-abdominal activity limits the use of this radionuclide in the assessment of intra-abdominal collections. Ga-67 can be used favourably if the radionuclide is complexed such that the mechanism of distribution is not iron analogue related. Ga-67-citrate also binds to other lesions such as neoplasms which have bleeding and necrosis which have likely increases in transferrin deposition, thus limiting its specificity (Peters and Saverymuttu 1987). The long physical half-life of Ga-67-citrate of 78 h and the fact that only 10–25 % is excreted renally in the first 24 h, and thence elimination is primarily faecal, also lead to a higher radiation dose to the patient.

The most commonly used isotopes currently are In-111, which has a half-life of 67 h, and Tc-99m, which has a half-life of 6 h. In-111 was first complexed to 8-hydroxyquinolone (oxine) to radiolabel leukocytes (McAfee and Thakur 1976). The complex forms a neutral and lipophilic compound (3:1 with indium), which diffuses readily across the cell membrane. Indium then disassociates and binds to intracellular components whilst some of the oxine leaves the cell leaving the leukocytes stably labelled (Thakur et al. 1977). In-111-oxine also binds to plasma transferrin and in order to obtain high labelling efficiency cells must be removed from plasma before labelling, which risks their activation. In contrast to Ga-67-citrate, there is no renal or bowel excretion making indium scintigraphy a useful tool for the localisation of intra-abdominal inflammation or infection. Tropolone was first used as a ligand for indium in 1982 and may be incubated with cells in autologous plasma at lower concentrations of leukocytes (Danpure et al. 1982; Danpure and Osman 1988). It has since been used widely to label leukocytes, platelets, and erythrocytes and is certainly now the chelate of choice for neutrophil, eosinophil, and mixed leukocyte studies using In-111.

Technetium bound to hexamethylpropyleneamineoxime (HMPAO) was originally used to assess cerebral perfusion but has since been adapted to radiolabel leukocytes. Tc-99m-HMPAO forms a neutral lipophilic complex, which passively diffuses into the cell. It is then converted into a hydrophilic form that is unable to cross the cell membrane, thereby trapping the technetium within the cell (Ellis 2011). Despite some initial elution of the label from the cells and a degree of

non-specific bowel activity arising from excretion via the renal and hepatobiliary tract, the use of ^{99m}Tc-HMPAO allows for higher resolution images and a reduction in the radiation dose delivered to the patient relative to In-111 (Robins et al. 2000). These techniques lead to indiscriminate labelling of cells although ligands may vary in their affinity for different cell types (Puncher and Blower 1994). It is therefore important that the cells of interest are purified prior to the radiolabelling process.

Factors influencing labelling efficiency (LE) of cells include the presence or the absence of plasma, concentration of ligand mixed with the radionuclide, pH of the labelling medium, incubation time, temperature, and cell concentration (Danpure and Osman 1988). Labelling cells in buffered saline can achieve high LE but again risks activating the cells. In contrast, labelling with In-111-troponolate or Tc-99m-HMPAO in plasma protects the cells whilst maintaining satisfactory LE (Ellis 2011). LE increases with cell concentration but falls if high volumes of plasma are used during the incubation as there is competition between plasma and cells for In-111-troponolate. Labelling 1×10^8 granulocytes in 1 ml of 90 % plasma gives an LE of 90 % (Danpure and Osman 1988). Radiolabelling for at least 15 min at room temperature and a pH in the range 7–7.6 are the optimal conditions for both LE and maintaining the viability of the cells. As both oxine and tropolone form a 3:1 complex with indium, an excess of ligand is required to saturate the radionuclide. An excess of HMPAO is also required for the formation of technetium complexes.

Once the cells of interest have been radiolabelled they are centrifuged and the supernatant containing unbound radionuclide is discarded to minimise the uncomplexed radioisotope from being co-injected along with the desired radiolabelled cells (Peters and Saverymuttu 1987).

Paramount to obtaining the in vivo outcomes is the retention of functionality and viability of the purified radiolabelled cells. Successful in vivo functionality must be correlated with in vitro functionality. In vitro functional assessment includes determining the ability of the cells to phagocytose (e.g. granulocytes) and to replicate (e.g. lymphocytes) (Ellis 2011). Another in vitro assessment of viability involves staining cells with trypan blue, which only permeates the cell membrane of non-viable cells and provides a way to quantify the percent viability. In vivo assessment is considered a better marker of leukocyte function, and includes observing the circulating characteristics of radiolabelled cells and the 45-min recovery, which is the percentage of radiolabelled cells injected that are still present in the freely circulating blood pool at 45 min post injection. Activated or damaged cells demonstrate a far slower transit through the lung and increased uptake in the liver (Saverymuttu et al. 1983a) and hence give rise to a much reduced 45-min recovery.

Once re-injected, the radiolabelled cells distribute within the circulating blood volume. Counts derived from subsequent small-volume blood samples are then corrected to a blood volume calculated according to the subject's height, weight, and gender. An individual's drug history is also important as agents such as antibiotics or corticosteroids may influence the chemotaxis of leukocytes to areas of infection and inflammation (Ackrill 2011). Corticosteroids reduce the transcription of cytokines (e.g. interleukins (IL)-4, -5, -13, chemokines, such as IL-8, regulated upon activation, normal cell expressed, and secreted (RANTES), eotaxins, and adhesion

molecules such as intercellular adhesion molecule-1 (ICAM-1), vascular cell adhesion molecule-1 (VCAM-1), and E-selectin (Barnes et al. 2003), which are important in the recruitment of leukocytes to areas of inflammation through rolling of the leukocytes on the vascular endothelium). Another factor which may affect the initial isolation and labelling process includes the erythrocyte sedimentation rate (ESR), which can vary in disease states. Leukocytes are also susceptible to mechanical damage during the isolation process by way of shear forces experienced in passage through needles, shaking, and centrifugation and these steps should be strictly controlled to reduce this variable.

8.2.1 Buffy Coat Leukocytes

Buffy coat leukocytes were the cells initially used to establish the technique of leukocyte radiolabelling. They have the advantage of being relatively easy to isolate from whole blood with minimal activation when isolated in plasma. They were used to determine normal leukocyte migration and kinetics in vivo and can localise to sites of focal infection such as abscesses and osteomyelitis (Palestro et al. 2006) as well as focal inflammation in conditions including rheumatoid arthritis (Peters and Saverymuttu 1987).

The effect on cell labelling, trafficking, and abscess or infection localisation by existing or novel non-specific anti-inflammatory drugs (NSAIDs) in vivo could be tested using buffy coat leukocytes.

8.2.2 Granulocytes

Both neutrophils and eosinophils are important mediators of infective and inflammatory processes. Neutrophils, which represent 50–60 % of circulating leukocytes, and eosinophils play a role in airway inflammation and also asthma (Busse et al. 1992) (Sampson 2000). Granulocytes are also important in the pathogenesis of other conditions such as bronchiectasis (Currie et al. 1987), pneumonia, chronic obstructive pulmonary disease (COPD) (Ruparelia et al. 2011), IBD (Cheow et al. 2005), systemic vasculitis (Jonker et al. 1992), and acute respiratory distress syndrome (ARDS) (Ware and Matthay 2000).

In the presence of ongoing neutrophilia, a mixed leukocyte preparation may be sufficient for the detection of focal infection and inflammation. The localisation of low-grade infections or inflammation, such as chronic osteomyelitis, however is enhanced if purified granulocytes are used (Peters and Saverymuttu 1987). Other situations in which pure granulocytes are superior to mixed leukocytes include intravascular sepsis (as it avoids detecting signal from contaminating labelled platelets and erythrocytes in the circulation), neutropenic patients, and if quantitative studies are required such as In-111-granulocyte excretion in IBD (Peters 1994).

Radiolabelled granulocytes can also be used to assess the effects of drugs on the circulating physiology of these cells and their impact on the conditions described. This technique would be particularly useful, for example, if specific anti-neutrophil strategies are being tested.

8.2.3 Eosinophils

Eosinophils account for only 1–3 % of circulating leukocytes and higher volumes of peripheral whole blood are required to isolate them. Eosinophilic inflammation is the pathological hallmark of asthma and allergic inflammation. Eosinophilia is present and pathogenic in a wide range of conditions including parasitic infection, cancer and organ-specific diseases affecting the lung- allergic bronchopulmonary aspergillosis (ABPA), eosinophilic pneumonia; the gastrointestinal tract- IBD, radiation enteritis; the skin- eczema and cellulitis and the vasculitic condition eosinophilic granulomatosis with polyangiitis (EGPA).

The radiolabelling of autologous human eosinophils remains experimental at this stage but is now an active area of research with significant applications to the pharmaceutical industry. A greater understanding of eosinophil kinetics and trafficking in health, and in conditions such as asthma, will likely allow for lower "N" studies (fewer animals or patients) in proof of concept (POC) studies to quantify the impact of novel therapeutics on allergic inflammation.

8.2.4 Lymphocytes

The radiolabelling of lymphocytes has been severely limited due to the extreme sensitivity of these cells to radiotoxicity, both when the whole body is irradiated as well as when directly radiolabelling the cells. This is especially notable in studies of replication. Whole-body irradiation results in lymphopenia, which is thought to be secondary to loss of a predominant T-cell population, although all populations are affected (Campbell et al. 1976). Initial studies suggested that In-111-oxine-labelled lymphocytes could be used to track the migration of the cells to lymphoid organs of healthy individuals and those with Hodgkin's disease (Lavender et al. 1977). However, subsequent studies have demonstrated that radiolabelling with In-111-oxine impairs lymphocyte function with reduced H-3 thymidine incorporation suggesting impeded cell proliferation (Segal et al. 1978) and alters the normal migration of these cells. This results in increased activity in the spleen and liver, and minimal activity in the lymph nodes (reduction in cells with POS migratory functionality), suggesting the sequestration of damaged cells (Chisholm et al. 1979). Chisholm et al. have also demonstrated a dose-dependent reduction in the ability of the HeLa S3 cell line to proliferate and form colonies as a result of the radiation emitted from In-111. Caution should also be recognised in that the chelating agent itself that is used to complex indium (oxine) may also lead to direct lymphotoxicity (Segal et al. 1978).

Although less cellular damage occurs when lymphocytes are radiolabelled with Tc-99m-HMPAO (Ellis 2011), studies have suggested that labelling mixed leukocytes with Tc-99m-HMPAO may still cause chromosomal abnormalities in the lymphocyte fraction (Ilknur et al. 2002).

8.2.5 Monocytes

Circulating monocytes represent 5–10 % of circulating leukocytes and have the capacity to migrate to areas of inflammation where they differentiate over a period of days into tissue macrophages and dendritic cells. The half-life of human monocytes in the blood is 3 days (Whitelaw 1972); and it is suggested that this short half-life can be explained by the continuous replenishment of the macrophage and dendritic cell population, although some organ macrophages may renew their populations independently from blood monocytes, e.g. alveolar macrophages (Tacke et al. 2006). It has been demonstrated in patients with rheumatoid arthritis that monocytes may be purified from 100 mL of whole blood by positive selection using CD14 cell surface marker reagents (Van Hemert et al. 2007; Bennink et al. 2008). Radiolabelled monocytes have also been used to investigate the pathogenesis of atherosclerosis (Dorffel et al. 2001) and acute myocardial infarction (Leuschner et al. 2012). There have again been concerns about the cytotoxicity and possible inhibition of monocyte differentiation into tissue macrophages by radiolabelling with tropolone or oxine. The use of tropolone as a chelator, rather than oxine, however, allows for the use of higher concentrations of In-111 in labelling suggesting that oxine is an important source of cytotoxicity (Van Hemert et al. 2009).

8.3 Methods for Quantifying Leukocyte Transit Time/Migration

The radiolabelling isotopes discussed in the previous section (i.e. In-111, Cr-51, Tc-99m) are unstable isotopes that emit energy in the form of gamma radiation when they decay to a more stable state. The radiation is readily detected with scintillation instruments in the form of probes, well counters, whole-body counters (WBC), and gamma cameras. These instruments have two principal components in common: the first is the scintillation crystal, commonly thallium-doped sodium-iodide (NaI(Tl)), which converts the energy of gamma photons into visible light; the second is the photomultiplier tube, which converts the energy of the visible light to electrons, and accelerates these through a high-voltage cascade to multiply the weak original signal to create a measurable electrical signal. Other crystals such as bismuth geranium oxide crystals have been utilised in other systems such as PET and have used photomultiplier tubes to generate high-pixel images.

8.3.1 Skin Patches

Micropore filters placed on skin abrasions have been used to capture radiolabelled granulocytes migrating to such sites, which can then be quantified and imaged (Pinching et al. 1990).

Skin abrasions were made on healthy volunteer's forearms using a dental drill. Micropore filters were placed on the abrasion and autologous In-111-tropolonate granulocytes injected at different time points between 4 and 20 h following the abrasion. Filter papers were changed at regular intervals and the radioactivity absorbed was measured by a well counter. The rise and fall of the pad radioactivity can be taken to represent granulocyte migration into the abrasion as plasma exudation of In-111 as cell-free circulating indium is persistently low. The ratio of radioactivity detected on the filter paper compared to blood cell-bound radioactivity was used to quantify the granulocyte presence in the abrasion. Abrasions of all ages demonstrated peak radioactivity levels 2–4 h following re-injection with the older abrasions having higher peaks. Physical exercise reduced the migration of labelled granulocytes to the abrasion due to diverted blood flow from the skin to exercising muscles and demargination of granulocytes at the sites of abrasion.

The ability to quantify granulocyte migration into skin abrasions supports the use of these non-invasive techniques to assess inflammatory diseases affecting the skin. It may also be used to assess the effect of treatment with local or systemically delivered drugs on the migration of granulocytes to the skin.

8.3.2 Scintillation Probe Counting

Scintillation probes, as body surface or as isolated tissue counters, containing a single, small NaI(TI) crystal and photodiode have been used in the detection of radioactivity in vivo, for example during surgical procedures where modest isolation of a target tissue may be procured allowing for improved target-to-non-target ratios of counts. These kinds of probes generally comprise a handheld modestly shielded detector (focused probe) coupled to an electronic display unit (e.g. analogue-to-digital counter or rate meter).

8.3.3 The Whole-Body Counter and Body Fluid Sampling

A WBC system allows assessment of total body radioactivity to be measured and quantified, and theoretically provides a way to study whole-body retention of radiolabelled products. The patient lies supine between highly sensitive anteriorly and posteriorly placed scintillation detectors containing sodium iodide crystals.

Fig. 8.3 Imaging modalities. (**a**) Planar gamma camera; (**b**) whole body counter; and (**c**) SPECT/CT

These detectors move and record radioactivity counts from head to toe. The WBC chamber is made with pre-1945 steel with 3 mm lead shielding on the inner walls from which no detectable isotopes are emitted during counting. Such shielding minimises background interference and allows the administration of ultra-low radiation doses to the patient (Fig. 8.3b).

This technique has been used to detect whole-body granulocyte distribution in healthy individuals and in those with bronchiectasis, asthma, and COPD where measuring the radioactivity in the sputum at the same time demonstrates the migration of granulocytes into the airway and loss from the body (Szczepura et al. 2011). Whole-body counting has also been used in patients with IBD (Carpani de Kaski et al. 1992) and is an accurate alternative to measuring the radioactivity of stool samples collected over 4 days. Loss of granulocytes through faeces correlates with disease activity in IBD (Saverymuttu et al. 1983c).

8.3.4 Planar Imaging

The first scintillation gamma camera was introduced in 1958 and is known as the Anger gamma camera (Anger 1958) (Fig. 8.3a). Visible light produced in a large-area (unitised) scintillation crystal reaches several photomultipliers arranged in a precise array behind the crystal, resulting in varying total signal strengths across the array depending on the photon annihilation location within the crystal and thus a depreciative electronic signal in photomultipliers away from the immediate scintillation point. The "centre of mass" (maximal photonic translation) of these signals is calculated to give the position of interaction of the original gamma photon. A collimator comprising multiple narrow, parallel holes in a thick sheet of lead limits detection to photons travelling at near-perpendicular trajectories toward the crystal. Gamma photons not in such line with the collimator holes are scattered to lower energies or absorbed by the lead. Thus, unimpeded and detected photons bear a spatial relationship to the "source" of the radiation, and hence an image can be constructed. The image, however, is a projection of photons from a 3-D object translated as a single 2-D plane view of the overlaying and underlying organ systems within the field of view.

Static planar images have been used to identify and quantify sites of infection and inflammation in numerous conditions including bronchiectasis, COPD, asthma, IBD, and rheumatoid arthritis where reduction in radioactivity in the joints can be demonstrated following effective treatment. Using a combination of whole-body counting, leukocyte scintigraphy, and body fluid sampling, there is an improvement in the appearance of the In-111-leukocyte scan and a reduction in the faecal loss of labelled granulocytes following treatment of Crohn's patients with oral fluticasone (Carpani de Kaski et al. 1991). Such techniques could therefore be used to assess the efficacy of new anti-inflammatory treatments in other conditions.

8.3.5 Dynamic Planar Imaging

Dynamic (imaging over time) gamma camera imaging entails the acquisition of multiple image frames generally in a short space of time (seconds to minutes), which for example allows the assessment of the initial distribution and subsequent margination of labelled leukocytes. The radioactivity is quantified through digital acquisitions and regions of interest (ROI) organ time–activity curves by drawing defined ROI over the organs of interest and recording their respective counts per pixel within the ROI. The use of short-lived radioisotopes requires these ROI collections to be decay-corrected with respect to the radionuclide used.

This technique has been used to assess the normal distribution of ex vivo radiolabelled and re-injected leukocytes, granulocytes, eosinophils, monocytes, and lymphocytes in healthy individuals and has led to knowledge about the in vivo kinetics of circulating as well as marginated cell pools as well as sites of cell destruction.

Dynamic imaging can also be used to assess lung transit time and alterations of normal cell kinetics and pools in disease states. For example, when In-111-troponolate-labelled granulocytes are re-injected into patients with IBD and imaged dynamically with a gamma camera it has been observed that these cells can localise in sites of inflammation within 10 min post injection (Saverymuttu et al. 1983b).

8.3.6 Single-Photon Emission Computed Tomography

As previously described in Sect. 8.3.4, planar scanning can only generate two-dimensional images, in which it can be difficult to distinguish specific organ borders or uptake within overlying structures within the ROI. The revolution of emission tomographic imaging allows for three-dimensional imaging of the distribution of radioactivity in vivo and thus specific organ uptake and potentially distribution information within an organ or a region of uptake (e.g. infection).

In SPECT, one or more gamma camera heads rotate around the patient and acquire planar images from several angles, which are then mathematically reconstructed to form cross-sectional (bread-slice) images through the body providing now volume pixels, or voxels, defined by the slice thickness of the system, of count information (Hutton 2011) (Fig. 8.3c). Sequential SPECT has been used to quantify the migration of labelled granulocytes into regions of the lung of patients with COPD whereby collecting data at regular intervals allows the calculation of granulocyte flux into the lung (Ruparelia et al. 2011). Sequential SPECT has also been used to quantify disease activity in IBD (Weldon et al. 1995b) and can theoretically be applied to other conditions characterised by inflammation.

SPECT has recently been coupled to X-ray CT, which can provide more quantitative data by allowing for correction of photon attenuation (loss of signal by scatter and absorption by tissue density) in the subject, and also allowing for imaging a merged anatomical (CT) and functional (SPECT) co-registration making it easier to determine the actual location of anatomic structures relative to the site of photon origination (radiolabelled cell localisation). SPECT/CT has been used in combination with either Ga-67- or In-111-labelled leukocyte scintigraphy to provide this additional co-registration information aiding diagnosis, precise localisation, and better assessment of disease or extent of infection (Bar-Shalom 2006). The use of SPECT/CT following the re-injection of autologous Tc-99m-granulocytes has also led to more accurate diagnoses of left-ventricular-assist-device infection (Litzler et al. 2010).

Dynamic SPECT is also possible and involves the rapid acquisition of image frames to create dynamic images of physiological or pathophysiological processes. It is important to note that the accumulation of a single-slice SPECT image is far greater in time than the acquisition time of a CT scan and thus very fast functional dynamic images are difficult to acquire. Very rapid functional dynamic imaging is better accomplished with PET (Sect. 8.3.7).

8.3.7 Positron Emission Tomography

An alternative method of functional scintillation tomographic detection is with PET scanners, which have a ring (single or multiple) of detectors (original PET systems had as few as 280 crystals in one ring (Derenzo 1980) to modern systems of more than 16 rings with over 32,000 detectors) around the patient for coincidence detection of the two 511 keV gamma photons. These gamma photons are created by the annihilation of nuclear emitted positrons which interact with the outer shell electrons causing release of two photons in opposite (180°) orientation (Hutton 2011). Radioligands such as F-18-fluorodeoxyglucose (F-18-FDG) is a widely used reagent for PET scanning of cardiac and neurologic conditions. The absence of a collimator as needed in planar imaging makes the technique more sensitive than SPECT. The detectors are again linked to photomultipliers, which convert the gamma signal into a digitised light signal that is used as in SPECT to reconstruct the tomographic image. The ability to localise lesions with PET is, as seen with SPECT, aided if coupled to CT, which also allows absolute quantification of the activity again by providing a mechanism for attenuation correction. Original PET systems used a ring of Ge-68, which is also a position isotope, as a low count rate tool (relative to X-ray CT) to correct for structural/anatomical attenuation.

Retrospective studies have suggested a role for F-18-FDG PET in the investigation of fever of unknown origin (FUO) and in patients with suspected focal infection or inflammation (Bleeker-Rovers et al. 2004). A recent review summarises the utility of PET in the investigation of malignancies, the diagnosis of chronic osteomyelitis (particularly of the axial skeleton) and infections associated with prostheses, and opportunistic infections in AIDS (Zhuang and Alavi 2002). The same review describes the use of PET to monitor disease activity in sarcoidosis and to detect vasculitis, and inflammation in IBD. F-18-FDG is also able to discriminate between infection and rejection in lung transplantation patients (Jones et al. 2004) and uptake has also been shown to be greater in the lungs of COPD patients but not in asthmatics (Jones et al. 2003).

Despite its advantages, it has been shown that elevated uptake of F-18-FDG by neutrophils detected by PET is a post-migratory event (likely related to metabolic activity of the locale) and may not always correlate with the extent of neutrophilic infiltration to the site of inflammation (Jones et al. 1997). Neutrophil migration and activation (although not NADPH oxidase activity) is thought to be responsible for increased F-18-FDG uptake. Another disadvantage of PET is that because no suitable metabolically stable PET radiolabels have yet been developed, it does not allow the quantification of cell trafficking to sites of inflammation in the same way that leukocyte scintigraphy with lower energy isotopes has performed. Furthermore, although the PET signal is thought to represent increased granulocyte glucose uptake, it is likely that other metabolically active cells at the site of inflammation contribute to the signal as noted above.

8.4 Biodistribution and Intravascular Lifespan of Leukocytes

8.4.1 Granulocytes

Granulocytes are formed from pluripotent stem cells in the bone marrow before being released into the circulation. As neutrophils mature from CD34-positive myeloid progenitors, they acquire new surface markers such as CD16b, CD35, and CD10 (Elghetany 2002). Early work with the diisopropylfluorophosphate (DFP^{32})-labelled granulocytes demonstrated that 50 % of the cells re-injected into healthy volunteers disappear rapidly from the circulation with a half-life of 6.6 h (Mauer et al. 1960). Following re-injection, radiolabelled cells are distributed in dynamic equilibrium between circulating and marginated granulocyte pools (Athens et al. 1960) (Fig. 8.4a). These two pools form a larger pool known as the total blood granulocyte pool (TBGP), which is twofold greater than that calculated from the

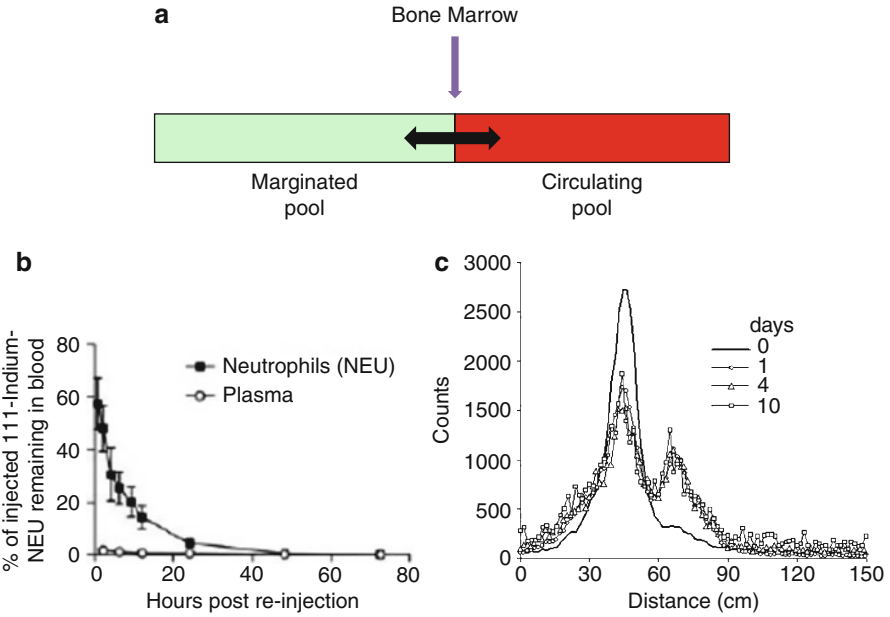

Fig. 8.4 Biodistribution and intravascular lifespan of granulocytes. (**a**) Schematic representation of the biodistribution of granulocytes between the bone marrow, marginated, and circulating pools. (**b**) Graph indicating the exponential decline in radiolabelled neutrophils from the circulation (Farahi et al. 2012). (**c**) Whole-body count profiles at increasing distances in cm from the head (*left*) to feet (*right*) in a normal subject at 45 min (day 0), 24 h, and 4 and 10 days following re-injection of In-111-labelled neutrophils. The *tallest peak* represents radioactivity in the liver and spleen and the *smaller peak* corresponds to radioactivity within the pelvic bone marrow. Physiological redistribution of labelled neutrophils from the liver and spleen to the bone marrow is demonstrated by 24 h following re-injection (Ruparelia et al. 2011)

peripheral blood granulocyte count and blood volume alone. Since the original work, In-111-granulocytes have been shown to have a mean intravascular residence time (MIRT) of 10 h with a half-life of 7 h (Saverymuttu et al. 1985b). It is thought that the marginated pool equilibrates with the circulating pool over a period of approximately 30 min and so use of the 45-min blood recovery value provides a sensitive biomarker of the functional viability of these cells (Peters 1994). As 50 % of the TBGP is immediately distributed to the marginated pool, the 45-min recovery will always be less than 50 % and in most studies has been shown to approximate 35–40 % for both In-111- and Tc-99m-HMPAO-granulocytes.

There is evidence that a large proportion of the marginated pool lies within the spleen (hence a dosimetry concern). Within 5 min of the re-injection of labelled granulocytes, the marginated pool accounts for 54 % of the total blood granulocyte pool (Peters et al. 1985a). Of this early marginated pool, the granulocytes are distributed between the spleen, liver, lung, and the remainder of the body. Whilst liver and splenic uptake increases with time, this uptake appears to be reversible suggesting a dynamic transit of granulocytes through these organs (Peters et al. 1985b). Hence adrenaline and exercise are both able to mobilise granulocytes from the marginated into the circulating pool, while in opposition, prednisolone increases the size of both pools, and endotoxin causes a shift of granulocytes from the freely circulating into the marginated pool (Athens et al. 1961). Following the injection of adrenaline, the use of Cr-51-labelled granulocytes demonstrates a fall in splenic activity and a corresponding rise in peripheral blood activity (McMillan et al. 1968). This illustrates the dynamic movement of granulocytes in the spleen and suggests that the initial margination seen in the spleen is physiological rather than a result of cell activation or damage (Peters and Saverymuttu 1987).

Intravascular transit time is estimated at 10 min in the spleen and 2 min in the liver; the persistent radioactive signal detected in the spleen beyond this represents both pooled and destroyed (or damaged) granulocytes (Peters 1998). Inflammatory conditions lead to a fall of activity detected in the spleen as granulocytes are diverted to sites of inflammation (Peters et al. 1985b). Although the liver normally represents a smaller part of the marginated pool, there is increased uptake if granulocytes are activated or damaged, which suggests that the destruction of granulocytes occurs within the reticuloendothelial system.

Granulocytes have a rapid transit through the lung under normal physiological circumstances (Saverymuttu et al. 1983a) and a mean transit time of between 20 s in the capillary blood (Doershuk 2000). Others have reported longer capillary transit times as much as 3–5 min (Peters 1998). There has been considerable debate regarding the size of the pulmonary granulocyte pool: it has been suggested that marginated granulocytes within the lung exist in two pools, one in which the granulocytes are moving quickly at the speed of erythrocytes and another pool in which granulocytes are met with obstruction as they do not deform as readily as erythrocytes as they travel through the vasculature (Peters 1998). For example, fully dilated capillaries have a diameter of 7.5 ± 2.3 μm whereas neutrophils have a diameter of 6.8 ± 0.8 μm; larger neutrophils are therefore restricted by smaller capillaries causing a 60–100-fold slower transit through the pulmonary capillary system relative to erythrocytes, which travel through in less than a second (Hogg 1994).

The same review suggests that these slower moving neutrophils increase their concentration within the pulmonary circulation relative to erythrocytes, and form the marginated, neutrophil pulmonary pool. Inhaled platelet-activating factor (PAF) leads to marked pulmonary sequestration of ^{111}In-labelled neutrophils, which again illustrates the capacity for activated neutrophils to be retained in the lung due to cytokines or other bioactive molecules (Tam et al. 1992).

In addition to dynamic movement of granulocytes within the spleen, a similar process of margination occurs in the bone marrow which has an intravascular transit time for granulocytes of 10 min (Ussov et al. 1995). A method using H-3 thymidine has provided insight into bone marrow neutrophil kinetics (Dancy et al. 1976). This study suggests a daily generation of 0.85×10^9 post-mitotic neutrophils per kg body weight within the bone marrow. Furthermore, the paper demonstrates that this post-mitotic pool of neutrophils contains adequate number of maturing and storage neutrophils to maintain the turnover of 0.85×10^9/kg/day for 6.6 days, therefore demonstrating a bone marrow transit time of just under 7 days. This is consistent with the observed neutropenia resulting from total body radiation where the nadir of cell counts in the peripheral circulation is 5–7 days post irradiation.

Using a WBC, the approximate distribution of In-111-labelled granulocytes can be detected using extremely low administered activities of the radioisotope (Szczepura et al. 2011). Neutrophils have a 45-min recovery time of approximately 40 % (due to their distribution between the marginated and freely circulating intravascular pools) and are then removed from the circulation in a mono-exponential manner (zero order) with final localisation in the liver, spleen, and bone marrow, which is evident at 24 h, reflecting their sites of destruction (Fig. 8.4b, c).

Tc-99m-HMPAO-granulocytes have identical kinetics through the lung, liver, and spleen as In-111-granulocytes. The half-life, however, of Tc-99m-HMPAO-leukocytes is lower at 4 h than that of In-111-granulocytes, which is thought to be an artefact, and represents Tc-99m elution from the circulation. Correction of such elution by in vitro stability experiments demonstrates a half-life approximating 6 h (Peters 1994). Non-specific bowel, urinary, and hepatobiliary activity is seen due to the excretion of hydrophilic complexes of Tc-99m-HMPAO and this must be taken into consideration in the analysis of abdominal scans performed in IBD or to localise abdominal collections. Early and sequential imaging is therefore important in IBD to avoid such non-specific bowel activity, which is not usually seen until at least 2 h following re-injection.

8.4.2 Eosinophils

To date there has been only one published study examining the kinetics of circulating radiolabelled eosinophils in healthy individuals (Farahi et al. 2012). Two early papers used intravenous injection of tritiated thymidine (H-3 thymidine) in patients with eosinophilia following surgical treatment for oesophageal cancer, bladder cancer (Parwaresch et al. 1976), glioblastoma, and chronic lymphocytic leukaemia

(Steinbach et al. 1979). Two patients with eosinophilia of unknown aetiology have also been studied although in one case, sarcoidosis was suspected (Herion et al. 1970). In Herion's paper leukocytes were separated by dextran sedimentation followed by hypotonic lysis of erythrocytes and then labelled with sodium radiochromate (Cr-51) before being re-injected. In-111-oxine-labelled eosinophil-enriched cells have also been used to assess eosinophil kinetics in one patient with Churg–Strauss syndrome and one with hypereosinophilic syndrome (Yamauchi et al. 1989). In the latter studies eosinophils accounted for only 87 % of the "eosinophil-enriched cells" that were purified and labelled, and neither technique isolated cells in autologous plasma as is our practice. Other disadvantages of the experimental methods used in these studies include the poor image resolution derived with the use of Cr-51, the potentially cytotoxic effect of In-111-oxine, and the risk of leukocyte clumping induced by heparin.

More recently however, eosinophil intravascular half-life has been determined using human mixed leukocytes that have been purified in autologous plasma and radiolabelled with In-111-tropolonate before re-injection. Subsequent blood sampling followed by isolation of "ultra-pure" eosinophils has indicated an intravascular residence time for these cells of approximately 25 h (Farahi et al. 2012). These investigators also studied purified eosinophils (prepared by discontinuous Percoll gradients and CD16-negative selection) radiolabelled with In-111-troponolate. In preliminary studies, the use of dynamic and static planar gamma camera imaging demonstrated rapid eosinophil transit through the lungs and margination in the liver and spleen (and to a far lesser extent bone marrow) with evidence of some recirculation of eosinophils from the liver (Farahi et al. 2012). This technological advance and knowledge about the circulation of eosinophils in healthy subjects provide an opportunity for pharmaceutical companies to test the impact of new drugs on eosinophil kinetics. Given the important role of eosinophils in allergic inflammation, this has wide applications in common conditions such as asthma and other conditions characterised by eosinophilic inflammation.

8.4.3 Lymphocytes

Lymphocyte kinetic studies have been limited by the use of suboptimal radionuclides such as Cr-51 and concerns about the lymphotoxicity of the oxine ligand used for In-111-oxine. It has been suggested that restricting the dose of radionuclide (either lower counts or higher specific radioactivity) allows lymphocytes to behave physiologically and unencumbered by the presence of oxine (Chisholm et al. 1979). Although In-111-oxine has been used to assess lymphocyte trafficking in man (Wagstaff et al. 1981), the amount of In-111-oxine label per 10^8 lymphocytes used in this study exceeds the level that has been shown to be lymphotoxic, particularly after 24 h. Lymphocytes were purified using a cell separator in the absence of autologous plasma. This produced lymphocytes that were greater than 95 % pure and 90 % viable. Following re-injection, serial blood samples demonstrated an initial

rapid clearance from the blood followed by a rise at 3–4 h which plateaued for 4–8 h before a second fall. Gamma camera imaging indicated a lack of uptake in the lungs and a distribution of activity between the liver and spleen by 4 h leading to the initial rapid clearance. There was a subsequent reduction in the splenic signal, which correlated with an increase in lymph node activity suggesting the recirculation of lymphocytes from the spleen into the circulation and thence to the lymph nodes. Heat-damaged lymphocytes demonstrate altered kinetics with significant lung and liver uptake and low activity in lymph nodes relative to controls suggesting that the In-111-oxine-labelled lymphocytes were behaving relatively physiologically.

8.4.4 Monocytes

Tritiated thymidine has been used to study monocyte kinetics in seven healthy individuals and this demonstrated a circulating half-life of 71 h (Whitelaw 1972), considerably longer than neutrophils. The use of Tc-99m-HMPAO-labelled monocytes to assess their biodistribution when re-injected into patients with rheumatoid arthritis has also shown initial margination in the lung followed by the re-distribution to the liver, spleen, and bone marrow (Bennink et al. 2008).

8.5 Migration Characteristics of Leukocytes

Following re-injection, the migration characteristics of labelled autologous leukocytes can clearly be seen to alter in pathological conditions such as abscesses and other systemic inflammatory processes. The pathological situations which involve leukocyte migration can be separated broadly into three categories according to the migratory behaviour of these cells: firstly, conditions in which leukocytes migrate to sites of infection and inflammation and remain localised such as abscesses; secondly, conditions in which leukocytes travel to such sites but continue to migrate into the lumen of the airway or the bowel such as bronchiectasis, COPD, and IBD; and thirdly, conditions such as community-acquired pneumonia (CAP) where re-injected leukocytes fail to migrate to the inflamed site because of early termination of such migration in the disease history.

8.5.1 Solid Abscess

Ga-67 citrate has been used previously to localise abscesses, but despite high sensitivity, it lacks specificity due to transferrin and other iron-binding sources which gallium also follows. Furthermore, renal and gastrointestinal excretion of radiogallium leads to non-specific bowel activity, which makes the detection of

intra-abdominal collections difficult. The delay of 24–72 h before the result of such a scan is available is also generally clinically unacceptable.

In-111-leukocytes have been used since the late 1970s for the localisation of abscesses and results are generally interpreted within 24 h; although faster than Ga-67, not all NM Departments offer this service and the time requirement still remains a disadvantage relative to other imaging modalities such as computed tomography (CT) although CT is non-specific and relates only to anatomical density discrimination or tissue/organ displacements. Intra-abdominal abscesses are identified with the use of a planar gamma camera as focal activity outside the normal distribution with intensity greater than that of the liver (Peters and Saverymuttu 1987). Only 33 % of abscesses are identified within 1–4 h of re-injection but 95 % are true positives (TP) at 18–24 h. The use of In-111-tropolone-labelled granulocytes can however generate false-positive (FP) images in conditions such as IBD, haematomas, tumours, non-rejecting renal allografts, and uncomplicated bowel anastomosis (Peters and Saverymuttu 1987).

In-111-labelled leukocytes would be the modality of choice in the investigation of an abscess in the gastrointestinal tract as ultrasound, and to some extent CT images, may be difficult to interpret because of overlying bowel gas and the distinction between an abscess and thickened or dilated loops of bowel. Comparison between In-111-troponolate-granulocytes, Tc-99m-HMPAO-leukocytes, and ultrasound scanning for the detection of intra-abdominal abscess has shown that Tc-99m-HMPAO scanning is at least as accurate as In-111-troponolate scanning and that both have a greater sensitivity and specificity than ultrasound scanning, although scintigraphy is less effective at detecting or discriminating hepatic abscesses (Weldon et al. 1995a, b). The physiological uptake of labelled leukocytes in the liver makes the detection of hepatic abscesses more difficult; however, sequential imaging may demonstrate a gradual increase in radioactivity within a septic focus whereas the physiological liver uptake falls between 1 and 4 h (Cousins et al. 2003a). Figure 8.5 demonstrates the use of In-111-labelled granulocytes to localise a communicating abscess.

The use of In-111-labelled autologous granulocytes is also able to detect pulmonary (Saverymuttu et al. 1985a) and brain (Peters et al. 1980) abscesses. Tc-99m-labelled leukocytes have also been used to detect brain abscesses (Grimstad et al. 1992) and both techniques may help distinguish infective or malignant lesions at this site.

8.5.2 Intrathoracic Disease

Re-injected radiolabelled autologous leukocytes usually demonstrate a rapid transit through the lungs unless the cells have been activated in vivo (for example, in graft-versus-host disease (GVHD) or septicaemia) or damaged ex vivo. Leukocyte trafficking in the lung however is altered under several disease conditions, such as in ARDS, COPD, bronchiectasis, and lobar pneumonia.

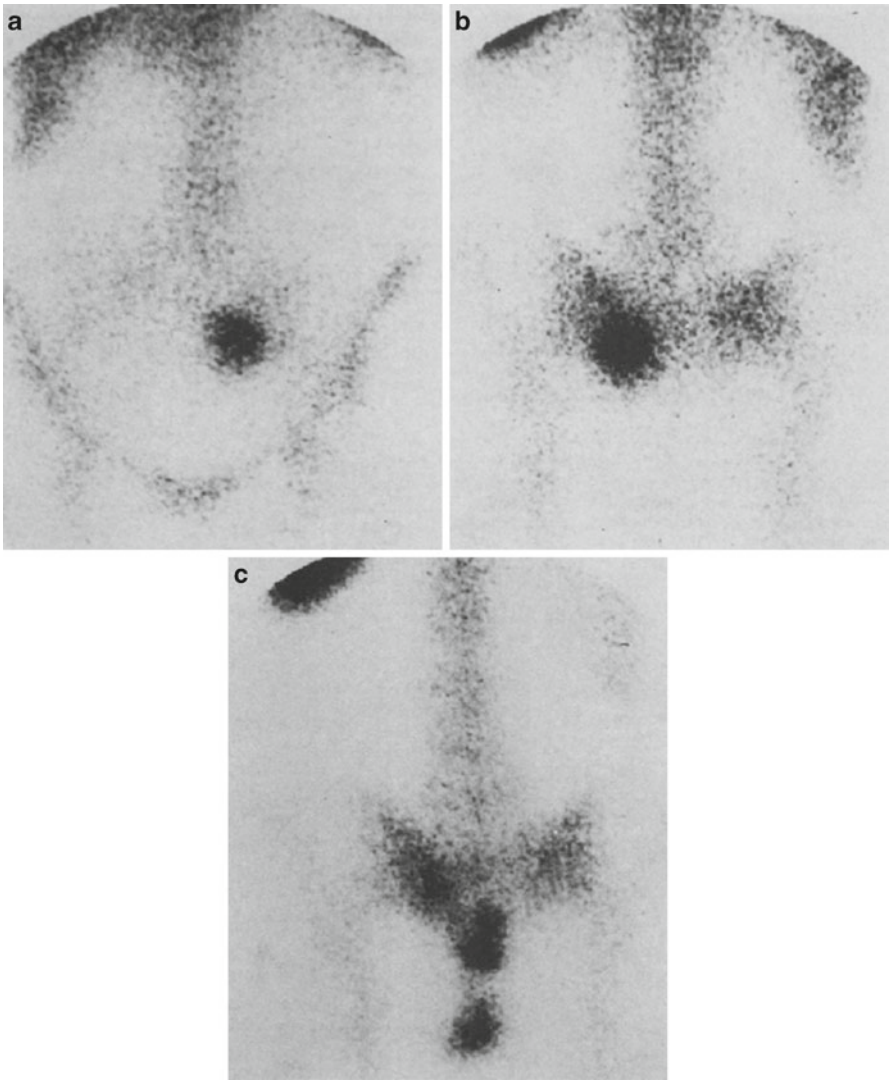

Fig. 8.5 In-111-granulocyte scans taken 3 h following injection. (**a**) Anterior planar camera view and (**b**) posterior planar camera view of an abscess in the left iliac fossa anterior to the left sacro-iliac joint. (**c**) The same individual scanned at 24 h indicating residual activity at the site of the abscess but also new activity in the distal colon because of a communicating abscess (Peters 1994)

8.5.3 ARDS

Neutrophils play a vital role in the pathogenesis of acute lung injury (Ware and Matthay 2000). The histological appearance of the lungs of patients with ARDS demonstrates the presence of neutrophils in the lung interstitium, alveolar space,

and vascular compartment, as well as structural damage to the endothelium and epithelium. These anatomical distributions and structural alterations are postulated to affect the barrier function of the alveolar capillary endothelium leading to lung injury (Downey et al. 1999). Granulocytes dual-labelled with both In-111 and Tc-99m have been used to determine pulmonary granulocyte kinetics in individuals with systemic inflammation characterised by increased soluble E-selectin levels, a marker of vascular activation (Ussov et al. 1999). Individuals with systemic inflammation demonstrate a larger pulmonary granulocyte pool but of note, these cells do not migrate into the interstitium unless the pulmonary endothelium is also activated. The re-injection of In-111-labelled autologous granulocytes into patients with ARDS demonstrates pulmonary retention even in the context of concurrent steroid treatment (Warshawski et al. 1986).

8.5.4 COPD

Neutrophils are abundant in the airways and lung parenchyma of individuals with COPD and are believed to be involved in the pathogenesis of the condition. The assessment of neutrophil kinetics in the lungs of patients with COPD has been determined using In-111-troponolate- and Tc-99m-HMPAO-labelled granulocytes combined with WBC and SPECT, which measures neutrophil clearance from the blood into the lung parenchyma (Ruparelia et al. 2011). At 45 min post re-injection, WBC data demonstrates a peak of radioactivity within the liver and spleen region followed by a second peak in the pelvic bone marrow. By 24 h, the peak within the liver and spleen is reduced whereas the bone marrow peak is higher, consistent with the known physiological re-distribution of neutrophils (Fig. 8.4c). The mean whole body loss of In-111-tropolonate in COPD patients over 7 days is less than 10 % and similar to healthy non-smokers; by contrast currently smoking COPD patients displayed a greater whole body In-111-tropolonate cell loss (Fig. 8.6b). SPECT images also demonstrate significant time-dependent and quantifiable migration of neutrophils into the lungs of patients with COPD (Figs. 8.6c and 8.7a) and this signal offers considerable promise as a marker of drug efficacy in this condition.

8.5.5 Bronchiectasis

The re-injection of In-111-troponolate-granulocytes followed by gamma camera imaging and whole-body counting has been used to assess granulocyte kinetics in patients with bronchiectasis (Currie et al. 1987). This demonstrates the migration of granulocytes to actively inflamed bronchiectatic areas of the lung within the first 24 h. These labelled cells then continue to migrate into the airway lumen and are expectorated in the sputum (Fig. 8.6a). Patients with severe bronchiectasis can lose

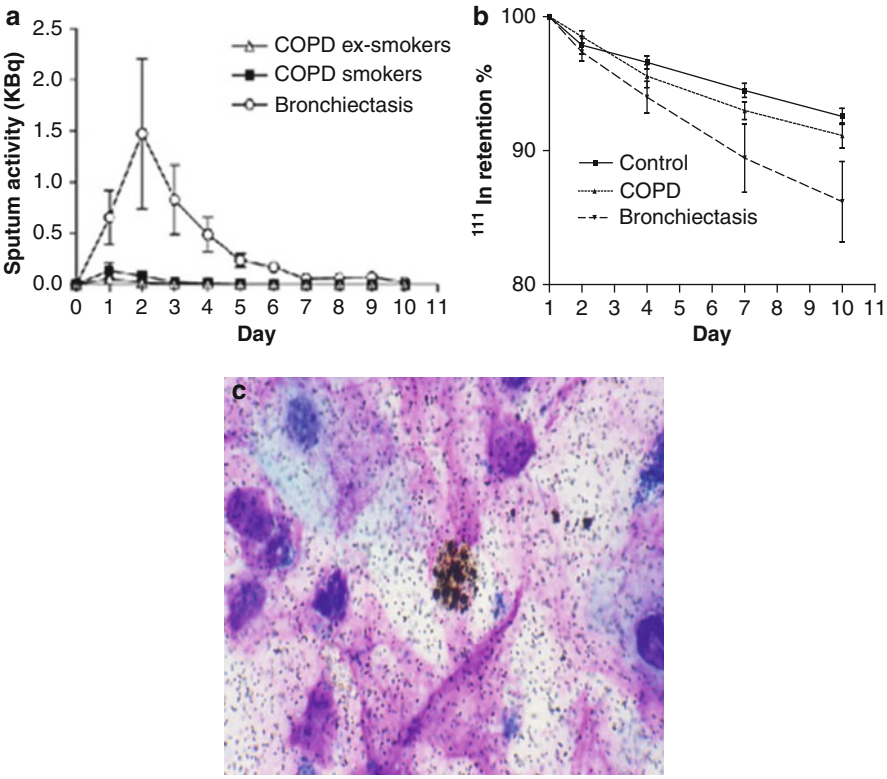

Fig. 8.6 Migration of In-111-labelled neutrophils into the sputum of patients with COPD and bronchiectasis. (**a**) The radioactivity of expectorated sputum in each 24-h period. (**b**) The percent of In-111 retention over a 10-day period in healthy volunteers (controls) and in patients with COPD and bronchiectasis. A higher level of In-111 loss from the body is demonstrated in those with bronchiectasis and COPD compared to controls. (**c**) Autoradiograph of an ^{111}In-labelled neutrophil in the expectorated sputum of a patient with COPD (Ruparelia et al. 2011)

>50 % of the re-injected labelled neutrophils in the sputum (Currie et al. 1987). As a consequence, radioactivity may be detected in the gastrointestinal tract of patients with severe bronchiectasis due to swallowed sputum containing In-111-labelled cells. In-111 uptake however is not present in all segments of bronchiectatic lung demonstrated on CT and such areas presumably reflect focally quiescent disease. The use of In-111-labelled granulocytes followed by WBC scanning demonstrates that bronchiectatic patients with active disease have a higher 7-day whole body loss of In-111, approximating 25 %, compared to less than 10 % in those with quiescent disease, which is similar to the loss seen in healthy non-smokers (Ruparelia et al. 2011) (Fig. 8.6b).

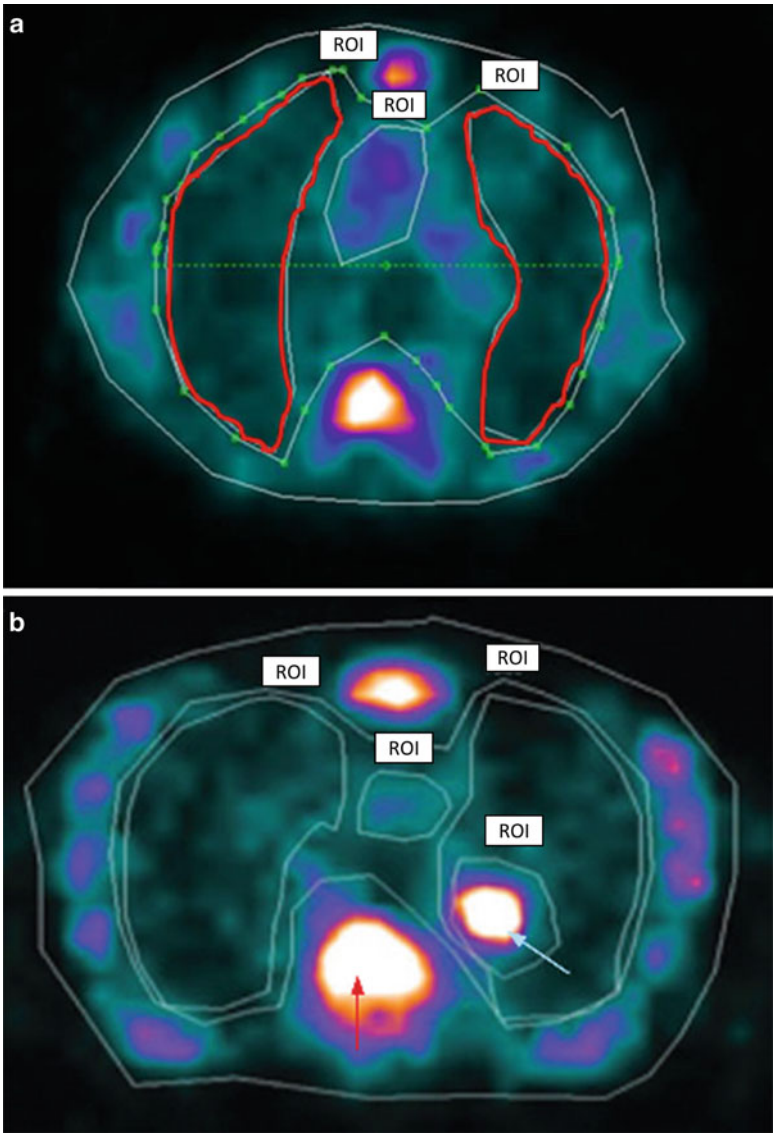

Fig. 8.7 (**a**) SPECT image demonstrating increased Tc-99m-labelled neutrophil uptake in the lung parenchyma of COPD patients. Regions of interest highlighted over the lungs (*red outline*), heart, and bone marrow (ribs, sternum, and vertebral body) (Ruparelia et al. 2011). (**b**) SPECT image indicating focal uptake of Tc-99m-labelled neutrophils in the left lower lobe of the lung (*blue arrow*). The *red arrow* indicates physiological uptake in the vertebral bone marrow) (Ruparelia et al. 2009)

8.5.6 *Lobar Pneumonia*

Although In-111-labelled leukocytes can be used to detect and localise abscesses in the lung and elsewhere, no signal is detected by gamma camera imaging in patients with uncomplicated lobar pneumonia. This is likely related to the extremely early (less than 6 h) termination of granulocyte migration in this disease (Saverymuttu et al. 1985a). The injection of Tc-99m-labelled autologous neutrophils followed by SPECT imaging in a patient with COPD, who was clinically well at the time of injection, incidentally demonstrated focal uptake in the lung at 4 hours after injection (Ruparelia et al. 2009) (Fig. 8.7b). Within 48 h the patient under study developed symptoms of dyspnoea, fever, and purulent sputum and clinical signs of consolidation confirmed by chest radiograph along with a positive sputum culture. This represents the capacity of these techniques to identify a pneumonic focus at a very early time point in the natural history of this condition before neutrophil migration has ceased.

8.5.7 *Inflammatory Bowel Disease*

IBD is a chronic inflammatory disease of the bowel and includes Crohn's disease, which may affect any part of the bowel, and ulcerative colitis (UC), which is usually confined to the rectum and colon.

In-111-labelled granulocyte scintigraphy in IBD has the ability to detect, anatomically locate, and define the severity of active inflammation and can image both the small and large bowel (Peters and Saverymuttu 1987). It has also been shown to correlate reliably with endoscopic findings and the histologically defined disease extent and activity (Saverymuttu et al. 1986). The intensity of uptake in the bowel in comparison to the uptake of the liver and spleen has been shown to correlate with clinical markers of severity (Peters and Saverymuttu 1987). The severity of IBD has also been shown to correlate with faecal granulocyte loss provided the stool collections are complete.

In the same way that granulocytes are lost in the sputum of patients with bronchiectasis and COPD, faecal loss of granulocytes occurs in IBD over the course of 4 days post injection and indicates the extent of migration of cells into the bowel lumen and subsequent loss from the body (Saverymuttu et al. 1983c). This may be demonstrated by the gradual reduction in image signal as the radiolabelled cells leave the body. Scanning with a WBC over 4 days also has the distinct advantage that it allows the administration of much lower levels of indium to quantify inflammation in IBD and the retention and loss of labelled cells (Cheow et al. 2005). It has been shown to be an accurate alternative to measuring the faecal excretion of these cells (Carpani de Kaski et al. 1992).

Tc-99m-HMPAO-labelled granulocytes are used more frequently in IBD due to the lower radiation dose of Tc-99m, greater image resolution, and capacity to detect small bowel pathology, which indium-scanning can miss (Fig. 8.8). Due to non-specific intestinal activity typical of Tc-99m-HMPAO-labelled granulocytes, false positives are possible when patients are scanned late particularly after 3 h; it is

Fig. 8.8 Tc-99m-HMPAO scan in a patient with severe ulcerative colitis demonstrating severe colitis (Cheow et al. 2005)

important therefore that an early image is taken followed by sequential images. The sensitivity of Tc-99m-HMPAO for the detection of acute inflammation ranges from 91 to 95 % (Weldon 2003). Used in conjunction with SPECT, this approach has been shown to accurately quantify the extent of inflammation in IBD (Weldon et al. 1995a, b). Faecal counting with Tc-99m is not possible due to its short half-life (6 h) and the extent of non-specific gastrointestinal excretion (>24 h).

Tc-99m-labelled granulocytes can also be used to assess disease reactivation and to identify complications in Crohn's disease such as abscess formation and fistulae although imaging must be performed early in suspected colo-vesical fistulae due to the urinary activity caused by renal excretion (Peters 1994). The signal from a Crohn's abscess remains persistent at 24 h and can be distinguished from non-specific bowel activity, the signal from which diminishes with time. False positives may be seen in recent bowel anastomosis and gastrointestinal bleeding.

8.5.8 Nephrological Disease

Abnormal renal uptake has been demonstrated by In-111-leukocyte scintigraphy in patients with renal transplant rejection with a sensitivity of 73 % (Forstrom et al. 1981). However, many individuals with chronic renal disease referred for pyrexia of unknown origin (FUO) do not show renal uptake (Cousins et al. 2003b). Given the extent of renal uptake of secondary Tc-99m-HMPAO complexes in the kidney, imaging of the renal parenchyma should always be undertaken with In-111-labelled cells. Diffuse renal uptake of In-111 has also been seen in systemic vasculitis (Jonker et al. 1992).

8.5.9 Orthopaedic Infections

Osteomyelitis is an infection of the bone arising from haematological seeding, direct spread from adjacent soft tissue and joints, or direct infection through trauma and/or orthopaedic surgery. Without prompt diagnosis and treatment complications may occur including the progression to chronic osteomyelitis.

The use of labelled leukocytes in the detection of bone infection is made more difficult by the previously discussed physiological uptake of leukocytes by the bone marrow. Negative scans are also possible in cases of chronic osteomyelitis, where granulocyte migration can be impeded by poor blood flow to osteomyelitis and thus provide minimal signal (Peters and Saverymuttu 1987).

The use of In-111-oxine-labelled leukocytes has however been used to detect osteomyelitis with a sensitivity of 0.91 and specificity of 0.62 (Palestro et al. 2002). These values are improved further if white cell scanning is combined with Tc-99m sulphur colloid. Limitations again include negative scans in chronic infections, and the local uptake of labelled leukocytes in lymph nodes (e.g. in the groin), which can confuse the interpretation of joint infection (Palestro et al. 2006).

Within the axial skeleton, the detection of abnormal uptake in the bone depends on the demonstration of leukocyte activity in the absence of colloid uptake (bone scintigraphy) (Peters 1994). Leukocyte scintigraphy in cases of vertebral body osteomyelitis will paradoxically demonstrate reduced uptake in affected areas due to comparatively greater physiological uptake in the bone marrow of adjacent healthy vertebral bodies (Seabold and Nepola 2003). Although the bone marrow in the peripheral skeleton is not usually a problem for the detection of osteomyelitis, it can sometimes be difficult to differentiate bone infection from adjacent soft tissue infection. CT or MRI anatomical discrimination may be of assistance together with the localised leukocyte uptake. Leukocyte scintigraphy may also be used to assess the response to treatment with antibiotics and to detect infection of and loosening of joint prostheses resulting in non-specific inflammation.

8.5.10 Rheumatoid Arthritis

Rheumatoid arthritis (RA) is a symmetrical, inflammatory polyarthropathy characterised by the accumulation of inflammatory cells in the synovial tissue of joints leading to chronic inflammation and destruction of joints.

Imaging of Tc-99m-HMPAO-labelled monocytes in patients with active RA has demonstrated similar initial kinetics to those seen with labelled mixed leukocytes with initial margination to the lungs followed by margination in the liver and spleen (Bennink et al. 2008). Within 2 h however, the labelled monocytes accumulate in the large and small joints of the hands and feet. Tc-99m-HMPAO-labelled lymphocytes have also been shown to migrate to joints and a positive joint scintigram is predictive of active synovitis (Jorgensen et al. 1995).

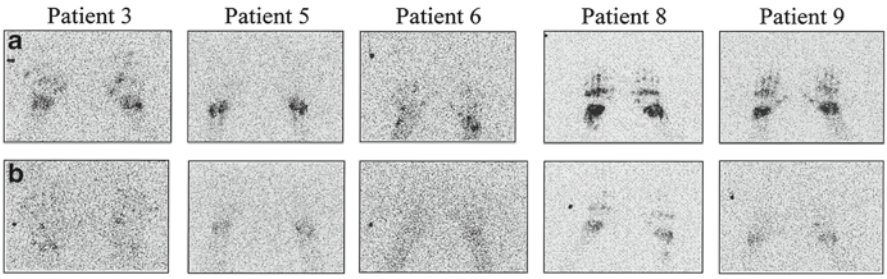

Fig. 8.9 In-111 scans of the hands and wrists of five patients taken 22 h after injection (**a**), before and (**b**) after a single intravenous bolus of anti-tumour necrosis factor α antibody. A reduction in the signal detected is demonstrated after treatment in all five patients (Taylor et al. 2000)

Leukocyte scintigraphy has also been used to assess the response to treatment in RA. In-111-granulocyte scintigraphy has been carried out in RA patients before and after treatment with agents targeting the tumour necrosis factor-α (TNFα) pathway. Following such treatment, granulocyte counts within the synovial fluid of patient samples are lower and this is accompanied by a significant reduction of the In-111-granulocyte signal in the knees, hand, and wrist joints (Taylor et al. 2000) (Fig. 8.9).

8.5.11 Systemic Vasculitis

Systemic vasculitis is associated with marked changes in granulocyte kinetics involving both the lung and spleen (Jonker et al. 1992). Patients with granulomatosis with polyangitis (GPA) and microscopic polyarteritis (MP) studied with autologous Tc-99m-HMPAO- or In-111-troponolate-labelled leukocytes, demonstrate diffuse lung uptake which is most marked in GPA patients. Activity can also be detected in the nose of GPA patients, and one such patient with rapidly progressive glomerulonephritis had diffuse uptake of indium-labelled cells in the kidneys. There was also abnormal splenic uptake in patients with systemic vasculitis.

8.6 Summary

Modern imaging modalities with ever-impressive improvements in spatial resolution and methods to interpret cell kinetics, have led to a revolution in leukocyte imaging via scintigraphy, and such methods have allowed for the quantitative interpretation of cell trafficking and migration of leukocytes under both physiological and pathological conditions.

Published studies have clearly demonstrated the utility of radioscintigraphy to assess the response of disease conditions (and normal physiology) to pharmacological intervention. Careful leukocyte preparation and radiolabelling, coupled to modern imaging modalities such as SPECT/CT, now provides an exciting platform to test the efficacy of new drugs and biologics, as well as novel cell therapies, in altering the migration characteristics and kinetics of inflammatory cells. The ability to image the anti-inflammatory responses to treatment with existing and novel drugs and biologics will continue to be innovative and a valuable asset in the understanding of how we can best control or treat infection and inflammation.

Acknowledgements Part of the work presented is supported by grants from the Medical Research Council, Wellcome Trust, Asthma UK, British Lung Foundation, GlaxoSmithKline, Biotechnology and Biological Science Research Council, Cambridge NIHR Biomedical Research Centre, MedImmune, and Academy of Medical Sciences.

We also thank the Nuclear Medicine Department at Addenbrooke's Hospital, the Wellcome Trust Clinical Research Facility, Cambridge, and Cambridge Biomedical Research Centre Core Biochemistry Assay Laboratory and acknowledge the support of the National Institute for Health Research, through the Comprehensive Clinical Research Network.

References

Ackrill (2011) The effect of patient medication and other factors on the biodistribution of radiopharmaceuticals. In: Theobald, Sampson's textbook of radiopharmacy, 4th edn. Pharmaceutical Press, London, pp 541–553

Anger (1958) Scintillation camera. Rev Sci Instrum 29(1):27–33

Athens et al (1960) Leukokinetic studies III. The distribution of granulocytes in the blood of normal subjects. J Clin Invest 40:159–164

Athens et al (1961) Leukokinetic studies IV. The total blood, circulating and marginal granulocyte pools and the granulocyte turnover rate in normal subjects. J Clin Invest 40:989–995

Bar-Shalom (2006) SPECT/CT using 67-Ga and 111-in-labeled leukocyte scintigraphy for diagnosis of infection. J Nucl Med 47:587–594

Barnes et al (2003) How do corticosteroids work in asthma? Ann Intern Med 139:359–370

Bennink et al (2008) Biodistribution and radiation dosimetry of 99mTc–HMPAO–labeled monocytes in patients with rheumatoid arthritis. J Nucl Med 49:1380–1385

Bleeker-Rovers et al (2004) Clinical value of FDG PET in patients with fever of unknown origin and patients suspected of focal infection and inflammation. Eur J Nucl Med Mol Imaging 31:29–37

Busse et al (1992) Eosinophils in asthma. Ann Allergy 68(3):286–290

Campbell et al (1976) Characteristics of the lymphopenia induced by radiotherapy. Clin Exp Immunol 23:200–208

Carpani de Kaski et al (1991) Fluticasone propionate in Crohn's disease. Gut 32:657–661

Carpani de Kaski et al (1992) Indium 111 whole body retention: a method for quantification of disease activity in inflammatory bowel disease. J Nucl Med 33(5):756–762

Cheow et al (2005) Quantification of disease activity in patients undergoing leucocyte scintigraphy for suspected infammatory bowel disease. Eur J Nucl Med Mol Imaging 32:329–337

Chisholm et al (1979) Cell damage resulting from the labelling of Rat lymphocytes and HeLa S3 cells woth in-111 oxine. J Nucl Med 20:1308–1311

Cousins et al (2003a) Imaging intra-abdominal sepsis. In: Peters A (ed) Nuclear medicine in radiological diagnosis. Martin Dunitz, London, pp 726–734

Cousins et al (2003b) Undiagnosed fever. In: Peters A (ed) Nuclear medicine in radiological diagnosis. Martin Dunitz, London, pp 703–713
Currie et al (1987) Indium 111-labelled granulocyte accumulation in the respiratory tract of patients with bronchiectasis. Lancet 1:1335–1339
Dancy et al (1976) Neutrophil kinetics in Man. J Clin Invest 58:705–715
Danpure et al (1982) The labelling of blood cells in plasma with 111-In-troponolate. Br J Radiol 55:247–249
Danpure, Osman (1988) Optimum conditions for radiolabelling human granulocytes and mixed leukocytes with 111-in-troponolate. Eur J Nucl Med 13:537–542
Derenzo (1980) Method for optimizing side shielding in positron-emission tomographs and for comparing detector materials. J Nucl Med 21:971–977
Doershuk (2000) Leukocyte trafficking in alveoli and airway passages. Respir Res 1(3):136–140
Dorffel et al (2001) Preactivated monocytes from hypertensive patients as a factor for atherosclerosis. Atherosclerosis 157:151–160
Downey (1994) Mechanisms of leucocyte motility and chemotaxis. Curr Opin Immunol 6(1): 113–124
Downey et al (1999) Regulation of neutrophil activation in acute lung injury. Chest 116(uppl1):465
Elghetany (2002) Surface antigen changes during normal neutrophilic development: a critical review. Blood Cells Mol Dis 28(2):260–274
Ellis (2011) Radiolabelling of blood cells: theory and practice. In: Theobald T (ed) Sampson's Textbook of radiopharmacy. Pharmaceutical Press, London, pp 420–445
Farahi et al (2012) Use of 111-Indium-labelled autologous eosinophils to establish the in vivo kinetics of human eosinophils in healthy subjects. Blood 120(19):4068–4071
Forstrom et al (1981) Indium-111-labeled leukocytes in the diagnosis of rejection and cytomegalovirus infection in renal transplant patients. Clin Nucl Med 6:146–149
Frier (1994) Leucocyte radiolabelling techniques: practical aspects. Scand J Gastroenterol 29(S203):32–35
Froelich, Swanson (1984) Imaging of inflammatory processes with labelled cells. Semin Nucl Med 14(2):128–140
Grimstad et al (1992) 99mTc-hexamethylpropyleneamine oxime leukocyte scintigraphy and C-reactive protein levels in the differential diagnosis of brain abscesses. J Neurosurg 77(5): 732–736
Gupta, Gupta (2005) Synthesis and surface engineering of iron oxide nanoparticles for biomedical applications. Biomaterials 26(18):3995–4021
Hansel et al (1991) An improved immunomagnetic procedure for the isolation of highly purified human blood eosinophils. J Immunol Methods 145(1–2):105–110
Herion et al (1970) Eosinophil kinetics in two patients with eosinophilia. Blood 36:361–370
Hoffer (1980) Gallium:mechanisms. J Nucl Med 21:282–285
Hogg (1994) The traffic of polymorphonuclear leukocytes through pulmonary microvessels in health and disease. AJR Am J Roentgenol 163:769–775
Hutton (2011) Physics applied to radiopharmacy:imaging instruments for nuclear medicine. In: Theobold T (ed) Sampson's textbook of radiopharmacy. Pharmaceutical Press, London, pp 61–71
Ilknur et al (2002) Labeling of mixed leukocytes with 99mTc-HMPAO causes severe chromosomal aberrations in lymphocytes. J Nucl Med 43(2):203–206
Jones et al (1997) Dissociation of neutrophil emigration and metabolic activity in lobar pneumonia and bronchiectasis. Eur Respir J 10:795–803
Jones et al (2003) In vivo assessment of lung inflammatory cell activity in patients with COPD and asthma. Eur Respir J 21:567–573
Jones et al (2004) Use of 18Fdg Pet to discriminate between infection and rejection in lung transplant recipients. Clin Transplant 77(9):1462–1464
Jonker et al (1992) A retrospective study of radiolabelled granulocyte kinetics in patients with systemic vasculitis. J Nucl Med 33:491–497

Jorgensen et al (1995) Radiolabelled lymphocyte migration in rheumatoid synovitis. Ann Rheum Dis 54:39–44
Lavender et al (1977) Kinetics of indium-111 labeled lymphocytes in normal individuals and those with Hodgkin's disease. Br Med J 2:797–799
Leuschner et al (2012) Rapid monocyte kinetics in acute myocardial infarction are sustained by extramedullary monocytopoiesis. J Exp Med 209(1):123–137
Litzler et al (2010) Leukocyte SPECT/CT for Detecting Infection of Left-Ventricular-Assist Devices:Preliminary Results. J Nucl Med 51(7):1044–1048
Mauer et al (1960) Leukokinetic Studies II. A method for labeling granulocytes in vitro with radioactive diisopropylfluorophosphate (DFP-32). J Clin Invest 39:1481–1486
McAfee, Thakur (1976) Survey of radioactive agents for the in vivo labelling of phagocytic leukocytes. I Soluble agents. II. Particles. J Nucl Med 17:408–488
McMillan et al (1968) Leukocyte labelling with 51-chromium. Technique and results in normals. Blood 32:738–754
Palestro et al (2002) Osteomyelitis: Diagnosis with 99mTc-labeled Antigranulocyte Antibodies Compared with Diagnosis with 111In-labeled Leukocytes—Initial Experience. Radiology 223:758–764
Palestro et al (2006) Combined labelled leukocyte and technetium 99m sulfur colloid bone marrow imaging for diagnosing musculoskeletal infection. Radiographics 26(3):859–870
Parwaresch et al (1976) The peripheral kinetics of human radiolabelled eosinophils. Virchows Arch B Cell Pathol 21:57–66
Peters (1994) The Utility of 99mTc-HMPAO-Leukocytes for Imaging Infection. Semin Nucl Med XXIV(2):110–127
Peters (1998) Just how big is the pulmonary granulocyte pool? Clin Sci 94:7–19
Peters, Saverymuttu (1987) The Value of Indium-labelled Leucocytes in Clinical Practice. Blood Rev 1:65–76
Peters et al (1980) Diagnosing cerebral abscess with 111-indium labelled autologous leukocytes. Lancet 2:309–310
Peters et al (1985a) Quantification of the distribution of the marginating granulocyte pool in man. Scand J Haematol 34(2):111–120
Peters et al (1985b) Splenic pooling of granulocytes. Clin Sci 68(3):283–289
Pinching et al (1990) Quantification of radiolabelled granulocyte migration in vivo. J Immunol Methods 126:7–11
Puncher, Blower (1994) Autoradiography and density gradient separation of technitium-99m-Exametazime (HMPAO) labelled leukocytes reveals selectivity for eosinophils. Eur J Nucl Med 21:1175–1182
Robins et al (2000) Biodistribution and Radiation Dosimetry of Stabilized 99mTc-Exametazime-Labeled Leukocytes in Normal Subjects. J Nucl Med 41(5):934–940
Ruparelia et al (2009) 99m Technitium-labelled neutrophil scanning in pneumonia. Thorax 64(1):92
Ruparelia et al (2011) Quantification of neutrophil migration into the lungs of patients with chronic obstructive pulmonary disease. Eur J Nucl Med Mol Imaging 38:911–919
Sampson (2000) The role of eosinophils and neutrophils in inflammation. Clin Exp Allergy 30(Sup 1):22–27
Saverymuttu et al (1983a) Lung Transit of 111-Indium-Labelled Granulocytes. Scand J Haematol 30:151–160
Saverymuttu et al (1983b) Measurement of granulocyte migration and accumulation in inflammation in man. Clin Exp Immunol 52:607–612
Saverymuttu et al (1983c) Quantitative faecal 111-indium leucocyte excretion in the assessment of disease activity in Crohn's disease. Gastroenterology 85:1333–1339
Saverymuttu et al (1985a) Indium 111 autologous leucocyte scanning in lobar pneumonia and lung abscesses. Thorax 40:925–930
Saverymuttu et al (1985b) The kinetics of 111-indium distribution following injection of 111-indium labelled autologous granulocytes in man. Br J Haematol 61:675–685

Saverymuttu et al (1986) Indium 111-granulocyte scanning in the assessment of disease extent and disease activity in inflammatory bowel disease. A comparison between colonoscopy, histology and faecal indium 111-granulocyte excretion. Gastroenterology 90:1121–1128
Seabold and Nepola (2003) Infection in the peripheral skeleton. In: Peters A (ed) Nuclear Medicine in Radiological Diagnosis. Martin Dunitz, London, pp. 65–77
Segal et al (1978) Indium-111 labeling of leukocytes: a detrimental effect on neutrophil and lymphocyte function and an improved method of cell labeling. J Nucl Med 19:1238–1244
Steinbach et al (1979) Estimation of Kinetic Properties of Neutrophilic. Eosinophilic and Basophilic Granulocytes in Human Blood. Blut 27–38
Szczepura et al (2011) Measuring whole-body neutrophil redistribution using a dedicated whole-body counter and ultra-low doses of 111-indium. Eur J Clin Invest 41(1):77–83
Tacke et al (2006) Migratory fate and differentiation of blood monocyte subsets. Immunobiology 211:609–618
Tam et al (1992) Inhaled platelet-activating factor causes pulmonary neutrophil sequestration in normal humans. Am Rev Respir Dis 146:1003–1008
Taylor et al (2000) Reduction of Chemokine Levels and Leukocyte Traffic to Joints by Tumour Necrosis Factor a Blockade in Patients with Rheumatoid Arthritis. Arthritis Rheum 43(1):38–47
Thakur et al (1977) Indium-111-Labelled Cellular Blood Components: Mechanisms of Labelling and Intracellular Location in Human Neutrophils. J Nucl Med 18:1020–1024
Ussov et al (1995) Granulocyte margination in bone marrow: comparison in the spleen and liver. Scand J Clin Lab Invest 55(1):87–96
Ussov et al (1999) Pulmonary granulocyte kinetics in relation to endothelial and granulocyte activation. Clin Sci 96:525–531
Van Hemert et al (2007) Labelling of autologous monocytes with 99mTc-HMPAO at very high specific radioactivity. Nucl Med Biol 34(8):933–938
Van Hemert et al (2009) Labeling monocytes for imaging chronic inflammation. J Nucl Med Mol Imaging 53:78–88
Von-Bruhl et al (2012) Monocytes, neutrophils and platelets cooperate to initiate and propagate venous thrombosis in mice in vivo. J Exp Med 819–825
Wagstaff et al (1981) A method for following human lymphocyte traffic using indium-111 oxine labelling. Clin Exp Immunol 43:435–442
Ware, Matthay (2000) The Acute Respiratory Distress Syndrome. N Engl J Med 342:1334–1349
Warshawski et al (1986) Abnormal neutrophil-pulmonary interaction in the adult respiratory distress syndrome. Quantitative assessment of neutrophil kinetics in humans with in vivo 111 indium neutrophil scintigraphy. Am Rev Respir Dis 133(5):797–804
Weldon M (2003) Radiological investigation of inflammatory bowel disease. In: Peters A (ed) Nuclear Medicine in Radiological Diagnosis. Martin Dunitz, London, pp 291–303
Weldon et al (1995a) Comparison of 99m technetium hexamethylpropylene-amine oxime labelled leucocyte with 111 indium troponolate labelled granulocyte scanning and ultrasound in the diagnosis of intra-abdominal abscess. Gut 37:557–564
Weldon et al (1995b) Quantification of inflammatory Bowel Disease Activity using technetium-99m HMPAO labelled leucocyte single photon emission computerised tomography (SPECT). Gut 36:243–250
Whitelaw (1972) Observations on human monocyte kinetics after pulse labelling. Cell Prolif 5(4):311–317
Yamauchi et al (1989) Kinetics of Indium-III-labeled eosinophils in two patients with eosinophilia. Eur J Nucl Med 15:274–278
Zhuang, Alavi (2002) 18-fluorodeoxyglucose positron emission tomographic imaging in the detection and monitoring of infection and inflammation. Semin Nucl Med XXXII:47–59

Chapter 9
Application of Bioluminescence Imaging (BLI) to the Study of the Animal Models of Human Infectious Diseases

Hana Golding and Marina Zaitseva

Abstract Traditional approaches in measuring the efficacy of antimicrobials, antivirals, antifungals, and antiparasitic therapies have limitations which contribute to noise in efficacy assessment. These include the following: (1) large number of animals must be sacrificed at multiple time points to assess the effects of therapy on pathogen titers in the organs; (2) weight loss of 25–30 % in animals requires ethical animal euthanasia which may be unscheduled and skew sampling; and (3) the organ titers are based upon ex vivo culture or analysis. Such limitations can lead to erroneous conclusions regarding drug efficacy versus spontaneous recovery. One needs to evaluate dissemination of the pathogen in vivo within the same animal to truly measure efficacy. Bioluminescence imaging (BLI) has been developed as a new method to monitor infections in small animal models. BLI is based on noninvasive measurement of biomarkers possessing a light-producing luciferin or other light-emitting metabolic substrates. This imaging platform is now a widely used technique in oncology, tumor metastasis, establishing efficacy of anticancer and anti-infective therapies, detecting protein–protein interactions, detecting transgene expression in vivo, and many more. BLI, importantly, enables each animal to be used as its own control over time, thus limiting the number of animals required in studies and minimizing animal-to-animal variations which improves statistical precision of efficacy outcomes. In this chapter we describe applications of BLI in the study of infection, reveal important limitations of the technique, and summarize recent work in murine microbial and viral models.

This book chapter reflects the views of the authors and should not be construed to represent FDA's views or policies.

H. Golding, Ph.D. • M. Zaitseva (✉)
Division of Viral Products (DVP), Center for Biologics Evaluation and Research (CBER), Food and Drug Administration (FDA), Bethesda, MD, USA
e-mail: marina.zaitseva@fda.hhs.gov

B.R. Moyer et al. (eds.), *Pharmaco-Imaging in Drug and Biologics Development*, AAPS Advances in the Pharmaceutical Sciences Series 8, DOI 10.1007/978-1-4614-8247-5_9,

9.1 Brief Description of the BLI Principles and Methodology of the Experiments Utilizing BLI as a Tool to Study Infections in Mice

9.1.1 Tissue Optics

The optical properties of the tissue to a large degree determine the sensitivity of deep-tissue imaging that utilizes fluorescent or bioluminescent probes. For example wavelengths of less than 600 nm are strongly quenched by hemoglobin molecule, while water absorption quenches wavelengths above 900 nm. In addition, endogenous chromophores such as elastin, collagen, tryptophan, NADH, porphyrins, and flavins in animal tissues and in the skin are subjected to autofluorescence upon excitation in wavelengths below 600 nm. Therefore, although fluorescent signals are generally brighter than bioluminescent signals, the very low autoluminescent levels usually result in superior signal-to-background ratios for bioluminescent imaging, particularly compared with fluorescent imaging in the green to red part of the spectrum (Lin et al. 2009; Troy et al. 2004). Based upon this fundamental differences in the signal-to-noise ratio, bioluminescent reporters remain to date more sensitive than fluorescent reporters for deep-tissue imaging applications.

9.1.2 Luciferases

Production of visible light is a natural phenomenon observed in some marine and terrestrial species. The mechanism responsible for light production is similar between these organisms and involves oxidation of an aldehyde substrate which is catalyzed by the enzyme luciferase. The major differences in the produced light between species are based on the source of the substrate, and on the kinetics and wavelength of the emitted light.

Genomes of bacteria such as Gram-negative bacteria *Photorhabdus luminescen*s and *Xenorhabdus luminescens* contain *lux* operon that encodes genes to synthesize luciferase and substrate luciferin, thus omitting the need to provide the substrate exogenously. Bacteria expressing the *lux* operon constitutively produce light with a peak emission at 490 nm. *Lux* operon has been widely used for bioluminescence imaging (BLI) of bacterial infections.

The luciferase enzymes from the North American firefly (Fluc) (*Photinus pyralis*) and from click beetle (*Pyrophorus plagiophthalamus*) are most widely used for BLI. These enzymes are monomeric proteins encoded by a single gene (*luc*). Modified firefly luciferase is expressed in the cytoplasm with a half-life of about 3 h. Luciferase catalyzes chemical reaction where exogenously provided D-luciferin substrate is oxidized in the presence of ATP-Mg^{+2} and O_2-generating oxyluciferin, CO_2, AMP, and light with a broad spectral emission that peaks at 560 nm but that

also includes a significant fraction of light above 600 nm (Gould and Subramani 1988). The luciferase enzymes from click beetle have been optimized to produce green-orange (544 nm) or red (611 nm) light after oxidizing luciferin. The longer wavelength light in the orange-red spectrum exhibits better penetration in living tissue and is therefore optimally suited for use in whole-animal imaging modality. The currently available methods allow detection of $>2.4 \times 10^5$ molecules of luciferase (Gould and Subramani 1988). The firefly luciferase is an oxygen scavenger. Due to the high homology to endogenous enzymes in mammalian cells, firefly luciferase is poorly immunogenic.

D-Luciferin substrate is a small molecule which penetrates across cell membranes and the blood–brain barrier. The mechanism of cellular uptake of luciferin is not fully elucidated and the role of specific membrane transporters in inward delivery and efflux of luciferin has been recently suggested (Zhang et al. 2012). Following injection of the substrate via intraperitoneal (IP) route, signal peaks around 15 min followed by a plateau phase of 15–20 min after which it steadily declines (Paroo et al. 2004). Studies that used radiolabeled D-luciferin showed that the kinetics of uptake and biodistribution varied significantly depending on the route of administration (Berger et al. 2008; Lee et al. 2003). The D-luciferin is not metabolized and is excreted via the kidneys within 2 h post injection.

Luciferase from marine organisms, *Renilla* (sea pansy) and *Gaussia* (copopod) luciferases, utilize coelenterazine substrate to produce light with emission peak at approximately 480 nm. The availability and in vivo distribution of the coelenterazine substrate is more limited than of the D-luciferin and therefore the coelentrazine may not be easily available for cells infected with *Renilla* luciferase-expressing pathogens. Bioluminescence from *Renilla* luciferase differs in kinetics from firefly luciferase peaking in about 1 min followed by decline in 10 min after i.v. injection (Paroo et al. 2004).

9.1.3 Detection and Measurement of Bioluminescence In Vivo in Live Animals

First bioimaging experiments utilizing photonic detection of light-emitting bacteria were performed in mice infected with luciferase-expressing *Salmonella typhimurium* (Contag et al. 1995). The same study also compared the sensitivity of bioluminescence measurements performed in live animals and in extracted organs and determined a five- to tenfold reduction in luminescence per cm of tissue, thus setting up the limitations for imaging of organs that are located deep in the body. The advancement in detector technologies greatly increased the sensitivity of charge-coupled device (CCD) cameras that can be cooled to −120 °C to maximally suppress dark current/noise allowing detection of minute amounts of bioluminescent light. As mammalian tissues are mainly absorbing in the blue, green, and yellow regions, the cooled CCD cameras are designed to detect red and near-red light (Contag and Bachmann 2002).

In a typical experiment, mice are infected with luciferase-expressing pathogen, receive a single dose of a luciferin substrate (the substrate is not injected when bacteria expressing *lux* operon are used), and are imaged while under anesthesia. Light emitted by infected organ(s) is captured by a CCD device during preset exposure time, is converted to numerical values using specific software, and is displayed on the monitor in pseudotyped colors scaled to reflect intensity of the captured light. During analysis of recorded images, the areas in the image that exhibit color are marked as regions of interest (ROIs) and the amount of light within designated ROIs is quantified as photon fluxes. Often, to adjust for various exposure times and sizes of ROIs, fluxes are normalized per unit of time and per area and are expressed as flux/s/cm^2. While normalization provides some advantage for comparison of luminescence signals between groups, one needs to remember that measured bioluminescence is relative and comparisons cannot be applied to tissues that are located at various depths of the organism. Therefore, in most studies, a set of ROIs is established for each site/organ, and groups of mice are compared and followed using the same ROIs throughout the study. Once these limitations are taken into consideration, it can be expected that BLI can measure luminescence signals in vivo with high sensitivity and reproducibility. The emitted fluxes can be used as quantitative measurements for statistical analyses. However, the correlation between bioluminescence and viral loads needs to be established for each organism/infection model.

Early studies using cell lines stably expressing luciferase showed that BLI can detect as few as approximately 30 cells in vitro and 1×10^3 cells in a mouse (Sweeney et al. 1999). However, it is important to note that the strength of promoters used to drive luciferase expression in recombinant viruses or bacteria may affect limits of detection. Therefore, it is essential to generate correlation curves for each luciferase-expressing pathogen used in the study. Our own data as well as reports published by other investigators have shown that measurements of photon fluxes emitted by recombinant viruses expressing luciferase correlated in linear fashion with viral loads measured in organs isolated from infected mice, thus supporting the notion that bioluminescence provides a direct measure of in-host viral replication and dissemination (Cook and Griffin 2003; Luker et al. 2002; Luker and Luker 2008; Zaitseva et al. 2009). It is also important to note that because luciferase requires ATP for generating light from luciferin, the IVIS system measures luciferase activity only in cells. Luciferase in the plasma is not measured and any signal acquired is from the organ not the blood.

9.2 BLI for Monitoring Viral Infections

The introduction of the luciferase gene into the genome of vaccinia virus (VACV) was the first attempt to use measurements of emitted light as an alternative approach to traditional plaque assay to quantify DNA viruses (Rodriguez et al. 1988). At a high infection rate, recombinant VACV produces about 10,000 particles per cell, which contributes to the 1,000-fold higher sensitivity in detecting VACV in vitro by

measuring luciferase activity compared with β-galactosidase as reporter-gene system (Rodriguez et al. 1988). Several studies used luciferase-expressing VACV to assess viral–host interactions. BLI of IFNα receptor knockout (KO) or TLR4 knockout mice infected with VACV-reporter virus showed that mutant mice had increased dissemination and higher levels of bioluminescence signal in internal organs that correlated with lower survival rates (Hutchens et al. 2008; Luker et al. 2005). More severe pathogenesis was observed in the TLR4 KO mice, and was attributed to increased lung inflammation. It suggested that innate immune receptors play a major role in limiting in-host dissemination of VACV (Hutchens et al. 2008). In our laboratory, BLI was extensively used to evaluate effects of anti-smallpox vaccine and antiviral treatments on dissemination of two strains of recombinant VACV expressing luciferase, WRvFire, and IHD-J-Luc, and the results of these studies are summarized at the end of this chapter (Zaitseva et al. 2009, 2011).

In vivo dissemination of a herpes simplex virus type I (HSV-1) was monitored using a recombinant strain of KOS HSV-1 virus that encoded both *firefly* luciferase and *Renilla* luciferase under the control of an early gene promoter (Luker et al. 2002). The validity of this model to study HSV-1 pathogenesis was confirmed by showing that valacyclovir, a potent inhibitor of HSV-1 replication, reduced bioluminescence in the eyes of mice in vivo and reduced viral titers in the tear film material ex vivo following KOS HSV-1 infection via corneal scarification. The same study also pointed to several limitations of the BLI; the activity of *Renilla* luciferase could be detected only after direct inoculation of the substrate (coelenterazine) in infected eyes but not after systemic administration. In addition, due to low spatial resolution of the 2-D imaging system, bioluminescence from the site of infection in the cornea could not be separated from the subsequent spread of infection to the periocular tissues (Luker et al. 2002). In the follow-up studies, BLI was used to study the role of IFNα in protection from HSV-1 infection using mice lacking IFNα R1 and mice lacking TLR9 and MyD88, known inducers of IFNα (Krug et al. 2004; Luker et al. 2003). IFNα R1 KO mice infected with reporter virus exhibited higher bioluminescence in internal organs compared with wild-type mice confirming that dissemination of HSV-1 was controlled by IFNα (Luker et al. 2003). In contrast, luminescence was not increased in mice lacking TLR9 or MyD88 suggesting that TLR9/MyD88 pathway was not involved in controlling viral replication in vivo (Krug et al. 2004).

While large DNA viruses such as poxviruses and HSV virus allow for insertion of a large portion of foreign DNA, the insertion of a reporter gene in RNA viruses is more challenging. Nevertheless, several laboratories reported successful construction of recombinant RNA viruses expressing luciferase and development of animal models where infection with recombinant RNA viruses was monitored by BLI.

Dengue virus (DENV) is a global disease threat for which there are no approved antivirals or vaccines. A recent report described an infectious recombinant *fluc-expressing* DENV that was sensitive to neutralizing antibodies and to antiviral agents, adenosine nucleoside NITD008 and mycophenolic acid in vitro (Schoggins et al. 2012). However, of the two compounds, only NITD008 but not mycophenolic acid suppressed virus replication in vivo, thus demonstrating that BLI may be a

useful drug discovery tool to identify compounds that target DENV in vivo (Schoggins et al. 2012).

BLI was used to study infections of mice with two members of the family of alphaviruses, Venezuelan equine encephalitis virus (VEEV) and Sindbis virus (SV), that are an important cause of encephalitis in the Americas, causing disease in horses, birds, and humans. Following intranasal infection of mice with TC83-luciferase, a highly attenuated strain of VEEV that replicates in mouse brain, bioluminescence was detected in the CNS at least 3 days before the onset of clinical signs of disease, including encephalitis and meningitis, thus allowing humane treatment of animals (Patterson et al. 2011). Moreover, this model was successfully utilized to show that human antiviral drug and TLR3 agonist Ampligen effectively inhibited viral dissemination after intraperitoneal but not intranasal delivery (Patterson et al. 2011). In the SV infection model, BLI enabled authors to visualize invasion of CNS by TRNSV-Luc recombinant SV from peripheral sites of viral replication following subcutaneous (s.c.) inoculation (Cook and Griffin 2003). Replication of SV was detected in the noses of mice at day 1 post infections followed by lower spinal cords and brains, thus providing evidence for the previously suggested nasal neuroepithelium as the initial site for replication of the SV prior to entering of the CNS (Cook and Griffin 2003).

An interesting application for BLI was recently reported in infection of mice with highly contagious respiratory parainfluenza virus (PIV) as a surrogate model for transmission of respiratory syncytial virus (RSV) in humans (Burke et al. 2011). Here authors utilized BLI to follow animal-to-animal transmission of a negative-RNA strand recombinant rSeV-luc(M-F*) virus that was phenotypically similar to wild-type Sendai virus (Burke et al. 2011). The study revealed important differences in the role of viral replication in pathogenesis versus transmission: infection of the upper respiratory tract and trachea were associated with animal-to-animal transmission while infection in the lungs was associated with pathogenesis (weight loss and mortality) (Burke et al. 2011).

9.3 BLI for In Vivo Monitoring of Bacterial Infections and Antibacterial Treatments

Bacterial *lux* operon contains genes coding for both luciferase and its substrate, and therefore BLI of bacterial infections in animal models does not require injections of the substrate. Yet, creating Gram-positive bioluminescent bacteria is complicated due to inability of the ribosomes in Gram-positive (G+) bacteria to bind and translate mRNA of the *lux* operon from Gram-negative *Photorhabdus luminescens*. Therefore two approaches were developed to adapt G+ bacteria for BLI. The G+ ribosome-binding sites were installed above each gene of the *P. luminescens lux* operon and the created cassette was inserted into the chromosome of G+ bacteria; this technique was implemented in animal models of infections with *Staphylococcus aureus* and *Streptococcus pneumoniae* (Francis et al. 2000, 2001; Kadurugamuwa et al. 2003;

Xiong et al. 2005). In other studies, *lux* operon was provided within the reporter plasmids to follow replication and dissemination of *S. aureus, Yersinia pestis*, and *Francisella tularensis* (Bernthal et al. 2010; Bina et al. 2010; Nham et al. 2012; Sha et al. 2013).

The antimicrobial effects of several antibiotics were evaluated by BLI in the mouse and in the rat models of *S. aureus* bacterial biofilm infections, commonly associated with implantation of prosthetic devices in humans and with *S. aureus* endocarditis (Kadurugamuwa et al. 2003; Xiong et al. 2005). In the first study, catheter colonized with luminescent *S. aureus* XEN 29 was implanted s.c. in mice. Bacterial growth and sensitivity to rifampin but not tobramycin or ciprofloxacin were determined by BLI and were confirmed by colony counts in extracted catheters ex vivo. Importantly, after the rifampin was discontinued, the rebound of the signal was observed, and was mediated by growth of the rifampin-resistant staphylococci (Kadurugamuwa et al. 2003). In the rat model of aortic infective endocarditis (IE), the effects of several anti-staphylococcal agents on *S. aureus* XEN 29 bacterial burden in cardiac vegetations were monitored by BLI. Microbial relapse due to discontinuation of vancomycin therapy was correctly predicted based on increased cardiac bioluminescence (Xiong et al. 2005). In addition, bioluminescent SH1000 *S. aureus* strain containing the *lux* genes within a plasmid was used to evaluate effectiveness of antibiotic treatment in a model of post-arthroplasty *S. aureus* joint infection in genetically engineered mice with fluorescent neutrophils (LysEGFP mice) (Bernthal et al. 2010). Following inoculation of the SH1000 *S. aureus* into the mouse joint containing orthopedic implant, increased bioluminescence, swelling of the affected leg, and increased EGFP-neutrophil fluorescence were observed. Importantly, bioluminescence and fluorescence were substantially lower in mice that received implants pre-coated with antibiotic-eluting polymers suggesting that bacterial biofilm and inflammatory responses could be prevented if sufficient concentrations of antibiotics are constitutively present at the surface of the implant (Bernthal et al. 2010).

The potential use of multidrug-resistant *Yersinia pestis* as a biological warfare and the reappearance of human plague in countries where no cases have been reported for decades renewed interest in the development of anti-*Y. pestis* drugs and vaccine. Virulent variants of *Y. pestis* C092 containing *lux* operon within pGEN-luxCDABE or within pUTmini-TN::luxKM2 reporter plasmids were recently generated and used in mouse models of bubonic plague and pneumonic plague, respectively (Nham et al. 2012; Sha et al. 2013). To mimic the natural route of transmission of bubonic plague in humans via flea bite, the bioluminescent *Y. pestits* C092 was inoculated into mice s.c. at *linea alba*. Using BLI, the in-host progression of the infection was monitored in real time. The data showed that after initial multiplication at the injection site, bacteria migrated from one lymph node to another via the lymphatic stream and once it reached the lymph nodes, the bacteria progressed very rapidly throughout the body (septicemic phase) leading to death within 2 days (Nham et al. 2012). In the mouse model of pneumonic plague, following intranasal inoculation, bioluminescent *Y. pestis* C092 established infection in the lungs prior to dissemination to the liver and spleen. Importantly, using this model, the authors

demonstrated that daily treatments with levofloxacin (10 mg/kg/day) starting 24 h post infection protected mice from lethality and completely reduced bioluminescence, indicating that this antimicrobial treatment killed bacteria early in the course of infection and prevented its dissemination (Sha et al. 2013).

Recently, BLI was employed in the mouse model of *E. coli*-induced infectious diarrhea (Rhee et al. 2011). In the first study, Enteropathogenic *E. coli* (EPEC) was transformed with *lux* operon-containing plasmid and used to localize intestinal sites where bacteria disseminate following oral administration. To allow for consistent EPEC colonization, mice were pretreated with streptomycin for 1 day prior to bacterial infection. In addition, because luciferase requires oxygen to induce bioluminescence, the entire intestine (duodenum–rectum) was excised, aerated, and subjected to BLI ex vivo. The study showed that cecum and colon, but not rectum, were the main sites of colonization by EPEC (Rhee et al. 2011). Human infections with EPEC are often studied using a genetically relevant murine *Citrobacter rodentium* which induces transmissible colitis and colonic epithelial cell hyperplasia in mice. A combination of a 2D BLI with a 3D diffuse light imaging tomography with μCT imaging (DLIT-μCT) (to determine the exact location of the BL foci in vivo) was employed for the first time to evaluate the effects of prophylactic treatment with *Bifidobacterium breve* UCC2003 probiotics on *C. rodentium* dissemination (Collins et al. 2012). The results showed that *C. rodentium* forms focal infection in the cecum, followed by colonization of the large intestine. Interestingly, pretreatment with *B. breve* did not prevent *C. rodentium* colonization, but significantly reduced distribution within the large intestine and ameliorated intestinal inflammation (as was confirmed by histological analysis of the lamina propria) (Collins et al. 2012).

9.4 BLI for In Vivo Monitoring of Infections with Parasites and Fungi

Recent reports demonstrated the utility of BLI in following infections of mice with parasites and fungi. The recombinant protozoan parasites *Leishmania donovani*, *Leishmania major*, and *Leishmania amazonensis* with genomic expression of firefly luciferase gene were shown to infect bone marrow-derived macrophages in vitro and to form lesions upon intradermal infection of mice in vivo (Lang et al. 2005; Roy et al. 2000). Importantly, light produced by in vitro-infected macrophages and light detected in lesions following in vivo infections correlated in linear fashion with the number of parasites measured by culture-based assay. In addition, the in vitro infection was shown to be useful for rapid screening of anti-Leishmania agents (Lang et al. 2005).

Interesting results were obtained with bioluminescent luciferase-expressing *Toxoplasma gondii* in the study of parasite reactivation after latency in chronically infected mice (Saeij et al. 2005). BLI of live mice showed that the parasites emerged in different anatomical sites: in the head and neck area in mice that were infected with highly virulent *T. gondii* and in the abdomen of mice infected with low-virulence *T. gondii*, thus linking virulence with anatomical location of the parasite (Saeij et al. 2005).

For visualization of *Candida albicans* fungal infections, clinical isolate of *Candida albicans* was stably transformed with a codon-optimized luciferase gene (Doyle et al. 2006). Chronic infections were established in mice and bioluminescence in vaginal tissue correlated with fungal loads assayed in vaginal lavage. Importantly, clearance of the infection following treatment with the antifungal drug, miconazole, as determined by imaging in vivo was confirmed in the ex vivo detection of fungal loads (Doyle et al. 2006). This study was further extended by expressing a synthetic version of the *Gaussia princeps* luciferase gene as part of the *C. albicans* GPI-linked cell wall protein (Enjalbert et al. 2009). In this construct, luciferase is expressed on cell surface and is readily accessible to the substrate irrespectively of whether the fungus is in the yeast or in the hyphal form, and thus omitting the problem of limited permeability of the hyphal cells for luciferin substrate (Enjalbert et al. 2009).

9.4.1 Conclusion

In conclusion, BLI of small rodents infected with pathogens engineered to express luciferase enzymes provides a useful tool to study pathogen–host interactions and for drug discovery and preclinical testing of therapies and vaccines. In all of these studies there are several issues that need to be taken into consideration while planning the experiments and interpreting the data. These factors include but are not limited to the following: susceptibility to the infection can be affected by genetics of the mouse strain, the intensity of the recorded signal is strongly affected by the color of the mouse fur and underlying skin, introduction of the luciferase gene may attenuate pathogenicity, and animal-to-animal variability in signal intensity and between anatomical sites.

It is important to also note that the improvements in gene sequences of luciferase enzymes and optimization of the expression techniques during the past several years dramatically expanded the panel of pathogens expressing luciferase reporter genes, enabling in vivo imaging during preclinical studies. As described above, some bioluminescent pathogens were already tested in prototype models for drug evaluation and others such as *Mycobacterium tuberculosis*, *Vibrio cholerae*, and *Bacillus anthracis* were already engineered for in vivo luminescence imaging and future studies will show their usefulness for preclinical studies of antibacterial treatments (Andreu et al. 2010; Glomski et al. 2007; Morin and Kaper 2009).

9.5 Bioimaging of Mice Infected with Recombinant Vaccinia Viruses Expressing Luciferase

Smallpox, a highly lethal disease with nearly 30 % mortality rate, is caused by infection with variola virus. Smallpox is highly contagious and is thought to be transmitted as an aerosol and via fomites, causing lung infection followed by viremic phase and development of classic disseminated rash or "pocks" (Fenner et al. 1988; Henderson et al. 1999).

Vaccination of the general public against smallpox was discontinued in the USA in 1972 after the massive worldwide vaccination campaign that eradicated smallpox. Yet the threat of potential release of variola virus as a bioterrorist agent and the emergence of monkeypox virus infections in humans have led to renewed interests in the development of antiviral drugs and safer vaccines (Henderson et al. 1999; Rimoin et al. 2010; Whitley 2003). The currently licensed smallpox vaccine containing replicating VACV (that belongs to the same family of orthopoxviruses as variola virus) poses a significant risk to individuals with certain skin disorders or immunodeficiency conditions (Baker et al. 2003; Belongia and Naleway 2003). To manage cases of vaccine-associated complications and for treatments of accidental exposures, new antiviral compounds are being investigated in animal models and in clinical trials in humans (Neyts and De Clercq 2003).

Preclinical testing of new anti-smallpox vaccines and therapeutics is performed using several animal models as surrogate models of variola virus infection in humans including infection of macaques with monkeypox virus (Edghill-Smith et al. 2005; Hooper et al. 2004; Panchanathan et al. 2007). However, due to the expense and requirement for Biosafety Level 3 facilities, nonhuman primate models cannot be widely used for smallpox vaccine development. The majority of preclinical testing and initial characterization of smallpox vaccines and therapies are performed with the Western Reserve (WR) strain of VACV or with ectromelia virus, which is highly lethal in mice. Various endpoints are used to follow infections in mice and include weight loss, pox lesion scoring, and viral load measurements by plaque formation on sensitive cell lines. These endpoints are not optimal as they cannot avoid morbidity or accurately predict lethality of individual animals. They require large number of animals in order to determine survival rates and to quantify viral loads in internal organs. Lethality was frequently used as an endpoint in the past, but is no longer acceptable.

To get an inside view on the pharmacology and mechanism of protection from lethality provided by vaccines against smallpox and antiviral therapies, our laboratory developed a complex approach where we employ bioluminescence to record dissemination and replication of VACV in live mice in the presence of antiviral treatments. In the experiments, mice are infected with a recombinant VACV which expresses firefly luciferase (emission peak at 560 nm), such as the WR (WRvFire) or International Health Department J (IHD-J-Luc) strains via intranasal (IN) route. Following infection, mice are observed for lethality and for weight loss and bioluminescence is recorded daily or as specified following administration of D-luciferin substrate via IP route each time prior to imaging. The recorded bioluminescence within ROI (as described above in Sect. 9.1.3) is converted into numerical values of photon fluxes using Living Image 3.2 software (PerkinElmer Inc., Hopkinton, MA, USA) and is analyzed using a panel of statistical tools. This chapter describes four experiments that illustrate the imaging approach we have employed combined with various types of statistical analyses that can be applied to understand how bioluminescence data can answer pharmacology questions which depend on the type of treatment and the scientific question one is trying to resolve.

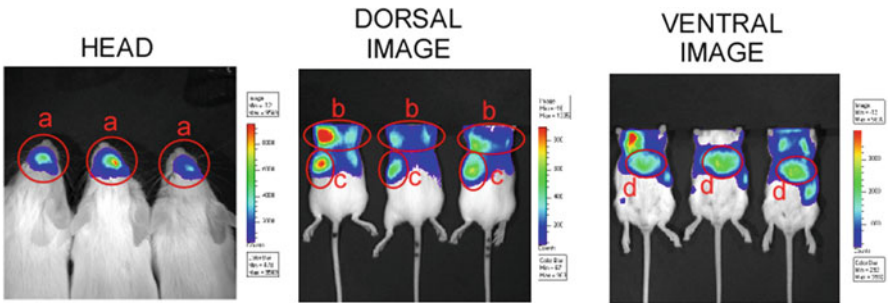

Fig. 9.1 Images of 5-week-old BALB/c mice infected with WRvFire VACV. Representative images of the heads (*left*), ventral torso (*center*), and dorsal torso (*right*) of mice infected with 10^5 pfu of WRvFire via the intranasal route are shown. Strong bioluminescence signals were noted in the nasal cavity (**a**), lungs (**b**), spleen (**c**), and liver (**d**). *Circles* mark the regions of interest (ROI) used to calculate total fluxes for subsequent analyses

9.5.1 Usage of Bioluminescence Recordings to Predict Lethality

The objective of the first approach was to determine whether a bioluminescence marker recorded using the IVIS 50 bioluminescence imaging instrument (PerkinElmer, Hopkinton, MA) in selected organs of infected mice (i.e., nasal cavity, lungs, spleen, and liver as shown in Fig. 9.1) was predictive of infection outcome, lethality versus survival. To answer this question, normal BALB/c mice (nine per group) were immunized with a licensed Dryvax vaccine that is considered a "gold standard" due to the long-lasting immune response in humans (Amanna et al. 2006; Hammarlund et al. 2003) or received PBS (control group) via IP injection, and 2 weeks later were challenged with a lethal dose of WRvFire (10 LD_{50}) via the IN route (Fig. 9.2) (Zaitseva et al. 2009). Control mice succumbed within 1 week post infection (p.i.), while all mice that received Dryvax survived (Fig. 9.2a, closed circles and open squares, respectively). In Dryvax-vaccinated mice, bioluminescence (photon flux) was not detected in the spleens and livers (data not shown). In the nasal cavity and lungs, photon fluxes were recorded on day 1 p.i., and were similar between control mice (closed circles) and immunized mice (open squares) (Fig. 9.2b, c, respectively).[1] Starting from days 3 to 4 p.i., photon fluxes were dramatically reduced in vaccinated but not in control mice suggesting that strong antiviral response induced by Dryvax vaccine protected mice from dissemination of WRvFire to the spleen and liver and rapidly cleared infection from the upper respiratory tract.

[1] Each curve represents specific wavelength photon fluxes recorded in one mouse on subsequent days.

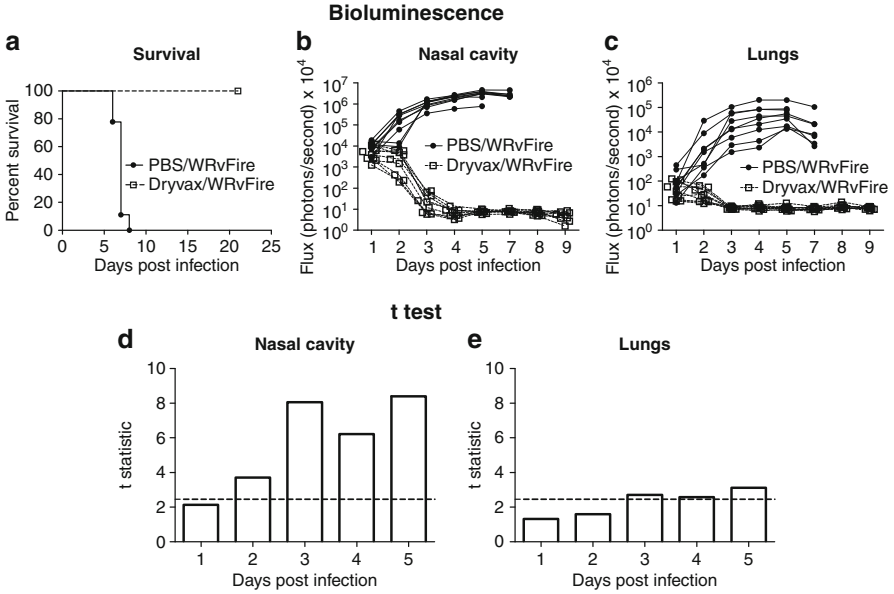

Fig. 9.2 Survival curves (**a**), bioluminescence in the nasal cavity (**b**), and lungs (**c**), and *t* statistics of the mean fluxes measured in the nasal cavity (**d**) and lungs (**e**) in mice that were challenged with WRvFire following immunization with Dryvax vaccine (on week 2). **b** and **c** illustrate the differences in the means of total fluxes between control animals (unimmunized, *closed circles*, $n=9$) and mice that were immunized with Dryvax vaccine (*open squares*, $n=9$) and survived challenge. **d** and **e** show significant differences in fluxes between Dryvax-vaccinated and control mice on days 2–5 in the nasal cavity and on days 3–5 for the lungs, $t \geq 2.12$ (shown as *dashed line*)

Mean photon fluxes were compared between control and immunized mice using *t* tests. Values of the *t* statistic above 2.12 (Fig. 9.2d, e, dashed lines) correspond to significant differences ($p<0.05$) for groups of nine mice. Calculated *t* values were above this critical value for the photon fluxes in the Dryvax-vaccinated mice on days 2–5 and 3–5 in the nasal cavity and lungs, respectively (Fig. 9.2d, e). These data showed that Dryvax-immunized mice all survived lethal challenge and had either no bioluminescence signal in internal organs or significantly lower signals in the upper respiratory track compared with control mice. Therefore, in this scenario, representing sterilizing immunity due to a potent vaccine, a direct comparison of means of photon fluxes using *t*-tests can be sufficient to support the efficacy of treatment.

9.5.2 Usage of Bioluminescence Recording to Predict Lethality When 100 % Effectiveness of Treatment Is Not Expected

To illustrate a situation when treatment protects only a proportion of animals or, in other words, only a proportion of animals "respond" to treatment with a desirable outcome, we employed a more suitable statistical approach. Two hundred (200) BALB/c mice

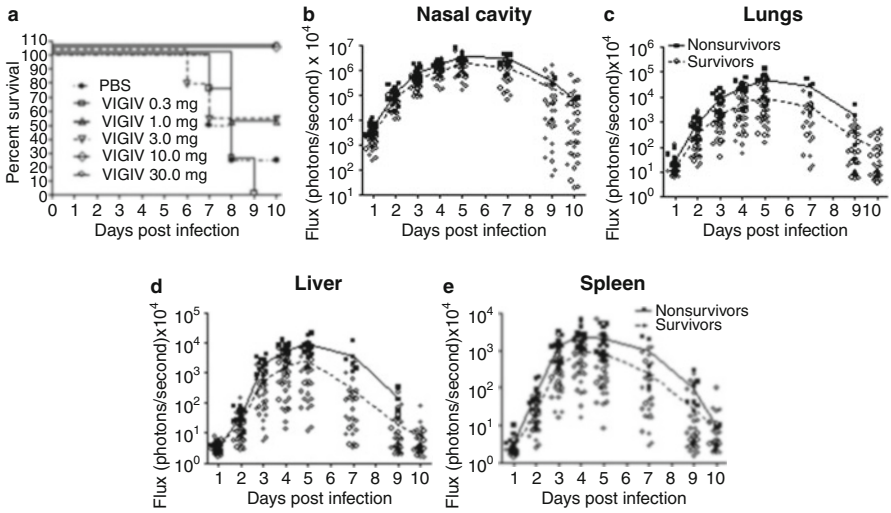

Fig. 9.3 Survival and bioluminescence in WRvFire-challenged mice that received pretreatment with VIGIV. Two hundred BALB/c mice (4–6 per group) received i.p. injections of VIGIV at doses 0.3, 1.0, 3.0, 10.0, and 30.0 mg per animal (or PBS in controls) 2 days before intranasal challenge. (**a**) The number of live mice was recorded each day and was used to calculate the percent survival. (**b–e**) The bioluminescence data per site/organ were obtained from six experiments. Daily fluxes in internal organs of surviving (*open circles*) and non-surviving mice (*closed circles*) of individual animals are shown. Total fluxes in the nasal cavity (**b**), lungs (**c**), liver (**d**), and spleen (**e**) were used to calculate means of total fluxes for surviving (*broken lines*) and non-surviving animals (*solid lines*). Total fluxes of 25 % of non-surviving (*closed symbols*) and 25 % surviving animals (*open symbols*) at each time point were randomly chosen using Excel's sampling for plotting in the graph

were treated IP with human Anti-Vaccinia Immunoglobulin for Intravenous use (VIGIV, Cangene Corporation, Winnipeg, Canada) at 5 doses ranging from 0.3 to 30 mg/animal or with PBS in controls, and 2 days later all mice were challenged with a lethal dose of WRvFire (Zaitseva et al. 2009). The study resulted in a true dose–response of none to 100 % of the lethally challenged mice to prophylaxis treatment with VIGIV (Fig. 9.3a). Bioluminescence recordings were acquired in all animals daily and mean photon fluxes in 4 organs of survived mice ($n=147$) and non-survived mice ($n=53$) were determined (Fig. 9.3b–e, closed vs. open symbols, respectively). Statistical analysis involved a *t* test of the means of fluxes recorded in individual mice. Although *t*-tests showed that mean fluxes were significantly different between surviving and non-surviving mice in all organs, some overlap in the signals was noted among the groups. These data prompted us to identify a statistical tool predictive of protection from lethality based on *threshold bioluminescence.*

Receiver operating characteristic (ROC) curve analysis is a graphical statistical tool that quantifies the ability of a prediction score to distinguish between "responders" and "nonresponders" by plotting *sensitivity* versus *1-specificity* for a binary classifier system as its discrimination threshold varies. As demonstrated in Fig. 9.4, four scenarios are possible for each predicted outcome: (1) bioluminescence in mice that did not survive could be above threshold (true positive, TP) or

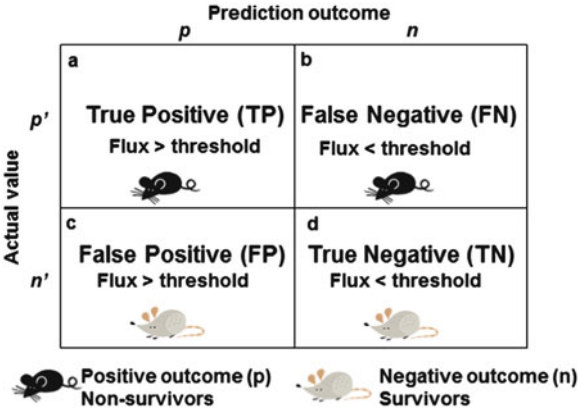

Fig. 9.4 *Confusion matrix* describing actual and predicted lethality in BALB/c mice challenged with WRvFire after they received prophylaxis treatment with VIGIV. This table explains the possible outcomes of a binary prediction rule. Study animals fall into four possible categories: (**a**) True positives are mice that died (positive outcome, p′) and were correctly predicted to die based on the levels of bioluminescence above threshold (positive prediction, p); (**b**) false negatives are mice that died (p′) and were incorrectly predicted to survive (negative prediction, n) based on the levels of bioluminescence below threshold; (**c**) false positives are mice that survived (negative outcome, n′) and were incorrectly predicted to die (p); (**d**) true negatives are mice that survived (n′) and were correctly predicted to survive (n)

(2) below threshold (false negative, FN); similarly, (3) mice that survived could exhibit signal below threshold (true negative, TN) or (4) exhibit signal above threshold (false positive, FP). Based on this assumption, the *sensitivity* of a prediction threshold is calculated as the ratio of the number of mice correctly predicted to die based on the level of bioluminescence to the number of all mice that died, TP/(TP+FN), and *specificity* is calculated as the ratio of the number of mice that had signal below threshold and survived to the total number of survived mice, TN/(FP+TN). Knowing the lethality/survival outcome for all 200 animals, sensitivity was plotted against 1-specificity for each value of recorded flux to calculate area under the ROC curve (AUC) for predictions based on bioluminescence levels in each of the four organs and for each of the days 1–5 following VACV challenge. The 5-day time frame for AUC analysis was selected based on the observation that all mice were alive during the first 5 days p.i. (Fig. 9.3a). Thus, bioluminescence recordings obtained during the first 5 days could be compared between mice that eventually survived or did not survive the challenge (Fig. 9.5). The highest AUC of 0.88–0.91 and of 0.91–0.87 were calculated for days 3–5 in the liver and spleen, respectively, suggesting that measurements of bioluminescence in these organs at these time points predicted lethality with greatest accuracy (Fig. 9.5). This approach showed that ROC analysis of the bioluminescence recordings can serve as a useful prediction tool when 100 % effectiveness of the treatment is not expected.

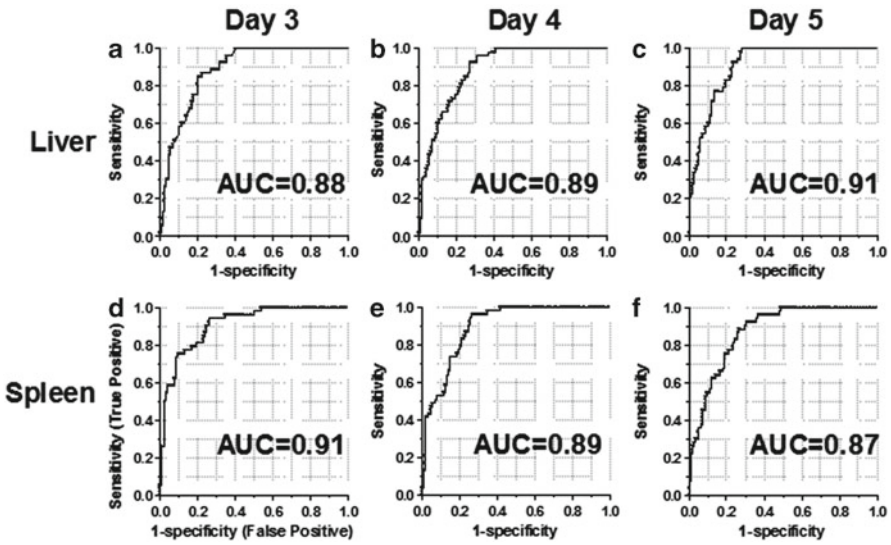

Fig. 9.5 ROC analyses of total fluxes in surviving and non-surviving mice. AUC values for liver (**a–c**) and spleen (**d–f**) were computed on days 3, 4, and 5 using fluxes recorded in mice described in the legend of Fig. 9.3 on days 1–5 post infection. This figure illustrates graphic format of ROC analysis

9.5.3 Usage of Bioluminescence to Assess the Effects of Doses on the Outcome of Treatment

In the third scenario, we used *t*-tests to determine the effects of treatment doses on viral loads (as assayed by recorded bioluminescence) in a given organ on a given day post challenge (Fig. 9.6). Groups of BALB/c mice (12 animals per group) received VIGIV at 30 mg/animal (open triangles) or 3 mg/animal (open squares) or PBS in controls (closed circles) 2 days prior to lethal challenge with WRvFire (Fig. 9.6a–e) or with IHD-J-Luc VACV (Fig. 9.6f–j) (Zaitseva et al. 2011). All control mice died within 1 week (Fig. 9.6a, f, closed circles); VIGIV at 30 mg protected 100 % of animals in both infections (Fig. 9.6a, f, open triangles). However, VIGIV at 3 mg protected only 33 and 17 % of mice infected with WRvFire or with IHD-J-Luc, respectively (Fig. 9.6a, f, open squares). Bioluminescence was recorded in all animals daily and mean photon fluxes per organ per group were calculated and plotted. As can be seen in Fig. 9.6b–e and g–j, viral loads in all survived mice returned to baseline levels on days 10–14.

To determine if treatment with the two doses of VIGIV significantly affected viral loads in each organ, mean photon fluxes were compared between control and treated mice using *t*-tests (*t* critical value = 2.07 for groups of 12 mice; dotted lines in Fig. 9.6k–r). In the nasal cavity, there were no significant differences in viral

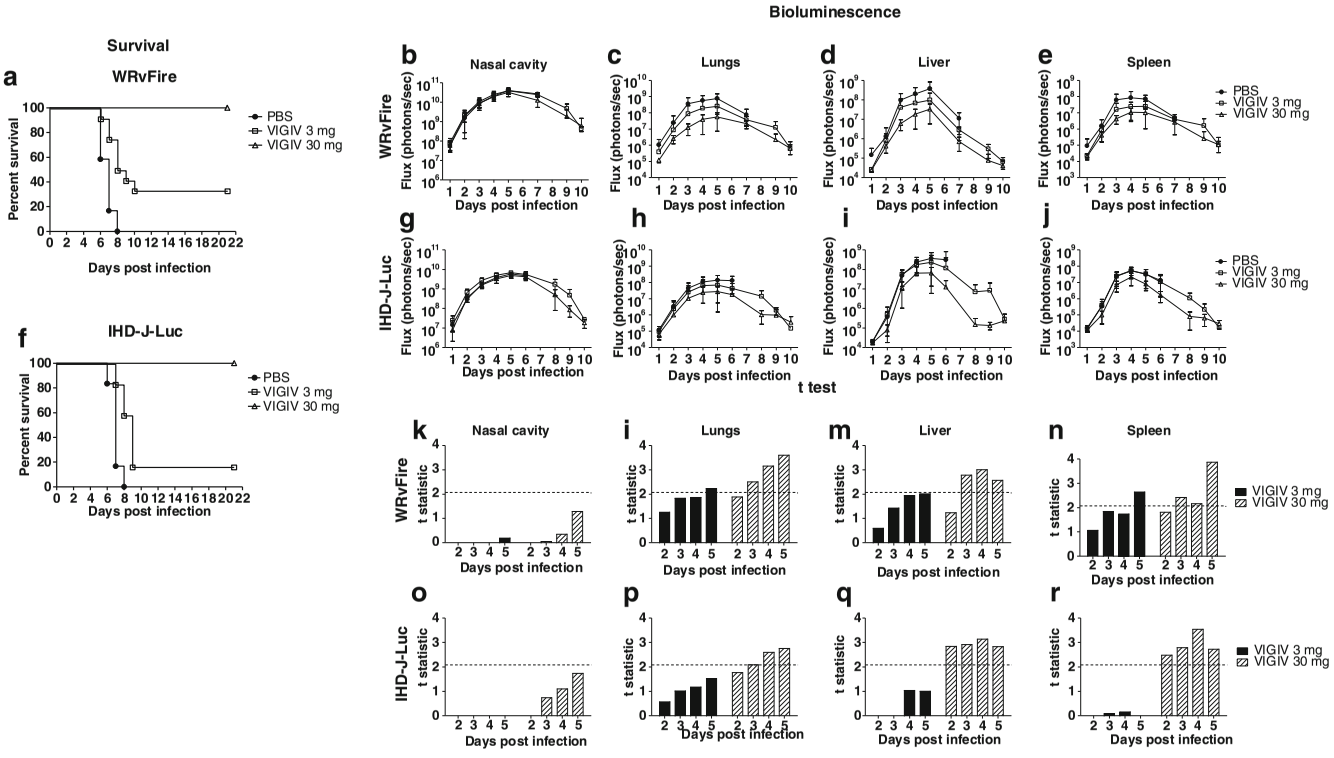

Fig. 9.6 (**a**–**f**) BALB/c mice (12 animals per group) received VIGIV at 30 mg/animal (*open triangles*) or 3 mg/animal (*open squares*) or PBS in controls (*closed circles*) 2 days prior to lethal challenge with WRvFire. Lethality Kaplan–Meier survival curves. (**b**–**e**) and (**g**–**j**). Bioluminescence, and *t*-tests of means of fluxes in mice that were treated with VIGIV and challenged with WRvFire or IHD-J-Luc VACV. Six BALB/c mice per group received PBS (*closed circles*) or VIGIV at 30 mg/animal (*open triangles*) or at 3 mg/animal (*open squares*) and were challenged 2 days later with WRvFre (**a**–**e**) or with IHD-J-Luc (**f**–**j**). Bioluminescence was recorded and used to calculate mean fluxes ± STDEV in the nasal cavity (**b**, **g**), lungs (**c**, **h**), liver (**d**, **i**), and spleen (**e**, **j**). (**k**–**n**, **o**–**r**) Significant differences (*t* values above *dotted lines*) between fluxes recorded in control mice and mice that received 3 mg (*solid bars*) or 30 mg (*hatched bars*) of VIGIV per animal and that were challenged with WRvFire or with IHD-J-Luc are shown in panels **k**–**n** and **o**–**r**, respectively. This figure illustrates a relationship between protection from lethality conferred by 30 mg of VIGIV and significant reduction in viral loads in three organs (lungs, liver, and spleen) on three consecutive days, days 3, 4, and 5

loads between VIGIV-treated and control mice for either dose of VIGIV at any time points in either virus infection (Fig. 9.6 panels k and o). In the lungs, liver, and spleen, viral loads were significantly different between mice that were treated with a 30 mg dose but not with 3 mg dose of VIGIV and control mice (hatched and solid bars, respectively), between days 3 and 5 (panels i–n in WRvFire infection and panels p–r in IHD-J-Luc infection). These statistical analyses demonstrated a correlation between protection from lethality and significant reduction in viral loads in 3 organs (lungs, liver, and spleen) on 3 consecutive days (days 3–5 p.i.). It also showed that significant reduction in viral loads for only 1 or 2 days in any individual site, as shown for VIGIV at 3 mg, did not confer protection from lethality (Fig. 9.6 panels i, m, and n, filled bars). Furthermore, these analyses underscore the conclusion that measurements of bioluminescence at a single time point may not be sufficient for assessing the efficacy of treatment. Accurate prediction of drug effectiveness might be improved by bioimaging at multiple time points and in several key organs as illustrated below.

9.5.4 Calculation of Areas Under the Flux Curve (AUC) for the Entire Survival Period Post Challenge

In the fourth scenario, we employed analysis of bioluminescence in infected mice to relate the efficacy of post-challenge treatment to the day of treatment initiation. In this approach, BALB/c mice were infected with IHD-J-Luc VACV and were treated IP with the antiviral drug Cidofovir (100 mg/kg dose) at 1, 2, 3, or 4 days post challenge. Controls were administered PBS (Fig. 9.7). Cidofovir is approved for treatment of cytomegalovirus (CMV) retinitis in AIDS patients and is the only antiviral compound approved by CDC for postexposure treatment of smallpox virus infections; see the Web site: http://www.bt.cdc.gov/agent/smallpox/vaccination/mgmt-adv-reactions.asp. All no-treatment control mice succumbed within 1 week (Fig. 9.7a, black curves), while all mice that received Cidofovir starting on day 1, 2, or 3 p.i. survived (Fig. 9.7a, red, blue, and green curves, respectively). Five out of six mice (83 %) survived when treatment was initiated on day 4 p.i. (Fig. 9.7a, purple curves). Mice were subjected to bioimaging daily and the recorded bioluminescence from individual mice was used to calculate and to plot mean photon fluxes for groups of six mice per group in the nasal cavity, lungs, liver, and spleen (Fig. 9.7b–e). As depicted in Fig. 9.7b–e, the bioluminescence signal returned to background levels in the lungs, liver, and spleen in all survived animals by day 14 p.i. and in the nasal cavity by day 30 (data not shown). Yet, there were clear differences in shapes of flux curves between groups suggesting that the delay in initiation of Cidofovir treatment post challenge might affect the kinetics of virus clearance.

To determine which delay in Cidofovir treatment significantly affected IHDJ-Luc viral loads, areas under the flux curves (AUC) were calculated for days 1–6 for all mice. These AUCs reflect the combined fluxes per organ per mouse representing cumulative viral loads during the observation period when all animals were still

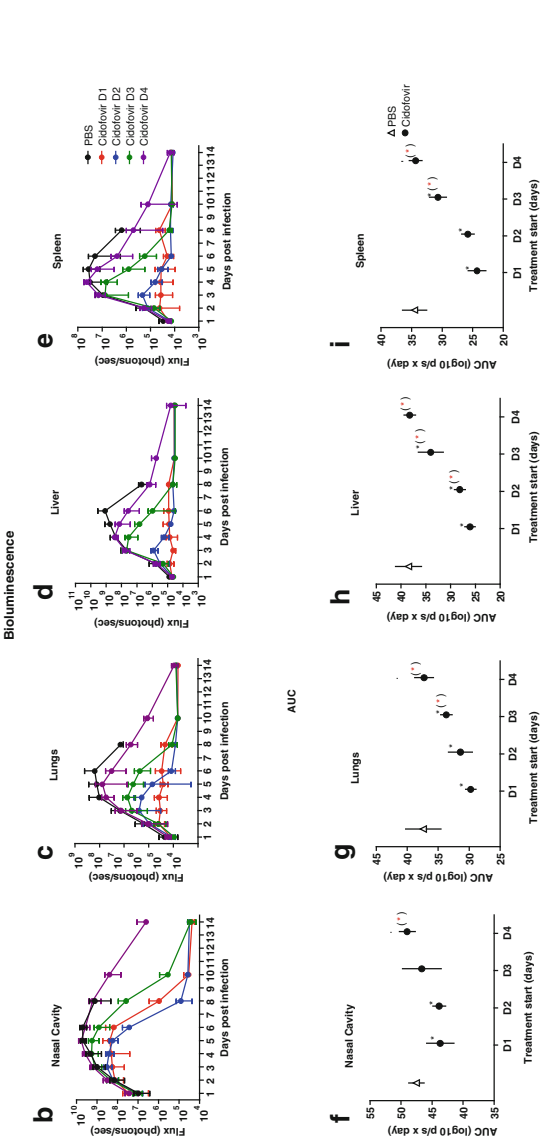

Fig. 9.7 (**a**–**i**) Survival curves, bioluminescence, and *t*-tests of the AUC for fluxes recorded in mice that received Cidofovir post challenge. BALB/c mice were infected with IHD-J-Luc and were treated with Cidofovir at 100 mg/kg on day 1 (*red curves*), day 2 (*blue curves*), day 3 (*green curves*), or day 4 (*purple curves*), or with PBS on day 1 (*black curves*) p.i. Mice were observed for survival (**a**) and bioluminescence was recorded and used to calculate mean fluxes ± STDEV in the nasal cavity (**b**), lungs (**c**), liver (**d**), and spleen (**e**). AUC for fluxes recorded between days 1 and 6 in the nasal cavity (**f**), lungs (**g**), liver (**h**), and spleen (**i**) in control mice (*open triangles*) and in mice that received Cidofovir at days 1, 2, 3, or 4 were computed and comparisons were made with *t*-tests. Black asterisks denote significant differences in AUC (viral loads) between control mice (*open triangles*) and mice that received Cidofovir (*closed circles*); asterisks in parenthesis denote significant differences in AUC (viral loads) between mice that received Cidofovir on day 1 versus day 2, 3, or 4 ($p \leq 0.05$)

alive (days 1–6 p.i.). Mean AUCs for groups of mice were compared with *t*-tests. AUCs in the lungs, liver, and spleen were significantly different between untreated control mice (open triangles) and mice that received Cidofovir (closed circles) starting on day 1, 2, or 3 post challenge (Fig. 9.7g–i). In the nasal cavity, AUCs were significantly different between control and treated mice only when treatment was delayed for 1 or 2 days (Fig. 9.7f). Although treatment initiated on day 4 p.i. rescued 83 % of animals from lethality, it failed to significantly reduce AUC (as a depiction of viral loads) compared to control mice in any of the organs that exhibited bioluminescence. We also compared AUCs between treatment groups only and found significant differences in the AUC in mice that initiated Cidofovir treatment on day 1 compared with day 3 or 4 (in the lungs, spleen, and liver). There were no significant differences in lethality or in viral loads if Cidofovir was administered on day 1 or 2 p.i. However, longer delay of ≥ 3 days was found to be protective from lethality, but was less efficient in reducing viral loads in all four organs.

9.6 Conclusions

Altogether our data showed that the use of bioluminescence imaging as a quantitative tool for assessing replication and dissemination of VACV in live mice, combined with a set of statistical tools (the *t* test, AUC, and ROC analysis), allowed us to (1) conserve significantly in the number of animals needed, (2) monitor dissemination of the virus within the same host over time including assessment of replication in hard-to-access anatomical sites within reasonable limits of detection, (3) generate models for prediction of lethality, and (4) gain insight regarding the effects of antiviral treatments on virus distribution over time and the quantitation of organ burdens (proportional to light intensity) as it relates to protection from lethality. Dissemination to the skin (i.e., pox formation) was also monitored. The bioimaging provides additional important information on the drug–pathogen–host interactions that correlate with organ pathology and between-host transmissibility that cannot be fully appreciated with the traditional models.

References

Amanna IJ, Slifka MK, Crotty S (2006) Immunity and immunological memory following smallpox vaccination. Immunol Rev 211:320–337

Andreu N, Zelmer A, Fletcher T, Elkington PT, Ward TH, Ripoll J, Parish T, Bancroft GJ, Schaible U, Robertson BD, Wiles S (2010) Optimisation of bioluminescent reporters for use with mycobacteria. PLoS One 5:e10777

Baker RO, Bray M, Huggins JW (2003) Potential antiviral therapeutics for smallpox, monkeypox and other orthopoxvirus infections. Antiviral Res 57:13–23

Belongia EA, Naleway AL (2003) Smallpox vaccine: the good, the bad, and the ugly. Clin Med Res 1:87–92

Berger F, Paulmurugan R, Bhaumik S, Gambhir SS (2008) Uptake kinetics and biodistribution of 14C-D-luciferin–a radiolabeled substrate for the firefly luciferase catalyzed bioluminescence reaction: impact on bioluminescence based reporter gene imaging. Eur J Nucl Med Mol Imaging 35:2275–2285

Bernthal NM, Stavrakis AI, Billi F, Cho JS, Kremen TJ, Simon SI, Cheung AL, Finerman GA, Lieberman JR, Adams JS, Miller LS (2010) A mouse model of post-arthroplasty Staphylococcus aureus joint infection to evaluate in vivo the efficacy of antimicrobial implant coatings. PLoS One 5:e12580

Bina XR, Miller MA, Bina JE (2010) Construction of a bioluminescence reporter plasmid for Francisella tularensis. Plasmid 64:156–161

Burke CW, Mason JN, Surman SL, Jones BG, Dalloneau E, Hurwitz JL, Russell CJ (2011) Illumination of parainfluenza virus infection and transmission in living animals reveals a tissue-specific dichotomy. PLoS Pathog 7:e1002134

Collins JW, Akin AR, Kosta A, Zhang N, Tangney M, Francis KP, Frankel G (2012) Pre-treatment with Bifidobacterium breve UCC2003 modulates Citrobacter rodentium-induced colonic inflammation and organ specificity. Microbiology 158:2826–2834

Contag CH, Bachmann MH (2002) Advances in in vivo bioluminescence imaging of gene expression. Annu Rev Biomed Eng 4:235–260

Contag CH, Contag PR, Mullins JI, Spilman SD, Stevenson DK, Benaron DA (1995) Photonic detection of bacterial pathogens in living hosts. Mol Microbiol 18:593–603

Cook SH, Griffin DE (2003) Luciferase imaging of a neurotropic viral infection in intact animals. J Virol 77:5333–5338

Doyle TC, Nawotka KA, Kawahara CB, Francis KP, Contag PR (2006) Visualizing fungal infections in living mice using bioluminescent pathogenic Candida albicans strains transformed with the firefly luciferase gene. Microb Pathog 40:82–90

Edghill-Smith Y, Golding H, Manischewitz J, King LR, Scott D, Bray M, Nalca A, Hooper JW, Whitehouse CA, Schmitz JE, Reimann KA, Franchini G (2005) Smallpox vaccine-induced antibodies are necessary and sufficient for protection against monkeypox virus. Nat Med 11:740–747

Enjalbert B, Rachini A, Vediyappan G, Pietrella D, Spaccapelo R, Vecchiarelli A, Brown AJ, d'Enfert C (2009) A multifunctional, synthetic Gaussia princeps luciferase reporter for live imaging of Candida albicans infections. Infect Immun 77:4847–4858

Fenner F, Henderson DA, Arita I, Jezek Z, Ladnyi ID (1988) Smallpox and its iradication. World Health Organization, Geneva, Switzerland

Francis KP, Joh D, Bellinger-Kawahara C, Hawkinson MJ, Purchio TF, Contag PR (2000) Monitoring bioluminescent Staphylococcus aureus infections in living mice using a novel luxABCDE construct. Infect Immun 68:3594–3600

Francis KP, Yu J, Bellinger-Kawahara C, Joh D, Hawkinson MJ, Xiao G, Purchio TF, Caparon MG, Lipsitch M, Contag PR (2001) Visualizing pneumococcal infections in the lungs of live mice using bioluminescent Streptococcus pneumoniae transformed with a novel gram-positive lux transposon. Infect Immun 69:3350–3358

Glomski IJ, Piris-Gimenez A, Huerre M, Mock M, Goossens PL (2007) Primary involvement of pharynx and peyer's patch in inhalational and intestinal anthrax. PLoS Pathog 3:e76

Gould SJ, Subramani S (1988) Firefly luciferase as a tool in molecular and cell biology. Anal Biochem 175:5–13

Hammarlund E, Lewis MW, Hansen SG, Strelow LI, Nelson JA, Sexton GJ, Hanifin JM, Slifka MK (2003) Duration of antiviral immunity after smallpox vaccination. Nat Med 9:1131–1137

Henderson DA, Inglesby TV, Bartlett JG, Ascher MS, Eitzen E, Jahrling PB, Hauer J, Layton M, McDade J, Osterholm MT, O'Toole T, Parker G, Perl T, Russell PK, Tonat K (1999) Smallpox as a biological weapon: medical and public health management. Working Group on Civilian Biodefense. JAMA 281:2127–2137

Hooper JW, Thompson E, Wilhelmsen C, Zimmerman M, Ichou MA, Steffen SE, Schmaljohn CS, Schmaljohn AL, Jahrling PB (2004) Smallpox DNA vaccine protects nonhuman primates against lethal monkeypox. J Virol 78:4433–4443

Hutchens MA, Luker KE, Sonstein J, Nunez G, Curtis JL, Luker GD (2008) Protective effect of Toll-like receptor 4 in pulmonary vaccinia infection. PLoS Pathog 4:e1000153

Kadurugamuwa JL, Sin LV, Yu J, Francis KP, Kimura R, Purchio T, Contag PR (2003) Rapid direct method for monitoring antibiotics in a mouse model of bacterial biofilm infection. Antimicrob Agents Chemother 47:3130–3137

Krug A, Luker GD, Barchet W, Leib DA, Akira S, Colonna M (2004) Herpes simplex virus type 1 activates murine natural interferon-producing cells through toll-like receptor 9. Blood 103: 1433–1437

Lang T, Goyard S, Lebastard M, Milon G (2005) Bioluminescent Leishmania expressing luciferase for rapid and high throughput screening of drugs acting on amastigote-harbouring macrophages and for quantitative real-time monitoring of parasitism features in living mice. Cell Microbiol 7:383–392

Lee KH, Byun SS, Paik JY, Lee SY, Song SH, Choe YS, Kim BT (2003) Cell uptake and tissue distribution of radioiodine labelled D-luciferin: implications for luciferase based gene imaging. Nucl Med Commun 24:1003–1009

Lin MZ, McKeown MR, Ng HL, Aguilera TA, Shaner NC, Campbell RE, Adams SR, Gross LA, Ma W, Alber T, Tsien RY (2009) Autofluorescent proteins with excitation in the optical window for intravital imaging in mammals. Chem Biol 16:1169–1179

Luker GD, Bardill JP, Prior JL, Pica CM, Piwnica-Worms D, Leib DA (2002) Noninvasive bioluminescence imaging of herpes simplex virus type 1 infection and therapy in living mice. J Virol 76:12149–12161

Luker GD, Prior JL, Song J, Pica CM, Leib DA (2003) Bioluminescence imaging reveals systemic dissemination of herpes simplex virus type 1 in the absence of interferon receptors. J Virol 77:11082–11093

Luker KE, Hutchens M, Schultz T, Pekosz A, Luker GD (2005) Bioluminescence imaging of vaccinia virus: effects of interferon on viral replication and spread. Virology 341:284–300

Luker KE, Luker GD (2008) Applications of bioluminescence imaging to antiviral research and therapy: multiple luciferase enzymes and quantitation. Antiviral Res 78:179–187

Morin CE, Kaper JB (2009) Use of stabilized luciferase-expressing plasmids to examine in vivo-induced promoters in the Vibrio cholerae vaccine strain CVD 103-HgR. FEMS Immunol Med Microbiol 57:69–79

Neyts J, De Clercq E (2003) Therapy and short-term prophylaxis of poxvirus infections: historical background and perspectives. Antiviral Res 57:25–33

Nham T, Filali S, Danne C, Derbise A, Carniel E (2012) Imaging of bubonic plague dynamics by in vivo tracking of bioluminescent Yersinia pestis. PLoS One 7:e34714

Panchanathan V, Chaudhri G, Karupiah G (2007) Correlates of protective immunity in poxvirus infection: where does antibody stand? Immunol Cell Biol 86:80–86

Paroo Z, Bollinger RA, Braasch DA, Richer E, Corey DR, Antich PP, Mason RP (2004) Validating bioluminescence imaging as a high-throughput, quantitative modality for assessing tumor burden. Mol Imaging 3:117–124

Patterson M, Poussard A, Taylor K, Seregin A, Smith J, Peng BH, Walker A, Linde J, Salazar M, Paessler S (2011) Rapid, non-invasive imaging of alphaviral brain infection: reducing animal numbers and morbidity to identify efficacy of potential vaccines and antivirals. Vaccine 29:9345–9351

Rhee KJ, Cheng H, Harris A, Morin C, Kaper JB, Hecht G (2011) Determination of spatial and temporal colonization of enteropathogenic E. coli and enterohemorrhagic E. coli in mice using bioluminescent in vivo imaging. Gut Microbes 2:34–41

Rimoin AW, Mulembakani PM, Johnston SC, Lloyd Smith JO, Kisalu NK, Kinkela TL, Blumberg S, Thomassen HA, Pike BL, Fair JN, Wolfe ND, Shongo RL, Graham BS, Formenty P, Okitolonda E, Hensley LE, Meyer H, Wright LL, Muyembe JJ (2010) Major increase in human monkeypox incidence 30 years after smallpox vaccination campaigns cease in the Democratic Republic of Congo. Proc Natl Acad Sci USA 107:16262–16267

Rodriguez JF, Rodriguez D, Rodriguez JR, McGowan EB, Esteban M (1988) Expression of the firefly luciferase gene in vaccinia virus: a highly sensitive gene marker to follow virus dissemination in tissues of infected animals. Proc Natl Acad Sci USA 85:1667–1671

Roy G, Dumas C, Sereno D, Wu Y, Singh AK, Tremblay MJ, Ouellette M, Olivier M, Papadopoulou B (2000) Episomal and stable expression of the luciferase reporter gene for quantifying Leishmania spp. infections in macrophages and in animal models. Mol Biochem Parasitol 110:195–206

Saeij JP, Boyle JP, Grigg ME, Arrizabalaga G, Boothroyd JC (2005) Bioluminescence imaging of Toxoplasma gondii infection in living mice reveals dramatic differences between strains. Infect Immun 73:695–702

Schoggins JW, Dorner M, Feulner M, Imanaka N, Murphy MY, Ploss A, Rice CM (2012) Dengue reporter viruses reveal viral dynamics in interferon receptor-deficient mice and sensitivity to interferon effectors in vitro. Proc Natl Acad Sci USA 109:14610–14615

Sha J, Rosenzweig JA, Kirtley ML, van Lier CJ, Fitts EC, Kozlova EV, Erova TE, Tiner BL, Chopra AK (2013) A non-invasive in vivo imaging system to study dissemination of bioluminescent Yersinia pestis CO92 in a mouse model of pneumonic plague. Microb Pathog 55:39–50

Sweeney TJ, Mailander V, Tucker AA, Olomu AB, Zhang W, Cao Y, Negrin RS, Contag CH (1999) Visualizing the kinetics of tumor-cell clearance in living animals. Proc Natl Acad Sci USA 96:12044–12049

Troy T, Jekic-McMullen D, Sambucetti L, Rice B (2004) Quantitative comparison of the sensitivity of detection of fluorescent and bioluminescent reporters in animal models. Mol Imaging 3:9–23

Whitley RJ (2003) Smallpox: a potential agent of bioterrorism. Antiviral Res 57:7–12

Xiong YQ, Willard J, Kadurugamuwa JL, Yu J, Francis KP, Bayer AS (2005) Real-time in vivo bioluminescent imaging for evaluating the efficacy of antibiotics in a rat Staphylococcus aureus endocarditis model. Antimicrob Agents Chemother 49:380–387

Zaitseva M, Kapnick SM, Meseda CA, Shotwell E, King LR, Manischewitz J, Scott J, Kodihalli S, Merchlinsky M, Nielsen H, Lantto J, Weir JP, Golding H (2011) Passive immunotherapies protect WRvFire and IHD-J-Luc vaccinia virus-infected mice from lethality by reducing viral loads in the upper respiratory tract and internal organs. J Virol 85:9147–9158

Zaitseva M, Kapnick SM, Scott J, King LR, Manischewitz J, Sirota L, Kodihalli S, Golding H (2009) Application of bioluminescence imaging to the prediction of lethality in vaccinia virus-infected mice. J Virol 83:10437–10447

Zhang Y, Pullambhatla M, Laterra J, Pomper MG (2012) Influence of bioluminescence imaging dynamics by D-luciferin uptake and efflux mechanisms. Mol Imaging 11:499–506

Chapter 10
Preclinical Imaging in BSL-3 and BSL-4 Environments: Imaging Pathophysiology of Highly Pathogenic Infectious Diseases

Lauren Keith, Svetlana Chefer, Laura Bollinger, Jeffrey Solomon, Srikanth Yellayi, Jurgen Seidel, David Thomasson, and Peter Jahrling

Abstract Structural and functional imaging are emerging as powerful tools for studying highly pathogenic infectious disease processes. Nuclear imaging modalities and sophisticated radiolabeled probes can be used to track physiological or biochemical processes associated with viral infection. Magnetic resonance imaging can provide anatomical images with exquisite soft tissue contrast, while magnetic resonance spectroscopy can measure the relative amounts of certain metabolites in a given tissue. However, conducting medical imaging studies in a high-containment laboratory requires advanced applications and modification not only of image acquisition and analysis processes but also of the imaging equipment. Processes such as ex vivo labeling of cells are hampered by the personal protective equipment required for the safety of laboratory personnel. Modification of medical imaging equipment can prevent contamination of the equipment. Regardless of the challenges involved, medical imaging could provide valuable information to researchers developing therapeutics against highly pathogenic infectious diseases.

L. Keith, Ph.D. (✉) • S. Chefer, Ph.D. • L. Bollinger • J. Solomon, Ph.D
S. Yellayi, B.V.Sc., Ph.D. Diplomate ACVP • J. Seidel, Ph.D. • D. Thomasson, Ph.D.
Integrated Research Facility, National Institutes of Allergy and Infectious Diseases, National Institutes of Health, Frederick, MD, USA
e-mail: Lauren.keith@nih.gov

P. Jahrling, Ph.D.
Integrated Research Facility, National Institutes of Allergy and Infectious Diseases, National Institutes of Health, Frederick, MD, USA

Emerging Viral Pathogens Section, National Institute of Allergy and Infectious Diseases, National Institutes of Health, Bethesda, MD, USA

B.R. Moyer et al. (eds.), *Pharmaco-Imaging in Drug and Biologics Development*, AAPS Advances in the Pharmaceutical Sciences Series 8, DOI 10.1007/978-1-4614-8247-5_10,

10.1 Benefits of Medical Imaging in Infectious Disease Research and Drug Development

In vivo medical imaging is emerging as a powerful supplement to conventional studies of viral pathogenesis and treatment. Imaging techniques have the potential to become influential and informative tools that could be applied to many steps in the drug development process. In general, one substantial benefit associated with medical imaging in highly pathogenic infectious disease research and drug development is the potential for longitudinal studies in a single subject with minimal interference with physiological processes and disease development. As opposed to conventional studies based around euthanasia and necropsy of infected subjects at various time points along the disease process, this longitudinal approach could increase the statistical relevance while decreasing the number of subjects needed to assess the efficacy of an investigational drug or treatment (Rudin and Weissleder 2003).

The drug development process is a time-consuming and expensive venture that involves many steps prior to approval. Both the financial and temporal burdens of many of the required phases might be mitigated with the use of medical imaging technologies. For example, the first step in the development of a new drug or biologic is the identification of the drug target, such as proteins and enzymes encoded by viruses. By developing and using specialized probes that bind to the drug targets, medical imaging could verify the presence and characterize the spatial and temporal distribution of intended targets (Willmann et al. 2008). After a target is chosen, high-throughput screening of compound libraries identifies experimental drugs or chemicals that have the desired effect on the target (Willmann et al. 2008; Valadon et al. 2006). Molecular imaging techniques could assess gene–protein interactions during this step of compound identification (Luker et al. 2003; Sharma et al. 2002). Also, by labeling investigational drugs, imaging could characterize the pharmacokinetics (e.g., accumulation and distribution over time) using various routes of administration and dosing schedules (Viglianti et al. 2004; Garg et al. 2008; Di Mascio et al. 2009; Bray et al. 2010; Ferro-Flores et al. 2012). The biodistribution of a drug interpreted from an image might give the first indication of the drug interacting with the intended target (Valadon et al. 2006). For example, small interfering RNAs (siRNAs) used to produce a therapeutic effect could be radiolabeled or conjugated to magnetic nanoparticles to verify tissue distribution or delivery of the molecules to the intended target using nuclear or magnetic resonance imaging (MRI) (Liu et al. 2007; Kumar et al. 2010). Furthermore, imaging techniques have the potential to quantify viral burden, assess the severity of infection or inflammation, track the host response to disease processes, and evaluate treatment outcomes throughout the life of the subject (Bray et al. 2010; Schellingerhout et al. 1998; Nahrendorf et al. 2006; Dotti et al. 2009; Jubeli et al. 2012). Biological, physiological, and molecular parameters assessed or quantified by imaging modalities may aid the drug development process by predicting the efficacy or safety of a new drug and serving as a surrogate for a clinical endpoint in controlled studies (Willmann et al. 2008; Wang and Deng 2010). Development of these parameters, collectively referred to as imaging biomarkers, could also facilitate evaluations of novel drug therapy (Rudin and Weissleder 2003).

Other considerations for the development of drugs and therapies for high consequence pathogens include the implementation of the FDA's "Animal Rule" (US Food and Drug Administration 2002). This rule applies to new drugs or biologics that are intended to treat or prevent disease that are either (1) very rare or (2) life-threatening or permanently debilitating. In the first case, clinical studies involving large patient populations are impractical, and historical data on these diseases are limited. In the second case, human studies are unethical, for obvious reasons. In these situations, investigators may forgo clinical trials if efficacy of a new drug or treatment procedure is evidenced by adequate well-controlled animal studies. Medical imaging could be used to support the assertion that the pathogenesis of the disease under question in selected animal models is similar to that in humans.

10.2 Image Acquisition and Analysis Strategies for Infectious Disease Research

10.2.1 Nuclear Imaging

Nuclear imaging modalities such as positron emission tomography (PET) and single-photon emission computed tomography (SPECT) are powerful, noninvasive techniques to visualize both location and number of infectious and inflammatory foci throughout the body. These techniques track physiological or biochemical processes at cellular and molecular levels. Application of nuclear imaging modalities focusing specifically on viral infection and diseases associated with biosafety level-3 (BSL-3) or BSL-4 pathogens has been limited. However, molecular imaging could provide a better understanding of viral infection progression and specific physiologic and metabolic changes that correspond to the efficacy of pharmaceutical therapies.

Clinically, a host response to infection can be studied by use of available isotopes and radiotracers that are not specific for a viral infection. Common features of most immune responses to an infection include increased blood supply, local or systemic changes in vascular permeability, and enhanced transudation. Beginning in the 1970s, cytomegalovirus pneumonitis and other infections in immunodeficient patients could be detected by administering an intravenous dose of Ga-67, which binds to circulating transferrin, and the in vivo biodistribution can be subsequently imaged with a gamma camera (Hamed et al. 1979; Reinders Folmer et al. 1986). Similar to other radiolabeled macromolecules such as proteins, polysaccharides, and polyamine derivatives proposed for imaging inflammation, Ga-67-transferrin complex extravasates at the site of inflammation as a result of increased blood flow and enhanced vascular permeability.

Other approaches to imaging infection include the intravenous infusion of In-111- or Tc-99m-labeled polyclonal human immunoglobulin (IgG), which is retained at sites of inflammation due to specific binding of IgG with Fc receptors

expressed on leukoctyes, which accumulate at the site of infection (Rubin and Fischman 1994). Radiolabeled IgG accumulation at infectious foci is mainly attributable to nonspecific extravasation or leakage of the labeled protein associated with increased vascular permeability. IgG radiolabeled with In-111 appears to have both high sensitivity and specificity for imaging human immunodeficiency virus (HIV)-infected patients (Buscombe et al. 1995).

A common practice in nuclear imaging is to use radiolabeled leukocytes that migrate to sites of infection and localize the sites of inflammation (Kumar 2005). Two approaches can be used for leukocyte labeling: in vivo and ex vivo. In vivo leukocyte labeling can be based on either antibody–antigen interaction or leukocyte receptor binding. Ex vivo labeling requires drawing a blood sample from the subject, isolating and purifying leukocyte population, radiolabeling with the appropriate radionuclides such as Tc-99m or In-111, and reinjecting the leukocytes into the subject. Ex vivo labeling requires additional lab space and equipment, is time intensive, and can subject laboratory staff to increased risk if blood samples contain a pathogenic agent. Therefore, ex vivo leukocyte labeling is not optimal for a BSL-4 environment. Regardless of the labeling strategy, imaging with radiolabeled leukocytes provides up to 90 % sensitivity for detection of both acute and chronic infection in the clinical setting (Wanahita et al. 2007).

Another way to image sites of viral infection or inflammation is with F-18 fluorodeoxyglucose (F-18 FDG), a nonspecific PET radiotracer that is trapped in cells in proportion to glycolytic activity. F-18 FDG PET imaging can be used to develop and evaluate new drugs for infectious diseases and monitor immune responses to newly developed treatments. Early in the HIV pandemic, for example, PET imaging with F-18 FDG demonstrated that regional or generalized alterations of cerebral glucose metabolism accompanying functional brain impairment in acquired immunodeficiency syndrome (AIDS) dementia can be reversed after effective antiviral (zidovudine) therapy (Yarchoan et al. 1987; Brunetti et al. 1989). The same technique has shown that peripheral lymph nodes have a greater glucose uptake in untreated HIV-infected patients than in patients on antiretroviral therapy, indicating that lymph nodes are a site of viral replication (Brust et al. 2006) or, alternatively, the increase could be due to uptake of F-18 FDG by clonal expanding lymphocytes. Computed tomography (CT) and F-18 FDG PET imaging of a patient with severe swine-origin H1N1 influenza indicated an intense inflammatory response revealed by an increase in F-18 FDG uptake in areas of dense pulmonary consolidation (characterized by higher Hounsfield units on CT images) as well as in regions of aerated lung (Bellani et al. 2010).

However, F-18 FDG is a nonspecific probe and incapable of differentiating inflammation from an infectious process. Therefore, other radiotracers that specifically quantify or characterize cell proliferation have been developed. For example, F-18 fluoro-3-deoxy-3-L-fluorothymidine (F-18 FLT) is monophosphorylated by thymidine kinase 1 (TK1) and remains trapped inside cells (Bading and Shields 2008). Since TK1 concentrations increase during the synthesis phase of the cell cycle, the uptake of F-18 FLT is believed to correlate with cell proliferation rather than with metabolic activity. Thus, F-18 FLT might be useful for identifying more

specific processes and mechanisms associated with immune response. Nevertheless, neither F-18 FDG nor F-18 FLT has any specificity towards any particular cell or tissue type. In contrast, 1-(29-deoxy-29-18F-fluoro-b-L-arabinofuranosyl)cytosine (F-18 FAC) represents a specific probe for lymphoid tissue (Bray et al. 2010; Shu et al. 2010). This probe targets deoxycytidine kinase, an enzyme involved in DNA synthesis through deoxyribonucleoside salvage pathway. Since deoxycytidine kinase is primarily expressed in lymphoid cells, F-18 FAC is considered a specific probe to study immune activation in vivo.

A different application of molecular imaging in infectious disease research is to label viruses directly using specific probes that bind to or are incorporated into viruses. The value of virus-specific radiopharmaceuticals is not only in the development of therapeutics against dangerous pathogens in animal models but also is to diagnose and formulate clinical decisions regarding therapy. New and improved radiotracers are being developed from several efficient antiviral drugs known to inhibit viral replication by binding to specific virion structural proteins or to the active sites of a viral enzyme. In addition, some antibodies are active against viral proteins expressed on the surface of infected cells. Such drugs and antibodies have been proposed for use as radiolabeled probes for the detection of viral infection (Bray et al. 2010) to visualize sites of viral replication in the body by in vivo imaging. Bray et al. identified a number of processes unique to viral replication that might serve as targets for radiolabeled, pathogen-specific tracers. They reviewed nine different DNA and RNA virus families and identified approved and experimental antiviral drugs that target virus-encoded molecules that might have potential as radiolabeled probes. A current example of this approach is the PET imaging of herpes simplex virus infections, in which the viral thymidine kinase phosphorylates thymidine analogues labeled with several different radionuclides, including C-11 or I-131, trapping them within infected cells (Gambhir et al. 2000). Finally, virus particles can be radiolabeled and tracked by in vivo imaging, providing a quantitative measure of viral burden (Schellingerhout et al. 1998; Rojas and Thorne 2012; Penheiter et al. 2012).

10.2.2 Magnetic Resonance Imaging

In contrast to other imaging modalities, MRI offers high, potentially submillimeter spatial resolution. Also, MR images exhibit superior soft tissue contrast compared to other imaging modalities, since the magnetic characteristics of tissues with similar electron densities can differ considerably. Magnetic resonance spectroscopy (MRS) measures the presence and relative amounts of certain metabolites based on the resonant frequencies of the metabolites present within a sample. Furthermore, unlike nuclear imaging, MR images can be obtained by exploiting only endogenous sources of contrast; exogenous and potentially harmful contrast agents are not a necessity. However, as will be discussed below, contrast agents can be used to probe certain cellular or molecular interactions. In general, an appreciable amount of flexibility is

associated with magnetic resonance techniques. This flexibility makes the modality appealing for infectious disease research in BSL-3 or BSL-4 environments.

Many viral hemorrhagic fevers (VHFs) are caused by pathogens that must be contained within a BSL-3 or BSL-4 environment. As the name suggests, VHFs are characterized in part by overall damage to the vascular system, often accompanied by hemorrhage and an increase in vascular permeability. A number of MRI techniques assess vascular permeability, integrity of the blood–brain barrier, and prevalence of hemorrhages in other nonviral diseases. Previously, dynamic contrast-enhanced MRI has been using to assay and quantify vascular permeability (Padhani et al. 2000; Floris et al. 2004; O'Connor et al. 2007; Cyran et al. 2012). Using an FDA-approved gadolinium diethylenetriaminepentaacetate (Gd-DTPA) contrast agent, Floris et al. reported a statistically significant increase in T1 values on quantitative T1 maps that were hypothesized to result from increased vascular permeability and subsequent leakage of the contrast agent. These measurements were used to objectively measure blood–brain barrier integrity (Floris et al. 2004). Cyran et al. used a macromolecular contrast medium and a dynamic image acquisition to estimate vascular permeability of tumors using a two-compartment model (Cyran et al. 2012). The calculated coefficients for endothelial permeability correlated with immunohistochemical measurements of vascular endothelial growth factor. Also, susceptibility-weighted imaging (Haacke et al. 2004) has been shown to be more sensitive in detecting hemorrhages and differentiating them from other physiological processes than classic T2*-weighted imaging techniques (Lobel et al. 2010). Liu et al. have used quantitative susceptibility mapping to objectively measure and assess the presence of as well as the physiologic burden of cerebral microhemorrhage (Liu et al. 2012). Approaches similar to these techniques would be beneficial to tracking both the loss of vascular integrity and prevalence and burden of hemorrhage with the progression of VHFs.

In addition to quantifying vascular permeability, MRI could potentially be used to track cell migration during viral infections. Recently, strategies for imaging cellular migration with MRI have been applied to tracking the distribution of stem cell therapies (Hoehn et al. 2007). In order to achieve a detectable level of contrast, cells of interest must be labeled prior to imaging. Many different, well-documented in vitro labeling strategies exist (Frank et al. 2003; Modo et al. 2005). However, similar to PET imaging tracers described above, in vivo labeling is preferred in a BSL-4 environment due to increased simplicity of the labeling process and avoidance of the risks associated with handling infected cells or tissue. Spontaneous, in vivo labeling of monocytes, macrophages, and other phagocytic cells can be achieved by systemic injection of a contrast agent that subsequently is incorporated into the cell by phagocytosis. Labeled cells then infiltrate areas of inflammation. Iron oxide nanoparticles, specifically ultrasmall paramagnetic iron oxides (USPIOs) or superparamagnetic iron oxides (SPIOs), have been successfully used as contrast agents to label phagocytic cells. Iron oxides produce areas of signal void, or hypointensity, in T2- or T2*-weighted MR images. In vivo labeling has been used to track macrophage infiltration in rat models of antigen-induced arthritis (Beckmann et al. 2003), inflammatory neurological disorders (Stoll et al. 2004), and ischemic brain

lesions (Kleinschnitz et al. 2003). Macrophage tracking would be extremely beneficial in the investigation of many infectious diseases. However, one challenge associated with this technique is the difficulty in distinguishing between SPIO-labeled cells and endogenous blood derivatives associated with hemorrhage that also exhibit hypointensity (Bulte 2009). This difficulty with detection of SPIO-induced loss of signal intensity may limit the efficacy of using SPIO-labeled cells for imaging viral hemorrhagic fevers or other diseases caused by BSL-3 or BSL-4 pathogens that are associated with hemorrhage.

Although viral hemorrhagic fevers or diseases caused by other exotic, high-consequence (BSL-4) viruses have not been imaged with MRI, patients infected with certain neurotropic viruses (BSL-3 viruses) have been imaged using MRI in the clinical setting. Japanese encephalitis virus is endemic in Southeast Asia (Umenai et al. 1985). Bilateral hemorrhagic thalamic involvement (Kumar et al. 1997) and bilateral white matter lesions (Shoji et al. 1994) have been detected by MRI in such virus-infected patients. Large outbreaks of West Nile virus disease occurred in United States in 2002 and 2003 (Hayes and Gubler 2006). Hyperintense lesions in the leptomeninges, cortex, subcortical white matter, brainstem, thalamus, and substantia nigra can be observed on T2-weighted clinical images (Jeha et al. 2003; Sejvar et al. 2003; Burton et al. 2004). While these publications are an appreciable benefit to clinical practice, well-controlled, experimental MRI studies in high-containment laboratories have not characterized the radiological presentation of these diseases. Such studies would be advantageous to both clinical diagnosis and drug treatment development.

10.2.3 Image Analysis

Many robust medical image processing techniques have been developed and validated in human subjects and phantoms in clinical and preclinical settings. To integrate medical imaging and infectious disease research in a BSL-3 or BSL-4 laboratory, techniques optimized for humans outside of containment need to be translated to small animals in high-containment environments. This translation is not without challenges.

For longitudinal studies of disease progression, all temporal scans of the subject should be aligned to the same spatial coordinate system using registration techniques. Such alignment is critical in providing quantitative data of rate of change of features during disease progression. This alignment is normally performed by automated image registration methods that benefit from considerable care in positioning the subject correctly and reproducibly in the scanner. In BSL-3 and BSL-4 environments, optimal subject placement is inherently more difficult due to restrictions of movement of personnel wearing positive-pressure suits or other personal protective equipment. Therefore, image registration methods must be robust to larger positional differences in subject orientation across scanning sessions in high containment than that occurring during sessions outside containment.

Atlas-based segmentation has become a common method to delineate anatomy in a medical image. For example, atlases of liver, brain, and other organs are used for image overlays in human research studies. In BSL-3 and BSL-4 environments, new animal atlases must be developed to utilize these segmentation strategies. Image segmentation is also more difficult in small animals than in humans due to the significantly smaller anatomy and corresponding decrease in the number of volume elements, or voxels, which represent a given area of interest within the image.

Many of the medical image analysis methods that have been developed and extensively validated were designed for the initial purpose of neuroimaging research (e.g., traumatic brain injury). These neuroimaging analysis methods must be translated to other organ systems necessary for the characterization of infectious disease and development of treatment.

10.2.4 Discovery and Validation of Imaging Biomarkers for Infectious Disease

Increasingly, medical imaging modalities provide either imaging biomarkers or surrogate endpoints for the costly and time-consuming process of drug development (Pien et al. 2005). An imaging biomarker is defined by extension of the Biomarkers Definitions Working Group (Biomarkers Definitions Working Group 2001) as "any anatomical, physiological, biochemical or molecular parameter detectable by one or more imaging modalities used to establish the presence or severity of disease" (Richter 2006). For example, the number of lesions identified on a T2-weighted MR image has been used as a surrogate endpoint for evaluating treatment response in patients with multiple sclerosis (Smith et al. 2003). Dynamic contrast-enhanced MRI markers, including blood flow, vessel permeability, or blood volume, have been used to assess reduction of vascularization of tumors in studies of antiangiogenic drugs (O'Connor et al. 2007). Enhanced standardized uptake value determined from an F-18 FDG PET image has been used as an imaging biomarker for tumor metabolism (O'Connor et al. 2008).

Traditionally, investigations into infectious disease pathogenesis or the development of vaccinations or therapeutics against these diseases rely heavily upon clinical assessments, clinical assays, standard techniques of virology and immunology, and histopathological findings in animal models. An appreciable challenge to integrating medical imaging into research conducted in high containment is the determination, development, and validation of imaging biomarkers that will quantify disease processes associated with the pathogens. Imaging studies performed with the intent of biomarker development must be prudently designed to correlate imaging biomarker data with at least one other, well-established method to prove the accuracy, precision, and sensitivity of the imaging biomarker (Smith et al. 2003). The risks of relying upon imaging biomarkers that have not been sufficiently validated beyond an individual study can be highly prejudicial, as these unvalidated biomarkers could negatively impact future studies.

Current and potential applications of clinical imaging modalities to infectious disease research have been reviewed above; however, the applications discussed were not necessarily designed to fulfill the requirements of an imaging biomarker. In an experimental study of nonhuman primate monkeypox virus (MPXV) disease model of human variola infection, serial F-18 FDG PET imaging has been used to identify inflammatory patterns of MPXV infection as predictors of disease outcome (Dyall et al. 2011, 2012). Multiple processes can contribute to lymph node activation. Such processes include, but are not limited to, immune cell proliferation as a part of a normal immune response, inflammation from cytocidal effects of MPXV, or cytotoxicity associated with the infiltration of activated immune cells.

Various imaging modalities have been used to identify biomarkers in animal models of infectious diseases. For example, magnetic resonance spectroscopy was used to identify changes in metabolic markers of neuronal integrity, such as N-acetylaspartate or creatine, during minocycline therapy of simian immunodeficiency virus-induced encephalitis (Ratai et al. 2010). In another study, the disease pathogenesis of neuroAIDS in nonhuman primates was monitored using C-11 (R)-1-(2-chlorphenyl)-*N*-methyl-*N*-(1-methylpropyl)-3-isoquinoline-carboxamide, a PET radioligand for peripheral benzodiazepine receptors abundant on macrophages. Increased binding of this radioligand has been proposed as a biomarker of neurodegenerative disease (Venneti et al. 2004).

10.3 Containment Strategies to Incorporate Imaging Platforms

The integration of modern medical imaging technologies within a high-containment biological laboratory is a relatively new concept that has not been widely undertaken. This lack of integration is mainly due to concerns over breaching the biocontainment barrier, contaminating the imaging equipment and potentially harming the imaging equipment with harsh decontamination chemicals. Furthermore, many of the pathogens for which vaccines or therapies are actively sought pose significant health risks to humans and therefore call for high levels of biosafety in highly specialized laboratory spaces. Such laboratory spaces require specialized ventilation and air treatment systems, controlled-access zones, air locks at laboratory entrances, and separate building modules to isolate the laboratory (US Department of Health and Human Services, Centers for Disease Control and Prevention, National Institutes of Health 2009).

Several containment strategies integrate medical imaging into the theatre of infectious disease research within a BSL-3 or BSL-4 laboratory. The majority of these strategies fall under one of two categories: imaging equipment that is fully contained within BSL environment or the BSL environment is extended to include only necessary components of the imaging equipment. Some advantages and difficulties inherent to each strategy are discussed below.

10.3.1 Fully Contained Equipment

One method for the integration of medical imaging and biological hazards is the inclusion of the entire imaging instrument within a high-containment laboratory. This method differs from the others discussed in this section in that there is no physical biocontainment barrier between imaging equipment and infected subject. As such, full containment of imaging instruments is only practical in circumstances when the instrument in question is dedicated to infectious disease imaging. Such containment would not only limit the use of the imaging device but would also be associated with a relatively large footprint within the BSL laboratory. A major concern in employing this configuration is the ability to decontaminate and service the devices without voiding warranties.

This containment configuration would require service engineers to have access to the high-containment laboratory to perform maintenance or service tasks. Such access could be granted in one of two scenarios. First, the service engineers are trained in BSL-3 or BSL-4 laboratory practices, and they perform required tasks using these practices, including donning personal protective equipment. The entry and training requirements for work within a BSL-3 or BSL-4 laboratory are not trivial, especially when certain high consequence pathogens are involved (US Department of Agriculture 2005). Requiring this training for each service engineer would be time consuming and inefficient. Furthermore, maintenance or repair activities could require work with tools or objects that may increase the risk of a tear in the positive-pressure suit or other breaches of personal protective equipment.

Alternatively, the imaging suite could be decontaminated prior to planned maintenance or repair by service engineers who are not trained in BSL practices. Subjecting the imaging device to decontamination procedures may increase the risk of damage. Many chemicals used in decontamination of a BSL-3 or BSL-4 laboratory (US Department of Health and Human Services, Centers for Disease Control and Prevention, National Institutes of Health 2009) could harm the device. Caustic etching of detectors, progressive degradation of device wiring insulation, and corrosion of solder points are only a few of the risks. Therefore, neither of these scenarios (i.e., entry of trained service engineers, decontamination) is optimal.

10.3.2 Containment Extension Strategy

Containment extension strategies are those that aim to keep the imaging device itself, or a large portion of it, outside the high-containment zone. Such strategies are solutions for imaging modalities that are large and not easily integrated into the BSL-3 or BSL-4 laboratory for the reasons described above, for example, clinical CT, PET, SPECT, and MRI systems. Containment is maintained by creating an extension of the high-containment laboratory within the bore or surrounding the subject table of the imaging device. This extension could be confluent to the BSL

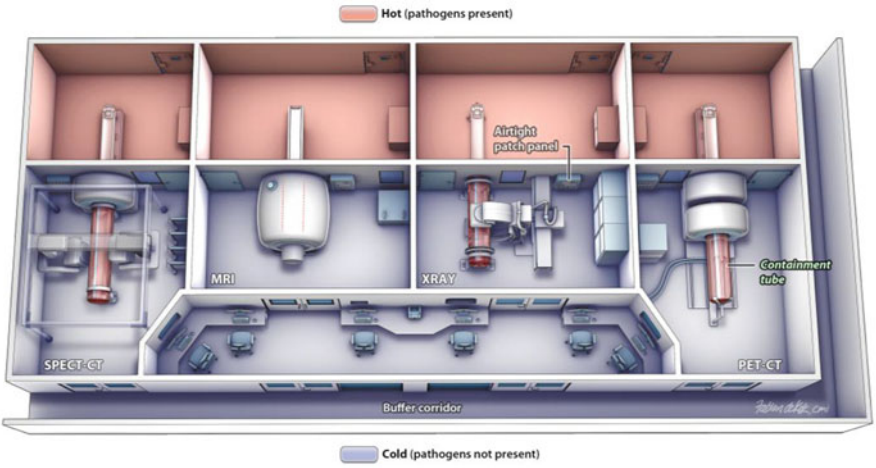

Fig. 10.1 Schematic of medical imaging suite with clinical SPECT/CT, MRI, X-ray, and PET/CT systems integrated into a biosafety level-4 laboratory using the containment tube strategy. The barrier wall and the containment tube separate the high-containment areas (*mauve*) from the non-containment rooms (*blue*). All rights reserved. Reprinted with permission from the American Biological Safety Association (ABSA), Mundelein, IL. Originally published in *Applied Biosafety: Journal of the American Biological Safety Association, 16*(2), p. 59. Copyright © 2011. Visit http://www.absa.org for more information

laboratory, as in the containment tube strategy that will be discussed below, or could involve an encapsulation of the infected subject (Jain et al. 2010).

The National Institute of Allergy and Infectious Diseases Integrated Research Facility (IRF) at Fort Detrick, MD, pursued a biocontainment extension design that located only those imaging elements that are absolutely necessary inside the high-containment zone. The IRF is equipped with clinical SPECT/CT, PET/CT, diagnostic X-ray, and MRI systems. The high-containment zone is extended into the bore of each imaging device with the use of transparent biocontainment tubes made of polycarbonate resin thermoplastic (Philips Bioshield™, North Ryde, Australia) (Fig. 10.1) (de Kok-Mercado et al. 2011). The subject is placed on the imaging table in the high-containment side of the barrier wall that then advances into the biocontainment tube prior to imaging. The bulk of the imaging device and associated electronic equipment remain outside of high containment and are therefore accessible to service engineers under normal maintenance and repair conditions. All electrical signals necessary for the imaging modality are sent through an airtight patch panel to the control room on the cold side of the barrier wall (Fig. 10.2). In addition to providing biocontainment, this containment extension tube strategy protects the imaging equipment from gases and chemicals that are used to decontaminate the high-containment laboratory, such as formaldehyde gas, hydrogen peroxide vapor, or chlorine dioxide gas. However, since placing the subject on the imaging table requires access to the hot zone, this containment strategy requires the imaging systems to be dedicated to infectious disease imaging.

Fig. 10.2 Airtight patch panel through which electrical signals are sent to electronic components on the cold side of the barrier wall. This eliminates the need for electronic components to be on the hot side and subjected to decontamination chemicals

The BSL-4 environment itself, along with the containment strategy chosen, will introduce issues unique to each imaging modality. Some of the issues that pertain to the containment extension tube strategy are discussed, and solutions are explored below for SPECT/CT, C-arm diagnostic X-ray, and MRI.

10.3.2.1 SPECT/CT System

The containment extension tube integrated into the SPECT/CT imaging equipment (Fig. 10.3) is 0.6-cm thick with an outer diameter of 61.0 cm. In nuclear imaging with parallel-hole collimators, spatial resolution degrades with increasing distance between source and collimator (Cherry et al. 2003). In a typical clinical environment, one can optimize spatial resolution by minimizing the distance between patient and collimator. With the containment tube strategy, this option is no longer available since the radius of the circular SPECT orbit is restricted to 33.0 cm or larger. The standard low-energy high-resolution (LEHR) collimator routinely used in the clinic is expected to provide inadequate spatial resolution at this operating distance. To overcome this limitation, the manufacturer of the SPECT scanner custom-designed a unique "ultra-ultra high-resolution" (UUHR) collimator for use at the IRF. Characteristics of the UUHR and LEHR collimators are listed in Table 10.1 (Leyson et al. 2012). System spatial resolution is expressed as full width at half maximum of the line spread function of data acquired from imaging Tc-99m-filled capillary tubes. Spatial resolution degradation with increasing distance from the collimator is less severe with the UUHR collimator than with the LEHR collimator (Fig. 10.4).

Fig. 10.3 Photograph of the SPECT/CT equipment with containment extension tube

Table 10.1 Characteristics of the UUHR and LEHR collimators

	UUHR	LEHR
Hole size (flat-to-flat)	1.22 mm	1.22 mm
Hole length	48 mm	27 mm
Septa thickness	0.15 mm	0.15 mm
System spatial resolution at 10 cm distance*	5.3 mm	7.3 mm
Sensitivity*	56 cpm/mCi	168 cpm/mCi

*Data presented were measured with 140 keV photons and 5/8″ NaI(TI) crystal; *cpm* counts per minute

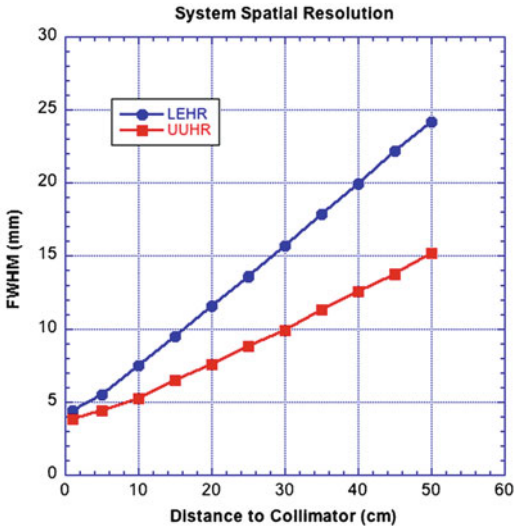

Fig. 10.4 System spatial resolution expressed as full width at half maximum of line spread functions versus distance to collimator using standard low-energy high-resolution (LEHR) and ultra-ultra high-resolution (UUHR) collimators

Fig. 10.5 Diagnostic X-ray installed with containment extension tube

With the UUHR collimator, system resolution at a source-to-collimator distance of 35 cm, an orbital radius that allows room for the biocontainment tube, is comparable to the resolution achieved at 20 cm with the standard parallel-hole LEHR collimator. However, the improved spatial resolution capabilities of the UUHR collimator come at the expense of a substantially reduced planar sensitivity that is nearly one-third that of standard collimators. The reduced sensitivity may be compensated for by administration of a higher dose of injected radioactivity or by a longer acquisition time than required with the LEHR collimator.

10.3.2.2 Diagnostic X-Ray

The implementation of the containment tube strategy into diagnostic X-ray imaging is relatively straightforward (Fig. 10.5). However, one important consideration is the potential for collision between the C-arm gantry and the containment tube that increases the risk of a biocontainment breach. One strategy for collision prevention is to use optical sensors to immediately stop all motion of the device if an object interrupts the optical laser light beam. Such sensors prevent collision of the imaging device with the containment tube as well as the wall of the high-containment laboratory (Fig. 10.6) (de Kok-Mercado et al. 2011).

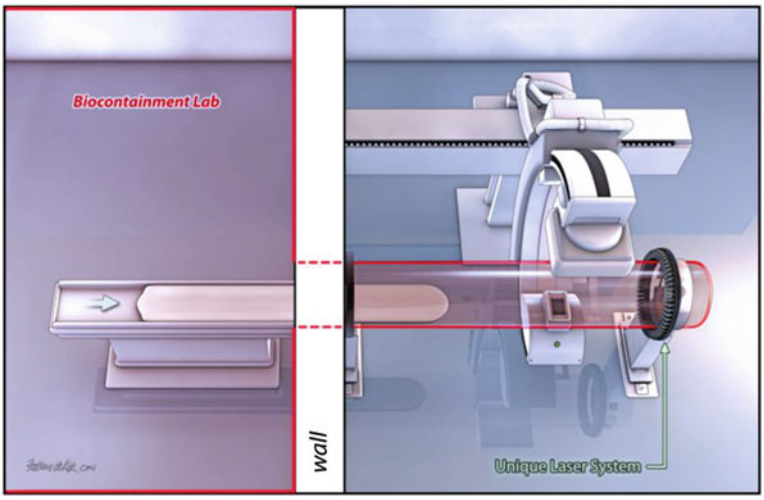

Fig. 10.6 X-ray gantry with its containment tube and unique laser system (black collar around containment tube) to prevent the movable X-ray head from striking the tube as its position is adjusted. If the X-ray head interrupts any laser beam, the power is immediately shut off. The barrier wall and containment tube separate the equipment from the laboratory. All rights reserved. Reprinted with permission from the American Biological Safety Association (ABSA), Mundelein, IL. Originally published in *Applied Biosafety: Journal of the American Biological Safety Association, 16*(2), p. 60. Copyright © 2011. Visit http://www.absa.org for more information

10.3.2.3 Magnetic Resonance Imaging

MRI presents a unique challenge when it comes to the integration of the modality with infectious disease research at high biosafety levels (Fig. 10.7). Even with the implementation of the containment extension tube strategy, MRI can require imaging equipment to be housed and operated within the containment zone. Most commercial MR scanners come equipped with a body radio frequency (RF)-receiver coil housed within the main bore, which is outside the containment tube in the containment extension strategy described above. In contrast, external RF-receiver coil arrays can appreciably improve signal-to-noise ratio and decrease scan time by taking advantage of an accelerated MR acquisition strategy called parallel imaging (Blaimer et al. 2004). Specialized external RF coils dedicated to a specific anatomical region or imaging protocol are commonly used. However, clinical RF-receive coils are costly and are not designed to withstand the autoclaving process associated with removal from biocontainment should repair be required. Possible solutions to repairing RF coils include use of off-the-shelf coils that can sustain the decontamination process or are inexpensive to replace should the coils become unusable (Dannels et al. 2008). Alternatively, custom, in-house coils could be designed such that coil maintenance can be performed in the biocontainment suite. Another option is the reliance on the body coil if external RF coils are damaged or worn.

Fig. 10.7 High-containment side of the magnetic resonance imaging room at the National Institute of Allergy and Infectious Diseases Integrated Research Facility at Fort Detrick, MD. The *black ring* around the bore entrance is a gasket that seals the connection between the containment tube and the barrier wall

Beyond issues with the MRI equipment, the associated strong magnetic field introduces a unique, additional hazard into a high-containment facility. The chance of ferrous objects entering the magnet room is always a risk in clinical MRI. Typically, the danger with this scenario is injury due to ferrous objects flying into the bore of the magnet. While this danger remains present with high-containment MRI, an additional risk of biocontainment breach is possible due to missile objects. Extreme care and caution must be used to avoid these dangerous events (Chaljub et al. 2001; Zimmer et al. 2004).

10.4 Conclusion

Regardless of the challenges involved with integrating medical imaging equipment into high-containment laboratory spaces, structural and functional imaging could serve as an integral tool in the development of therapeutics against highly pathogenic infectious diseases. Using nuclear imaging probes that are currently available, SPECT and PET imaging can identify foci of increased cell metabolism or proliferation after infection. The development of a greater number of more specialized and specific probes would make these modalities even more influential. Certain MRI techniques have the advantage of not requiring administration of exogenous contrast agents, which decreases risk of exposure from accidental needle sticks. Also advantageous is the possibility of cell

labeling and tracking with SPIOs or USPIOs as contrast agents. New, meaningful image biomarkers are being developed in animals to characterize infectious disease processes and efficacy or safety of a new drug. However, care must be taken to validate these imaging biomarkers thoroughly prior to implementation.

Following image acquisition, standard image analysis processes must be optimized for imaging experimentally infected small animals in longitudinal studies in a high-containment laboratory. Such optimization in part will require the development of new, small animal atlases for automated segmentation algorithms as well as rigorous image registration routines. As positioning of infected small animals is hampered by personal protective equipment required for the safety of laboratory personnel, image registration methods must be utilized in order to minimize larger positional differences in subject orientation across scanning sessions.

Numerous strategies are available to physically integrate and install medical imaging equipment into BSL-3 and BSL-4 laboratory spaces. The advantages and disadvantages associated with each strategy may differ depending on the requirements of each facility. An assessment of the laboratory necessities is recommended for new high-containment laboratories. As a result of such assessment and deliberation, personnel from the Integrated Research Facility in Fort Detrick, MD, elected for the containment tube strategy described above. With the containment tube strategy, repair of imaging equipment does not require entry into high containment. The containment tube assures the safety of imaging and repair personnel by preventing exposure to highly pathogenic agents.

By using the same imaging techniques throughout the drug development process, the translation from basic science biodefense research to clinical evaluation will be streamlined in a way that could decrease the approval time for an investigational agent. Imaging biomarkers identified in animals could be used as surrogate markers in clinical evaluation. Image analysis techniques used to track progression of viral infection and therapeutic response to a drug candidate could also be applied to tracking response of patients to a therapeutic intervention. The integration of temporal, spatial, functional, and metabolic information gained from medical imaging modalities in combination with standard evaluation of antiviral drug candidates will have a great impact on the course of future drug development.

Acknowledgments The authors thank Fabian de Kok-Mercado for his contribution to this work. The content of this chapter does not necessarily reflect the views or policies of the US Department of Health and Human Services or of the institutions and companies affiliated with the authors. This work was supported by the Integrated Research Facility, Division of Clinical Research, National Institute of Allergy and Infectious Diseases (NIAID), and Battelle Memorial Institute's prime contract with NIAID (HHSN272200200016I).

References

Bading JR, Shields AF (2008) Imaging of cell proliferation: status and prospects. J Nucl Med 49(Suppl 2):64S–80S

Beckmann N et al (2003) Macrophage infiltration into the rat knee detected by MRI in a model of antigen-induced arthritis. Magn Reson Med 49(6):1047–1055

Bellani G et al (2010) Imaging of lung inflammation during severe influenza A: H1N1. Intensive Care Med 36(4):717–718
Biomarkers Definitions Working Group (2001) Biomarkers and surrogate endpoints: preferred definitions and conceptual framework. Clin Pharmacol Ther 69(3):89–95
Blaimer M et al (2004) SMASH, SENSE, PILS, GRAPPA: how to choose the optimal method. Top Magn Reson Imaging 15(4):223–236
Bray M et al (2010) Radiolabeled antiviral drugs and antibodies as virus-specific imaging probes. Antiviral Res 88(2):129–142
Brunetti A et al (1989) Reversal of brain metabolic abnormalities following treatment of AIDS dementia complex with 3′-azido-2′,3′-dideoxythymidine (AZT, zidovudine): a PET-FDG study. J Nucl Med 30(5):581–590
Brust D et al (2006) Fluorodeoxyglucose imaging in healthy subjects with HIV infection: impact of disease stage and therapy on pattern of nodal activation. AIDS 20(7):985–993
Bulte JW (2009) In vivo MRI cell tracking: clinical studies. Am J Roentgenol 193(2):314–325
Burton JM et al (2004) Neurological manifestations of West Nile virus infection. Can J Neurol Sci 31(2):185–193
Buscombe JR, Oyen WJ, Corstens FH (1995) Use of polyclonal IgG in HIV infection and AIDS. Q J Nucl Med 39(3):212–220
Chaljub G et al (2001) Projectile cylinder accidents resulting from the presence of ferromagnetic nitrous oxide or oxygen tanks in the MR suite. Am J Roentgenol 177(1):27–30
Cherry SR, Sorenson JA, Phelps ME (2003) The gamma camera: performance characteristics. In: Physics in nuclear medicine. Saunders, Philadephia, PA
Cyran CC et al (2012) Permeability to macromolecular contrast media quantified by dynamic MRI correlates with tumor tissue assays of vascular endothelial growth factor (VEGF). Eur J Radiol 81(5):891–896
Dannels WR et al (2008) Integrated system of MRI RF loop coils plus spacing fixtures with biocontainment tubes. WIPO Patent Application. PCT/US2008 073512, filed June 19, 2008
de Kok-Mercado F, Kutlak F, Jahrling PB (2011) The NIAID integrated research facility at Fort Detrick. Appl Biosafety 16(2):58–66
Di Mascio M et al (2009) Antiretroviral tissue kinetics: in vivo imaging using positron emission tomography. Antimicrob Agents Chemother 53(10):4086–4095
Dotti G et al (2009) Repetitive noninvasive monitoring of HSV1-tk-expressing T cells intravenously infused into nonhuman primates using positron emission tomography and computed tomography with 18F-FEAU. Mol Imaging 8(4):230–237
Dyall J et al (2011) Evaluation of monkeypox disease progression by molecular imaging. J Infect Dis 204(12):1902–1911
Dyall J et al (2012) Assessment of longitudinal changes in 18FDG uptake in bone marrow and lymph node and in lymph node volume in nonhuman primate model of monkeypox infection. World Molecular Imaging Congress Dublin, Ireland, Sep 5–8 2012
Ferro-Flores G, Ocampo-Garcia BE, Melendez-Alafort L (2012) Development of specific radiopharmaceuticals for infection imaging by targeting infectious micro-organisms. Curr Pharm Des 18(8):1098–1106
Floris S et al (2004) Blood-brain barrier permeability and monocyte infiltration in experimental allergic encephalomyelitis: a quantitative MRI study. Brain 127(Pt 3):616–627
Frank JA et al (2003) Clinically applicable labeling of mammalian and stem cells by combining superparamagnetic iron oxides and transfection agents. Radiology 228(2):480–487
Gambhir SS et al (2000) Imaging transgene expression with radionuclide imaging technologies. Neoplasia 2(1–2):118–138
Garg M et al (2008) Radiolabeling, pharmacoscintigraphic evaluation and antiretroviral efficacy of stavudine loaded 99mTc labeled galactosylated liposomes. Eur J Pharm Sci 33(3):271–281
Haacke EM et al (2004) Susceptibility weighted imaging (SWI). Magn Reson Med 52(3): 612–618
Hamed IA et al (1979) Pulmonary cytomegalovirus infection: detection by Gallium 67 imaging in the transplant patient. Arch Intern Med 139(3):286–288

Hayes EB, Gubler DJ (2006) West Nile virus: epidemiology and clinical features of an emerging epidemic in the United States. Annu Rev Med 57:181–194
Hoehn M et al (2007) Cell tracking using magnetic resonance imaging. J Physiol 584(Pt 1):25–30
Jain NK et al (2010) Biosafety level (BSL)-3 life support cell for studying live animals. Patent Application. PCT/US20100313821, filed June 16, 2010
Jeha LE et al (2003) West Nile virus infection: a new acute paralytic illness. Neurology 61(1):55–59
Jubeli E et al (2012) E-selectin as a target for drug delivery and molecular imaging. J Control Release 158(2):194–206
Kleinschnitz C et al (2003) In vivo monitoring of macrophage infiltration in experimental ischemic brain lesions by magnetic resonance imaging. J Cereb Blood Flow Metab 23(11):1356–1361
Kumar V (2005) Radiolabeled white blood cells and direct targeting of micro-organisms for infection imaging. Q J Nucl Med 49(4):325–338
Kumar S et al (1997) MRI in Japanese encephalitis. Neuroradiology 39(3):180–184
Kumar M et al (2010) Image-guided breast tumor therapy using a small interfering RNA nanodrug. Cancer Res 70(19):7553–7561
Leyson C et al (2012) Performance comparison of ultra-ultra high resolution collimators to low-energy high resolution collimators. J Nucl Med 53(suppl 1):2409
Liu N et al (2007) Radiolabeling small RNA with technetium-99m for visualizing cellular delivery and mouse biodistribution. Nucl Med Biol 34(4):399–404
Liu T et al (2012) Cerebral microbleeds: burden assessment by using quantitative susceptibility mapping. Radiology 262(1):269–278
Lobel U et al (2010) Three-dimensional susceptibility-weighted imaging and two-dimensional T2*-weighted gradient-echo imaging of intratumoral hemorrhages in pediatric diffuse intrinsic pontine glioma. Neuroradiology 52(12):1167–1177
Luker GD, Sharma V, Piwnica-Worms D (2003) Visualizing protein-protein interactions in living animals. Methods 29(1):110–122
Modo M, Hoehn M, Bulte JW (2005) Cellular MR imaging. Mol Imaging 4(3):143–164
Nahrendorf M et al (2006) Noninvasive vascular cell adhesion molecule-1 imaging identifies inflammatory activation of cells in atherosclerosis. Circulation 114(14):1504–1511
O'Connor JP et al (2007) DCE-MRI biomarkers in the clinical evaluation of antiangiogenic and vascular disrupting agents. Br J Cancer 96(2):189–195
O'Connor JP et al (2008) Quantitative imaging biomarkers in the clinical development of targeted therapeutics: current and future perspectives. Lancet Oncol 9(8):766–776
Padhani AR et al (2000) Dynamic contrast enhanced MRI of prostate cancer: correlation with morphology and tumour stage, histological grade and PSA. Clin Radiol 55(2):99–109
Penheiter AR, Russell SJ, Carlson SK (2012) The sodium iodide symporter (NIS) as an imaging reporter for gene, viral, and cell-based therapies. Curr Gene Ther 12(1):33–47
Pien HH et al (2005) Using imaging biomarkers to accelerate drug development and clinical trials. Drug Discov Today 10(4):259–266
Ratai EM et al (2010) Proton magnetic resonance spectroscopy reveals neuroprotection by oral minocycline in a nonhuman primate model of accelerated NeuroAIDS. PLoS One 5(5):e10523
Reinders Folmer SC et al (1986) Gallium-67 lung scintigraphy in patients with acquired immune deficiency syndrome (AIDS). Eur J Respir Dis 68(5):313–318
Richter WS (2006) Imaging biomarkers as surrogate endpoints for drug development. Eur J Nucl Med Mol Imaging 33(Suppl 1):6–10
Rojas JJ, Thorne SH (2012) Theranostic potential of oncolytic vaccinia virus. Theranostics 2(4):363–373
Rubin RH, Fischman AJ (1994) The use of radiolabeled nonspecific immunoglobulin in the detection of focal inflammation. Semin Nucl Med 24(2):169–179
Rudin M, Weissleder R (2003) Molecular imaging in drug discovery and development. Nat Rev Drug Discov 2(2):123–131
Schellingerhout D et al (1998) Mapping the in vivo distribution of herpes simplex virions. Hum Gene Ther 9(11):1543–1549

Sejvar JJ et al (2003) Neurologic manifestations and outcome of West Nile virus infection. JAMA 290(4):511–515
Sharma V, Luker GD, Piwnica-Worms D (2002) Molecular imaging of gene expression and protein function in vivo with PET and SPECT. J Magn Reson Imaging 16(4):336–351
Shoji H et al (1994) Magnetic resonance imaging findings in Japanese encephalitis. White matter lesions. J Neuroimaging 4(4):206–211
Shu CJ et al (2010) Novel PET probes specific for deoxycytidine kinase. J Nucl Med 51(7):1092–1098
Smith JJ, Sorensen AG, Thrall JH (2003) Biomarkers in imaging: realizing radiology's future. Radiology 227(3):633–638
Stoll G et al (2004) In vivo monitoring of macrophage infiltration in experimental autoimmune neuritis by magnetic resonance imaging. J Neuroimmunol 149(1–2):142–146
Umenai T et al (1985) Japanese encephalitis: current worldwide status. Bull World Health Organ 63(4):625–631
US Department of Agriculture (2005) Agriculture bioterrorism protection act of 2002; possession, use and transfer of select agents and toxins, final rule. Fed Regist 70(52):13294
US Department of Health and Human Services, Centers for Disease Control and Prevention, National Institutes of Health (2009) In: Chosewood LC, Wilson DE (eds) Biosafety in microbiological and biomedical laboratories, 5th edn. US Government Printing Office: Washington, DC. http://www.cdc.gov/biosafety/publications/bmbl5/. Accessed 5 Dec 2012
US Food and Drug Administration (2002) New drug and biological drug products; evidence needed to demonstrate effectiveness of new drugs when human efficacy studies are not ethical or feasible. Fed Regist 67(105):37988–37998
Valadon P et al (2006) Screening phage display libraries for organ-specific vascular immunotargeting in vivo. Proc Natl Acad Sci USA 103(2):407–412
Venneti S et al (2004) PET imaging of brain macrophages using the peripheral benzodiazepine receptor in a macaque model of neuroAIDS. J Clin Invest 113(7):981–989
Viglianti BL et al (2004) In vivo monitoring of tissue pharmacokinetics of liposome/drug using MRI: illustration of targeted delivery. Magn Reson Med 51(6):1153–1162
Wanahita A et al (2007) Diagnostic sensitivity and specificity of the radionuclide (indium)-labeled leukocyte scan. J Infect 55(3):214–219
Wang YX, Deng M (2010) Medical imaging in new drug clinical development. J Thorac Dis 2(4):245–252
Willmann JK et al (2008) Molecular imaging in drug development. Nat Rev Drug Discov 7(7):591–607
Yarchoan R et al (1987) Response of human-immunodeficiency-virus-associated neurological disease to 3′-azido-3′-deoxythymidine. Lancet 1(8525):132–135
Zimmer C et al (2004) Near-miss accident during magnetic resonance imaging by a "flying sevoflurane vaporizer" due to ferromagnetism undetectable by handheld magnet. Anesthesiology 100(5):1329–1330

Chapter 11
Magnetic Resonance as a Tool for Pharmaco-Imaging

Brian R. Moyer, Tom C.-C. Hu, Simon Williams, and H. Douglas Morris

Abstract Imaging technologies in the nonclinical laboratory have been greatly bolstered by the ever-improving methods available with magnetic resonance (MR) imaging. Small animal systems have been growing in capability even while becoming more amenable to use by biologists, revolutionizing how we can study pathophysiology and follow a drug or biologic therapy. MR's ability to characterize many anatomical and physiological processes, based on their underlying influence on tissue magnetization properties, has led, for example, to discoveries in the psychopharmacology of attention deficit and cognitive drug therapies and in recording changes of oxygenation, blood flow and vessel permeability in acute studies, or the chronic remodeling of tissue water diffusion following therapy. This is a short and clearly abbreviated discussion of the applications of MRI in the nonclinical

B.R. Moyer, M.S. (Pharm), M.S. (Tox), C.N.M.T. (✉)
BRMoyer & Associates, LLC, 23 Hawk Drive, Bedford, NH 03110, USA
e-mail: bmoyernh@gmail.com

T.C.-C. Hu, Ph.D., M.B.A.
Health and Human Services (HHS), Office of the Assistant Secretary for Preparedness and Response (ASPR), Biomedical Advanced Research and Development Authority (BARDA), Washington, DC 20201, USA

Nuclear and Radiological Engineering/Medical Physics Program, George W. Woodruff School of Mechanical Engineering, Georgia Institute of Technology, North Avenue, Atlanta, GA 30332, USA
e-mail: tom.hu@hhs.gov

S. Williams, D.Phil.
Department of Biomedical Imaging, Genentech, Inc., 1 DNA Way, South San Francisco, CA 94080, USA
e-mail: williams.simon@gene.com

H.D. Morris, Ph.D.
NIH Mouse Imaging Facility, National Institute of Neurological Disorders and Stroke, National Institutes of Health, 10 Center Drive, B1D-69, Bethesda, MD 20892, USA
e-mail: dmorris@nih.gov

B.R. Moyer et al. (eds.), *Pharmaco-Imaging in Drug and Biologics Development*,
AAPS Advances in the Pharmaceutical Sciences Series 8, DOI 10.1007/978-1-4614-8247-5_11,

(and clinical) drug development laboratory, and it is meant to introduce the reader to the concepts and how this specific imaging modality likely offers the most versatile of all imaging modalities as well as being one with very high resolution.

Abbreviations

ADC	Apparent diffusion coefficient—the diffusion of molecules in tissues is modulated by many mechanisms that restrict or impose tortuosity around obstacles and such as blood flow in small vessels or cerebrospinal fluid in ventricles and other contributions to MR signal attenuation. Images are "weighted" by the "apparent" diffusion processes. Note that the ADC concept has been extremely successful in tumor biology to demonstrate necrosis, especially for clinical applications. The basic ADC approach has been challenged recently, as new, more comprehensive models of diffusion in biological tissues have been introduced. Also, the rADC, or relative ADC, is a ratio of lesions to control brain ROIs
B_0	Static main magnetic field provided by the MR system magnet
B_1	Secondary magnetic field perpendicular to B_0 transiently created during an experiment by the system's radiofrequency coils and gradient sets
BOLD	Blood oxygen level dependent (a particular contrast mechanism)
Chemical shift	The resonant frequency of nuclei in some chemical environment relative to those in a standard environment (e.g., the protons of benzene)
CNR	Contrast-to-noise ratio—the CNR is directly linked to statistical measures such as the *t*-values, but it does not depend on the number of points or runs as do the *t*-values; in fMRI it is made up of the functional signal change and the temporal signal change as the average signal change (task related) over the non-task-related variability over time (time-series noise)
FT	Fourier Transform—a mathematical treatment of the FID or echo signal from a modern pulsed MR experiment to convert the recorded time-domain data into usable spatial frequency-domain data and hence images; an MR image consists of a matrix of pixels based on the number of lines filed in "K-space" (phase matrix) and the number of data points in each line (frequency matrix)
FID	Free induction decay—the signal observed during the process of relaxation that follows an excitation of nuclei induced by a pulse of radiofrequency energy
FOV	Field of view—physical dimensions of the imaged volume

fMRI	Functional magnetic resonance imaging—generally for cerebral blood flow
Gradient	A (relatively small) magnetic field that increases in strength with distance from the center of the image; these are created transiently by pulses from the gradient coils to impart the magnetic spins with frequency and phase information to facilitate image formation
K-space	A spatial frequency domain where information on the frequencies of a signal and where it comes from (on the gradient) in the patient is located; this information is in radians per cm; often called the chest of drawers for how the data is stored
NMR	Nuclear magnetic resonance—general term for the analytical chemistry of chemical shift analysis and the former term of MR as "NMR imaging"
phMRI	Physiologic or pharmacologic imaging using MRI
Pulse sequences	A programmed sequence of magnetic field pulses and time delays from the radiofrequency coil and the gradient set during the imaging experiment which manipulate the spin behavior of nuclei; changes to the induction and relaxation can be exploited to reveal properties of the tissue of interest
Relaxation	Process by which a population of excited (high-energy) nuclei give up RF energy and return to their ground (low-energy) state. This emitted energy is detected to form the images
Relaxivity	The ability of magnetic compounds to increase the relaxation rates of the surrounding water proton spins. Relaxivity is used to improve the contrast of the image and to study tissue-specific areas where the contrast agent better diffuses; view http://www.youtube.com/watch?v=Osx8Ced9Eyw
RF	Radiofrequency—the resonant frequency of protons at commonly used magnetic field strengths is in the radiofrequency range, e.g., 64 MHz at 1.5 Tesla
SNR	Signal-to-noise ratio
T_1	Longitudinal relaxation occurs when a population of excited nuclei give up their extra energy to the surrounding electronic environment; the time constant "T_1" (63 % of the longitudinal magnetization to recover) for this process is also known as the "spin–lattice" relaxation time constant. T_1 values are typically on the order of a second
T_2	Transverse relaxation occurs when a population of excited nuclei exchange energy with their neighbors; the time constant "T_2" (63 % of the longitudinal magnetization to recover) for this process is also known as the "spin–spin relaxation" time constant. In biological tissues T_2 values are typically on the order of tenths of a second

T_2*	The observed decay of the FID signal following the RF excitation pulse; it is faster than T_2 as it is the combination of the T_2 decay superimposed on dephasing phenomena such as magnetic field inhomogeneity
Tesla	One weber per meter squared; the SI unit of magnetic field strength
TOF	Time of flight—flowing nuclei present in a slice of interest which has an excitation pulse applied; more or less signal is recovered depending on their velocity; useful in magnetic resonance angiography
	A full listing of definitions is available at http://cis.rit.edu/htbooks/mri/gloss.html (8 pages of glossary terms)

11.1 Introduction to Magnetic Resonance Imaging

The field of modern biomedical imaging has been heavily influenced by the maturation of nuclear magnetic resonance (NMR) away from its roots as an analytical chemists' spectroscopic tool into the medical application known as magnetic resonance imaging (MRI). As a disclaimer we must acknowledge that this chapter cannot even begin to teach all the fundamentals of MR chemistry, physics, and mathematics nor even biology; MR is a field in its own right. For an excellent treatise with full coverage of the topic of magnetic resonance imaging and excellent illustrations of the physics, instrumentation and equipment imaging techniques and examples of various imaging artifacts, and safety, we refer the reader to the book entitled *MRI in Practice* by Westbrook, Roth, and Talbot (4th Ed., 2011, a Wiley-Blackwell publication).

The role of magnetic resonance imaging in drug development has grown exponentially as the instrumentation has become more refined, more widely available, and easier to use. This has been driven in part by the rapidly expanding clinical utility of MRI and the prospect of having a bench-to-bedside translation for many important experiments. Wise and Tracey (2006) have provided a comprehensive view of how one aspect of MRI, functional MRI (fMRI), is being used in drug development, specifically in brain functional assessments under drug challenges and therapies. More will be discussed on fMRI in the field of psychotherapy and neuropharmacology in a later section. It is the premise of this book that imaging has over the past 50–60 years advanced the portfolio of imaging agents, contrast agents, and other imaging probes and has begun the new exploitation of biomarkers—elements of physiologic expression—using the many radiotracers, US-CT-MR contrast agents, optical probes, and more and the imaging platforms of CT and MR as tools to dissect disease. We have an armament of tools at our disposal and one of the most versatile is magnetic resonance imaging. Advances in phMRI (physiologic MRI) are making huge strides in our understanding of drug effects on brain function, tumor susceptibility to novel therapeutics, cardiac imaging and blood/vascular

imaging (especially in stroke and deep vein thrombosis, or DVT), and even lung function such as pulmonary fibrosis and ventilation.

Modern clinical radiological imaging relies on the existence of useful image contrast between tissue types. Even before the field of MRI was developed, alterations were noted in the spin–lattice (T_1) and spin–spin (T_2 and T_2*) relaxation times of solutions containing paramagnetic ions. The significance of this alteration for the development of MRI was that small differences in the local magnetic properties of substances could be detected in spectroscopic changes of the surrounding water. In particular, Damadian observed that the relaxation times for tumors in rats presented differently than normal tissue as a function of the decrease in water constrained in tumor tissue (Damadian et al. 1977; Geva 2006). In a 1973 seminal paper, Paul Lauterbur demonstrated spatial localization via NMR, which he called "zeugmatography," and the utility of relaxometry in imaging. The first images were of two capillary tubes in a NMR spectrometer (Lauterbur 1973). One capillary contained a solution of $MnSO_4$ in order to reduce the T_1 of the observed hydrogen nuclei in water. By increasing the power of the RF transmission, two different images ("zeugmatograms") were acquired, which showed variation in the image intensity for the $MnCl_2$ solution capillary compared to water only, and demonstrated the feasibility of using T_1 variation as an image contrast. Lauterbur further postulated that all NMR visible phenomena, such as chemical shifts, diffusion, and dipolar couplings, can be "visible" in an image form.

As illustrated in the example above, intrinsic relaxometric differences in tissue can serve as image contrast, and furthermore, contrast can be enhanced by agents with different affinities for pathological and healthy tissue. Useful qualities of a contrast agent include (a) physical properties that affect the local magnetic environment sensitively and (b) chemical properties that allow the contrast agent to travel to the appropriate region of interest for imaging. MRI continues to be dominated by detection of the protons in tissue water, and our discussion will focus on these widespread ^{1}H MR techniques. However, we note that MRI with less common nuclei such as ^{23}Na or ^{19}F have been investigated and may have niche roles to play in fields such as imaging brain function or tissue oxygenation, respectively.

11.1.1 Pulse Sequences

Pulse sequences are the tools of the MRI imaging scientist. They can be thought of as a way to "sculpt" or "paint" the images using a wide variety of "paint brushes." These sequences are a series of RF pulses and magnetic field gradient applications spaced at carefully defined intervals so that the whole sequences excite or rephrase the resonance response following field perturbation. One "paints" with alterations in pulses and gradients. The brushes are simply how we address and make the RF pulses interact with the magnetic field both temporally and spatially. There are many pulse sequences in practice, and they each take some knowledge of the pathology of interest to select and customize appropriately; there may not be a single choice that is optimal.

Table 11.1 describes some frequently encountered pulse sequences, their most common abbreviations, and basically what they are directed to do in the generation of an image. Each pulse sequence is designed to accomplish a specific purpose, such as eliminating signal from static structures to reveal motion; this is not always to create a "better" image, but rather to improve image quantification and to emphasize particular aspects of the physiology being studied. The advantages and disadvantages of each pulse sequence are too complex to cover in this chapter; however, the reader is invited to review the textbook of Westbrook, Roth, and Talbot, *MRI in Practice*, published by Wiley-Blackwell, 2011 (Chap. 5 in the 3rd edition). Another textbook to review, especially for small animal imaging examples, is *Practical Small Animal MRI*, also published by Wiley-Blackwell by Gavin and Bagley (2009).

11.1.2 Potential Uses of MRI for Pharmaceutical Imaging

The pharmaceutical industry has for years investigated drug and biologics in development by measuring changes intrinsic to the physiologic behavior of the systems being targeted, such as the receptor-mediated generation of a biochemical signal that leads to some behavioral, functional, biochemical, or biophysical change to the system. MR imaging takes full advantage of the later phenomena, with the relaxation properties of tissue water greatly influenced by subtle variations in the presence of blood, oxygen, lipid membranes, proteins in solution or in aggregates, the anisotropic orientation of nerve fibers, etc. The intrinsic behavior of hydrogen (a dipole magnet in itself with a POS proton and a NEG electron forming a dipole; essentially encumbered as water) can be mapped in biophysical terms and exploited to create a signal of metabolic change (chemical exchanges in a chemical reaction, e.g., magnetic resonance spectroscopy; see Chap. 12 of this book) or as an anatomic change (tissue-type transitions and edge detection) and even as a measure of flow as magnetized blood elements flow through a tissue. Each of these behaviors allows an investigator to use nonionizing electromagnetic fields (B_1) in a magnetic field (B_0) to interrogate biologic systems. On top of this rich variety of intrinsic tissue contrast are all the additional contrast mechanisms available to us through the introduction of extrinsic contrast agents. We commonly apply contrast agents in CT and X-ray imaging, but contrast agents can also be used to enhance MRI. Contrast agents differ from radioactive tracers (say) in that they are not detected by the system directly but rather by their alteration of the local magnetic fields and the resultant change in resonant frequency (chemical shift) or relaxivity, properties which can be differentiated with an appropriate pulse sequence.

The magnetic properties of tissue and even contrast agents vary with the magnetic field strength. Higher field strengths lead to inherently higher detection sensitivity because a greater net polarization of the nuclear spins is achieved, but this comes with the potentially unwelcome complications of increased T_1 and decreased T_2 relaxation times which makes it more difficult to maintain (and image) transverse magnetization, adversely affecting the use of pulse sequences with long echo trains

Table 11.1 Pulse sequences, abbreviations (common—manufacturers may use different acronyms for the same sequence, refer to the manufacturer terms of use), mechanisms, and purpose

Pulse sequence name	Abbreviations	Purpose
Spin-echo types		
Conventional	SE	The "gold standard" In general, T_1 for anatomy and T_2 for pathology (tissues that are diseased may have more edema or vasculature)
Fast or turbo	FSE, TSE	A spin-echo scan with shorter scan times; by virtue of how it fills K-space it is useful in "stationary" organ systems; not so useful in chest, or abdomen (K-space will be defined for the reader in the next section)
Inversion recovery	IR	Good for accurate T_1 measurements and contrast on low-field systems
Fast inversion recovery	FIR	A modification of IR where multiple lines of K-space are filled as in FSE
Short tau inversion recovery	STIR	Important in musculoskeletal imaging as bone marrow and bruising are suppressed as well as fat
Fluid attenuated inversion recovery	FLAIR	Useful for attenuating signal from CSF in brain and spinal imaging to emphasize periventricular and spinal cord injuries
Gradient echo types		
Conventional	GE	Variable flip angles so that the TR (and scan time) can be reduced; used for T_2* and T_1 and proton density weighted images; sensitive to flow and thus useful for angiography
Steady-state/echo formation	SSEF	Steady state = TR is shorter than the T_1 or T_2 relaxation times (no time for transverse magnetization to occur); steady state sequences have high signal when T_1/T_2 ratios approach 1.0)
Coherent gradient echo	GRASE, FFE, FISP, FAST	Coherent = residual transverse magnetization (from previous RF pulses) is in phase; rapid images of T_2* weighted; used for vessel patency assessments or fluid (cystic) identity
Incoherent gradient echo (or spoiled)	SPGR, T_1FFE, FLASH	Incoherent = residual transverse magnetization (from previous RF pulses) is out of phase; RF spoiled pulses product T_1 or proton density images; useful T_1 anatomy with Gd contrast

(continued)

Table 11.1 (continued)

Pulse sequence name	Abbreviations	Purpose
Steady-state free precession	SSFP	Used for true T_2 weighting; brain and joints for 2D and 3D volumetric imaging; fast spin echo (FSE), however, is often a better choice as it has better T_2 weighting plus short scan times
Balanced gradient echo	BGE	Modified coherent gradient echo; corrects for rephasing in flowing blood; imaging the heart and great vessels and spinal images, especially the auditory meatus and cervical spine reservoirs
Fast gradient echo	FGE	Single breath-hold technique for very fast pulse sequences and volume acquisitions; multiple slices in respiratory scans, esp. dynamic contrast enhanced lung lesions; also for the abdomen and the breast
Echo planar imaging	EPI	A method that collects all the data required for a full K-space acquisition and from a single echo train. Very efficient at low magnetic field strengths and widely used in clinical imaging. But it is technologically very demanding on the hardware since filling K-space in this situation requires rapidly and continuously slewing the readout gradients. Can be combined with "magnetization preparation" pulses to create a variety of alternative relaxation images. Safety can be an issue with rapid gradient switching leading to nerve stimulation. EPI becomes difficult at higher fields due to distortion and chemical shift artifacts
Parallel imaging techniques		
Parallel imaging	ASSET, SENSE, iPAT, SMASH	Sensitivity encoding; fills K-space efficiently by multiple lines acquired via coupled coils enabled to acquire data simultaneously; systems are available with 2, 4, 6 and 8 coil couplings can be employed. Requires advanced hardware but an important technique that shortens scan times but may suffer from chemical shift artifacts from mismatched resonant coil frequencies

like EPI and altering the impact of contrast agents. Because building magnets with higher field strengths or larger diameters is relatively expensive, magnets which have to be large enough to accommodate human patients typically operate at lower field strengths (0.5–3 T) than those commonly found in small animal imaging laboratories (4.7–11 T). Very high-field magnets, such as the 21.1 T system at the National High Magnetic Field Laboratory in Florida, help to quantify the benefits and challenges that come with increasing field strength, and some clinical research centers have magnets of 9.4 T and higher. Because rapid imaging with EPI and the use of contrast-enhancing agents are important for some applications, and this is easier to achieve at relatively low fields such as 1 T, a new generation of relatively affordable low-field small animal imaging systems is being made available by manufacturers traditionally associated with high-field magnets, such as Bruker. Exploration of small animal imaging at field strengths beyond 9.4 T is mostly of academic interest at present but is very much application-dependent. Other technological developments also aim to increase the sensitivity of the MR experiment, such as more precise RF electronics, low-noise detector design, especially with cryogenic cooling of the RF coil and receiver electronics, and the design of coils with application-specific forms for maximum efficiency such as the multi-element spine coils common in the clinic and now being implemented in small animal systems. These developments may offer sensitivity improvements at lower cost and with fewer consequences than continually increasing the magnetic field strength.

Fundamental questions facing drug and biologics developers when testing a NCE into an animal model for advanced development may be answered using imaging applications. The listing below (and this list is certainly not exhaustive) addresses some imaging points about inclusion of an imaging approach to development questions:

- MR, like CT, addresses anatomy and distortions of anatomy very well (see Chap. 7 in oncology).
- Also, like CT, disease model natural history progression (i.e., tumor growth and RECIST determination) assessment is possible but with a distinct advantage in chemical characterization, such as discriminating lean from fatty tissues.
- Risk of different drug/biologic activities related to circadian rhythms may be imaged (i.e., neurologic changes in day–night sleep patterns and even hibernation).
- Biologic signal response times: Long duration versus immediate measures.
- Blood flow in tumors, angiogenesis, chemotherapeutic, and radiation effects.
- Appropriateness of use of multimodal imaging reagents/platforms.
- *Cell therapies*: Methods for labeling of cells ex vivo and in vivo and methods to follow stem cell tracking.
- Noninvasive imaging of proliferation and necrosis; histologic slice correlates.
- Changes in metabolic activity (and with circadian rhythms).
- Choosing the appropriate functional and/or quantitative platform.
- *Lung*: Noninvasive imaging of oxidative stress and lung function/fluid clearance, volume changes, capacity, macrophage activity, and changes in compliance due to fibrotic changes.

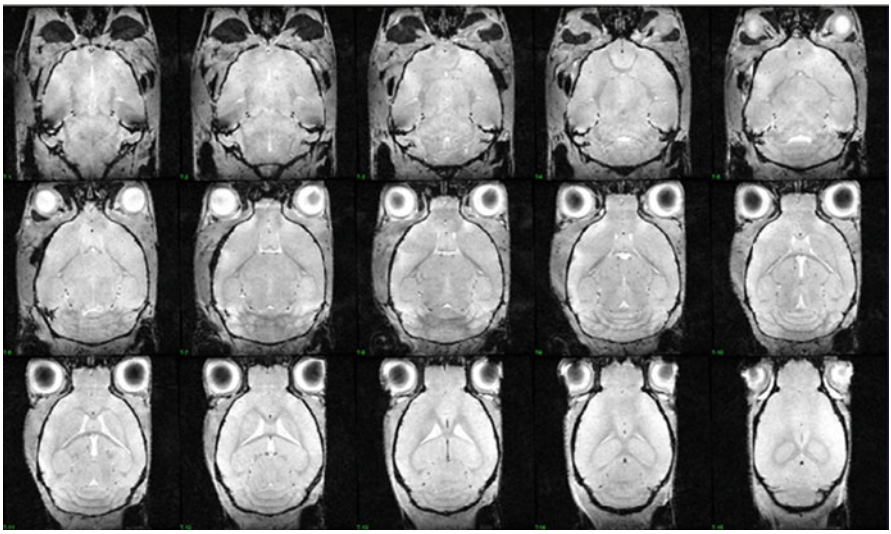

Fig. 11.1 Depiction of the mouse brain from the floor of the cranium (*upper left*) to the superior aspect above the ventricles (*lower right*) using a very high-magnetic-field system. From: Florida State University, National High Magnetic Field Laboratory using their 900 MHz system at 62×62 micron resolution in 150 micron slices; Resources include: Initial in vivo rodent sodium and proton MR imaging at 21.1 T. Schepkin VD, Brey WW, Gor'kov PL, Grant SC. *Magn Reson Imaging*. 2010; 28(3):400–407. With permission. http://www.magnet.fsu.edu/usershub/scientificdivisions/nmr/probes/probe_900mri.html

- *Kidney/liver*: Renal blood flow, clearance of drugs based upon renal function, liver metabolic changes, biliary flow, blood flow, tubular secretion.
- *GI tract*: Drug dissolution, segmental analysis/function, GI transit time, blood flow, crypt and villus apoptosis, GI lesions of various etiologies.
- *Wound* healing: Hematopoietic trafficking, clotting, stem cell arrival times, flow.
- *Liver*: Quantitation of fibrosis and changes in tissue elasticity accompanying disease progression.
- Hyperpolarization or chemical shift imaging applications; applicable to lungs.
- *Limits* of resolution in image fusion: Optical, X-ray, PET/SPECT, and MR images.
- Regulatory: Validation of the platform(s) and novel imaging biomarkers.
- Cost: Appropriateness; always include a cost analysis.

A general view of what MRI can achieve in the small animal setting is seen in Fig. 11.1 which displays a set of serial slices (floor of the cranium up to the ventricles) of the mouse brain. This is a high-resolution high-field image set utilizing a 62×62 micron resolution in 150 micron slices. Typical small animal imaging, even in a 1.5 T machine, can achieve a useful resolution in a mouse and is a first-line approach in drug development imaging. Higher-field systems may be better suited to applications where sensitivity is limiting, but care must be taken to avoid neural stimulation when gradients are switched rapidly.

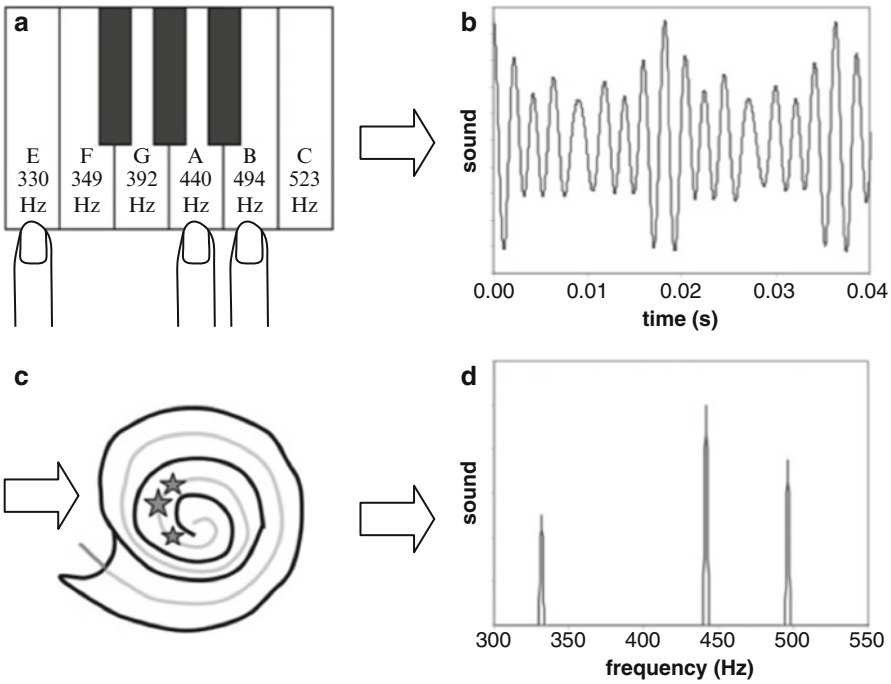

Fig. 11.2 Sound is produced as oscillations in air as a function of time and perceived as tones of specific frequencies. If three piano keys are struck (**a**), the vibration of the strings causes the air and thus the tympanic membrane of the ear to oscillate with time. If we measure these oscillations, they might look like the graph in panel (**b**). These sound waves produce an oscillation within the basilar membrane in the cochlea (**c**) where specific regions of the membrane (*indicated by stars*) respond maximally to the principal frequencies of the sound burst. The tonotopic mapping of the cochlea allows the brain to perceive the relative loudness of each specific frequency (or *piano key*), as shown in the spectrum (**d**). Both graphs (**b**) and (**d**) represent the sound produced by the piano and are related by the FT. The cochlea performs a natural FT. In an analogous way, the gradients of an MR scanner make tissues at different keys (locations) resonate at different frequencies, giving off a time signal measured by the receive coil that might look like the graph in panel (**b**). A computer, rather than a cochlea, performs the FT to reveal an image of the relative signal strength of each key (tissue location), analogous to the graph in (**d**). Reprinted from Paschal and Morris (2004). With permission

The physics of MR is complex and challenging, but the basic principle is simple: a population of hydrogen nuclei will behave like tiny magnets, each aligning with or against the static magnetic field B_0, and the whole having a small net magnetization vector precessing at the Larmor frequency around B_0. A perpendicular pulse of radiofrequency energy along the B_1 axis and at the same Larmor frequency causes the net magnetization vector to "tip" and reorient along B_1. After the B_1 pulse is turned off, the magnetization returns by T_1 and T_2 relaxation to the B_0 axis, emitting radiofrequency electromagnetic energy which allows a remote coil to sense the energy; based upon the induction field strength and the pulse sequence of the initiating radiofrequency, the exact position of the response can be mapped in what is termed K-space (Fig. 11.2).

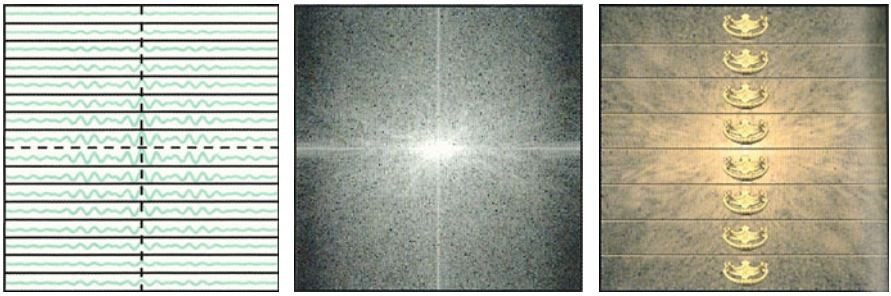

Fig. 11.3 A pictorial description of "K-space" for one slice of an image. The graphic shows a map of phase versus the frequency. That is, the graphic shows a spatial frequency domain where location of the signal within the subject is contained. Frequency is defined here in terms of phase change over distance (measured in radians). The units of K-space are radians per cm

MRI signals are similar to sound in that they can be presented in two equal ways, as either functions of time (t) or frequency (Hz or $1/t$). The reciprocal relationship between these variables is no accident and carries with it a great deal of physical and mathematical utility. If we strike a chord on a piano, several strings vibrate at a specific frequency. These frequencies mix to form a superposition of waves that we can pickup in a microphone or the tympanic membrane of our middle ear. The oscillations can then be decoded by the cochlea due to its frequency-specific mapping. Mathematically we can perform the same operation to recover the individual pure tone and amplitude of the keys in the chord.

In this fashion, MRI signals produce a superposition of all components in the RF-excited portion of the patient/animal which is then detected and digitized. The spatial information that is available in this signal has been encoded by the MRI scanner in such a way to fill a grid line (or K-line) in K-space. Each successive acquisition will fill another K-line such that we will fill our image K-space uniformly. Using a mathematical technique known as Fourier analysis, we can transform the signal into a number of weighted coefficients that will make up the intensities of our image. Thus we have used the Fourier transform to "transform" our K-space time-varying data to an image based on frequencies. MRI has a great deal of flexibility on how it fills in K-space and a great deal of image contrast, resolution, and clarity can occur due to the manner in which K-space is filled. The popular technologist training book, *MRI in Practice*, uses an interesting paradigm as a "chest of drawers" to describe the orthogonality of the phase versus frequency axes of K-space. In this manner, we can think of each drawer as being a rapidly scanned K-line and we sequentially acquire each "drawer of information" as an acquisition (Fig. 11.3).

The leftmost image in Fig. 11.3 shows the ordering and line information describing the K-space data of phase versus frequency. K-space itself is not the image; rather, it is an information package of an image. The "diagrammatic" representation highlights the acquisition order for a rectilinear MR K-space strategy. The actual data shown in Fig. 11.3b demonstrates the center-out character of K-space where the

low-frequency components of the image (contrast, total signal amplitude, etc.) are located around the K(0,0) point. Following Fourier transform (FT) computation in one or more directions, the "package" converts the K-space phase versus frequency into frequency amplitudes which is actual positional information.

Figure 11.4 is a demonstration of this positional transformation as it shows an image derived out of K-space order (Fig. 11.4a). By removing the center points of K-space (Fig. 11.4b), the resulting image consists of short-range or high-frequency edge transitions that show only line like image structures without any image contrast. Similarly, when transforming only the low-frequency components (Fig. 11.4c) results in a near-interpretable image based on contrast and large scale structures but at low spatial resolution.

A large number of methods or sequences have been developed to acquire MRI images and thus fill K-space most efficiently for the application and results desired. Simply by changing the K-space filling order from edge-to-edge sequentially, center-out, or center-in K-line ordering, it is possible to change the contrast of the image especially when changes in state to the imaging region are in progress (i.e., contrast agent washout). Table 11.2 includes some of the most common K-space filling orders in currently in clinical use. The major types, sequential rectilinear, EPI, and parallel imaging, account for a vast majority of the K-space ordering used. Some knowledge of these techniques will allow the reader to be more discerning about the strengths and weaknesses of each method when encountered in the literature.

11.2 Contrast Agents for Pharmacological Imaging

The field of MR imaging has greatly been improved, and indeed expanded, in capability with the introduction of contrast agents. Not unlike CT with X-ray contrast media such as the iodinated products, MRI has contrast-enhancing products. Unlike CT contrast agents which are electron dense and directly affect the X-ray absorption, MR contrast agents are typically not "seen" per se; rather, they affect the magnetic susceptibility and thus the tissue water imaging properties (not the media itself). Magnevist (formerly Schering AG, now Bayer) was approved for use by the FDA in 1988 and it revolutionized the kinds of imaging approaches one could take on then-typical systems with limited field strength and often stability and homogeneity issues too. Since that time there have been many other contrast media products introduced (Table 11.2). The products are termed "linear" or "macrocyclic" and "nonionic" and "ionic" to describe their chemistries; the macrocycles are supposedly more chemically stable than the linear variants, while nonionic agents in bolus form may be less perturbing to the heart, for example. These kinds of agents generally require a paramagnetic atom or ion: gadolinium (Gd), dysprosium (Dy), iron (Fe), and manganese (Mn), among others, have been employed for this purpose.

The Fe ion is, of course, intrinsic as a physiologic element predominantly in hemoglobin, myoglobin, and red blood cells. It is also very effective in what are

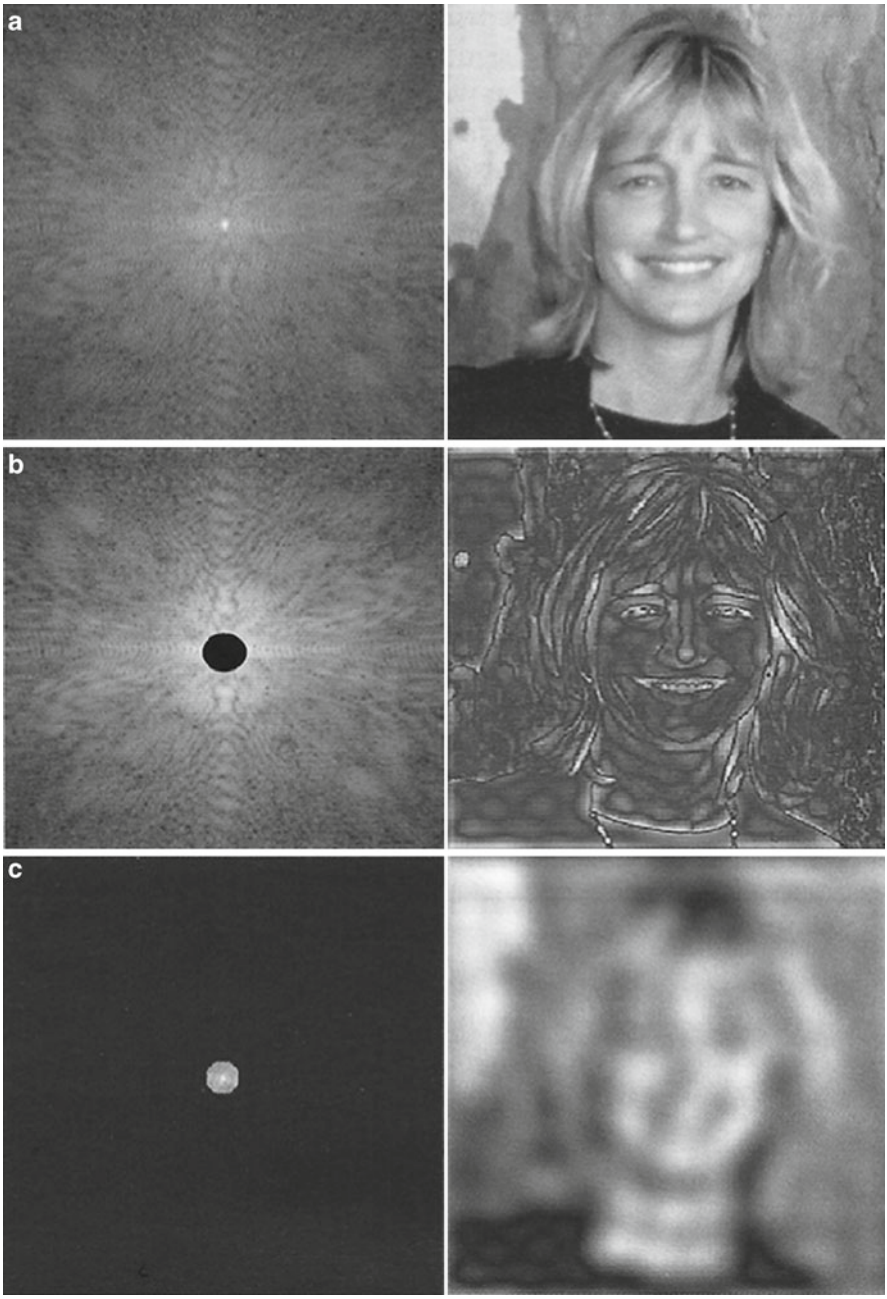

Fig. 11.4 A depiction of the spatial information contained in K-space. The entire K-space information is passed through a Fourier transform to which transforms frequency amplitude to frequency-domain (positional) space to create the image in where (**a**) is the entire K-space, (**b**) is everything but the center information (high resolution but poor content), and (**c**) is the center information only (poor resolution with high content). Magnetic field gradients spatially locate signals according to their frequency and converts to amplitude (positional intensity). From: Westbrook et al. (2011); with permission

Table 11.2 Clinically relevant K-space filling strategies. This table summarizes the some common methods for filling K-space, organized according to trajectory

Trajectory	Variants	Rationale	Utility
Non-EPI rectilinear	Sequential	Every k_y step is acquired as a individual readout ordered from top to bottom of K-space	All standard imaging sequences where contrast is constant over excitations (steady state imaging)
	Centric	Every k_y step is acquired as a individual readout starting with the center line ($k_y = 0$) and alternating ($+k_y$ and $-k_y$) on subsequent excitations	Used for applications where initial transient contrast dominate the image (i.e., a preparatory RF stage or contrast injection—non-steady state)
	Reverse centric	Every ky step acquired in a separate readout, starting with the outer lines of K-space ($k_y = +k_{y,\,maximum}$ and $-k_{y,\,maximum}$) and working inward from either edge in successive excitations	The final relative contrast dominates the image contrast, typically used after a preparatory pulse such as inversion (non-steady-state imaging)
	View-sharing	Incomplete sets of k_y lines acquired for different cine phase images. Share k_y lines between temporally adjacent readouts to fill K-space for each cine phase image	Cine applications use short scan times and high temporal resolution with good spatial resolution. A consequence is temporal blurring (heart and abdominal scans)
	Partial or half Fourier	More than have the k_y lines are acquired and using K-space symmetry estimate the missing data	Rapid scan requirements such as cardiac, interventional or dynamic contrast applications. Results in a reduction of ~2 in scan time at the cost of 1/sqrt(2) reduction in signal-to-noise ratio
	Zero filling or Fourier interpolation	Central k_y lines are acquired (minimally half the desired matrix size) and substitute zero for the missing data points. "Zero filling" in K-space is equivalent to a perfect interpolation of a low resolution image to a higher resolution image without linear or polynomial limitations	Rapid scan requirements such as cardiac, interventional or dynamic contrast applications also. Results in a reduction of N in scan time at the cost of 1/sqrt(N) reduction in signal-to-noise ratio

(continued)

Table 11.2 (continued)

Trajectory	Variants	Rationale	Utility
EPI—echo planar imaging	Single shot—blipped	Traverse all of K-space, starting in one corner, sweeping across the k_x axis for a given k_y value, turning ("blipping" or formally "boustrophedon") to the adjacent k_y line and sweeping back across the readout axis. Following the boustrophedon to the next k_y line and so forth until K-space is completed	Very high speed applications such as functional MRI (fMRI), stroke (DWI) or diffusion tensor neuroimaging (DTI). Distortions and T_2*-dependent signal loss limit the acquisition of a high-resolution image
	Multi-shot—blipped	Increase the granularity of K-space travel, beginning at one edge acquiring a readout turning the boustrophedon to the next non-adjacent k_y line and acquiring the readout, and so forth. Using a fraction of K-space equal to $1/N_{shots}$). N_{shots} excitations used to complete the image	Not as fast as single-shot EPI. Used for rapid applications (fMRI, DTI) for higher resolution images. Less distortion and higher signal-to-noise ratio than single-shot EPI
Parallel imaging	GRAPPA	Uses specific receiver coil geometries create additional K-space data without added scans. Auto-calibrates using central K-space lines	Used for reduction in imaging time where a reduction in image SNR is offset by high efficiency receiver coils
	SENSE	Receiver coil sensitivity maps are used to compute additional k_y lines in K-space from unders-ampled (factor of 2–8) data	Rapid scanning applications that use the high efficiency receiver coil arrays to reduced SNR losses due to scan time reduction

termed SPIO (super paramagnetic iron oxide) applications. SPIO magnetic resonance imaging can be used in liver pathologies, i.e., nonalcoholic fatty liver disease, as a way to evaluate Kupffer cell phagocytic function. Iron oxide (as SPIOs) can be also used in cell labeling and thus tracking cells and their homing capacity. With typical pulse sequences and at the relatively high field strengths common in small animal imaging, iron is usually considered to be a specific T_2 imaging agent meaning that its principal effect is to shorten the tissue T_2 causing a signal "drop out" (reduction) rather than giving a signal enhancement such as might be expected with a T_1 contrast agent.

In the ionic form, manganese (Mn), gadolinium (Gd) and dysprosium (Dy) from the lanthanide series exert a dramatic effect on the relaxation properties of water. This effect results from unpaired electrons in the *d* or *f* atomic shells, which give rise to a strong magnetic moment. Other elemental examples include Cr^{3+} (3 unpaired electrons), Fe^{3+} (5 unpaired), Ni^{2+} (2 unpaired), Cu^{2+} (1 unpaired, with dipole contributions from the *d* shell), Eu^{3+} (6 unpaired), Gd^{3+} (7 unpaired), and Dy^{3+} (5 unpaired, with contributions from the *f* shell). Although the properties of each ion govern its utility in imaging, the strength of an ion's effect on contrast will depend upon the strength of the magnetic moment.

The effect of these ions on the excited ^1H nuclei (which comprise the MRI signal) depends on multiple components. First, the dipoles of the ions may interact with nuclear ^1H dipole, which in turn stimulates spin–flip transitions and accelerates T_1 relaxation of ^1H. The strength of this interaction depends on the approach distance between ^1H and the ion. If the ion is part of a larger molecule (e.g., deoxyHb), large distance leads to a small interaction. The effect magnitude of the dipole–dipole interaction is also modulated by the correlation time which determines the duration of the coupling between ^1H and ionic dipole. To increase coupling, the rotational rate of the ion or chelating molecule should be similar to the excitation frequency of ^1H. If the ion is not chelated, it will have a wide range of rotational velocities compared to the excitation frequency of ^1H. In this case, the dipole–dipole interaction is weaker. For suitable rotational rates, the correlation time will depend on the electron spin relaxation time of the agent, where slower electronic relaxation results in greater coupling of the dipoles. Ultimately, relaxation rates should be comparable to the ^1H Larmor frequency for an agent to be effective at increasing T_1 relaxation. Electron spin relaxation times for ionic Mn and Gd are ~10^{-8} to 10^{-10} s and appropriate for the range of Larmor precessional frequencies in clinical scanners. Larmor precession refers to the precession of the magnetic moments of electrons, atomic nuclei, and atoms about an external magnetic field. Those effects which lead to spin–flip transitions also result in randomization of ^1H phase after de-excitation and result in increased local T_2 relaxation. Finally, the presence of the paramagnetic dipoles around less mobile ^1H nuclei (e.g., water in the hydration shells of tissue macromolecules) alters the local precessional frequency, which further increases T_2 relaxation.

Consideration of all these effects together determines the ratio of T_1 and T_2 relaxation rates for a given concentration. Like other forms of emission spectroscopy, these characteristic relaxation processes return the nuclear magnetization back to

the equilibrium distribution after being excited. Ions with longer spin relaxation time (e.g., Mn^{2+}, Gd^{3+}) tend to stimulate spin–flip transitions effectively and are useful for enhancing contrast positively on T_1-weighted images. At higher concentrations, they are also useful for increasing T_2 relaxation resulting in local loss of signal in the image. Increased signal is particularly useful because it usually has a higher dynamic range and can be quantified more accurately than a loss of signal. Typically, paramagnetic agents, such as chelated Gd, increase T_1 and T_2 relaxation at the same rate per mM. Since this rate is the same, the change of T_1 relaxation per mM is larger by proportion than the change in T_2 relaxation. On the other hand, ions with shorter spin relaxation times, such as dysprosium (Dy^{3+}), do not stimulate spin–flip transitions readily. These ions function primarily to vary the local Larmor frequency (they are said to act as "chemical shift agents") and therefore to decrease the intensity on T_2-weighted images which are formed from protons precessing at or very close to the original Larmor frequency. While Mn^{2+} may not have as strong of a magnetic moment as other agents such as Gd^{3+}, the T_2 relaxation rate (R_2) of water containing Mn^{2+} ions at 1.5 T grows at 10× the rate per mM as compared to the T_1 relaxation rate (R_1). This makes Mn^{2+} a valuable agent for both T_2 and T_1 imaging, the effect depending on the field strength and the local concentration of agent in the tissue.

Another avenue to increase the T_1 relaxivity is to chelate the paramagnetic ions to a larger molecule so as to decrease their rotational velocity and increase the rotational correlation time. An added benefit of using a chelate is that for less chemically reactive but toxic metals, such as Gd, the chelated complex is excreted from the body within a short timescale (approximately a few hours). This greatly decreases potential toxic side effects, although in some patients with altered kidney function gadolinium contrast agents have been associated with severe toxicities causing the FDA to require a black-box warning to be included in the label (see Sect. 11.2.1. Nephrogenic Syndrome). Examples of chelates that have been used include Gd-DTPA, Gd-DPDT, Gd-DOTA, and other macromolecules such as MnDPDP, Cr-EDTA, and Dy-EDTA. Nonionic molecules have also been utilized to prevent the release of the ion and to decrease the rotational velocity.

Manganese dipyridoxyl diphosphate (MnDPDP) is approved as an i.v. contrast agent for MR imaging of the liver. MnDPDP is a chelate consisting of the organic ligand dipyridoxyl diphosphate (DPDP) and Mn^{2+}. Following i.v. injection, MnDPDP is metabolized by a process involving dephosphorylation of MnDPDP to MnPLED (manganese dipyridoxyl ethylamine) and exchange of Mn^{2+} for Zn^{2+} (Toft et al. 1997) with the consequent release of manganese ions. In humans the rate of total manganese plasma clearance is multiphasic (Toft et al. 1997). The initial clearance half-life lasts for less than 20 min, with the longer terminal elimination phase occurring between 5 and 11 h. Following i.v. injection of MnDPDP, the released manganese accumulates in the liver, bile, pancreas, kidneys, and cardiac muscle (Hustvedt et al. 1997). Following oral intake the manganese accumulation occurs only in the liver and bile (Thomsen et al. 2005). Due to its T_1 relaxation effect, the released Mn^{2+} ions act as an MR contrast agent (Cory et al. 1987; Mendonca-Dias et al. 1983) which allows MnDPDP to be used as an MR contrast agent.

11.2.1 Gadolinium Nephrogenic Syndrome

Gadolinium ions have known toxicities and as such any use of Gd requires the chemistry of the contrast agent keep the ion "caged" in chelation to maintain safety. The safety issue for gadolinium is known as nephrogenic syndrome (fibrosis) (Kanal 2008). It is primarily a skin phenomenon but can affect internal organs as well. Originally termed nephrogenic fibrosing dermopathy (NFD) due to its proclivity for the skin, it was eventually found to actually include systemic tissues and organs. Gadolinium-based MR contrast agents (GBMCAs) which have received FDA approval include, for example, Omniscan™ (gadodiamide) which is the one agent that accounts for most of the nephrogenic syndrome reports. There are two others that contribute to the total incident count and they are Magnavist™ (gadopentetate) and Optimark™ (gadoversetamide). It is apparent that most of the patients developing this syndrome are also in end stage renal disease, are >60 years of age and have a history of diabetes or a history of severe hepatic disease/liver transplant or pending liver transplant. Present recommendations from the ACR MR safety committee can be found at http://www.acr.org/mr_safety (Kanal et al. 2013). An excellent review of the safety of contrast agents in MR is provided by Kirchin and Runge (2008).

11.3 MRI and Functional MRI (fMRI) Applications

MRI and fMRI have advanced their footprint in the drug development laboratory with increasing improvements in system adaptations to small animals and novel imaging pulse sequences which have expanded both anatomical and functional capabilities. Functional MR imaging (fMRI) is an imaging technique that can evaluate blood flow when at rest and following stimulation. It is particularly useful in the brain because of the well-defined and largely symmetric anatomy and the tight anatomic and physiological relationship between neural and vascular tissues, but it has been applied to other tissues. Two or more sets of images collected under different conditions (with and without some stimulus, e.g.) can be related mathematically and can be statistically correlated with each other to reveal the areas showing changes as a result of the stimulus, for example, the altered blood flow patterns in regions of the brain performing mental activation tasks. This methodology has been extended to brain studies where drugs (rather than physical or mental stimuli) can alter the activity of regional centers to show blood flow changes in the affected areas of the cerebral cortex. In the early days of fMRI, the change in flow was mostly seen using contrast agents but now the blood itself, and its intrinsic sensitivity to MR fields (oxyhemoglobin is diamagnetic vs. deoxyhemoglobin which is paramagnetic) allows one to image blood flow without contrast. Venous blood contains an almost equal mix of oxy and deoxyhemoglobin. With exercise (change in oxygenation) more oxygen is needed and thus the oxy component is extracted from the capillaries changing the "delta." Paramagnetic deoxyhemoglobin creates an inhomogeneous magnetic field in the immediate vicinity in the brain and this in turn increases the T_2* decay and attenuates the MR signal. The MR signal intensity change is called the BOLD or "blood-oxygen-level-dependent" effect.

The notion that MRI could be sensitive enough to measure brain activity, in addition to brain anatomy, is only about 20–25 years old. An observation was made that when neural activity was seen to increase in a particular area of the brain, the area had a measurable MR signal that also increased by a small amount. Although this effect had a magnitude change of close to 1 %, it was seen to be consistent and measurable with high accuracy and is now a major basis as to why fMRI has taken off as a very useful MR tool in neurologic diseases, chemical injuries, blood–brain barrier breaches, and even in psychopharmacology in cognitive neuroscience. The applications of fMRI in translational medicine and clinical practice are becoming an important tool to measure plasticity of neural recovery (surgery and trauma) and maintenance of brain function under stresses and disease.

In its simplest form, fMRI places a subject under conditions where the subject alternates between periods of doing a particular task and placing himself back into a stable (cognitively speaking) control state. This could, for example, be structured as 30 s blocks looking at a visual stimulus alternating with 30 s blocks with eyes closed. The fMRI data is analyzed to identify brain areas in which the MR signal has a matching pattern of changes and these areas are taken to be activated by the stimulus (in this example, the visual cortex at the back of the head).

It is not because the MR signal is directly sensitive to the neural activity. Instead, the MR signal change is an indirect effect related to the changes in blood flow that follow the changes in neural activity. The picture of what happens is somewhat subtle and depends on two effects. The first effect is that oxygen-rich blood and oxygen-poor blood have different magnetic properties related to the hemoglobin that binds oxygen in blood. This has a small effect on the MR signal, so that if the blood is more oxygenated, the signal is slightly stronger. The second effect relates to an unexpected physiological phenomenon. For reasons that we still do not fully understand, neural activity triggers a much larger change in *blood flow* rather than in *oxygen metabolism*, and this leads to the blood being more oxygenated when neural activity increases. This somewhat paradoxical *blood-oxygen-level-dependent* (BOLD) effect is the basis for fMRI (Fig. 11.5).

The orderly and sequential accretion of cognitive milestones in the typically developing child constitutes a most fascinating facet of childhood development. The establishment and use of cognitive developmental screening instruments such as the Denver Developmental Screening Test and the Wechsler Intelligence Scale for Children (WISC-R[1]) reflect the normalized and chronologic pattern of cognitive development documented in children. Recent advances in neurobiology have provided new understanding of cellular events that underlie neuronal function in the central nervous system. While this critical information sheds light upon function of the brain at a microanatomic level, it sheds little light upon the ways in which the neural tissue of the brain functions as an interrelated network of subsystems to produce human behavior and cognition.

[1] Refer to Wechsler Intelligence Scale for Children http://www.pearsonassessments.com/HAIWEB/Cultures/en-us/Productdetail.htm?Pid=015-8979-044.

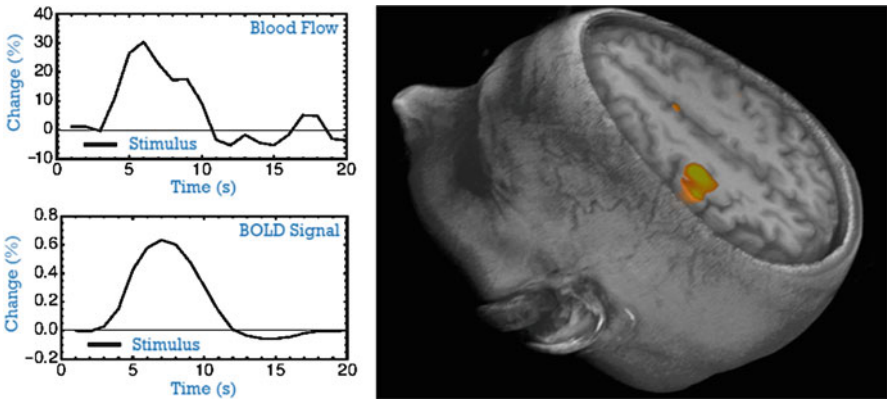

Fig. 11.5 fMRI is a way to describe and image changes in localized blood oxygenation. Depicted in the figure is a theoretical location in the brain where blood flow is measured and the concomitant BOLD signal parallels the time course and relative area and modulation profile. UCSD, Center for Functional MRI, *Why is the MR Signal Sensitive to Changes in Brain Activity?* http://fmri.ucsd.edu/Research/whatisfmri.html. *Left image*: reproduced from Buxton (2010), based on data from Miller et al. (2001); *Right image*: reproduced from Buxton (2002)

11.3.1 Small Animal and Pediatric Applications of fMRI

One of the major uses of fMRI is in early childhood development in the assessment of disease, cognitive impairments, and functional deficits. This is even true in the fetal subject where certain regions of the brain can be assessed for blood flow preterm. Table 11.3 gives a time line of major development events and anatomical information can be collected via MR imaging and the cofunctional component may also be explored using fMRI. In fetal imaging blood flow changes can be monitored using metronomic sounds as a form of stimuli. The use of anesthetics to prevent motion during a scan may be necessary with small children but it is common in small animal imaging; care must be taken that the anesthesia does not unduly perturb the physiology being studied (there are effects on cerebral blood flow and blood glucose levels to consider, e.g.). Again, the reader is encouraged to seek further information on small animal imaging with MRI in the textbooks of Westbrook et al. (2011) and Gavin and Bagley (2009).

The regional blood flow in young children can be measured using task-oriented tests (reading, writing, physical movement) or passive testing such as auditory stimuli, tactile sensory stimuli, smells, and perturbations in light exposure. Each of these activities can change blood flow associated with the brain region of interest. Rivkin provides some examples in these tests in Fig. 11.6. fMRI has pediatric challenges but it also has issues of reproducibility in the aged and in certain diseases such as dementia where comprehension is required (D'Esposito et al. 2003).

Table 11.4 on the pediatric neuroanatomy development schedule and Fig. 11.7 showing pediatric brain blood flow using fMRI are presented as examples of the complexity involved in pediatric MR imaging. Age dependent brain anatomic

Table 11.3 Major Gd and Mn contrast agents and their physical attributes for imaging[a, b]

Characteristic	Magnevist	ProHance	Omniscan	MultiHance	Gadovist	OptiMARK	TeslaScan
Type	Linear, ionic	Cyclic, nonionic	Linear, nonionic	Linear, ionic	Cyclic, nonionic	Linear, nonionic	Complex cage see figure "a" below[c]
Paramagnetic ion	Gd	Gd	Gd	Gd	Gd	Gd	Mn; MnDPDP
Metal chelate (mg/mL)	469	279	287	334	605	331	2.75
Dosage concentration	0.5 mol/L	0.5 mol/L	0.5 mol/L	0.5 mol/L	1.0 mol/L	0.5 mol/L	5 μmol/kg
Osmolality (Osm/kg)	1.96	0.63	0.65	1.97	1.6	1.11	2.98
Viscosity (mPa s @ 37 °C)	2.9	1.3	1.4	5.3	4.96	2.0.	Not available
T_1 relaxivity L/mmol s @ 0.47 T in plasma	4.9	4.6	4.8	9.7	5.6	Not available	r1 = 2.3, r2 = 4.0 (@ B_0 = 1.0 T)

[a]Table adapted from Kanal (2008)

[b]Note: Fe paramagnetic products include SPIO (superparamagnetic ion oxide; particles) for cell labeling and other applications

[c]Figure "a": The MnDPDP structure. For Gadolinium contrast agent cage structures the reader is referred to Faulkner (2008):

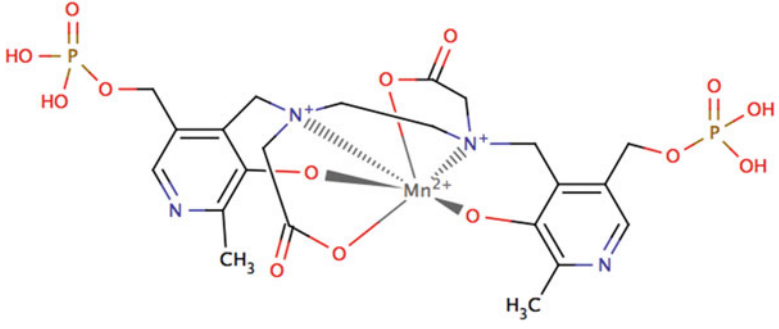

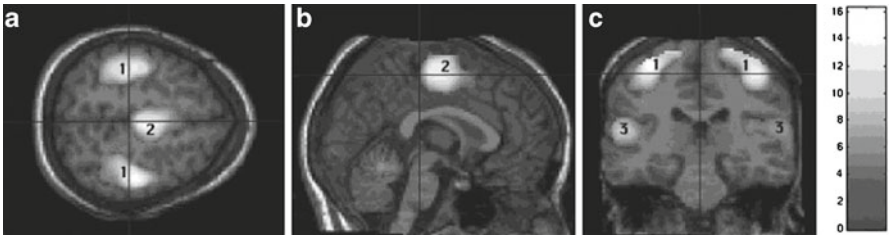

Fig. 11.6 fMRI imaging in pediatric (nonverbal task) conditions. Group analysis of data obtained during fMRI study of four 9- to 10-year-old normal volunteer children. The children were instructed to perform bimanual alternating finger tapping to match the rhythm of a metronome beat delivered to them simultaneously by earphones. The statistical color map of regional activation is rendered upon the high-resolution T_1W image of one of the subjects. The axial image (**a**) demonstrates activation of primary motor cortex (areas marked by 1) and supplementary motor cortex (area marked by 2). The sagittal image (**b**) provides a medial view of supplementary motor cortex (area marked by 2). The coronal image in (**c**) reveals the same regions of primary motor cortex (areas marked by 1) activation found in (**a**). In addition, the superior temporal gyri (areas marked by 3) reveal significant activation indicative of their role in hearing the metronome beat (from: Rivkin 2000). The nonverbal task approach is applicable to small animal studies

Table 11.4 Major events in human brain development and peak times of occurrence[a]

Major development event	Peak time of occurrence
Primary neurulation	3–4 weeks' gestation
Prosencephalic development	2–3 months' gestation
Neuronal proliferation	3–4 months' gestation
Neuronal migration	3–5 months' gestation
Apoptosis	6 months' gestation-1 month postnatal
Synaptogenesis and organization	5 months gestation-years postnatal
Myelination	Birth-years postnatal

[a]Adapted from Rivkin (2000)

changes in newborns can confound image interpretation of blood flow patterns. Brain tissue arterial input and venous drain (i.e., flowing blood) is what is imaged in fMR. As blood passes through a selected brain slice an RF pulse is applied to the slice and the blood within the slice experiences a phase change which allows for localized angiographic evaluation.

In brain cancer, fMRI has a practical application (Young and Knopp 2007). fMRI provides activation maps of the brain cortex that reflect hemodynamic activity related to neuronal activity. As discussed preciously, the BOLD signal of local tissue oxygenation measures the magnetic property changes of hemoglobin as blood traverses through a vascular network as an intrinsic contrast agent. The effect of oxygenation of a brain voxel element is an increased diamagnetic oxyhemoglobin and decreased paramagnetic deoxyhemoglobin. Measurements within the brain locations for speech, language, comprehension, memory, and motor skills which may be altered by tumor invasion can be measured and efficacy of treatment assessed. Preoperative fMRI can help the physician (or nonclinical investigator) to better determine the BOLD valuations of the tumor margins, control regions of the brain, supplemental cortex, and globally the bilateral hemispheres. Increased tumor

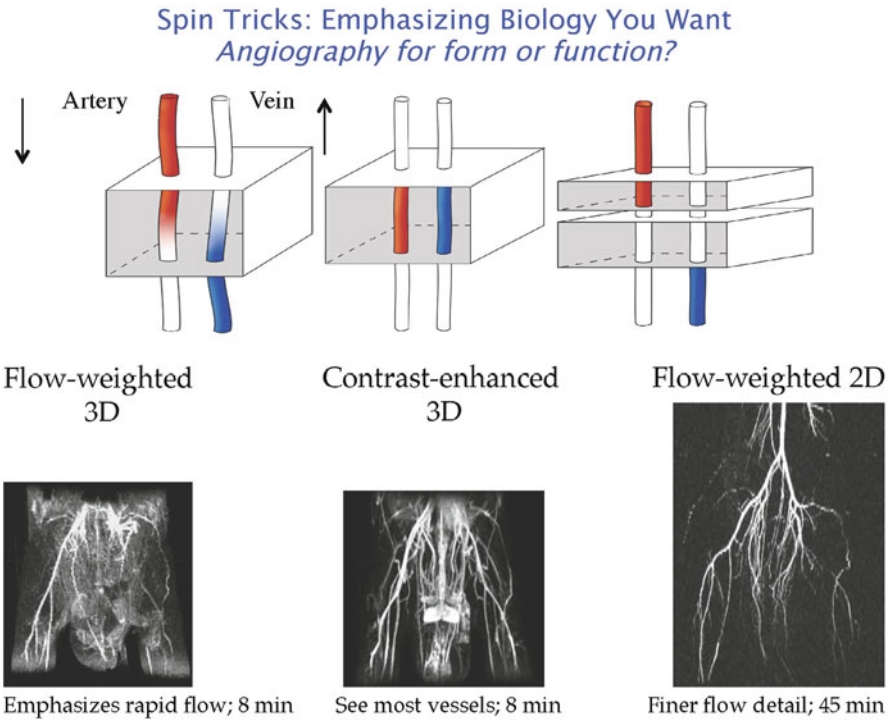

Fig. 11.7 Depiction of flow, where magnetic transference occurs within an MR image slice, which may be mapped to show relative change through a targeted vessel. Courtesy of Simon Williams, Genentech, So. San Francisco

vascularity provides a measure of the grade of the tumor. The interpretation of the BOLD signal, however, requires some caution toward use as a clinical or translational tool for assessing drug-induced differences in fMRI images (Logothetis and Wandell 2004; Matthews et al. 2006)

Ferrari et al. (2012) provide an excellent review of an experimental protocol for rats and mice to evaluating pharmacologic fMRI changes (phMRI, *ph*armacologic or *ph*ysiologic MRI). They discuss the role of anesthetics (isoflurane and halothane) and chemical use, animals and the constraints on the animal models, animal preparation, tracheotomy (for controlled ventilation), vessel cannulations appropriate for the MR contrast agent administration and blood gas determinations in the MR environment, arterial gas measurements, relative cerebral volume (rCBV), use of a 4.7 Tesla system T_2-weighted anatomical images using RARE sequence (RARE; rapid acquisition with relaxation enhancement) as well as conventional spin-echo sequences, and use of the blood pool contrast agent Endorem® (Guerbet, France). The methods they report are limited in that this is not set up for chronic measurements. However it has excellent applications in the study of neuroscience and psychopharmacology. Figure 11.8 depicts physiologic (or pharmacologic) phMRI images (Becerra et al. 2013).

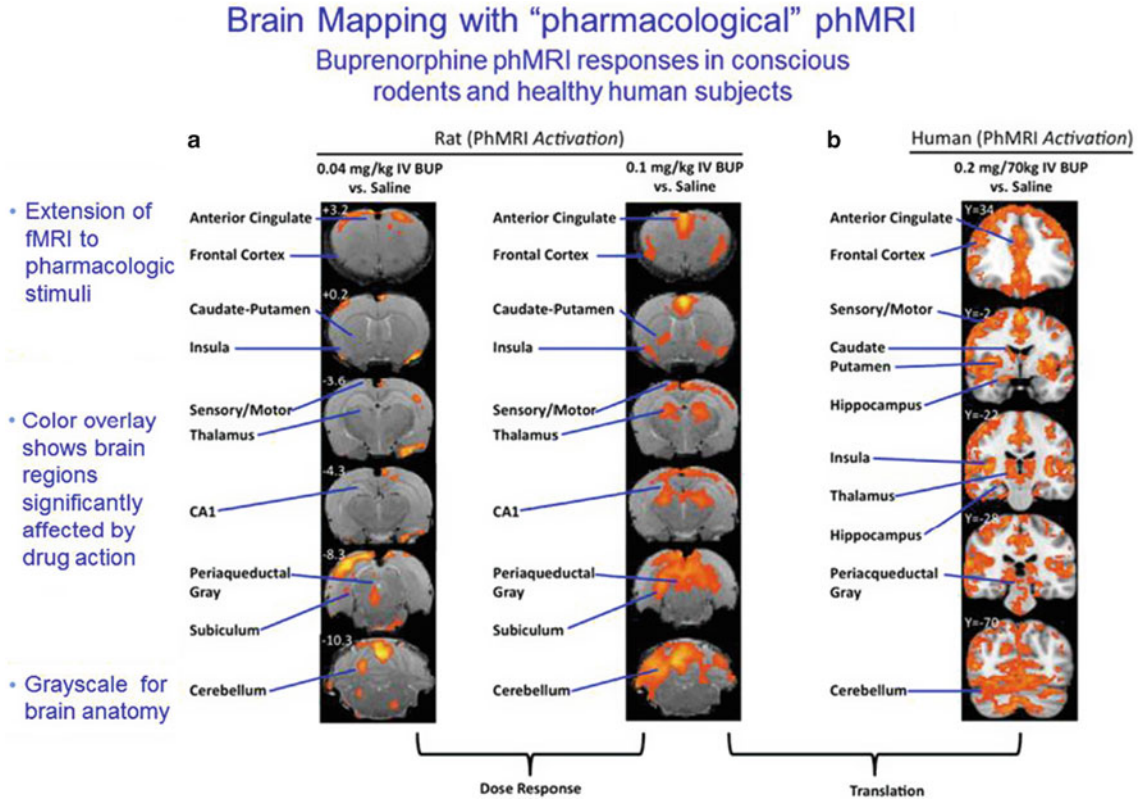

Fig. 11.8 Physiologic/pharmacologic MRI. phMRI for brain mapping of drug intervention in the rat (**a**) and in the human (**b**) conscious brain. Images depict both rodent and human response maps of activation by buprenorphine (BUP). From: Becerra et al. (2013); with permission

11.3.2 MR Imaging and Psychopharmacology

Yurgelun-Todd et al. (2005) describe in their paper a study of fMRI imaging in schizophrenic patients during word production and the pharmacologic effects of D-cycloserine (D-CS). D-CS, a partial agonist at the glycine recognition site of the n-methyl D-aspartate (NMDA) receptor, can improve primary negative symptoms in schizophrenics. Rats administered the drug MK-801, an NMDA antagonist, have been shown to have a deficit in spatial memory which can be reversed by D-CS. D-CS thus serves as a neuroleptic for the structural and functional abnormalities in the frontal and temporal cortex of schizophrenics. The effect of D-CS in cognition is less well understood. Previous work using verbal cognitive challenge testing an fMRI in controls and schizophrenics showed control subjects had greater activation of the left dorsolateral prefrontal cortex region relative to the schizophrenics. Schizophrenics exhibit hypo-frontality and neuroleptic therapy increases activation in the left temporal lobes relative to nonpsychiatric controls. Using fMRI they were able to show that D-CS plus neuroleptics augmented temporal lobe activation in schizophrenic patients relative to neuroleptics alone. They were also able to surmise that enhanced temporal lobe activation was negatively associated with a reduction in negative symptoms. Word fluency was effectively augmented in subjects administered D-CS, and the fMRI results demonstrated that the temporal lobe activation directly correlated with the temporal drug induced change in blood flow which characterized the temporal lobe activation.

Roe and Chen (2008) provide a very good paper on high-resolution fMRI maps of cortical activation in nonhuman primates (NHP), a very prominent model in testing brain changes due to drug activity, i.e., psychopharmacology. They were addressing a method to map high spatial (submillimeter) resolution of cortical activity in the NHP brain. They note that other methods have been able to report at this level such as with optical imaging which has contributed in confocal microscopy in brain layers at the mm-plus dimension. Can fMRI also map the NHP brain at such resolution? Their hypothesis was "yes." They studied the ability of BOLD fMRI to measure submillimeter resolution of the NHP cortex. Digital (hand, digit 3, D3, e.g.) stimulation leads to focal activation at the cortical location of D3 activation/stimulation and also stimulation of D4 was mapped to the D4 location in the cortex—using optical probes. The stimulation of D3 and D4 should lead to two activation spots, but what was observed was only *one* central location stimulation suggesting an illusionary perception. They observed that stimulation of the skin is not only a *surface topography* map but also a *perception* map. The brain serves as an integrator of signals for general "perception." This was observed using optical probes and set the standard resolution required to test their hypothesis of obtaining similar information using fMRI. Consistent with the optical experiments, simultaneous stimulation of D3 and D4 in squirrel monkeys produced a single fMRI central focal cortical activation with 0.5 mm resolution image of the central stimulation spot. This kind of resolution has potentially profound implications in measuring psychopharmacologic drug interventions in the NHP model.

Mitterschiffthaler et al. (2006) discuss the utility of fMRI in psychiatry. The utility of psychiatric assessments in translational species remains in question but certainly changes in their physiologic parameters (as phMRI; refer to Fig. 11.8) by drug induced physiologic actions can be imaged and quantified in the non-clinical setting.

11.3.3 The Apparent Diffusion Coefficient (ADC) and Stroke

As most clinical and preclinical MRI is based on looking at the hydrogen nuclei of large concentration compounds such as water and fat, it is possible to sensitize the image to the structure below the level of the image resolution. One of the strengths of MRI is the ability to make relatively small changes in pulse sequence to be sensitive to certain physical effects. In this manner, we can make the sequence diffusion-weighted image (DWI). DWI is can probe the integrity of cell membranes, the changes in microvascularity in tumors, and changes due to osmotic shock as in strokes or thrombosis. Diffusion sensitivity is produced by adding strong gradient pulses that encode nonlinear movement due to Brownian motion of water molecules traversing the local environment. The diffusion length scale can probe dimensions as small as a micron or as long as 10 s of microns by varying the length, amplitude, and spacing of the diffusion gradients. Using this flexibility other applications of diffusion sensitized MRI can be detecting and following neuronal fiber tracts in the brain, spine, or major nerves. In like manner, diffusion-based methods can be used to track muscle fibers in skeletal and cardiac muscle. All of this done without any external contrast compound needed to be added. The basic diffusion-weighted image (DWI) technique, the Stejskal–Tanner sequence, uses a pair of high-amplitude gradient pulses in a spin-echo sequence with increasing amplitude,

$$I = I_0 \times \exp\left(-bD\right),$$

where $b = f(G, \delta, \Delta)$ and where G = gradient amplitude, δ = gradient spacing, Δ = gradient duration.

The signal, I, is reduced in amplitude from I_0 based on the amount of diffusive motion the water molecules undergo. In this technique, any motion produces a reduction in signal amplitude, I. Thus, it is possible to encode motion such as perfusion or in some limited case flow as a complicating effect. This apparent diffusion coefficient (ADC) yields a method to probe the microstructural integrity of tissue at a cellular level (Moseley et al. 2009). The ADC map can be obtained as a slope of a series of diffusion-weighted images with changing gradient strength (i.e., images collected at $b = 0$ s/mm^2), then, for example, $b = 250$, then $b = 500$, then $b = 700$, then $b = 1000$ s/mm^2, and then the natural log of the ratio of each image to the first image ($b = 0$) as log[Image "$b = X_o$"/Image "$b = 0$")] is plotted versus "b" to obtain the decrement in regional intensity with increasing gradient strength (Fig. 11.9). In stroke, the apparent diffusion is measurably slower (thus relative hyperintensity is retained in the infarcted area in the diffusion image) compared to normal brain areas by as

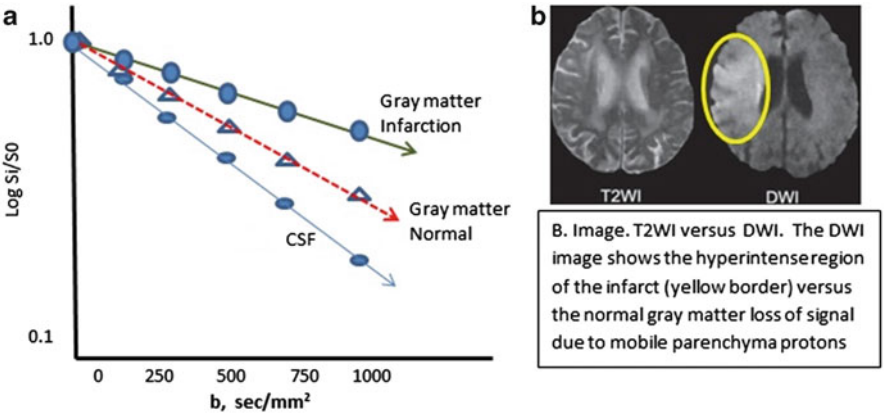

Fig. 11.9 The ADC profile (cm^2/s, or m^2/s). (**a**) *Plot*: An ADC map is obtained from a series of DW images with increasing *b* value (s/mm^2) here plotted as a series of regional area ratio values from $b = 0–1{,}000$. The ADC is the slope of the profile. Gray matter has a slope is less than the CSF (cerebrospinal fluid) and is commonly 1×10^{-5} cm^2/s, where the average displacement along one direction in the image is 8–9 μm observed over a 30–50 ms period. ADC regional decreases are highly correlated with areas of infarction (more mobile extracellular water protons). (**b**) *Image*: T_2WI versus DWI where the DWI shows the ADC hyperintense region of an ischemic stroke (*yellow circle*) (From: Neil (2008), with permission)

much as 30–60 % decreases in the slope (a flattening of the slope) versus normal. Figure 11.9 depicts an infarcted region which remains hyperintense in a DW image versus that same slice imaged as a T_2-weighted image.

In the case of stroke, cerebral blood flow is compromised from the normal 12–20 mL/110 g/min to usually <12 or, at later time points, the region may be affected by increased flow, i.e., "luxury" perfusion, a condition called reactive hyperemia, where CBF is greater than 20 mL/110 g/min. Changes in CBF that are less than 12 will result in a hyperintense region of the DWI image (as seen in Fig. 11.9) which is a consequence of a decline in the apparent diffusion coefficient of water in passing through the brain parenchyma. In the chronic stroke brain environment (<12 mL/110 g/min), the ADC is elevated due to extracellular water content and low diffusibility.

In a trial conducted by Schlaug et al. 1997), they evaluated the relative ADC (rADC; a useful measure in preclinical studies as well), a ratio of lesions to control brain ROIs; they found that in stroke there are two phases for the rADC. That is, the rADC is reduced and lasts about 96 h staying at about 50 % of normal from the time of stroke onset. Then after 96 h an increasing trend in the rADC is observed from 50 % of normal to normal and then to elevation of rADC at times >7 days in excess of 200 % of normal. The persistent reduction in rADC in the first 4 h is suggested to indicate progressive cytotoxic edema rather than extracellular edema and cell lysis. Such an observation can thus allow investigations of rADC in test animal models with induced cerebral stroke (e.g., reperfusion injury following middle cerebral artery balloon occlusion rat models; Yang and Betz 1994).

Changes to the Fickian Diffusion model (Gaussian intensity decay) can be described using other DWI methods. One of the simplest methods is termed "diffusion kurtosis imaging" (DKI) where the deviations from Gaussian signal decay are mapped out using a kurtosis term to the normal (single mode) distribution (Jensen et al. 2005). This method purports to detect additional changes to the diffusion image which are masked by the ST model. A number of papers in recent years have applied this methodology to studies in neurology and oncology as a more sensitive detection for disease processes.

11.3.4 The ADC Applied to Conditions in Oncology

The reader is again referred to the Oncology chapter of this volume (Chap. 7) for a view of imaging platforms used in oncology and where the MR platform is described. MRI can be quite flexible in describing the tissue heterogeneity, vascularity, and microstructural changes found in tumor environments. Standard characterizations such as tumor perfusion, vascular bed integrity, and hypoxia can be measured via MRI based on water motion as tracked via diffusion or perfusion. Here we will specifically address the ADC and tumor blood flow/perfusion (and indirectly angiogenesis and blood volume). Krupnick et al. (2012) describe MRI protocols for the study of mouse lung tumors and these kinds of studies may be very valuable in the assessment of new chemical entities that target lung cancer in vivo. Indeed, their models are also quite relevant to the study of other lung pathologies including radiation injury which may include normal and lung cancer tissue responses. Physiologic and/or pharmacologic MRI can greatly help define the dose and schedule of treatments used for lung cancers, pleural effusions resulting from treatments and induction of cytokine overexpression, syndromes such as asthma or other immunologic compromises of the lung, and many more similar pathologies. The air spaces of the lung can create very large magnetic susceptibility artifacts and it has traditionally been very difficult to image small structures (like nascent tumors) accurately. Using MR techniques that reduce the image sensitivity to susceptibility diphase such as spin-echo variants can yield image clarity which is competitive with CT detection. This enables lung parenchymal imaging and makes MRI somewhat competitive with X-ray CT in these applications (Stolzmann et al. 2013).

DWI techniques can be used to observe image changes in tissue with such as carcinoma or tumor heterogeneity by changes in the diffusion sensitivity. These techniques can produce a secondary and confirmatory contrast for other techniques that depend on discrimination via T_1 or T_2 changes. This use of ADC has been shown to be a good marker for radiosensitivity as this generally tracks the hypoxic environments in tumors (Williams et al. 2013). The use of ADC without the use of contrast agent provides a stable longitudinal biomarker for therapeutic evaluation without complications due to imaging timing or animal preparation. Likewise ADC DWI can be used to determine rapidly occurring changes due the tumor vascularity and changes due to angiotensive factors producing disordered vascular permeability. Figure 11.10 below shows the ADC tracking changes in glioma growth model in

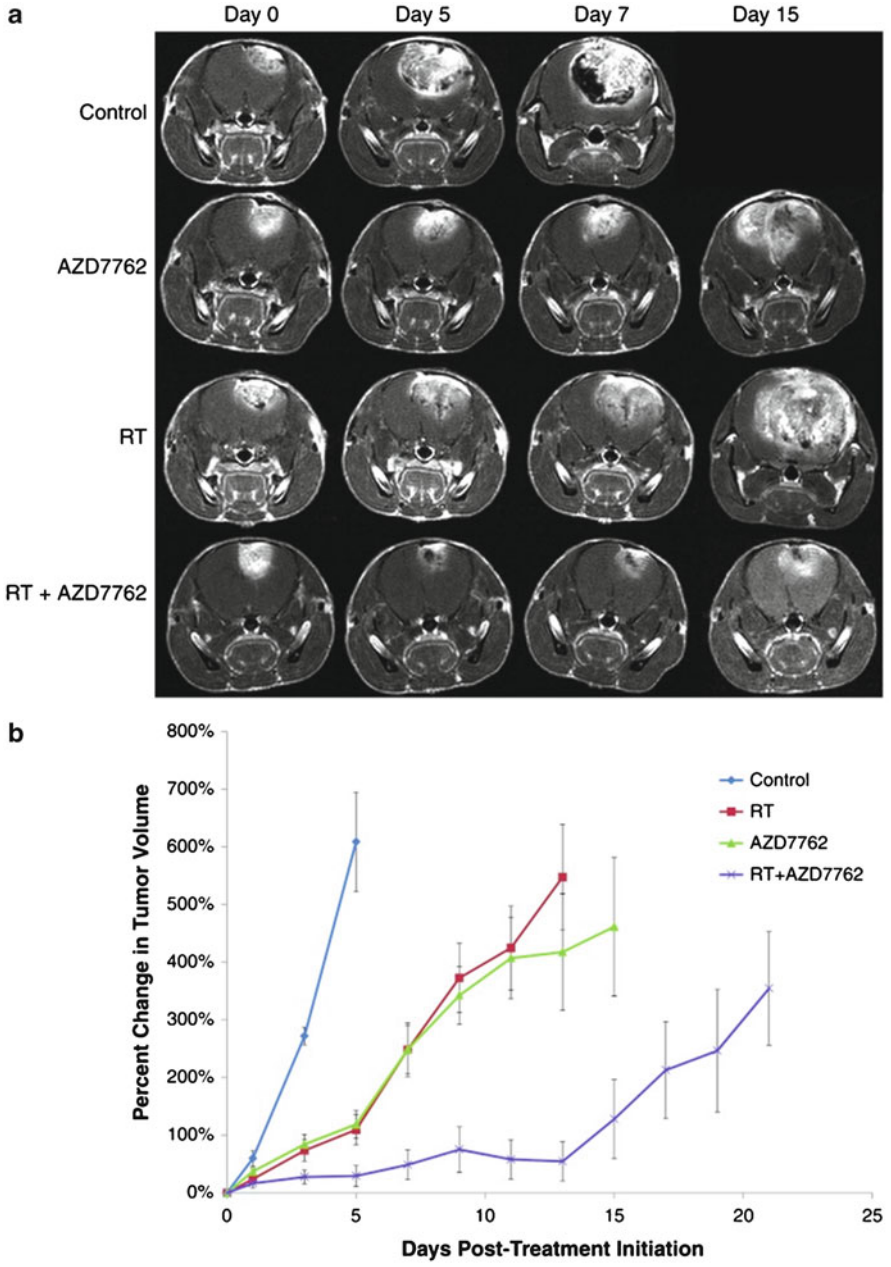

Fig. 11.10 MR images of rat cerebral tumors and treatment response. (**a**) MRI data consist of anatomic contrast-enhancing coronal T_1-weighted images for representative animals from each of the treatment groups from pretreatment (day 0) to days 5, 7, and 15. Day 15 is not shown for the control animal due to the rapid tumor growth for untreated animals. (**b**) MRI-determined intracerebral tumor volumes over time for each treatment group. Treatments occurred for 10 days total, 5 days/week. MRI was performed every other day during treatment and thereafter to determine tumor volume until end of study period for (1) control ($n=7$), (2) 15 mg/kg AZD7762 ($n=10$), (3) RT ($n=10$), or (4) AZD7762+RT ($n=12$). Error bars represent SEM. All tumor volumes were significantly different ($P<0.05$) from control tumor volumes beginning at day 3 post-treatment initiation. The combined therapy group was also significantly different ($P<0.05$) from the other three groups beginning at day 3 post-treatment initiation. Reproduced from: Williams et al. (2013) with permission

rodents with and without the administration of a radiosensitivity agent (i.e., selectively sensitizing tumors to DNA-damaging agents, kinase inhibitors).

Other related changes to the tumor environment such as perfusion can be detected via MRI. These perfusion-weighted imaging techniques can be used to determine the standard Kety equation parameters for bulk blood flow into tissue with quantification that is similar to PET 18-O-H_2O measurements. Quantified perfusion measurements via arterial spin labeling (ASL) techniques require additional time for the perfused spins to exchange with the tumor vascular bed and ECF (Wolf et al. 2005).

Other pulse sequences may find other applications in oncology as they can help to detect signal-loss image artifacts in the vicinity of other potentially attenuating structures such as iron-rich sites of necrosis or hemorrhage which are relatively common in tumors. The technique known as susceptibility-weighted imaging (SWI) is quite sensitive for detecting the changes that occur from necrosis and hemorrhage (Mittal et al. 2009). SWI, a post processing technique, detects the small local magnetic fields that distort the MRI signal phase on very short distance scales while retaining the high SNR of a standard gradient echo MRI.

11.4 Quality Control, Noise, Performance Monitoring, Contrast-to-Noise Ratio (CNR)

11.4.1 Noise and Artifacts in MRI

Noise and artifacts are part of the landscape of any analytical system. MRI has many that are intrinsic and many that are outside of the instrument and can be, in part, controlled by the operator and through environmental forethought in the design of the laboratory. There are additive elements of noise in MRI. These include thermal noise from the body which is the summation of thermal vibration of ions, electrons, etc., and this is the dominant noise in most MRI systems. There is also simple digital quantized noise from the analog to digital (A/D) devices and controllers, preamplifiers, and other sources of electronic noise. The RF coils have their own inherent thermal noise. A/D devices, preamps, and electronic noise and thermal noise in the RF coils are more limiting factors for very small objects such as for MRI microscopy. The use of higher fields is usually intended to achieve higher SNR, but this is dependent on the pulse sequence and the relaxation properties of the system being imaged; higher fields can sometimes reduce the SNR especially if the pulse sequence relies on prolonged periods of transverse magnetization such as in EPI. Major sources of nonthermal noise or variation in fMRI include cardiac and pulmonary variations, head movement, low-frequency noise, spontaneous neural and vascular fluctuations (BOLD noise), and behavior variations (subject and system). Sources of variation generally become more significant with increasing field strength. If one wants lower spatial resolution, then the thermal noise elements become less significant. Temporal

noise is also something that should be considered and is mostly related to time of day, system operating times (durations), variations in system support (heating, environmental controls cycling, HVAC, electrical power loads), and other variables.

In fMRI, Geissler et al. (2007) suggest that the contrast-to-noise ratio (CNR) may be a useful quality check. The contrast-to-noise ratio (CNR) is directly linked to statistical measures such as the *t*-values, but it does not depend on the number of points or number of runs (scans) as do the *t*-values themselves. In fMRI, the CNR is made up of the functional signal change and the temporal signal change as the average signal change (task related) over the non-task-related variability over time (time-series noise). The CNR is thus a useful intuitive parameter to estimate fMRI performance and may be useful in comparing fMRI images across imaging sessions and potentially across institutions.

11.4.2 ACR Practice Guidelines and Medical Physics Performance Monitoring

The American College of Radiology (ACR) has published Guidelines on MRI equipment and on performance standards for the performance and interpretation of MRI imaging (ACR 2003; ACR 2004). The Medical Physics Performance document (2004) sets goals for performance to produce consistency of the MR instrumentation and associated peripherals. They suggest the following performance characteristics be monitored:

- Physical and mechanical inspection
- Phase stability
- Magnetic field homogeneity
- Magnetic field gradient calibration
- Radiofrequency (RF) calibration for all coil
- Image signal-to-noise ratio (SNR) for all coils
- Intensity uniformity for all volume coils
- Slice thickness and location accuracy
- Spatial resolution and low contrast object detectability
- Artifact evaluation
- Film processor quality control (if applicable)
- Hard copy fidelity
- Soft copy fidelity
- MRI safety checks—environmental postings and controls

In addition, they recommend the following quality control programs for fMRI (and by association MRI in general):

- Physical and mechanical inspections
- Magnetic field gradient calibration
- RF calibration for the head coil (in fMRI, and brain imaging)
- Image SNR and uniformity for the head coil

- Film processor QC
- Hard and soft copy fidelity

Initial performance checks should be performed on installation and more comprehensive that the annual and the period performance checks. Acceptance testing should include the evaluation of all coils with reproducible but realistic phantom subjects since coil performance depends on the size, position, and conductivity of the sample. It must be clear that the peripherals are often not associated with the quality program and as such often are weak links in image quality and interpretation and may lead to errors in image evaluations. For systems of MRS (spectroscopy) an MRS series of quality checks in addition to these are recommended. The reader is directed to Chap. 12 on MRS techniques for further information.

The ACR Guidance for Performing and Interpreting MRI (2003) defines the staffing and training requirements (incl. medical physicists), technologists, and others. In addition, the document serves to guide the requirements on system documentation, equipment specifications, safety guidelines, quality control programs, and also such topics as infection control and imaging subject education and allowances for concerns (Kanal et al. 2013).

Friedman and Glover (2006) have provided an excellent review on approaches they have observed and recommend for multicenter fMRI quality assurance protocols. fMRI acquisitions are highly dependent on temporal stability. BOLD signals are changes on only a few percent in magnitude, and as such thermal or environmental change can affect the system and wipe out collected data by simply added noise. Stability across days, weeks, and months is necessary for fMRI systems. Friedman and Glover provide specific examples of what they term FIRST-BIRN fMRI and they provide sequence parameters using EPI or "spiral gradient echo recalled" (see Table 11.1 in Sect. 1.1). The authors of the paper discuss the phantom used in the Glover stability QA protocol as a 17 cm diameter spherical plastic vessel (Dielectric Inc., Madison, WI) filled with a doped agar gel designed to approximate the brain in terms of T_1 and RF conductivity. The reader is encouraged to review their paper and develop familiarity with their approaches.

11.5 Conclusions

MRI technology continues to develop in ways that make it more available and more relevant to the drug and biologics development laboratory. As it moves from "nice to have" to being an essential readout, it will have a significant impact on the way we approach regulatory approvals and it will be an incredibly versatile part of the investigative "tool chest" of development, not unlike what PCR did to molecular biology.

Oncology, psychopharmacology, physiologic and pharmacologic MR (phMRI) intervention, stroke, and many other applications and investigative approaches of MR are available to the drug and biologics drug development teams. It is the

application of this extraordinarily versatile imaging modality that can deliver both anatomy and function that has added major new avenues of noninvasive imaging toward understanding of the complexities of biology. It is expected that MRI will be one of the most accessible imaging technologies used in drug and biologic development.

The uses and image value of MRI are only as good as the quality checks and performance standards that are executed. There are primary quality control checks that are important to remain diligent. It is possible that use of the contrast-to-noise ratio (CNR), especially for fMRI (Sorenson 2006), may help serve as a uniform quality check that can work across studies and even across institutions.

Contrast agents are available, but they must be administered in high concentrations that can be toxic in some individuals who are compromised by pathologies affecting hepatic or renal function. Gd, Dy, and Mn are the important paramagnetic elements employed in commercial contrast agents for MR imaging. These agents are not the image "content" post-administration as is common of CT and X-ray imaging, but rather their *effects* on tissue water relaxivity is what actually creates the image. It is important, especially for Gd ions, to remain caged within the chelate structure to avoid an associated nephrogenic systemic fibrosis which is generally observed in the elderly and especially in renal disease with reduced clearance capacity.

References

ACR practice guideline: performing and interpreting MRI, ACR technical standard for performing and interpreting magnetic resonance imaging (MRI), 1992 (Res 14), amended 1995, 96, 2000, 2001, 2002, effective 1/1/2003, pp 29–33

ACR technical standard: MRI equipment, ACR technical standard for diagnostic medical physics performance monitoring of magnetic resonance imaging (MRI) equipment, 1999 (Res 19), revised 2004 (Res 17b), pp 743–745

Becerra L, Upadhyay J, Chang P-C et al (2013) Parallel buprenorphine phMRI responses in conscious rodents and healthy human subjects. J Pharmacol Exp Ther 345:41–51

Buxton RB (2002) Introduction to functional magnetic resonance imaging: principles and techniques. Cambridge University Press, Cambridge. Second revised edition published in October 2009

Buxton RB (2010) Interpreting oxygenation-based neuroimaging signals: the importance and the challenge of understanding brain oxygen metabolism. Front Neuroenergetics 2:8

Cory DA, Schwartzentruber DJ, Mock BH (1987) Ingested manganese chloride as a contrast agent for magnetic resonance imaging. Magn Reson Imaging 5(1):65–70

Damadian R, Goldsmith M, Minkoff L (1977) NMR in cancer: XVI. FONAR image of the live human body. Physiol Chem Phys 9:97–100

D'Esposito M, Deouell LY, Gazzaley A (2003) Alterations in the BOLD fMRI signal with ageing and disease: a challenge for neuroscience. Nat Rev Neurosci 4:863–872

Faulkner W (2008) Gadolinium based contrast agents. SMRT Educ Sem 11(2):5–10

Ferrari L, Turrini G, Crestan V, Bertani S, Cristofori P, Bifone A, Gozzi A (2012) A robust experimental protocol for pharmacological fMRI in rats and mice. J Neutrosci Methods 204:9–18

Friedman L, Glover GH (2006) Report on a multicenter fMRI quality assurance protocol. J Magn Reson Imaging 23:827–839

Gavin PR, Bagley RS (eds) (2009) Practical small animal MRI. Wiley-Blackwell, Ames, IA

Geva T (2006) Magnetic resonance imaging: historical perspective. J Cardiovasc Magnet Reson 8:573–580
Geissler A, Gartus A, Foki T, Tahamtan AR, Beisteiner R, Barth M (2007) Contrast-to-Noise ratio (CRN) as a quality parameter in fMRI. J Magn Reson Imaging 25:1263–1270
Hustvedt SO, Grant D, Southon TE, Zech K (1997) Plasma pharmacokinetics, tissue distribution and excretion of MnDPDP in the rat and dog after intravenous administration. Acta Radiol 38 (4 Pt 2):690–699
Jensen JH, Helpern JA, Ramani A, Lu H, Kaczynski K (2005) Diffusional kurtosis imaging: the quantification of non-gaussian water diffusion by means of magnetic resonance imaging. Magn Reson Med 53:1432–1440
Kanal E (2008) Nephrogenic syndrome fibrosis. SMRT Educ Sem 11(2):11–14
Kanal E, Expert Panel on MR Safety et al (2013) ACR guidance document on MR safe practices. J Magn Reson Imaging 37:501–530
Kirchin MA, Runge VM (2008) Contrast agents for magnetic resonance imaging: safety update. SMRT Educ Sem 11(2):15–23
Krupnick AS, Tidwell VK, Engelbach JA, Alli VV, Nehori A, You M, Vikis HG, Gelman AE, Kreisel D, Garbow JR (2012) Quantitative monitoring of mouse lung tumors by magnetic resonance imaging. Nat Protoc 7(1):128–142
Lauterbur PC (1973) Image formation by induced local interactions: examples employing nuclear magnetic resonance. Nature 242:190–191
Logothetis NK, Wandell BA (2004) Interpreting the BOLD Signal. Annu Rev Physiol 66: 735–769
Matthews PM, Honey GD, Bullmore ET (2006) Applications of fMRI in translational medicine and clinical practice. Nat Rev Neurosci 7:732–744
Mendonca-Dias MH, Gaggelli E, Lauterbur PC (1983) Paramagnetic contrast agents in nuclear magnetic resonance medical imaging. Semin Nucl Med 13(4):364–376
Miller KL, Luh WM, Liu TT, Martinez A, Obata T, Wong EC, Frank LR, Buxton RB (2001) Nonlinear temporal dynamics of the cerebral blood flow response. Hum Brain Mapp 13:1–12
Mittal S, Wu Z, Neelavalli J, Haacke EM (2009) Susceptibility-weighted imaging: technical aspects and clinical applications, part 2. AJNR Am J Neuroradiol 30:232–252
Mitterschiffthaler MT, Ettinger U, Mehta MA, Mataix-Cols D, Williams SCR (2006) Applications of functional magnetic resonance imaging in psychiatry. J Magn Reson Imaging 23:851–861
Moseley ME, Liu C, Rodriguez S, Brosnan T (2009) Advances in magnetic resonance neuro-imaging. Neuro Clin 27:1–19
Neil JJ (2008) Diffusion imaging concepts for clinicians. J Magn Reson Imaging 27:1–7
Paschal CB, Morris HD (2004) K-space in the clinic. J Magn Reson Imaging 19:145–159
Rivkin MJ (2000) Developmental neuroimaging of children using magnetic resonance techniques. Ment Retard Dev Disabil Res Rev 6:68–80
Roe AW, Chen LM (2008) High resolution fMRI maps of cortical stimulation in nonhuman primates: correlation with intrinsic signal optical images. ILAR J 49(1):116–123
Schepkin VD, Brey WW, Gor'kov PL, Grant SC (2010) Initial in vivo rodent sodium and proton MR imaging at 21.1 T. Magn Reson Imaging 28:400–407
Schlaug G, Stewart B, Benfield A, Edelman RR, Warach S (1997) Time course of the apparent diffusion coefficient (ADC) abnormality in human stroke. Neurology 49(1):113–119
Sorenson AG (2006) Future prospects for fMRI in the clinic. J Magn Reson Imaging 23:941–944
Stolzmann P et al (2013) Detection rate, location, and size of pulmonary nodules in trimodality PET/CT-MR. Invest Radiol 48:241–246
Thomsen HS, Loegager V, Noerrgaard H, Chabanova E, Moller J, Sonne J (2005) Oral manganese for liver and bile imaging. Acad Radiol 12(Suppl 1):S21–S23
Toft KG, Hustvedt SO, Grant D et al (1997) Metabolism and pharmacokinetics of MnDPDP in man. Acta Radiol 38(4 Pt 2):677–689
UCSD, Center for Functional MRI, why is the MR signal sensitive to changes in brain activity? http://fmri.ucsd.edu/Research/whatisfmri.html. Accessed 13 May 2013

UK (2005) (now in 4th edition, 2011: http://www.westbrookmriinpractice.com/)
Westbrook C, Roth CK, Talbot J (2011) MRI in practice, 3rd edn. Blackwell, Oxford
Williams TM et al (2013) DW-MRI as a predictive biomarker of radiosensitization of GBM through targeted inhibition of checkpoint kinases. Transl Oncol 6:133–142
Wise RG, Tracey I (2006) The role of fMRI in drug discovery. J Magn Reson Imaging 23: 862–876
Wolf RL et al (2005) Grading of CNS neoplasms using continuous arterial spin labeled perfusion MR imaging at 3 Tesla. J Magn Reson Imaging 22:475–482
Yang GY, Betz AL (1994) Reperfusion-induced injury to the blood-brain barrier after middle cerebral artery occlusion in rats. Stroke 25:1658–1664
Young RJ, Knopp EA (2007) Brain MRI: tumor evaluation, in, update: MRI of the brain. SMRT Educat Sem 10(4):23–38
Yurgelun-Todd DA, Coyle JT, Gruber SA, Renshaw PF, Silveri MM, Amico E, Cohen B, Goff DC (2005) Functional magnetic resonance imaging studies of schizophrenic patients during word production: effect of D-cycloserine. Psychiatry Res 138:23–31

Chapter 12
Technologies and Principles of Mass Spectral Imaging

Kevin A. Douglass, Demian R. Ifa, and Andre R. Venter

Abstract The field of imaging is rapidly becoming more of an analytical chemistry tool. Included in this is the capability of mass spectrometry (MS) to give anatomical and metabolic information. Mass spectrometry has also entered the imaging world as an analytical chemistry tool. This chapter will attempt to cover a variety of techniques using mass spectral approaches for metabolic imaging such as MALDI, SIMS, DESI, LAESI, AP-fs-LDI, LA-FAPA, PESI, and LMJ-SSP. Each of these will be covered with their respective physics as well as the mechanics of how to employ these in the drug and biologics development setting as alone or as alongside of other inclusive imaging modalities. The reader should also investigate Chap. 6 (Autoradiography; Solon and Moyer) in this volume for some of the classical approaches to metabolic imaging.

12.1 Introduction

Determining the distribution of drugs and drug metabolites in tissues is a necessity for drug discovery and development. Many kinds of studies rely on this information, including absorption, distribution, metabolism, and excretion (ADME), pharmacokinetic (PK), and toxicology studies. Traditionally, this information has been obtained using radiographic imaging methods such as whole-body autoradiography (WBA) and positron-emission tomography (PET). In these radiographic methods, the drug compound is given a radioactive label which is detected within the imaging

K.A. Douglass • A.R. Venter (✉)
Department of Chemistry, Western Michigan University, 1903 W Michigan Avenue, Kalamazoo, MI 49008-5413, USA
e-mail: andre.venter@wmich.edu

D.R. Ifa
Department of Chemistry, York University, 4700 Keele Street, Toronto, ON, M3J 1P3, Canada

B.R. Moyer et al. (eds.), *Pharmaco-Imaging in Drug and Biologics Development*, AAPS Advances in the Pharmaceutical Sciences Series 8, DOI 10.1007/978-1-4614-8247-5_12,

experiment. Recently, mass spectral imaging (MSI) has emerged as an attractive alternative.

MSI offers several advantages over WBA and PET. MSI does not require the use of compounds labeled with radioactive isotopes, which can be expensive, time-consuming to prepare, and have a short window of use. Since WBA and PET detect the decay of the radioactive isotope instead of molecules, they are unable to distinguish between the parent compound and its metabolites. MSI, on the other hand, can be used to determine the localization of the parent drug and its metabolites as well as other biologically relevant compounds present in the tissue sample, all in one imaging experiment. In addition, many MSI instruments are capable of high-accuracy mass measurements and/or MS/MS experiments, offering confident identification of drugs and their metabolites simultaneously with the imaging experiment without requiring subsequent LC-MS experiments.

12.1.1 What Is Mass Spectral Imaging?

MSI is a surface analysis technique in which the distribution of chemicals on a surface are determined to create a chemical image for one or more dimensions. Initially, the area to be imaged is divided into several smaller areas, or pixels. This process is illustrated in Fig. 12.1 where a sample image (a) is divided into a 10×10 grid of 100 pixels (b). Each individual pixel is then analyzed, and one mass spectrum becomes associated with it (c). After the entire area has been interrogated, an average mass spectrum of all the pixels can be created that represents all of the ions that were present on the total surface area of all pixels. Using imaging software, peaks in the mass spectrum can be selected to generate chemical distribution maps or chemical images based on their distribution on the surface. For instance, the simple image in Fig. 12.1a is comprised of three molecules, each of which is localized in a separate area of the image. By selecting to display an individual ion peak, a representative chemical image for the corresponding compound is created (d). These individual images can be overlaid to generate a single image of the chemicals on the surface (e).

12.1.2 Important Terms for Mass Spectral Imaging

12.1.2.1 Lateral (Spatial) Resolution

Lateral, or spatial, resolution is the minimum distance in which two distinct objects can be resolved on the surface, similar to optical resolution. A typical strategy to measure resolution is to compare features of known dimensions present on a sample, determined using microscopic methods, with the chemical image obtained by MSI. A sample is sometimes prepared solely for this purpose, with typical choices being a printed grid (Kertesz and Van Berkel 2008; Shelley et al. 2008;

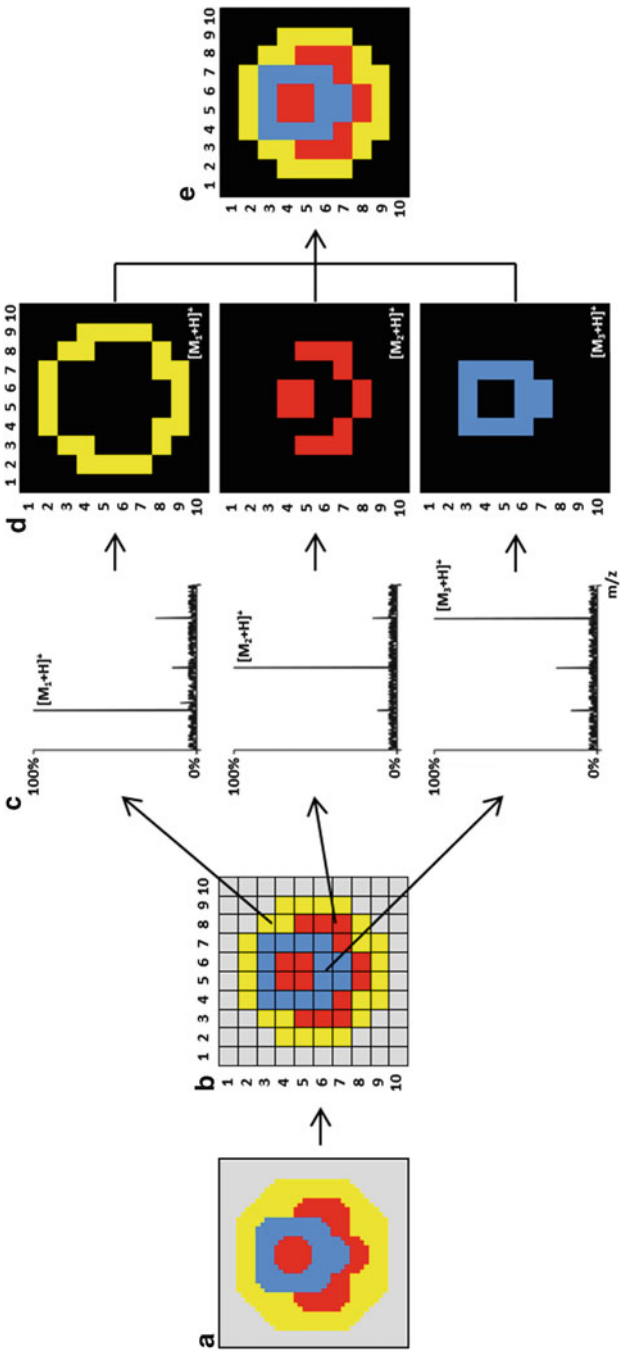

Fig. 12.1 An outline of the IMS experiment. An image (**a**) is initially divided into the desired number of pixels (**b**) and a mass spectrum is then obtained for each pixel (**c**). A chemical image can be created by plotting the intensity of a selected peak within each pixel (**d**), and these images can then be combined into a single image (**e**)

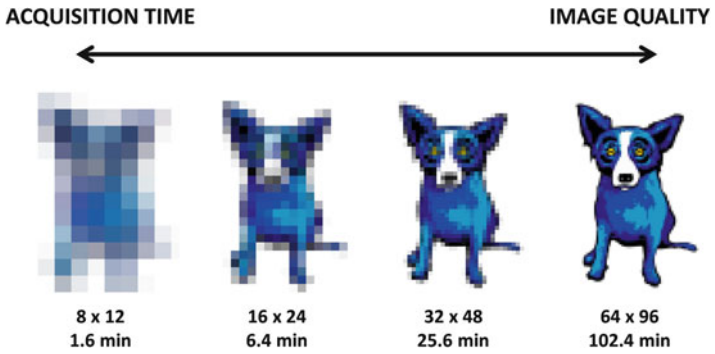

Fig. 12.2 Image quality is inversely related to acquisition time. It is best to choose the resolution that has the shortest acquisition time while still able to adequately answer the question at hand. The Blue Dog Series is a group of original paintings by George Rodrigue (Reproduced with permission of the copyright owner Rodrigue Studios, LLC)

Ovchinnikova et al. 2010; Laskin et al. 2012) or a set of lines with increasing width along one dimension (Ifa et al. 2007; Liu et al. 2010). In most cases, spatial resolution is limited by the probe dimensions, although a theoretical limit exists for the pixel size where the amount of material present in a pixel is below the detectable limit, in which case the pixel size is limited by the sensitivity of the mass spectrometer.

One factor to consider when increasing the pixel count by increasing the resolution is that acquisition time (AT) increases quadratically with pixel count as shown in Eq. (12.1), where ST is the scan time and X and Y are the vertical and horizontal dimensions:

$$\mathrm{AT} = \mathrm{ST}\frac{X * Y}{(\text{pixel size})^2} \tag{12.1}$$

Therefore, MSI analysis is typically a balance between image quality and acquisition time. For example, Fig. 12.2 shows several images of a dog at different resolutions. The image farthest on the left is 8×12 pixels. If the scan time is 1 s, the image would take 96 s (or 1.6 min) to acquire. However, the image resolution is poor and may not be adequate to answer the question the image was supposed to answer. On the other hand, the image farthest on the right is composed of 64×96 pixels and would take 102 min to acquire with the same scan time of 1 s. The level of detail is now very good, but the acquisition time has increased dramatically. In practice, one should choose a resolution that is adequate to answer the question at hand while minimizing acquisition time. One approach is to use a constant number of pixels per inch, or pixel density. The acquisition time scales with area for images with identical pixel densities, so good resolution can be obtained for a small area of interest while keeping the acquisition time short.

Table 12.1 The resolving powers of several mass analyzers

Mass analyzer	Resolving power (FWHM)
FT-ICR	1,000,000
FT-Orbitrap	100,000–300,000
TOF	10,000–40,000
Quadrupole/iontrap in ultrazoom mode	10,000
Quadrupole/iontrap	1,000

12.1.2.2 Depth Resolution

Depth resolution describes the thickness of the layer of material that is removed from the sample with each analysis. For some MSI techniques, such as secondary ion mass spectrometry (SIMS) or laser ablation electrospray ionization (LAESI), it is possible to continue resampling the sample spot after an initial desorption event to obtain information about successive layers of the sample. In this way, layer by layer can be removed and analyzed to create a three-dimensional chemical image. For other techniques, such as matrix-assisted laser desorption/ionization (MALDI) and desorption electrospray ionization (DESI), it is possible to obtain a three-dimensional image by dividing the sample into thin slices and imaging each slice (Eberlin et al. 2010a). Several factors affect the depth resolution, such as sample preparation, the energy and destructiveness of the chosen ionization source, the required signal intensity, the scan time, and the time for analysis.

12.1.2.3 Mass Resolution

Mass resolution refers to the ability of a mass analyzer to separate two adjacent mass spectral peaks. Different types of mass analyzers have different resolving powers r (Table 12.1), where m designates a mass value and Δm is the peak width necessary for separation at m:

$$r = m / \Delta m$$

Figure 12.3 shows two spectra for the short peptide bradykinin at two different resolving powers. At a resolving power of 1,000, there is no differentiation of the isotopic peaks, but at a resolving power of 5,000, the individual isotope peaks are distinguished. Mass resolution is an important performance parameter that determines the ability to obtain information about chemical species whose mass spectral peaks have very similar m/z values. For example, Fig. 12.4 shows the distribution of phospholipids in the sagittal sections of a rat brain (Manicke et al. 2010). Ions used to form the images in the left panel (A,C,E,G) have m/z values very similar to the corresponding ions used to form the images on the right panel (B,D,F,H). Without adequate mass resolution, the two species would have appeared as a single peak, and the resulting image would be a combination of the two separate chemical images.

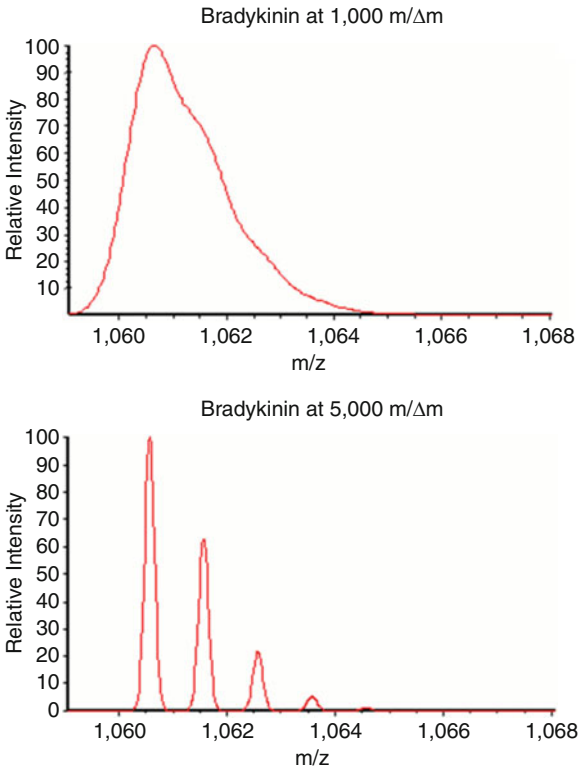

Fig. 12.3 Bradykinin at two resolving powers

12.1.3 General Equipment Needed to Perform Mass Spectral Imaging

12.1.3.1 Sample Preparation

For MSI, the typical ADME workflow begins with the dosing of an animal with the compound of interest. The animal is then sacrificed at a designated time interval, and slides are prepared. If performing whole-body analysis, which gives information about the distribution of the compound within the entire animal, the whole body is sectioned. This may require the use of an embedding medium to rigidify the animal, the most popular choice being carboxymethylcellulose (Ullburg et al. 1977). Alternatively, individual organs or other tissue samples may be removed and sectioned. Transfer of the sections to slides requires the use of adhesive tape or paper (Prideaux et al. 2010). Adhesive tape is not amenable to MSI techniques which require a conductive substrate, such as MALDI, unless a conductive matrix is applied to the sample, but paper suffers the disadvantages of incomplete transfer and sample distortion. A washing step is sometimes applied to the sample prior to analysis in order to remove interfering salts or other suppressants (Shariatgorji et al. 2012). Care must be taken to minimize the solubility of the target compound in the

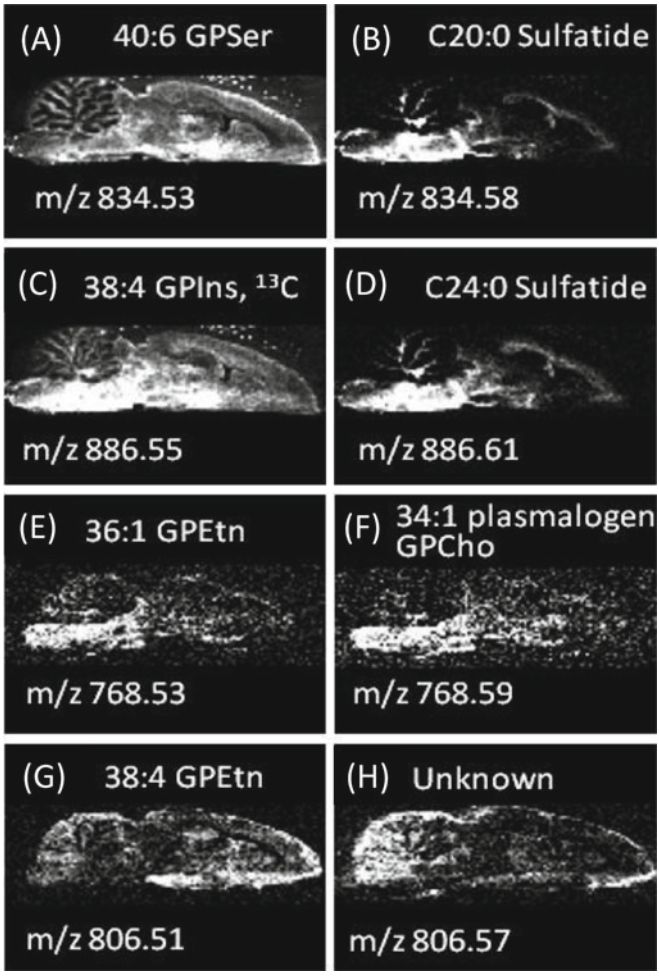

Fig. 12.4 The distribution of phospholipids in the sagittal sections of a rat brain. The panels on the left (A,C,E,G) and the adjacent panels on the right (B,D,F,H) have highly similar m/z values, requiring a high resolution mass analyzer for differentiation

wash solution to minimize removal and delocalization. Once prepared, samples should be analyzed immediately to minimize sample degradation in the open laboratory environment (Goodwin et al. 2012).

The sample may or may not require additional sample preparation depending on the nature of the sample and the MSI technique that will be used. Ambient mass spectrometry ionization methods such as DESI require little to no sample preparation, while methods such as MALDI require considerable sample preparation. In general, the imaged surface should be flat, and the sample must meet the analytical requirements of the specific technique that is used. For instance, some techniques require that the sample be placed in a vacuum chamber for analysis, while some require that the analyte of interest be soluble in a particular solvent system.

12.1.3.2 Sample Positioning Stage

In an imaging experiment, the desorption/ionization source and mass spectrometer are typically held stationary while the sample is moved relative to them. To accurately raster a sample, a moving stage is required. The moving stage is an important part of the experimental setup to consider as the quality of the image depends on the robustness and repeatability of the sampling. Typical moving stages use computer-controlled stepping motors in the x and y dimensions. For samples analyzed under ambient conditions, a height adjustment is also required for optimizing the sample position relative to the ionization source and mass spectrometer inlet. The minimum step size determines the minimum lateral resolution, while the minimum and maximum velocities impact the time required for analysis. In the case of spray desorption methods such as DESI (discussed below), a smooth scanning motion is required, as these techniques typically acquire data as line scans. For techniques which use a laser or a probe device for desorption, data is acquired one pixel at a time, and a fast movement to the following pixel is desired. The reproducibility of sample placement is also important for indexing of pixels.

12.1.3.3 Desorption/Ionization Source and Mass Analyzer

The desorption/ionization source is important because it desorbs the sample, generates the gas-phase ions that are ultimately detected, and sets limits on the lateral and depth resolutions. There are many kinds of desorption and ionization agents available, such as lasers, ion beams, plasmas, liquid microjunctions, solid probes, and solvent sprays. Many sources are a combination of two or more of these agents (Huang et al. 2011).

There are many kinds of mass analyzers available as well, such as the triple quadrupole, Q-trap, orbitrap, or time of flight (TOF). Different mass analyzers have different mass ranges and mass resolutions. Analyzers with high mass resolution can be used to determine the elemental composition of the detected compounds, which enables unambiguous identification simultaneous with the imaging experiment. Similarly, analyzers with MS/MS capabilities can be used to fragment a peak of interest for identification purposes. In some cases, fragments can be selected and fragmented again, offering structural information about the parent compound. Most sources can be paired with any mass analyzer, but some common configurations exist, such as MALDI-TOF.

12.1.3.4 Post-processing

Computer software is used to process the imaging data after it has been collected. The software allows the visualization of the chemical image and includes features for data manipulation. Various commercial programs, as well as many programs developed in-house, exist for processing MSI data. A popular software option is BioMAP

(http://www.maldi-msi.org/), which can be downloaded for free from the Internet. Depending on the resolution of the mass analyzer and the pixel count, imaging files can become quite large. Therefore, the processing speed and storage capabilities of the computer used for data acquisition and processing must be considered before performing an MSI experiment. The processing of MSI data typically includes (1) concatenating individual mass spectra into a single file, (2) building a table of all the ions detected over the entire image, (3) extracting the ions of interest, and (4) displaying the distribution of these particular ions across one or more images.

12.2 MSI Methods

The lateral, depth, and mass resolutions, as well as sample preparation, can vary significantly between the different MSI methods, so the choice of which method to use depends on the application. Established techniques for the MSI of drug distributions in tissues include secondary ion mass spectrometry (SIMS) and matrix-assisted laser desorption/ionization (MALDI). These techniques offer the advantages of high sensitivity and high spatial resolution, but typically require a substantial amount of sample preparation. The introduction of desorption electrospray ionization (DESI) (Takats et al. 2004) and direct analysis in real time (DART) (Cody et al. 2005) instigated a rapid emergence of the so-called ambient ionization techniques. Ambient methods such as DESI and laser ablation electrospray ionization (LAESI) are becoming increasingly popular choices for MSI. These techniques require little-to-no sample preparation, allowing high-throughput analysis to be done in the open environment. Ambient ionization techniques are able to analyze samples directly because they include both desorption and ionization capabilities. While these two events can be accomplished with a single agent in some cases, most ambient methods use separate agents for desorption and ionization. Many permutations of the desorption and ionization agents have been achieved (Huang et al. 2011; Venter et al. 2008). The desorption processes of most ambient ionization methods are localized, so these methods have the ability to be used for MSI (Wu et al. 2013).

A figure containing schematics for several MSI techniques discussed below is presented at the end of the chapter.

12.2.1 Common MSI Techniques Used for Drug Discovery

12.2.1.1 Secondary Ion Mass Spectrometry (SIMS)

In SIMS, an ion beam is used to bombard a sample in vacuum. Ions are liberated from the surface and subsequently detected. Many ion beam choices are available, including mono- and polyatomic clusters. Polyatomic clusters and molecular ions

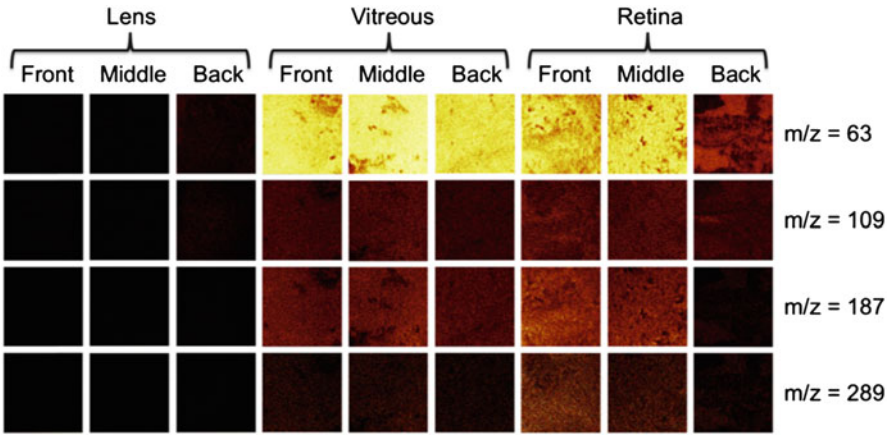

Fig. 12.5 The distribution of dexamethasone sodium phosphate drug fragments in various sections of the lens, vitreous humor, and retina of perfused ovine ocular tissue determined using Bi3+ cluster TOF-SIMS. (From Mains et al. 2011; with permission)

such as C_{60} reduce the amount of fragmentation that is common during SIMS. Both the spatial and depth resolutions are very good for SIMS, as low as 100 nm (Pacholski and Winograd 1999) and 15 nm (Cheng and Winograd 2005), respectively, making it an ideal choice if high resolution is required. SIMS can be operated in one of two modes by adjusting the density of ions bombarding the surface. Static SIMS, achieved with a low density of ions, is minimally destructive. Dynamic SIMS, which is more destructive, occurs with a high density of ions. Dynamic SIMS can be used to remove layers of the sample to construct a 3D chemical image of the sample (Seeley and Caprioli 2012). SIMS is typically used for low molecular weight molecules, although interference from fragmentation can be quite severe in the low mass range of the spectrum, making the interpretation of the data difficult.

Figure 12.5 shows an example of using Bi_3^+ cluster TOF-SIMS to map the distribution of dexamethasone sodium phosphate drug fragments in various sections of the lens, vitreous humor, and retina of perfused ovine ocular tissue (Mains et al. 2011). By comparing the distributions with those obtained from non-perfused tissue, the authors were able to show that the movement of dexamethasone through the eye is not the result of diffusion alone. The images are 500 × 500 μm, demonstrating the extremely high resolution of this technique.

12.2.1.2 Matrix-Assisted Laser Desorption/Ionization (MALDI)

MALDI is another vacuum method with high spatial resolution. Resolutions as low as 30 μm (Burnum et al. 2008) have been attained, although resolutions around 200 μm are more typical. MALDI is usually paired with TOF mass analyzers and as such offers a large mass range, 600 Da to 1 MDa. The ionization agent is a laser pulse. As the name implies, MALDI requires the application of a matrix compound

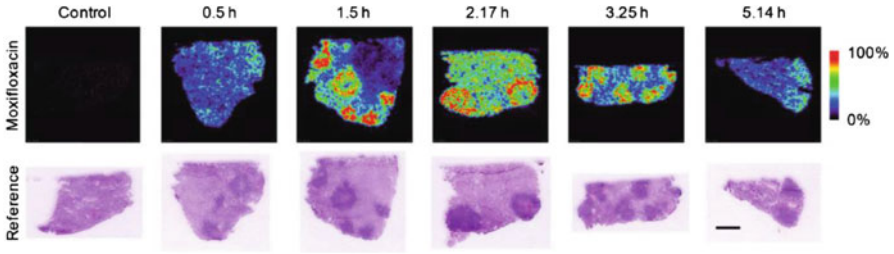

Fig. 12.6 The distribution of moxifloxacin in tuberculosis-infected rabbit lung biopsies determined using MALDI-TOF. The scale bar in the reference image at 5.14 h represents 5 mm. (From Prideaux et al. 2011; with permission)

prior to analysis to absorb the laser energy and aid with ionization, which usually occurs through protonation or deprotonation reactions. There are many matrix compounds used in MSI MALDI, and the choice of matrix depends on the application (Kaletaş et al. 2009). For instance, 2,5-dihydroxybenzoic acid (DHB) is usually used for sugars or peptides, while sinapinic acid is used for proteins or lipids. There are several methods for applying the matrix, including droplet deposition, dry coating, sublimation, and electrospray (Kaletaş et al. 2009). Choosing the correct matrix compound and applying it are critical to the success of MALDI. When the matrix dries, crystals are typically formed and the size and homogeneous distribution of these crystals are important for obtaining good spatial resolution when attempting MSI by MALDI. One drawback of MALDI is the interference in the low mass range from the formation of matrix clusters, making the interpretation of data for lower molecular mass compounds difficult. However, higher molecular weight compounds can ionize easily in MALDI, making it ideal for the study of biopolymers such as proteins, DNA, or RNA.

Figure 12.6 shows the distribution of the tuberculosis drug moxifloxacin in infected rabbit lung biopsies (Prideaux et al. 2011). The drug was shown to accumulate in the granulomatous lesions over time, preferentially in the outer regions known to contain active microphages as opposed to the central necrotic caseum, where lower levels were detected. Since extracellular bacteria populations are thought to reside in this central area, this information may be clinically relevant. The scale bar for these images is 5 mm, so the pixel size is much larger than what can be attained by SIMS, but the resolution is adequate to show the various distributions of the target compound.

Many modifications to the traditional MALDI setup have been used for MSI. The laser pulse is typically applied from above the plane of the sample, but by using a transparent MALDI substrate, it is possible to apply the laser pulse from behind. This enables the sample to be placed much closer to the mass spectrometer inlet to improve ion transmission (Vertes et al. 1990). Mass spectral imaging has been demonstrated in the transmission geometry (Richards et al. 2011). Laser desorption ionization (LDI) is a method operationally similar to MALDI (McMahon 1985), with the exception that it is not necessary to apply a matrix to the sample prior to

analysis. LDI has been used to image metabolites in plant tissues (Cha et al. 2009), lipid distributions in mouse brain tissues (Goodwin et al. 2011), and antibiotic compounds on the surface of beewolf larval cocoons (Kroiss et al. 2010). Finally, intermediate and atmospheric pressure MALDI (AP-MALDI) sources have been used for the MSI of lower molecular weight compounds (Guenther et al. 2011; Garrett et al. 2007).

12.2.1.3 Desorption Electrospray Ionization (DESI)

DESI, one of the pioneering ambient techniques, (Takats et al. 2004) is performed by directing an electrosprayed solvent at the sample section. Initial droplets create a thin liquid film into which material is dissolved. Subsequent droplets impact this film and produce secondary droplets which fly towards the mass spectrometer inlet (Costa and Graham 2008). Ionization from these secondary droplets occurs in the same way as traditional electrospray ionization (Takáts et al. 2005). For compounds not easily analyzed by DESI, reagents can be added to the electrospray to react with these molecules and form product molecules that are more easily ionized and detected. This method is called reactive DESI (Cotte-Rodriguez et al. 2005). The typical resolution for a DESI MSI experiment is around 200 μm, although a resolution as high as 40 μm has been reported (Kertesz and Van Berkel 2008).

Of all the ambient methods, DESI has been developed the most as a MSI technique, especially for the analysis of lipids in tissue samples (Eberlin et al. 2011). The three-dimensional analysis of lipids has been demonstrated for the lipids in rat brain tissue (Eberlin et al. 2010a) as well as the mapping of lipids (Paglia et al. 2010) after two-dimensional high-performance thin-layer chromatography (2D-HPTLC) separation and peptides (Pasilis et al. 2008) after one-dimensional HPTLC. DESI MSI analysis has also included the mapping of drug distributions in tissues (Kertesz et al. 2008), natural products imaging (Lane et al. 2009; Li et al. 2011; Muller et al. 2011; Thunig et al. 2011; Ifa et al. 2011), and cancerous tissue discrimination (Dill et al. 2009; Eberlin et al. 2010b). In addition, reactive DESI has been used to image cholesterol in adrenal gland tissue (Wu et al. 2010), a compound not amenable to standard DESI analysis.

A comparison between the whole-body imaging of a mouse sagittal section by DESI-MS/MS and WBA (Kertesz et al. 2008) is shown in Fig. 12.7. The specimen was intravenously dosed with 7.5 mg/kg of propranolol and euthanized 60 min after dosing. Each pixel in the DESI-MS/MS image corresponds to an area of approximately 140 μm by 200 μm in size. Comparison of panels B and D shows that DESI-MS/MS was able to detect propranolol in the brain, lung, and stomach regions. The autoradioluminograph obtained by WBA showed accumulation in the liver, kidney, and salivary gland as well, which was not picked up by DESI-MS/MS, but this signal may have resulted from the detection of propranolol metabolites, which WBA cannot distinguish from the parent drug.

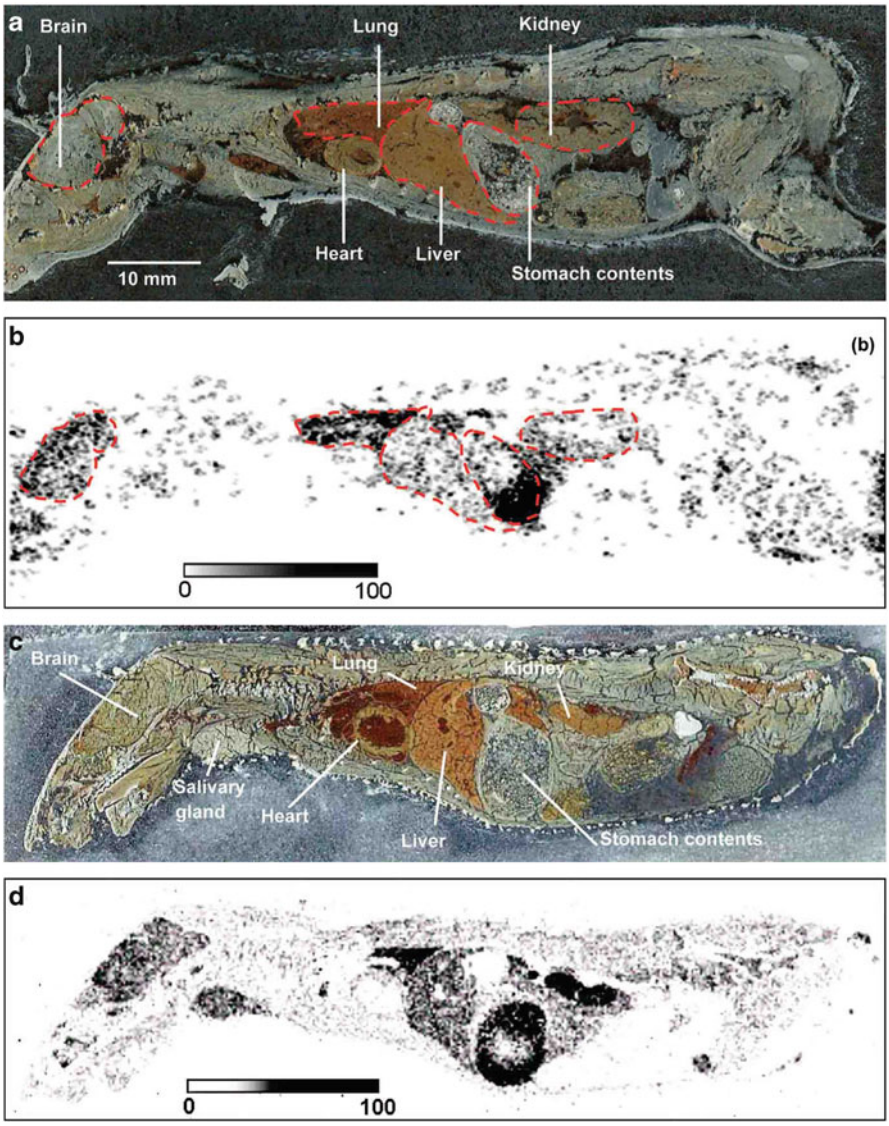

Fig. 12.7 (**a**) and (**c**) are optical images of whole-body tissue sections of a mouse dosed with 7.5 mg/kg propranolol and euthanized 20 min after dosing. (**b**) Distribution of propranolol determined using DESI-MS/MS. (**d**) Distribution of propranolol determined using WBA. (From Kertesz et al. 2008; with permission)

12.2.2 Other Techniques

Besides the MSI techniques commonly used for drug discovery, many other desorption/ionization techniques have been developed that have high potential for MSI. Many of these techniques are part of the boom of ambient techniques that began

with DESI and DART and share the advantages common to all ambient techniques, such as operation at atmospheric pressure and limited sample preparation. While ambient ionization is a relatively young field compared to SIMS and MALDI, it is currently receiving a lot of attention and is developing rapidly. Besides DESI, some methods have already become commercially available, such as LAESI and LMJ-SSP. The following section contains a brief introduction for various MSI techniques which have shown the potential to be used for drug discovery and development. They are divided according to the desorption mechanism of their ionization source, the parameter which typically has the largest impact on lateral resolution.

12.2.2.1 Laser Desorption Techniques

In each of the following ambient techniques, a laser is directed towards the sample and material is ablated with the firing of the laser, similar to MALDI or LDI. After ablation, ionization is achieved by one of several methods, depending on the technique.

Laser Ablation Electrospray Ionization (LAESI)

During LAESI analysis (Nemes and Vertes 2007), material is ablated from the sample using a mid-infrared laser at 2,940 nm. The ablated material then coalesces with the droplets of an electrospray that is directed towards the mass spectrometer inlet. Ionization occurs by the typical electrospray ionization mechanisms (Nemes and Vertes 2007). The amount of material that is ablated can be controlled by adjusting the number of laser pulses applied to each sample position. This makes it possible to perform 3D imaging experiments using this method (Nemes et al. 2009).

The bio-applications demonstrated by LAESI have included the ability to map both the 2D (Nemes et al. 2008) and 3D (Nemes et al. 2009) distributions of plant metabolites present in *Aphelandra squarrosa* leaves (Fig. 12.8), the mapping of small metabolites and lipids in rat brain tissue sections (Nemes et al. 2010), and the in vitro analysis of metabolites in the electric organ of the fish *Torpedo californica* (Sripadi et al. 2009). In addition, the in situ analysis of single cells (Shrestha and Vertes 2009; Shrestha et al. 2011) has also been demonstrated by LAESI.

Laser Ablation Inductively Coupled Plasma Mass Spectrometry (LA-ICPMS)

LA-ICPMS (Durrant 1999) begins by using a laser to ablate material on the sample. This material is then transferred via a flow of gas to a plasma source for ionization, where the high temperature of the plasma breaks the material into individual atoms, some of which are ionized. A lateral resolution of 4 μm has been reported (Durrant 1999). Because it uses a plasma ionization source, this technique is very good for elemental analysis. For example, Fig. 12.9 shows the distribution of Cu, Fe, Zn, and Mn in a rat brain at 2 h, 7 days, and 28 days after the administration

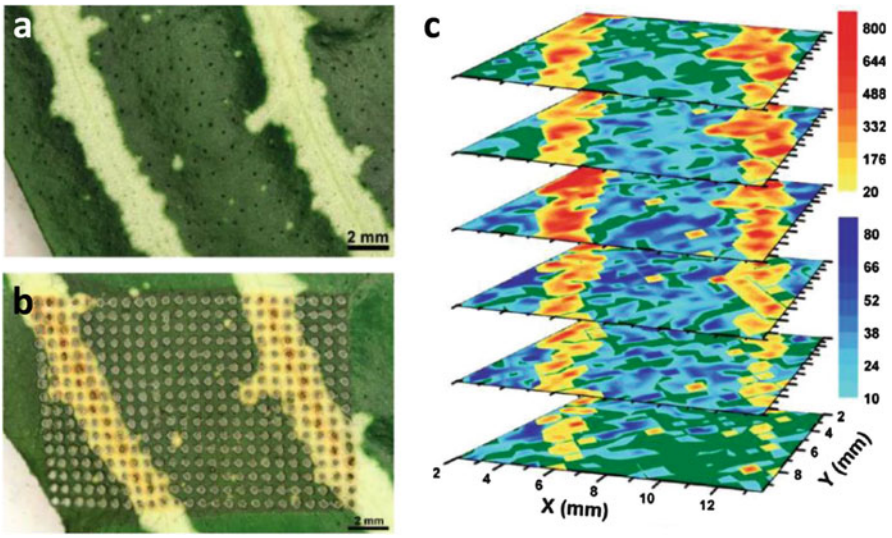

Fig. 12.8 Optical image of an *Aphelandra squarrosa* leaf before (**a**) and after (**b**) LAESI analysis. The 3D distribution of kaempferol/luteolin (**c**) followed the variegation pattern of the optical images. (From Nemes et al. 2009; with permission)

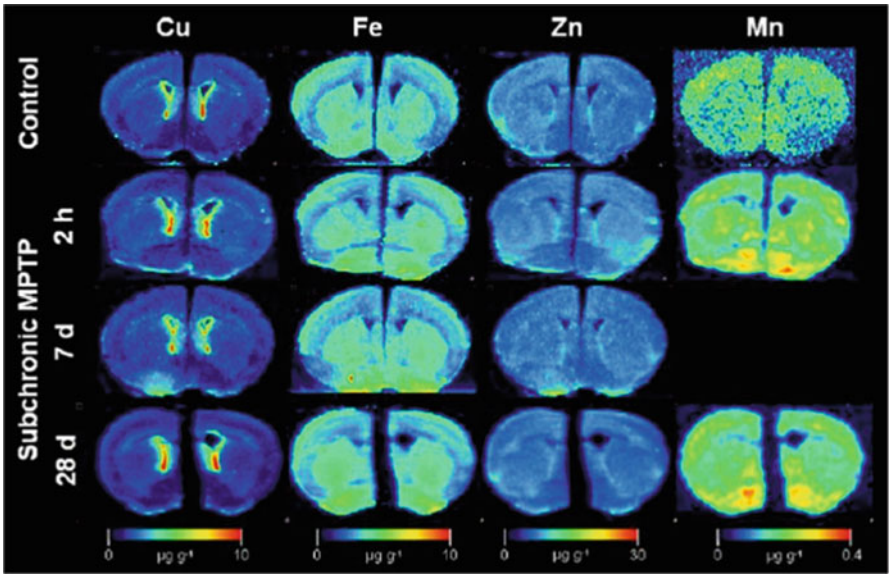

Fig. 12.9 Cu, Fe, Zn, and Mn distributions in rat brain sections at various time points following administration of 1-methyl-4-phenyl-1,2,3,6-tetrahydropyridin (MPTP). (From Matusch et al. 2010)

of 1-methyl-4-phenyl-1,2,3,6-tetrahydropyridin (MPTP), a drug used to model Parkinson's disease (Matusch et al. 2010). It was possible to observe an increase of Fe over time in the interpeduncular nucleus as well as a significant decrease of Cu in the periventricular zone and fascia dentate at 2 h and 7 days followed by over-compensation at 28 days.

Infrared Laser Ablation Metastable-Induced Chemical Ionization (IR-LAMICI)

Similar to LAESI, a mid-infrared laser at 2,940 nm is used to ablate material during IR-LAMICI (Galhena et al. 2010). However, unlike LAESI, after ablation the material is introduced to a metastable plume directed towards the mass spectrometer inlet, where ionization occurs by gas-phase chemical ionization. IR-LAMICI has been used for natural product imaging on biological surfaces (Galhena et al. 2010) as well as the small molecule imaging of drug tablets (Galhena et al. 2010).

Atmospheric Pressure Femtosecond Laser Desorption Ionization (AP fs-LDI)

AP fs-LDI uses near-infrared laser pulses with high peak power densities to desorb and ionize the sample (Coello et al. 2010). Because the sample absorbs the laser energy directly, sample fragmentation can occur (Lozovoy et al. 2008). Similar to LAESI, AP fs-LDI can be combined with an electrospray, a technique referred to as laser electrospray mass spectrometry in the literature (LEMS) (Judge et al. 2010). The mass range for AP fs-LDI is limited at around *m*/*z* 400, but it has the best reported spatial resolution of the laser-based ambient techniques at around 20 μm (Coello et al. 2010). The ability to analyze biological tissues was demonstrated for AP fs-LDI by imaging a monolayer of onion epidermis, which allowed the visualization of individual cells (Fig. 12.10) (Coello et al. 2010).

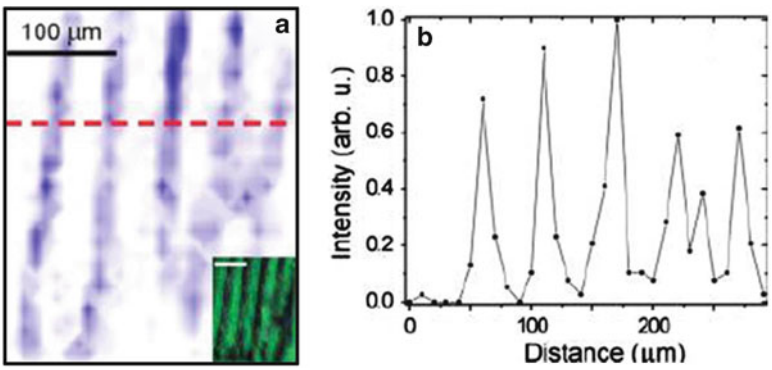

Fig. 12.10 Individual onion epidermis cells visualized using AP fs-LDI. Panel (**a**) shows the MSI chemical image and corresponding optical image (inset). Panel (**b**) shows the intensity distribution for scan represented by the red dashed line in panel (**a**). (From Coello et al. 2010)

Laser Ablation Coupled to Flowing Atmospheric-Pressure Afterglow (LA-FAPA)

The last of the laser desorption methods is LA-FAPA (Shelley et al. 2008). LA-FAPA uses an ultraviolet laser to ablate material. This material is subsequently carried by a nitrogen stream to the afterglow of a helium atmospheric pressure glow discharge ionization source where analyte molecules are mixed with the plasma and ionized. LA-FAPA can be used to analyze molecules up to 1 kDa with a spatial resolution as low as 20 μm, depending on the size of the laser spot. LA-FAPA has been used for drug tablet analysis as well as the imaging of tissue loaded with lidocaine (Shelley et al. 2008).

12.2.2.2 Plasma and Vapor Desorption Methods

Low-Temperature Plasma Source (LTP)

The low-temperature plasma source (LTP) (Harper et al. 2008) uses plasma for both desorption and ionization. In the LTP source, an alternating voltage is applied between two electrodes separated by a dielectric layer, generating a low-temperature plasma which is then applied to the surface to desorb and ionize the sample at a spatial resolution as low as 250 μm (Liu et al. 2010).

Desorption Atmospheric Pressure Photoionization (DAPPI)

DAPPI (Haapala et al. 2007) uses a heated jet containing solvent vapor to desorb material from the sample, which is then ionized by photoionization using a photoionization lamp. The heated jet increases the temperature of the sample where it is applied, a parameter important for efficient desorption (Luosujärvi et al. 2008). For this reason, substrates with low thermal conductivity are best. Pharmaceutical and illicit drugs have been detected using DAPPI (Haapala et al. 2007; Luosujärvi et al. 2009), and MSI analysis of phytocompounds from plant leaves, as well as the selective ionization of a sterol lipid from a brain tissue sample, has also been demonstrated with a spatial resolution of 1 mm (Pól et al. 2009).

12.2.2.3 Probe Electrospray Ionization (PESI)

During PESI (Hiraoka et al. 2007), a solid needle is used to penetrate the surface of the sample, some of which adheres to the needle on extraction. The needle is then moved to a position in front of an spray emitter, where droplets from the spray wet the needle tip containing the desorbed material. A high voltage applied to the needle then initiates an electrospray at the needle tip, which ionizes the sample and transfers it to the mass spectrometer. Once the ionization event is finished, the needle is moved to the next sample position, and the process is repeated.

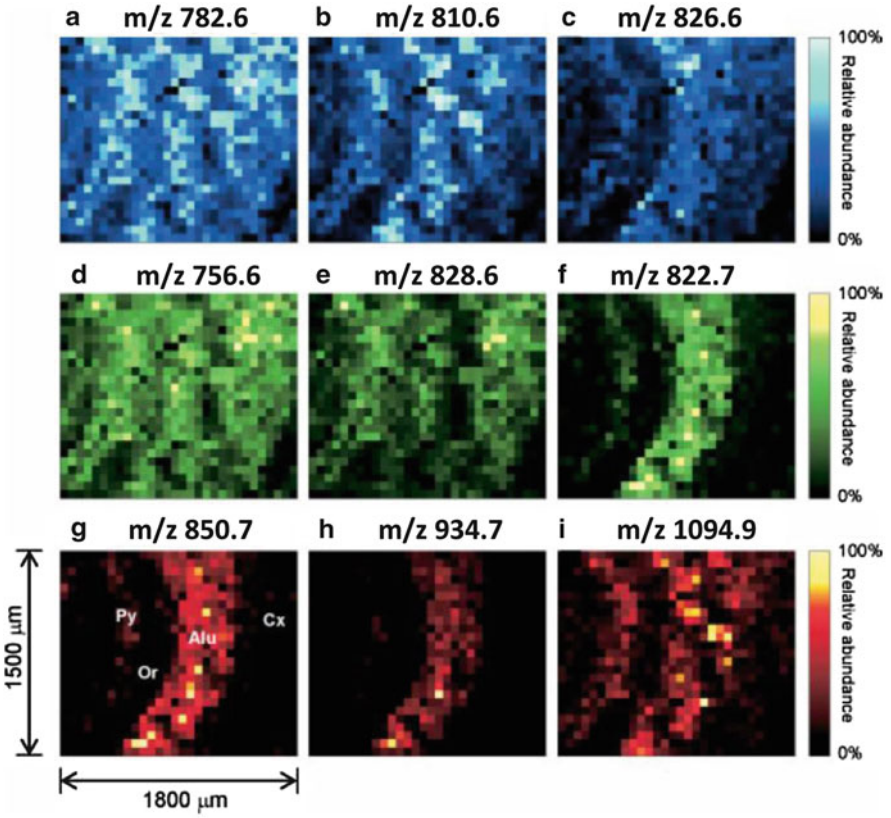

Fig. 12.11 Chemical images of phospholipids (**a**–**e**), galactosylceramides (**f**–**h**), and an ion at *m*/*z* 1,094.9 present in a mouse brain section determined using PESI (**i**). (From Chen et al. 2009; with permission)

The lateral resolution is limited by the size of the probe, which is typically around 100 µm or less. Depth profiling is also possible using PESI, although carryover resulting from increasing hole size during subsequent punctures makes quantitative measurement difficult (Chen et al. 2009). PESI has been used to analyze phospholipids and galactosylceramides from mouse brain sections (Fig. 12.11) with a lateral resolution of 60 µm (Chen et al. 2009).

12.2.2.4 Liquid Microjunction Methods

Several closely related ambient methods have been developed where a liquid junction is formed between the sample and a probe, including the liquid microjunction surface-sampling probe (LMJ-SSP), the nanospray desorption electrospray ionization (nano-DESI) source, and the liquid extraction surface analysis (LESA) source. Solvent is delivered directly to the sample, and material from the sample is

dissolved into the junction. The solvent containing the sample is then transferred to a position where it is ionized by electrospray ionization.

Liquid Microjunction Surface-Sampling Probe (LMJ-SSP)

The LMJ-SSP (Van Berkel et al. 2008) uses a set of coaxial capillaries where solvent from the outer capillary forms the junction with the sample while the inner capillary transfers solvent sampled from the junction to a pneumatically assisted electrospray. A noncontact method of LMJ-SSP called proximal probe thermal desorption/secondary ionization has been developed where the continuous flow probe is positioned immediately above the surface, catching material from a transmission mode laser ablation event (Ovchinnikova et al. 2011). Traditional LMJ-SSP has demonstrated tissue imaging capabilities (Van Berkel et al. 2008), though the lateral resolution is larger than many other ambient techniques at 670 μm. Proximal probe thermal desorption/secondary ionization has a lateral resolution around 50 μM (Ovchinnikova et al. 2010), similar to other methods using laser desorption.

Nanospray Desorption Electrospray Ionization (Nano-DESI)

The nano-DESI source (Roach et al. 2010) forms a liquid microjunction between the sample and two closely positioned capillaries, one that delivers solvent and another with a self-aspirating nanospray at the other end, which is positioned in front of the mass spectrometer inlet. The analysis of human carcinoma and rat brain tissues (Laskin et al. 2012) has demonstrated nano-DESI's ability to achieve a lateral resolution as low as 12 μm (Fig. 12.12).

Liquid Extraction Surface Analysis (LESA)

During LESA (Eikel et al. 2011), the probe is first positioned close to the surface. When in position, the probe extrudes a droplet to form a liquid microjunction with the sample. The droplet is then retracted back into the probe and transferred to a position from where it is subsequently electrosprayed. A lateral resolution of 1 mm was demonstrated for the imaging of the pharmaceutical product terfenadine and its metabolite fexofenadine in whole-body mouse sections (Eikel et al. 2011).

12.2.3 Summary Table

A summary of the MSI methods is presented in Table 12.2. The table summarizes reported lateral and depth resolutions. It also illustrates applications of the various MSI methods. Figure 12.13 is also provided as a simplified depiction of several of

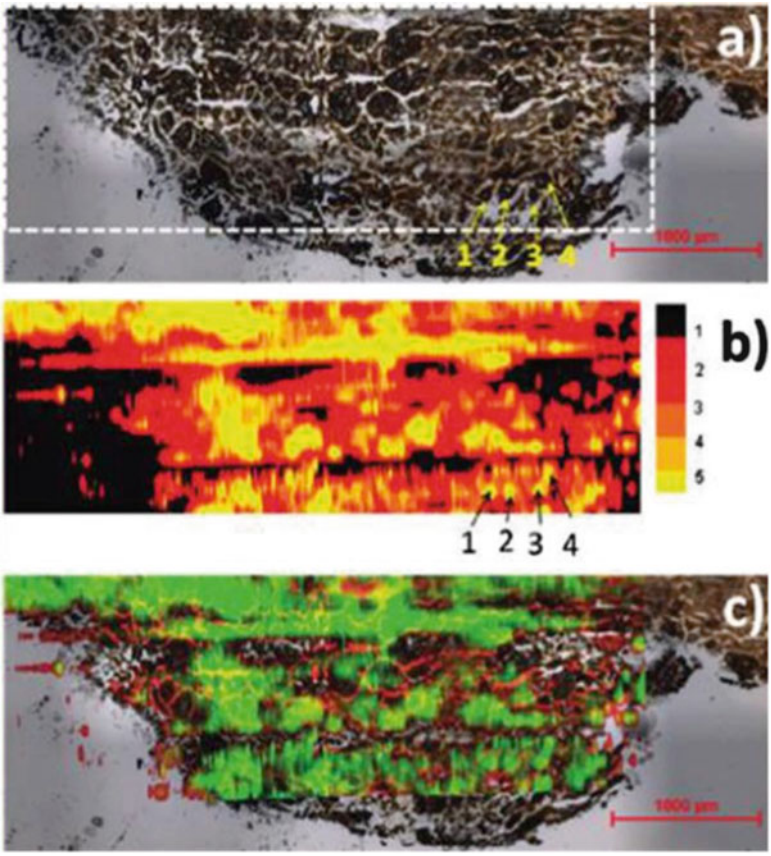

Fig. 12.12 (**a**) Optical image of a papillary renal cell carcinoma human tissue sample. (**b**) Ion image of the cholesteryl ester at *m*/*z* 687.5 obtained using nano-DESI. (**c**) Overlay of the optical image and chemical image. The scale bar represents 1 mm. (From Laskin et al. 2012, with permission)

the IMS methods presented in this chapter. Many methods have been used for biomedical applications, and others listed are likely to be used for such applications soon. While no other method has yet to approach the lateral resolution capable by SIMS, most have reported lateral resolutions of 200 μm or less, adequate for many imaging applications at tissue level.

12.3 Concluding Remarks

MSI has become a valuable tool which can provide complementary data to radiographic and optical studies of drug distributions. As the field of mass spectrometry continues to expand, the already extensive collection of available ionization sources and mass

Table 12.2 Summary of mass spectrometry methods that have been used for imaging experiments

Technique	Desorption agent	Ionization agent[a]	Spatial resolution[b]	Depth resolution[b]	Applications
SIMS	Ion beam	Ion beam	100 nm (Pacholski and Winograd 1999)	15–20 nm (Cheng and Winograd 2005)	Pharmaceuticals, various bio-applications. Several recent reviews (Seeley and Caprioli 2012; Barnes et al. 2011; Lee et al. 2012)
MALDI	Laser	*	30 µm (Burnum et al. 2008)	–	Tissue analysis, plant proteins, drug development, etc. Several recent reviews (Seeley and Caprioli 2011, 2012; Lagarrigue et al. 2011; Goto-Inoue et al. 2011; Grassl et al. 2011; Balluff et al. 2011; Bonnel et al. 2011; Fernández et al. 2011; Kaspar et al. 2011)
LA-ICPMS	Laser	Plasma	4 µm (Durrant 1999)	–	Bioaccumulation of metals in tissues (Matusch et al. 2010)
LAESI	Laser	Electrospray	200 µm (Nemes et al. 2010)	30 µm (Nemes et al. 2009)	Plant products (Nemes et al. 2008, 2009), tissue analysis (Sripadi et al. 2009)
IR-LAMICI	IR-laser	Metastable plume	300 µm (Galhena et al. 2010)	–	Natural products (Galhena et al. 2010), pharmaceuticals (Galhena et al. 2010)
AP fs-LDI	Laser	*	20 µm (Coello et al. 2010)	–	Tissue imaging (Coello et al. 2010)
LA-FAPA	UV-laser	Metastable plume	20 µm (Shelley et al. 2008)	36 µm (Shelley et al. 2008)	Pharmaceuticals (Shelley et al. 2008), tissue imaging (Shelley et al. 2008)
LTP	Plasma	*	250 µm (Liu et al. 2010)	–	

(continued)

Table 12.2 (continued)

Technique	Desorption agent	Ionization agent[a]	Spatial resolution[b]	Depth resolution[b]	Applications
DAPPI	Solvent vapor	Photochemical ionization	1 mm (Pól et al. 2009)	–	Pharmaceuticals (Haapala et al. 2007), drugs (Luosujärvi et al. 2009), lipids (Pól et al. 2009), plant products (Pól et al. 2009)
PESI	Solid probe	Electrospray	60 µm (Chen et al. 2009)	–	Tissue imaging (Chen et al. 2009)
LMJ-SSP	Liquid microjunction[c] laser[d]	Electrospray	670 µm[c] (Van et al. 2008) 50 µm[d] (Ovchinnikova et al. 2010)	–	Tissue imaging (Van et al. 2008)
Nano-DESI	Liquid microjunction	Nanospray	12 µm (Laskin et al. 2012)	–	Tissue imaging (Laskin et al. 2012)
LESA	Liquid microjunction	Electrospray	1 mm (Eikel et al. 2011)	–	Tissue imaging (Eikel et al. 2011)
DESI	Electrospray	*	40 µm (Kertesz and Van Berkel 2008)	–	Pharmaceuticals (Kertesz et al. 2008), lipids (Eberlin et al. 2011), peptides (Pasilis et al. 2008), natural products (Lane et al. 2009; Li et al. 2011; Muller et al. 2011; Thunig et al. 2011; Ifa et al. 2011)

[a]An "*" indicates desorption/ionization occur together using the desorption agent
[b]Lowest reported value found in the literature. An "–" indicates no available data
[c]Contact mode LMJ-SSP
[d]Proximal probe LMJ-SSP

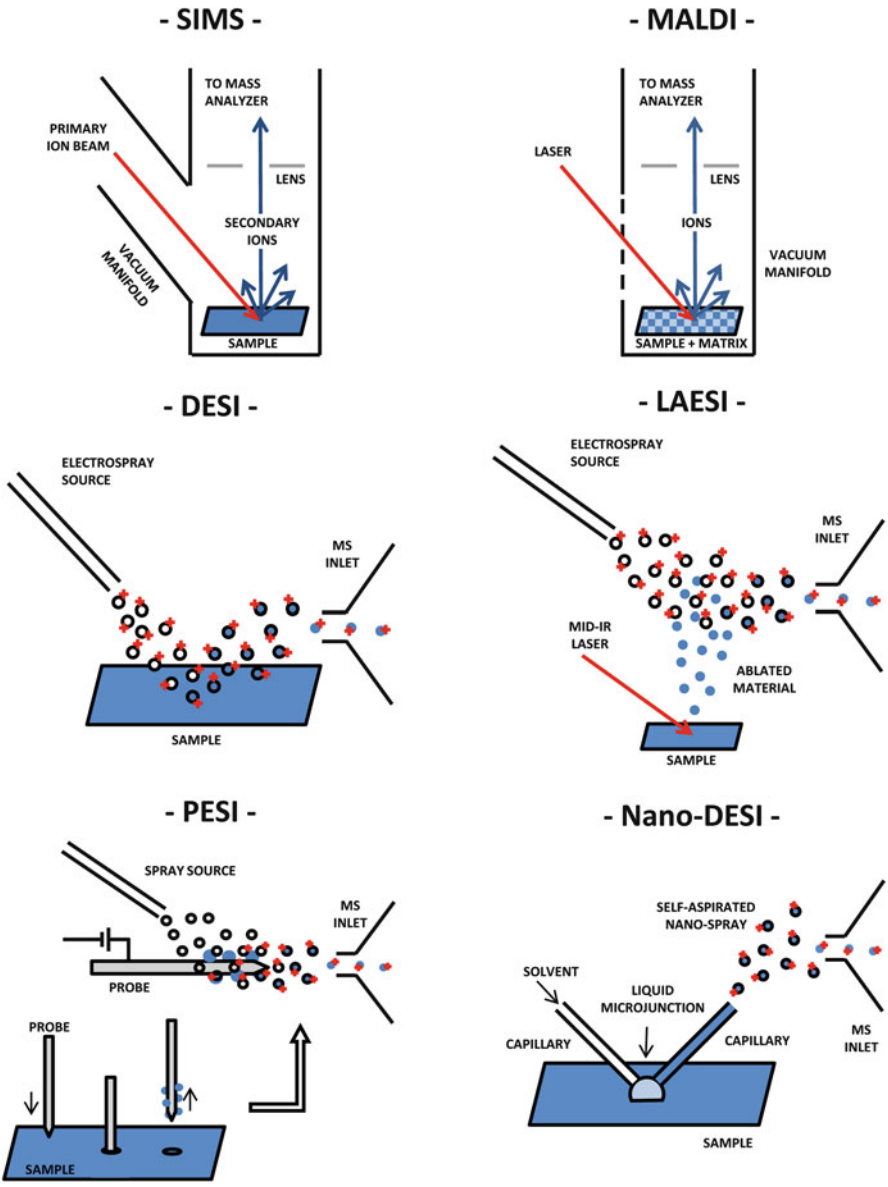

Fig. 12.13 Schematics of various ionization/desorption methods used for MSI

analyzers, the number of possible techniques with which to perform MSI, will continue to grow as well. As we have shown, many recently introduced ambient ionization sources have already found utility in MSI for drug discovery. With continued development, they will increasingly present an attractive alternative to established techniques such as MALDI and SIMS. The ambient methods offer several advantages over SIMS

as well as MALDI. For many applications, the ambient methods offer satisfactory resolution while requiring much less sample preparation, improving the time of analysis.

Wu et al. have identified several target areas in which progress would aid the adoption of the ambient MSI techniques into the field of drug discovery and development (Wu et al. 2013). These areas include:

1. A better understanding of ion suppression and matrix effects which are common in ambient mass spectrometry
2. Increased robustness in ambient MSI source design and experimental setup to increase reproducibility
3. Increased use of high-resolution mass analyzers and tandem mass spectrometry for molecular identification
4. The development of imaging software and other tools for handling increasingly large sets of imaging data
5. Improved spatial resolution of the ambient methods
6. The development of quantitative methods, such as the inclusion of internal standards

References

Burnum KE, Frappier SL, Caprioli RM (2008) Matrix-assisted laser desorption/ionization imaging mass spectrometry for the investigation of proteins and peptides. Annu Rev Anal Chem 1(1):689–705

Balluff B et al (2011) MALDI imaging mass spectrometry for direct tissue analysis: technological advancements and recent applications. Histochem Cell Biol 136(3):227–244

Bonnel D et al (2011) MALDI imaging techniques dedicated to drug-distribution studies. Bioanalysis 3:1399–1406

Barnes TJ, Kempson IM, Prestidge CA (2011) Surface analysis for compositional, chemical and structural imaging in pharmaceutics with mass spectrometry: a ToF-SIMS perspective. Int J Pharm 417(1–2):61–69

Coello Y et al (2010) Atmospheric pressure femtosecond laser imaging mass spectrometry. Anal Chem 82(7):2753–2758

Cha S et al (2009) Direct profiling and imaging of epicuticular waxes on arabidopsis thaliana by laser desorption/ionization mass spectrometry using silver colloid as a matrix. Anal Chem 81: 2991–3000

Costa AB, Cooks RG (2008) Simulated splashes: elucidating the mechanism of desorption electrospray ionization mass spectrometry. Chem Phys Lett 464:1–8

Cotte-Rodriguez I et al (2005) Desorption electrospray ionization of explosives on surfaces: sensitivity and selectivity enhancement by reactive desorption electrospray ionization. Anal Chem 77(21):6755–6764

Chen LC et al (2009) Ambient imaging mass spectrometry by electrospray ionization using solid needle as sampling probe. J Mass Spectrom 44:1469–1477

Cheng J, Winograd N (2005) Depth profiling of peptide films with TOF-SIMS and a C60 probe. Anal Chem 77(11):3651–3659

Cody RB, Laramée JA, Durst HD (2005) Versatile new ion source for the analysis of materials in open air under ambient conditions. Anal Chem 77(8):2297–2302

Durrant SF (1999) Laser ablation inductively coupled plasma mass spectrometry: achievements, problems, prospects. J Anal At Spectrom 14(9):1385–1403

Dill AL et al (2009) Lipid profiles of canine invasive transitional cell carcinoma of the urinary bladder and adjacent normal tissue by desorption electrospray ionization imaging mass spectrometry. Anal Chem 81(21):8758–8764
Eberlin LS et al (2010a) Three-dimensional vizualization of mouse brain by lipid analysis using ambient ionization mass spectrometry. Angew Chem Int Ed 49(5):873–876
Eberlin LS et al (2011) Desorption electrospray ionization mass spectrometry for lipid characterization and biological tissue imaging. Biochim Biophys Acta Mol Cell Biol Lipids 1811(11): 946–960
Eberlin LS et al (2010b) Cholesterol sulfate imaging in human prostate cancer tissue by desorption electrospray ionization mass spectrometry. Anal Chem 82(9):3430–3434
Eikel D et al (2011) Liquid extraction surface analysis mass spectrometry (LESA-MS) as a novel profiling tool for drug distribution and metabolism analysis: the terfenadine example. Rapid Commun Mass Spectrom 25(23):3587–3596
Fernández J et al (2011) Matrix-assisted laser desorption ionization imaging mass spectrometry in lipidomics. Anal Bioanal Chem 401(1):29–51
Goodwin RJA, Iverson SL, Andren PE (2012) The significance of ambient-temperature on pharmaceutical and endogenous compound abundance and distribution in tissues sections when analyzed by matrix-assisted laser desorption/ionization mass spectrometry imaging. Rapid Commun Mass Spectrom 26:494–498
Galhena AS et al (2010) Small molecule ambient mass spectrometry imaging by infrared laser ablation metastable-induced chemical ionization. Anal Chem 82(6):2178–2181
Guenther S et al (2011) AP-MALDI imaging of neuropeptides in mouse pituitary gland with 5 μm spatial resolution and high mass accuracy. Int J Mass Spectrom 305:228–237
Goodwin RJA et al (2011) Matrix-free mass spectrometric imaging using laser desorption ionization Fourier transform ion cyclotron resonance mass spectrometry. Rapid Commun Mass Spectrom 25:969–972
Grassl J, Taylor N, Millar AH (2011) Matrix-assisted laser desorption/ionisation mass spectrometry imaging and its development for plant protein imaging. Plant Meth 7(1):21
Goto-Inoue N et al (2011) Imaging mass spectrometry for lipidomics. Biochim Biophys Acta (BBA) Mol Cell Biol Lipids 1811(11):961–969
Garrett TJ et al (2007) Imaging of small molecules in tissue sections with a new intermediate-pressure MALDI linear ion trap mass spectrometer. Int J Mass Spectrom 260:166–176
Huang MZ et al (2011) Ambient ionization mass spectrometry: a tutorial. Anal Chim Acta 702(1):1–15
Harper JD et al (2008) Low-temperature plasma probe for ambient desorption ionization. Anal Chem 80(23):9097–9104
Haapala M et al (2007) Desorption atmospheric pressure photoionization. Anal Chem 79(20): 7867–7872
Hiraoka K et al (2007) Development of probe electrospray using a solid needle. Rapid Commun Mass Spectrom 21(18):3139–3144
Ifa DR et al (2007) Development of capabilities for imaging mass spectrometry under ambient conditions with desorption electrospray ionization (DESI). Int J Mass Spectrom 259(1–3):8–15
Ifa DR et al (2011) Tissue imprint imaging by desorption electrospray ionization mass spectrometry. Anal Meth 3(8):1910–1912
Judge EJ et al (2010) Analysis of pharmaceutical compounds from glass, fabric, steel, and wood surfaces at atmospheric pressure using spatially resolved, nonresonant femtosecond laser vaporization electrospray mass spectrometry. Anal Chem 82(8):3231–3238
Kroiss J et al (2010) Symbiotic streptomycetes provide antibiotic combination prophylaxis for wasp offspring. Nat Chem Biol 6:261–263
Kaspar S et al (2011) MALDI-imaging mass spectrometry—an emerging technique in plant biology. Proteomics 11(9):1840–1850

Kertesz V et al (2008) Comparison of drug distribution images from whole-body thin tissue sections obtained using desorption electrospray ionization tandem mass spectrometry and autoradiography. Anal Chem 80(13):5168–5177
Kaletaş BK et al (2009) Sample preparation issues for tissue imaging by imaging MS. Proteomics 9(10):2622–2633
Kertesz V, Van Berkel GJ (2008) Improved imaging resolution in desorption electrospray ionization mass spectrometry. Rapid Commun Mass Spectrom 22(17):2639–2644
Laskin J et al (2012) Tissue imaging using nanospray desorption electrospray ionization mass spectrometry. Anal Chem 84(1):141–148
Liu Y et al (2010) Imaging mass spectrometry with a low-temperature plasma probe for the analysis of works of art. Angew Chem Int Ed 49(26):4435–4437
Lozovoy VV et al (2008) Control of molecular fragmentation using shaped femtosecond pulses. J Phys Chem A 112(17):3789–3812
Luosujärvi L et al (2008) Desorption and ionization mechanisms in desorption atmospheric pressure photoionization. Anal Chem 80(19):7460–7466
Luosujärvi L et al (2009) Analysis of street market confiscated drugs by desorption atmospheric pressure photoionization and desorption electrospray ionization coupled with mass spectrometry. Rapid Commun Mass Spectrom 23(9):1401–1404
Lee YJ et al (2012) Use of mass spectrometry for imaging metabolites in plants. Plant J 70(1):81–95
Lagarrigue M et al (2011) Matrix-assisted laser desorption/ionization imaging mass spectrometry: a promising technique for reproductive research. Biol Reprod 86(3):74
Lane AL et al (2009) Desorption electrospray ionization mass spectrometry reveals surface-mediated antifungal chemical defense of a tropical seaweed. Proc Natl Acad Sci 106(18): 7314–7319
Li B et al (2011) Characterization of barley leaf tissue using direct and indirect desorption electrospray ionization imaging mass spectrometry. J Mass Spectrom 46:1241–1246
Muller T et al (2011) Direct plant tissue analysis and imprint imaging by desorption electrospray ionization mass spectrometry. Anal Chem 83(14):5754–5761
Manicke NE et al (2010) High-resolution tissue imaging on an orbitrap mass spectrometer by desorption electrospray ionization mass spectrometry. J Mass Spectrom 45(2):223–226
Mains J, Wilson CG, Urquhart A (2011) ToF-SIMS analysis of dexamethasone distribution in the isolated perfused eye. Invest Ophthalmol Visual Sci 52:8413–8419
Matusch A et al (2010) Cerebral bioimaging of Cu, Fe, Zn, and Mn in the MPTP mouse model of Parkinson's disease using laser ablation inductively coupled plasma mass spectrometry (LA-ICP-MS). J Am Soc Mass Spectrom 21(1):161–171
McMahon JM (1985) The analyses of six common vitamins by laser desorption mass spectroscopy. Anal Biochem 147(2):535–545
Nemes P, Vertes A (2007) Laser ablation electrospray ionization for atmospheric pressure, in vivo, and imaging mass spectrometry. Anal Chem 79(21):8098–8106
Nemes P et al (2008) Ambient molecular imaging and depth profiling of live tissue by infrared laser ablation electrospray ionization mass spectrometry. Anal Chem 80(12):4575–4582
Nemes P, Woods AS, Vertes A (2010) Simultaneous imaging of small metabolites and lipids in rat brain tissues at atmospheric pressure by laser ablation electrospray ionization mass spectrometry. Anal Chem 82(3):982–988
Nemes P, Barton AA, Vertes A (2009) Three-dimensional imaging of metabolites in tissues under ambient conditions by laser ablation electrospray ionization mass spectrometry. Anal Chem 81(16):6668–6675
Ovchinnikova OS, Kertesz V, Van Berkel GJ (2010) Molecular surface sampling and chemical imaging using proximal probe thermal desorption/secondary ionization mass spectrometry. Anal Chem 83(2):598–603

Ovchinnikova OS, Kertesz V, Van Berkel GJ (2011) Combining transmission geometry laser ablation and a non-contact continuous flow surface sampling probe/electrospray emitter for mass spectrometry based chemical imaging. Rapid Commun Mass Spectrom 25:3735–3740

Prideaux B, Staab D, Stoeckli M (2010) Applications of MALDI-MSI to pharmaceutical research. Meth Mol Biol 656:405–413

Pasilis S et al (2008) Using HPTLC/DESI-MS for peptide identification in 1D separations of tryptic protein digests. Anal Bioanal Chem 391(1):317–324

Paglia G et al (2010) Desorption electrospray ionization mass spectrometry analysis of lipids after two-dimensional high-performance thin-layer chromatography partial separation. Anal Chem 82:1744–1750

Pacholski ML, Winograd N (1999) Imaging with mass spectrometry. Chem Rev 99(10): 2977–3006

Pól J et al (2009) Automated ambient desorption–ionization platform for surface imaging integrated with a commercial Fourier transform ion cyclotron resonance mass spectrometer. Anal Chem 81(20):8479–8487

Prideaux B et al (2011) High-sensitivity MALDI-MRM-MS imaging of moxifloxacin distribution in tuberculosis-infected rabbit lungs and granulomatous lesions. Anal Chem 83:2112–2118

Richards AL et al (2011) Imaging mass spectrometry in transmission geometry. Rapid Commun Mass Spectrom 25:815–820

Roach PJ, Laskin J, Laskin A (2010) Nanospray desorption electrospray ionization: an ambient method for liquid-extraction surface sampling in mass spectrometry. Analyst 135(9):2233–2236

Shariatgorji M et al (2012) Controlled-pH tissue cleanup protocol for signal enhancement of small molecule drugs analyzed by MALDI-MS imaging. Anal Chem 84:4603–4607

Seeley EH, Caprioli RM (2012) 3D imaging by mass spectrometry: a new frontier. Anal Chem 84(5):2105–2110

Sripadi P et al (2009) In vitro analysis of metabolites from the untreated tissue of *Torpedo californica* electric organ by mid-infrared laser ablation electrospray ionization mass spectrometry. Metabolomics 5(2):263–276

Shrestha B, Vertes A (2009) In situ metabolic profiling of single cells by laser ablation electrospray ionization mass spectrometry. Anal Chem 81(20):8265–8271

Shrestha B, Patt JM, Vertes A (2011) In situ cell-by-cell imaging and analysis of small cell populations by mass spectrometry. Anal Chem 83(8):2947–2955

Shelley JT, Ray SJ, Hieftje GM (2008) Laser ablation coupled to a flowing atmospheric pressure afterglow for ambient mass spectral imaging. Anal Chem 80(21):8308–8313

Seeley EH, Caprioli RM (2011) MALDI imaging mass spectrometry of human tissue: method challenges and clinical perspectives. Trends Biotechnol 29(3):136–143

Takats Z et al (2004) Mass spectrometry sampling under ambient conditions with desorption electrospray ionization. Science 306(5695):471–473

Takáts Z, Wiseman JM, Cooks RG (2005) Ambient mass spectrometry using desorption electrospray ionization (DESI): instrumentation, mechanisms and applications in forensics, chemistry, and biology. J Mass Spectrom 40(10):1261–1275

Thunig J, Hansen SH, Janfelt C (2011) Analysis of secondary plant metabolites by indirect desorption electrospray ionization imaging mass spectrometry. Anal Chem 83(9):3256–3259

Ullburg S (1977) The technique of whole-body autoradiography: cryosectioning of large specimens, in special issue on whole-body autoradiography. Instr J Sci Tools. O. Elvefeldt (ed) LDK-Producter AB, Bromma, Sweden, pp 2–29

Vertes A, Balazs L, Gijbels R (1990) Matrix-assisted laser desorption of peptides in transmission geometry. Rapid Commun Mass Spectrom 4(7):263–266

Venter A, Nefliu M, Cooks RG (2008) Ambient desorption ionization mass spectrometry. TrAC Trends Anal Chem 27(4):284–290

Van Berkel GJ et al (2008) Liquid microjunction surface sampling probe electrospray mass spectrometry for detection of drugs and metabolites in thin tissue sections. J Mass Spectrom 43(4): 500–508

Chapter 13
Regulatory Considerations Involved in Imaging

Brian R. Moyer, Narayan P.S. Cheruvu, and Tom C.-C. Hu

Abstract Today's revolution in imaging technologies in the biomedical sciences has raised much needed hope for improved diagnostics, therapeutics, and the eventual cure of many debilitating illnesses. Imaging itself has become the seed technology that has fostered the development of many novel diagnostic approaches as well as helping point the way to witnessing the mechanism of action of drugs and biologics. The advancement of new drugs and biologics will be undertaken in the future with surrogate biomarkers, and many of these will be in the form of imaging. Imaging of pharmacodynamic responses to therapies such as changes in RECIST, cerebral glucose utilization, MRI BOLD changes reflecting neurologic activity, and many other novel approaches are opportunities for the imaging community to work with the regulatory community to contribute to the advancement of novel agents. As stated by Dr Steven Larson (2007) "*We are experiencing a paradigm shift from anatomic towards biomarker (molecular imaging) as the primary means for assessing treatment response in oncology*" and as such the regulatory environment for this to happen must be considered and developed to maximize the potential which imaging brings to medical diagnosis and to clinical decision making.

B.R. Moyer, M.S. (Pharm), M.S. (Tox), C.N.M.T. (✉)
BRMoyer and Associates, LLC, 23 Hawk Drive, Bedford, NH 03110, USA
e-mail: bmoyernh@gmail.com

N.P.S. Cheruvu, Ph.D., M.B.A.
Covidien Inc., Hazelwood, MO 63042, USA

T.C.C. Hu, Ph.D.
Health and Human Services (HHS), Office of the Assistant Secretary for Preparedness and Response (ASPR), Biomedical Advanced Research and Development Authority (BARDA), Washington, DC 20201, USA

Nuclear and Radiological Engineering/Medical Physics Program, George W. Woodruff School of Mechanical Engineering, Georgia Institute of Technology, North Avenue, Atlanta, GA 30332, USA

B.R. Moyer et al. (eds.), *Pharmaco-Imaging in Drug and Biologics Development*,
AAPS Advances in the Pharmaceutical Sciences Series 8, DOI 10.1007/978-1-4614-8247-5_13,

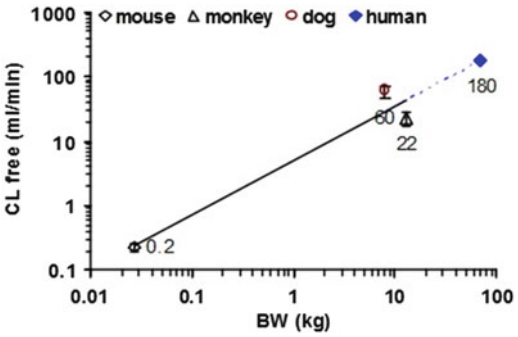

Fig. 13.1 Human clearance of drug "X" relative to other species. Linearity for human and three other species is shown for a log–log relationship of body weight (BW and clearance of free drug Cl-free). A key factor for the best estimation of clearance is the use of the log of the body weight as this provides linearity that covers at least two log range across species. See Chap. 5 in this volume for more detail on the use of clearance in species dose scaling (from Onthank 2005; figure from dissertation; unrestricted)

13.1 The Regulatory Issues in Translational Biology

One of the most confounding issues for the pharmaceutical industry is not at the regulatory approval end of the development spectrum but rather somewhere "in the middle" where costs begin to accelerate, decisions on what is the drug or biologic's market share (potential revenue), what constraints on the indication will be appropriate or required (due to safety findings), and decisions to let go of programs that may have marginal efficacy or too low a therapeutic index (Paul et al. 2010; Muller and Milton 2012).

13.1.1 The Concept of Translational Biology: Predicting Human from Animals

While science rests predominantly on drug development using animal models of disease, including murine genetic knock-in and knock-out models (genetically engineered mouse models; or GEMMs), there has been a long history of skepticism on the relevance of animal models (European Commission, 2010). Although mice share 99% genetic equivalency to man there is still the relationships of gene expressions and the pathologic outcomes may be temporally different from man as well as pharmacologically (receptor affinities, etc). It is important to investigate the prediction of a drug behavior across several species to obtain a linear profile of the drug clearance across those species such that a true estimate of the drug behavior in man may be predicted (Fig. 13.1). Ensuring a range of body weights across selected species is an important factor to consider when applying allometric scaling. If the selected body weights of the species tested have less than a one- to tenfold (1 log)

range, then the value of the extrapolated slope for the estimate is not well defined and the data may skew the determined human value. It is also very important to recognize that in addition to renal flow differences and nephron count in the renal cortex (both are additional allometric parameters for consideration) that can affect rates of drug clearance, some drug elimination rates are a function of *total* drug rather than *free* (unbound) drug concentration in the eliminating region. Changes in drug binding either in blood or in the eliminating region (receptor-mediated clearance) will influence the species clearance from the blood. In the "big picture" of PK across species, it is apparent that tissue binding is far less important in pharmacokinetics than is drug binding to the plasma proteins (Gibaldi and Koup 1981). It thus important to assess protein binding and make corrections to the clearance estimates. In terms of clearance across species, Mordenti (1986) provides a graph showing the linearity of antipyrine clearance versus body weight in 11 species. This relationship across species allows one to do comparative pharmacology and PK studies using this observed relationship as a reference clearance "gold standard." Ritschel and Banerjee (1986) show a similar relationship, as with Mordenti using 11 species, for the volume of distribution (V_β) of antipyrine. Again, a useful "gold standard" for interpreting across species.

From a regulatory perspective, it is prudent to determine the in vitro plasma binding of a drug in several species (including human) in addition to the standard pharmacokinetic parameter estimates as these two considerations form a significant basis for correlation to the human dose. Muller and Milton (2012) describe how to consider plasma protein binding and tissue exposures. We recommend inspection of their paper on the importance of establishing a reliable across species therapeutic index (TI) in drug and especially biologics development. They point out that there is always some likelihood that the in vitro target specificity may not correlate with the therapeutic index. They provide where this is the case where they describe the drug pergolide for Parkinsonism. Pergolide is a dopamine receptor agonist which was found (after approval) to have an additional off-target agonal receptor affinity for the 5-HT_{2b} receptor which was contributing to valvular heart disease complications in some patients. Pergolide has a 36-fold higher affinity for the dopamine receptor than for the 5-HT_{2b} receptor, but in vivo conditions of clearance and overall drug exposure (likely cardiac surface percent flow >> pituitary blood flow) led to an actual therapeutic index of less than 1. For a more current review of dose translation employing body surface area (BSA), we direct the reader to Reagan-Shaw et al. (2007).

Mordenti (1986) provided a log-log plot of multiple species with respect to the logarithm of each species urinary clearance of intrinsic unbound antipyrine (in L/MLP $\times 10^5$), where MLP is maximum lifetime potential in years, vs the logarithm of body weight and demonstrates that this is a highly linear function (r = 0.989) (Fig. 13.2).

Onthank (2005) found in his dissertation that if clearance was taken as the primary PK value, the weight-based allometric scaling, with addition of the protein-binding adjustment, was predictive within 12.5 % based on a retrospective analysis. Work by Tang and Mayersohn (2005a, b) reported predicting human clearance values within 78 % with a method using only rat and human data. They also reported that accuracy using simple allometric scaling was within 323 % and using the rule of exponents

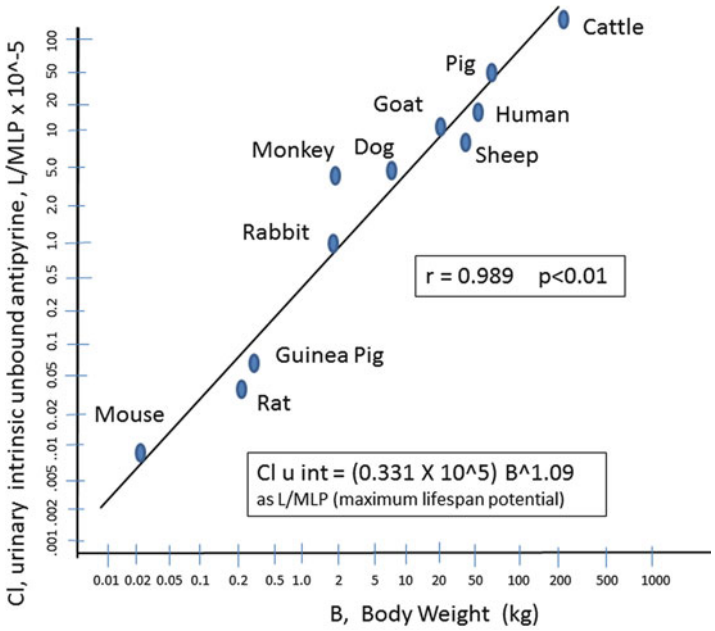

Fig. 13.2 Antipyrine clearance versus BW (kg) versus body weight (BW) over 11 species (log–log plot). Note the similar log–log relationship as was seen for Clearance (from Mordenti 1986; with permission). A similar plot of antipyrine volume of distribution (V_β) versus BW is available from Ritschel and Banerjee (1986)

alone it was within 185 %. Thus, the method of Onthank showing a 12.5 % prediction accuracy based upon clearance and weight-based scaling is an excellent method for providing human clinical dose estimates.

13.1.2 Immunogenicity and Biologics

Immunogenicity, and indeed nearly all drug and biologic toxicologic occurrences, has prompted regulatory attention which has mobilized into specific recommendations and guidance documents (Bass et al. 2011; FDA Guidance for Industry, UCM33856, 2013). Figure 13.3 depicts the history of safety guidance documents over the past 30 years. Imaging is a small part of this as it has generally been in the tracer dose category and thus generally with wide therapeutic indexes. However, of late there has been development of highly biologically active radiotracers and the CT, US, optical, and MR imaging platform industries have been making more biologically active contrast agents which could have deleterious biological activities and thus reasonable suggestion of concern for safety. The development of small radiotracer peptides with exceptionally high (sub-nanomolar) receptor affinities has resulted in products with potentially narrow therapeutic index values. The institution of the Phase "0" trials (see FDA reference: *Exploratory IND studies*, G6384dft.pdf, April

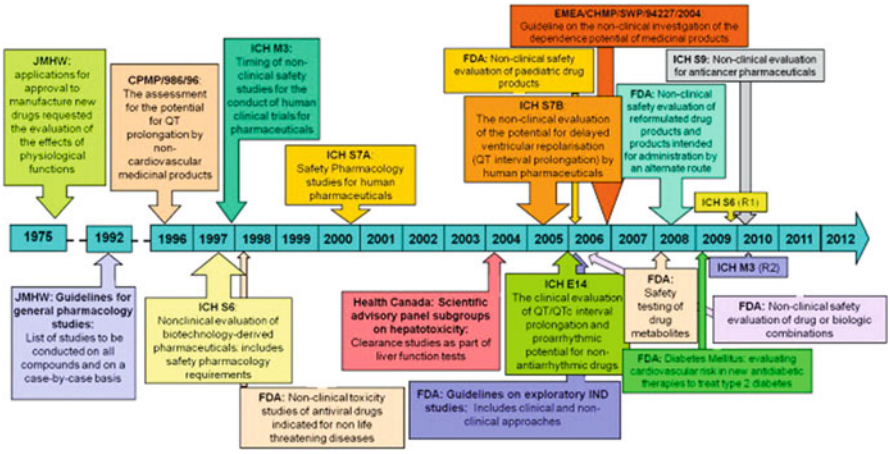

Fig. 13.3 Scope and implementation date of regulatory guidance documents referring entirely or in part to safety pharmacology over the last 30 years. Over the last decade there has been an increase in number and scope of regulatory guidance referring to safety pharmacology end points reflecting increasing regulatory concerns. *FDA* Food and Drug Administration, *ICH* International Conference on Harmonization, *JMHW* Japanese Ministry of Health and Welfare, *FDA* United States Food and Drug Administration, *EMEA* European Agency for the Evaluation of Medicinal Products, *CPMP* Committee on Proprietary and Medicinal Products, *CHMP* Committee on Medicinal Products for Human Use (from Bass et al. 2011, with permission)

2005) allows investigators with purportedly "safe" radiotracers (indeed potentially benign contrast agents as well—documented with GLP toxicology supporting documents) to enter into a dose escalation safety trial. More will be discussed on this post-IND avenue later in the chapter. This kind of early human trial has profound implications in the advancement of new imaging agents and also the potential for use of existing radiotracers and contrast agents with known high therapeutic index values to be employed as companion diagnostics in new clinical indications.

13.1.2.1 The TeGenero Incident: Implications in Imaging

Shankar et al. (2006), as well as Nada and Somberg (2007), has addressed some very important points of scientific as well as regulatory aspects on the immunogenicity of first-in-man (FIM) biologics which have additional implications in their use as diagnostic imaging agents or use as surrogate biomarker end points to explore or defend the efficacy and safety of a biologic. The efficacy and the safety of biologics in human studies has inherent risk with the potential appearance of immune responses. A tragic case of this was the TeGenero TNG1214 incident. Immunogenicity studies are now critical elements of study in the preclinical setting of biologic development following this clinical trial experience. The Nada article is detailed in how clinical trials must change in light of the TeGenero failed FIM dose adjustments.

In 2006 (March 13th) a clinical trial began as a small (<10 patient) Phase 1 trial that was designed based upon preclinical experience. TGN1412 was an agonal

monoclonal antibody (humanized IgG4/kappa) for the human CD28 cell surface marker. As an IgG4 antibody it binds with low affinity to Fc receptors and does not mediate ADCC (antibody-dependent cell-mediated cytotoxicity) or CDC (complement-dependent cytotoxicity) activity. The study was a proposed dose escalation, single IV dose in escalating cohorts covering a 0.1–5 mg/kg dose range. Patients ($n=6$ plus 2 controls) were separated in time for dosing by 10 min. All six patients receiving the lowest dose experienced severe life-threatening toxicities and all within 90 min, and by 21 h all the subjects experienced multiorgan failure (Rellahan 2009).

What are the implications of this biologic, tested in multiple species with general safety assessment sufficient for trial initiation? Clearly this is similar to testing a biologic imaging agent in a Ph "0" trial where the dose is termed "non-efficacious" or even "non-significant" since it binds as a tracer. What are the limits of a safe "tracer dose"? How can we properly test biologics to assure a safe undertaking for a new biologic in the clinic? This is never going to be answered sufficiently for every new product, but there are procedures to give more attention.

The results of the TeGenero incident showed that a 28-day repeated dose study in cynomolgus monkeys gave a NOAEL (no observed adverse event level) of 50 mg/kg—the highest dose to be tested in the clinical setting. Looking closely at the data, however, there were signs of risk. There were elevations in IL-2, IL-6, and IL-5 (an anti-inflammatory) which were dose dependent. There were no signs of TNF-α or INF-γ. The company responsible for the trial saw the rise in IL-2 and IL-6 but was more driven to move the product forward by the observed lack of increases in TNF-α or INF-γ which were considered more important "threat" biomarkers. The long-term consequences of the safety picture were emphasized rather than anything that might occur acutely. Literature sources were known that described the T cell activation in nonhuman primates (NHPs) as muted to that of human but this too was not queried. Lack of toxicity in NHPs does not mean T cell agonists will not be toxic in humans.

An allometric pharmacodynamic response paradigm might well have been useful to consider. There would have been a better prediction of the eventual outcome if the company had not used the NOAEL but rather employed MABEL. MABEL is an acronym for "Minimal Anticipated Biological Effect Level." The intent of the use of MABEL is to more appropriately justify a dose for a biologic effect based upon actual pharmacology –i.e. adjust the dose for anticipated exposure in man by including an anticipated duration of effect which allows for adjustments based upon interspecies differences in product affinity as well as potency. Simms (2009) provides an excellent outline of the TGN1214 analysis for the first dose in man and defined the anticipated safety window based on NOAEL and MABEL appropriate safety factor based on potential risk at 0.001 mg/kg rather than the 0.1 mg/kg (2-log lower) which was the NOAEL-only determination.

Typically, a clinical dose is arrived at as a series of steps (per the FDA Guidances):

- Step 1: Determine "no observed adverse effect level" (NOAEL).
- Step 2: Convert NOAEL to a "human equivalent dose" (HED)—generally normalized to body surface area (BSA).
- Step 3: Select HED from the most appropriate species—additional factors: metabolism, receptors, binding epitopes—*default*: most sensitive species (lowest HED).

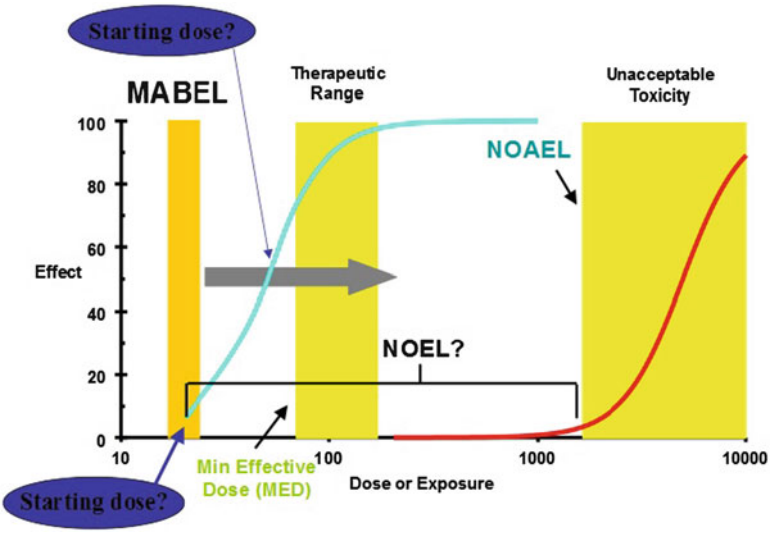

Fig. 13.4 MABEL as an improved paradigm to assist in the decision of a biologic's human starting dose versus the classic approach from NOAEL versus NOEL (no observed event level) methods (from Simms 2009; with permission)

- Step 4: Apply a safety factor (>tenfold) to give a "maximum recommended starting dose" (MRSD).
- Additional NEW STEP using MABEL:
- Step 5: Adjust MRSD based on the pharmacologically active dose.

Clinical first dose, probably more for biologics than drugs, actually needs to change the above paradigm to use the approach provided by MABEL where MABEL asks the question: "why start with the highest dose you think is safe?—Better to start with the lowest dose you think is active." In brief, the decision on the first dose in humans needs to ask about BOTH toxic observations and pharmacologic observations. Figure 13.4 depicts what MABEL actually looks like in the setting of determining the first dose in humans.

13.1.2.2 Companion Diagnostics (CDx) and Imaging

Imaging platforms are fast becoming aids as clinical and non-clinical diagnostic tools for evaluating drug and biologic responses in-vivo (Bocan 2010). In the very near future they will be required as companion tools for identifying and quantifying surrogate endpoints in oncology and a wide variety of diseases (Ellenberg and Hamilton 1989; Carver 2010). Imaging uses in the drug and biologics development arena are being exploited to inform on the risk and benefit of further investment in a candidate drug or in a surrogate biomarker for companion development. An example of a surrogate marker of cancer is circulating tumor cells (CTCs). These cells may offer promise as a surrogate source of representative cells from the

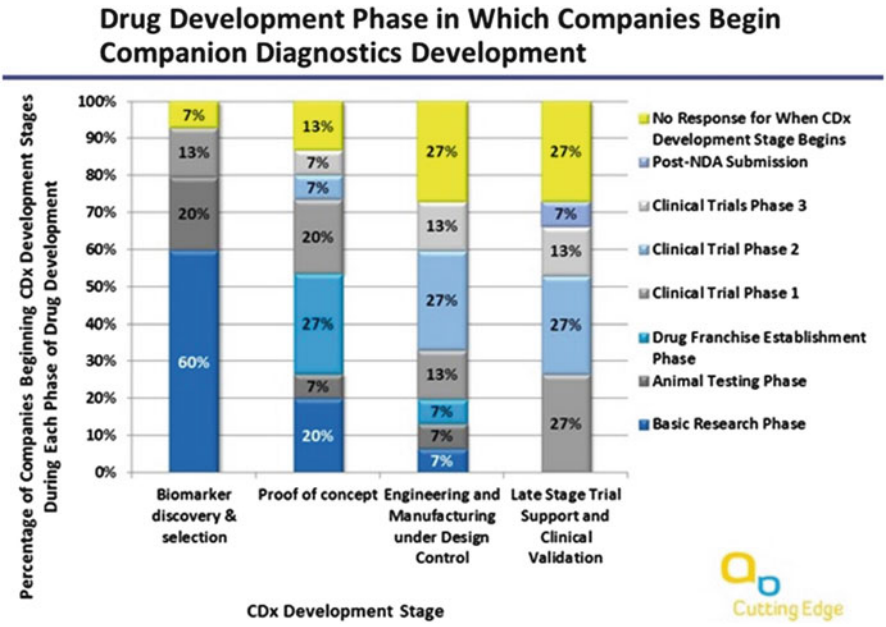

Fig. 13.5 When do companies begin using companion diagnostics? It is apparent that in early discovery 60 % are employing some form of a companion diagnostic for their basic research (likely POS controls), while approximately 40–50 % are using CDx in the animal testing, drug franchising (new companies; or bought by established "Big Pharma"), and thence in Phase 1 (from Cutting Edge Information®, **PH169 Companion Diagnostics and Biomarker Development**; 2012; with permission)

disease that can be obtained in real time and may provide opportunities to evaluate predictive biomarkers, i.e., genetic markers, that can guide treatment decisions. In this review, we consider some of the technical hurdles around surrogate markers such as CTC capture and their analysis platforms for biomarker evaluations but not simply as laboratory assays but as clinically relevant tracking tools that can be employed in imaging and allow the real-time clinical measurements that decide treatment rationale as well as measure treatment success or failure. This chapter will hopefully suggest to the reader novel paths for codevelopment of anticancer therapeutics with image-based diagnostics that could enable clinical validation and qualification of biomarker-based assays as companion diagnostics. Companion diagnostics—tests that provide information about a patient's genetic and genomic characteristics that are used to make therapeutic treatment decisions—hold great promise for "personalizing" medicine and streamlining drug development (Carver 2010).

When are biomarkers explored in the drug development phase as a "companion diagnostics"? In a survey conducted by "Cutting Edge Innovation" (2012), four stages of CDx use were identified: (1) biomarker and discovery, (2) proof of concept (efficacy), (3) engineering and manufacture under design control, and, in (4) late stage trial, support and clinical validation (see web site: http://www.cuttingedgeinfo.com/2012/pharma-stages-new-drug-companion-diagnostic-development/c-5/). The majority of companies begin CDx utilization in early discovery, and this likely is in the form of validating

positive controls. Figure 13.5 depicts the corporate approaches to when they introduce the concept of a companion diagnostic to the primary drug indication.

13.2 Biomarkers and Animal Models: Regulatory Considerations

13.2.1 The Animal Model and Biomarker Qualification Programs at the FDA

It is important to recognize the advancements in regulatory policy at the FDA. Three major "initiatives" over the past several years have made the FDA a true partner in drug discovery, development, and review. The first of these we want to discuss is the "*Critical Path*" *Initiative* dated March of 2004 (and updated 2006; web link: http://www.fda.gov/ScienceResearch/SpecialTopics/CriticalPathInitiative/ucm076689.htm). The publication "Innovation/Stagnation: Challenge and Opportunity on the Critical Path to New Medical Products" identified several reasons for a widening gap in the time between scientific discovery and the appearance of a drug or biologic that changes medical practices. The FDA found that innovations and development of novel medical products were fraught with difficulty and unpredictability (and thus commensurate failure), and the report concluded that the pharmaceutical industry needed to (1) modernize its approaches in the areas of scientific and technical tools and (2) include more advanced information technologies. By implementing actions on these two areas alone, the FDA felt that there would be a significant stimulus to innovation and improve the throughput of drug/biologic evaluations that predict the safety, effectiveness, and manufacturability of medical products.

In March 2006, the FDA's Commissioner announced the release of FDA's Critical Path Opportunities List which resulted from wide public participation. The list described 76 specific areas where the sciences of product development had the greatest need for improvement. The specific areas included genomics, informatics (computer science and statistical techniques), and *imaging*.

Subsequent to the Critical Path Initiative, the FDA has recently launched three important initiatives which have direct connection with imaging. These include qualification programs[1] called the "*Biomarker Qualification Consortium of Best Practices*," the "*Animal Model Qualification Program,*" and the "*Drug Development Tools* (*DDT*) *Qualification Program*." In these initiatives, the FDA actually fosters development in these three directions. The "*Biomarker Qualification Consortium of Best Practices*"[2] offers an opportunity to formally develop and rigorously test a

[1] CDER has developed DDT Qualification Programs directed toward the following types of DDTs: biomarkers, clinical outcome assessments (COAs), and animal models.

[2] Biomarker qualification program: http://www.fda.gov/Drugs/DevelopmentApprovalProcess/DrugDevelopmentToolsQualificationProgram/ucm284076.htm; The Biomarker Qualification

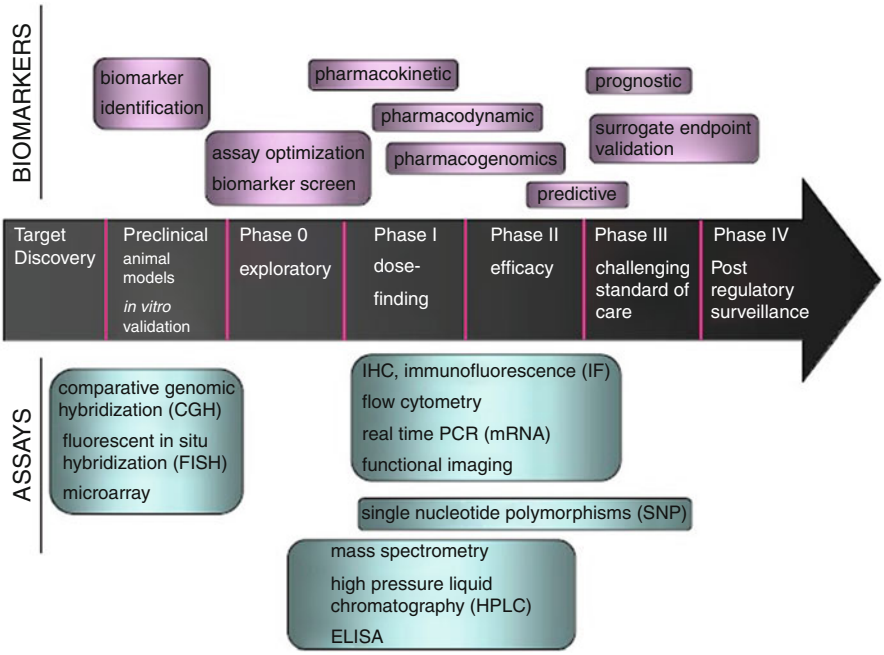

Fig. 13.6 A different view of the regulatory process by viewing a separation of "biomarkers" from "analytical assays." The distinction is not always clear (from Dhani and Siu 2008; with permission)

candidate biomarker for use as part of a candidate drug or biologic's regulatory process. The goals of the CDER Biomarker Qualification Program are to:

- Provide a framework for scientific development and regulatory acceptance of biomarkers for use in drug development.
- Facilitate integration of qualified biomarkers in the regulatory review process.
- Encourage the identification of new and emerging biomarkers for evaluation and utilization in regulatory decision-making.
- Support outreach to relevant external stakeholders to foster biomarker development.

Biomarkers under considered for qualification must be measurable and conceptually independent of the specific test performing the measurement. The distinction of what is a "biomarker"—i.e., a chemical analysis? a "method"? "Biomarkers" are defined differently from "assays" and are more broadly defined as parts of systems which can represent something about the pathology of interest such as being a "predictive" or "prognostic" indicator, i.e., a future trend or outcome versus an advance indication or portent of a future event, respectively. Figure 13.6 depicts

Process is described fully in this link: http://www.fda.gov/Drugs/DevelopmentApprovalProcess/DrugDevelopmentToolsQualificationProgram/ucm284621.htm.

this separation of "biomarkers" from "assays" with distinction of biomarkers as terms under larger definitions and assays as specific platforms that can help define a biomarker through the development process. A good reference on how the regulatory authorities have evolved on biomarker qualification is Goodsaid and Papaluca (2010). Another reference discussing "companion diagnostics" is that of Kern and Thomae (2013) and for examples of "surrogate endpoints" in clinical trials see Prentice (1898). A "roadmap for biomarker qualification" can be found in Warnock and Peck (2010).

The Drug Development Tools (DDT) offered by the FDA allows CDER to work with submitters (the public, pharma, etc.) to guide them as they develop or refine a novel DDT for a specific use or indication. Not unlike a grant or contract, CDER then will rigorously evaluate the submission (review) for use in the regulatory process. Qualifying a "tool" (aka DDT) within this FDA program will then allow drug/biologic candidate sponsors to use the "tool" in the qualified context of use during their drug development without requesting that CDER reconsider and reconfirm the suitability of the "tool" for the qualified context of use as it will already be available "off the regulatory shelf." The mission and objectives of the DDT Initiative include the following points:

- To qualify and make DDTs publicly available for a specific context of use to expedite drug development and review of regulatory applications.
- To provide a framework for scientific collaboration to facilitate DDT development.
- To facilitate integration of qualified DDTs in regulatory review.
- To encourage development of DDTs for contexts of use with unmet needs.
- To encourage the formation of collaborative groups to undertake DDT development programs to increase the efficiency and lessen the individual resource burden incumbent with DDT development.
- To encourage innovation in drug development.
- The Animal Model Qualification (AMQ) program is evolving. The program is voluntary and models qualified through this program will be made public. The process described below is subject to change as the Qualification Review Teams (QRTs) work with a number of submitters.

The "Animal Model Qualification" (AMQ) program is sponsored through both CDER and CBER. It is intended to provide added impetus and support for developing improved animal models for drug and biologics. In general, these are sponsored for development under the Animal Rule (21 CFR 314.600 for drugs; 21 CFR 601.90 for biological products[3]), but this need not be an exclusive approach. The AMQ program is to foster animal models of disease which have well-characterized natural histories, reasonably well-understood pathophysiological mechanisms of the disease as related to a pathogen, drug or biologic, and use of the animal model in mitigating or controlling disease. In general, the FDA wishes to see such model interpretations

[3] Concept paper from the FDA: Animal Models—Essential Elements to Address Efficacy Under the Animal Rule http://www.fda.gov/downloads/Drugs/GuidanceComplianceRegulatoryInformation/Guidances/ucm072214.pdf.

show "translation," or rational species cross over, in more than one animal species for the expected response that is predictive for human benefit. A single animal species can serve as the model if it is sufficiently well characterized for an accurate predictive response in humans. In the Animal Rule, the primary study end point is generally "enhancement of survival" (or prevention of major morbidity). The animal model may also simply serve to define the kinetics and pharmacodynamics of the product in humans and to facilitate in the selection of an effective dose in humans as per the Animal Rule.

Product-independent animal models, i.e., animal models which utilize imaging agents, can be evaluated and qualified as part of the qualification program outlined for Drug Development Tools (DDTs) (see 2010 draft *Guidance for Industry*: *Qualification Process for Drug Development Tools*). In this case "imaging" may have a direct tie to drug success in development. A potentially very good example of this is the utility of F-18 FDG in defining cancer metabolic behavior following drug or biologic therapy (see Chap. 7 for oncology-directed imaging). Figure 13.7 depicts a flow diagram of the process for advancement of a DDT through the FDA qualification pathway.

We will not be covering the "Clinical Outcomes Assessment Tools" (COAT) in much depth in this chapter simply as clinical use of imaging is far too comprehensive a treatise to cover with everything else we need to cover in support of the previous chapters. The reader is encouraged to visit the FDA COAT web site for further information.[4] The primary goal of this book, and indeed this chapter, is to inform the Reader of the *non-clinical* regulatory environment.

13.2.2 Quality Systems Guidance for Imaging Platforms

13.2.2.1 PET, SPECT, MR, CT, and Optical Platforms and the Need for FDA Compliance

In the laboratory setting, imaging platforms are relegated to being simply part of the analytical instruments repertoire—except they are often left out of the formalism tied to quality controls for the corporate analytical services such as ELISA's and other set-aside and managed support services.

Imaging can potentially play a major role in the interpretation of the outcomes depicted in Fig. 13.8 where imaging can (1) provide the initial diagnosis and subsequent additional diagnostic information (on multiple platforms) on the genetics and physiologic character of the cancer prior to treatment (Shields 2008); provide the time rate of change in the RECIST or other measurable property of a cancer whereby a measure of treatment success can be provided (Wahl et al. 2009), and (3) provide a documentation of therapeutic success and resolution of the cancer (Weber 2009).

[4] Clinical Outcomes Assessment Qualification Program (COAQ): http://www.fda.gov/Drugs/DevelopmentApprovalProcess/DrugDevelopmentToolsQualificationProgram/ucm284077.htm.

Fig. 13.7 The Drug Development Tool (DDT) program and a representative regulatory pathway whereby upon full qualification the "Tool" becomes publically available to foster development of future drugs and biologics (from Davis J, FDA presentation at NIH; BARNCATS meeting, Office of Counter-Terrorism and Emergency Coordination, CDER, FDA January 25, 2013; with permission)

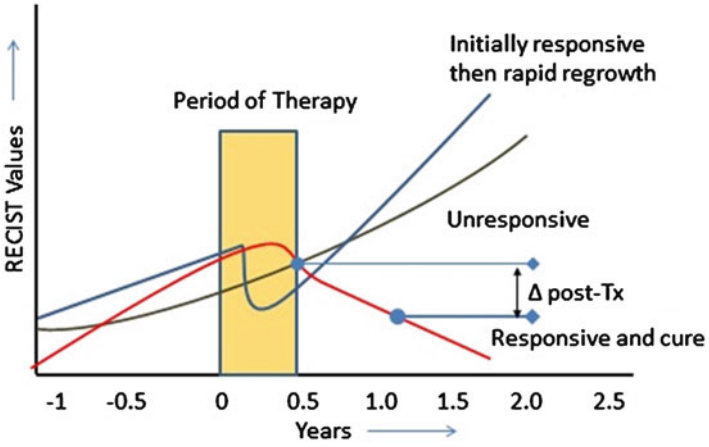

Fig. 13.8 A cartoon depiction of three theoretical cases of cancer development, adjudication with therapy, and the response to the therapy (poor with progression, unresponsive, and successful response with resolution). The change in tumor RECIST values post-therapy can be indicative of success

To achieve these clinical end points and like any analytical system-based laboratory service, there is a requirement of providing validated imaging systems, image collection procedures (time(s) post-administration, acquisition times for statistical purposes, acquisition protocols, other quality assurances), image processing and validated processing algorithms, image interpretation (reader training and interpretation skills), and the appropriate medium to present the findings must also be validated (color maps, windowing of the images, film versus digital screens, etc.). A discourse of these important regulatory concerns is provided below in Sects. 13.2.2.2 and

13.2.2.3. Hoffman (2009) provides a very good walk through of the use of F-18 fluorothymidine (FLT) as an imaging agent for measuring tumor proliferative responses to therapy. He also provides an excellent review of the various IND processes and the role and responsibilities of the physician in using imaging for evaluating new chemical entities (NCEs) in post-IND trials (Hoffman 2012).

13.2.2.2 Image Platform Validations

This topic is too involved to cover adequately in this short section; however, a fine review of an often overlooked aspect of imaging platform validations is provided on medical imaging "processing" by Jannin et al. (2006). The reader is also invited to seek manufacturer guidelines and device applications that are recognized as validated by the FDA medical devices section (see http://www.fda.gov/MedicalDevices/DeviceRegulation andGuidance/GuidanceDocuments/default.htm). The medical devices section covers radiation-emitting devices including MR (for electromagnetic fields), CT, and PET/SPECT with self-contained attenuation correction sources and optical imaging agent sensors (laser sources and near infrared cameras (NIR), etc.). Image platform validations are inherently the responsibility of the manufacturers. However, operationally, the instruments are governed by operating procedures, technical support in the operations, and these all involve operator training and validation of the instruments prior to use in controlled (i.e., FDA acceptable) studies. There are specific limits in performance, and operating the imaging platform will be limited to the inherent resolution of the system, noise of the system (ability to maintain stable electronics), the choices of reconstruction algorithms in 3-D projections, field homogeneity for MR systems as well as coil performance, laser intensity control and reflectivity for optical probes, etc. A "quality control" checklist is appropriate in any imaging platform. Here is an example of a simplified MR system quality operations checklist where there will be a PET imaging correlate. Table 13.1 shows that the aggregate scoring is done through a spider graph representation of the total scores from each topical QC element.

13.2.2.3 Quality Control of Radiotracers, Contrast Agents, and Optical Probes

The Chemical, Manufacturing and Control (CMC) elements of any drug are a critical section of the IND and the NDA/BLA filings. There are multiple guidance documents on the CMC of drugs and biologics,[5] and any imaging agent must in turn satisfy the expectations of stability, purity, stability, excipient control, assay validations of manufacturing processes, starting materials, and composition of the product. There are specific CMC documents which contain sample formats for documentation radiotracers such as for F-18 FDG (cardiac brain and cancer indications), Na F-18

[5] FDA CMC Guidance documents can be found at http://www.fda.gov/drugs/guidancecomplianceregulatoryinformation/guidances/ucm064979.htm.

Table 13.1 Quality assurance principles for an MR study with a PET (F-18 FDG) correlation

1.0 Staff responsibilities and qualifications
1. Designated operational personnel
2. Designated personnel for patient management
3. Training logs/SOP manual
4. Operational roles defined
5. Contact lists and postings
2.0 Peripheral instruments and devices, reagents, supplies
1. Specifications of peripherals
2. Receipt and login of reagents/controls/devices
3. Radioisotope receipt/RSO controls (PET studies)
4. Storage conditions
5. Drug handling and drug delivery methods
3.0 MRI camera maintenance
1. Specifications of system defined
2. Manufacturer maintenance records
3. Automated equipment controls
4. Table movement and alignment tests
4.0 MRI camera quality assurance testing
1. Specifics from protocol outlined
2. Electronic stability assessments prior to study
3. Safety check prior to study
4. RF field map of room and magnet
5. Quality assurance tests—(weighting factors are adjustable)
Item A. 30 %
Item B. 30 %
Item C. 20 %
Item D. 20 %
5.0 Contrast agent and image ROI correlations
1. MR contrast agent log-in and prescription
2. PET radioactive drugs—RSO involvement
3. Image acquisitions timed for contrast agent
4. ROI selection criteria defined
5. Patient dosing records (non-electronic)
6.0 F-18 FDG-PET correlation option
1. Objective of study defined for fMRI staff
2. FDG blood draw protocol defined for magnet
3. FDG blood sampling procedure training
4. Draw volumes and dead volume corrections
5. Radiation survey procedures for post-study

(continued)

Table 13.1 (continued)

7.0 Image acquisition and archiving

1. BOLD protocol defined

2. Reconstruction methods defined/validated

3. Patient image ROI methodology: study to study

4. Image archiving method security

5. Image registration with other modality (CT, PET)

The resultant spider graph (no scoring entered) provides a snapshot of the overall quality package

injection (bone uptake), and ammonia N-13 injection (see http://www.fda.gov/downloads/Drugs/GuidanceComplianceRegulatoryInformation/Guidances/ucm078740.pdf). The Society of Nuclear Medicine in 2008 also issued a CMC document for radiotracers that is quite useful (Harapanhalli 2008). Nanoparticle contrast agents, particularly for MRI and ultrasound products, that provide improved contrast and favorable biodistribution, i.e., superparamagnetic iron oxide nanoparticles for use as MRI contrast agents and cell labeling, may require additional and different CMC support documentation. Optical imaging agents are entering the clinical arena, and they too will require additional CMC directed at the photostability and the photon decay characteristics of these imaging agents.

13.3 The FDA Review Process: Translational Responsibilities

13.3.1 The Selection of an Imaging Platform to Defend Drug Approval

The FDA approval process is rigorous but not insurmountable. Figure 13.9 describes a full development scenario where a drug enters basic research and finishes with FDA approval and launch (and Phase 4 (not shown)) commitments if there are any post-marketing safety measures the agency wishes to determine after giving their approval to market. In contrast to the average time for the approval for drug or biologic which is 1–13 years, a typical development timeframe for approval of a radiotracer imaging agent may be as little as 7–8 years as it is often supported by a wide therapeutic index (high-dose MR, CT, and other contrast agent face standard safety therapeutic index

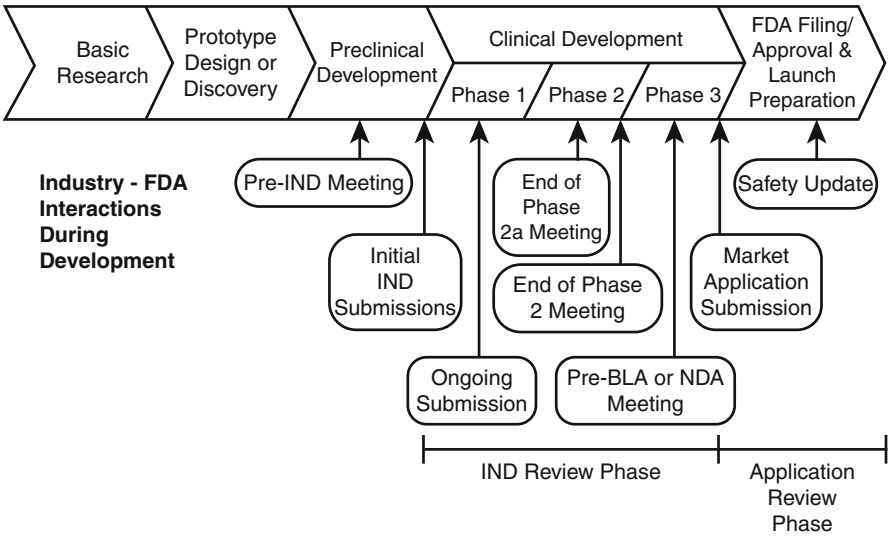

Fig. 13.9 *The FDA Review Process*. A timeline for Sponsor—FDA interaction schedules from early discovery through the NDA/BLA application/approval and launch of product. The paradigm fits any imaging agent as well, but nuclear and very low-dose contrast agents do have the opportunity for the Phase "0" trial (see Sect. 13.2.1) (from FDA, Critical Path Initiative 2004)

concerns). However, this is changing as noted previously due to the advent of biologics as imaging agents and their propensity for immunogenicity. The FDA encourages sponsors to engage with them "early and often," and this can be hugely beneficial in both cost control and study design and outcomes and eventual acceptances for product approval.

13.3.2 Phase "0" Clinical Trials

Prior to entering a clinical study, novel drugs and biologics have been through extensive preclinical safety and efficacy evaluations. Imaging agents, particularly PET and SPECT agents (due to low mass content in the drug), are best studied in a Phase "0" trial where the predictive risk is low due to the less than pharmacologically active concentrations required to produce their clinical determinant (usually uptake over time or relative to a control tissue, i.e., SUV; see Chap. 7). Tomaszewski (2007) provides a very good walk through the process of moving from the preclinical stage into the Phase "0" trial (Fig. 13.10). Marchetti and Schellens (2007) also provide an excellent perspective on FDA versus European (EMEA) regulatory and scientific considerations of Phase "0" trials for drugs and biologics. An important concern they pose is that there are few validated biomarkers for demonstrating anticancer activity. Pharmacological, biological, or imaging measurements at very low exposure levels of novel new anticancer agents (which are often very potent) are required, but unfortunately few reliable and validated assays are currently available. The high potency of new biologic anticancer molecules requires the use of low

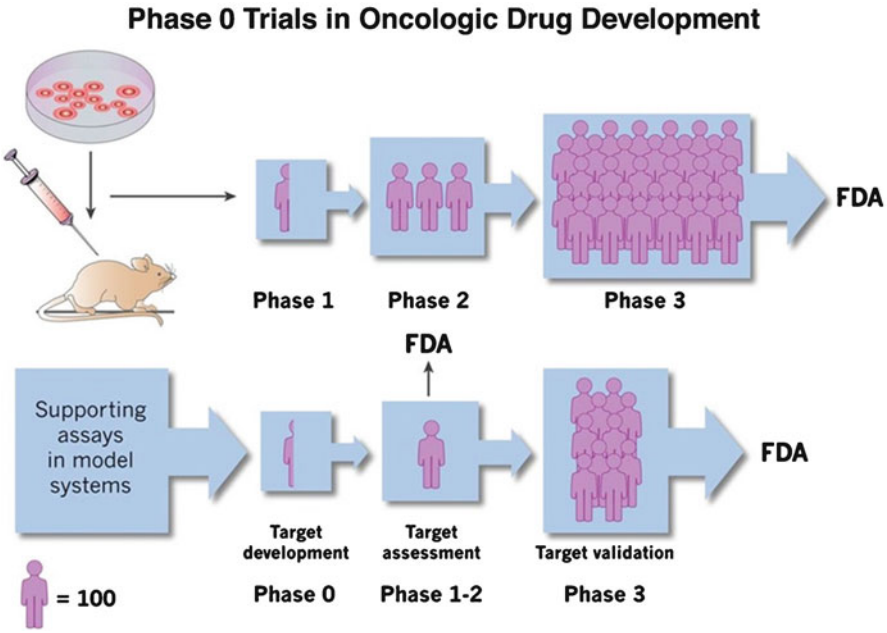

Fig. 13.10 Companion diagnostics, CDx (e.g., an imaging agent): the supporting CDx assays (i.e., and image) represent an agent that is codirected with the investigation of a new drug or biologic as a surrogate biomarker. As a "companion" for the indication, the imaging agent may support changes in a therapeutic approach. The Phase "0" is typically an imaging study with a PET/SPECT or other "tracer" platform but can be done with benign, high-dose imaging agents such as for MR, CT, US, or optical (from Murgo 2007, with permission)

First-In-Man (FIM) doses that are often significantly lower that what had been done for the traditional anticancer agents, potentially as low as three-log lower doses. Micro-dose studies must use very sensitive analytical assays for pharmacokinetic assessments, or may use medical imaging such as PET, SPECT, MR, MRS (magnetic resonance spectroscopy) as "analytical tools". Currently, most imaging techniques are not fully accepted as analytical companion diagnostic tools. Wahl et al. (2009) summarize the emerging considerations for PET imaging as it has become a test venue for imaging as a tool for oncologic response criteria.

The reader is directed to an online series of slide shows from the NCI DCTD (Division of Cancer Therapy and Diagnosis) Programs on Cancer Imaging Programs and Translational Research Programs entitled "Phase 0 Trials in Oncologic Drug Development" (September 5, 2007, Natcher Conference Center, NIH Bethesda, MD) with a web link as http://dctd.cancer.gov/MajorInitiatives/Sep0507Phase0Workshop/workshop.htm. In this series of lectures there is a wealth of reference material with respect to imaging equipment, software and data management, and biostatistical considerations. Imaging examples as well as a series of slides by Dr. Mankoff on the requirements one should anticipate with respect to imaging acquisition and analysis. Figure 13.11 is a selected slide from the NCI series on Phase "0" trials by Dr. Mankoff (2007) where he describes imaging as dynamic

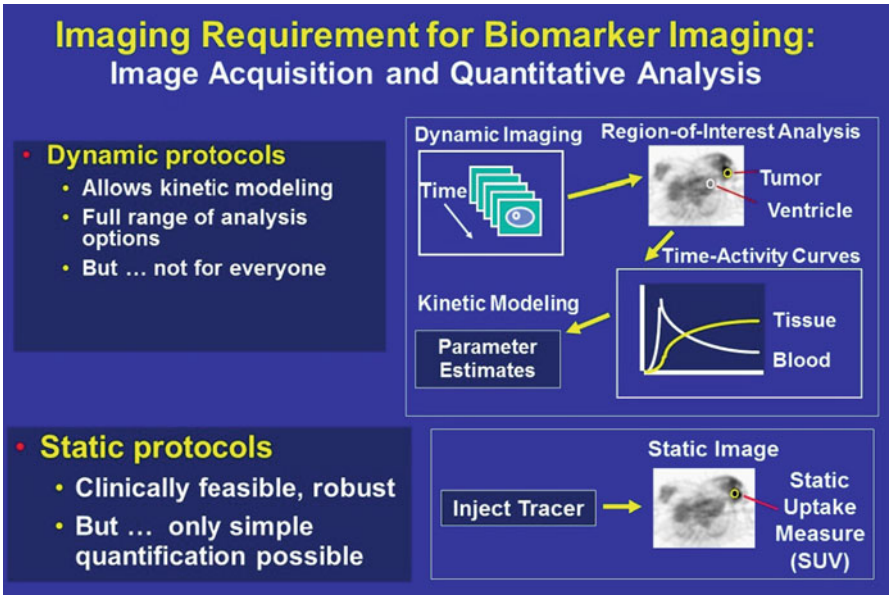

Fig. 13.11 A slide from Mankoff (2007) in the NCI series of talks on the conduct of Phase "0" trial. The figure describes dynamic/static protocols (time series of images), region-of-interest (ROI) analysis of test regions versus control, and kinetic modeling for parameter estimates (time–activity modeling). Each step in the process has critical regulatory implications (from Mankoff 2007; with permission)

protocols (time series of images as well as static imaging), region-of-interest (ROI) analysis (uptake areas vs. control regions), kinetic modeling for parameter estimates, and display of the kinetic data for selected and quantified regions of interest (ROIs).

Medical imaging agents generally are governed by the same regulations as other drug and biological products. In that they must undergo all the scrutiny of CDM, safety, use, and employment under the proper clinical indication, so too is the process one would need to employ an imaging platform on the development of a non-imaging drug or biologic. The imaging system employed will essentially be a diagnostic to govern therapy, a way to visualize a biomarker of either efficacy or safety, and the platform must operate under the rule not unlike a CLIA laboratory certification and validation. Just like a complete blood count, the instrumentation, the training of personnel, the maintenance of the instrument, and the calibration of the instrument at the time of use are critical issues for use of the data for submission toward approval. If a drug or diagnostic imaging agent is to be used in clinical concert, then they need to be developed simultaneously for the indication. The three-part Guidance for developing medical imaging drugs and biologics (FDA, Imaging Guidance Parts 1, 2, and 3, June 2004; see Guidance references) outlines the important aspects and details of imaging agent approval. What this book has been focusing on is a 180° view of this paradigm where the imaging agent is directing the approval of a new novel drug or biologic. Thus, the imaging system

and all associated reagents, platform preparation, platform controls, and platform validation as well as the biomarker (imaging tracer or contrast agent—or simply the physics of an imaging system itself), reagents, chemical preparation, shelf life of a biomarker imaging agent, and metabolic behavior of the tracer or contrast agent in health and disease hold for the use of the platform for associated regulatory documentation.

13.3.2.1 Clinical Trials: Image Analysis via the Blinded Read

Once a drug has moved beyond preclinical to the IND and a human clinical effort, the imaging agent performance must be measurable, quantifiable, and nonsubjective (as much as possible), and readers of the images (radiologists generally) must be consistent and require limited adjudication on the interpretation of the image(s). The performance measures of an imaging agent or imaging system are not different form a therapeutic. An imaging "system," i.e., the device alone or with tracer or contrast, is measured in a clinical trial for its ability to define a pathology, measure a mitigation via a change in pharmacodynamics or metabolism, or change metabolic behavior of the pathology (aka benefit).

Core Labs: Charters, Blinded Reads, Reader Adjudication, and ROC Curves

Before Imaging: Develop a Charter. Before beginning an imaging trial one must first set up the process and statistical analysis plan (SAP) which will provide the overall decisional outcomes from the trial images. The images must be collected appropriately, stored and displayed as required, and read by trained and unbiased readers. To this end the CORE laboratory performing these analyses will need to set up an "Imaging Charter." This is an important document which should comprise a comprehensive, detailed description of the clinical trial imaging methodology. Sponsors of the study should generally regard the Imaging Charter as an integral component of the protocol, much as the SAP. Submit the Charter to the FDA with the complete clinical protocol, including the final SAP, and include important supportive documents. The content of the Charter should include an **Executive Summary** of the trial design and the role of imaging in the trial. This is followed by the **Image Acquisition Standards** which include:

- *Equipment standardization and operation*, i.e., vendor-specific equipment/platforms (e.g., injectors, scanners, software)
- *Equipment technical settings* to be used at each site
- *Role of the technicians* in operation, including identification of faulty or unacceptable images and the need to repeat imaging
- *Phantoms to be used* for site qualification and image quality monitoring
- *Patient preparation*, positioning, and comfort measures
- Imaging *dates and times* and alternatives

- Handling of *off-protocol images*
- Imaging *risks to the patient*
- *Site qualification* process
- *Acquisition quality* control monitoring process
- *Data* storage, transfer, and site display
- Image interpretation (Clinical Trial Standards)
  - *Trained readers*, radiology, and/or nuclear medicine specialists
  - *Image transfer*, *receipt documentation*, *and initial quality assessment*
  - *Image display and interpretation*
  - *Selection of images* for interpretation, display sequence, and randomization
  - *Readers*: background qualifications (reader training)
  - *Timing of image reads* and the read process
  - *Imaging case report forms*; imaging data lock process
  - *Quality control* of the image display and interpretation process

Then there is the "before," "during," and "after" CORE Lab imaging analysis considerations:

- Before imaging—Charter Modifications
  - Charter will describe the process for modification.
  - Charter will describe the process for transfer of information to the sponsor, including needed support activities for the statistical analysis.
- During imaging—Monitoring and Charter Modifications
  - Record of modification of the imaging procedures
- After imaging—QA and documentation
  - Transfer of images (known fidelity of process) and archived as a usual component of patient care and as clinical trial source documents and with limited access
  - Retained for potential inspection and auditing
  - Clinical sites or a core facility analysis (QA/QC; reads and determination of reader interpretation consistency)

The Imaging Charter forms the "rigor" of the study. Within the Charter structure the FDA will find the holes, the gaps in oversight, that will raise questions, and thus, it is imperative that the CORE Laboratory services you enroll in your drug or biologics development have the history, the experience, and the staff that are schooled in these disciplined activities. One should be most careful of the image processing validation within the Charter's oversight. Processor validation is an often overlooked feature as they are frequently "packaged" and called "validated." The processing system employed needs to be tested rigorously with positive and negative control approaches as it is imperative to understand and highlight the intrinsic characteristics and behavior of the method. Critical elements include the evaluation of system performance (i.e., reproducibility, error propagation, especially from image to image

in a kinetic study) and biomarker performance (repeatability in a system and also subject to subject variance using that system), and to fully understand the limitations to the information the targeted imaging objective can convey clinically for the indication of interest (Jannin et al. 2006). Validation is a multifaceted process and it generally is best operationally to include simulated images. Simulated images actually allow for highly predictive outcomes, and if processing becomes askew these images will generally provide reasonable information to recognize the need to realign the software or electronic processors. These kinds of images help define behavior of the method and defend or explain observed intersubject variability.

The Receiver Operating Characteristic (ROC) Curve: Example Using the SUV

The Receiver Operating Characteristic (ROC) curve is a statistical tool of analysis that is utilized to measure the observer (image reader) or to test the performance of the image readings. Duarte et al. (2002) have provided a very useful example in the image analysis setting where the objective was to discern via reading FDG-PET images of bone metastases, that is, to discern malignant versus benign lesion using the observed distributions of the tracer in bone and standardized uptake values (SUV) (see Chaps. 1, 5, and 6) valuations.

In their study they examined ninety-nine bone sites in 33 patients who received F-18 FDG. The "gold standard" reference for the study was "confirmation on a bone scan (PET)" where a positive (POS) finding was a three out of four result. By these criteria the population of 99 lesions were 39 malignant and 60 benign. The SUV valuations from the readers were 61 different grades of uptake from 1.0 to 7.0. The reader valuations were classified as true positive (TP), true negative (TN), false-positive (FP), and false-negative (FN), and the TP and FP fractions were calculated for each threshold value. These comprise the ROC curve (Fig. 13.12) seen below. The optimal SUV of 2.5 produced a true positive (TP) rate (*y*-axis; sensitivity) of ~0.75 and a 1 false-positive rate (*x*-axis; 1-specificity) of <0.1 showing there was little additional benefit (e.g., a sensitivity for malignancy >75 % sensitivity when the SUV is >2.5) from higher SUV values (2.5–7.0) in the ability of a reader to recognize malignancy from benign lesions. An ROC analysis should be an integral part of the Imaging Charter and certainly part of the statistical analysis plan for an imaging clinical trial as it identifies the optimal crossover of scoring that delineates "presence of disease" from that of "no disease."

One must take caution on "statistical significance" when interpreting images (and any other scientific query). Always ask the question "What is the importance of the observed significance?" and then, more critically, assess the actual "significance of importance" (Riegelman 1979). This may read as a "play on words" but these words are indeed a critical point of understanding. The educated (but often subjective) review of an image by a trained reader still has bias and interpretive actions that can quite easily lead to FP and FN readings. The region of interest (ROI) for the assigned or recognized lesion is solely based upon the reader's judgment of edge or the fall off

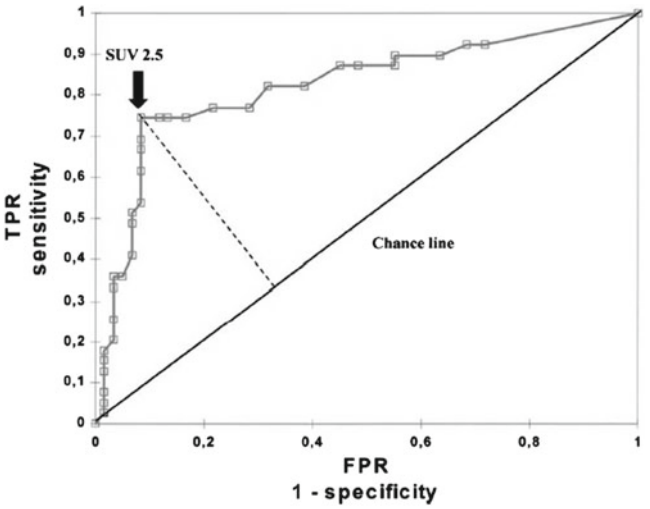

Fig. 13.12 The Receiver Operating Characteristic (ROC) curve depicts the overall performance of readers in terms of their ability to shape the ROC curve to a TPR of 1 and FPR of 0. The AUC of the curve above the "chance line" (50:50 call) improves with reader training. The curve depicts the ability to discern malignancy (>2.5 SUV) from a PET F-18 FDG study. In this case the TPR is nearly a plateau when SUV is >2.5 (from Duarte et al. 2002; with permission)

of intensity of signal. This can add several pixels (picture elements or voxels for PET/SPECT or MR for volume elements; slice volumes) that weaken or strengthen the counts acquired in that ROI, and against the background ROI the standardized uptake value (SUV) for, for instance, an F-18-FDG signal can push or retract an SUV into benign or malignant categorization. This is the inherent "noise" of reader interpretations and is highly dependent on training and common image analysis techniques that need to be harmonized as much possible during the reader trainings. Tests of the readers to attain the required skills need to be performed for reader qualification to actually participate in the blinded read of a trial images. Such training, the documentation of the test images, the reader training, and qualifying examinations of the readers need to be retained for FDA review as part of the Imaging Charter and trial documentation. It is important to remember that one must ask what is the importance of the observed differences (TP from FP and the inverse), especially if any differences are narrow, because finding a difference in small SUV valuations may or may not actually be a true correlation to benign versus malignant and actually represent another contribution to the observed uptake, i.e., infection or differences in regional blood flow. It is important in small imaging trials to remember that the presence of statistically significant difference tells little about the inherent variance expected in each group, i.e., benign uptake versus malignant uptake.

13.3.2.2 Managing the Image Review and Analysis

Effective Management Tools for the Independent Imaging Review Process

Bates and Williams (2007) provided a short but concise article on "effective management" of the independent imaging review process in oncology clinical trials that involve imaging. They key to a successful program is to prospectively define the methodology that will define the clinical outcome. A defined review process must first be implemented, knowledge of the reviewers biases and technical capacity to perform the review, the data that is expected and that the proper reader output will be provided for the statistical analysis and the kind of assessment that the readers will be required to provide. Documentation alone is not sufficient. Unrealistic expectations, lack of experience, and expertise and numerous other issues can make for a waste of investment and may lead to improper conclusions.

There are three key documents that establish the Imaging Core Lab's ability to have success. They include a Project Plan, the Imaging Charter, and the Investigator Site Manual. The Project Plan is a key first document that defines the timelines and the budgets. It can also serve as a guide for the communication plans as well as data management plans. It will aid in the process of qualifying a clinical site, the investigator, and the methodology of sponsor and core lab communications. The first objective of the Project Plan is to identify the risks to the program and establish a risk mitigation strategy to avoid the pitfalls that can be identified.

The Imaging Charter (aka Independent Review Charter, IRC) should be developed in tandem with the Project Plan as it is responsible for the overall review process, image collection and scheduling, types of images (structure/format; i.e., DICOM), the clinical data to be collected, the analysis of the reads, reader training, and reader adjudications (resolution of reader interpretations; partnered reader scoring, image scoring operations). The Charter is often lacking in operational logistics at the sacrifice of getting regulatory or medical issues resolved for the conduct of the trial. Care should be exercised to make sure all participants—clinical, regulatory, data management, statistics, and the core lab for image processing and reading—are included and have opportunities to manage the creation of the document. Very rigorous data collection and management to assure compliance of the "moving parts" often gets "relaxed" after a period of time when specific items become operationally consistent and repeatable.

The Investigator Site Manual is another document that can have severe repercussions if not appropriately constructed and managed. This document goes to the core lab and to the imaging clinical sites. It has a dual purpose: (1) to establish exact imaging protocols and parameters and (2) to provide logistical instructions to the clinical operations team. This document is often far more detailed than the actual clinical protocol. Imaging parameters such as slice size in MR and PET/SPECT, contrast agent or radiotracer administration timing with image acquisition, improper anatomical coverage, and suboptimal baseline image collection or poor attenuation corrections are common imaging trial errors and often cause patient exclusion from the analysis.

Prospectively designing the independent review process is a critical operation for a successful imaging trial. It is imperative that the leadership of the trial demand and

assure the three documents are properly created, clearly written, and vetted with each participating operational entity. The handling of pitfalls in the management of a trial using image analysis is only successful when the operational and communication questions are fully vetted, detailed with solutions with each participant, and a risk mitigation strategy generated.

13.3.2.3 Program Management for Drug and Biologic (and Imaging) Development

Program management is the lead oversight of all operations. Clinical operations, regulatory oversight, statistical planning and analysis, clinical research associates (CRAs) attending to drug or biologic supplies as well as imaging agent or contrast agents and coordination of deliveries with the clinical site (refrigeration required?, etc.), case report form design, technical staff and management communications to the sites, pharmacology and toxicology advisors from the non-clinical IND efforts, the data management team and coordination of the imaging core lab, and selection of talented radiologists (or other appropriate scientists) trained to read the images—all are under the leadership of the program manager. The clinical site principal investigator (PI) should be instructed on trial expectations, anticipated enrollment, scheduling, and expectations of data delivery and data quality. These points are often deferred from clear discussion with the expectation that the PI is either an "expert in the field" and knows what is expected. This is a common mistake as each trial has its own idiosyncrasies and thus requires the program manager and the clinical manager communicate fully and candidly with the clinical site PI.

13.4 A View of "FDA Perspectives" from Outside the FDA

Janet Woodcock has presented a talk on the regulatory (FDA/CDER) perspectives (Woodcock 2010) where she cites the importance of standardization of image acquisition, interpretation (procedure for reading an image), and the management of data through multicenter trials. These elements are critical for accurate diagnosis and assurance to the FDA that the CDx (aka, image) has merit to assess the response of a condition to a therapeutic intervention. Coincident to these requirements is, of course, the requirement of standardization, e.g., of the imaging agent and the imaging platform, and in the non-clinical setting as defense to the agency we need standardization of the routine method of the animal model preparation, the disease model, and imaging parameters that help define the biomarker of interest with respect to the disease, and we need to do this all within corporate and academic budgets which often look at imaging as "that luxury."

Outside the FDA in imaging forums and imaging societies, such as the Radiologic Society of North America (RSNA), scientists and regulatory professionals that support corporate and legal aspects of drug development have formed a task force called the "Quantitative Imaging Biomarkers Alliance" (QIBA) Task Force, and it

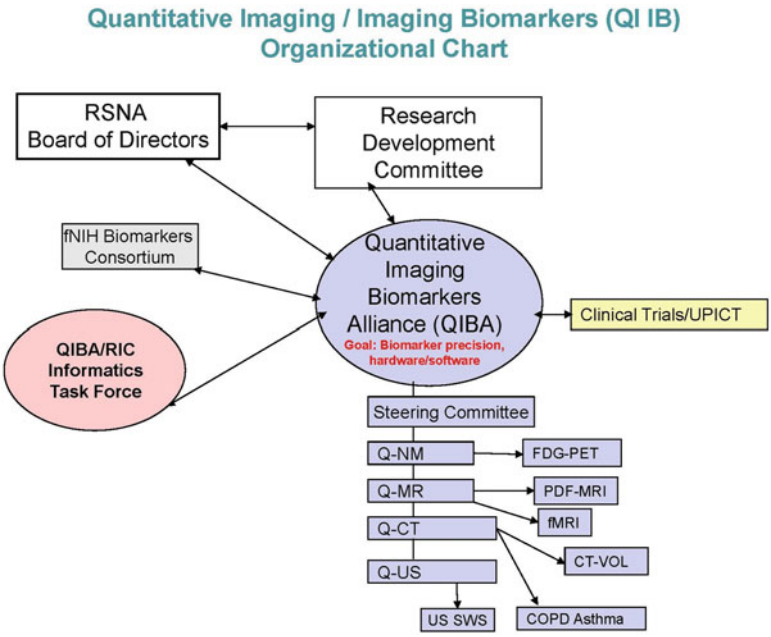

Fig. 13.13 The Quantitative Imaging Biomarkers Alliance (BIQA) within RSNA. A diagram offering a view of the multiple inputs that this organization has recruited to assist the medical community in deriving regulatory acceptance of biomarkers employed in imaging (from RSNA BIQA Report of Aug. 25, 2011, see RSNA in the references)

is comprised of over 20 individuals with active participation in the imaging sciences. Their organizational and FDA-supportive framework is given in Fig. 13.13 as they were set up within the RSNA as a reporting body to the Board of Directors in 2011. As can be seen, the FDA is an important contributor to the QIBA imaging roundtable advisory body feeding into the QIBA feedback from multiple players in the imaging industry on biomarker precision and hardware requirements to achieve regulatory acceptances and validation of biomarkers in imaging. Such organization as the QIBA, as a form of representation as a body to the FDA, has been invaluable toward FDA inclusion and acceptance of imaging in such activities as the DDT and the *Critical Path Initiative*.

13.5 Concluding Remarks

This chapter has been an attempt to introduce the reader to the regulatory environment that surrounds the activities we call "Imaging." The reader must feel, however, the term "imaging" is almost "missed" in the concepts of regulatory activities, and the reader may be correct in that observation. Imaging is a discipline not unlike an

"analytical chemistry toolbox." We "inject on one side and the analysis comes out the other" is not too far from the truth. Imaging is a multidisciplined art and we think the reader has come to appreciate the wide variety of imaging platforms, imaging agents, imaging modalities, imaging quality, image resolution, and "imaging ideas" that all translate to "imagination." "Imagination" is the limiting factor for "imaging" in the pharmaceutical industry, and the advancement of any product can be enhanced through the regulatory process, regulatory rigor, and regulatory oversight. Imaging agents as radiopharmaceuticals (Agdeppa and Spilker 2009; Dunphy and Lewis 2009; SNM 2008; Shields 2008; Zhao et al. 2009), MR contrast agents (Strijkers et al. 2007), and optical probes (Rice and Contag 2009; Boddington 2010) offer the reader excellent reviews on the practical applications and clinical indications of these imaging agents and their respective platforms. Boddington (2010) also discusses cell tracking with optical systems using an FDA alternative for luciferase. Bristow (2008) also provides an excellent overview on the state of the art of biomarkers used in clinical trials.

It is inevitable that imaging sciences will play more of a role in the development of drugs and biologics (Hoffman 2012). Wagner et al. (2006) have pointed out how many "nanomolecular" agents are being developed, and many of these are imaging agents. The ease of monitoring—in a single animal—the pharmacodynamics, the toxicokinetics, and the overall "image" (picture) of a drug as it transits or depots in the body will make drug development much more like an analytic service, more of a step-by-step laboratory operation, and a key way to observe how "a" leads to study "b" which leads to study "c," etc. The availability of small animal imaging platforms (with associated cost reduction from increased market volume), better and more licensed contract service organizations (CROs) that will offer imaging services, and the subcontracting market to provide maintenance of these devices (especially with the advances in novel electronics, detector system, and software), "human" imaging systems are being miniaturized and being implemented as cost-effective laboratory additions. The FDA Initiatives for Biomarkers, Drug Development Tools (aka imaging platforms), and the Animal Models Directives are financially and scientifically creating new opportunities for the imaging sciences. Soon there will be a sufficient number of "off the shelf" validated biomarkers and animal models that will revolutionize clinical medicine and especially drug and biologics development. Companies with products to develop will eventually use these libraries of imaging models and validated imaging tools/tracers/agents, which the FDA is familiar with and possibly co-developed with their "Tools" initiatives. The goal is to avoid "re-invention" of an already validated animal model with a new imaging approach and biomarker—all very likely not validated. The initiatives will actually populate the nonclinical environment with validated and well-characterized models where the disease natural histories are fully defined and imaging tools can be applied appropriately. These tools will be validated across academic institutions and corporate entities, including private CROs, as well as "big" and "little" (one product or venture capital funded) pharma. Table 13.2) is provided as a resource of regulatory approaches, web sites and links, imaging platform tools and and we have also

Table13.2 Regulatory web-based resources important for use of imaging platforms and products in drug and biologics development

Regulatory references and comments on imaging	Web access
Guidance for Industry: Developing Medical Imaging Drug and Biological Products	
• *Part 1: Conducting safety assessments*, FDA—Food and Drug Administration; Center for Drug Evaluation and Research (CDER); Center for Biologics Evaluation and Research (CBER), June 2004	http://www.fda.gov/downloads/Drugs/…/Guidances/ucm071600.pdf; last accessed 25 Apr 2013
Comment: Each of these (Part 1–3) deals with the development and the approval process for an imaging agent (PET tracer, MR contrast, Optical, etc., and thus are not specifically for approval of a combination diagnostic or a surrogate drug or biologic used for approval of another	
• *Part 2: Clinical indications,* FDA- Food and Drug Administration; June 2004	http://www.fda.gov/downloads/Drugs/GuidanceComplianceRegulatoryInformation/Guidances/ucm071603.pdf; last accessed 25 Apr 2013
Comment: as above	
• *Part 3: Design, analysis, and interpretation of clinical studi*es, FDA- Food and Drug Administration; June 2004	http://www.fda.gov/downloads/Drugs/GuidanceComplianceRegulatoryInformation/Guidances/UCM071604.pdf; 25 Apr 2013
Comment: As above	
Carver, KH. "Companion diagnostics: Evolving FDA regulation and issues for resolution." *In Vitro Diagnostics: The Complete Regulatory Guide, 2010,* Chapter 8, pp 149–184	http://www.cov.com/files/Publication/e5c4b3dc-1832-4742-9937-84f965052b44/Presentation/PublicationAttachment/7795d260-621d-4d13-bd29-863acac00254/Companion%20Diagnostics%20-%20Evolving%20FDA%20Regulation%20and%20Issues%20for%20Resolution.pdf; last accessed 27 Apr 2013
Comment: An important guidance to help frame the language of translation of a diagnostic in the analytical laboratory to a diagnostic in the imaging laboratory	
Guidance for industry: *Guidance for industry standards for clinical trial imaging endpoints;* FDA- Food and Drug Administration; June 2011	http://www.fda.gov/downloads/Drugs/GuidanceComplianceRegulatoryInformation/Guidances/UCM268555.pdf; last accessed 25 Apr 2013
• Comment: A guide on what is expected in reading images. The purpose of the guidance is to assist sponsors in the use of endpoints that depend on the results of imaging tests in clinical trials of therapeutic drugs and biological products[a]	
• This guidance focuses on the imaging standards that are regarded as important *when imaging is used to assess a primary endpoint*, or an endpoint component, in a clinical trial intended to confirm a drug's efficacy[b]	

Guidance for Industry, Investigators and Reviewers: *Exploratory IND studies*, G6384dft.pdf, April 2005 • *Comment: A guide on the Phase "0" trial and what the FDA expects of the CMC requirements as well as animal safety*	http://www.fda.gov/downloads/Drugs/GuidanceComplianceRegulatoryInformation/Guidances/ucm078933.pdf; last accessed 25 Apr 2013
Guidance for Industry and Reviewers: *Estimating the safe starting dose in clinical trials for therapeutics and adult healthy volunteers*; CDERguid/3814dft.pdf; Dec 2002 *Comment: A useful guidance for basic allometry*	http://www.fda.gov/OHRMS/DOCKETS/98fr/02d-0492-gdl0001-vol1.pdf; last accessed 4/25/2013
Guidance for Industry: *Codevelopment of two or more unmarketed investigational drugs for use in combination*; December 2010; *COMMENT: This guidance is very applicable to the use of unapproved, but available, imaging agents for use in the defense of unmarketed drugs or biologics. Imaging agents may be used as defense of (1) finding a pathology, (2) monitoring the treatment success (or failure) of a second product on that acts on the pathology, and (3) where the imaging agent can defend the resolution or progression of the pathology under the treatment product*	http://www.fda.gov/downloads/Drugs/GuidanceComplianceRegulatoryInformation/Guidances/UCM236669.pdf; last accessed 2 Feb 2013
Feng Q, *Clinical trial efficacy endpoints for molecular Imaging Products Development*, Div. Medical Imaging Products (DMIP), June 11, 2012 *Comment: A useful document which frames the objectives of the FDA's Medical Imaging Products Division (MIPD)*	http://www.fda.gov/downloads/Drugs/ScienceResearch/ResearchAreas/Oncology/UCM314270.pdf; last accessed 25 Apr 2013
John J. Smith, Medical Imaging: The Basics of FDA Regulation Published: August 1, 2006; • *Comment: Device approvals—Imaging platform approval recommendations Devices that use medical imaging are increasingly prevalent. OEMs must know how to navigate the regulatory pathway to get such devices approved. Medical imaging is playing a large and increasing role in modern healthcare delivery. Understanding FDA's regulatory construct that governs medical imaging is crucial to manufacturers operating in this exciting and challenging environment*	http://www.mddionline.com/article/medical-imaging-basics-fda-regulation; last accessed 25 Apr 2013
RSNA, Report on the Quantitative Imaging Biomarkers Alliance Task Force, August 25, 2011 *Comment: A critical assessment on quantitation of imaging biomarkers that the Reader will benefit from in applying to their own systems*	http://qibawiki.rsna.org/images/2/25/QIBA_task_force_report_11-3-11.pdf; last accessed 5 May 2013

(continued)

Table 13.2 (continued)

Regulatory references and comments on imaging	Web access
FDA, *Critical path initiative: innovation/stagnation- challenge and opportunity on the critical path to new medical products*, 2004 *Comment: A document on FDA revitalization and change in regulatory approaches*	http://www.fda.gov/ScienceResearch/SpecialTopics/CriticalPathInitiative/CriticalPathOpportunitiesReports/ucm077262.htm; main page: http://www.fda.gov/ScienceResearch/SpecialTopics/CriticalPathInitiative/ucm076689.htm (updated 12/2012); last accessed 28 Apr 2013
Statistical principles for clinical trials—EMEA, Human Medicines Evaluation Division, ICH Topic 9, Note for Guidance, London, 18 March 1998, CPMP/ICH/363/96 • *Comment: a useful reference on statistical approaches which are in FDA favor.*	http://www.emea.europa.eu/docs/en_GB/document_library/Scientific_guideline/2009/09/WC500002928.pdf; last accessed 25 Apr 2013
Immunogenity in Animal and Clinical Research —FDA Guidance: Guidance for Industry: Immunogenicity Assessment for Therapeutic Protein Products • *Comment: Immune responses to therapeutic protein products may pose problems for both patient safety and product efficacy. Immunologically based adverse events, such as anaphylaxis, cytokine release syndrome, so-called "infusion reactions," and nonacute immune reactions such as immune complex disease (see Appendix C), have caused sponsors to terminate the development of therapeutic protein products or limited the use of otherwise effective therapies. Both patient-related and product-related factors may affect immunogenicity of therapeutic protein products. These factors provide the starting point for an immunogenicity risk assessment*	http://www.fda.gov/downloads/drugs/guidancecompliance%20regulatoryinformation/guidances/UCM338856.pdf Feb 2013; last accessed 25 Apr 2013
Simms, J, PAD/MABEL: Calculation of the minimum anticipated biological effect level (MABEL) and first dose in human, 2009 *Comment: This document brings the concept of animal testing and clinical assurance of efficacy and safety in first in human trials where the animal model and pathophysiology play an important role in dose adjustment and selection across species (improved allometry)*	http://www.emea.europa.eu/docs/en_GB/document_library/Presentation/2009/11/WC500010862.pdf; last accessed 25 Apr 2013

Woodcock J, *Medical Imaging: CEDR's Perspective*, Radiologic Society North. America Workshop, Bethesda, MD, April 13–14, 2010 *Comment: A useful treatise on the way the FDA views imaging agents. Not a reference in the context of this book which advocates imaging for the development of other agents*	http://www2.rsna.org/re/TwoTopicImagingWorkshopPresentations/Index%20Files/Woodcock%20CDER%20Perspective.pdf; last accessed 25 Apr 2013
Woodcock J, An FDA perspective on the drug development process, *Food Drug Law J* 1997;52(2):145–161 *Comment: A brief discussion on the rules of law and the drug development process; intellectual property, regulations, pathways to approval*	Not formally available through the web. Seek the Food Drug Law Journal
Woodcock: FDA to Consider Approving Some Drugs Using Just One Phase I Clinical Trial; Latest News | Posted: 12 February 2013; • *Comment: consideration of the new category of* Breakthrough Products *designation. The pathway is intended for any product (*including an imaging product that supports a companion designation, *Editorial comment) that is "intended, alone or in combination with one or more other drugs, to treat a serious or life-threatening disease or condition and for which preliminary clinical evidence indicates that the drug may demonstrate substantial improvement over existing therapies on one or more clinically significant endpoints."* • *The "Breakthrough Products" designation may provide incentive for companies to develop imaging agents that directly expose efficacious responses in a Phase "0" of other type study. This is category is added to the already in place incentives such as fast-track status, priority review and accelerated approval*	http://www.raps.org/focus-online/news/news-article-view/article/2853/woodcock-fda-to-consider-approving-some-drugs-using-just-one-phase-i-clinical-t.aspx; last accessed 25 Apr 2013
Woodcock J, *Developing a Qualified Biomarker: Regulatory Considerations*; Institute of Medicine of the National Archives, Perspectives on Biomarker and Surrogate Endpoint Evaluation - Discussion Forum; Summary Released: January 18, 2011 *Comment: A surrogate endpoint is expected to predict clinical benefit (or harm, or lack of benefit) based on epidemiologic, therapeutic, patho-physiologic or other scientific evidence*	http://www.iom.edu/~/media/Files/Activity%20Files/Research/NeuroForum/Woodcock.pdf; last accessed 25 Apr 2013

(continued)

Table 13.2 (continued)

Regulatory references and comments on imaging	Web access
Brian Malkin and Scot Pittman, The Drug/Biologics Approval Process: An FDLI (Food Drug and Law Institute) Primer**,** January 2013 • *Comment: This publication will help explain the FDA approval processes for drugs and biologics. It describes various FDA premarket requirements and pathways for drug and biologics application reviews, including changes enacted under the Food and Drug Administration Safety and Innovation Act (FDASIA). Topics addressed include the New Drug Application (NDA) process, non-NDA routes to market, generic drugs and the abbreviated new drug application process, as well as over-the-counter drugs and biologics*	http://www.fdli.org/products-services/~/resources/resources-order-box-detail-view/the-drug-biologics-approval-process-an-fdli-primer; last accessed 25 Apr 2013
Phase "0" Trials: Tomaszewski J, The Pre-Clinical Pathway to the Phase 0 Trial, in, Workshop: *Phase 0 Trials in Oncologic Drug Development*, Natcher Conference Center, NIH, Bethesda, MD; Div of Cancer Treatment and Diagnosis; September 5, 2007 • *Comment: A useful reference on moving a pre-clinical candidate toward the IND/NDA through Phase "0" planning and preparation in terms of studies and approaches.* Larson S, Herceptin as a Phase 0 Imaging Example, in, Workshop: *Phase 0 Trials in Oncologic Drug Development*, Natcher Conference Center, NIH, Bethesda, MD; Div. of Cancer Treatment and Diagnosis; September 5, 2007 • *Comment: An excellent example of an imaging Phase "0" trial* Mankoff D, Imaging to Guide Early Drug Trials, in, Workshop: *Phase 0 Trials in Oncologic Drug Development*, Natcher Conference Center, NIH, Bethesda, MD; Div. of Cancer Treatment and Diagnosis; September 5, 2007 *Comment: Also a part of a full meeting at the National Institutes of Health on the Phase "0" Trial approach. The Reader is encouraged to review all the talks form this event and they are web accessible.*	http://dctd.cancer.gov/MajorInitiatives/Sep0507Phase0Workshop/workshop.htm; last accessed 5 May 2013 http://dctd.cancer.gov/MajorInitiatives/Sep0507Phase0Workshop/workshop.htm; last accessed 25 Apr 2013 http://dctd.cancer.gov/MajorInitiatives/Sep0507Phase0Workshop/workshop.htm; last accessed 25 Apr 2013

[a]*drugs* incl. human drugs and therapeutic biological products

[b]A "confirmatory trial" is an adequately controlled trial

provided short summaries of regulatory documents and Guidances. The imaging world is fast expanding from the clinical environment into the early drug and biologic laboratory and it will be important in the future for pharmaceutical developers to contribute their own "imagination" as to how they want to apply imaging tools as potential anaytical tools to provide solutions in answering their scientific questions.

References

Agdeppa ED, Spilker ME (2009) A review of imaging agent development. AAPS J 11(2): 286–299

Bass AS, Vargas HM, Valentin J-P, Kinter LB, Hammond T, Wallis R, Siegl PKS, Yamamoto K (2011) Safety pharmacology in 2010 and beyond: survey of significant events of the past 10 years and a roadmap to the immediate-, intermediate- and long-term future in recognition of the tenth anniversary of the Safety Pharmacology Society. J Pharm Toxicol Meth 6(1):7–15

Bates S, Williams K (2007) Effective management of the independent imaging review process. Appl Clin Trials 16(Suppl 5):6–11

Bocan T (2010) Platform imaging biomarkers: applications across pre-clinical drug discovery with a focus on neuroscience, oncology, cardiovascular and future horizons. Amer Pharm Rev, 01 August 2010; http://www.americanpharmaceuticalreview.com/Featured-Articles/115057-Platform-Imaging-Biomarkers/

Boddington SE (2010) Labeling human embryonic stem cell-derived cardiomyocytes with indocyanine green for non-invasive tracking with optical imaging: an FDA compatible alternative to firefly luciferase. Cell Transplant 19(1):55–65

Bristow RG (ed) (2008) Special issue: biomarkers of clinical trials using molecular inhibitors and radiotherapy: state-of-the-art approaches. Cancer Metastasis Rev 27(3):335–539

Carver KH (2010) Companion diagnostics: evolving FDA regulation and issues for resolution. In vitro diagnostics: the complete regulatory guide Chap. 8, pp 149–184. http://www.cov.com/files/Publication/e5c4b3dc-1832-4742-9937-84f965052b44/Presentation/PublicationAttachment/7795d260-621d-4d13-bd29-863acac00254/Companion%20Diagnostics%20-%20Evolving%20FDA%20Regulation%20and%20Issues%20for%20Resolution.pdf. Accessed 4/27/13

Dhani N, Siu LL (2008) Clinical trials and biomarker development with molecularly targeted agents and radiotherapy. Cancer Metastasis Rev 27(3):339–349

Duarte PS, Zhuang H, Castellucci P, Alavi A (2002) The receiver operating characteristic curve for the standard uptake value in a group of patients with bone marrow metastasis. Mol Imag Biol 4(2):157–160

Dunphy MPS, Lewis JS (2009) Radiopharmaceuticals in preclinical and clinical development for monitoring of therapy with PET. J Nucl Med 50(Suppl 5):106S–121S

Ellenberg SS, Hamilton JM (1989) Surrogate endpoints in clinical trials. Cancer Stat Med 8(4):405–413

European Commission (May 2010) "Of Mice and Men—Are mice relevant models for human disease?" Outcomes of a European Commission Workshop "Are mice relevant models for human disease" held in London, UK, 21 May 2010. http://ec.europa.eu/research/health/pdf/summary-report-25082010_en.pdf. Accessed 5/10/2013

FDA (2004) Critical path initiative: innovation/stagnation-challenge and opportunity on the critical path to new medical products. http://www.fda.gov/ScienceResearch/SpecialTopics/CriticalPathInitiative/CriticalPathOpportunitiesReports/ucm077262.htm; main page: http://www.fda.gov/ScienceResearch/SpecialTopics/CriticalPathInitiative/ucm076689.htm (last updated Dec 2012). Accessed 4/28/2013

Feng Q (2012) Clinical trial efficacy endpoints for molecular imaging products development. Div. Medical Imaging Products (DMIP). http://www.fda.gov/downloads/Drugs/ScienceResearch/ResearchAreas/Oncology/UCM314270.pdf. Accessed 25 Apr 2013

Gibaldi M, Koup JR (1981) Pharmacokinetic concepts—drug binding, apparent volume of distribution and clearance. Eur J Clin Pharm 20(4):299–305

Goodsaid F, Papaluca M (2010) Evolution of biomarker qualification at the health authorities. Nat Biotechnol 28(5):441–443

Guidance for industry, investigators and reviewers: exploratory IND studies, G6384dft.pdf, 2005. http://www.fda.gov/downloads/Drugs/GuidanceComplianceRegulatoryInformation/Guidances/ucm078933.pdf. Accessed 4//25/13

Guidance for industry and reviewers: estimating the safe starting dose in clinical trials for therapeutics and adult healthy volunteers; CDERguid/3814dft.pdf, 2002. http://www.fda.gov/downloads/Drugs/Guidances/UCM078932.pdf. Accessed 5/2/2013

Guidance for Industry: developing medical imaging drug and biological products part 1: conducting safety assessments, FDA Food and Drug Administration; Center for Drug Evaluation and Research (CDER); Center for Biologics Evaluation and Research (CBER), 2004. http://www.fda.gov/downloads/Drugs/…/Guidances/ucm071600.pdf. Accessed 4/25/2013

Guidance for industry: developing medical imaging drug and biological products part 2: clinical indications, FDA Food and Drug Administration; Center for Drug Evaluation and Research (CDER); Center for Biologics Evaluation and Research (CBER), 2004. http://www.fda.gov/downloads/Drugs/GuidanceComplianceRegulatoryInformation/Guidances/ucm071603.pdf. Accessed 4/25/2013

Guidance for industry: developing medical imaging drug and biological products part 3: design, analysis, and interpretation of clinical studies, FDA Food and Drug Administration; Center for Drug Evaluation and Research (CDER); Center for Biologics Evaluation and Research (CBER), 2004. http://www.fda.gov/downloads/Drugs/GuidanceComplianceRegulatoryInformation/ Guidances/UCM071604.pdf. Accessed 4/25/2013

Guidance for industry: guidance for industry standards for clinical trial imaging endpoints; FDA Food and Drug Administration; Center for Drug Evaluation and Research (CDER); Center for Biologics Evaluation and Research (CBER), 2011. http://www.fda.gov/downloads/Drugs/GuidanceComplianceRegulatoryInformation/Guidances/UCM268555.pdf. Accessed 4/27/2013

Guidance for industry: immunogenicity assessment for therapeutic protein products, FDA Food and Drug Administration; Center for Drug Evaluation and Research (CDER); Center for Biologics Evaluation and Research (CBER), 2013. http://www.fda.gov/downloads/Drugs/GuidanceComplianceRegulatoryInformation/Guidances/UCM338856.pdf. Accessed 4/27/2013

Strijkers GJ, Mulder WJM, van Tilborg GAF, Nicolay K (2007) MRI contrast agents: current status and future perspectives. Anticancer Agents Med Chem 7(3):291–305

Harapanhalli RS (2008) Bench to bedside: the roadmap chemistry, manufacturing, and controls issues in radiopharmaceutical applications, 55th Annual meeting of the society of nuclear medicine, New Orleans, LA, June 14–18, 2008. http://apps.snm.org/docs/CME/PresenterItems/EventID_41/PresenterItemTypeID_1/CMC%20Issues-%20Harapanhalli.pdf. Accessed 5/10/2013

Hoffman JM (2012) IND research: the process and responsibilities of the MD, web page; Society of Nuclear Medicine. http://www.snm.org/docs/mwm12/Presentations/Friday/IND%20Research%20-%20The%20Process%20and%20Responsibilities%20of%20the%20MD-Clinical%20TrialsNetwork.pdf. Accessed 25 Apr 2013

Hoffman JM (2009) FLT centralized IND: standardized imaging protocol, web page, Society of Nuclear Medicine. http://interactive.snm.org/docs/SNMCTN/Monday/1100%20-%201115%20-%20Hoffman,%20John/Hoffman%20Final%20Clinical%20Trials%20Presentation%202%209%2009.pdf. Accessed 5/1/2013

ICH Topic 9, Note for guidance on statistical principles for clinical trials, EMEA, Human Medicines Evaluation Division, London, 18 Mar 1998, CPMP/ICH/363/96. http://www.emea.europa.eu/docs/en_GB/document_library/Scientific_guideline/2009/09/WC500002928.pdf. Accessed 4/27/2013

Jannin P, Krupinski E, Warfield S (2006) Validation in medical image processing. IEEE Trans Med Imag 25(11):1405–1409

Kern D, Thomae M (2013) Companion diagnostics and the FDA pre-submission programme. Regulatory Rapporteur 10(2):5–7

Larson S (2007) Herceptin as a phase 0 imaging example. In: Workshop: phase 0 trials in oncologic drug development, Natcher Conference Center, NIH, Bethesda, MD, Div. of Cancer Treatment and Diagnosis. http://dctd.cancer.gov/MajorInitiatives/Sep0507Phase0Workshop/workshop.htm. Accessed 4/25/2013

Mankoff D (2007) Imaging to guide early drug trials. In: Workshop: phase 0 trials in oncologic drug development, Natcher Conference Center, NIH, Bethesda, MD, Div. of Cancer Treatment and Diagnosis. http://dctd.cancer.gov/MajorInitiatives/Sep0507Phase0Workshop/workshop.htm. Accessed 25 Apr 2013

Marchetti S, Schellens JHM (2007) The impact of FDA and EMEA guidelines on drug development in relation to phase 0 trials. Brit J Cancer 97:577–581

Mordenti J (1986) Man versus beast: pharmacokinetic scaling in mammals. J Pharm Sci 75(11): 1028–1040

Muller PY, Milton MN (2012) The determination and interpretation of the therapeutic index in drug development. Nat Rev Drug Discov 11:751–761

Murgo AJ (2007) Clinical trial design, biostatistics, ethics, and recruitment. In: Workshop: phase 0 trials in oncologic drug development, Natcher Conference Center, NIH, Bethesda, MD, Division of Cancer Treatment and Diagnosis. http://dctd.cancer.gov/MajorInitiatives/Sep0507Phase0Workshop/workshop.htm. Accessed 4/27/2013

Nada A, Somberg J (2007) First-in-man (FIM) clinical trials post-TeGenero: a review of the impact on the TeGenero trial on the design, conduct and ethics of FIM trials. Am J Therap 14:594–604

O'Neal M (2010) Imaging charters and reader metrics in independent radiology review, CMO, RadPharm Imaging Core Lab, CoreLab Partners, Inc., Radiologic Society of America (RSNA) Presentation. http://www2.rsna.org/re/TwoTopicImagingWorkshopPresentations/Index%20Files/O%27Neal%20Panel%20Img%20Interp.pdf. Accessed 5/7/2013

Onthank DC (2005) Prediction of "First dose in human" for radiopharmaceutical/imaging agents based on allometric scaling of pharmacokinetics in pre-clinical animal models, Ph.D. Dissertation, Worchester Polytechnic Institute. http://www.wpi.edu/Pubs/ETD/Available/etd-011006-132234/unrestricted/2Onthank-Dissertation.pdf. Accessed 26 Apr 2013

Paul SM, Mytelka DS, Dunwiddie CT, Persinger CC, Munos BH, Lindborg SR, Schacht AL (2010) How to improve R&D productivity: the pharmaceutical industry's grand challenge. Nat Rev 9:203–214

Prentice RL (1898) Surrogate endpoints in clinical trials: definitions and operational criteria. Stat Med 8(4):431–440

Reagan-Shaw S, Nihal M, Ahmad N (2007) Dose translation from animal to human studies revisited. FASEB J 22:659–661

Rellahan B (2009) The TeGenero Incident March 13, 2006 UK; TGN1412—a superagonist anti-CD28 antibody, FDA presentation. http://www.ctti-clinicaltrials.org/resources/2009-fda-clinical-investigator-training-course/Rellahan%20case%20study.pdf. Accessed 5/6/2013

Rice BW, Contag CH (2009) The importance of being red. Nat Biotechnol 27(7):624–625

Riegelman R (1979) The importance of significance and the significance of importance. Postgraduate Med 66(1):119–124

Richardson D, Report PH (2012) Companion diagnostics and biomarker development. Partnership strategies and benchmarks, Fig. 1.16, p 39; entitled: Timing Diagnostic and Drug Development Processes, Cutting Edge Information®. http://www.cuttingedgeinfo.com/2012/pharma-stages-new-drug-companion-diagnostic-development/. Accessed 5/13/2013

Ritschel WA, Banerjee PS (1986) Physiological pharmacokinetic models: principles, applications, limitations and outlook. Exp Clin Pharmacol 8(10):603–614

RSNA (2011) Report on the quantitative imaging biomarkers alliance task force. http://qibawiki.rsna.org/images/2/25/QIBA_task_force_report_11-3-11.pdf. Accessed 5/5/2013

Shankar G, Shores E, Wagner C, Mire-Sluis A (2006) Scientific and regulatory considerations on the immunogenicity of biologics. Trends Biotechnol 24(6):274–280

Shields AF (ed) (2008) Special issue: imaging of molecular pathways associated with cancer. Cancer Metastasis Rev 27(4):541–750

Simms J (2009) PAD/MABEL: calculation of the minimum anticipated biological effect level (MABEL) and 1st dose in human. http://www.emea.europa.eu/docs/en_GB/document_library/Presentation/2009/11/WC500010862.pdf. Accessed 4/27/2013

SNM, Society of Nuclear Medicine (2008) Molecular imaging of cancer: from molecules to humans (special supplement) J Nucl Med (Suppl 2):1S–195S

Tang H, Mayersohn M (2005a) A novel model for prediction of human drug clearance by allometric scaling. Drug Metab Disp 33:1297–1303

Tang H, Mayersohn M (2005b) Accuracy of allometrically predicted pharmacokinetic parameters in humans: role of species selection. Drug Metab Disp 33:1288–1293

Tomaszewski J (2007) The pre-clinical pathway to the phase 0 trial. In: Workshop: phase 0 trials in oncologic drug development, Natcher Conference Center, NIH, Bethesda, MD, Division of Cancer Treatment and Diagnosis. http://dctd.cancer.gov/MajorInitiatives/Sep0507Phase0Workshop/workshop.htm. Accessed 5/5/2013

Wagner V, Dullaart A, Bock A-K, Zweck A (2006) The emerging nanomedicine landscape. Nat Biotechnol 24(10):1211–1217

Wahl RL, Jacene H, Kasamon Y, Lodge MA (2009) From RECIST to PERCIST: evolving considerations for PET response criteria in solid tumors. J Nucl Med 50(Suppl 5):122S–150S

Warnock DG, Peck CC (2010) A roadmap for biomarker qualification. Nat Biotechnol 28(5):444–445

Weber WA (2009) Assessing tumor response to therapy. J Nucl Med 50(Suppl 5):1S–10S

Woodcock J (1997) An FDA perspective on the drug development process. Food Drug Law J 52(2):145–161

Woodcock J (2013) Developing a qualified biomarker: regulatory considerations, Institute of Medicine. http://www.iom.edu/~/media/Files/Activity%20Files/Research/NeuroForum/Woodcock.pdf. Accessed 5/5/2013

Woodcock J (2010) Medical imaging: CEDR's perspective, Radiologic Society North America Workshop, Bethesda, MD. http://www2.rsna.org/re/TwoTopicImagingWorkshopPresentations/Index%20Files/Woodcock%20CDER%20Perspective.pdf. Accessed 4/25/2013

Zhao B, Schwartz LH, Larson SM (2009) Imaging surrogates of tumor response in therapy: anatomic and functional biomarkers. J Nucl Med 50:239–249

Author Biography

Mr. Brian R. Moyer is the Sr. Science Advisor for HHS/BARDA (the Biomedical Advanced Research and Development Authority, Washington, DC) in radiation and chemical injury countermeasures. He is the Owner and President of BRMoyer & Associates, LLC, Bedford, NH, specializing in medical imaging applications in drug/biologics development, radiation and chemical injuries, and pharmacokinetic and toxicokinetic consulting services. Mr. Moyer holds an MS in Pharmacology from the University of California, San Francisco, an MS in Toxicology from the University of San Francisco, and is board certified in nuclear medicine technology. He has over 80 publications in the field of imaging and has 6 drug approvals (1 BLA, 5 NDAs). He is the current chairperson of the Pharmaco-Imaging Focus Group (PIFG) for the American Association of Pharmaceutical Scientists (AAPS), is an active Rotarian, and he resides in Bedford, NH, with his wife Carol.

Dr. Narayan P.S. Cheruvu is a Sr. Principal Clinical Pharmacologist at Covidien, St. Louis, MO. He earned his Bachelor's in Pharmacy from Andhra University and Masters in Pharmacy from Institute of Technology—Banaras Hindu University, India, and Doctor of Philosophy in Pharmaceutical Science from Nebraska Medical Center, Omaha. He has over 9 years of experience in drug discovery and development in the areas of preclinical and clinical pharmacology. He has over 20 publications and has contributed to 3 drug approvals. Dr. Cheruvu is a member of numerous professional organizations, including American Association of Colleges of Pharmacy, American Society of Pharmacometrics, and American Association of Pharmaceutical Scientists. Dr. Cheruvu is the founding chair of the Pharmaco-Imaging Focus Group (PIFG) for the American Association of Pharmaceutical Scientists (AAPS).

Dr. Tom C.-C. Hu received a Bachelor's degree in Chemistry, *Magna Cum Laude*, with an emphasis in Biology from the University of Pittsburgh in 1996. Dr. Hu then went on to receive his M.S. and Ph.D. in Chemistry from Carnegie Mellon University in 1999 and 2001, respectively. Dr. Hu then moved to the National Institutes of Health as an Intramural Research Training Award (IRTA) Fellow. After his IRTA Fellowship, he went on to GlaxoSmithKline PLC as a Principal Scientist and also

B.R. Moyer et al. (eds.), *Pharmaco-Imaging in Drug and Biologics Development*,
AAPS Advances in the Pharmaceutical Sciences Series 8, DOI 10.1007/978-1-4614-8247-5,

earned an MBA from Villanova in 2005. During this time he was awarded the ASPET Division of Systems and Integrated Pharmacology (DSIP) Award in 2003. In March 2005, Dr. Hu became an Assistant Professor of Radiology and the Founding Director for the Small Animal Imaging Program at the Medical College of Georgia. In 2009, he joined the Biomedical Advanced Research and Development Authority (BARDA) as a Project Officer involving national implementation of medical countermeasure therapeutics and diagnostics for Chemical and Radiological/Nuclear threats. Dr. Hu is an invited Reviewer on the Process Validation Review Panel at the Chemical and Biological Defense Program (CBDP) Science and Technology (S&T) Process. He serves as an associate editor and an ad hoc reviewer for many peer-reviewed journals. He has also chaired several scientific meeting sessions at various national and international conferences. Dr. Hu is currently a Project Officer in the Office of the Assistant Secretary for Preparedness and Response (ASPR), U.S. Department of Health and Human Services (HHS) and an Adjunct Assistant Professor of Nuclear and Radiological Engineering/Medical Physics Program, The George W. Woodruff School of Mechanical Engineering, Georgia Institute of Technology.

Index

B.R. Moyer et al. (eds.), *Pharmaco-Imaging in Drug and Biologics Development*, AAPS Advances in the Pharmaceutical Sciences Series 8, DOI 10.1007/978-1-4614-8247-5,